AGSO JOURNAL
OF AUSTRALIAN GEOLOGY & GEOPHYSICS

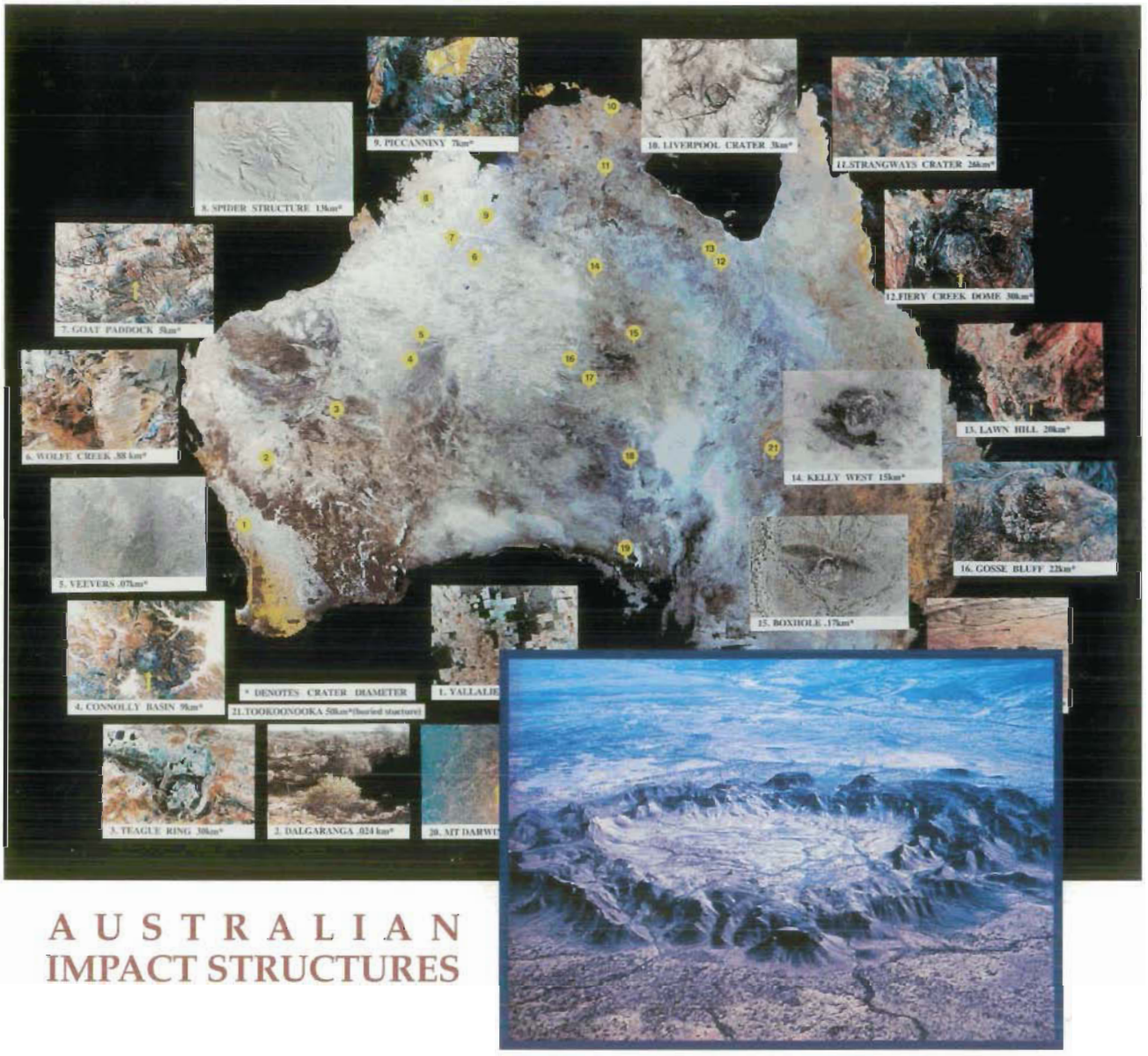

AUSTRALIAN IMPACT STRUCTURES

VOLUME 16, NUMBER 4
1996

AGSO Journal of Australian Geology & Geophysics

Editor: Ian Hodgson, Corporate Publications, Australian Geological Survey Organisation

Policy

The *AGSO Journal of Australian Geology & Geophysics* is a quarterly journal of geoscientific research results relating to the program and interests of the Australian Geological Survey Organisation (AGSO). It complements other earth science journals by focusing on Australia, and includes papers covering the broader Australasian and SW Pacific region.

The *Journal's* target audience is the world-wide geoscientific community, catering for the interests of the resource, exploration and environmental industries, as well as those of researchers in universities and State and Federal agencies.

The Editorial Board is responsible for the scientific policies and standards of the *Journal,* which will publish papers on fundamental research, applied research and review topics. Contributions are invited from anyone. Scientific excellence and relevance to the broad aims of AGSO are the main criteria for acceptance of manuscripts for publication. Peer review and editorial and production standards are similar to those of leading international journals.

Guide for contributors

Submission of a paper to the *Journal* implies that the paper is original and unpublished, and is not being considered for publication elsewhere. Papers published in the *AGSO Journal of Australian Geology & Geophysics* become Commonwealth copyright. Authors are responsible for obtaining permission to reproduce any material, especially a figure, that has been published previously.

All submissions will be peer-reviewed. Submissions by AGSO authors will normally be reviewed by non-AGSO referees; those by non-AGSO authors, by at least one AGSO referee.

When your paper has been accepted you will be asked to supply a copy on an IBM-compatible diskette. Do not send this until it is requested.

Submission of manuscripts

- Three copies of the complete manuscript should be sent to the Editor.
- Your manuscript should be double-spaced, with margins of at least 25 mm, on one side only of A4 paper, with all pages numbered. Single-spaced copies are not suitable for refereeing or editing and will not be accepted.
- Use a straightforward print-out in Times or Courier font. Do not use desktop publishing software to prepare your manuscript.
- Photocopies of draft figures are acceptable when the manuscript is first submitted, as long as they are clear enough for the reviewers. Final versions of figures must be supplied when the final version of the manuscript is accepted for publication.
- Photographs should be supplied as glossy prints.

Style

Contributions should be written in English, and spelling should follow the latest edition of *The Macquarie Dictionary.* Refer to a recent issue of the *Journal* for further guidance on general style. But note that a revised style for references is being introduced with these instructions. Heading hierarchy should be indicated in the margin by ringed capital letters; A for main headings, B for second level headings, etc.

Abstract

An abstract is required at the beginning of the manuscript. It should provide an informative summary of the main results and conclusions contained in the manuscript. It should not exceed 300 words. (An abstract is not adequate if it states that certain work was done, but fails to summarise the outcomes.).

References

The Journal does not cite 'in prep' references. References 'in press' are acceptable only if the journal and issue can be supplied. References to unpublished data, if necessary, should be quoted as personal communications, giving the affiliation of the person being quoted and the date of communication. References should be cited in the text by author(s) and year in the normal Harvard style. For example: 'Ernest (1976, p. 312) showed that...' or as described by earlier workers (Zagreb 1931; Ernest 1976; Melway & Murray 1977; Melway et al. 1978). References should be listed at the end of the text, in alphabetical order and in the style shown below. Please note that all journal titles are spelt out in full.

Continued inside back cover

AGSO JOURNAL

OF AUSTRALIAN GEOLOGY & GEOPHYSICS

VOLUME 16, NUMBER 4, 1996

Thematic issue: Australian impact structures*

* In honour of Robert S. Dietz (1914–1995) — pioneer of astrobleme research — and of Eugene M. Shoemaker and Carolyn S. Shoemaker for their major contributions to the study of Australian impact structures.

Guest associate editor: Andrew Y. Glikson

A.Y. Glikson
Preface 371

A.Y. Glikson (compiler)
A compendium of Australian impact structures, possible impact structures, and ejecta occurrences 373

R.S. Dietz
The significance of extraterrestrial impacts with reference to Australia 377

E.M. Shoemaker & C.S. Shoemaker
The Proterozoic impact record of Australia 379

R.A.F. Grieve & M. Pilkington
The signature of terrestrial impacts 399

A.W.R. Bevan
Australian crater-forming meteorites 421

G.E. Williams, P.W. Schmidt, & D.M. Boyd
Magnetic signature and morphology of the Acraman impact structure, South Australia 431

M.W. Wallace, V. Gostin, & R.R. Keays
Sedimentology of the Neoproterozoic Acraman impact-ejecta horizon, South Australia 443

D.J. Milton, A.Y. Glikson, & R. Brett
Gosses Bluff — a latest Jurassic impact structure, central Australia. Part 1: geological structure, stratigraphy, and origin 453

D.J. Milton, B.C. Barlow, A.R. Brown, F.J. Moss, E.A. Manwaring, E.C.E. Sedmik, G.A. Young, & J. Van Son
Gosses Bluff — a latest Jurassic impact structure, central Australia. Part 2: seismic, magnetic, and gravity studies 487

P.R. Tingate, J.F. Lindsay, & S.J. Marshallsea
Impact structures as potential petroleum exploration targets: Gosses Bluff, a Late Jurassic example in central Australia 529

J.D. Gorter, R.J. Korsch, & R.S. Nicoll
Thermal history of the Gosses Bluff impact structure, central Australia, from conodont colour-alteration indices: implications for hydrocarbon prospectivity and erosional history 553

P.W. Haines
Goyder impact structure, Arnhem Land, Northern Territory 561

F.L. Sutherland
The Cretaceous/Tertiary-boundary impact and its global effects with reference to Australia 567

A.Y. Glikson
Mega-impacts and mantle-melting episodes: tests of possible correlations 587

General paper

D.H. Blake
Structural interpretations of the Wonga Belt in the Proterozoic Mount Isa Inlier of northwest Queensland — a review 609

Map (in back pocket):

D.J. Milton
Geology of the central uplift, Gosses Bluff impact structure, Northern Territory (1:7500 geological map)

ISSN 1320–1271

Subscriptions to the AGSO Journal are available through the Australian Geological Survey Organisation (GPO Box 378, Canberra ACT 2601; tel. 06 249 9642, fax 06 249 9982).

Other matters concerning the Journal should be sent to the Editor, AGSO Journal

Editor, AGSO Journal: Ian Hodgson
Editor of this number of the AGSO Journal: Geoff Bladon
Cover design and figures prepared by AGSO Cartographic Services Unit unless otherwise indicated.
Prepared for publication by Green Words, Canberra

Printed in Australia by National Capital Printing, Fyshwick, A.C.T. 2609

AUSTRALIAN GOVERNMENT PUBLISHING SERVICE CANBERRA 1996

Month of issue, June 1996

Front-cover illustration: **A poster, 'Australian impact structures — a photographic catalogue'*, by A. Buchanan[1], A.W.R. Bevan[2], & R. Shaw[1], and (inset) an aerial view looking northwest at the circular ridge of the Gosses Bluff structure, central Australia.**

The poster was produced by photographic compilation of satellite images and aerial photographs showing the geographic distribution of known Australian impact structures as catalogued by Shoemaker & Shoemaker (1988: Lunar and Planetary Science, XIX, 1079–1080). Owing to the sizes of many of these structures, and the cryptic surface expressions of some of them, they can be best viewed from data recorded on satellite platforms and in aircraft. The locality and reference image for the photographic catalogue is a digital mosaic of images acquired from the AVHRR sensor on the NOAA series of satellites. This sensor has a swath width of 3000 km and a ground spatial resolution of 1.1 km.

Photographs numbered 3, 4, 6, 7, and 19 were acquired by the Multispectral Scanner System (MSS) sensor aboard the Landsat 4/5 spacecraft. These satellites are part of an American series specifically designed for land-use studies. The Landsat MSS instrument has a swath width of 185 km and a ground spatial resolution of 80 m. Photographs numbered 1, 9, 11, 12, 13, and 16 were acquired by the Landsat Thematic Mapper sensor which has a swath width of 185 km and ground spatial resolution of 30 m.

The satellite imagery was provided by the Australian Centre for Remote Sensing and the Leeuwin Remote Sensing Application Centre, Department of Land Administration (DOLA), Western Australia. Vertical aerial photographs numbered 10, 14, 15, 18, and 20 were provided by and reproduced with the permission of the General Manager, Australian Surveying & Land Information Group, Department of Administrative Services, Canberra, ACT. The oblique aerial photograph no. 17 was provided by M. Freeman. The field photograph no. 2 was supplied by Ken Leighton of Rangeland Survey, DOLA. The aerial photograph no. 20 was supplied from Tasmap, Department of Environment and Planning, Tasmania. The Australian NOAA AVHRR mosaic was produced by A. Wyllie at the Leeuwin Remote Sensing Application Centre.

The poster was presented at the 6th Australasian Remote Sensing Conference, 1992, Wellington, New Zealand.

* The Fiery Creek dome, portrayed on the cover, has been shown not to be of an impact origin (E.M. Shoemaker, personal communication 1996)

1 Leeuwin Remote Sensing Application Centre, Western Australian Department of Land Administration.

2 Department of Earth and Planetary Sciences, Western Australian Museum.

Thematic issue: Australian impact structures

Preface

Studies of structures produced by impacts of asteroids and comets, and of the thermal, atmospheric, hydrospheric, and biological effects of mega-impacts, have led to an increased understanding of the repercussions of these events on terrestrial evolution. Since the recognition of small recent craters and their associated meteoritic materials early in the century (e.g., Barringer crater, Arizona, and the Henbury craters, Northern Territory), the identification of impact sites has been advanced by the use of shatter cones as diagnostic criteria (e.g., for the Vredefort, Sudbury, and Gosses Bluff structures), as pioneered by Robert Dietz. The introductory article in this issue is possibly the last paper Robert Dietz wrote before he passed away in May 1995. Since the early 1980s, the scope of impact studies has expanded with the discovery of distant ejecta deposits and with the characterisation of the atmospheric, hydrospheric, and biological consequences of large impacts. The outstanding example is the coeval Chicxulub impact structure in the Yucatan Peninsula, Mexico, the associated global Cretaceous–Tertiary-boundary ejecta layer marked by iridium anomalies, and the related mass extinction.

This thematic issue has grown from a plan to publish the principal results, including detailed maps, of the joint AGSO (formerly BMR)/United States Geological Survey study of the Gosses Bluff impact structure, in central Australia. Some of the results of this study have been documented in technical reports and short articles, but the bulk of them have until now remained unpublished.

The Australian continent is uniquely placed with regard to the study of ancient impact scars, an observation that reflects two factors: firstly, the preservation of vast tracts of little-deformed Precambrian strata; and, secondly, the arid conditions and low relief, which enhance the preservation of both ancient and recent impact signatures, often shown on satellite images and aerial photographs. Recognising these factors, Eugene and Carolyn Shoemaker have, since the mid-1980s, undertaken numerous trips to remote parts of this land in an indefatigable search for evidence of impacts. AGSO is honoured that these distinguished scientists accepted our invitation to publish some of their results in the *AGSO Journal*.

One of the most exciting discoveries was that of the Acraman impact structure, South Australia, found by George Williams. Acraman is a prime example of an impact structure correlated with coeval regional ejecta, found in the Bunyeroo Formation and its equivalents. Both the impact structure and the ejecta are documented in papers in this issue.

This number of the *AGSO Journal* is fortunate to have a review by Richard Grieve & Mark Pilkington on the criteria for recognising extraterrestrial impact structures. The economic significance of impact structures has been recently highlighted by Grieve & Masaitis (1994: International Geology Review, 36, 105–151). Petroleum reservoirs include those at the Ames Hole and Red Wing Creek (USA) and Viewfield (Canada) structures, for example. The Tookoonooka and Talundilly structures in the Eromanga Basin (Queensland) might have influenced the migration of oil and gas. Grieve & Pilkington point out that about 25 per cent of the known terrestrial impact craters are associated with economic resources, including metalliferous mineral deposits such as the Ni–Cu ores at Sudbury, Ontario. Preservation of the Witwatersrand gold deposits is attributed to their structural location in the ring structural depression of the Vredefort impact structure. The current exploitation of petroleum and minerals associated with impact structures in North America is estimated to be valued at $5 billion per year.

The catastrophic consequences of major impacts on the terrestrial atmosphere, hydrosphere, and biosphere, as well as their structural effects, have been increasingly evident from studies over the last 10 years or so. The last two papers in this issue are concerned with the Cretaceous–Tertiary-boundary extinction, and the potential tectonic and magmatic effects of major asteroid and comet impacts.

This preface has benefited from the comments of E.M. Shoemaker. I am personally indebted to the late R.S. Dietz for his encouragement, and to E.M. and C.S. Shoemaker for their contribution to and support of this issue. My sincere thanks to R.A.F. Grieve, M. Pilkington, A.W.R. Bevan, and F.L. Sutherland for providing invited review papers. I am grateful to C.E. Barton, chairman of the Editorial Board of the *AGSO Journal*, for inviting me to edit this issue; to J.C. Dooley and A.N. Yeates for processing the original Gosses Bluff monograph; to G.E. Williams for generous help with reviews; and to D.J. Milton for coming to Australia to help with the preparation of the Gosses Bluff material. I thank G.M. Bladon for meticulous editorial processing; K.A. Barrett for cartographic work; and I.M. Hodgson and K.H. Wolf for editorial advice. Grateful acknowledgments are due to A.W.R. Bevan, D.M. Boyd, J. Claoué-Long, R.A.F. Grieve, A.R. Hildebrand, D.M. Hoatson, J. Leven, J.F. Lindsay, M. Pilkington, J.W. Sheraton, A.J. Stewart, S.R. Taylor, A.M. Therriault, M.W. Wallace, J. Webb, A.T. Wells, and G.E.Williams for reviewing papers included in this issue. My sincere thanks to R. Shaw for help with providing material for the cover of this issue.

Andrew Y. Glikson
February 1996

AGSO Journal of Australian Geology & Geophysics, 16 (4), 373–375

A compendium of Australian impact structures, possible impact structures, and ejecta occurrences[1]

Compiled by A.Y. Glikson[2]

1. Meteorite craters and astroblemes

Structure and site	*Lat./long.*	*Diameter (km)*	*Impact criteria**	*Age (Ma)*	*References*
1. Dalgaranga, Yalgoo, WA	27°40'S 117°17'E	0.024	abm	<0.003?	Bevan (this issue); Nishiizumi et al. (unpublished; E.M. Shoemaker personal commmunication 1995)
2. Snelling, Kimberley, WA	19°21'S 127°46'E	0.029 × 0.022	ab	<0.005?	Shoemaker & Shoemaker (unpublished)
3. Veevers, Canning Basin, WA	22°58'S 125°22'E	0.070	abm	≤0.02	Yeates et al. (1976); Bevan (this issue); Nishiizumi et al. (unpublished; E.M. Shoemaker personal communication 1995)
4. Henbury, central Australia, NT	24°35'S 133°10'E	13 or 14 craters; 0.006-0.18	abesm	0.0042 ± 0.0019	Bevan (this issue); Attrep et al. (1991)
5. Boxhole, NT	22°37'S 135°12'E	0.17	am	0.03	Bevan (this issue); Shoemaker et al. (1988); Shoemaker et al. (1990)
6. Wolfe Creek, Kimberley, WA	19°10'S 127°46'E	0.88	aems	0.3	Bevan (this issue); Attrep et al. (1991); E.M. Shoemaker (personal communication 1995
7. Mount Darwin, Tas. west coast	42°18'S 145°40'E	1.0	aeg	0.74 ± 0.04	Fudali & Ford (1979); Shoemaker & Shoemaker (1988)
8. Mount Toondina, Oodnadatta area, SA	27°57'S 132°22'E	4	agx	<35	Plescia et al. (1994); Shoemaker & Shoemaker (unpublished)
9. Goat Paddock, Kimberley, WA	18°20'S 126°40'E	5	abe	~55	Shoemaker & Shoemaker (1988)
10. Connolly Basin, Gibson desert, WA	23°32'S 124°45'E	9	abg	<60	Shoemaker & Shoemaker (1989); Shoemaker et al. (1989)
11. Yallalie Basin, west Yilgarn, WA	30°27'S 115°46'E	13	bgu	~90	Dentith et al. (1992); E.M. Shoemaker (personal communication 1995)
12. Tookoonooka, Eromanga Basin, Qld	27°20'S 142°49'E	~55	begu	128 ± 5	Gorter et al. (1989)
13. Talundilly, Eromanga Basin, Qld	24°44'S 144°37'E	~30	gu	128 ± 5	Longley (1989)
14. Liverpool, Arnhem Land, NT	12°24'S 134°03'E	~3?	ab	>140?	Shoemaker & Shoemaker (1988)
15. Gosses Bluff, Amadeus Basin, NT	23°49'S 132°18'E	24	abegx	142.5 ± 0.8	Milton et al. (this issue)
16. Piccaninny, Kimberley, WA	17°25'S 128°25'E	7	ab	<360	Beere (1983); Shoemaker & Shoemaker (1988); E.M. Shoemaker (personal communication 1995)
17. Kelly West, Tennant Creek region, NT	19°56'S 133°57'E	8–20	abx	Neo-proterozoic	Shoemaker & Shoemaker (this issue)

[1] Based principally on updated information kindly provided by E.M. Shoemaker and C.S. Shoemaker, papers included in this issue, and comments by A.W.R. Bevan and G.E. Williams. The structures and distal meteoritic occurrences are listed in an approximate age or maximum age sequence. Only the more recent references, including papers in the present issue, are listed here. For original and other references for each occurrence consult reference lists in papers in this issue.

[2] Division of Regional Geology & Minerals, Australian Geological Survey Organisation, P.O. Box 378, Canberra, ACT 2601.

1. Meteorite craters and astroblemes

Structure and site	*Lat./long.*	*Diameter (km)*	*Impact criteria**	*Age (Ma)*	*References*
18. Acraman, Gawler craton, SA	32°01'S 135°27'E	85–90	abefgx	~590	Williams et al. (this issue)
19. Spider, Kimberley, WA	16°44'S 126°05'E	13 × 11	ax	>700	Shoemaker & Shoemaker (this issue)
20. Strangways, Arnhem Land, NT	15°12'S 133°35'E	>26	abesx	1000?	Shoemaker & Shoemaker (this issue)
21. Goyder, Arnhem Land, NT	13°28'S 135°02'E	7-25	as	<1400	Haines (this issue)
22. Lawn Hill, NW Qld	18°41'S 138°39'E	20	abex	<1670; pre-Middle Cambrian	Shoemaker & Shoemaker (this issue)
23. Teague Ring, Wiluna region, WA	25°52'S 120°53'E	30	abgx	1630 ± 5	Shoemaker & Shoemaker (this issue)

2. Some circular structures, including buried structures, whose *potential* impact origin requires testing

Structure and site	*Lat./long.*	*Diameter (km)*	*Impact criteria*	*Age (Ma)*	*References*
Dirranbandi, Qld	28°35'S 148°10'E		multiple craters		Binns (1967)
Spring Range, Barrow Creek, NT	21°52'S 134°18'E	0.3	(type of planar deformation feature [PDF] requires confirmation)		Haines (1989)
Mulkarra,west Eromanga Basin, SA	27°50'S 138°55'E	17	gu	105 ± 3	Flynn (1989)
Camooweal, NW Qld	19°15'S 138°07'E	~30	gu (requires confirmation through drilling)	>550	Glikson (unpublished)

3. Spherule/ejecta units and siderophile-element anomalies of demonstrated and *possible* impact origin

Age/stratigraphy	*Location*	*Lithology/texture/impact criteria*	*Reference*
Frasnian–Fammenian (Late Devonian)	north Canning Basin, WA	iridium anomaly; extensive extinctions; interpreted in terms of biogenic concentrations of siderophiles	Hurley & Van der Voo (1990)
~0.59 Ga ejecta unit within shale; Bunyeroo Formation	Flinders Ranges, SA	fragmental ejecta (including shatter-coned fragments); spherules; siderophile-element anomalies; shock lamellae in quartz	Wallace et al. (this issue)
~2.5 Ga Dales Gorge Member, Brockman Iron Formation	Hamersley Basin, WA	spherules mixed with volcaniclastics	Simonson (1992)
~2.6 Ga Carawine Dolomite	Hamersley Basin, WA	a spherule component within dolomixtite	Simonson (1992)
~2.6 Ga upper Wittenoom Formation	Hamersley Basin, WA	12–130-cm-thick spherule-bearing unit in turbidite; pronounced iridium anomaly	Simonson (1992); B.M. Simonson (personal communication 1995)
~3.45 Ga upper Warrawoona Group	Miralga Creek, north Pilbara Block, WA	0.1-0.75-mm-diameter spherules in 15-50-cm-thick current-bedded arenite within chert intercalated with mafic volcanics	Lowe & Byerly (1986)

***Impact criteria**

a geologic structure
b impact breccia (including distal ejecta) and/or shock metamorphism (cf. shock lamellae in quartz)
e impact melt
f siderophile elements in fallout layer
g geophysical evidence
m associated meteorites
s siderophile elements in impact melt
u buried structure
x shatter cones

References

Attrep, M. Jr., Orth, C.J., Quintana, L.R., Shoemaker, C.S., Shoemaker, E.M. & Taylor, S.R., 1991. Chemical fractionation of siderophile elements in impactites from Australian meteorite craters. Lunar and Planetary Science, XXII, 39–40.

Beere, G.M., 1983. Piccaninny structure — a cryptoexplosion feature in the Ord Basin, East Kimberley. Geological Survey of Western Australia, Record 1983/6

Binns, R.A., 1967. Possible meteorite craters near Dirranbandi, Queensland. 30th Annual Meeting of the Meteoritic Society, Moffett Field, California, Program.

Dentith, M.C., Bevan, A.W.R., McInerney, K.B., 1992. A preliminary investigation of the Yallalie Basin: a buried 15 km diameter structure of possible impact origin in the Perth Basin, Western Australia. Meteoritics, 27, 214.

Flynn, M., 1989. The Mulkarra structure: a possible buried impact crater in the western Eromanga Basin, Australia. In: O'Neil, B.J. (editor), The Cooper and Eromanga Basins, Australia. Proceedings of the Petroleum Exploration Society of Australia, the Society of Petroleum Engineers, and the Australian Society of Exploration Geophysicists (SA Branches), Adelaide, 431–439.

Fudali, R.F. & Ford, R.J., 1979. Darwin glass and Darwin crater: a progress report. Meteoritics, 14, 283–296.

Gorter, J.D., Gostin, V.A. & Plummer, P.S., 1989. The enigmatic subsurface Tookoonooka complex in south–west Queensland: its impact origin and implications for hydrocarbon accumulations. In: O'Neil, B.J. (editor), The Cooper and Eromanga Basins, Australia. Proceedings of the Petroleum Exploration Society of Australia, the Society of Petroleum Engineers, and the Australian Society of Exploration Geophysicists (SA Branches), Adelaide, 441–456.

Haines, P.W., 1989. Probable impact structure near Barrow Creek, Northern Territory. Australian Journal of Earth Science, 36, 13

Hurley, N.F. & Van der Voo, R., 1990. Magnetostratigraphy, Late Devonian iridium anomaly and impact hypotheses. Geology, 18, 291–294.

Longley, I.M., 1989. The Talundilly anomaly and its implications for hydrocarbon exploration of Eromanga astroblemes. In: O'Neil, B.J. (editor), The Cooper and Eromanga Basins, Australia. Proceedings of the Petroleum Exploration Society of Australia, the Society of Petroleum Engineers, and the Australian Society of Exploration Geophysicists (SA Branches), Adelaide, 473–490.

Lowe, D.R. & Byerly, G.R., 1986. Early Archean silicate spherules of probable impact origin, South Africa and Western Australia. Geology, 14, 83–86.

Plescia, J.B., Shoemaker, E.M. & Shoemaker, C.S., 1994. Gravity survey of the Mount Toondina impact structure, South Australia. Journal of Geophysical Research, 99, 13167–13179.

Shoemaker, E.M., Roddy, D.J., Shoemaker, C.S. & Roddy, J.K., 1988. The Boxhole meteorite crater, Northern Territory. Lunar and Planetary Science, XIX, 1081–1082.

Shoemaker, E.M. & Shoemaker, C.S., 1988. Impact structures of Australia. Lunar and Planetary Science, XIX, 1079–1080.

Shoemaker, E.M. & Shoemaker, C.S., 1989. Geology of the Connolly Basin impact structure, Western Australia. Lunar and Planetary Science, XX, 1008–1009.

Shoemaker, E.M., Shoemaker, C.S., Nishiizumi, K., Kohl, C.P., Arnold, J.R., Klein, J., Fink, D., Middleton, R., Kubik, P.W. & Sharma, P., 1990. Ages of Australian meteorite craters — a preliminary report (abstract). Meteoritics, 25, 409.

Shoemaker, E.M., Shoemaker, C.S. & Plescia, J.B., 1989. Gravity investigation of the Connolly Basin impact structure, Western Australia. Lunar and Planetary Science, XX, 1010–1011.

Simonson, B.M., 1992. Geological evidence for a strewn field of impact spherules in the early Precambrian Hamersley Basin of Western Australia. Geological Society of America, Bulletin, 104, 829–839.

Yeates, A.N., Crowe, R.W.A. & Towner, R.R., 1976. The Veevers crater — a possible meteoritic feature. BMR Journal of Australian Geology & Geophysics, 1, 77–88.

AGSO Journal of Australian Geology & Geophysics, 16 (4), 377–378

The significance of extraterrestrial impacts with reference to Australia

Emeritus Professor Robert S. Dietz, 1914–1995

An impact by an asteroid or comet on the surface of a planet or Moon is the closest natural answer to the physical conundrum as to what happens when an irresistible force collides with an immovable object: the strata open up like a giant flower with a central crater eye and petal-like streaks of ejecta. Whereas plate tectonics outline ongoing mantle–crustal processes, cosmic impacts are the wild cards that perturb both terrestrial crustal history and the evolution of life; they result in the paradigm of astrocatastrophism, and link Earth science with astronomy. Over the aeons, the face of the Moon has looked down on Earth with a fixed stare, while mother Earth has constantly modified her smile through plate tectonics.

The role of extraterrestrial impact in Earth history with its catastrophic scenario has been and remains an anathema to many geologists who follow uniformitarian Lyellian views. The British astronomer H.A. Proctor in 1873 was probably the first to offer an impact interpretation of the lunar craters, but withdrew the idea because such craters were not evident on Earth. In 1893, G.K. Gilbert, chief geologist of the United States Geological Survey, described the lunar craters as meteoritic in origin, but in 1896 opined that the Barringer crater, Arizona, was of volcanic origin. In 1969, G.J.H. McCall wrote: 'It is not in dispute that impact explosions have had some role in geology, though it must appear to most geologists, weighing the geologic record without sentiment, that their role has been very insignificant'. McCall regarded the Wolfe Creek Crater in the Kimberley region of northwest Australia, as of volcanic origin. The Apollo missions, initially biased toward a volcanic interpretation of the lunar craters, resulted in a ringing victory for 'impactology'. More recently, clear distinctions have been made between impact and volcanic features on Venus.

The gradual recognition between 1930 and 1950 that the Barringer crater (Meteor crater) was truly a prototype asteroidal crater aroused much interest, and by mid-century eleven craters associated with meteoric debris had been recognised, four of them in Australia — namely Dalgaranga, Henbury, Boxhole, and Wolfe Creek. The 24-m-diameter Dalgaranga crater was first discovered in 1923, but fifteen years passed before E.S. Simpson published in 1938 a description of this crater and the associated mesosiderite fragments, which contrasted with the nickel–iron fragments associated with craters elsewhere. In 1932, the Henbury cluster of craters was described by A.R. Alderman. The 152-m-diameter Boxhole crater was identified by C.T. Madigan in 1937. Most remarkable of all was the Wolfe Creek crater (averaging 880 m across, and 45 m deep), discovered from the air in 1947. A decade would pass before the first of the astroblemes — ancient eroded impact structures — would be identified from their structural type and shock indicators. To date, some 23 putative craters and astroblemes have been verified on the Australian continent (see compendium, this issue).

The reality of planetary impacts by cosmic bolides was emphasised by the apparition of the 1994 comet Shoemaker–Levy 9, which had been disrupted into a 'string of pearls' by Jupiter's tidal attraction. As calculated, the fragments slammed into Jupiter's southern hemisphere over several days in July 1994, at 60 km s^{-1}, creating immense explosions. These impacts resulted in the greatest recorded display of celestial fireworks since the telescope was invented by Galileo. Within ten seconds of impact of each fragment, an immense fireball rose above the horizon and into telescopic view. The plumes of debris arced in ballistic trajectories expanding to thousands of kilometres. The end result of this impact series amounted to Earth-size dark splotches which persisted for several months. Had such impacts impinged on Earth, the effects would compare with those of the 65 Ma Cretaceous/Tertiary boundary events when over two-thirds of terrestrial species were wiped out by the effects of an asteroid that formed the Chicxulub crater in Yucatan.

The role of mega-impact in earliest planetary history is manifested for example by the probable extraction of the Moon from Earth by a Mars-size body, and by the interpretation of Miranda, Saturn's satellite, as a churned body coalesced from fragments blown apart by impact. The retrograde rotation of Venus is possibly explained by early capture of a satellite about half the size of the Moon. Space probes reveal that impact craters dominate the surface morphology of most of the terrestrial planets and their 27 satellites; some of the best examples engrave the surface of Venus and the Moon, where the near-absence of erosion ensures the pristine structure of these scars. Earth is exceptional among the planets since its volcanic–tectonic activity and severe surface erosion over the aeons eliminate or extensively mask the effects of impacts. Nevertheless, some 160 impact scars are revealed by the morphological and geological record, and each year several more are discovered.

Planets and satellites have been bombarded by cosmic debris for 4.6 Ga; evidence of the first 600 Ma of this process is furnished by the 30 000 craters on the Moon, testifying to an asteroid/comet flux about two orders of magnitude greater than at present. Scant terrestrial evidence for this period — the Hadean — includes relict 4.27-Ga zircon grains in sediments in the Gascoyne Province of Western Australia, 3.96-Ga tonalite gneiss and amphibolite of the Acasta gneiss (Slave Province, Northwest Territories, Canada), and gneisses of similar age in Antarctica.

Comparative planetology offers new perspectives on the history of the Earth; sometimes we must leave home to learn from whence we came! Remnant Hadean surfaces of Mercury, Mars, and the Moon hold clues to the Earth's earliest history. Yet Earth remains unique, thanks to its surface temperature range allowing the preservation of liquid water and thereby the evolution of life. Mars lacks sufficient atmospheric pressure to hold liquid water, while the Venusian mantle was probably catastrophically degassed. The Goldilocks paradigm prevails: Earth is stressful, but this hastens the arrow of evolution. Remarkable discoveries lie ahead.

The lunar record reveals early accretionary growth through impacts, culminating in saturation bombardment ending about 3.9 Ga when the giant maria basins were blasted out. The 1994 Clementine mission to the Moon has greatly enhanced the knowledge of this satellite. Even more important was the grand tour of the Solar System by Voyager 1 and 2, followed recently

by the Magellan mapping of Venus. Venus reveals three impact craters larger than 150 km across (Mead, Meitner, and Isabella), as does the Earth (Vredefort, 2.0 Ga; Sudbury, 1.85 Ga; and Chicxulub, 65 Ma). Remarkably, although impact ejecta have been identified at the Cretaceous–Tertiary boundary in over 100 sites worldwide since 1980, it took another decade to find Chicxulub — in 1990 —buried beneath a kilometre of limestone in the Yucatan Peninsula, Mexico. How many more covered or deformed impact structures await discovery? The crater count on Venus is about 1000, and Earth should have at least a similar number of craters. The scattered pages of Precambrian stratigraphy might have preserved some impact effects — including diamictites, microtektites (spherule beds), superheated magmas, and impact-related deformational events. Shatter cones and mineral planar deformational features may be preserved locally.

The first fall recognised as meteoritic in origin occurred in 1803, when 3000 fragments fell at L'Aigle, France. On Kitt Peak near Tucson, Arizona, a program called Spacewatch uses a special telescope for detecting meteoroids passing near the Earth. Eighty-two small objects had been discovered over five years to the end of 1994. On 8 December 1994, a 10-m rock designated '1994xM1' hurtled past Earth at 43 000 km h^{-1} at a record-setting close approach of 102 000 km — about one-quarter the distance between the Earth and the Moon. Had this cosmic cannonball struck Earth, a 150-m-diameter crater would have resulted. Although crater-forming impacts are historically rare, recent examples include the Sikhote–Alin event, which showered 23 t of nickel–iron fragments on Kamchatka, Siberia, in 1947. In 1954, at Sylacuaga, Alabama, a 3.86-kg chondrite crashed through the roof of a house and ricocheted to hit a woman on the hip. In 1984, a 1.5-kg chondrite knocked a mailbox off its post in Claxton, Georgia, USA. In 1991, a 1-m iron created a 10-m percussion crater at Sterlitamak, Russia. Two cars have been hit recently by small meteorites: one at Peekskill, New York (1992); the other in Japan (1995). No deaths have been reported to have been caused by meteorites, but a gram-size fragment soft-landed on the head of a small boy during the 1992 M'bali fall in Uganda.

My own principal contact with Australian impact structures was a one-week study of Gosses Bluff in 1967, while en route to join the US Coast and Geodetic survey's research vessel *Oceanographer* in Perth (Dietz 1967: Nature, 216, 1082–1084). I recognised that it was an astrobleme *par excellence* and one of the world's finest examples. Gosses Bluff is an exhumed circular ring structure of up-ended strata with a 4.5-km central uplift enclosing a central eroded basin. Surrounding the uplift is an annular-ring syncline, providing an overall diameter to the disturbance of 24 km. The structure is truncated by mesas constituting the relics of a Mesozoic peneplain. Gosses Bluff includes a spectacular display of shatter cones created by the impact shock wave. The shatter cones are oriented upwards at high angles relative to the bedding at the centre, and at low angles to the bedding at the peripheries of the structure. These attitudes represent shock effects propagated from the centre at a shallow depth beneath the palaeosurface. Shatter-coned breccia clasts suggest that deformation and uplift immediately followed the passage of a shock front. The structure and scale of Gosses Bluff resemble those of the Sierra de Cangalha astrobleme in Brazil.

Two other Australian astroblemes are of special interest to me. The first is the large late Precambrian Acraman structure. Like Chicxulub, ejecta blankets of the Acraman impact containing shatter cones and shock lamellae are recognised in stratigraphic records located hundreds of kilometres away from the crater. The second remarkable astrobleme is the Spider structure — so named because of the numerous sandstone ridges which radiate from its central uplift. Spider promises to tell us much about the mechanics of central rebound uplift, typical of many astroblemes.

With the exception of Antarctica, Australia with its dry desert climate is the world's finest site for the collection of meteorites. With about 447 Australian meteorites now known, Australia ranks third in meteoritic finds after Antarctica and the USA. The meteorites range from nickel–iron masses to friable stones. They include soft carbonaceous chondrites — even rare pre-biotic organic compounds — and samples from the Moon and the Asteroid Vesta (Eucrites). Australian finds include Calcalong Creek, the only known lunar-derived meteorite, and the Murchison CM2 carbonaceous chondrite. Meteorites offer an insight into the metallic cores of planets, form the basis for determining the age of the Solar System and the Earth, and yield information on cosmic radiation.

The vast Australasian tektite strewn field, which extends northwestward between Australia and southeast Asia, consists of small bits of anhydrous natural glass splashed from a cometary impact about 780 000 years ago from an unidentified locus. These tektites are aerodynamically sculptured by their molten passage through the atmosphere. Flanged buttons are found in Australia. These indicate flight into near space for at least several minutes to allow molten spheres to congeal and then, upon re-entry, partly remelt on their front faces to form flanges. A former interpretation of tektites in terms of impact ejection from the Moon has been discarded on geochemical criteria. It is possible that the comet that generated the Australian tektites broke into several fragments before impact, laying down a swath of small craters or possibly just searing the ground along a path extending from Hainan Island, China, and striking across southeast Asia to Thailand. Large layered blobs of glass termed Muong Nong tektites from a type locality in Laos occur along this path. In 1967, I made the suggestion that the 20-km Elgygytgyn crater in Siberia might be the source of the Australasian strewn field, but subsequent dating of this crater as 4 Ma shows that it is too old to be the source of this field.

A 1961 paper by W.F. Cannon entitled 'Impact of uniformitarianism' examines the role of this principle laid down by Charles Lyell in his 1830 'Principles of geology'. Nowadays a paper entitled 'The impact of impacts' would seem to be in order in view of the catastrophic role played by the collision of bolides with Earth, causing craters, wild fires, and extinctions. As the planetologist and historian of science Ursula Marvin has pointed out, bolide impacts are a geological process of major importance which, by its very nature, demolishes uniformitarianism as a basic principle in geology. To regard bolide impacts as uniformitarianism, imposing a modern usage on an 1830s Lyellian term, would amount to an exercise in 'newspeak'.

AGSO Journal of Australian Geology & Geophysics, 16 (4), 379–398

The Proterozoic impact record of Australia

Eugene M. Shoemaker[1] & Carolyn S. Shoemaker[1]

Six impact structures of known or probable Proterozoic age have been identified in Australia: (1) the Teague Ring structure in central Western Australia, 30 km in diameter and possibly about 1630 Ma in age; (2) the Spider structure in northern Western Australia, 11 km wide, 13 km long, and probably Meso- to Neoproterozoic in age; (3) the Kelly West structure in the central Northern Territory, possibly between 8 and 20 km in diameter and Neoproterozoic in age; (4) the Strangways structure in the northern Northern Territory, possibly 40 km in diameter and about 1000 Ma in age; (5) the Lawn Hill structure in northwestern Queensland, 20 km in diameter and probably of Neoproterozoic age; and (6) the Acraman structure, probably about 35 to 40 km in diameter and about 590 Ma in age.

Discovery of impact structures in *exposed* gently to mildly deformed stratified Proterozoic rocks in Australia is estimated to be complete or close to complete at diameters equal to or greater than 20 km. From the four known structures with diameter ≥20 km, the estimated area of exposed Proterozoic strata (~1.15×10^6 km^2), and the estimated mean time of exposure (~900 Ma), the cratering rate is estimated at $(3.8 \pm 1.9) \times 10^{-15}$ km^{-2} y^{-1}. This estimate for the production of craters ≥20 km during the Proterozoic is consistent with the mean cratering rate for the last 3.2 Ga on the Moon, and somewhat below the estimated present cratering rate on Earth.

Introduction

The most complete record on Earth of Precambrian impact structures has been found on the Australian craton. This circumstance is due to two factors. Firstly, epicontinental basins of Proterozoic age that contain gently to moderately deformed, largely unmetamorphosed sedimentary rocks are extensively exposed in Australia. Structural deformation by impact is fairly readily recognised in these basins. Secondly, much of the Australian craton has been exceptionally stable, not only during the Phanerozoic but also during a considerable part of Proterozoic time. Hence many large impact structures have been neither too deeply eroded nor too deeply buried to render them undetectable. We present here a summary of six structures of known or probable Proterozoic age (Fig. 1), and the implications that may be drawn from these structures for the cratering rate in Proterozoic time.

Criteria for recognising impact structures

Impact structures can be recognised by a diagnostic suite of structural features and shock effects. Many of these features are illustrated by the Gosses Bluff structure, Northern Territory (Milton et al. 1996a, b in this issue). Gosses Bluff is the most thoroughly explored impact structure in Australia.

Fresh impact craters generally have rims of structurally uplifted bedrock overlain, in turn, by coarse fragmental material ejected on ballistic trajectories and, finally, by a fallout deposit of finer debris, much of which is intensely shocked. This rim sequence has been eroded away from most ancient impact structures, and is entirely missing at the Proterozoic impact sites of Australia. The interiors of impact craters generally are lined with a lens of breccia; large craters contain a sheet or irregular body of impact-melt rock that rests on or interfingers with the breccia or locally may rest directly on coherent rocks uplifted in the centre of the crater. When erosion has been deep, both the breccia lens and the melt rocks may also be missing.

At all impact sites on Earth larger than about 4 km, the initial deep transient cavity excavated by impact has collapsed. Material that underlay the transient cavity wall and rim has been displaced downward and inward, and the central floor of the cavity has risen in a complex dome or uplift. A central uplift and surrounding ring structural depression are the most readily recognised structural features of all deeply eroded large impact structures formed in stratified target rocks. Because the central uplift has been forced upward by the convergent flow of the collapsing transient cavity walls, strata on the flanks of the uplift are circumferentially shortened by faults and steeply plunging folds. This deformation is somewhat similar to the puckering of a cloth pulled up through a ring. At many impact sites, the convergent flow has led to the repetition of beds along thrust-faults, where material from the collapsing walls has ramped up on the flanks of the central uplift.

The topographic rim of complex impact structures in the size range we describe in this report coincides with or lies just outside the outer margin of the ring structural depression. Erosion of the crater initially leads to outward migration of the rim. Very deep erosion, on the other hand, can lead ultimately to a decrease in size of the remaining structure. For the structures described here, we take the diameter of the outer margin of the ring structural depression as the best estimate of the diameter of the original crater.

Most of the displaced rocks underlying impact craters are more intensely fractured than the rocks in the surrounding terrain. Hence there is a decrease in the density of the rocks within the

Figure 1. Locations of Proterozoic impact structures.

[1] Lowell Observatory, Flagstaff, Arizona 86001, USA; and US Geological Survey, 2255 North Gemini Drive, Flagstaff, Arizona 86001, USA

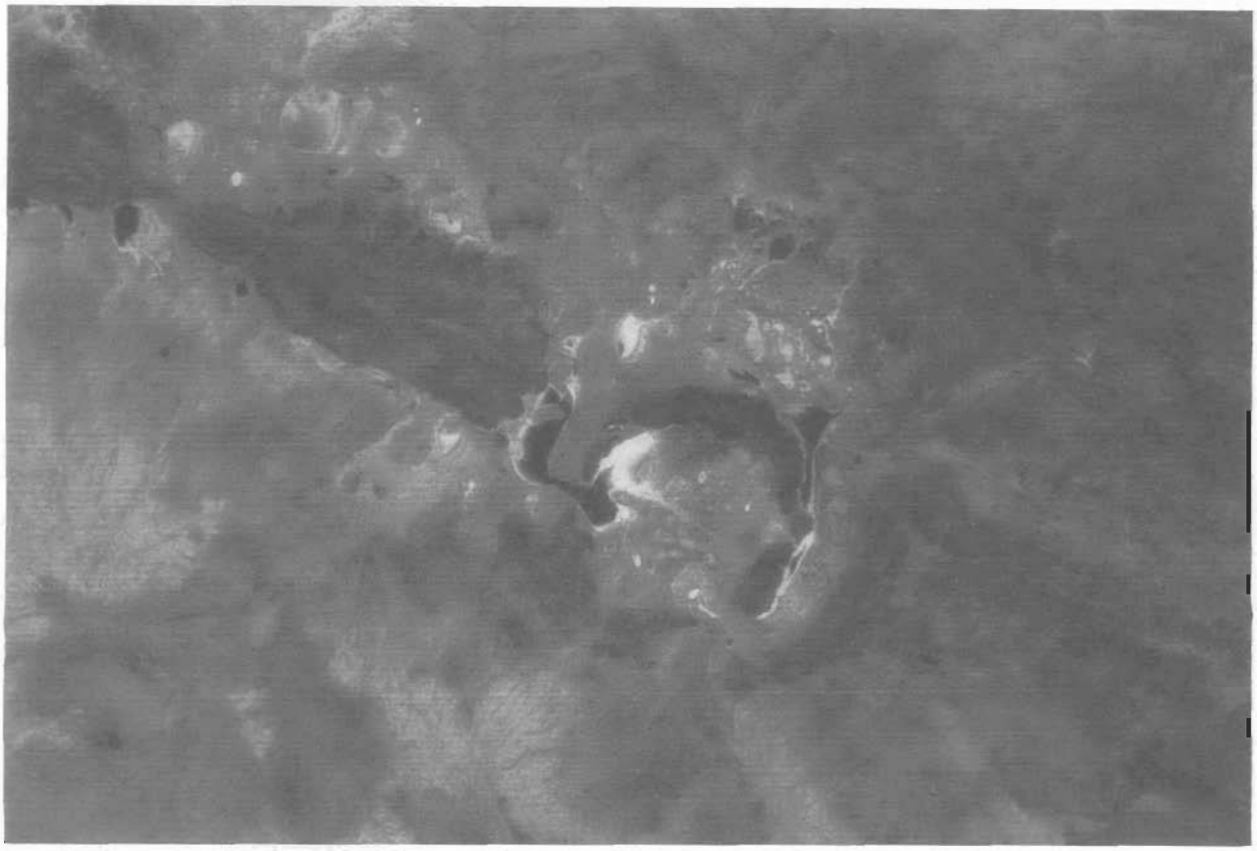

Figure 2. Landsat image of the Teague Ring structure (WA).

structure, and this is generally reflected in a negative Bouguer gravity anomaly (Pilkington & Grieve 1992; Grieve & Pilkington this issue). In some structures, dense rocks brought up from considerable depth in the central uplift give rise to a Bouguer gravity high that is typically surrounded by a broader gravity low (Shoemaker et al. 1989; Plescia et al. 1994). Gravity surveys have proved to be an important adjunct to structural investigations of impact structures, particularly where exposures are limited or where the structure is entirely buried.

In addition to the distinctive structural pattern, many petrological features are associated with impact structures (French & Short 1968; Grieve 1987, 1991). The most intensely shocked materials found at impact sites are the impact-melt rocks. Melting is due not only to the passage of the shock wave but also to viscous heating during flow of the shocked material along the transient cavity wall and frictional heating at the boundaries of structural units. In very large impact structures, the preserved melt rock may have the form of a thick lens or sheet that has crystallised with ordinary igneous textures (Grieve et al. 1991; Simonds et al. 1978). More commonly, melt rocks occur in a breccia, termed suevite, in which the clasts consist of a mixture of unmelted, partly melted, and completely melted material (Shoemaker & Chao 1961; Pohl et al. 1977). Generally, the parent lithology of the partly and completely melted clasts can be identified. Contamination of some impact melts by constituents of the impacting body is recognised by an enhancement of siderophile elements (Palme 1982). The noble metals, in particular, have proved to be useful tracers of the impactors.

At stresses below the threshold for melting, shock-metamorphic effects include the solid-state transformation of minerals to distinctive glasses (diaplectic glass) that preserve the texture of the original grains (e.g., the transformation of plagioclase to maskelynite). High-pressure polymorphs, such as coesite, stishovite, and diamond, also are formed; generally these high-pressure phases are found in the breccia lens or in the suevite. At still lower stresses, the effects of shock most easily observed petrographically are multiple sets of planar deformation lamellae, shock mosaicism, grain-crushing, and kink-banding in mica. Planar lamellae produced by shock in quartz occur as multiple sets in diagnostic preferred crystallographic directions (Alexopoulos et al. 1988), and are readily distinguished from the lamellae commonly found in tectonically deformed quartz and reported in rare instances from quartzose tuffs. Low-pressure shock effects can be found in structurally coherent rocks of the central uplift, as well as in the breccias.

Shatter cones, which are distinctive striated conical fractures produced at shock stresses of about 2.5 to 25 GPa (Milton 1977), are particularly useful indicators of impact structures, as they can be recognised easily in the field. They are found in the central uplift of each of the known Proterozoic impact structures in Australia. As demonstrated in laboratory (Shoemaker et al 1961; Schneider & Wagner 1976) and field (Bunch & Quaide 1968; Roddy & Davis 1977) experiments, shatter cones are formed under conditions of compression in the direction of shock propagation, and extension (owing to divergence of flow in the expanding shock wave) in directions normal to shock propagation. The apices of shatter cones statistically point initially toward the shock origin; they are subsequently rotated during uplift of the transient cavity floor. Where they are well developed, shatter cones commonly are found out to distances from the centre of an impact structure about equal to one-third the radius of the entire structure. They also occur at greater distances in crater-floor breccias and have been found in crater ejecta.

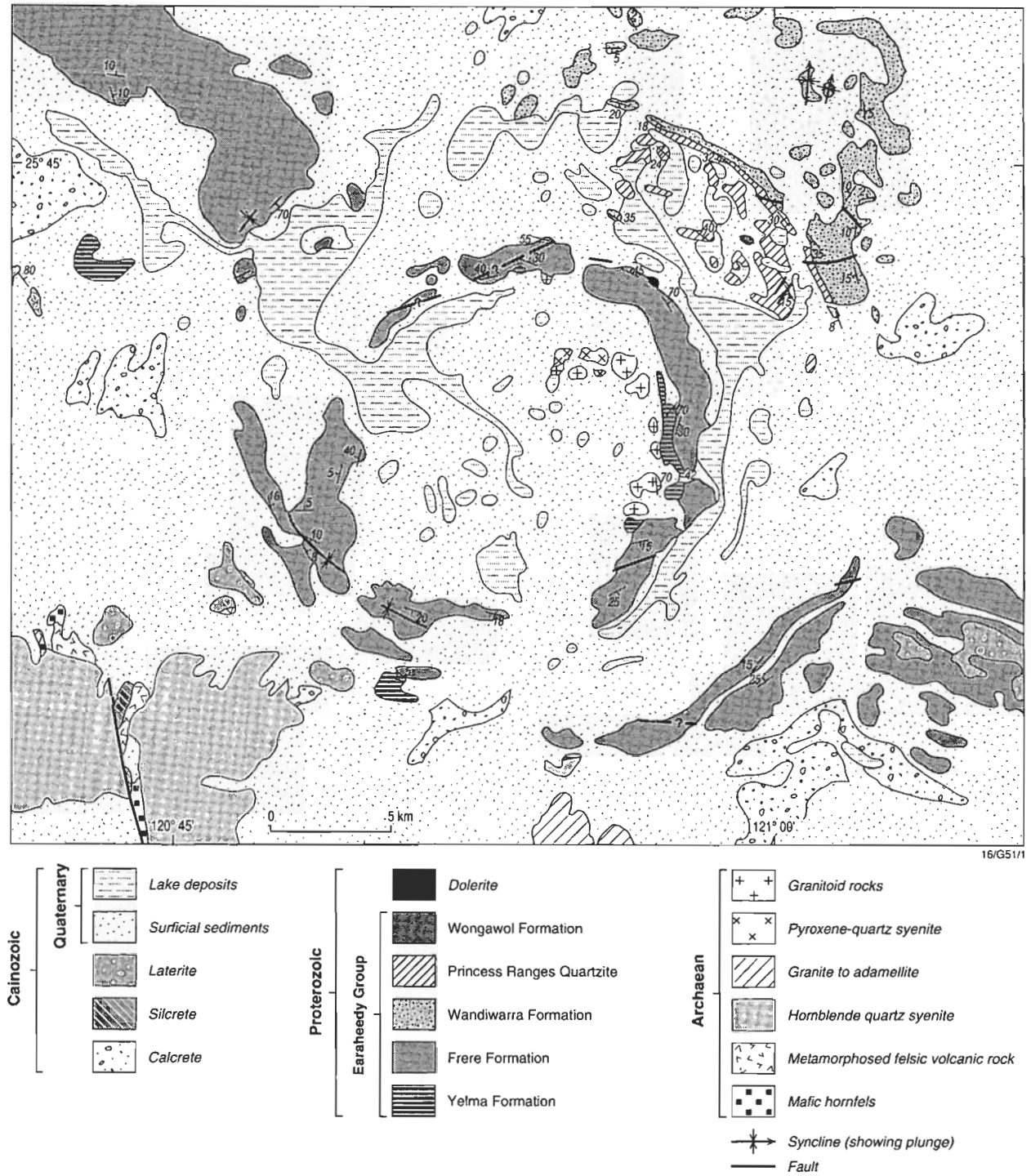

Figure 3. Geology of the Teague Ring structure (WA), adapted from Bunting et al. (1982).

Teague Ring structure (WA)

Possibly the oldest known impact structure in Australia is the 30-km-diameter Teague Ring (lat. 25°52'S, long. 120°53'E[1]), first reported by Butler (1974). It was later mapped in somewhat greater detail by Bunting et al. (1982). Located on the southern margin of the Nabberu Basin, the Ring is a prominent feature as seen from orbit in Landsat images (Fig. 2), and has been observed and photographed by astronauts.

Strata belonging to the lowermost 4 km of the Earaheedy Group of Palaeoproterozoic age (Hall et al. 1977; Bunting et al. 1977; Hall & Goode 1978) are dropped down in a ring syncline that surrounds a central uplift of Archaean crystalline rocks (Fig. 3). Inward-dipping, dark, ferruginous beds (banded iron formation) of the Frere Formation, near the base of the Earaheedy Group, mark the margin of the structure around more than 180° of the circumference. These same beds, steeply upturned on the flank of the central uplift, form a prominent dark collar around Archaean rocks in the centre.

[1] All coordinates given in this paper are for the centres of the impact structures.

Figure 4. False-colour Landsat image of the Spider structure (WA).

As found in the central uplifts of nearly all other impact structures formed in stratified rocks, the beds in the collar of the central uplift at Teague Ring are puckered in steeply dipping faulted folds. A hint of these folds can be seen in the map pattern of the Frere Formation portrayed at 1:250 000 scale (Fig. 3) by Bunting et al. (1982), but larger-scale mapping, some of which we carried out in 1986 and 1995, is required to delineate the structural details. Not only is there circumferential shortening but the beds of the collar are also ramped up and are repeated by thrusts. Shatter cones are present in the banded iron formation of the Frere Formation in the upturned collar, but generally they are poorly developed and fairly rare.

The uplifted crystalline rocks in the centre of the structure — comprising leucogranite, quartz syenite, and sparse vein quartz — generally are not strongly shocked. The granite is locally shattered or brecciated, especially near the contact with the Earaheedy Group. Bunting et al. (1980) described multiple sets of planar deformation lamellae in quartz grains in the granite, but did not identify the crystallographic orientation of the lamellae. Very thin veins of pseudotachylite also cut the crystalline rocks (Bunting et al. 1980). Remarkably, we found a shatter cone in vein quartz, a rock type not expected to be susceptible to this type of fracturing. A reconnaissance gravity survey that we made in 1986 revealed a broad negative gravity anomaly over the central uplift. The anomaly may be due in part to extensive deep fracturing or brecciation of the crystalline rocks, consistent with gravity observations at many other impact structures, but may also reflect the presence of low-density granite in the central uplift.

The Earaheedy Group preserved on the southern edge of the Nabberu Basin dips 5 to 10° north-northeast, toward the axis of the basin. The entire Teague Ring structure is similarly tipped to the north-northeast, and truncated by the present, nearly horizontal land surface. Only the Frere Formation and a thin underlying sequence of beds of the Yelma Formation fill the ring syncline on the southwest side of the structure, whereas a much thicker stack of strata fills the syncline on the northeast. Apparently the Teague Ring structure has been fairly deeply eroded; intensely shocked rocks that probably were located near the original crater floor have been eroded away. However, most of the crystalline rocks in the centre are covered by Quaternary deposits, which might conceal further shock-metamorphic features.

The available information on the age of the Teague Ring structure is derived entirely from the work of Bunting et al. (1980). An apparent whole-rock Rb–Sr 1630-Ma isochron was obtained for four relatively fresh to moderately altered samples of quartz syenite in the central uplift. This was interpreted as either a likely age of intrusion of the syenite or a metamorphic age. Similar syenites, including one dated at 2360 Ma, are found in the Yilgarn Block south of Teague Ring, and a substantial body of quartz syenite that apparently has normal Archaean Rb–Sr systematics is exposed just to the southeast of the Teague Ring structure. A single shatter cone found in the syenite of the central uplift by J. Ferguson (Bunting et al. 1980) indicates that the syenite predates the impact and probably is a normal component of the local Archaean terrane. We consider that the apparent 1630-Ma age is the most likely age of the impact structure, and that the Rb–Sr system in the syenite probably was re-equilibrated during an extended pulse of heat induced by impact. The suggested age for the impact structure is somewhat younger than

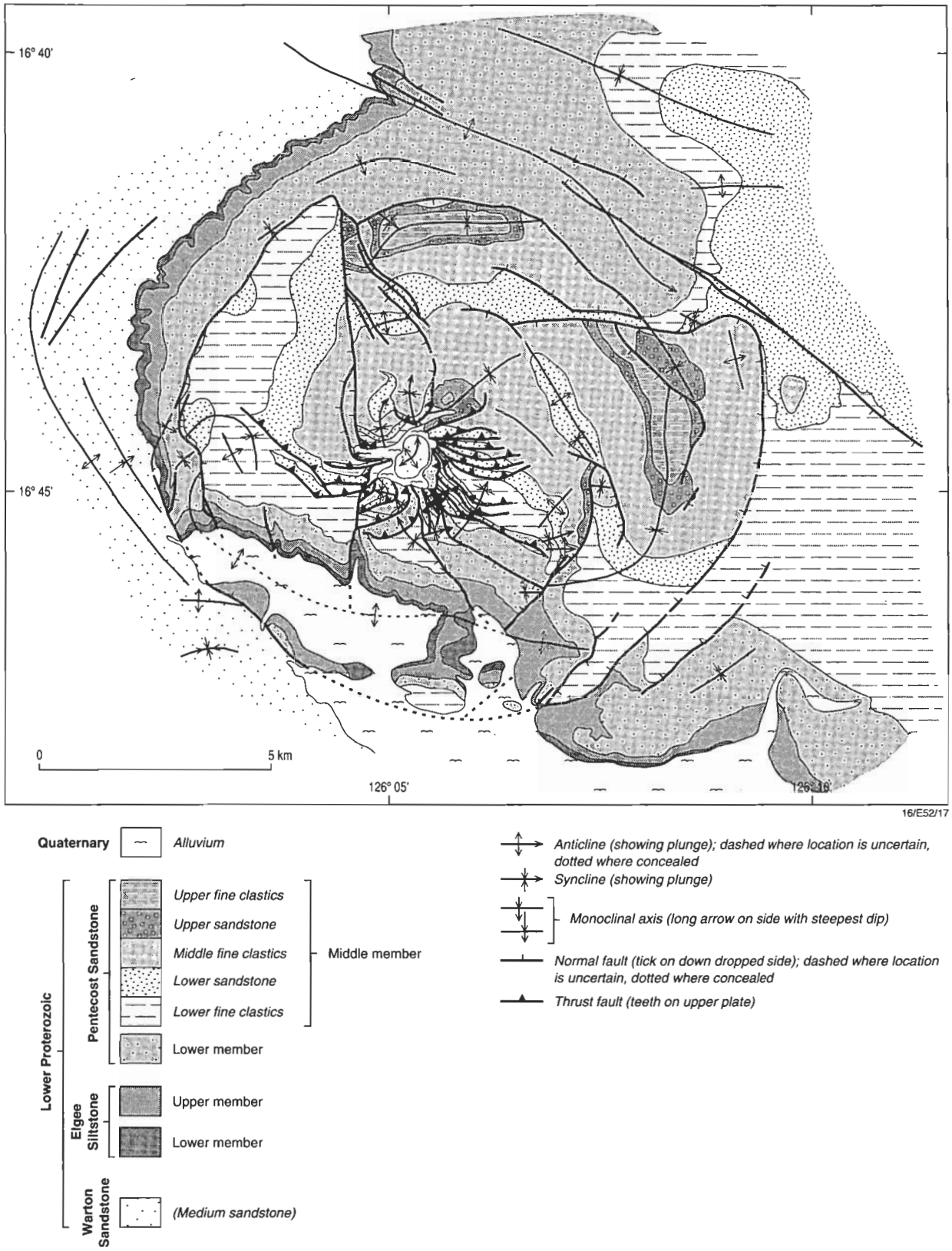

Figure 5. Geology of the Spider structure (WA), mapped by E.M. Shoemaker and C.S. Shoemaker, 1984–1985.

the 1700–1800 Ma age inferred for the Earaheedy Group (Bunting et al. 1977).

A second apparent whole-rock Rb–Sr isochron of 1260 Ma was obtained by Bunting et al. (1980) for four samples of moderately to severely altered syenite and granite from the central uplift. They suggested that this age reflects an episode of intense weathering. If this is correct, it indicates that the crystalline rocks now exposed in the central uplift were near the surface, and that the Teague Ring structure was already deeply eroded, by Mesoproterozoic time. Further chronological studies at the Teague Ring structure clearly are desirable.

Figure 6. Oblique aerial view of the centre of the Spider structure (WA) from the west. Photo by D.J. Roddy and E.M. Shoemaker.

Figure 7. Large shatter cones in quartzite on the central uplift of the Spider structure (WA).

Spider structure (WA)

The Spider impact structure (Fig. 4), located on the Kimberley plateau of northern Western Australia and centred at latitude 16°44'S, longitude 126°05'E, was first recognised by J.E. Harms (Harms et al. unpublished manuscript) about 35 years ago; the occurrence of shatter cones was briefly reported by Harms et al. (1980). Some of the local structural deformation was noticed in the course of 1:250 000-scale mapping of the Mount Elizabeth Sheet area by Roberts & Perry (1969). We mapped the central part of the structure at a scale of ~1:25 000 in 1984 and the remainder of the structure at ~1:50 000 in 1985 (Shoemaker & Shoemaker 1988b).

The Spider structure is developed in sedimentary rocks, chiefly sandstone, of the Kimberley Group of Palaeoproterozoic age; it occurs in an area of gently dipping beds near the axis of the broad, open Mount Barnett Syncline. The impact structure is bounded by a series of normal faults and monoclines that delimit a complex, structurally depressed region 11 km wide and about 13 km long (Fig. 5). Although the boundary is somewhat irregular, the long axis of the structure is oriented roughly northwest–southeast. A steep-sided fault-bounded structural dome about 0.5 km across occurs at the centre of the structural depression. In comparison with other impact structures of similar size, the central uplift is anomalously small and low in structural relief.

The most remarkable feature of the entire impact structure is a series of about twenty thin, overlapping thrust-sheets that occupy the lowest part of the structural depression surrounding the central dome. Most thrust-displacement is roughly from the north to the south. Repetition and upturning of three different sandstone units in the Pentecost Sandstone is responsible for the unusual twenty-legged appearance of the 'spider' (Fig. 6). Well-developed shatter cones (Fig. 7) occur in rocks of both the central uplift and the surrounding thrust-sheets over an area about 2 km in diameter.

We interpret the Spider structure to have been formed by low oblique impact from the north or northwest. Rocks evidently were 'skidded' to the south-southeast beneath the floor of the transient cavity before the collapse and the development of the central uplift. Some additional thrust-displacement possibly occurred during inward flow of material along the walls of the collapsing transient cavity.

The Spider structure appears to have been fairly deeply eroded. Our detailed mapping revealed no impact-melt rocks or breccias that may have formed close to the initial crater floor. An estimated thickness of 2000 to 2500 m of Palaeoproterozoic (1700–1800 Ma) sedimentary beds of the Kimberley and Bastion Groups inferred to have been deposited in the vicinity of the structure have been eroded away.

About 20 to 25 km east of the Spider structure, mildly deformed rocks of the Kimberley Group are truncated and overlain unconformably by nearly flat-lying beds of the Walsh Tillite of Neoproterozoic age (Roberts & Perry 1969). In places, the unconformity at the base of the tillite is at about the same elevation as the highest topographic features in the Spider structure, and rests on beds equivalent to those found on the edge of the structure. The impact structure and immediately surrounding area probably were eroded nearly to the level of the present topographic summits before the Precambrian tillite accumulated.

The small size and amplitude of the central uplift, and the small area occupied by shatter cones, suggest that the present level of exposure lies near the base of the impact disturbance. However, low-oblique impact may have resulted in anomalously shallow deformation. Hence the Spider structure may have been formed either before or moderately late in the history of Precambrian denudation of the region.

Kelly West structure (NT)

The Kelly West structure (lat. 19°56'S, long. 133°57'E) was first recognised by Tonkin (1973) from the presence of shatter cones. Were it not for the strikingly developed and abundant shatter cones (Fig. 8), Kelly West would have escaped detection as an impact site. The feature mapped by Tonkin is part of the central uplift, which we remapped in detail in 1989 (Fig. 9).

Impact was centred roughly on the axis of a synclinal inlier of quartzitic sandstone of the Palaeo- to Mesoproterozoic Hatches Creek Group, which rests with marked angular unconformity on the Warramunga Group of Palaeoproterozoic age. Uplift at the centre of the structure partly unfolded the pre-existing syncline in the Hatches Creek Group. The uplift is demonstrated by the rotation of shatter-cone axes. Apices of the shatter cones are rotated outward, away from the centre of uplift. We documented this rotation by measuring the orientations of cone axes for 86 in-situ shatter cones distributed over the exposed beds. Other deformation at Kelly West typical of central uplifts includes outward-plunging radial folds and, along the southeast flank of the uplift, the duplication of strata by overthrust displacement toward the centre of the uplift. Across the centre of the uplift, beds are crumpled in northwest- to northeast-trending folds. Close to the centre of the exposed Hatches Creek Group, the quartzitic sandstone is intensely brecciated.

A sedimentary breccia that contains clasts of both impact breccia and fairly intensely shocked sandstone rests unconformably on the deformed rocks of the Hatches Creek Group. This breccia is an ancient colluvial deposit that may have formed early in the erosional history of the Kelly West structure or, conceivably, in the original crater. It is overlain by Cambrian marine deposits.

Extremely limited exposure of the less resistant beds of the Warramunga Group surrounding the central uplift has prevented accurate determination of the size of the Kelly West impact structure from observations of outcrops. Shatter cones are distributed over the entire exposure of the Hatches Creek Group quartzitic sandstone, which is 2 km long. From the well-exposed part of the central uplift, we estimate that the diameter of the whole structure is not less than about 8 km and probably not greater than 20 km. In an attempt to overcome the limitations of exposure, a preliminary gravity survey was conducted in collaboration with J.B. Plescia in 1989. The intrinsic character of the gravity field is so complex, however, that we were unable to isolate the gravity signature of the impact structure.

The age of the Hatches Creek Group is considered to be close to the 1862 ± 45-Ma U–Pb age of the Epenarra Volcanics dacites, which occur at its base unconformably over the Waramunga Group (Page 1988). Near Kelly West, more than 5 km of the Hatches Creek Group was deposited, folded, and then largely eroded away in Precambrian time (Smith 1970). The impact almost certainly occurred after this episode of deep erosion had been largely completed, perhaps during the Neoproterozoic.

Figure 8. Shatter cone in quartzite at the Kelly West structure (NT).

By Early Cambrian time, the resistant quartzitic sandstone of the Hatches Creek Group in the central uplift formed a monadnock that was then buried by cherty limestone of the Gum Ridge Formation during the early Middle Cambrian. This formation onlaps the sides of the monadnock, and preserved remnants of it fill palaeovalleys in the monadnock. Half a billion years after burial, the exhumed monadnock remains a prominent hill on the landscape today (Fig. 10).

Strangways structure (NT)

The Strangways structure (lat. 15°12'S, long. 133°35'E), Northern Territory, was first mapped at 1:250 000 scale by Dunn (1963). It was recognised by Guppy et al. (1971) as an impact structure from its prominent central uplift, which is locally *intensely shatter*-coned, and from the impact-melt rocks exposed near the centre. The central uplift of the structure was later remapped by Ferguson et al. (1978) at a scale of 1:50 000; details of the geology in the centre were mapped by E.M. and C.S. Shoemaker and M.R. Dence in 1990. Clastic sedimentary rocks of the Roper Group of Meso- to Neoproterozoic age and the granite basement on which they rest were deformed by impact. Most of the central and southern part of the structure is concealed beneath Cainozoic, Cretaceous, and possibly older Phanerozoic beds. The Antrim Plateau Volcanics of Early Cambrian age appear to overlap the northern part of the structure.

As mapped by Ferguson et al., the central uplift at Strangways includes granite encircled by a collar of quartzites and other rocks of the Limmen Sandstone, Mainoru and Crawford? Formations, and Abner Sandstone (Fig. 11). The collar of upturned and overturned beds is at least 20 km in diameter. Most of the beds are overturned and dip at moderately low angles, as though the collar had been dragged outward along the wall of the transient cavity.

No well-defined ring structural depression surrounding the central uplift has been recognised, partly because so much of the structure is concealed beneath Phanerozoic deposits. Regional deformation of the Roper Group, possibly pre-impact, complicates the recognition of impact deformation in the strata surrounding the central uplift. The Strangways Fault (Dunn 1963), probably of post-impact age, may truncate the impact structure in the east. Ferguson et al. (1978) estimated the diameter of the Strangways impact structure to be 20 to 25 km; a diameter of 26 km was estimated by Shoemaker & Shoemaker (1988a, 1990) on the basis of the work of Ferguson et al. and our own work. In view of the size of the central uplift, however, we now think that this diameter is almost certainly too small. A more likely diameter for the impact-deformed beds is about 40 or more kilometres.

Near the centre of the Strangways structure, scattered outcrops of suevite (Fig. 12) rest on granite breccia or locally on shattered granite or shock-melted granite (Fig. 13). The granite breccia grades downward into shattered or coherent granite. At one point very near the centre, shock-melted granite grades directly downward into coherent granite. The suevite consists largely of shock-melted clasts of quartzite, shale, and granite. Some clasts are longer than a metre, and are drawn out and deformed by viscous flow (Fig. 14). The abundant siderophile elements in various components of the suevite indicate contamination by the impacting body (Morgan et al. 1981). Nickel is enriched in the melt rocks by factors of about 10 to 60 relative to the background abundances of the country rocks. Iridium is enriched generally by more than a factor of 20. Up to 2.8 ppb Ir was found in a shock-melted granite clast. Massive very coarse breccias with unmelted clasts of quartzite and granite also rest on the

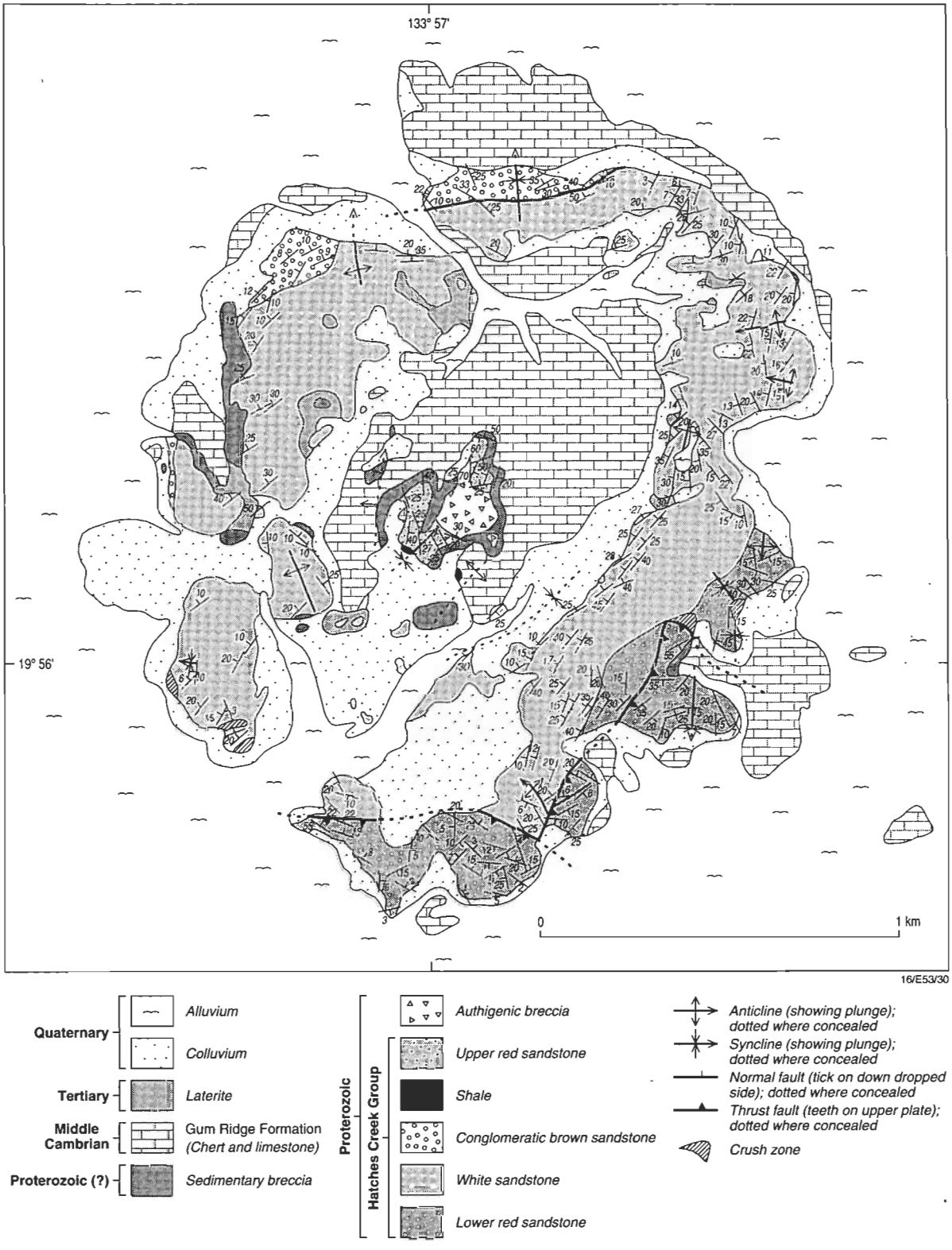

Figure 9. Geology of the central uplift of the Kelly West structure (NT), mapped by E.M. Shoemaker and C.S. Shoemaker, 1989.

granite along the northeast side of the granite outcrop area. These breccias were possibly emplaced by return flow of material down the wall of the transient cavity.

A Precambrian age for the Strangways structure is suggested by the overlap of undeformed Early Cambrian Antrim Plateau Volcanics on deformed beds of the Roper Group on the northern side of the structure. There, the highest preserved formation of the Roper Group (Bessie Creek Sandstone) probably lies within the ring structural depression. Rocks in the impact structure evidently were eroded down to a nearly level surface before the Antrim Plateau Volcanics erupted.

Ferguson et al. mapped — as the Tindall Limestone of Middle Cambrian age — carbonate rocks overlapping the central uplift. A careful re-examination of these rocks, however, shows that they consist of calcrete and freshwater limestone that bears late Cainozoic fossils. Almost precisely in the centre of the central

Figure 10. Oblique aerial view of the Kelly West structure (NT) from the south. Photo by D.J. Roddy and E.M. Shoemaker.

uplift, we found a poorly exposed sequence of chert and red sandstone of unknown age that lies above the granite and below sandstone beds of Cretaceous age. This sequence might be a preserved remnant of deposits laid down in the initial impact crater.

It should be possible to obtain accurate $^{40}Ar/^{39}Ar$ ages from the shock-melted granites at the Strangways structure, but attempts to do so have so far failed to yield unambiguous plateau ages. Bottomley (1982) and Bottomley et al. (1990) suggested an age of ~470 Ma on the basis of the youngest observed argon-release ages. This suggestion was influenced by the belief (now rejected) that mid-Cambrian limestones were deformed by impact. Crude plateaus in argon-release diagrams reported by Bottomley et al. (1990) suggest to us that the age of Strangways is in the neighbourhood of 1000 Ma. This age is somewhat younger than the inferred ages of the deformed beds of the Roper Group. Further $^{40}Ar/^{39}Ar$ studies on appropriate samples are needed.

Lawn Hill structure (Qld)

The Lawn Hill structure (lat. 18°41'S, long. 138°39'E) was first recognised as an impact structure by Stewart & Mitchell (1987), who described shatter cones and multiple sets of planar deformation lamellae in quartz grains from the central uplift. Both the shatter cones and the crystallographic orientation of the lamellae are indicative of mild shock pressures. The impact structure (Fig. 15) has been formed in clastic sedimentary rocks of the Lawn Hill and older formations of the McNamara Group (Sweet & Hutton 1982). These rocks were folded before impact; regional folds and faults extend into the rim of the structure. From the present topographic remnants, we estimate the rim to be about 20 km in diameter.

As at other impact structures, a central uplift is present, and beds on its flank are puckered in steeply plunging faulted folds, which we mapped in detail in 1990 and 1991 (Fig. 16). Beds also are ramped up and repeated along a series of small thrusts on the flanks of the uplift. Shatter cones are well-developed and fairly numerous on the uplift. A patch of suevite, first noticed by Stewart & Mitchell (1987), rests on deformed beds of the Lawn Hill Formation, almost precisely in the centre of the uplift (Fig. 16). The suevite consists of twisted impact-melted clasts of siltstone and sandstone up to tens of centimetres long embedded in a finer breccia matrix. Analyses of samples of the matrix that we submitted to C.J. Orth and Moses Attrep of the Los Alamos National Laboratory revealed only very weak (i.e., a factor of two to four) to negligible enrichment in siderophile elements.

A structural moat surrounding the central uplift is largely concealed beneath Middle Cambrian limestone and limestone breccia that rest on the folded Precambrian rocks. The impact structure was eroded before the Cambrian beds were deposited, but a substantial ring depression is present at the unconformity where the Cambrian fills the moat (Fig. 17). The ring of Cambrian rocks filling the moat drew early attention of geologists to the structure.

The age of the Lawn Hill structure is not yet tightly constrained, but future work could yield a satisfactory $^{40}Ar/^{39}Ar$ age from impact-melted clasts in the suevite. Beds of the McNamara Group correlate roughly with the Mount Isa Group, dated at about 1670 Ma (Page 1981). Impact postdates an episode of fairly tight folding of the McNamara Group and predates deposition of the Middle Cambrian beds. The Cambrian beds were deposited in a craterform feature that was breached on the northwest side, and also in the breach. Preservation of part of the topographic relief of the crater at the beginning of Cambrian

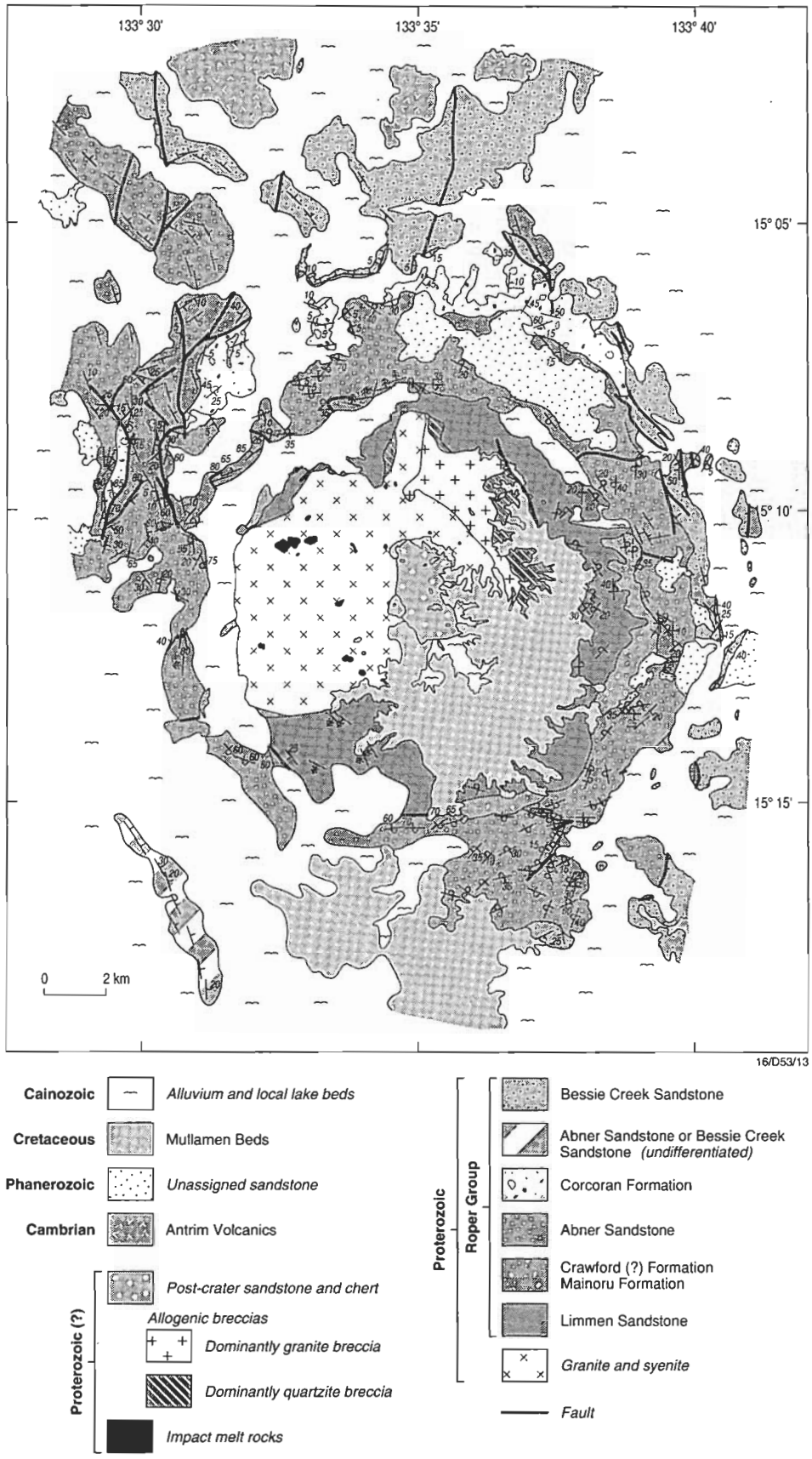

Figure 11. Geology of the central uplift of the Strangways structure (NT), adapted from an unpublished compilation by D.J. Milton and incorporating additions and modifications by E.M. Shoemaker, M.R. Dence, and C.S. Shoemaker, 1990.

Figure 12. Outcrop of suevite near the centre of the Strangways structure (NT).

deposition suggests that the impact occurred very late in the Proterozoic or possibly in the Early Cambrian. Even so, part of the relief of the crater is still preserved today, half a billion years later. Outcrops of the McNamara Group in the rim rise 60 to 100 m above the plain in the centre of the structure. Thus, the existence of craterform topography in Middle Cambrian time does not require that the age of the crater was close to that of the beds which fill it.

Acraman structure (SA)

The Acraman structure (lat. 32°01'S, long. 135°27'E) is one of the largest known Precambrian impact structures in Australia and also the best dated. It is discussed by G.E. Williams, the discoverer, and his collaborators in an accompanying paper (Williams et al. this issue), and fully described by him elsewhere (Williams 1994a, b). Williams suggests that the transient cavity may have been as much as 40 km in diameter, and that the final collapse crater may be marked by a conspicuous fault-controlled arcuate structure at 85–90 km diameter. From our own field observations, however, we think that the final crater probably was not much more than about 35 to 40 km in diameter, although some faulting or renewed displacement on old faults may well have occurred at the greater distances suggested by Williams. At a radius of 19 to 20 km from the centre of the structure, the well-exposed Yardea Dacite is essentially flat-lying and undeformed, and exhibits no recognised shock effects. We think it unlikely that the final crater could have been much larger than the present topographic basin in which Lake Acraman is located.

The Acraman structure was formed in Mesoproterozoic volcanic rocks, chiefly dacite. Distant fallout from the impact was discovered by Gostin et al. (1986) in the upper part of a ~10-km-thick sequence of sedimentary rocks of Neoproterozoic age in the Adelaide Geosyncline. The fallout layer occurs about 1100 m below strata known to contain an Ediacaran fossil assemblage and about 1500 m below Cambrian beds. Impact occurred very late in the Proterozoic, probably near 590 Ma.

False alarms

In our ten-year survey of impact structures in Australia, we examined many candidates found on Landsat images, 1:250 000-scale geological maps, and aerial photographs, and from discussions with other geologists. Three candidate impact structures of possible Precambrian age, which we have since rejected, seemed sufficiently promising to warrant mention after preliminary field examination: the Dampier and Pippingara structures in Western Australia, and the Fiery Creek Dome in Queensland.

The Dampier and Pippingara structures are circular or possibly circular features in the Pilbara Block and are recognisable on Landsat images and regional geological maps (Shoemaker & Shoemaker 1985). The Dampier structure occurs on the coast. If it is truly circular, only a segment is exposed on the mainland and in the Dampier Archipelago; the remainder is concealed beneath the Indian Ocean. The most striking component of this structure is the Gidley Granophyre (de Laeter & Trendall 1971), exposed in an arcuate outcrop belt. The granophyre occurs in a crudely stratiform sheet that rests on Archaean granite and dips toward the apparent centre of the structure. Local concentrations of sheared Archaean granite blocks are present near the base of the granophyre, which suggested to us that the granophyre might be an impact-melt sheet containing blocks of shocked Archaean basement rock. However, the granophyre is intrusive into overlying basalts assigned to the basal Mount Roe Basalt of the Fortescue Group, which we confirmed by detailed mapping of Enderby Island. Because of this intrusive relationship, it is unlikely that the granophyre is an impact-melt sheet.

The Pippingara structure, south of Port Hedland and 400 km east of Dampier, is underlain by Archaean granite that is partly

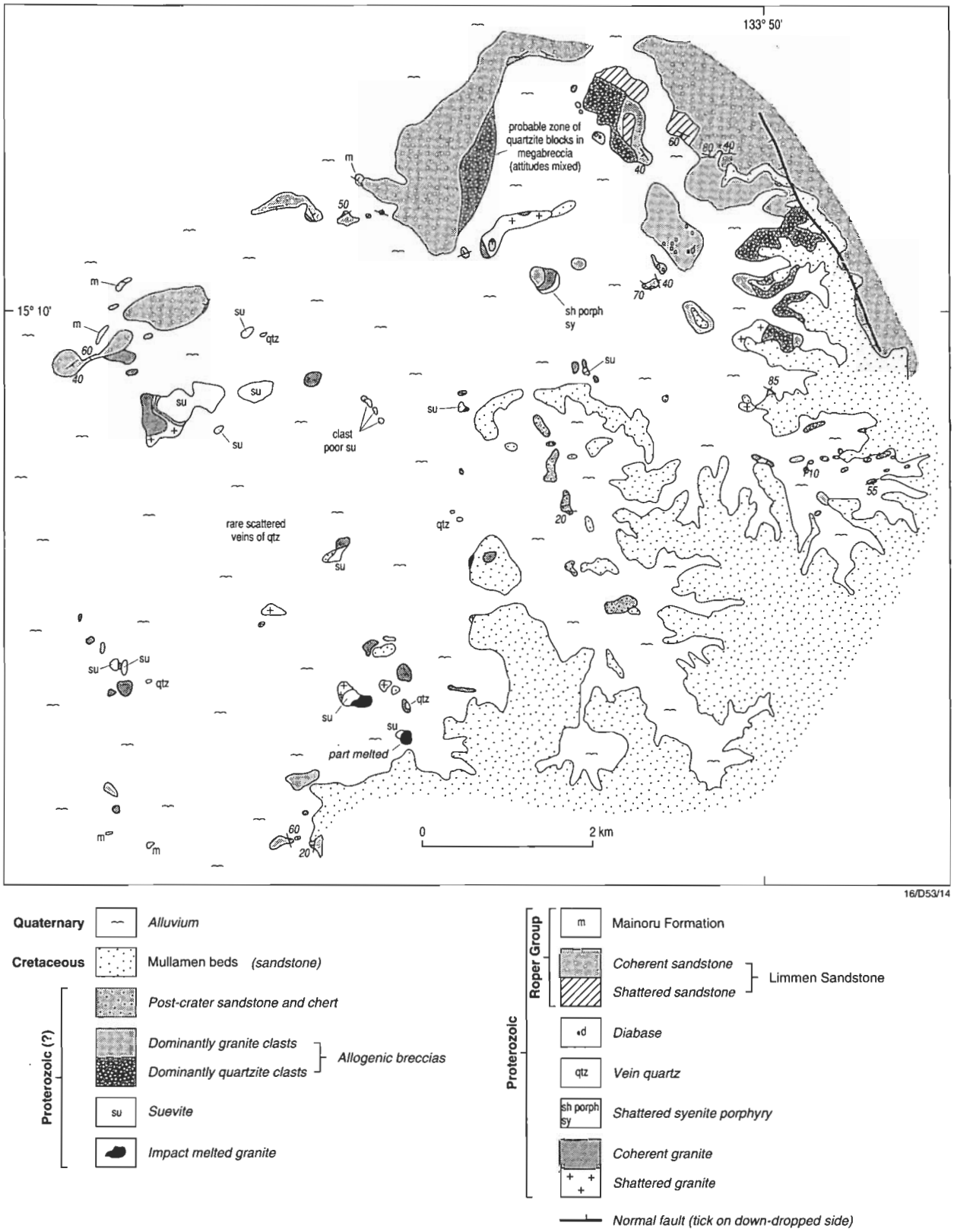

Figure 13. Detailed geology of the centre of the Strangways structure (NT), mapped by E.M. Shoemaker, M.R. Dence, and C.S. Shoemaker, 1990.

bounded by a collar of Archaean metasediments and mafic to ultramafic crystalline rocks. Extensive brecciation of the granite that we noted during reconnaissance examination, and a pronounced gravity low centred over the structure (Hickman & Gibson 1982), suggested to us that the granite might have been deformed and brecciated by impact. A search for shatter cones, particularly in fine-grained metasediments in the collar, was unsuccessful. The beds in the collar, moreover, show no evidence of the circumferential shortening that would be expected if the granite had been displaced in the central uplift of an impact structure. We conclude that the granite is a normal pluton of the Pilbara Block of unusually circular outline which,

Figure 14. Large clast of melted quartzite in suevite at the Strangways structure (NT).

though locally brecciated and sheared, exhibits no compelling evidence of impact deformation.

The Fiery Creek Dome (lat. 19°13'S, long. 139°13'E) is a circular structure 30 km in diameter consisting of a central uplift surrounded by a structural moat that has been modified by a younger regional network of closely spaced faults (Hutton & Wilson 1984). Our attention was drawn to the structure by Landsat images, and we interpreted it as a possible impact structure on the basis of a very brief reconnaissance examination in 1987 (Shoemaker & Shoemaker 1988a, 1990). In 1991 we mapped the centre of the structure in detail, and found that the dome is underlain by a previously unrecognised gabbroic laccolith. Beds on the flanks of the dome dip only moderately (10 to 25°), and are not circumferentially shortened by radial folds. No shatter cones are present, and we found no evidence of shock effects. Although the Fiery Creek Dome has broad similarities to eroded impact structures, it is not of impact origin.

Cratering rate during the Proterozoic

One of our principal goals in studying the impact structures of Australia has been to improve the understanding of Earth's impact history. We have been interested in the Precambrian history, in particular, because of an apparent discrepancy between the 3.2-Ga cratering record of the Moon, and estimates of the current cratering rate based on astronomical observations of Earth-crossing bodies and on the Phanerozoic terrestrial record of impact structures. Shoemaker et al. (1990) suggested that the production of impact craters larger than 20 km in diameter might have increased by a factor of about two during the Phanerozoic. They further suggested that this increase in cratering rate was due to an increase in the flux of stars that perturb the Oort cloud of comets.

The number of long-period comets crossing the orbit of the Earth is severely attenuated by the gravitational perturbations due to Jupiter, which efficiently expel Jupiter-crossing Oort cloud comets from the solar system (Hills 1981). New comets are delivered to Jupiter- and Earth-crossing orbits by the shuffling of orbits in the Oort cloud, by passing stars and other massive objects, and also by galactic tidal forces (Matese et al. 1995). Both the frequency of encounters with stars and the strength of the tidal forces depend heavily on the distance of the sun from the central plane of the galaxy.

In its trajectory around the galaxy, the sun oscillates in the direction perpendicular to the galactic plane (z oscillation) with a period of order 60 to 70 Ma (Bahcall & Bahcall 1985). The present amplitude of oscillation of the sun is anomalously low compared with that of stars of similar mass and age; a decrease in the z oscillation late in geological history would have increased the mean flux of stars in the solar neighbourhood (Shoemaker et al. 1990) and also the tidal perturbation of the Oort Cloud. This could have led to an increase by a factor of about two in the cratering rate if about half or more of the impact craters are produced by comets.

The cumulative size–frequency distribution for the six recognised Australian impact structures of Proterozoic age is illustrated by the solid line with 1-σ error bars in Figure 18. From an analysis of the size–frequency distribution of craters of Copernican and Eratosthenian age on the Moon mapped by Wilhelms (1987), and observations of Earth-crossing asteroids and comets (Shoemaker et al. 1990), we infer that the expected size–frequency distribution for Proterozoic impact structures on Earth, in the diameter range of 10 to 30 km, has a form represented approximately by the dashed line in Figure 18 ($N_D \propto D^{-2.27}$, where N_D is cumulative frequency and D is crater diameter in kilometres). A curve of this form passing through $N_D = 4$, where D = 20 km, represents the observed frequency between 20 and 40 km diameter satisfactorily (i.e., within the 1-σ errors). Alternatively, Grieve & Shoemaker (1994) have suggested that $N_D \propto D^{-1.8}$ fits the size distribution for known terrestrial impact structures larger than 20 km in diameter. A curve with the latter form, shown with a dotted line in Figure 18, is a somewhat better fit to the observed frequency.

We suggest that the discovery of *exposed* impact structures with a diameter equal to or larger than 20 km formed in Australia's gently to moderately deformed Proterozoic stratified rocks may be complete or close to complete. Our decade-long search, which included a review of Landsat images and the available 1:250 000 geological maps, did not reveal any other candidate structures that passed careful field investigation. The accepted impact structures in this size range were easily recognisable as candidates. At diameters below 20 km, on the other hand, many exposed Precambrian impact structures probably remain to be found. Extrapolation of the dashed and dotted curves suggests that perhaps as many as 8 to 13 impact structures larger than 10-km diameter still await discovery, provided that they have not been lost by erosion. Our experience indicates that 10 km is well below the threshold diameter for detection of impact structures from unprocessed Landsat images. A careful screening of Landsat images of Western Australia by Carolyn Shoemaker, without prior knowledge of the location of known structures,

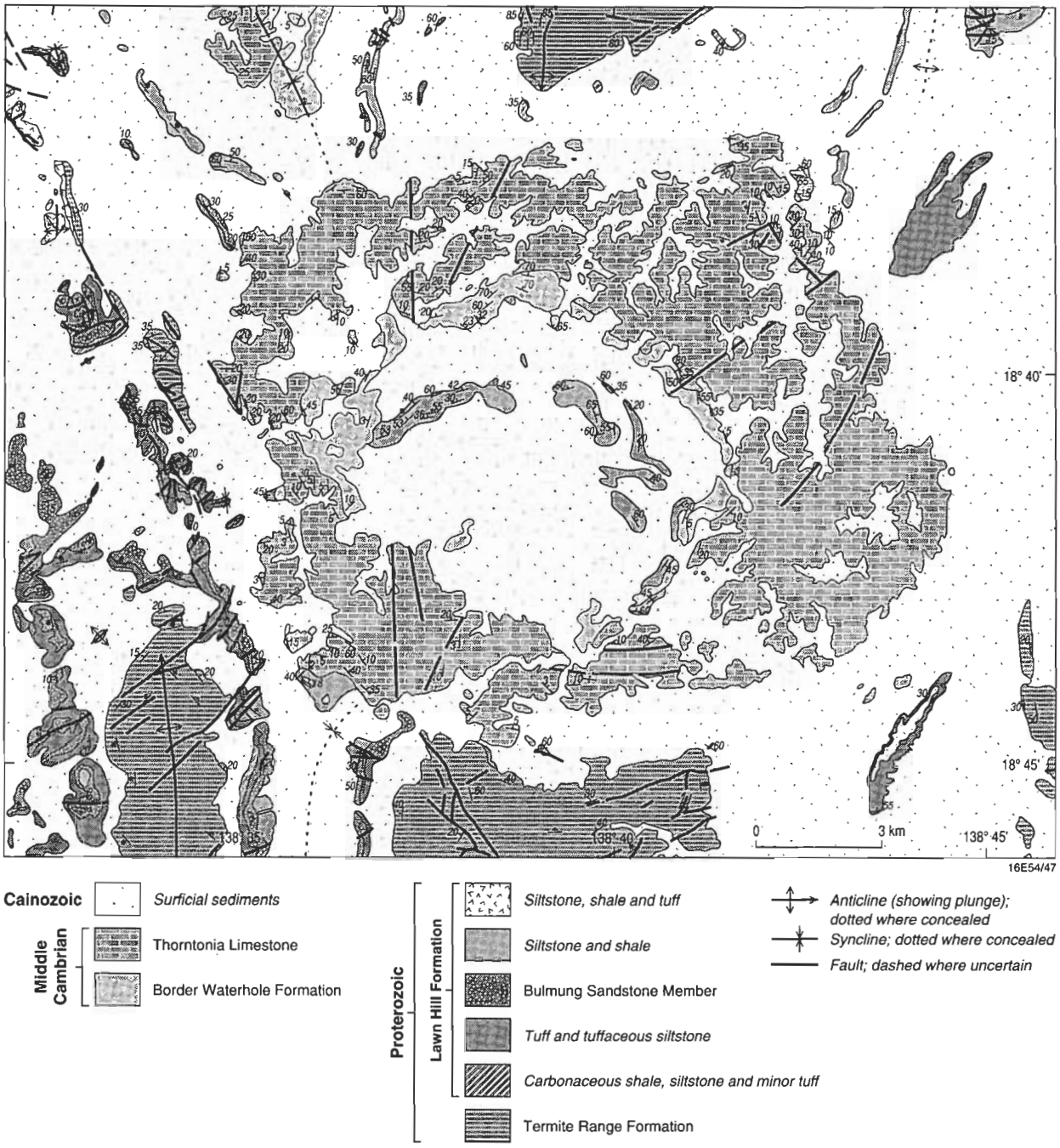

Figure 15. Geology of the Lawn Hill structure (Qld), adapted from Sweet & Hutton (1982).

easily detected the 30-km Teague Ring structure, for example, but not the 11–13-km Spider structure. Interestingly, 20 km is the approximate diameter threshold at which discovery of late Phanerozoic impact structures is thought to be complete for the North American and European cratons (Grieve 1984; Grieve & Shoemaker 1994).

The area of exposed (i.e., mappable at 1:5 000 000 scale) Proterozoic little-deformed sedimentary and volcanic rocks in Australia is about 1.15×10^6 km^2. We include in this figure the Gawler Range Volcanics, but not the Antrim Plateau Volcanics, which might be late Neoproterozoic. We include only stratified, little-deformed rocks, as experience to date indicates that impact structures are extremely difficult to recognise in complex metamorphic or plutonic terranes. Roughly similar areas of Palaeoproterozoic strata (2500 to 1600 Ma) and Mesoproterozoic strata (1600 to 1000 Ma) are exposed; Neoproterozoic strata (1000 to 545 Ma) are exposed over an extensive but somewhat subordinate area. The mean age of the exposed Proterozoic strata is about 1450 Ma. Assuming that most of the exposed Proterozoic strata have seldom been so deeply buried as not to record the structure associated with ≥20-km-diameter craters, we estimate that the mean time over which these rocks have been exposed to the production of impact structures during the Proterozoic is about 1450 – 545 = 905 Ma. The estimated mean Proterozoic crater production rate for craters ≥20 km diameter, then, is:

$$(4 \pm 2)/1.15 \times 10^6 \text{ km}^2/0.905 \times 10^9 \text{ y}$$

$$= (3.8 \pm 1.9) \times 10^{-15} \text{ km}^{-2} \text{ y}^{-1}.$$

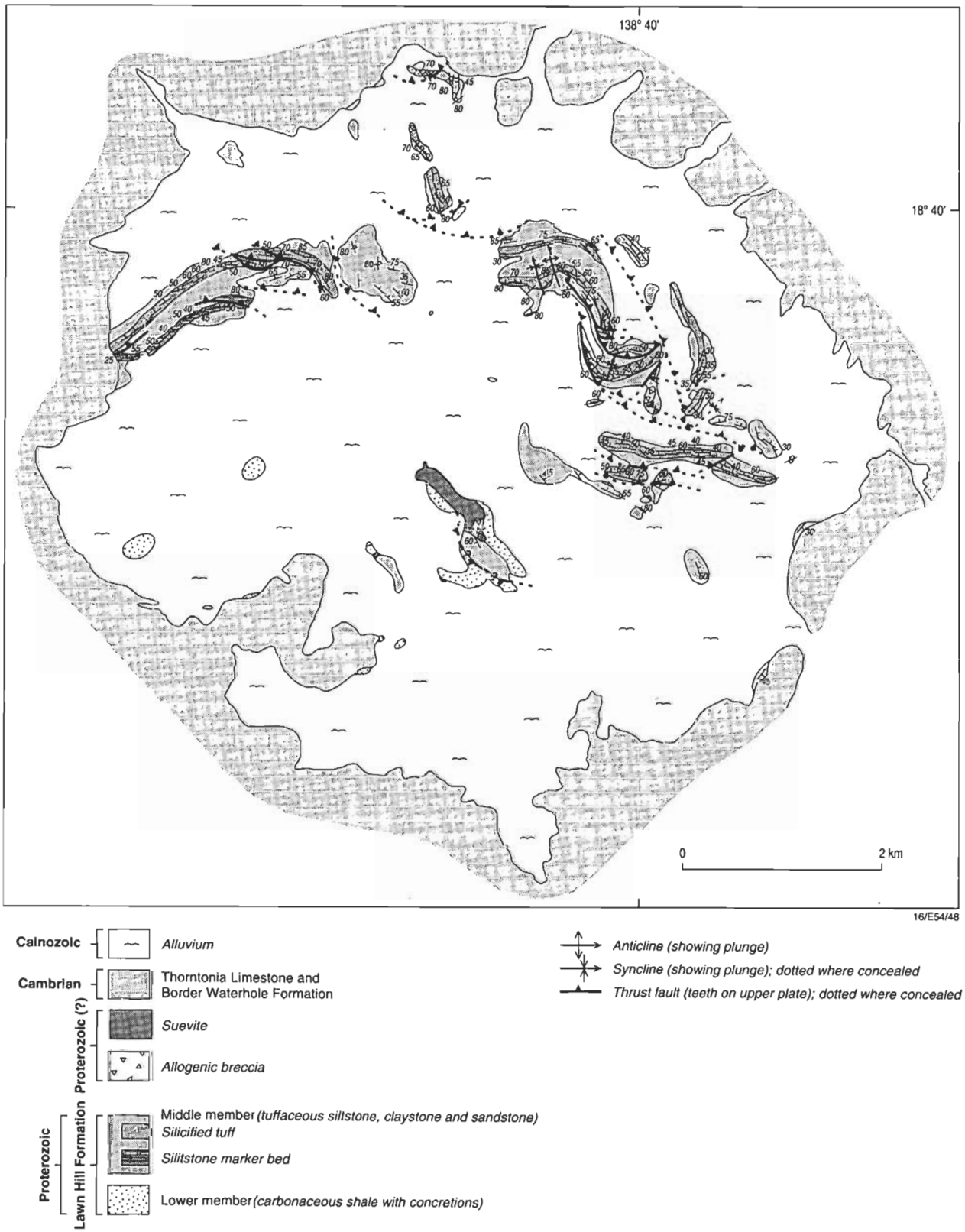

Figure 16. Geology of the central uplift of the Lawn Hill structure (Qld), mapped by E.M. Shoemaker and C.S. Shoemaker, 1990–1991.

This estimate is based strictly on *exposed* structures and the average age of *exposed* rocks. Any unknown impact structures buried by Proterozoic or Phanerozoic strata, which likely are numerous, are irrelevant to the calculation.

Our estimate of the Proterozoic cratering rate is close to the terrestrial crater production equivalent to the average rate of cratering on the Moon for the last 3.2 Ga (Table 1). According to Wilhelm's (1987) count of all 132 Eratosthenian and Copernican lunar craters (age ≤ 3.2 Ma) with D ≥30 km, and assumptions that (i) the impacting bodies had velocities like those of present-day Earth-crossing asteroids and (ii) $N_D \propto D^{-1.8}$ (20 km ≤D ≤ 30 km), the terrestrial production of craters at D ≥20 km diameter equivalent to the mean 3.2-Ga lunar cratering rate is:

$$4.3 \pm 0.4 \times 10^{-15}\ \text{km}^{-2}\ \text{y}^{-1}.$$

Figure 17. False-colour Landsat image of the Lawn Hill structure (Qld). A ring of Cambrian limestone and limestone breccia is shown in pale blue.

If half the impactors are comets, the equivalent terrestrial rate is:

$$3.9 \pm 0.3 \times 10^{-15}\ \mathrm{km^{-2}\ y^{-1}}.$$

Shoemaker et al. (1990) estimated the present terrestrial crater production from the combined impact of asteroids and comets at $4.9 \pm 2.9 \times 10^{-15}\ \mathrm{km^{-2}\ y^{-1}}$ for D ≥20 km. This rate was derived from estimates of the present population and flux of Earth-crossing asteroids and the flux of long-period comets. More recently, Shoemaker et al. (1994) have suggested that periodic comets contribute an additional ~20 per cent to the crater production, which raises the total estimated terrestrial cratering rate to $5.9 \pm 3.5 \times 10^{-15}\ \mathrm{km^{-2}\ y^{-1}}$. This estimate, based entirely on astronomical surveys, is in good agreement with the crater production for the last 120 Ma of $5.6 \pm 2.8 \times 10^{-15}\ \mathrm{km^{-2}\ y^{-1}}$, derived from dated impact structures ≥20 km diameter on the North American and European cratons (Grieve & Shoemaker 1994). It is also in good agreement with the record of Phanerozoic impact structures ≥10 km diameter in the central United States discussed by Shoemaker (1977). When extrapolated for $N_D \propto D^{-1.8}$, the ≥10-km cratering rate found by Shoemaker ($2.2 \pm 1.1 \times 10^{-15}\ \mathrm{km^{-2}\ y^{-1}}$) yields a ≥20-km cratering rate of $6.3 \pm 3.2 \times 10^{-14}\ \mathrm{km^{-2}\ y^{-1}}$. Each of the estimates of the recent or Phanerozoic cratering rate overlaps the inferred mean long-term rate, but the fact that all three estimates of the recent rate agree closely and are higher than that derived from the 3.2-Ga lunar crater record suggests that the cratering rate has increased in late geological time. For a discussion of the relationship between lunar and terrestrial cratering rates, see Grieve & Shoemaker (1994).

Although the statistical uncertainties are large, the Proterozoic cratering record of Australia is consistent with the long-term lunar cratering record. It is possible, of course, that the known Proterozoic impact structures are not broadly distributed in age. Within the present bounds on their ages, five of the six structures could be late Neoproterozoic and one could conceivably be Early Cambrian. The broad tracts of Palaeoproterozoic sedimentary terrane that we searched intensively in Western Australia yielded only two Proterozoic impact structures and only one greater than 20 km diameter. (There are, however, two impact-spherule horizons in the 2.6-Ga Wittenoom Formation and Carawine Dolomite and in the Brockman Iron Formation of the Hamersley Group (Simonson 1992), for which no source craters have been found.) Taken at face value, these observations hint at possible long-term fluctuations in the cratering rate. Most of the Proterozoic impact structures might have been produced after the onset of a suspected late surge in crater production. This would be consistent with observed high crater counts on the rim deposit of the ~800-Ma lunar crater Copernicus (Basaltic Volcanism Study Project 1981; Wilhelms 1987).

We conclude that the cratering rate might have increased in late geological time, perhaps as early as the Neoproterozoic; that the z oscillation of the sun might have decreased in the last billion years after having encountered one or more massive objects; and that the impact of comets might have produced as many as about half of the craters larger than 20-km in diameter during the postulated period of enhanced bombardment.

Table 1. Estimates of crater production rates on Earth

	Production of craters ≥20 km diameter[a] 10^{-15} *km*$^{-2}$ *y*$^{-1}$
Cratering rate on Earth equivalent to the 3.2-Ga crater record on the Moon	
(asteroidal impact velocities assumed)	4.3 ± 0.4
(50% asteroidal velocities and 50% cometary velocities assumed)	3.9 ± 0.3
Proterozoic cratering rate estimated from Australian impact structures	3.8 ± 1.9
Phanerozoic cratering rate estimated by extrapolation from impact structures ≥10 km diameter in central United States (Shoemaker 1977)	6.3 ± 3.2
Cratering rate for last 120 Ma estimated from dated impact structures on North American and European cratons (Grieve & Shoemaker 1994)	5.6 ± 2.8
Present cratering rate estimated from astronomical surveys	5.9 ± 3.5

a. Errors listed are 1 σ.

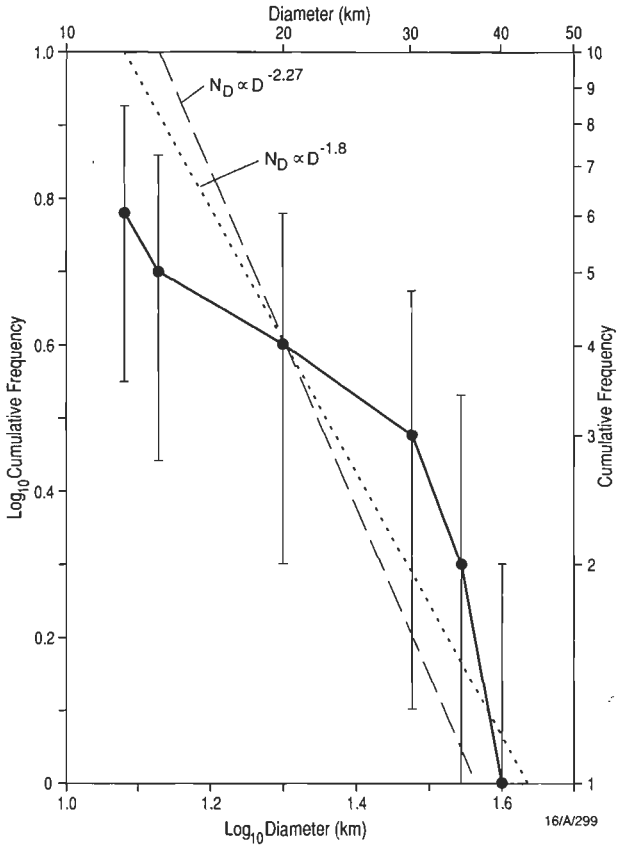

Figure 18. Cumulative size–frequency distribution of Proterozoic impact structures in Australia. The observed cumulative frequency with 1-σ error bars is depicted by the solid line; the inferred cumulative frequency proportional to $D^{-2.27}$ is depicted by the dashed line; the inferred cumulative frequency proportional to $D^{-1.8}$ is depicted by the dotted line.

Acknowledgments

We wish to thank numerous individuals and companies that have helped us over the last 11 years. The Geological Survey of Western Australia graciously loaned us a radio for communication on their network and stored our field equipment in the early years; Ray Connolly, Alex Trendall, and Phil Playford were especially helpful. Stockdale Prospecting Ltd gave us a lift by helicopter into the centre of the Spider structure in 1984. Chris Arndt and Joe Harms of Broken Hill Pty shared their unpublished report of the Spider structure, and provided the false-colour Landsat image (Fig. 4). Geologists of CRA kindly shared photographs, maps, and other data on the Lawn Hill structure. The warm hospitality of Barry and Di Kubala of Adels Grove, near Lawn Hill, is much appreciated. We thank all the station owners and managers for permission to enter, travel, and camp on their stations in the course of our studies. Dan Milton provided his compilation on the geology of the Strangways structure for our use in the field and as a source for preparing Figure 11. David Roddy contributed his skills as pilot and photographer to capturing aerial views of many structures. We thank George Williams for helpful review of the manuscript. AGSO's Cartographic Services Unit has been especially helpful in the preparation of the accompanying maps. The fieldwork for this investigation was supported by NASA funds transferred to the US Geological Survey.

References

Alexopoulos, J.S., Grieve, R.A.F. & Robertson, P.B., 1988. Microscopic lamellar deformation features in quartz: discriminative characteristics of shock-generated varieties. Geology, 16, 796–799.

Bahcall, J.N. & Bahcall, S., 1985. The Sun's motion perpendicular to the galactic plane. Nature, 316, 706–708.

Basaltic Volcanism Study Project, 1981. Basaltic volcanism on the terrestrial planets. Pergamon Press, New York.

Bottomley, R.J., 1982. $^{40}Ar/^{39}Ar$ dating of melt rock from impact craters. PhD Thesis, University of Toronto, Toronto, Ontario, Canada.

Bottomley, R.J., York, D. & Grieve, R.A.F., 1990. $^{40}Argon^{39}argon$ dating of impact craters. Proceedings of the 20th Lunar and Planetary Science Conference, 421–431.

Bunch, T.E. & Quaide, W.L., 1968. Shatter cones in the Danny Boy nuclear crater. In: French, B.M. & Short, N.M. (editors), Shock metamorphism of natural materials. Mono Book Corp., Baltimore.

Bunting, J.A., Brakel, A.T. & Commander, D.P., 1982. Nabberu, Western Australia — 1:250 000 Geological Series map and explanatory note. Geological Survey of Western Australia.

Bunting, J.A., Commander, D.P. & Gee, R.D., 1977. Preliminary synthesis of Lower Proterozoic stratigraphy and structure adjacent to the northern margin of the Yilgarn Block. Geological Survey of Western Australia, Annual Report for 1976, 43–48.

Bunting, J.A., de Laeter, J.R. & Libby, W.G., 1980. Evidence for the age and cryptoexplosive origin of the Teague Ring structure, Western Australia. Geological Survey of Western Australia, Annual Report for 1980, 125–129.

Butler, H., 1974. The Lake Teague ring structure, Western Australia: an astrobleme? Search, 5, 534–536.

de Laeter, J.R. & Trendall, A.F., 1971. The age of the Gidley Granophyre. Geological Survey of Western Australia, Annual Report for 1970, 62–67.

Dodson, R.G. & Gardener, J.E.F., 1978. Tennant Creek, Northern Territory — 1:250 000 Geological Series map and

explanatory notes, SF/53–6. Bureau of Mineral Resources, Australia.

Dunn, P.R., 1963. Hodgson Downs, Northern Territory — 1:250 000 Geological Series map and explanatory notes, SD/53–14. Bureau of Mineral Resources, Australia.

Ferguson, J., Brett, R., Milton, D.J., Dence, M.R., Simonds, C.H. & Taylor, S.R., 1978. Strangways cryptoexplosion structure, Northern Territory, Australia: preliminary results. Meteoritics, 13, 459–460.

French, B.M. & Short, N.M., 1968 (editors). Shock metamorphism of natural materials. Mono Book Corp., Baltimore.

Gostin, V.A., Haines, P.W., Jenkins, R.J.F., Compston, W. & Williams, I.S., 1986. Impact ejecta horizon within Late Precambrian shales, Adelaide Geosyncline, South Australia. Science, 233, 198–200.

Grieve, R.A.F., 1984. The impact cratering rate in recent time. Proceedings of the 14th Lunar and Planetary Science Conference: Journal of Geophysical Research, 89, B403–B408.

Grieve, R.A.F., 1987. Terrestrial impact structures. Annual Review of Earth and Planetary Science, 15, 245–270.

Grieve, R.A.F., 1991. Terrestrial impact: the record in the rocks. Meteoritics, 26, 175–194.

Grieve, R.A.F. & Pilkington, M., 1996. The signature of terrestrial impacts. AGSO Journal of Australian Geology & Geophysics (this issue).

Grieve, R.A.F. & Shoemaker, E.M., 1994. The record of past impacts on Earth. In: Gehrels, T. (editor), Hazards due to comets & asteroids. The University of Arizona Press, Tucson, Arizona, 417–462.

Grieve, R.A.F., Stöffler, D. & Deutsch, A. 1991. The Sudbury structure: controversial or misunderstood? Journal of Geophysical Research, 96, 22753–22764.

Guppy, D.J., Brett, R. & Milton, D.J., 1971. Liverpool and Strangways Craters, Northern Territory. Two structures of probable impact origin. Journal of Geophysical Research, 76, 5387–5393.

Hall W.D.M., Goode, A.D.T., Bunting, J.A. & Commander, D.P., 1977. Stratigraphic terminology of the Earaheedy Group, Nabberu Basin. Geological Survey of Western Australia, Annual Report for 1976, 40–43.

Hall, W.D.M. & Goode, A.D.T., 1978. The Early Proterozoic Nabberu Basin and associated iron formations of Western Australia. Precambrian Research, 7, 129–184.

Harms, J.E., Milton, D.J., Ferguson, J., Gilbert, D.J., Harris, W.K. & Goleby, B., 1980. Goat Paddock cryptoexplosion crater, Western Australia. Nature, 286, 704–706.

Harms, J.E., Wilson, J.G., Arndt, C.D. & Gilbert, D.J., undated. An unusual "spider" structure of probable impact origin in the Kimberley region, northwest Australia. Unpublished manuscript.

Hickman, A.H. & Gibson, D.L., 1982. Port Hedland–Bedout Island, Western Australia — 1:250 000 Geological Series map and explanatory notes. Bureau of Mineral Resources, Australia, and Geological Survey of Western Australia.

Hills, J.G., 1981. Comet showers and the steady-state infall of comets from the Oort cloud. Astronomical Journal, 86, 1730–1740.

Hutton, L.J. & Wilson, I.H., 1984. Mount Oxide region, Queensland — 1:100 000 geological map and commentary. Bureau of Mineral Resources, Australia, and Geological Survey of Queensland.

Matese, J.J., Whitman, P.G., Innanen, K.A. & Valtonen, M.J., 1995. Periodic modulation of the Oort cloud comet flux by the adiabatically changing galactic tide. Icarus, 116, 255–268.

Milton, D.J., 1977. Shatter cones — an outstanding problem in shock mechanics. In: Roddy, D.J., Pepin, R.O. & Merrill, R.B. (editors), Impact and explosion cratering. Pergamon Press, New York.

Milton, D.J., Barlow, B.C., Brown, A.R., Moss, F.J., Manwaring, E.A., Sedmik, E.C.E., Young, G.A. & Van Son, J., 1996a. Gosses Bluff — a latest Jurassic impact structure, central Australia. Part 2: Seismic, magnetic, and gravity studies. AGSO Journal of Australian Geology & Geophysics (this issue).

Milton, D.J., Glikson, A.Y. & Brett, R., 1996b. Gosses Bluff — a latest Jurassic impact structure, central Australia. Part 1: Geological structure, stratigraphy, and origin. AGSO Journal of Australian Geology & Geophysics (this issue).

Morgan, J.W., Wandless, G.A. & Petrie, R.K. 1981. Strangways Crater. Trace elements in melt rocks. Lunar and Planetary Science, XII, 714–716.

Page, R.W., 1981. Depositional ages of the stratiform base metal deposits at Mount Isa and McArthur River, Australia, based on U–Pb zircon dating of concordant tuff horizons. Economic Geology, 76, 648–658.

Page, R.W., 1988. Geochronology of Early to Middle Proterozoic fold belts in northern Australia: a review. Precambrian Research, 40/41, 1–19.

Palme, H., 1982. Identification of projectiles of large terrestrial impact craters and some implications for the interpretation of Ir-rich Cretaceous/Tertiary boundary layers. In: Silver, L.T. & Schultz, P.H. (editors), Geological implications of impacts of large asteroids and comets on the Earth. Geological Society of America, Special Paper 190, 223–233.

Pilkington, M. & Grieve, R.A.F., 1992. The geophysical signature of terrestrial impact craters. Reviews of Geophysics, 30, 161–181.

Plescia, J.B., Shoemaker, E.M. & Shoemaker, C.S., 1994. Gravity survey of the Mount Toondina impact structure, South Australia. Journal of Geophysical Research, 99, 13167–13179.

Pohl, J., Stöffler, D., Gall, H. & Ernstson, K., 1977. The Ries impact crater. In: Roddy, D.J., Pepin, R.O. & Merrill, R.B. (editors), Impact and explosion cratering. Pergamon Press, New York, 703–714.

Roberts H.G. & Perry, W.J., 1969. Mount Elizabeth, Western Australia — 1:250 000 Geological Series map and explanatory notes, SE/52–1. Bureau of Mineral Resources, Australia.

Roddy, D.J. & Davis, L.K., 1977. Shatter cones formed in large-scale experimental explosion craters. In: Roddy, D.J., Pepin, R.O. & Merrill, R.B. (editors). Impact and explosion cratering. Pergamon Press, New York, 715–750.

Schneider, E. & Wagner, G.A., 1976. Shatter cones produced experimentally by impacts in limestone targets. Earth and Planetary Science Letters, 32, 40–44.

Shoemaker, E.M., 1977. Astronomically observable crater-forming projectiles. In: Roddy, D.J., Pepin, R.O. & Merrill, R.B. (editors), Impact and explosion cratering. New York, Pergamon Press, 617–628.

Shoemaker, E.M. & Chao, E.C.T., 1961. New evidence for the impact origin of the Ries Basin, Bavaria, Germany. Journal of Geophysical Research, 66, 3371–3378.

Shoemaker, E.M., Gault, D.E. & Lugn, R.V., 1961. Shatter cones formed by high-speed impact in dolomite. US Geological Survey, Professional Paper 424–D, 365–368.

Shoemaker, E.M. & Shoemaker, C.S., 1985. Impact structures of Western Australia. Meteoritics, 20, 754–756.

Shoemaker, E.M. & Shoemaker, C.S., 1988a. Impact structures of Australia (1987). Lunar and Planetary Science, XIX, 1079–1080.

Shoemaker, E.M. & Shoemaker, C.S., 1988b. The Spider impact structure. Geological Society of America, Abstracts with Programs, 20, A147.

Shoemaker, E.M. & Shoemaker, C.S., 1990. Proterozoic impact record of Australia. In: Abstracts for the International Workshop on Meteorite Bombardment on the Early Earth. Lunar and Planetary Institute Contribution 746, 47–48.

Shoemaker, E.M., Shoemaker, C.S. & Plescia, J.B., 1989. Gravity investigation of the Connolly Basin impact structure, Western Australia. Lunar and Planetary Science, XX, 1010–1011.

Shoemaker, E.M., Weissman, P.R. & Shoemaker, C.S., 1994. The flux of periodic comets near Earth. In: Gehrels, T. (editor), Hazards due to comets and asteroids. University of Arizona Press, Tucson, Arizona, 313–335.

Shoemaker, E.M., Wolfe, R.F. & Shoemaker, C.S., 1990. Asteroid and comet flux in the neighborhood of the Earth. *In:* Sharpton, V.L. & Ward, P.D. (editors), Global catastrophes in Earth history; an interdisciplinary conference on impacts, volcanism, and mass mortality. Geological Society of America, Special Paper 247, 155–170.

Simonds, C.H., Floran, R.J., McGee, P.E., Phinney, W.C. & Warner, J.L., 1978. Petrogenesis of melt rocks, Manicouagan impact structure, Quebec. Journal of Geophysical Research, 85, 2773–2788.

Simonson, B.M., 1992. Geological evidence for a strewn field of impact spherules in the early Precambrian Hamersley Basin of Western Australia. Geological Society of America, Bulletin 104, 829–839.

Smith, K.G.,1970. Bonney Well, Northern Territory — 1:250 000 Geological Series map and explanatory notes, SE/53–14. Bureau of Mineral Resources, Australia.

Stewart, A. & Mitchell, K., 1987. Shatter cones at the Lawn Hill circular structure, northwestern Queensland: presumed astrobleme. Australian Journal of Earth Sciences, 34, 477–485.

Sweet, I.P., & Hutton, L.J., 1982. Lawn Hill region, Queensland — 1:100 000 geological map and commentary. Bureau of Mineral Resources, Australia.

Tonkin, P., 1973. Discovery of shatter cones at Kelly West near Tennant Creek, Northern Territory, Australia. Journal of the Geological Society of Australia, 20, 99–102.

Wilhelms, D.E., 1987. The geologic history of the Moon. US Geological Survey, Professional Paper 1348.

Williams, G.E., 1994a. Acraman: a major impact structure from the Neoproterozoic of Australia. In: Dressler, B.O., Grieve, R.A.F. & Sharpton, V.L. (editors), Large meteorite impacts and planetary evolution. Geological Society of America, Special Paper 293, 209–224.

Williams, G.E., 1994b. Acraman, South Australia: Australia's largest meteorite impact structure. Proceedings of the Royal Society of Victoria, 106, 105–127.

Williams, G.E., Schmidt, P.W. & Boyd, D.M., 1996. Magnetic signature and morphology of the Acraman impact structure, South Australia. AGSO Journal of Australian Geology & Geophysics (this issue).

AGSO Journal of Australian Geology & Geophysics, 16 (4), 399–420

The signature of terrestrial impacts

Richard A.F. Grieve[1] & Mark Pilkington[1]

The high level of endogenic geological activity makes the terrestrial record of impact difficult to read. Terrestrial processes, such as erosion, rapidly modify craterforms and ultimately remove the evidence of impact. In their largely uneroded states, terrestrial impact structures have the basic so-called simple and complex forms observed on other planetary bodies, but few of them have morphometric parameters, such as apparent and true depth and stratigraphic uplift, that can be defined. Erosion severely affects such parameters, and can even result in a positive topographic form due to differential erosion. The principal criterion for the recognition of terrestrial impact structures is, therefore, not their form, but the occurrence of shock-metamorphic effects. These are well-documented and are described briefly. In parautochthonous target lithologies, they are limited to the central portion of the original crater floor, and attenuate radially and with depth. Shock effects also occur in allochthonous lithologies, such as breccias and impact-melt rocks.

In addition to a characteristic geological signature, terrestrial impact structures have characteristic geophysical signatures. The most common is a Bouguer gravity low, which extends out to the rim. The low is due to impact-induced brecciation and fracturing. It increases in value with increasing size, reaching a limiting value of ~300 $\mu m\ s^{-2}$ (~300 g.u.). In large impact structures, it can be accompanied by a central relative high. The magnetic signature can be more varied but generally corresponds to a subdued low. Local intense magnetic anomalies can occur in the centres of large structures, D >40 km; these magnetic highs have various sources, but many are due to post-impact hydrothermal alteration. Impact can also lead to a reduction in seismic velocities and resistivity of the target rocks.

The geophysical, geological, and morphological characteristics at terrestrial impact structures are summarised in tabular form as an aid to the recognition of additional structures.

Introduction

During the last 25 years, our perspective of the planetary bodies of the solar system has changed from them being astronomical to geological objects. With volcanism and, to a lesser extent, tectonism, impact cratering is now recognised as a ubiquitous geological process affecting all the terrestrial planets. Its apparent importance relative to other geological processes is inversely proportional to planetary size. Smaller planetary bodies are less efficient at retaining their internal heat, and are thus less endogenically active over geological time than larger planetary bodies. Thus, they tend to preserve greater portions of their earliest crust. It is this crust that bears overwhelming evidence of the importance of impact, as it dates back to early times in planetary history when the impact flux was greater than two orders of magnitude higher than the present day (Hartmann 1995).

The Earth is the most endogenically active of the terrestrial planets, and thus has retained the poorest sample of the results of impacts which have occurred throughout geological time. The study of terrestrial impact structures does not have a long established tradition in the Earth sciences. In addition, it has, until recently, largely been the provenance of a small number of workers with strong ties to planetary geology. Although the known sample of terrestrial impact structures is small, terrestrial impact structures are the major source of ground-truth data on the geological and geophysical effects of hypervelocity impact at a variety of scales.

Recently, there has been a growing awareness in the more general Earth-science community as to the potential importance of impact for the terrestrial environment. This has been spurred by several recent realisations. They include: the discovery of chemical and physical evidence for the involvement of impact at the Cretaceous–Tertiary (KT) boundary and the associated mass extinction event (e.g., Alvarez et al. 1980; Smit & Hertogen 1980; Bohor et al. 1984) and their relation to the Chicxulub impact structure in the Yucatan Peninsula, Mexico (Table 1; Hildebrand et al. 1991); the resource potential of impact structures, some of which are related to world-class ore deposits, both spatially and genetically (Grieve & Masaitis 1994); and the disastrous consequences of impacts for human civilisation (Gehrels 1994). The detailed study of impact processes, however, is so recent that it is not yet part of the general knowledge base.

Impact involves the transfer of considerable energies to a spatially limited area of the Earth's surface in a very short time interval. As a consequence, local geology of the target area is only of secondary importance, and the geological and geophysical effects of impact are, to a first order, largely independent of the target. The effects are, however, scale-dependent on the size of the impact. The net result is that, at least before they are modified by post-impact endogenic processes, impacts of similar scale produce similar first-order results. Thus, even though the number of known terrestrial impact structures is small (~150; Grieve et al. 1995), we can derive some general observations with respect to their appearance and geological and geophysical signatures. This contribution outlines some of these observations. We hope that it permits known structures to be placed in context, and provides a guide to the recognition of features consistent with an impact origin at additional structures.

General appearance of terrestrial impact structures

Morphology

Impact structures on other planetary bodies are recognised by their characteristic forms. The morphology of impact structures is divided into simple and complex structures (Dence 1968). Simple structures have the form of a bowl-shaped depression with a structurally uplifted rim, which includes an overturned flap overlain by ejecta (Fig. 1). This bowl-shaped depression is sometimes referred to as the apparent crater. It is underlain by an allochthonous breccia lens, which is parabolic in cross-section and contained by fractured but mostly autochthonous target rocks (Fig. 1). The crater defined by the parautochthonous target rocks is referred to as the true crater. At larger diameters, collapse features in the rim area become more prominent, and the structure evolves into a so-called complex structure, which consists of a structurally complex rim, a downfaulted annular trough, and a structurally uplifted central area (Fig. 2).

[1] Geological Survey of Canada, 1 Observatory Crescent, Ottawa, Canada K1A 0Y3. Contribution 34795 from the Geological Survey of Canada.

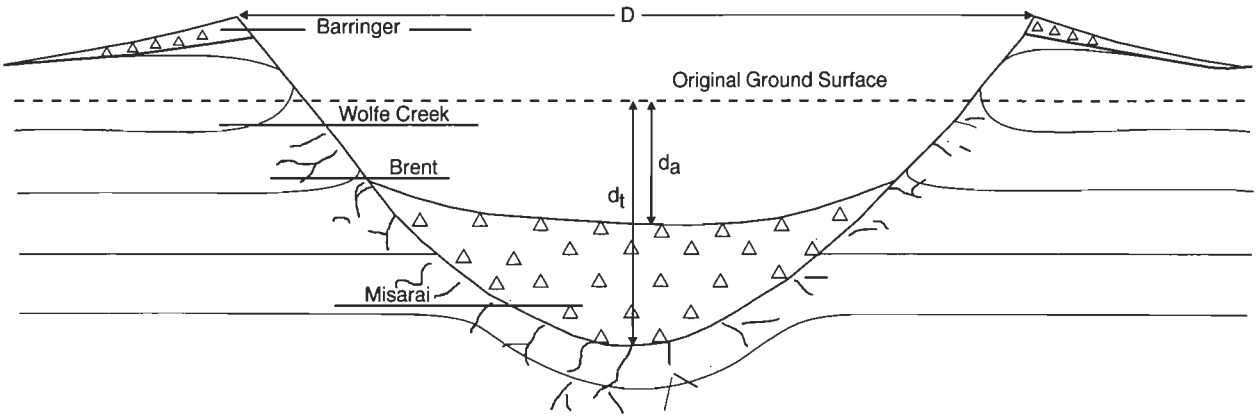

Figure 1. Schematic cross-section of a simple impact structure. Note the overturned flap on the rim overlain by ejecta (small triangles), and the interior allochthonous breccia (large triangles) partly filling the true crater. Present erosional levels of a number of terrestrial simple craters (Table 1) are indicated on the left side of the structure. Definitions of rim diameter (D), apparent depth (d_a), and true depth (d_t) are also indicated.

Table 1. Principal characteristics of terrestrial impact structures mentioned in the text

Structure	*Country*	*Latitude*	*Longitude*	*Diameter (km)*[a]	*Age (Ma)*[a]
Acraman	Australia	32°01'S	135°27'E	85–90	~590
Ames	USA	36°15'N	98°12'W	16	470 ± 30
Avak	USA	71°15'N	156°38'W	12	>95
Barringer	USA	35°02'N	111°01'W	1.2	0.049 ± 0.003
Boltysh	Ukraine	48°45'N	32°10'E	24	88.3
Bosumtwi	Ghana	6°30'N	1°25'W	10.5	0.3 ± 0.02
Brent	Canada	46°05'N	78°29'W	3.8	450 ± 30
Charlevoix	Canada	47°32'N	70°18'W	54	357 ± 15
Chesapeake Bay	USA	37°15'N	76°04'W	85	35.5 ± 0.6
Chicxulub	Mexico	21°20'N	89°30'W	180	64.98 ± 0.05
Connolly	Australia	23°22'S	124°45'E	9	<60
Couture	Canada	60°08'N	75°20'W	8	430 ± 25
Dellen	Sweden	1°55'N	16°39'E	8	89.0 ± 2.7
East Clearwater	Canada	56°05'N	74°07'W	26	290 ± 20
Gardnos	Norway	60°39'N	9°00'E	5	500 ± 10
Gosses Bluff	Australia	23°49'S	132°18'E	24	142.5 ± 0.5
Haughton	Canada	75°22'N	89°41'W	24	23 ± 1
Kara	Russia	69°12'N	65°00'E	65	73 ± 3
Lockne	Sweden	63°00'N	14°48'E	7	455
Misarai	Lithuania	54°01'N	24°34'E	3	570 ± 50
Mistastin	Canada	55°53'N	63°18'W	28	38 ± 4
Mjølnir	Norway	73°48'N	29°40'E	40	143 ± 20
Montagnais	Canada	42°53'N	64°13'W	45	50.5 ± 0.8
Puchezh-Katunki	Russia	57°06'N	43°35'E	80	220 ± 10
Ries	Germany	48°53'N	10°37'E	24	15.1 ± 1
Saint Martin	Canada	51°47'N	98°32'W	40	220 ± 32
Siljan	Sweden	61°02'N	14°52'E	53	368.0 ± 1.1
Slate Islands	Canada	48°40'N	87°00'W	30	<350
Sudbury	Canada	46°36'N	81°11'W	~250	1850 ± 3
Teague	Australia	25°52'S	120°53'E	30	1630 ± 5
Tookoonooka	Australia	27°20'S	142°49'E	~55	128 ± 5
Vredefort	South Africa	27°00'S	27°30'E	~300	2016 ± 10
West Hawk	Canada	49°46'N	95°11'W	2.44	100 ± 50
Wolfe Creek	Australia	19°10'S	127°46'E	0.88	0.3

a. Other diameter and age estimates have been presented for some of these structures — e.g., Sharpton et al. (1993) has estimated the diameter of Chicxulub to be 300 km.

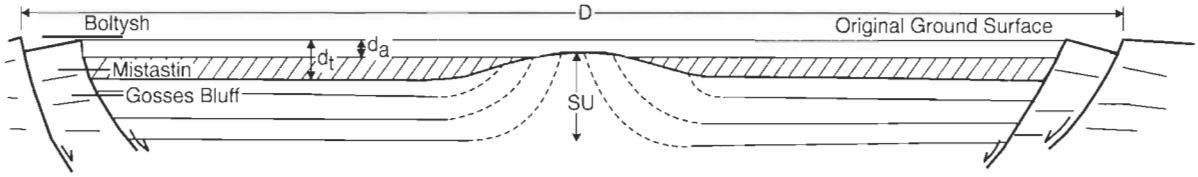

Figure 2. Schematic cross-section of a complex impact structure (not to scale). Note the faulted rim area, downfaulted annular trough, and uplifted centre. Present erosional levels of a number of terrestrial complex impact structures (Table 1) are indicated on the left side of the structure. Rim diameter (D), apparent depth (d_a), true depth (d_t), and amount of stratigraphic uplift (SU) are also indicated. Allochthonous materials (impact-melt rocks and/or breccias) partly filling the structure are indicated by diagonal lines.

Figure 3. Oblique aerial photograph of the 0.88-km-diameter Wolfe Creek Crater (Australia; Table 1), an example of a simple impact structure. Note that this structure, although only ~300 000 years old, has an eroded rim and is partly filled by sediments.

As with simple structures, complex structures are partly filled by allochthonous material, such as breccias and impact-melt rocks, and an apparent and true crater can be defined (Fig. 2). The uplifted central area has initially the topographic form of a central peak, which rises above the floor of the structure (Fig. 2) and has a height that generally does not exceed the depth from the rim to the floor (Pike 1977). With increasing diameter, the central peak is accompanied by a fragmentary ring (a central-peak basin). Larger structures have an interior ring with no peak (a peak-ring basin), and even larger-diameter structures have multiple inner rings (a multi-ring basin; Hartmann & Wood 1971; Wood & Head 1976). These forms and definitions, as well as much of the known morphometry, for the various types of impact structures are based on the planetary, particularly the lunar, record.

These terms are also used to describe terrestrial impact structures (Table 2). There are, however, a number of complicating factors in the terrestrial environment. Few terrestrial impact structures exposed at the surface have near-pristine forms. Near-pristine forms are restricted to the youngest terrestrial impact structures. As smaller impacts occur more frequently than larger ones, they are, therefore, limited to structures with the simple form. The best examples include Barringer (or Meteor) Crater (USA) and Wolfe Creek (Australia; Fig. 3; Table 1). Even they, however, have been modified to some degree by erosion and sedimentary infilling.

Most larger, complex structures are eroded to varying degrees (Fig. 4). There are, however, a number of complex impact structures which were buried by post-impact sediments almost immediately after formation (e.g., Chicxulub, Mexico; Montagnais, Canada; Puchezh-Katunki, Russia; Table 1), and presumably have a near-pristine form. They can, however, only be delineated by drillhole and geophysical data, and therefore the exact details of their morphologies are generally not well known. Only the largest terrestrial impact structures have the potential to be peak-ring basins or multi-ring basins. Unfortunately, the largest structures — Chicxulub; Sudbury, Canada; and Vredefort, South Africa (Table 1) — are either buried, tectonised, or eroded. Their original detailed morphology cannot be defined with confidence, although they are assumed to represent multi-ring or peak-ring basins (e.g., Sharpton et al. 1993; Hildebrand et al. 1995; Spray & Thompson 1995).

There is a tendency to compare terrestrial impact structures with, particularly, lunar impact structures (e.g., Pike 1985), and to assume a greater equivalence in detailed morphology than the observational data would suggest. However, the planetary environments evince important differences. For example, secondary target effects on Earth include the transition from simple to complex forms at diameters of ~2 km and ~4 km, depending on whether the target rocks are sedimentary or crystalline respectively; there are also mixed targets with sediments overlying crystalline basement. Some complex impact structures in mixed or largely sedimentary targets do not appear to develop a topographically high central peak. For example, Ries (Germany) and Haughton (Canada; Fig. 5) are of similar size and age (Table 1) and have no emergent central peak; in contrast, Boltysh (Ukraine; Table 1), which is of a similar size but in a crystalline target, has a central peak that is emergent from the surrounding ~300 m of impact lithologies filling the structure. All these structures have been affected by only minor erosion,

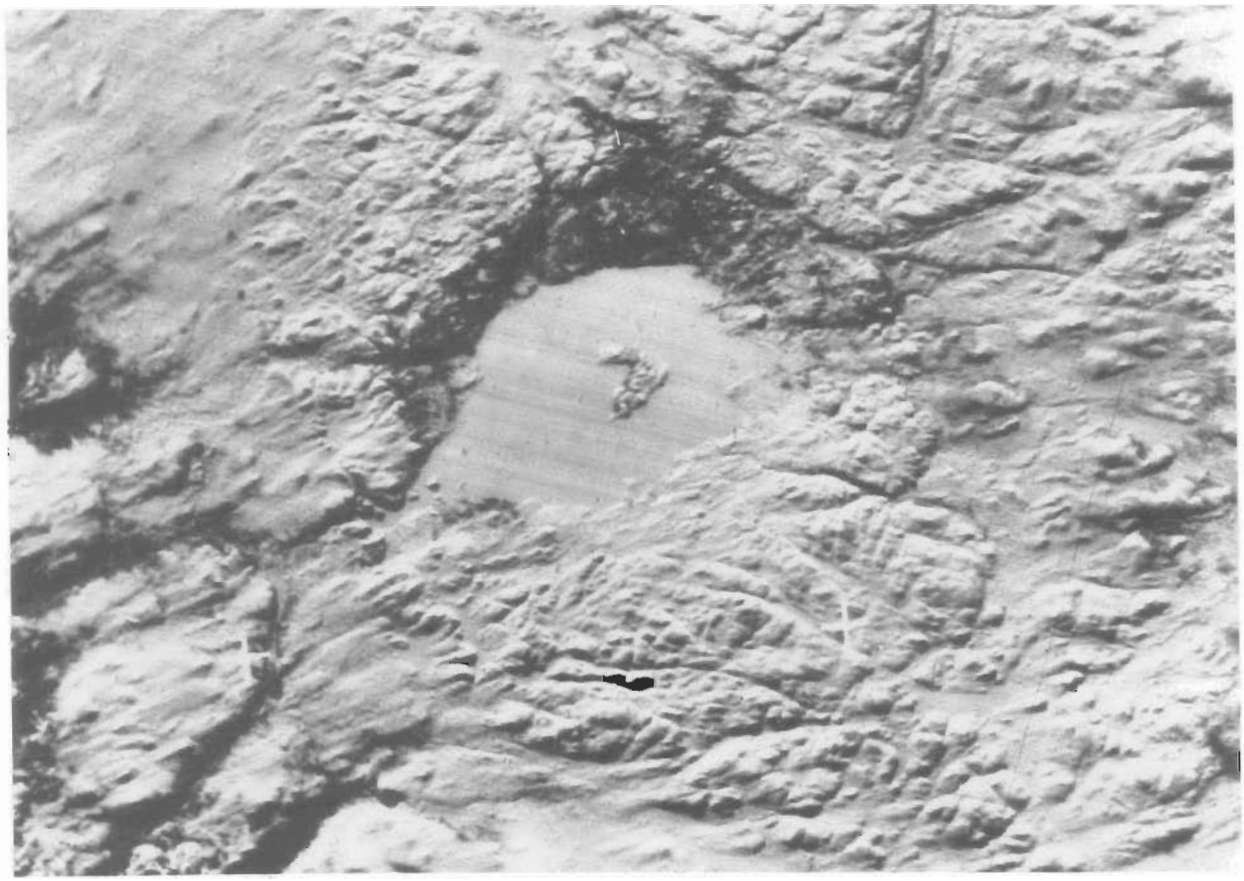

Figure 4. Landsat image of the 28-km-diameter Mistastin (Canada; Table 1) complex impact structure. The central uplift is represented as a 5-km-diameter horseshoe-shaped island; the annular trough is partly occupied by a (frozen) lake; and the rim is barely visible. The relative level of erosion is indicated in Figure 2.

and, at present, there is no clear explanation for this difference in their morphologies.

In addition, planetary gravity has an effect on cratering mechanics and, thus, morphologies. The lower lunar gravity (0.1645 g, where g is the average terrestrial value for gravitional acceleration) results in deeper impact structures on the moon compared with structures of an equivalent size on Earth. This is because gravity is the force acting against both the excavation of material and the formation of topography. In addition, the various forms of impact structures, and their diameter ranges, appear to be an inverse function of planetary gravity (Pike 1985). Thus, they form smaller diameters on Earth than on the moon. There is an additional effect due to gravity. Gravity is a variable in cratering mechanics, but it is not a variable in determining the volume of target material melted in a specific impact event. Thus, an impact into crystalline target rocks generates ~2.5 times more impact melt in a terrestrial than a lunar event resulting in a structure of equivalent size (Cintala & Grieve 1994). This additional melt, which in large part is retained within the impact structure, also has the effect of reducing observed topographic variations.

By far the greatest difference between planetary and terrestrial impact structures, however, is the effect of erosion and sedimentation in the terrestrial environment. Both processes effectively remove impact structures from the terrestrial record by destruction or burial of the craterform. It has been estimated that the signature of a 20-km impact structure can be removed from the record by erosion in <120 Ma if glaciation is one of the erosional agents (Grieve 1984). The effects of erosion are apparent even in low-erosional environments, such as Australia. For example, Wolfe Creek is only ~300 000 years old and occurs within a desert to semi-desert environment (Fig. 3). Nevertheless, it has had its topographic expression in terms of depth reduced by >100 m, or ~70 per cent, according to the present and original topography as constrained by gravity and crater models (Fudali 1979; Grieve et al. 1989). At the present rate of erosion and infilling, Wolfe Creek will cease to exist as a craterform in slightly over 100 000 years. This, however, does not necessarily mean that it would no longer be recognisable as the site of an impact. Impact results in characteristic geological and geophysical effects that are clearly recognisable, even after the original craterform has been removed. As such impact sites are still recognisable but are no longer, by definition, craters, they are referred to as impact structures. In order not to be forced to define when a terrestrial impact crater becomes an impact structure, we refer to all, by the more generic term, as impact structures.

Morphometry

Owing to erosion, few terrestrial impact structures have sufficient topographic information to define morphometric relations. The morphometry of the seven simple structures with the best available data (Grieve et al. 1989) define the relationships:

$$d_a = 0.13D^{1.06}, \text{ and}$$

$$d_t = 0.28D^{1.02},$$

Figure 5. Airborne X-band radar image of the 24-km-diameter complex impact structure at Haughton (Canada; Table 1). Although only slightly eroded, it has no evidence of a topographic central peak (cf. Fig. 4).

where d_a and d_t are the apparent and true depths as measured from the original ground surface to the top and bottom, respectively, of the infilling allochthonous breccia lens; D is the rim diameter as measured at the top of the rim; and units are kilometres (Fig. 1). As noted earlier, the largest terrestrial simple structures in crystalline targets have D ~<4 km. Thus, the amount of erosion required to remove the topographic expression of the largest simple structure on Earth is ~500 m. To remove essentially all geological expression of the structure and the allochthonous breccia lens (Fig. 1), however, requires >1 km of erosion.

There are even fewer good-quality topographic data on the original dimensions of complex structures. Grieve & Pesonen (1992) defined the relationships:

$$d_a = 0.12D^{0.30} \text{ and}$$

$$d_a = 0.15D^{0.43},$$

for sedimentary and crystalline targets respectively (Fig. 2). These relationships are based on data from only five structures and have considerable uncertainty. This uncertainty is due in part to the known examples of larger complex structures being generally older than simple structures, because of the cratering rate, and in part to their smaller d/D ratios (Fig. 2) being more sensitive to topographic changes due to erosion. Nevertheless, the general form of the relationships is similar to that for the moon, where $d_a \propto D^{0.3}$ for lunar complex structures (Pike 1977). On the basis of these relationships, the topography of a 20-km-diameter complex structure would be removed by erosion as little as 300–500 m deep. Like simple structures, such an eroded complex structure would still be recognisable by the geological effects of impact. Indeed, the site of a complex impact structure can be recognised even if it is eroded well below the parautochthonous rocks of the original floor of the structure. The stratigraphic uplift of material in the centre of complex impact structures can be recognised as a geological anomaly (Fig. 2).

The amount of stratigraphic uplift and the diameter of a complex structure maintain a moderately well-defined relationship:

$$SU = 0.06D^{1.1},$$

where SU is the amount of stratigraphic uplift undergone by the deepest lithology now exposed at the surface in the centre (Grieve et al. 1981). This relationship was based on data from 15 complex impact structures. We have revised it, here, according to data from our most recent compilation of terrestrial

Table 2. Morphological and geological signatures of terrestrial impact structures

	Simple	*Complex*
Morphology[a]	Bowl-shaped depression.	Flat floor with faulted rim and central structural uplift, which may be manifested as a topographic peak and/or interior ring(s).
Morphometry[a]	d_t ~$2d_a$ and 1/3 D. D ~<2 and 4 km in sedimentary and crystalline targets respectively.	d:D variable, but less than simple craters and decreasing with D. SU ~1/10 D.
Geology	Partly filled by allochthonous breccia lens with melt rocks. Fractured parautochthonous target rocks, possibly with various breccia and melt dykes.	Partly filled by relatively thin (with respect to D) impact-melt rocks and/or allochthonous breccia. Uplifted deeper lithologies in centre. Downfaulted lithologies in annular trough. Fractured parautochthonous target rocks with various breccia and melt dykes extending out to rim.
Shock metamorphism	In breccia lens; most highly shocked materials are concentrated at top and bottom. In parautochthonous target rocks, shock effects are limited to floor of true crater, and attenuate radially and with depth.	In allochthonous lithologies. In parautochthonous target rocks, shock effects are limited to central uplift (<0.5D), and attenuate radially and with depth.

a. For largely uneroded structures.

impact structures and their characteristics; the relationship is now based on data from 24 structures, and is redefined as:

$$SU = 0.086D^{1.03} \text{ (Fig.6).}$$

Therefore, after the removal of the topography associated with a 20-km-diameter complex structure, the geological expression of the structural uplift requires an additional ~2 km of erosion before it too is removed from the terrestrial record.

Differential erosion has removed all topographic expression of the craterform at a number of complex impact structures, and replaced it with a residual central positive structure. For example, geological and geophysical data indicate that the Gosses Bluff structure is 24 km in diameter (Table 1; Milton et al. this issue; Tingate et al. this issue). The present surface topographic expression of the structure, however, is restricted to a central 4.5-km-diameter annular ridge rising 200 m above the surrounding plain (Fig. 7). This annular ridge represents the remnant core of a central uplift containing erosionally resistant Ordovician–Devonian sandstone. Thus, the present form of Gosses Bluff owes as much to erosion and lithology, as to the original complex crater morphology.

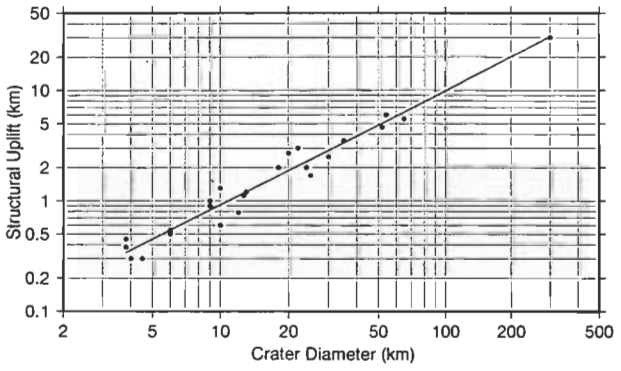

Figure 6. Structural uplift (SU) versus rim diameter (D) for 24 terrestrial complex impact structures in log–log space. Least-squares regression of the data gives the relation SU = 0.086 $D^{1.03}$.

The observation that eroded terrestrial complex impact craters can appear ultimately as neutral or even positive topographic features with uplifted lithologies has contributed historically to the reluctance of some workers to accept the impact origin of certain structures (e.g., Bucher 1963). There has been a recent increase in interest in the contrary hypothesis of a cryptoexplosion origin for certain complex impact craters. This is a direct consequence of the promotion of the argument that the causal agent of the mass extinction and the evidence at the KT boundary are not related to impact (e.g., Loper & McCartney 1988; Carter et al. 1990; Officer 1992). Previously advanced arguments, however, for an impact origin have been elegantly summarised recently by French (1990). These arguments are rooted largely in the geological characteristics of impact structures.

Geology of impact structures

Even though an anomalous circular topographic, structural, or geological feature may indicate the presence of an impact structure, there are other endogenic geological processes that can produce similar features in the terrestrial environment. An obvious craterform is an excellent indicator of a possible impact origin, particularly if it has the appropriate morphometry, but, as noted earlier, such features are rare and short-lived in the terrestrial environment. The burden of proof for an impact origin generally lies with the documentation of the occurrence of shock-metamorphic effects.

Few structures preserve physical evidence of the impacting body. They are limited to small, young, simple structures, where the impacting body (or fragments of it) has been slowed by atmospheric retardation, and impacts with less than its cosmic velocity. These are restricted generally to the impact of iron or stony-iron meteorites. Stony meteorites are weaker than their iron-bearing counterparts, and small ones are generally crushed in the atmosphere as a result of atmospheric interaction and the formation of a stress gradient from their leading to trailing edges (Melosh 1981). Larger impacting bodies (>100–150 m in diameter) survive atmospheric passage with undiminished velocity. Consequently, the peak shock pressures upon impact

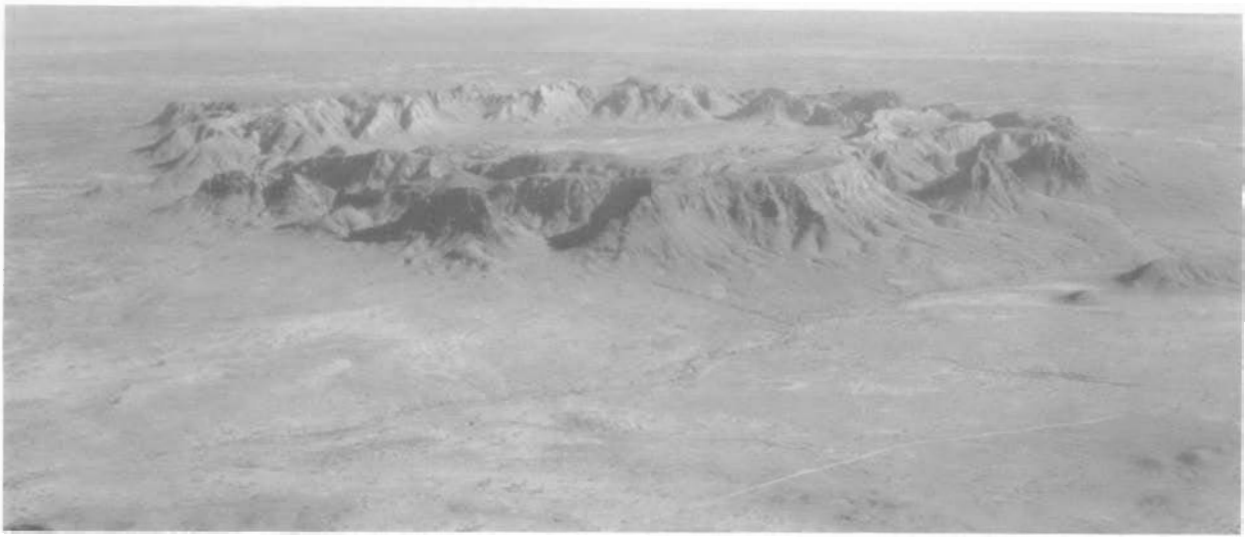

Figure 7. Oblique aerial photograph of Gosses Bluff (Australia; Table 1). This 24-km-diameter complex impact structure is eroded below the original floor (Fig. 2), and is now expressed as a 4.5-km-diameter topographically positive annulus of hills due to differential erosion.

are sufficient to result in the vaporisation of the impacting body, destroying it as a physical entity

Shock metamorphism is the progressive breakdown in the structural order of rocks and, more importantly, their constituent minerals, and is caused by the passage through them of a high-pressure shock wave. On impact, the bulk of the impacting body's kinetic energy is transferred to the target by means of a shock wave. This shock wave imparts kinetic energy to the target materials, which leads to the formation of a crater, and increases the internal energy of the target materials, which leads to the formation of shock-metamorphic effects. The details of the physics of impact and shock-wave behaviour, including cratering mechanics, are presented by Melosh (1989, and references therein), and are not repeated here.

Shock-metamorphic effects observed at terrestrial impact structures, and in shock-recovery experiments, are the net result of transient compression by the shock wave and then release to ambient pressure. Considerable pressure–volume work is done during compression, and pressure release is along an adiabat. Not all the pressure–volume is recovered on release, and the excess is manifested as waste-heat. The amount of trapped waste-heat increases with increasing shock pressure, and ultimately leads to the melting and vaporisation of a portion of the target rocks and, as noted previously, the impacting body. The exact physical conditions on impact are a function of the specific impact parameters. The density of the impacting body and the target, and the impact velocity, determine the peak pressure, which can be considerable. For example, the impact of a stony chrondritic body into granite at 25 km s^{-1} results in a peak pressure at the point of impact of ~900 GPa (9 million bars). The intensity of the shock wave attenuates with distance into the target, and the size of the impacting body determines the absolute radial distance in the target at which a specific shock pressure is achieved and, thus, at which shock-metamorphic effects occur.

Shock-metamorphic effects are well-described in papers in French & Short (1968) and Roddy et al. (1977), as well as by Stöffler (1971, 1972, 1974). They are discussed here only in general terms. Minimum shock pressures required for the production of diagnostic shock-metamorphic effects are 5–10 GPa for most silicate minerals. Shock metamorphism occurs at extremely high strain rates (~10^6–10^9 s^{-1}), and shock-pressure duration is measured in seconds, or less, in even the largest impact events (Melosh 1989). Thus, unlike endogenic terrestrial metamorphism, disequilibrium and metastability are common phenomena in shock metamorphism.

The only known diagnostic shock effect that is megascopic in scale is the occurrence of shatter cones (Dietz 1968). These conical striated fracture surfaces are best developed in fine-grained, structurally isotropic lithologies, such as carbonates and quartzites (Fig. 9). They do occur in coarse-grained crystalline rocks but are less common and poorly developed. Shatter cones are initiated most frequently in rocks that experienced moderately low shock pressures, 2–6 GPa, but have been observed in rocks that experienced ~25 GPa (Milton 1977). All other diagnostic, subsolidus, shock-metamorphic effects are microscopic in scale.

The most common documented shock-metamorphic effect is the occurrence of so-called planar microstructures in tectosilicates, particularly quartz (Hörz 1968). The utility of planar microstructures in quartz reflects the ubiquitous nature of the mineral and its stability, and the stability of the microstructures themselves, in the terrestrial environment, and the relative ease with which they can be documented. Planar elements in quartz are divided into planar fractures (PFs) and planar deformation features (PDFs). PDFs (Figs 8 and 9) are most common in crystalline targets, and, when fresh, most are filled with glass (Engelhardt & Bertsch 1969). These glass lamellae are moderately easily annealed, and are commonly manifested as linear chains of inclusions and bubbles, called decorated planar features, which are observed at all but the youngest impact structures. PDFs in quartz have specific orientations, which are a function of recorded shock pressure, and have been calibrated in large part by shock-recovery experiments. Major recent reviews of the nature of the shock metamorphism of quartz, with an emphasis on the nature and origin of planar microstructures in experimental and natural impacts, can be found in Stöffler & Langenhorst (1994) and Grieve et al. (1996).

The development of PDFs in quartz, which occurs over the pressure range of 5–10 to ~35 GPa, is accompanied by progressive changes in other optical and physical properties (Stöffler &

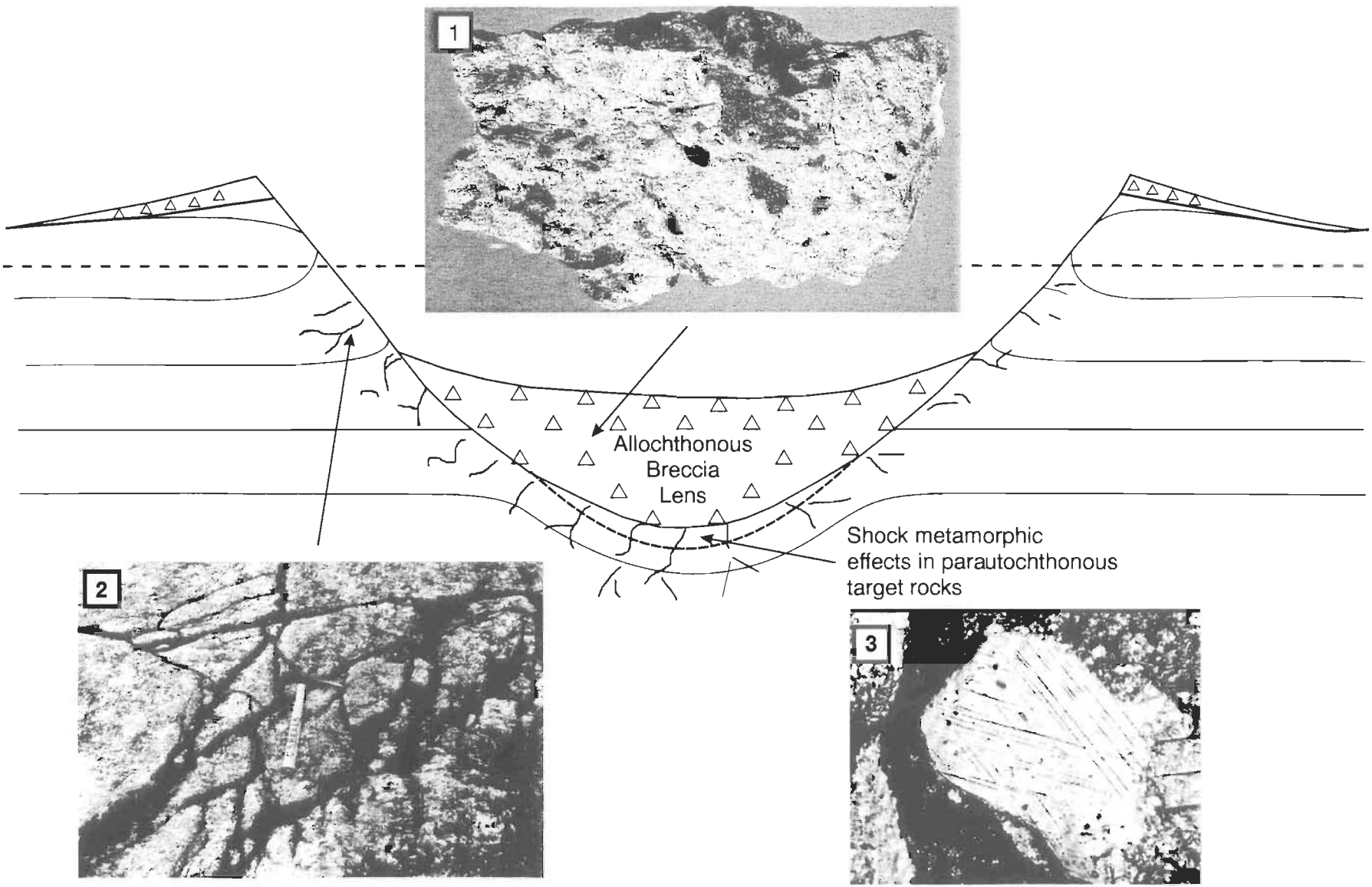

Figure 8. Schematic cross-section of a terrestrial simple impact structure, and the locations and nature of various shock-metamorphic effects: (1) allochthonous breccia with clasts (dark) of impact-melted target rock; (2) fractured parautochthonous target rock of the wall of the true crater; (3) planar deformation features in parautochthonous target rocks of the floor of the true crater.

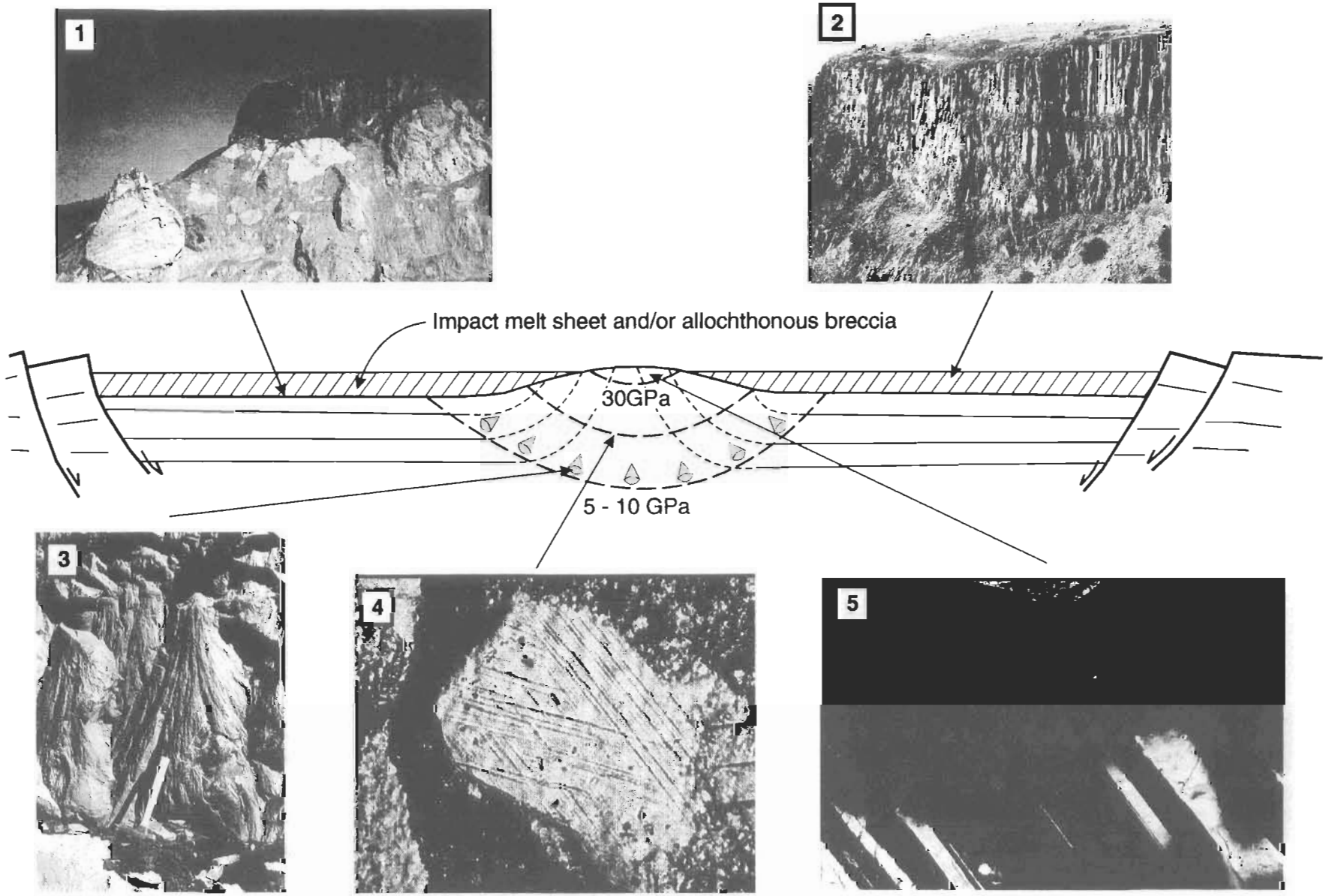

Figure 9. Schematic cross-section of a terrestrial complex impact structure, and the locations and nature of various shock-metamorphic effects: (1 and 2) allochthonous coherent impact-melt sheet overlying allochthonous breccia; (3) shatter cones; (4) planar deformation features in quartz; (5) development of diaplectic glass in feldspar. Also indicated are the general positions of shock isobars in parautochthonous target rocks of the central uplift. Note the spatial confinement of these shock effects to the centre of the structure, and their attenuation radially and with depth.

Langenhorst 1994). For example, asterism and line broadening — apparent from X-rays — reveal a progressive breakdown in structural order (e.g., Chao 1968; Hörz & Quaide 1973; Hanss et al. 1978).

Porous sedimentary rocks evince some differences in the response to shock compared with crystalline or compact sedimentary rocks. For example, quartz in sandstone exhibits more PFs and fewer PDFs, and certain PDF orientations, such as ω {10$\bar{1}$3}, tend to be suppressed relative to PDFs in quartz in shocked crystalline rocks (Fig. 10; Robertson 1980; Grieve & Therriault 1995). In addition, during shock compression, considerable pressure–volume work is done in collapsing pore space. As a result, more waste-heat is trapped in porous sedimentary rocks than in crystalline rocks shocked to equivalent pressure. This leads to enhanced intra- and inter-mineral melting at moderately low shock pressures. Details of some of these effects, as observed in the Coconino Sandstone at the Barringer structure, are presented by Kieffer (1971) and Kieffer et al. (1976).

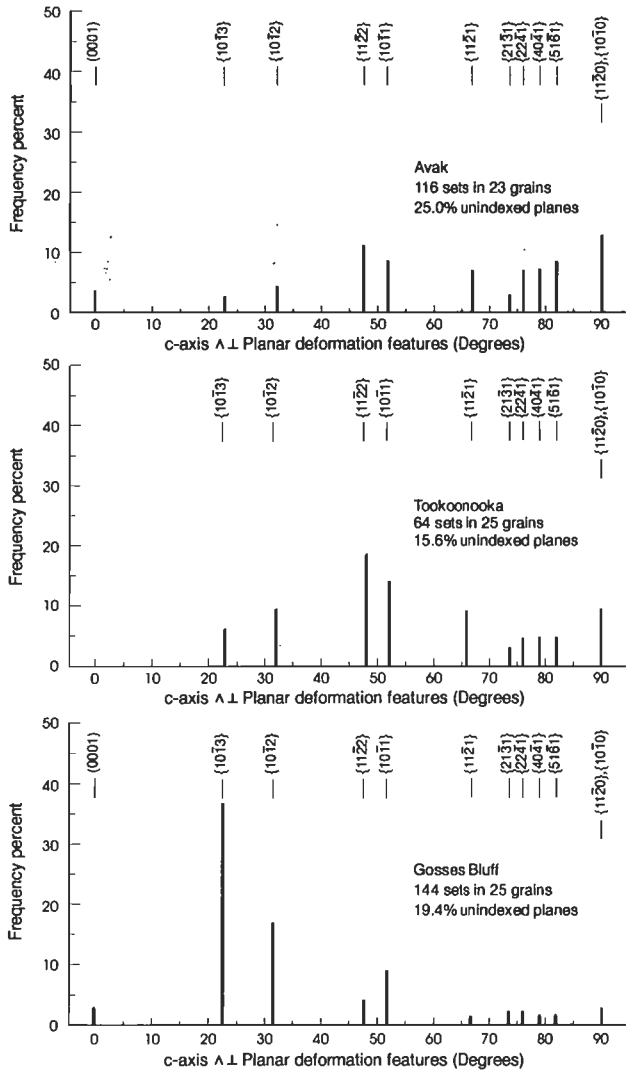

Figure 10. Frequency per cent of indexed orientations of planar deformation features in quartz from Avak (USA; Table 1), Tookoonooka (Australia; Table 1), and Gosses Bluff. Note the relative shortage of ω {10$\bar{1}$3} orientations at Avak and Tookoonooka compared with Gosses Bluff. This is believed to be a textural effect peculiar to porous sedimentary rocks.

The reason why certain orientations of PDFs in quartz are suppressed in porous sedimentary rocks is not known and is the subject of current study. Robertson (1980) suggested that, in the pressure range in which — for example — ω features are formed in crystalline rocks, PDFs do not form in porous sedimentary rocks, as the pressure–volume work due to compression is being adsorbed in closing pores. Clearly, these second-order differences in the behaviour of rocks subjected to shock are related to textural differences. For example, the relative abundances of certain PDF orientations in different sandstone units at Gosses Bluff are texture-dependent: units with an equigranular close-packed texture have relative orientation abundances similar to crystalline rocks (Fig. 10); others with more isolated quartz grains in a fine-grained matrix are similar, with respect to PDF orientations, to other more porous sandstones at other impact structures (Grieve et al. 1996).

Shock pressures of ~30 and ~35 GPa are sufficient to render feldspar and quartz, respectively, to glasses (Fig. 9). These are solid-state glasses with physical properties distinct from fusion glasses, and are generally referred to as a diaplectic glass (Stöffler & Horneman 1972). In addition, shock can result in the formation of metastable polymorphs, such as stishovite and coesite from quartz (Chao 1968) and diamond and lonsdaleite from graphite (Masaitis et al. 1972). Coesite and diamond are also products of endogenic terrestrial geological processes, including high-grade metamorphism (e.g., Dobrzhinetskaya et al. 1995), but the paragenesis and, more importantly, the geological setting are completely different.

By ~50 GPa individual minerals begin to decompose thermally or melt (Stöffler 1972, 1984), leading to the production of mixed mineral melts. Above ~60 GPa, the waste-heat is sufficient to result in whole-rock melting. Such melts occur as glass bombs in crater ejecta (Engelhardt 1990), as glassy to crystalline fragments and lenses in breccias (Fig. 8), and as coherent sheets (Fig. 9; Grieve et al. 1977). When crystallised, impact-melt sheets have igneous textures, but tend to be heavily charged with clastic debris towards their lower and upper contacts. They may, therefore, have a textural resemblance to endogenic igneous rocks. Impact-melt rocks, however, commonly have an unusual chemistry compared with endogenic volcanic rocks, as their composition depends on the melting of a mix of target rocks, as opposed to partial melting and/or fractional crystallisation relationships that apply to igneous rocks. Isotopic analyses also indicate that such parameters as $^{87}Sr/^{86}Sr$ and $^{143}Nd/^{144}Nd$ ratios reflect the pre-existing target rocks, while isochron dating methods indicate much younger crystallisation ages, which are related to the impact event (Jahn et al. 1978; Faggart et al. 1985).

Enrichments above target rock levels in siderophile elements and Cr have been identified in some impact-melt rocks (Palme 1982). These are due to an admixture of up to a few per cent of meteoritic material from the impacting body. In some such rocks, the relative abundances of the various siderophiles have constrained the composition of the impacting body to the level of meteorite class — for example, East Clearwater (Canada; Table 1), which was formed by a Cl chondrite (Palme et al. 1979). In other such rocks, no siderophile anomaly has been identified. This may be due to the inhomogeneous distribution of meteoritic material within the impact-melt rocks and sampling variations (Palme et al. 1981), or to differentiated non-siderophile-enriched impacting bodies, such as basaltic achondrites (Wolf et al. 1980). Most recently, high-precision

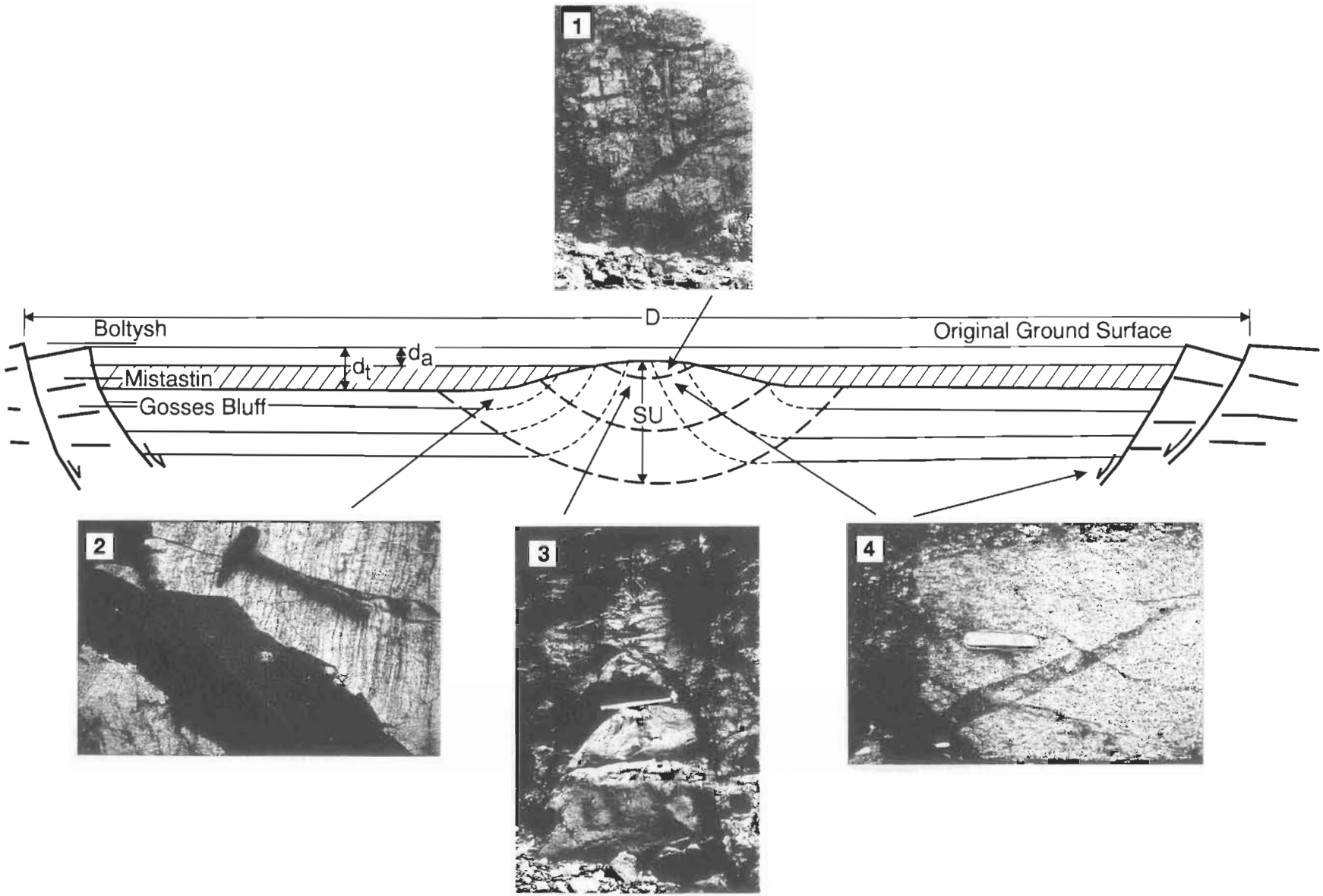

Figure 11. Schematic cross-section of a terrestrial complex impact structure, and the locations and nature of various impact-related lithologies in the parautochthonous rocks of the floor and central uplift: (1) vertically dipping uplifted beds in the central uplift; (2) impact-melt dyke in the floor; (3) clastic breccia dyke in the central uplift; (4) pseudotachylite in the central uplift. Pseudotachylite is also found associated with rim faults.

osmium-isotopic analyses have been used to detect a meteoritic signature at terrestrial impact structures (Koeberl et al. 1994). The sensitivity of this isotopic technique might help detect additional, faint meteoritic signals in impact lithologies. Osmium-isotopic ratios are, however, ineffective for discriminating between types of meteoritic bodies.

The proportion of recognisable impact-melt rocks at craters in sedimentary and some mixed targets is at least two orders of magnitude less than at similar-size terrestrial craters in crystalline targets (Kieffer & Simonds 1980). A polymict allochthonous breccia deposit in sedimentary targets occupies the equivalent stratigraphic position to an impact-melt sheet in crystalline targets (Fig. 9). These breccia deposits can contain highly shocked melted clasts and glass corresponding in composition to target rock sedimentary lithologies (Redeker & Stöffler 1988). These deposits are generally referred to as suevitic breccias, particularly by workers from the former USSR (Masaitis et al. 1980). Like the suevite deposits of Ries, which is in a mixed target and where the compositions of the melt glasses correspond to the underlying crystalline target rocks (Pohl et al. 1977; Stöffler et al. 1977), they contain clasts showing all levels of shock.

The lack of extensive coherent sheet-like impact-melt deposits at structures in sedimentary targets is perhaps unexpected, as theoretical considerations indicate that sedimentary lithologies melt under shock compression at equivalent, or even lower, shock pressures than crystalline lithologies. This absence, however, is not a function of the melting behaviour of the various target rock lithologies, but is believed to be due to the extensive expansion of volatiles from sedimentary rocks on their release from shock compression (Kieffer & Simonds 1980). For example, shock experiments indicate that ~50 per cent of the carbon dioxide in calcite is volatilised by shock pressures as low as 30 GPa (Lange & Ahrens 1986). Thus, the impact melt in sedimentary impacts is highly dispersed by gas expansion, which results in the production of mainly impact-melt-bearing suevitic breccia deposits instead of a coherent impact-melt sheet. In addition, the presence of volatiles results in enhanced alteration of the impact-melt glasses to carbonates and hydrated phases.

In addition to extensive deposits of polymict allochthonous breccia, other types of breccia are found at terrestrial impact craters. They include various types of dykes of allochthonous monomict and polymict breccias (Fig. 11) related to various stages of crater formation (Lambert 1981; Stöffler et al. 1988). Also, a large volume of mostly autochthonous monomict breccia and fractured target rocks make up the floor of impact structures. Pseudotachylite is also present at craters in crystalline targets (Fig. 11), the most spectacular occurrences being at Vredefort and Sudbury, where these frictional melt breccias occur over areas of ~5000 km^2 (Dressler 1984; Reimold & Colliston 1994). Pseudotachylite and various breccia deposits are characteristic of the geology of terrestrial impact structures. They are, however, not in themselves diagnostic indicators of impact, as they can be formed by other high-strain-rate endogenic geological processes. It is the occurrence of shocked clasts within these lithologies that designate them as being of impact origin.

Distribution of shock metamorphism

As cratering mechanics and shock metamorphism are largely governed by physics, the spatial distribution of shock-metamorphic effects at terrestrial impact structures is essentially invariant. There have been, however, few systematic and detailed studies of the variation in the recorded level of shock at impact structures. Nevertheless, the studies that have been conducted provide a moderately consistent picture of the spatial distribution of shock effects at terrestrial impact structures. In allochthonous lithologies, such as breccias and melt rocks, there can be a wide range of shock effects, ranging from none to melting in close spatial proximity. Apart from ejecta, which are rarely preserved in the terrestrial environment, such allochthonous lithologies are confined to within the rim and floor of both simple and complex impact structures (Figs. 8 and 9).

Short (1970) used PDFs in quartz as a parameter to create a 'shock index' for the allochthonous breccia lens at the simple West Hawk structure (Canada; Table 1). From the shock index, he noted a variation in the level of shock metamorphism; maximum shock levels occurred towards the top and base of the breccia lens. The shock-metamorphic effects in the breccia lens at Brent (Canada; Table 1) are similarly disposed (Dence et al. 1977; Grieve 1978). Most of the material in the breccia lenses at simple impact structures, however, does not display obvious shock-metamorphic features, and the range of shock levels is consistent with the allochthonous nature of the breccias. The concentrations of more highly shocked materials towards the base and upper zones in the centre are due to movements associated with the mechanics of cratering (e.g., Dence et al. 1977; Grieve et al. 1977; Melosh 1989).

To our knowledge, there has been only one example of a systematic study of variations in recorded shock in the parautochthonous rocks beneath a simple impact crater, and this is at Brent (Dence 1968; Dence et al. 1977; Robertson & Grieve 1977). Shock effects occur in the parautochthonous rocks of the floor of the impact structure only in the centre (Fig. 8). For ~15 m beneath an impact-melt lens at the base of the allochthonous breccia lens, all indications of shock metamorphism have been recrystallised. Below this depth, however, PDFs in quartz are apparent but progressively decrease in abundance with depth. Estimates of the shock pressures recorded by the PDFs range from 23.0 to 5.7 GPa over the 85 m where PDFs are apparent (Robertson & Grieve 1977).

At complex impact structures, such as Charlevoix and the Slate Islands (Canada; Table 1), variations in the orientations of PDFs in quartz indicate that recorded shock levels in the parautochthonous rocks of the crater floor attenuate from ~25 GPa at the centre to <5 GPa at radial distances of <0.5 the rim diameter (Fig. 9; Robertson & Grieve 1977). These estimates represent lower bounds, as both structures have been eroded below the original floor, but they do emphasise the observation that shock-metamorphic effects in parautochthonous target rocks of complex structures are, like those at simple structures, spatially limited to the central area, well within the original rim (Fig. 8 and 9). These types of relationships permit the relative spatial limitation of recorded shock to be used to estimate original morphological parameters at severely eroded structures, where there is little or no indication of the original rim. This has been done most recently at very large eroded complex structures, such as Sudbury (Grieve et al. 1991; Deutsch & Grieve 1994; Stöffler et al. 1994) and Vredefort (Therriault et al. 1993, 1995).

Systematic studies of variations in recorded shock with depth at complex structures are limited. There are generally few drill-cores of sufficient depth. Studies at the Ries structure indicate that the recorded shock pressure attenuates over the sampled ~600 m in the crystalline basement floor of the structure (Engel-

hardt & Graup 1977). They also indicate structural complexities with depth and that, as a whole, the section consists of parautochthonous materials which are faulted and displaced. Similarly, the recorded shock pressure, as determined from PDF orientation in quartz, decreases with depth in the parautochthonous rocks of the uplifted floor of the Kara structure (Sazonova 1981; Sazonova et al. 1981; Gurov & Gurova 1991). At the Puchezh-Katunki structure (Russia; Table 1), where samples from 5 km of core drilled in the centre are available (Pevzner et al. 1992), the estimated recorded shock-pressure levels decrease from ~40 GPa at the top of the central uplift to ~10 GPa at 5-km depth, and are, again, largely based on variations in PDF orientations in quartz (Ivanov 1994).

Systematic studies of the distribution of shocked quartz within ejecta are restricted to the Ries structure. In general, a decrease of the recorded shock level from top to bottom of the ejecta has been observed (Pohl et al. 1977; Schneider 1971). Suevite breccia is present on top. It contains abundant impact-melt bombs, and ranges down in recorded shock levels to quartz with coesite and stishovite to quartz with PDFs and PFs of the lowest shock stage or no evidence of shock. This assemblage changes discontinuously at the base of the suevite, where a second polymict breccia unit (called Bunte breccia at Ries) forms the main mass of the ejecta. Schneider (1971) found that the maximum shock level below the suevite is represented by diaplectic quartz glass, and that the abundance of quartz with PFs and PDFs continuously decreases with increasing depth in the Bunte breccia. A more recent study, however, failed to record any systematic distribution in the level of shock metamorphism in the Bunte breccia (Banholzer & Hörz 1979).

There have been no systematic studies of the spatial distribution of recorded shock at impact structures in (porous) sedimentary targets. The most comprehensive work is at Barringer (Kieffer 1971; Kieffer et al. 1976), and it concentrated on establishing a shock classification scheme for various shock-metamorphic effects in the Coconino Sandstone. All samples, however, were allochthonous in nature, and the highest levels of average recorded shock were apparent in the uppermost materials, which are considered to be samples of fall-back breccia.

Disregarding tektite and microtektite occurrences, we know of only two examples in which highly dispersed and well-removed ejecta are linked to a known impact site:

- ejecta from the Acraman structure (Australia; Table 1), which occur up to ~500 km from the impact site (Gostin et al. 1986; Wallace et al. this issue); and
- ejecta from the Chicxulub structure, which occur worldwide at the KT boundary (Bohor et al. 1984, 1987; Hildebrand et al. 1991).

A layer containing shocked quartz and shatter-cone fragments in dacite clasts in the shales of the Adelaide Geosyncline (South Australia) was the initial evidence for ejecta from the Acraman structure. Later work indicated an associated siderophile anomaly (Gostin et al. 1989; Wallace et al. 1990). There is very little documentation on the shock-metamorphic effects, except that the ejecta are PDFs (Gostin et al. 1986).

The initial indications of an impact origin for deposits at the KT boundary were geochemical (Alvarez et al. 1980; Ganapathy 1980). They were followed by the discovery of physical evidence of impact in the form of quartz with PDFs in KT boundary samples from the western interior of North America (Bohor et al. 1984). In addition to PDFs, some quartz grains in the KT boundary layer display reduced refractive indices and X-ray asterism (Bohor 1990), and coesite and stishovite have been identified (McHone et al. 1989; Boslough et al. 1995). Since the initial discoveries, quartz with PDFs, and other shocked minerals, have been recognised worldwide in KT boundary deposits (Bohor et al. 1987).

No systematic study has been undertaken to determine if there is any variation with location in the orientation of PDFs, and thus in the recorded shock pressure, in quartz from KT boundary layers worldwide. The maximum dimensions of the shocked quartz grains, however, tend to be larger and more of them contain PDFs at North American sites than elsewhere (Bohor et al. 1987), suggesting an impact site close to the Americas. This was confirmed by the discovery of the Chicxulub impact structure on the Yucatan Peninsula (Hildebrand et al. 1991).

There have been claims of shock-metamorphic effects in minerals from other biostratigraphic boundaries — e.g., Triassic–Jurassic (Badjukov et al. 1987; Bice et al. 1992). The observation basis for these claims, however, is not as strong as for the KT boundary event. Indeed, the observations are somewhat confusing, because the 'shocked' quartz at the Triassic–Jurassic boundary, for example, occurs in three separate beds (Bice et al. 1992). Recently, however, shocked quartz with PDFs, confirmed by both optical and TEM observations, has been recognised near the Eocene–Oligocene boundary at Massignano (Italy; Langenhorst & Clymer 1995).

There is other evidence of impact in the stratigraphic column. Most often, this is in the form of regional to local occurrences of tektite and microtektite bodies. Some of them are related to known impact structures — e.g., the moldavite tektites with Ries, and the Ivory Coast microtektites with Bosumtwi (Ghana; Table 1). The sources of other strewn fields is unknown, although there are a number of suggestions in the literature (e.g., Wasson 1991; Poag et al. 1994). Some of these strewn fields cover a considerable area of the Earth's surface. For example, the Australasian strewn field covers an area in excess of 50×10^6 km^2 (Koeberl 1994). A recent summary of evidence for impact in the stratigraphic column can be found in Grieve (1996a).

Geophysics of impact structures

Geophysical anomalies over terrestrial impact structures (Table 3) vary in their character and, in isolation, do not provide definitive evidence for an impact origin. About 30 per cent of known terrestrial impact structures are buried by post-impact sediments, and geophysical methods have provided the means for their initial discovery and subsequent exploration. Interpretation of a single geophysical data set over a suspected structure can be ambiguous but, when combined with complementary geophysical methods and the existing database over other known impact structures, a more definite assessment can be made. Since potential-field data are available over large areas, with almost continuous coverage (compared with seismic reflection lines), gravity and magnetic observations are the primary geophysical indicators used for evaluating the occurrence of possible terrestrial impact structures. Seismic data, although providing much better spatial resolution of subsurface structure, is used less, because it is generally unavailable. Electrical methods have been used even less, although they hold promise (e.g.,

Henkel 1992). Several recent discoveries of terrestrial impact structures were identified initially as geophysical anomalies — e.g., Chicxulub (Hildebrand et al. 1991), Mjølnir (Barents Sea; Table 1; Gudlaugsson 1993), and Chesapeake Bay (USA; Table 1; Poag et al. 1994). Their impact origin was confirmed, however, through geological evidence — i.e., the documented occurrence of shock-metamorphic effects.

Gravity signature

The most notable geophysical signature associated with terrestrial impact structures is a negative gravity anomaly (Fig. 12). When the regional fields are removed, these gravity lows are generally circular and extend to, or slightly beyond, the rim of the structure. They are due to the lithological and physical changes associated with the impact process. In uneroded structures, low-density sedimentary infill of the topographic depression of the crater contributes to the gravity low. In complex structures, low-density impact-melt sheets also can contribute to the negative gravity effect. Such lithological effects, however, are minor compared with density contrasts induced by fracturing and brecciation of the target rocks. Porosity levels within the allochthonous breccia deposits increase owing to the fragmentation and redistribution of target lithologies during crater formation. Shock-induced fracturing of parautochthonous target rocks beneath the crater floor also leads to increased porosity and, hence, reduced densities, compared with the surrounding undisturbed formations.

The amplitude of the maximum negative gravity anomaly associated with impact structures increases with the crater diameter (Fig. 13; Dabizha & Fedynsky 1975). The value of this negative anomaly is primarily determined by the density contrast and depth of the brecciated and fractured zones. The final character of the gravity anomaly at largely uneroded structures is determined by D and, to a lesser extent, the pre-impact density distribution of the target rocks. Post-impact processes, such as erosion, may cause further changes in anomaly shape and size. According to the data from 58 terrestrial impact structures, Pilkington & Grieve (1992) showed that erosional level and nature of target lithology (whether mainly sedimentary or crystalline) have only a secondary effect on gravity anomaly size. Erosional effects are most prominent when the structure has been eroded

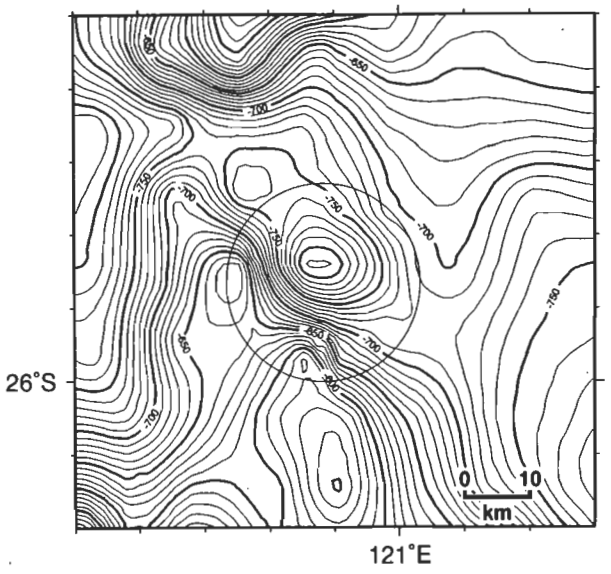

Figure 12. Observed Bouguer gravity field over Teague (Australia; Table 1); contour interval 10 μm s^{-2}. The outline of the rim of the structure is indicated by a circle. Note the interference with regional trends, and the presence of a gravity low over the structure.

to levels below the original crater floor. For example, in highly eroded large complex structures, only the central gravity high (see below) remains and the structure is characterised by only a positive anomaly — e.g., Connolly (Australia; Table 1; Shoemaker et al. 1989).

In general, simple craters and small complex craters (D <10 km) are characterised by a circular bowl-shaped residual negative anomaly — e.g., Wolfe Creek (Fudali 1979). For larger complex craters, the residual gravity low may be modified by the presence of a central gravity high, which is due to deeper denser crustal material being brought to the surface — e.g., Vredefort (Stepto 1990). The compressive regime in the central uplift of complex craters may also contribute to the central gravity high, through reduction in the initial impact-induced porosity (Grieve 1988). For larger structures (D >30 km) the maximum negative gravity anomaly reaches a limiting value of ~300 μm s^{-2} (Fig. 13).[1] This limit can be interpreted in terms of

Table 3. Geophysical signatures of terrestrial impact structures

	Simple	*Complex*
Gravity	Concentric low.	Concentric low. Central gravity high possible for D <30 km, probable for D >30 km. Central high <0.5D in diameter.
Magnetics	Simple low or subdued zone.	Simple low or subdued zone for D <10 km. Short-wavelength central anomalies possible for D = 10–40 km, probable for D >40 km. Central anomalies, generally, more localised than central gravity high.
Seismic	Low-velocity zone extending to ~>D.	Low-velocity zone coincident with structure. Possible high-velocity core for larger D. Zone of incoherent reflectors in target rocks at centre of structure and extending out to ~<0.5D; coherency increases with radial distance. Isotropic seismic zone corresponding to allochthonous deposits.
Electrical	Low-resistivity zone coincident with low-seismic-velocity zone.	Low-resistivity zone. Higher resistivities possible in central uplift of largest structures.

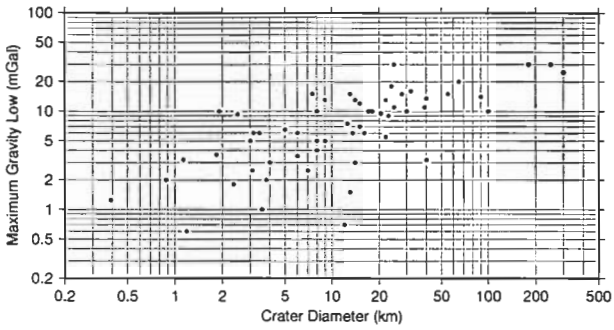

Figure 13. Maximum residual Bouguer gravity low relative to diameter for 58 terrestrial impact structures. Note the general trend of increasing gravity low with increasing diameter, until maximum values of ~300 μm s^{-2} are reached. Some of the scatter in the data is due to secondary effects, such as erosional level.

a maximum depth of fracturing associated with the structure (Basilevsky et al. 1983). For a density contrast of 0.1 t m^{-3} (100 kg m^{-3}), this corresponds to a depth of 8 km, below which it is expected that open fractures are essentially closed by lithostatic pressure (Perrier & Quiblier 1974).

Modelling of residual gravity data at simple craters (e.g., Fudali & Cassidy 1972; Grieve et al. 1989) shows that the apparent and true crater depths, d_a and d_t, are good estimates for model body dimensions, if the appropriate density contrasts are used. Hence, reduced densities due to extensive fracturing of autochthonous rocks beneath the crater floor do not appear to contribute significantly to the gravity anomaly at simple craters. In contrast, at complex structures, Pilkington & Grieve (1992) showed that the amount of stratigraphic uplift (SU) provides a useful estimate of the depth of the fractured zone, although, for D >30 km, this depth reaches a limiting value, as noted earlier, and the gravity effect is essentially constant.

Magnetic signature

Magnetic anomalies associated with terrestrial impact structures are generally more complex than associated gravity anomalies, and reflect the greater variation possible in the magnetic properties of rocks. The dominant effect at impact structures, however, is a magnetic low or subdued zone (Fig. 14; Dabizha & Fedynsky 1975; Clark 1983), which is commonly manifested as a truncation of the regional magnetic fabric. At larger structures, the magnetic low can be modified by the presence of shorter-wavelength large-amplitude localised anomalies which usually occur at or near the centre of the structure. These are generally small in areal extent, much less than that of the central gravity high, if present. Like the gravity signature, the magnetic signature does not reflect a one-to-one correspondence between the cross-sectional shape of the anomaly and the morphology of the impact structure. Furthermore, the existence of a central gravity high does not imply the presence of a central magnetic anomaly. Anomaly form, however, is somewhat dependent on the size of the structure: magnetic lows occur at small structures (D <10 km), and central high-amplitude anomalies at larger structures (D >40 km). There are also examples of structures with no obvious magnetic signature. For small impact structures in particular, aeromagnetic survey parameters may be inadequate to resolve the anomalous magnetic effects related to impact.

Magnetic anomalies related to impact may be caused by one or more of several mechanisms. Shock can serve to increase or decrease magnetisation levels. At peak pressures of ~1 GPa, shock demagnetisation can remove existing remanent magnetisation (e.g., Cisowski & Fuller 1978), and, at pressures of >10 GPa, magnetic susceptibility levels can be reduced. As well as a reduction in magnetisation levels, target rocks can also acquire a shock remanent magnetisation (SRM) in the direction of the Earth's field at the time of impact. The strength of SRM increases with ambient field intensity, and decreases with distance from the point of impact (Cisowski & Fuller 1978). SRM is most likely to occur in autochthonous target rocks that experience pressures >1 GPa and temperatures less than the Curie points of the magnetic phases present. Changes in magnetic properties due to mineralogical changes, particularly in mafic silicates, can occur at greater pressures (>30 GPa) — e.g., the production of magnetite from the thermal decomposition of amphibole and biotite (Fel'dman 1994). Similar effects can occur with ore minerals. For example, at lower pressures, titanomagnetite can result from the breakdown of ilmenite (Chao 1968).

As impact-melt rocks cool, they can acquire a thermoremanent magnetisation (TRM) in the direction of the Earth's magnetic field at the time of impact. This effect has led to several palaeomagnetic dating studies based on samples of impact-melt rocks and breccia (e.g., Robertson 1967; Pohl & Soffel 1971). A stable remanence and low directional scatter appear to be characteristics of palaeomagnetic data from impact-melt rocks, and reflect the rapid acquisition of the magnetisation (Pohl & Soffel 1971). Whole-rock melting can also result in the production of non-magnetic impact glasses (Pohl 1971).

The production of new magnetic phases resulting from elevated residual temperatures and hydrothermal alteration following impact may lead to the acquisition of a chemical remanent magnetisation (CRM) in the direction of the ambient field. The central magnetic anomaly at Saint Martin (Canada; Table 1) is attributed to the formation of hematite from the alteration of mafic silicates in the floor of the central uplift (Coles & Clark 1982). Residual post-impact heat and fracturing of the target rocks often result in the establishment of a local hydrothermal system, and the presence of oxygen favours higher magnetisation intensities. Post-impact processes — such as chemical weathering, leaching, and metamorphism — will further modify magnetic properties over longer time intervals.

Magnetisations have been observed in several different carriers — e.g., magnetite, hematite–ilmenite, and pyrrhotite. As expected, no one magnetic phase is characteristic of impact sites. Breccias and impact melt-rocks are characterised by Königsberger ratios (remanent/induced magnetisation) much larger than unity, so that induced magnetisation can be considered negligible, and observed magnetic anomalies are primarily due to remanent magnetisation levels. Several different sources producing the central magnetic anomalies are found at larger structures. At highly eroded structures (Vredefort), magnetic basement can be exposed in the central uplift. Anomalies can correspond to alteration zones within the central uplift area (Saint Martin), or the central anomaly can be caused by highly magnetic impact-melt rocks (Dellen, Sweden; Table 1) or suevite breccias (Ries).

[1] 1 μm s^{-2} = 1 g.u. = 0.1 mGal.

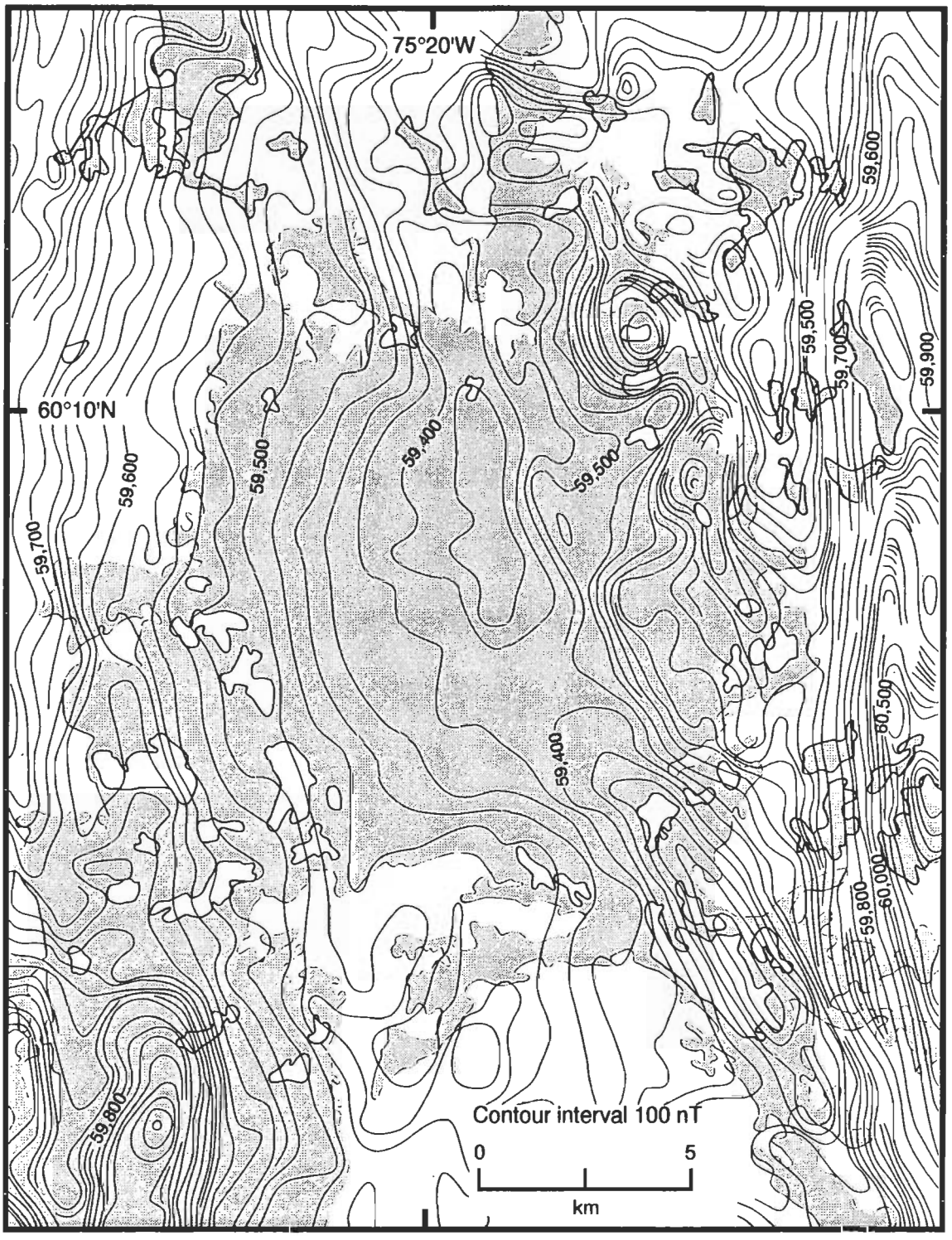

Figure 14. Observed magnetic field intensity over Couture (Canada; Table 1). Contour interval is 100 nT. Note the presence of a magnetic low over the area (shaded) of the roughly circular lake (the impact structure), and the lack of short-wavelength anomalies characteristic of the regional field.

The causes of magnetic lows at impact structures are not clear. The impact process undoubtedly results in a reduction in the magnetisation intensity of the target material. For uneroded craters, post-impact sedimentary infill will tend to be non-magnetic and so contribute to the reduced field intensity. This does not, however, explain the low fields over heavily eroded structures. By analogy with the gravity signature, an important contribution to the magnetic field must come from the parautochthonous target rocks beneath the floor of the structure. Recent studies of drillcore from several Canadian structures indicate that all impact lithologies show a reduction in both induced and remanent magnetisation levels, but this is not sufficient to produce all of the observed magnetic lows (Scott et al. 1995). The fractured target rocks also show diminished magnetisation levels at depths well below the floor, suggesting that the propagating shock wave is the likely cause.

Seismic signature

Seismic reflection and refraction data provide complementary information to potential-field data and geological observations on the characteristics of terrestrial impact structures. Reflection surveys allow for detailed imaging of the crater morphology, and for delineating seismically isotropic zones and incoherent reflections that are characteristic of brecciation and fracturing (e.g., at Tookoonooka; Gorter et al. 1989). The disturbance of coherent subsurface reflectors is most prominent in the central uplift of complex structures and decreases outward and downward from this zone (Brenan et al. 1975). As well as providing estimates of such morphological parameters as the dimensions of the central uplift, annular trough, and faulted blocks at the structural rim of complex structures, the depths to horizontal reflectors below the crater floor can be used to determine the amount of stratigraphic uplift (Fig. 2; Brown 1973).

The radial variation in impact-induced effects is also apparent on reflection seismic profiles. Where the transition between incoherent and coherent reflectors can be located, this provides an estimate of the dimensions of the so-called transient cavity (Melosh 1989; Juhlin & Pedersen 1987). The spatial density and penetration of faults decreases outwards from the annular trough at complex structures (Scott & Hajnal 1988). Towards the rim of complex structures, the moderately undeformed reflectors within downfaulted blocks allow such displacements to be mapped accurately (Brenan et al. 1975). As expected, the overall structural character of complex impact structures mapped by reflection seismic images corresponds to surface observations at exposed impact structures.

Refraction seismic surveys have proved useful for mapping the velocity distribution within terrestrial impact structures — specifically, zones of reduced velocities caused by fracturing and brecciation. At simple structures, velocity reductions of up to 50 per cent have been measured within the allochthonous breccia lens and sedimentary infill (Millman et al. 1960; Ackerman et al. 1975). In addition, at Barringer, the mapped lower-velocity zone also extends out beyond the rim of the structure. At complex structures, the low-velocity zone may extend well below the crater floor — e.g., at Ries (Pohl et al. 1977) — yet the uplift of deeper crustal material can lead to increased velocities, such as those occurring at Vredefort (Green & Chetty 1990).

Other signatures

As yet, electrical methods have been used little in the study of impact structures. The presence of fluids, however, in impact-induced fractures and pore spaces leads to decreased resistivity levels that can be mapped effectively by various methods. At the simple West Hawk structure, resistivities increase to 300 Wm at the crater rim, then up to ~800 Wm at one crater radius beyond the rim (Clark 1980). Studies within complex structures in crystalline targets have shown significant resistivity lows occurring within and extending out from the structural rim (Vishnevsky & Lagutenko 1986). At Siljan (Sweden; Table 1), Henkel (1992) has also mapped an increase in resistivity coinciding with the central uplift. Deeper investigations using magnetotelluric methods have not proved as informative, though low-resistivity zones have been mapped near several complex structures (e.g., Zhang et al. 1988; Mareschal & Chouteau 1990; Masero et al. 1994).

Summary and concluding remarks

We have attempted to summarise the basic signatures of terrestrial impact structures in Tables 2 and 3; by necessity, they represent a generalisation. Although local target rock geology has some importance, it tends to play only a second-order role in the character of terrestrial impact structures. Erosion is an important factor in the nature of the terrestrial impact record; it modifies the appearance of impact structures, even to the point of producing positive topographic features, and ultimately removes them from the record. Although it is probably premature to state that most of the obvious impact structures on the Earth's land surface have been discovered, some recent discoveries have resulted from the occurrence or re-examination of unusual lithologies rather than an obvious circular geological or topographic feature. For example, the breccias at Gardnos (Norway; Table 1) and Lockne (Sweden; Table 1) had been known for some time, but their shock-metamorphic effects were documented only recently, and they are now associated with the remnants of impact structures (Dons & Naterstad 1992; Lindström & Sturkell 1992; Therriault & Lindström 1995).

The occurrence of shock-metamorphic effects in association with some of the signature elements (Tables 2 and 3) provides the confirmatory evidence for an impact origin for somewhat enigmatic circular or quasicircular features at or near the Earth's surface. Several enigmatic structures bear some of the characteristics listed in Tables 2 and 3, but an impact origin remains to be confirmed for them through the documentation of shock-metamorphic features. One such feature is the Mount Toondina structure (Australia), which consists of a quasicircular 4-km-diameter central uplift; a report of the presence of shatter cones (E.M. Shoemaker, USGS, personal communication 1995) favours the prospect of Mount Toondina joining the growing list of confirmed terrestrial impact structures.

Terrestrial impact structures represent unusual geological events and, as such, they have resulted in local anomalous geological environments, some of which have produced significant economic deposits. About 25 per cent of known terrestrial impact structures have some form of economic deposit associated with them, and about half of these are currently exploited or have been exploited in the recent past. They range from local and now uneconomic (e.g., reserves of 300 000 t of hydrothermal Pb–Zn ores at Siljan) to world class (e.g., reserves of 1.6×10^9 t Ni–Cu–PGE ores at Sudbury). They also include hydrocarbon deposits (e.g., reserves of 50 million barrels of oil and 60 billion cubic feet of gas at Ames, USA; Table 1). The Ames impact structure not only produced the structural trap but also provided the source rocks, which are locally developed post-impact oil shales (Grieve 1996b). In addition, production includes hydrocarbons from non-traditional sources, such as the fractured crystalline rocks of the central uplift at Ames.

All currently known commercial hydrocarbon-producing impact structures and impact lithologies are located in North and Central America. There is, however, potential elsewhere. For example, the 55-km-diameter Tookoonooka structure has a zone of potential stratigraphic traps. Perhaps more importantly for hydrocarbon exploration, the Tookoonooka structure has created a shadow zone for hydrocarbon migration from the Eromanga Basin depocentre since the Early Cretaceous (Gorter et al. 1989). The early recognition of a hydrocarbon-prospective subsurface structure as an impact structure, with its moderately

invariant characteristics and potential for non-traditional sources, would significantly affect exploration strategies.

The level of knowledge concerning individual terrestrial impact structures is highly variable. The details for some are limited to the original discovery publication. As impact is such an important planetary geological process, and terrestrial impact craters are currently the only source of ground-truth data on large-scale impact events, this disregard is somewhat distressing. It is compensated, to some degree, by the fact that impact structures with similar dimensions and target rocks have the same major characteristics. Nevertheless, there is still much to be learnt about impact processes from terrestrial impact structures, particularly with respect to the third dimension. This is the property that is unobtainable from impact structures on other bodies in the solar system, and must be studied by remote-sensing methodologies.

Although the study of terrestrial impact structures has important ramifications for understanding impact processes, their study is not entirely an academic pursuit. The documentation of the terrestrial impact record provides a direct measure of the cratering rate on Earth (Grieve 1984), and thus a constraint on the hazard that impact presents to human civilisation (Gehrels 1994). The KT impact may have resulted in the demise of the dinosaurs as the dominant land-life form, and thus permitted the ascendency of mammals and, ultimately, humans. It is an inevitable fact, however, that if human civilisation persists into geological timescales it too will be subjected to a major impact-induced environmental crisis of immense proportions.

Acknowledgments

We thank M. Ford, J. Rupert, and J. Smith for their assistance in manuscript preparation. C. Tarlowski kindly provided the gravity data displayed in Figure 12. We gratefully acknowledge reviews by A. Hildebrand and A. Therriault.

References

Ackermann, H.D., Godson, R.H. & Watkins, J.S., 1975. A seismic refraction technique used for subsurface investigations at Meteor Crater, Arizona. Journal of Geophysical Research, 80, 765–775.

Alvarez, L.W., Alvarez, W., Asaro, F. & Michel, H.V., 1980. Extraterrestrial cause for the Cretaceous–Tertiary extinction. Science, 208, 1095–1108.

Badjukov, D.D., Lobitzer, H. & Nazarov, M.A., 1987. Quartz grains with planar features in the Triassic–Jurassic boundary sediments from Northern Limestone Alps. Lunar and Planetary Science, XVIII, 38–39 (abstract).

Banholzer, G. & Hörz, F., 1979. Distribution and shock metamorphism of crystalline clasts in the continuous deposits of the Ries crater, Germany. Lunar and Planetary Science, X, 63–65 (abstract).

Basilevsky, A.T., Ivanov, B.A., Florensky, K.P., Yakovlev, O.I., Fel'dman, V.I., Granovsky, L.V. & Sadovsky, M.A., 1983. Impact craters on the moon and planets (in Russian). Nauk Press, Moscow.

Bice, D.M., Newton, C.R., McCauley, S., Reiners, P.W. & McRoberts, C.A., 1992. Shocked quartz at the Triassic–Jurassic boundary in Italy. Science, 255, 443–446.

Bohor, B.F., 1990. Shock-induced microdeformations in quartz and other mineralogical indications of an impact event at the Cretaceous–Tertiary boundary. Tectonophysics, 171, 359–372.

Bohor, B.F., Foord, E.E., Modreski, P.J. & Triplehorn, D.M., 1984. Mineralogic evidence for an impact event at the Cretaceous–Tertiary boundary. Science, 224, 867–869.

Bohor, B.F., Modreski, P.J. & Foord, E.E., 1987. Shocked quartz in the Cretaceous–Tertiary boundary clays: evidence for a global distribution. Science, 236, 705–709.

Boslough, M.B., Cygan, R.T. & Izett, G.A., 1995. NMR spectroscopy of quartz from the K/T boundary: shock-induced peak boundaries, dense glass and coesite. Lunar and Planetary Science, XXVI, 149–150 (abstract).

Brenan, R.L., Peterson, B.L. & Smith, H.J., 1975. The origin of Red Wing Creek Structure: McKenzie County, North Dakota. Wyoming Geological Association, Earth Science Bulletin 8, 1–41.

Brown, A.R., 1973. A detailed seismic study of Gosses Bluff, Northern Territory. Bureau of Mineral Resources, Australia, Report 163.

Bucher, W.L., 1963. Are cryptovolcanic structures due to meteoritic impact? Nature, 197, 1241–1245.

Carter, N.L., Officer, C.B. & Drake, C.L., 1990. Dynamic deformation of quartz and feldspar: clues to causes of some natural crises. Tectonophysics, 171, 373–391.

Chao, E.C.T., 1968. Pressure and temperature histories of impact metamorphosed rocks — based on petrographic observations. In: French, B.M. & Short, N.M. (editors), Shock metamorphism of natural materials. Mono Book Corp., Baltimore, 135–158.

Cintala, M.J. & Grieve, R.A.F., 1994. The effects of differential scaling of impact melt and crater dimensions on lunar and terrestrial craters: some examples. In: Dressler, B.O., Grieve, R.A.F. & Sharpton, V.L. (editors), Large meteorite impacts and planetary evolution. Geological Society of America, Special Paper 293, 51–59.

Cisowski, S.M. & Fuller, M., 1978. The effect of shock on the magnetism of terrestrial rocks. Journal of Geophysical Research, 83, 3441–3458.

Clark, J.F., 1980. Geomagnetic surveys at West Hawk Lake, Manitoba, Canada. Canadian Department of Energy, Mines and Resources, Earth Physics Branch, Geomagnetic Series, 20, 1–11.

Clark, J.F., 1983. Magnetic survey data at meteoritic impact sites in North America. Geomagnetic Service of Canada, Earth Physics Branch, Open File, 83–5, 1–32.

Coles, R.L. & Clark, J.F., 1982. Lake St. Martin impact structure, Manitoba, Canada: magnetic anomalies and magnetizations. Journal of Geophysical Research, 87, 7087–7095.

Dabizha, A.I. & Fedynsky, V.V., 1975. The Earth's "star wounds" and their diagnosis by geophysical methods (in Russian). Zamlya Vselennaya, 3, 56–64.

Dence, M.R., 1968. Shock zoning at Canadian craters: petrography and structural implications. In: French, B.M. & Short, N.M. (editors), Shock metamorphism of natural materials. Mono Book Corp., Baltimore, 169–184.

Dence, M.R., Grieve, R.A.F. & Robertson, P.B., 1977. Terrestrial impact structures: principal characteristics and energy considerations. In: Roddy, D.J., Pepin, R.O. & Merrill, R.B. (editors), Impact and explosion cratering. Pergamon Press, New York, 247–275.

Deutsch, A. & Grieve, R.A.F., 1994. The Sudbury structure: constraints on its genesis from lithoprobe results. Geophysical Research Letters, 21, 963–966.

Dietz, R.S., 1968. Shatter cones in cryptoexplosion structures. In: French, B.M. & Short, N.M. (editors), Shock metamor-

phism of natural materials. Mono Book Corp., Baltimore, 267–285.

Dobrzhinetskaya, L.F., Eide, E.A., Larsen, R.B., Sturt, B.A., Tronnes, R.G., Smith, D.C., Taylor, W.R. & Posukhova, T.V., 1995. Microdiamond in high-grade metamorphic rocks of the Western Gneiss region, Norway. Geology, 23, 597–600.

Dons, J.A. & Naterstad, J., 1992. The Gardnos impact structure, Norway. Meteoritics, 27, 215 (abstract).

Dressler, B.O., 1984. General geology of the Sudbury area. In: Pye, E.G., Naldrett, A.J. & Giblin, P.E. (editors), The geology and ore deposits of the Sudbury structure. Ministry of Natural Resources, Toronto, 57–82.

Engelhardt, W.v., 1990. Distribution, petrography and shock metamorphism of the ejecta of the Ries crater in Germany — a review. Tectonophysics, 171, 259–273.

Engelhardt, W.v. & Bertsch, W., 1969. Shock induced planar deformation structures in quartz from the Ries Crater, Germany. Contributions to Mineralogy and Petrology, 20, 203–234.

Engelhardt, W.v. & Graup, G., 1977. Shock metamorphism in crystalline rocks from the Nördlingen 1973 research drill hole (in German). Geologica Bavarica, 75, 255–271.

Faggart, B.E., Basu, A.R. & Tatsumoto, M., 1985. Origin of the Sudbury complex by meteoritic impact: neodymium isotopic evidence. Science, 230, 436–439.

Fel'dman, V.I., 1994. The conditions of shock metamorphism. In: Dressler, B.O., Grieve, R.A.F. & Sharpton, V.L. (editors), Large meteorite impacts and planetary evolution. Geological Society of America, Special Paper 293, 121–132.

French, B.M., 1990. 25 years of the impact–volcanic controversy: is there anything new under the sun or inside the Earth? EOS, 71, 411–414.

French, B.M. & Short, N.M. (editors), 1968. Shock metamorphism of natural materials. Mono Book Corp., Baltimore.

Fudali, R.F., 1979. Gravity investigation of Wolf Creek crater, Western Australia. Journal of Geology, 87, 55–67.

Fudali, R.F. & Cassidy, W.A., 1972. Gravity reconnaissance at three Mauritanian craters of explosive origin. Meteoritics, 7, 51–70.

Ganapathy, R., 1980. A major meteorite impact on the Earth 65 million years ago: evidence from the Cretaceous–Tertiary boundary clay. Science, 209, 921–923.

Gehrels, T. (editor), 1994. Hazards due to comets and asteroids. University of Arizona Press, Tucson.

Gorter, J.D., Gostin, V.A. & Plummer, P.S., 1989. The enigmatic sub-surface Tookoonooka complex in south-west Queensland: its impact origin and implications for hydrocarbon accumulations. In: O'Neil, B.J. (editor), The Cooper and Eromanga Basins, Australia. Proceedings of the Petroleum Exploration Society of Australia, the Society of Petroleum Engineers, and the Australian Society of Exploration Geophysicists (SA Branches), Adelaide, 441–456.

Gostin, V.A., Haines, P.W., Jenkins, R.J.F., Compston, W. & Williams, I.S., 1986. Impact ejecta horizon within late Precambrian shales, Adelaide Geosycline, South Australia. Science, 233, 198–200.

Gostin, V.A., Keays, R.R. & Wallace, M.W., 1989. Iridium anomaly from the Acraman impact ejecta horizon: impact can produce sedimentary iridium peaks. Nature, 340, 542–544.

Green, R.W. & Chetty, P., 1990. Seismic refraction studies in the basement of the Vredefort structure. Tectonophysics, 171, 105–113.

Grieve, R.A.F., 1978. The melt rocks at Brent crater, Ontario, Canada. Proceedings of the 9th Lunar and Planetary Science Conference, 2579–2608.

Grieve, R.A.F., 1984. The impact cratering rate in recent time. Proceedings of the 14th Lunar and Planetary Science Conference. Journal of Geophysical Research, Supplement, 89, B403–B408.

Grieve, R.A.F., 1988. The formation of large impact structures and constraints on the nature of Siljan. In: Bodén, A. & Eriksson, K.G. (editor), Deep drilling in crystalline bedrock. Springer–Verlag, New York, 1, 328–348.

Grieve, R.A.F., 1996a. Extraterrestrial impact events: the record in the rocks and the stratigraphic column. Palaeogeography, Palaeoclimatology and Palaeoecology (in press).

Grieve, R.A.F., 1996b. Terrestrial impact structures: basic characteristics and economic significance, with emphasis on hydrocarbon production. Proceedings of the Ames Workshop, Oklahoma Geological Survey, Special Paper (in press).

Grieve, R.A.F., Dence, M.R. & Robertson, P.B., 1977. Cratering processes: as interpreted from the occurrence of impact melts. In: Roddy, D.J., Pepin, R.O. & Merrill, R.B. (editors), Impact and explosion cratering. Pergamon Press, New York, 791–814.

Grieve, R.A.F., Garvin, J.B., Coderre, J.M. & Rupert, J., 1989. Test of a geometric model for the modification stage of simple impact crater development. Meteoritics, 24, 83–88.

Grieve, R.A.F., Langenhorst, F. & Stöffler, D., 1996. Shock metamorphism of quartz in nature and experiment: II. Significance in geoscience. Meteoritics (in press).

Grieve, R.A.F. & Masaitis, V.L., 1994. The economic potential of terrestrial impact craters. International Geology Review, 36, 105–151.

Grieve, R.A.F. & Pesonen, L.J., 1992. The terrestrial impact cratering record. Tectonophysics, 216, 1–30.

Grieve, R.A.F., Robertson, P.B. & Dence, M.R., 1981. Constraints on the formation of ring impact structures, based on terrestrial data. In: Schultz, P.H. & Merrill, R.B. (editors). Multi-ring basins. Pergamon Press, New York, 37–57.

Grieve, R., Rupert, J., Smith, J. & Therriault, A., 1995. The record of terrestrial cratering. GSA Today, 5, 189, 194–196.

Grieve, R.A.F., Stöffler, D. & Deutsch, A., 1991. The Sudbury structure: controversial or misunderstood? Journal of Geophysical Research, 96, 22753–22764.

Grieve, R.A.F. & Therriault, A.M., 1995. Planar deformation features in quartz: target effects. Lunar and Planetary Science, XXVI, 515–516 (abstract).

Gudlaugsson, S.T., 1993. Large impact crater in the Barents Sea. Geology, 21, 291–294.

Gurov, E.P. & Gurova, E.P., 1991. Geological structure and composition of rocks in impact craters (in Russian). Nauk Press, Kiev.

Hanss, R.E., Montague, B.R., Davis, M.K., Galindo, C. & Hörz, G., 1978. X-ray diffractometer studies of shocked materials. Proceedings of the 9th Lunar and Planetary Science Conference, 2773–2787.

Hartmann, W., 1995. Planetary cratering: I. Lunar highlands and tests of hypotheses on crater populations. Meteoritics, 30, 451–467.

Hartmann, W.K. & Wood, C.A., 1971. Moon: origin and evolution of multi-ring basins. The Moon, 3, 3–78.

Henkel, H., 1992. Geophysical aspects of meteorite impact craters in eroded shield environment, with special emphasis on electric resistivity. Tectonophysics, 216, 63–90.

Hildebrand, A.R., Penfield, G.T., Kring, D.A., Pilkington, M., Camargo, A.Z., Jacobsen, S.B. & Boynton, W.V., 1991. Chicxulub crater: a possible Cretaceous/Tertiary boundary impact crater on the Yucatan Peninsula, Mexico. Geology, 19, 867–871.

Hildebrand, A.R., Pilkington, M., Connors, M., Ortiz-Aleman, C. & Chavez, R.E., 1995. Size and structure of the Chicxulub crater revealed by horizontal gravity gradients and cenotes. Nature, 376, 415–417.

Hörz, F., 1968. Statistical measurements of deformation structures and refractive indices in experimentally shock loaded quartz. In: French, B.M. & Short, N.M. (editors), Shock metamorphism of natural materials. Mono Book Corp., Baltimore, 243–253.

Hörz, F. & Quaide, W.L., 1973. Debye–Scherrer investigations of experimentally shocked silicates. The Moon, 6, 45–82.

Ivanov, B.A., 1994. Geochemical models of impact cratering: Puchezh–Katunki structure. In: Dressler, B.O., Grieve, R.A.F. & Sharpton, V.L. (editors), Large meteorite impacts and planetary evolution. Geological Society of America, Special Paper 293, 81–91.

Jahn, B., Floran, R.J. & Simonds, C.H., 1978. Rb–Sr isochron age of the Manicouagan melt sheet, Quebec, Canada. Journal of Geophysical Research, 83, 2799–2803.

Juhlin, C. & Pedersen, L.B., 1987. Reflection seismic investigations of the Siljan impact structure, Sweden. Journal of Geophysical Research, 92, 14113–14122.

Kieffer, S.W., 1971. Shock metamorphism of the Coconino Sandstone at Meteor Crater, Arizona. Journal of Geophysical Research, 76, 5449–5473.

Kieffer, S.W., Phakey, P.P. & Christie, J.M., 1976. Shock processes in porous quartzite: transmission electron microscope observations and theory. Contributions to Mineralogy and Petrology, 59, 41–93.

Kieffer, S.W. & Simonds, C.H., 1980. The role of volatiles and lithology in the impact cratering process. Reviews of Geophysics and Space Physics, 18, 143–181.

Koeberl, C., 1994. Tektite origin by hypervelocity asteroidal or cometary impact: target rocks, source craters, and mechanisms. In: Dressler, B.O., Grieve, R.A.F. & Sharpton, V.L. (editors), Large meteorite impacts and planetary evolution. Geological Society of America, Special Paper 293, 133–152.

Koeberl, C., Shirey, S.B. & Reimold, W.U., 1994. Re–Os isotope systematics as a diagnostic tool for the study of impact craters. In: New developments regarding the K/T event and other catastrophes in early Earth history. LPI Contribution 825, Lunar and Planetary Institute, Houston, 61–63 (abstract).

Lambert, P., 1981. Breccia dikes: geological constraints on the formation of complex craters. In: Schultz, P.H. & Merrill, R.B. (editors), Multi-ring basins. Pergamon Press, New York, 59–78.

Lange, M.A. & Ahrens, T.J., 1986. Shock-induced CO_2 loss from $CaCO_3$; implications for early planetary atmospheres. Earth and Planetary Science Letters, 77, 409–418.

Langenhorst, F. & Clymer, A., 1995. TEM examination of quartz from Massignano (Ancona, Italy). 4th International Workshop of the ESF Network on Impact Cratering and Evolution of Planet Earth, 107–108 (abstract).

Lindström, M. & Sturkell, E.F.F., 1992. Geology of the early Palaeozoic Lockne impact structure, central Sweden. Tectonophysics, 216, 169–185.

Loper, F.E. & McCartney, K., 1988. Shocked quartz found at the K/T boundary: a possible endogenous mechanism. EOS, 69, 961.

Mareschal, M. & Chouteau, M., 1990. A magnetotelluric investigation of the structural geology beneath Charlevoix Crater, Quebec. Physics of the Earth and Planetary Interiors, 60, 120–131.

Masaitis, V.L., Danilin, A.I., Mashchak, M.S., Raikhlin, A.I., Selivanovskaya, T.V. & Shadenkov, E.M., 1980. The geology of astroblemes (in Russian). Nedra Press, Leningrad.

Masaitis, V.L., Futergendler, S.I. & Gnevushev, M.A., 1972. Diamonds in impactites of the Popigai meteorite crater (in Russian). Zapiskio Vsesoyuznoge Mineralogicheskogo Obshchestva, 101, 108–112.

Masero, W., Schnegg, P.-A. & Fontes, S.L., 1994. A magnetotelluric investigation of the Araguainha impact structure in Mato Grosso–Goias, central Brazil. Geophysics Journal International, 116, 366–376.

McHone, J.F., Nieman, R.A., Lewis, C.F. & Yates, A.M., 1989. Stishovite at the Cretaceous–Tertiary boundary, Taton, New Mexico. Science, 243, 1182–1184.

Melosh, H.J., 1981. Atmospheric breakup of terrestrial impactors. In: Schultz, P.H. & Merrill, P.B. (editors), Multi-ring basins. Pergamon Press, New York, 29–35.

Melosh, H.J., 1989. Impact cratering: a geologic process. Oxford University Press, New York.

Millman, P.M., Liberty, B.A., Clark, J.F., Willmore, P. & Innes, M.J.S., 1960. The Brent crater. Ottawa Dominion Observatory, Publication 24, 1–43.

Milton, D.J., 1977. Shatter cones — an outstanding problem in shock mechanics. In: Roddy, D.J., Pepin, R.O. & Merrill, R.B. (editors), Impact and explosion cratering. Pergamon Press, New York, 703–714.

Milton, D.J., Glikson, A.Y. & Brett, R., 1996. Gosses Bluff — an end-Jurassic impact structure in central Australia. Part 1: geology. AGSO Journal of Australian Geology & Geophysics (this issue).

Officer, C.B., 1992. The relevance of iridium and microscopic dynamic deformation features toward understanding the Cretaceous/Tertiary transition. Terra Nova, 4, 394–404.

Palme, H., 1982. Identification of projectiles of large terrestrial impact craters and some implications for the interpretation of Ir-rich Cretaceous/Tertiary boundary layers. Geological Society of America, Special Paper 190, 223–233.

Palme, H., Goebel, E. & Grieve, R.A.F., 1979. The distribution of volatile and siderophile elements in the impact melt of East Clearwater (Quebec). Proceedings of the 10 th Lunar and Planetary Science Conference, 2465–2492.

Palme, H., Grieve, R.A.F. & Wolf, R., 1981. Identification of the projectile at Brent crater, and further considerations of projectile types at terrestrial craters. Geochimica et Cosmochimica Acta, 45, 2417–2424.

Perrier, R. & Quiblier, J., 1974. Thickness changes in sedimentary layers during compaction history: methods for quantitative evaluation. American Association of Petroleum Geologists, Bulletin 58, 507–528.

Pevzner, L.A., Kirjakov, A.F., Vorontsov, A.K., Masaitis, V.L., Mashchak, M.S. & Ivanov, B.A., 1992. Vorotilovskaya drillhole: first deep drilling in the central uplift of a large terrestrial impact crater. Lunar and Planetary Science, XXII, 1063–1064 (abstract).

Pike, R.J., 1977. Size-dependence in the shape of fresh impact craters on the moon. In: Roddy, D.J., Pepin, R.O. & Merrill, R.B. (editors), Impact and explosion cratering. Pergamon Press, New York, 489–509.

Pike, R.J., 1985. Some morphologic systematics of complex impact structures. Meteoritics, 20, 49–68.

Pilkington, M. & Grieve, R.A.F., 1992. The geophysical signature of terrestrial impact craters. Reviews of Geophysics, 30, 161–181.

Poag, C.W., Powars, D.S., Poppe, L.J. & Mixon, R.B., 1994. Meteoroid mayhem in Ole Virginny: source of the North American tektite strewn field. Geology, 22, 691–694.

Pohl, J., 1971. On the origin of the magnetization of impact breccias on Earth. Zeitschrift für Geophysik, 37, 549–555.

Pohl, J. & Soffel, H., 1971. Paleomagnetic age determination of the Rochechouart impact structure (France). Zeitschrift für Geophysik, 37, 857–866.

Pohl, J., Stöffler, D., Gall, H. & Ernston, K., 1977. The Ries impact crater. In: Roddy, D.J., Pepin, R.O. & Merrill, R.B. (editors), Impact and explosion cratering. Pergamon Press, New York, 343–404.

Redeker, H.J. & Stöffler, D., 1988. The allochthonous polymict breccia layer of the Haughton impact crater, Devon Island, Canada. Meteoritics, 23, 185–196.

Reimold, W.U. & Colliston, W.P., 1994. Pseudotachylites of the Vredefort Dome and the surrounding Witwatersrand Basin, South Africa. Geological Society of America, Special Paper 293, 177–196.

Robertson, P.B., 1980. Anomalous development of planar deformation features in shocked quartz of porous lithologies. Lunar and Planetary Science, XI, 938–940 (abstract).

Robertson, P.B. & Grieve, R.A.F., 1977. Shock attenuation at terrestrial impact structures. In: Roddy, D.J., Pepin, R.O. and Merrill, R.B. (editors), Impact and explosion cratering. Pergamon Press, New York, 687–702.

Robertson, W.A., 1967. Manicouagan, Quebec, paleomagnetic results. Canadian Journal of Earth Sciences, 4, 641–649.

Roddy, D.J., Pepin, R.O. & Merrill, R.B. (editors), 1977. Impact and explosion cratering. Pergamon Press, New York.

Sazonova, L.V., 1981. Planar deformations in quartz from authigenic breccia from the central uplift of the Kara meteorite crater (in Russian). Doklady Akadamii Nauk SSSR, 261, 731–734.

Sazonova, L.V., Karotayeva, N.N., Ponomarev, G.Y. & Dabizha, A.I., 1981. The Kara meteorite crater (in Russian). In: Marakusheva, A.A. (editor), Impactites. Moscow State University Press, Moscow, 93–135.

Schneider, W., 1971. Petrologic study of the Bunte breccia at the Nördlingen Ries (in German). Neues Jahrbuch für Mineralogie, Abhandlungen, 114, 136–174.

Scott, D. & Hajnal, Z., 1988. Seismic signature of the Haughton structure. Meteoritics, 23, 239–247.

Scott, R.G., Pilkington, M., Tanczyk, E.I. & Grieve, R.A.F., 1995. Magnetic properties of three impact structures in Canada. Meteoritics, 30, 576–577 (abstract).

Sharpton, V.L., Burke, K., Camargo-Zanoguera, A., Hall, S.A., Lee, D.S., Marin, L.E., Suarez-Reynoso, G., Quezada-Muneton, J.M., Spudis, P.D. & Urrutia-Fucugauchi, J., 1993. Chicxulub multiring impact basin: size and other characteristics derived from gravity analysis. Science, 261, 1564–1567.

Shoemaker, E.M., Shoemaker, C.S. & Plescia, J.B., 1989. Gravity investigation of the Connolly basin impact structure, Western Australia. Lunar and Planetary Science, XX, 1010–1011 (abstract).

Short, N.M., 1970. Anatomy of a meteorite impact crater: West Hawk Lake, Manitoba, Canada. Geological Society of America, Bulletin 81, 609–648.

Smit, J. & Hertogen, J., 1980. An extraterrestrial event at the Cretaceous–Tertiary boundary. Nature, 285, 158–200.

Spray, J.G. & Thompson, L.M., 1995. Friction melt distribution in terrestrial multi-ring impact basins. Nature, 373, 130–132.

Stepto, D., 1990. The geology and gravity field in the central core of the Vredefort structure. Tectonophysics, 171, 75–103.

Stöffler, D., 1971. Progressive metamorphism and classification of shocked and brecciated crystalline rocks in impact craters. Journal of Geophysical Research, 76, 5541–5551.

Stöffler, D., 1972. Deformation and transformation of rock-forming minerals by natural and experimental shock processes: I. Behavior of minerals under shock compression. Förtschritte der Mineralogie, 49, 50–113.

Stöffler, D., 1974. Deformation and transformation of rock-forming minerals by natural and experimental shock processes: II. Physical properties of shocked minerals. Förtschritte der Mineralogie, 51, 256–289.

Stöffler, D., 1984. Glasses formed by hypervelocity impact. Journal of Non-Crystalline Solids, 67, 465–502.

Stöffler, D., Bischoff, L., Oskierski, W. & Wiest, B., 1988. Structural deformation, breccia formation, and shock metamorphism in the basement of complex terrestrial impact craters: implications for the cratering process. In: Bodén, A. & Eriksson, K.G. (editors), Deep drilling in crystalline bedrock. Springer–Verlag, New York, 1, 277–297.

Stöffler, D., Deutsch, A., Avermann, M., Bischoff, L., Brockmeyer, P., Buhl, D., Lakomy, R. & Müller-Mohr, V., 1994. The formation of the Sudbury structure, Canada: towards a unified impact model. In: Dressler, B.O., Grieve, R.A.F. & Sharpton, V.L. (editors), Large meteorite impacts and planetary evolution. Geological Society of America, Special Paper 293, 303–318.

Stöffler, D., Ewald, U., Ostertag, R. & Reimold, W.U., 1977. Research drilling Nördlingen 1973, Ries: composition and texture of polymict impact breccias. Geologica Bavarica, 75, 163–190.

Stöffler, D. & Hornemann, U., 1972. Quartz and feldspar glasses produced by natural and experimental shock. Meteoritics, 7, 371–394.

Stöffler, D. & Langenhorst, F., 1994. Shock metamorphism of quartz in nature and experiment: 1. Basic observation and theory. Meteoritics, 29, 155–181.

Therriault, A.M., Grieve, R.A.F. & Reimold, W.U., 1995. How big is Vredefort? Meteoritics, 30, 586–587 (abstract).

Therriault, A.M. & Lindström, M., 1995. Planar deformation features in quartz grains from the resurge deposit of the Lockne structure, Sweden. Meteoritics, 30 (in press).

Therriault, A.M., Reid, A.M. & Reimold, W.U., 1993. Original size of the Vredefort structure, South Africa. Lunar and Planetary Science, XXIV, 1419–1420 (abstract).

Tingate, P.R., Lindsay, J.F. & Marshallsea, S.J., 1996. Impact structures as potential petroleum exploration targets: Gosses Bluff, a Late Jurassic example from central Australia. AGSO Journal of Australian Geology & Geophysics, this issue.

Vishnevsky, S.A. & Lagutenko, V.N., 1986. The Ragozinka astrobleme: an Eocene crater in the central Urals (in Russian). Doklady Akademii Nauk SSSR, 14, 1–42.

Wallace, M.A., Gostin, V.A. & Keays, R.R., 1990. Acraman impact ejecta and host shales: evidence for low-temperature mobilization of iridium and other platinoids. Geology, 18, 132–135.

Wallace, M.W., Gostin, V.A. & Keays, R.R., 1996. Sedimentology of the Neoproterozoic Acraman impact-ejecta horizon, South Australia. AGSO Journal of Australian Geology & Geophysics, this issue.

Wasson, J.T., 1991. Layered tektites: a multiple impact origin for the Australasian tektites. Earth and Planetary Science Letters, 102, 95–109.

Wolf, R., Woodrow, A.B. & Grieve, R.A.F., 1980. Meteoritic material at four Canadian impact craters. Geochimica et Cosmochimica Acta, 44, 1015–1022.

Wood, C.A. & Head, J.W., 1976. Comparison of impact basins on Mercury, Mars and the moon. Proceedings of the 7th Lunar Science Conference, 3629–3651.

Zhang, P., Rasmussen, T.M. & Pedersen, L.B., 1988. Electric resistivity structure of the Siljan impact region. Journal of Geophysical Research, 93, 6485–6501.

AGSO Journal of Australian Geology & Geophysics, 16 (4), 421–429

Australian crater-forming meteorites

A.W.R. Bevan[1]

Meteorites are associated with five impact structures in Australia. Three of them are group IIIAB irons (Wolf Creek, Henbury, and Boxhole), Veevers is a group IIAB iron, and material recovered from the crater at Dalgaranga is a mesosiderite stony-iron. The impacts range in age from a few thousand years (Dalgaranga, Henbury, Veevers, and Boxhole) to 300 000 years (Wolfe Creek Crater). Metallographic studies of the surviving fragments at some of the craters show that impact damage ranges from simple fracturing, through shock-hardening of metal, to plastic and shear deformation, reheating and attendant recrystallisation, and, ultimately, melting. Details of the microstructures of surviving fragments of iron meteorite from the craters suggest that shear deformation may have been an important mechanism in the disruption of the projectiles. Frictional heating from viscous drag between projectile and target, and from rapid shear deformation within the projectile, may be sufficient to melt and vaporise significant portions of the projectiles and account for the large deficit of meteoritic material from Australian impact craters.

Figure 1. Locations of Australia's described impact structures. Five (large solid dots) are clearly recognisable craters associated with meteorites; all of them are less than 300 000 years old. Authenticated and likely impact structures not easily recognisable because of great age, deep erosion, or burial are shown as open dots. One structure, Mount Darwin Crater in Tasmania, is undoubtedly of meteorite impact origin (Fudali & Ford 1979), but no meteorites have been collected from the site. The indicated diameters of structures are based on conspicuous topographic expression or geophysical evidence, and may not reflect the original dimensions of very old, eroded complex structures (from Shoemaker & Shoemaker 1988; Buchanan et al. 1992).

[1] Department of Earth and Planetary Sciences, Western Australian Museum, Francis Street, Perth, WA 6000.

Table 1. Australian impact craters associated with meteorites

Name	*Coordinates*	*Diameter (km)*	*Age (Ma)*	*Meteorite type/class*
Dalgaranga	27°40'S, 117°17.5'E	0.024	<0.003?[1]	Stony-iron, mesosiderite
Veevers	22°58'06"S, 125°22'07"E	0.07	<0.004?[1]	Iron, group IIAB
Henbury (Craters)	24°35'S, 133°10'E	0.006-0.18	0.0042 ± 0.0019[2,3]	Iron, group IIIAB
Boxhole	22°37'S, 135°12'E	0.17	0.0054 ± 0.0015[2]	Iron, group IIIAB
Wolfe Creek Crater	19°18'S, 127°46'E	0.88	~0.30[4]	Iron, group IIIAB

[1] Shoemaker & Shoemaker (1988). [2] Kohman & Goel (1963). [3] Goel & Kohman (1963). [4] Shoemaker et al. (1990).

Introduction

Of the 23 structures identified as having originated from the impact of extraterrestrial objects in Australia, five (Wolfe Creek Crater, Henbury, Dalgaranga, Veevers, and Boxhole) are associated with meteorites (Fig. 1). All five are simple bowl-shaped structures ranging in diameter from 24 m (Dalgaranga) to 880 m (Wolfe Creek Crater) and in age from a few thousand years (Dalgaranga, Henbury, and Boxhole) to 300 000 years (Wolfe Creek Crater; Table 1). At each crater, the impacting meteorites have been identified as follows: Wolf Creek[1] (group IIIAB iron); Henbury (group IIIAB iron); Dalgaranga (mesosiderite stony-iron); Veevers (group IIAB iron); and Boxhole (group IIIAB iron). Detailed modern metallographic descriptions have been presented by Buchwald (1975, and references therein) for the residual fragments of the impacting irons at Wolfe Creek Crater, Boxhole, and Henbury, by Bevan et al. (1995) for the Veevers meteorite, and by Nininger & Huss (1960) and McCall (1965a) for the Dalgaranga mesosiderite and its occurrence.

Numerous studies have examined the thermomechanical alteration of the crater-forming meteorites wrought by shock-metamorphism resulting from impact with the Earth, and several authors have considered the mechanism of disruption of the original projectiles during the impact event (e.g., Heymann et al. 1966, and references therein; Vdovykin 1973). However, despite extensive theoretical and experimental work in the field of cratering mechanics, geological studies of craters (Shoemaker 1960, 1963; Grieve 1987, 1991; Melosh 1989, and references therein), and shock-metamorphism (e.g., Stöffler 1971, 1972, 1974; French & Short 1968, and references therein; Roddy et al. 1977, and references therein; Alexopoulos et al. 1988) there is still much to be learnt about the phase changes that occur in the impacting bodies (both target and projectile) and the resulting disposition of the material at the point of impact.

The surviving fragmental material from some of the Australian impactors unfortunately has been extensively corroded (e.g., Wolf Creek), and much of the original structure of the fragments that might have given an insight to the mechanism of disruption has been lost. Nevertheless, at other sites — notably Henbury, Veevers, and Dalgaranga — fresh material survives to the present day in meteorite collections. The purpose of this paper is to review the data on Australian crater-forming meteorites, and, by comparison with examples from other parts of the world, to examine possible mechanisms of disruption of the impacting projectiles.

[1] Historical research has revealed that the surname of the person after whom the crater was named was 'Wolfe' not 'Wolf'. Consequently, the locality has been renamed Wolfe Creek Crater. However, according to the rules of meteorite nomenclature, the previously published name of Wolf Creek is retained for the meteorites found at the site.

Boxhole

The Boxhole crater, measuring about 170 m in diameter, is situated in the Northern Territory near the Plenty River at latitude 22°37'S, longitude 135°12'E. The crater, which was discovered in June 1937, is formed in schists and gneisses of Precambrian age, and has a rim raised about 3 m above the surrounding plain. Little fresh meteoritic material survives at the crater. During the first scientific examination of the crater, Madigan (1937) surveyed and described the structure. Two balls of 'iron-shale' (nodules of iron oxides representing the weathered remnants of fragments of the meteorite) and one fragment of meteoritic iron weighing about 100 g were found and analysed subsequently (Madigan 1940).

Since the discovery of the crater, much additional material, including one mass of 82 kg, has been recovered from the site. However, the total weight of fragments recovered from the crater that are documented in museum collections throughout the world is only around 280 kg (Graham et al. 1985). The largest single holding of material (178 kg) is at the South Australian Museum in Adelaide. Other collections have undoubtedly been made by private collectors; Buchwald (1975) estimated that perhaps as much as 500 kg of iron meteorites and around 50 kg of iron-shale have been recovered in total.

Soil in an area up to 1.5 km around the crater was sampled by Hodge & Wright (1970), who noted a spotty distribution of weathered meteorite particles similar to those discovered around the Henbury craters (Hodge 1971). Numerous shale-balls have been found buried in the soil around the crater, together with small fragments of less-weathered iron meteorite typically 50-200 g in weight (Buchwald 1975). Many of the small fragments are intensely deformed and twisted slugs of metal, or wedge-shaped fragments.

The metallography of the deformed fragments shows that the medium Widmanstätten pattern is bent and torn, that kamacite has been transformed by reheating and rapid cooling to unequilibrated α_2-kamacite, probably by the reaction α-γ-α_2, and that inclusions of schreibersite [$(Fe,Ni)_3P$] and troilite (FeS) are widely melted. Buchwald (1975) interpreted this alteration as

the result of thermomechanical treatment resulting from compression and heating of the meteorite during the cratering event. The metallographic features indicate that the residual temperature of the deformed slugs must have been briefly above 1000°C.

Whereas many specimens of Boxhole are apparently disrupted fragments from a larger body that fragmented on impact, Buchwald (1975) has shown that some fragments became detached from the projectile during atmospheric passage and were not involved in the crater-forming event. One such specimen is a 3.7-kg mass preserved at the National Museum of Natural History in Washington. A metallographic examination of the undeformed portions of the meteorite (Buchwald 1975) shows a well-developed medium octahedrite (kamacite bandwidth 1.00 ± 0.15 mm) Widmanstätten pattern and shock-hardened ε-kamacite. The latter feature indicates that the meteorite was subjected to shock-loading in excess of 13 GPa before impact with the Earth.

Boxhole has been chemically classified as a group IIIAB iron containing 7.64% Ni, 18.1 ppm Ga, 37.2 ppm Ge, and 8.2 ppm Ir (Wasson & Kimberlin 1967).

Wolf Creek

The Wolfe Creek Crater was discovered from the air in June 1947 by F. Reeves, N.B. Sauve, and D. Hart (Reeves & Chalmers 1949; Guppy & Matheson 1950). It is situated at latitude 19°10'S, longitude 127°46'E, on the margin of the Great Sandy Desert in Western Australia, and about 110 km south of Halls Creek. It measures 850–900 m (averaging 880 m) in diameter, and is the largest crater associated with meteorites known in Australia. Formed in Precambrian quartzites, it has a rim that rises up to 35 m above the surrounding sand plain, and about 50 m above the current flat crater floor. Depth/diameter relationships of simple impact craters (Melosh 1989), and a gravity survey by Fudali (1979), suggest that the crater is 140–150 m deep. It now contains an extensive aeolian sedimentary fill.

Fresh iron meteorite fragments are extremely rare at the crater (e.g., Cassidy 1954; McCall 1965b); only 1.3 kg of unoxidised material is known to have been collected. The most important specimens are a number of small masses discovered 4 km southwest of the crater and described by Taylor (1965). Several terrestrially produced secondary minerals have been described from the weathered material by White et al. (1967) and Faust et al. (1973). A substantial amount of iron-shale, including shale-balls weighing up to 300 kg (LaPaz 1954), has been recovered. Many of the shale-balls contain rare stringers and particles of fresh metal (Knox 1967), although Buchwald (1975) noted that corrosion has largely obscured the original structure of the meteorite. In all, several thousand kilograms of shale-balls have been recovered from the crater (McCall & de Laeter 1965).

An analysis of the fresh material (Scott et al. 1973) yielded 9.22% Ni, 18.4 ppm Ga, 37.3 ppm Ge, and 0.036 ppm Ir, showing that the meteorite belongs to chemical group IIIAB. Structurally, the Wolf Creek meteorite is a medium octahedrite with a kamacite bandwidth of 0.85 ± 0.15 mm (Buchwald 1975). Buchwald (1975) noted that the moderately fresh material consists of slugs of metal in which the Widmanstätten pattern is slightly distorted, particularly at the margins of the fragments, indicating plastic deformation associated with the break-up of the impacting body. Kamacite in Wolf Creek displays the

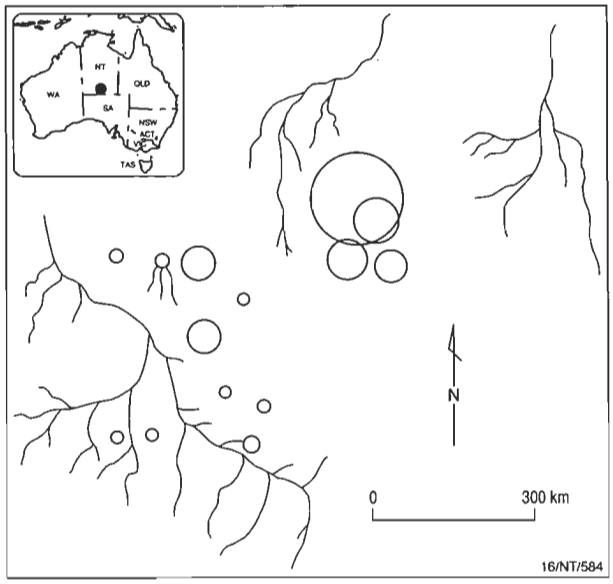

Figure 2. Schematic map of the crater strewn field at Henbury, Northern Territory (after Passey & Melosh 1980).

shock-hardened ε-structure which Buchwald (1975) attributed to pre-terrestrial shock-loading of the meteorite. Although the classified fragments were found at a considerable distance from the crater, Buchwald (1975) concluded that the material was consistent with the more deeply weathered remnants found nearer the crater, and that they were undoubtedly the same meteorite.

More recently, E.M. and C.S. Shoemaker found additional fresh iron meteorite fragments weighing 10.4, 2, and 0.9 g near the crater. These are deposited (WAM 13659) at the Western Australian Museum in Perth, and remain to be described. The 10.4-g sample was used for a terrestrial age determination. From the ratios of $^{36}Cl/^{10}Be$ and $^{41}Ca/^{36}Cl$ for the meteorite, Shoemaker et al. (1990) reported an age for the crater of 300 000 years.

Henbury

The group of impact craters near the Finke River south of the Macdonnell Ranges at latitude 24°35'S, longitude 133°10'E in the Northern Territory are among the best studied in Australia. The crater field was recognised in 1931, and subsequently described by Alderman (1932a). Early search parties independently organised by Alderman (1932b) and R. Bedford of the then Kyancutta Museum are reported to have recovered 1447 individual fragments of meteorite — ranging in weight from less than a gram to 132 kg, and totalling 649 kg — including some shale-balls. Many specimens collected by R. Bedford were sent to the British Museum (Natural History) in London, where they were described by Spencer & Hey (1933) and reside to the present day.

Thirteen or fourteen craters ranging in diameter from 6–180 m have been identified in a strewn field trending roughly northeasterly. The largest craters are at the northeastern end of the field (Fig. 2). Extensive fieldwork has been carried out at the craters (e.g., Hodge 1965), and Milton (1972) has provided a detailed account of the geology. A magnetic survey of the area conducted by Rayner (1939) revealed no large magnetic anomalies, from which he concluded that large masses of meteoritic iron were not represented at the site. However, small anomalies

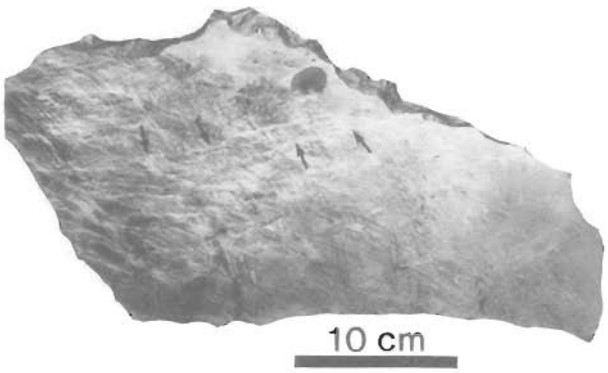

Figure 3. Polished and etched slice of a large mass of the Henbury meteorite showing flattening, distorted Widmanstätten pattern, and extensive zones of shear deformation (arrowed).

were associated with some iron fragments, and one weighing 18 kg was recovered from crater no. 5. Bedford had previously excavated three (nos. 10, 11, and 13) of the smallest craters. In the smallest crater (no. 13) he found four large masses of iron weighing 2.3, 10.9, 54.4, and 132.7 kg. Around and between the masses, 20 kg of iron-shale suggested that the four irons were corroded fragments of what was originally a single large mass (Spencer & Hey 1933; Buchwald 1975; Axon & Steele-Perkins 1975). Buchwald (1975) estimated that at least 1200 kg of meteorites have been recovered from the crater strewn field, most of which have been found in narrow zones of a few hundred metres around the craters.

Detailed metallographic examinations of numerous fragments of the Henbury meteorite (Buchwald 1975) have revealed an enormous range of internal structures that can be attributed to the impact. However, several of the large masses and some of the smaller fragments display unaltered Widmanstätten patterns, and do not appear to have been involved in the formation of the craters. These specimens retain regmaglypts, remnants of fusion crusts, and heat-affected zones as testimony to their independent flight through the atmosphere. The Henbury meteorite is a medium octahedrite with a bandwidth of 0.95 ± 0.1 mm, and belongs to chemical group IIIAB (Buchwald 1975; Wasson & Kimberlin 1967; Scott et al. 1973). Despite a chemical similarity between Henbury and Boxhole, and a suggestion that the two events were contemporaneous, Buchwald (1975) has shown that the metallurgy of the least damaged specimens of both meteorites have significant differences that seem to establish them as distinct. Moreover, Kohman & Goel (1963) and Goel & Kohman (1963) derived slightly different ages for the two cratering events.

Many masses of Henbury are intensely deformed and sheared (Fig. 3). These fragments are generally flattened, twisted, and torn with irregular sharp edges, and the surfaces of many display slickensides. The interior structures of deformed fragments show intensely bent and kneaded Widmanstätten patterns and varying degrees of annealing. Zones of shear deformation, some arranged en echelon, pervade the structures of the most intensely deformed fragments; they are accompanied by attendant recrystallisation of the metal. Kamacite in the smallest metallic slugs is generally transformed completely to α_2-kamacite, and the Widmanstätten structures of these specimens are indistinct and partly resorbed. Some fragments have been almost cleaved in half by shearing, and this has been accentuated by later terrestrial corrosion. Within the shear zones, accessory minerals such as troilite and schreibersite have been shock-melted and smeared out into veins. In the most severely shock-heated fragments, schreibersite has been largely resorbed.

Axon & Steele-Perkins (1975) studied a 5-kg slice from the 132.7-kg mass found in crater no. 13, and many of the shrapnel-like fragments from other craters generated by the impact. The large slice is traversed by a number of shear faults that parallel the outer surface of the section. Axon & Steele-Perkins (1975) suggested that the fracture surfaces of the mass could represent the extreme situation in which limited shear displacement gave way to physical separation along a faulted surface; this is supported by the observations of Buchwald (1975). From the morphology and metallography of the shrapnel-like fragments, Axon & Steele-Perkins (1975) concluded that fracturing of the impacting projectile probably occurred by separation along zones of intense shear deformation. Moreover, the thermal alteration of the surviving fragments was also generated by the rapid propagation of shear deformation.

The most severely deformed specimens have a high density of sheared surfaces. Shear zones vary from the microscopic (50–200 μm wide) to the macroscopic scale, in which shears with displacements of a few micrometres to several millimetres extend 40 cm across sections (Buchwald 1975; Axon & Steele-Perkins 1975). The impactor might have had larger zones of shear faulting, evidence of which would have been destroyed along with the bulk of the projectile.

Buchwald (1975) noted one heavily deformed Henbury fragment with a shear-ruptured slickensided surface covered by a thin fusion crust. He suggested that the crust formed when the fragment was hurled away from the impact site. However, it is more likely that the crust is a vestige of melted material that was generated by shearing during impact fragmentation.

Veevers

The Veevers meteorite impact crater (Fig. 4), measuring 70–80 m in diameter, was recognised in July 1975 (Yeates et al. 1976). The crater is situated between the Great Sandy and Gibson Deserts in Western Australia at latitude 22°58'06"S, longitude 125°22'07"E. At the time of discovery, the crater was surveyed, but no meteoritic material was recovered (Yeates et al. 1976). E.M. and C.S. Shoemaker visited the site twice, and recovered 36 metallic fragments and slugs (Fig. 5) weighing 298.1 g, mainly from near the rim to the north and east of the crater (Bevan et al. 1995).

Wasson et al. (1989) analysed the meteorite and showed that it is a normal member of chemical group IIAB containing 5.82% Ni, 57.7 ppm Ga, 160 ppm Ge, and 0.028 ppm Ir. Bevan et al. (1995) described the fragments as essentially single crystals of α-kamacite that have been partly or completely transformed by reheating to unequilibrated α_2-kamacite, particularly along zones of intense shear deformation. They concluded that the fragments represent individual kamacite lamellae which were separated from the original coarsest octahedral structure of the meteorite as the result of impact fragmentation; this conclusion confirmed earlier observations made by Wasson et al. (1989). Moreover, Bevan et al. (1995) suggested that the meteorite may have failed as the result of fracturing along zones of shear deformation. The pattern of shearing in some of the Veevers fragments locally indicates that the original octahedral structure of the meteorite may have influenced the selection of certain

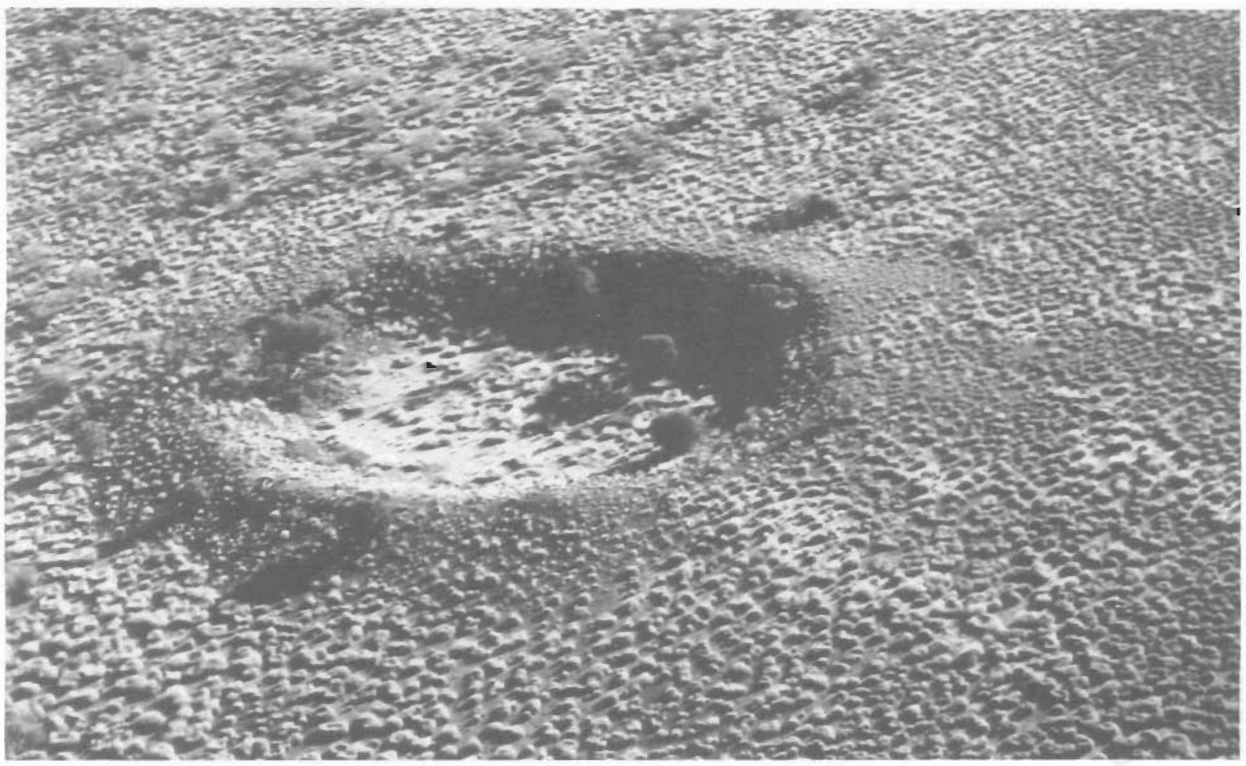

Figure 4. Oblique aerial view of the 70–80-m-diameter Veevers meteorite impact crater (named for geologist J.J. Veevers; photograph courtesy of A.N. Yeates, AGSO).

surfaces for shear faulting. From a metallographic study of the Veevers fragments, and comparisons with experimentally heat-treated samples of the Canyon Diablo meteorite, Bevan et al. (1995) suggested that terrestrial impact caused intense shock-loading which resulted in shearing and plastic deformation of the projectile and attendant localised shock-heating. The peak residual shock temperatures suggested by the surviving fragments is >800°C. As a result of the disruption of a portion of the meteorite along brittle-cracking paths, such as α–α crystal boundaries and schreibersite crystals, some of the energy of the impact might have been absorbed, allowing part of the original microstructure of the meteorite to be preserved.

Veevers is the only known crater-forming iron of group IIAB. The fall of another IIAB iron, Sikhote-Alin, which was observed in Siberia in 1947, resulted in 122 impact holes. However, Fesenkov & Krinov (1959) suggested that these are not true impact craters. Many of the recovered masses, totalling 23.2 t, display only the earliest stages of shock-metamorphism (Krinov 1963; Buchwald 1975).

Dalgaranga

The Dalgaranga crater, recognised in 1923 by G.E.P. Wellard, is the first such discovery known to have been caused by the impact of a meteorite in Australia (Fig. 6). Situated at latitude 27°40'S, longitude 117°17.5'E, the crater measures 24 m in diameter, and is around 3 m deep. Wellard is reported to have recovered numerous fragments of meteoritic material from the vicinity of the crater, but the whereabouts of the bulk of it is unknown. Additional collections made by H.H. Nininger and G.I. Huss of the American Meteorite Laboratory in 1959 and 1960 amounted to 207 specimens weighing 1098 g recovered from the area surrounding the crater, and 280 specimens weighing around 9.1 kg recovered from beneath the crater floor (Nininger & Huss 1960).

Simpson (1938) described the meteorite from a single fragment weighing 42 g, and concluded that it was an 'iron' with a medium octahedral structure. Later work by Nininger & Huss (1960) and McCall (1965a) showed that the impacting meteorite is a mesosiderite stony-iron. A modern analysis of the metallic portion of the meteorite — 8.8% Ni, 15.5 ppm Ga, 56 ppm Ge, and 4.2 ppm Ir (Wasson et al. 1974) — has confirmed a mesosiderite classification (Graham et al. 1985). A more recent analysis by Hassanzadeh et al. (1990) yielded 10.27% Ni, 12.7 ppm Ga, and 4.99 ppm Ir, showing that the metallic nodules in Dalgaranga vary in composition. This is reflected in structural variations of metallic nodules, which have Widmanstätten patterns ranging from finest to coarsest octahedrite.

Much of the material found at Dalgaranga, particularly the material from within the crater, is extensively altered by prolonged terrestrial weathering. Nevertheless, a substantial number of the fragments, including many metallic slugs, are well preserved. The metallic slugs display Widmanstätten patterns that are variably bent and deformed (Nininger & Huss 1960). The metallic portions of the meteorite locally show narrow zones of shear deformation along which metal has been finely recrystallised (Bevan & Griffin 1994). Other fragments show little effects of shock-metamorphism (Nininger & Huss 1960).

Discussion

Extensive studies of Meteor Crater in Arizona, USA (Shoemaker 1960, 1963), of the associated Canyon Diablo meteorite (Heymann et al. 1966; Vdovykin 1973), and of other simple impact structures throughout the world (e.g., Grieve 1991, and references therein), combined with experimental work on

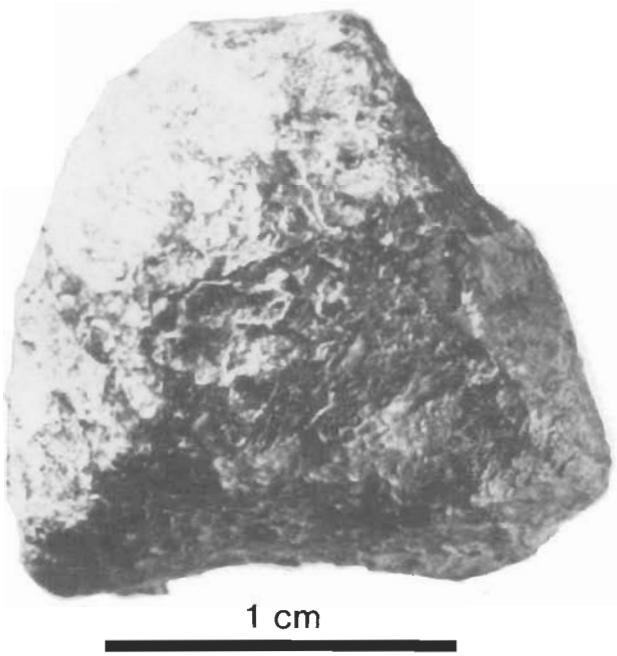

Figure 5. Fragment, weighing 8.9 g, of the Veevers crater-forming meteorite found by E.M. and C.S. Shoemaker in 1984.

Figure 6. Dalgaranga meteorite impact crater (24 m in diameter), Western Australia, viewed from the north at ground level (courtesy of W.H. Cleverly and M.K. Quartermaine).

hypervelocity impact (Melosh 1989, and references therein), have provided much information on the mechanics of cratering.

Shoemaker et al. (1963) disputed the widely held concepts that a large part of a projectile travelling at a high velocity and causing a Meteor Crater-size structure would vaporise as it impacted into rock, and that the explosive expansion of the vapour produces the resultant crater. Nininger (1956) suggested that the metallic spherules that occur at Meteor Crater were formed by the condensation of iron–nickel vapour. However, Blau et al. (1973) and Kelly et al. (1974) have since shown that the metallic spheroids are more likely to have been generated by shock-melting.

From an experimental impact of a small (4.76-mm-diameter) steel sphere travelling at 4.27 km s^{-1} into a block of Coconino Sandstone collected from Meteor Crater, Shoemaker et al. (1963) showed that, for those conditions, the fusion of the projectile could not be due to compressive heating alone, or to the conduction of heat from the shocked target, but could be accounted for by the production of heat by viscous drag and friction along the projectile/target interface, and by frictional heating along shear planes within the projectile.

Shoemaker et al. (1963) showed convincingly that shear-generated frictional heating of the experimental steel projectile appeared adequate to account for the melted material recovered from the experiment, and was the best explanation for the occurrence of fused steel on the striated surfaces of the larger recovered fragments. They concluded from this experiment that abundant metallic spheres from the melting of an iron projectile could be produced without the generation of any significant amount of vapour, and that more definitive evidence was required to show that a significant fraction of the Meteor Crater projectile had been vaporised on impact. However, some scaling problems arise from the extrapolation of small-scale experiments to hypervelocity impacts of iron meteorites weighing tens of thousands of tons and measuring tens of metres in diameter.

Only general limits of the pressures required for phase changes in complex multiphase geological materials under conditions of compressive shock-loading are known (Ahrens & O'Keefe 1977). For melting and vaporisation of iron to occur by compression, estimates indicate that the onset of melting occurs at 220 GPa and is complete by 260 GPa, whereas vaporisation starts at 420 GPa and is complete at 1680 GPa (Ahrens & O'Keefe 1977). In an impact event, the greatest shock pressures occur during the initial contact and compression stage (Melosh 1989). During the initial compression stage of the vertical impact of a body weighing 50 000 t travelling at 15 km s^{-1} into a crystalline (anorthositic) target, the highest shock pressures attained are estimated to be of the order of hundreds of gigapascals. Although they are much greater than the yield strength of the impactor and target, the compressive pressures fall far short of those required to vaporise a significant portion of the projectile. Compressive pressures (1590 GPa) capable of extensive vaporisation are attained only for large impactors travelling at velocities of 30 km s^{-1} or more (Melosh 1989).

Most impacts are not vertical (Shoemaker 1962), and the morphology of many of the Australian craters (notably Henbury) supports this assertion. The physics of oblique impacts differs markedly from that of vertical or near-vertical impacts (Wichman & Schultz 1994, and references therein; Yang & Ahrens 1995, and references therein). Melosh (1989) noted that the principal difference between vertical and oblique impacts is apparent in the effects on the projectile. In a moderately oblique impact, the projectile is first compressed by shock generated at the target–projectile interface. The shock is then propagated into the projectile, and thus reduces the vertical component of its velocity. However, the horizontal component of the projectile's velocity remains large (Melosh 1989). Melosh (1989) pointed out that one of the consequences of oblique impacts is that 'jetting' may play a significant role.

Experimental work has shown that even at impact velocities of around 6 km s^{-1}, which are theoretically too low to melt large portions of either projectile or target, jets of incandescent debris shoot away rapidly at a low angle from the impact site (Melosh 1989). At low impact velocities, the jetting phenomenon, first observed by D.E. Gault, is evidently due to molten material. Melosh (1989) suggested that, at higher impact velocities, superheated vapour may be ejected; he propounded that the melt/vapour ratio, and the projectile mass, scale as the square of the impact velocity. He also noted that the effect of oblique

impacts on the production of melt or vapour is not well known, although jetting may enhance the amount produced. However, recent work by Yang & Ahrens (1995, and references therein) has provided experimental data on impact-jetting during oblique impacts.

Differences in the dimensions and compositions of the known crater-forming meteorites, in the velocities and trajectories of the bodies, and in the nature of the target rocks have together led to large differences in the magnitudes of their impacting events and to a resultant enormous range of shock-induced features in the residual fragments. Observed damage of crater-forming irons ranges from simple fracturing, through shock-hardening of metal, to plastic and shear deformation, reheating, attendant recrystallisation, and, ultimately, melting. Nevertheless, Bevan et al. (1995) noted that there are some close similarities in the overall nature of the thermomechanical alteration and apparent mechanism of disruption suffered by many crater-forming irons.

Parting along zones of intense shear deformation and faulting appears to have been an important mechanism in the disruption of the Henbury and, to a lesser extent, Veevers projectiles (Axon & Steele-Perkins 1975; Bevan et al. 1995). Furthermore, heating and localised melting are demonstrably associated with shearing in residual fragments of both projectiles, and in the metallic portions of Dalgaranga. From their observations of Henbury, Axon & Steele-Perkins (1975) deduced that, once shearing is initiated on a selected surface, it is likely to be propagated by the local generation of heat and the superplastic lubrication of the small kamacite crystals in the zone of mylonitisation.

At all the crater sites in Australia, there is a large deficit of meteoritic material. Even at Meteor Crater in Arizona, the most comprehensively studied simple structure in the world, only around 30 t of fragmental material and an unknown weight of millimetre-size metallic iron–nickel spherules have been recovered from a projectile estimated to have weighed in the range 50 000–100 000 t (Shoemaker 1960, 1963; Vdovykin 1973; Melosh 1989). The question arises: where is the bulk of the impacting material? Substantial portions of the impacting projectiles must have been shock-melted; this assertion is supported by the occurrence of abundant metallic Fe–Ni spherules (or evidence of their pre-existence) at many of the sites. At Henbury, Fe–Ni globules have also been identified embedded in the impact-generated glasses (Taylor 1967; Gibbons et al. 1976), and the impactites generally contain significant concentrations of siderophile elements derived from the impactor (Attrep et al. 1991).

One possible reason for the paucity of meteoritic material at the impact sites is that much of the remnants of the projectiles are imbedded in impact breccias beneath the crater floors (E.M. Shoemaker, US Geological Survey, personal communication). However, the lack of sharp magnetic anomalies at the craters suggests that, if this is correct, the material must be very widely dispersed. Whether any significant portion of the material was vaporised in events of this scale has yet to be proved (e.g., Shoemaker et al. 1963).

Most frictional energy is dissipated as heat. Much of the heat is generated in the small areas of contact between the bodies, and the local temperatures may instantaneously be very high (Jaeger 1942). These transient high temperatures have been called 'flash temperatures'. Archard (1959) theorised that the maximum flash temperature which can be reached at a high-velocity steel–steel frictional contact, provided that the total load is borne by a single plastically deformed area, is of the order of 10 000°C (Arnell et al. 1991). Significantly, this temperature is well in excess of that required for vaporisation to occur.

Summary and conclusions

Metallographic evidence from the residual fragments of iron meteorites, and one stony-iron meteorite, from Australian simple impact craters provides strong support for the suggestion by Shoemaker et al. (1963), based on experimental work, that the bulk of the impact-generated thermal effects on high-velocity metallic projectiles are due to frictional heating. In surviving fragments of meteorites from Australian craters, thermal alteration appears to be largely associated with shear deformation. Whereas frictional heat is sufficient to melt parts of a small projectile, Shoemaker et al. (1963) have suggested that it is insufficient to vaporise a large part of it.

Despite the extensive terrestrial corrosion and disintegration of some of the meteorites, this process alone cannot account for the paucity of material at the sites of impact. Theoretical tribology (Arnell et al. 1991) suggests that high-velocity frictional contact can generate extreme temperatures locally, and may lead to jetting. The possibility that substantial portions of the projectiles were destroyed by vaporisation associated with the jetting phenomenon needs to be modelled mathematically, and the compounding effects of oblique impacts taken into account. Frictional contact between the projectile and target, and within shear zones in the projectile, are both sources of heat generation. Octahedral iron meteorites are composed of a trellis-work of interlocking plates of varying thicknesses, the Widmanstätten pattern. The interaction and collision of plates in the structure during the compressive stage of hypervelocity impact are, as yet, unknown.

The surviving fragments at the craters probably represent material scabbed from the outermost (perhaps rear) portions of the projectiles during the impact, and thrown with ejecta around the craters. However, some, particularly at the Henbury and Boxhole craters, represent fragments detached during atmospheric flight. Further studies, notably measurement of short-lived cosmogenic isotopes of both hand specimens and metallic spherules from Australian craters, may help to determine the spatial relationships between unmelted and melted material from the impacting projectiles.

Acknowledgments

I am grateful to S.R. Taylor and an anonymous reviewer for many helpful comments that greatly improved the text. Thanks are also due to D. Hendricks for the preparation of the figures, P. Downes for assistance, and A.N. Yeates (AGSO) for the photograph of Veevers crater.

References

Ahrens, T.J. & O'Keefe, J.D., 1977. Equations of state and impact-induced shock-wave attenuation on the moon. In: Roddy, D.J., Pepin, R.O. & Merrill, R.B. (editors), Impact and explosion cratering. Pergamon Press, New York, 639–656.

Alderman, A.R., 1932a. The meteorite craters at Henbury, central Australia. Mineralogical Magazine, 23, 19–32.

Alderman, A.R. 1932b. The Henbury (central Australia) meteoritic iron. Records of the South Australian Museum, 4, 561–563.

Alexopoulos, J.S., Grieve, R.A.F. & Robertson, P.B., 1988. Microscopic lamellar deformation features in quartz: discriminative characteristics of shock-generated varieties. Geology, 16, 796–799.

Archard, J.F., 1959. The temperature of rubbing surfaces. Wear, 2, 438–455.

Arnell, R.D., Davies, P.B., Halling, J. & Whomes, T.L., 1991. Tribology — principles and design applications. Macmillan, London.

Attrep, M. Jr., Orth, C.J., Quintana, L.R., Shoemaker, C.S., Shoemaker, E.M. & Taylor, S.R., 1991. Chemical fractionation of siderophile elements in impactites from Australian meteorite craters. Lunar and Planetary Science Conference, XXII, 39–40.

Axon, H.J. & Steele-Perkins, E.M., 1975. Fracture mechanism of Henbury meteorite by separation along surfaces of shear faulting. Nature, 256, 635.

Bevan, A.W.R. & Griffin, B.J., 1994. Re–examination of the Murchison Downs meteorite: a fragment of the Dalgaranga mesosiderite? Journal of the Royal Society of Western Australia, 77, 45–49.

Bevan, A.W.R., Shoemaker, E.M. & Shoemaker, C.S., 1995. Metallography and thermo–mechanical treatment of the Veevers (IIAB) crater-forming iron meteorite. Records of the Western Australian Museum, 17, 51–59.

Blau, P.J., Axon, H.J. & Goldstein, J.I., 1973. Investigation of the Canyon Diablo metallic spheroids and their relationship to the breakup of the Canyon Diablo meteorite. Journal of Geophysical Research, 18, 363–374.

Buchanan, A., Bevan, A.W.R. & Shaw, R., 1992. Australian impact structures — a photographic catalogue. Proceedings of the 6th Australasian Remote Sensing Conference, 1, 238–248.

Buchwald, V.F., 1975. Handbook of iron meteorites. University of California Press, Los Angeles.

Cassidy, W.A., 1954. The Wolf Creek, Western Australia, meteorite crater. Meteoritics, 1, 197–199.

Faust, G.T., Fahey, J.F., Mason, B.H. & Dwornik, E.J., 1973. The disintegration of the Wolf Creek meteorite and the formation of pecoraite, the nickel analogue of clinochrysotile. US Geological Survey Professional Paper 384C, 1–35.

Fesenkov, V.G. & Krinov, E.L. (editors), 1959. Sikhote–Alinskij zheleznyi meteoritnyi dozhd. Books 1 (1959) & 2 (1963).

French, B.M. & Short, N.M. (editors), 1968. Shock metamorphism of natural materials. Mono Book Corporation.

Fudali, R.F., 1979. Gravity investigation of Wolf Creek Crater, Western Australia. Journal of Geology 87, 55–72.

Fudali, R.F. & Ford, R., 1979. Darwin glass and Darwin Crater: a progress report. Meteoritics 14, 283–296.

Gibbons, R.V., Hörz, F., Thompson, T.D. & Brownlee, D.E., 1976. Metal spherules in Wabar, Monturaqui and Henbury impactite. Geochimica et Cosmochimica Acta, Supplement, 7, 1, 863–880.

Goel, P.S. & Kohman, T.P., 1963. Cosmic ray exposure history of meteorites from cosmogenic Cl^{36}. In: Radioactive dating. International Atomic Energy Agency, Vienna, 413–432.

Graham, A.L., Bevan, A.W.R. & Hutchison, R., 1985. Catalogue of meteorites (with special reference to those represented in the collection of the British Museum [Natural History]), 4th edition. BMNH and University of Arizona Press.

Grieve, R.A.F., 1987. Terrestrial impact structures. Annual Reviews of Earth and Planetary Sciences, 16, 245–270.

Grieve, R.A.F., 1991. Terrestrial impact: the record in the rocks. Meteoritics, 26, 175–194.

Guppy, J.D. & Matheson, R.S., 1950. Wolf Creek Crater, Western Australia. Journal of Geology, 58, 30–36.

Hassanzadeh, J., Rubin, A.E. & Wasson, J.T., 1990. Compositions of large metal nodules in mesosiderites: links to iron meteorite group IIIAB and the origin of mesosiderite subgroups. Geochimica et Cosmochimica Acta, 54, 3197–3208.

Heymann, D., Lipschutz, M.E., Nielsen, B. & Anders, E., 1966. Canyon Diablo meteorite: metallographic and mass spectrometric study of 56 fragments. Journal of Geophysical Research, 71, 619–641.

Hodge, P.W., 1965. The Henbury meteorite craters. Smithsonian Contributions to Astrophysics, 8 (8), 199–213.

Hodge, P.W., 1971. Meteoritic particles in the soil surrounding the Henbury meteorite craters. Journal of Geophysical Research 76, 3880–3895.

Hodge, P.W. & Wright F.W., 1970. Meteoritic spherules in the soil surrounding terrestrial impact craters. Nature, 225, 717–718.

Jaeger, J.C., 1942. Moving sources of heat and the temperature of sliding contacts. Journal and Proceedings of the Royal Society of New South Wales, 76, 203–224.

Kelly, W.R., Holdsworth, E. & Moore, C.B., 1974. The chemical composition of metallic spheroids and metallic particles within impactite from Barringer Meteorite Crater, Arizona. Geochimica et Cosmochimica Acta, 38, 533–543.

Knox, R. Jr., 1967. Surviving metal in meteoritic iron-oxide from the Wolf Creek, Western Australia, meteorite crater. Meteoritics, 3, 235–238.

Kohman, T.P. & Goel, P.S., 1963. Terrestrial ages of meteorites from cosmogenic C^{14}. In: Radioactive dating. International Atomic Energy Agency, Vienna, 395–411.

Krinov, E.L., 1963. In: Middlehurst, B. & Kuiper, G.P. (editors), The Solar System, Volume IV: Moon, meteorites and craters. University of Chicago Press, Chicago, 208–234.

LaPaz, L., 1954. Meteoritic material from the Wolf Creek, Western Australia, Crater. Meteoritics, 1, 200–203.

McCall, G.J.H. & de Laeter, J.R., 1965. Catalogue of Western Australian meteorite collections. Western Australian Museum, Special Publication 3.

McCall, G.J.H., 1965a. New material from, and reconsideration of, the Dalgaranga meteorite and crater, Western Australia. Mineralogical Magazine, 37, 476–487.

McCall, G.J.H., 1965b. Possible meteorite craters — Wolf Creek, Australia and analogs. Annals of the New York Academy of Sciences, 123, 970–998.

Madigan, C.T., 1937. The Box Hole crater and the Huckitta meteorite (central Australia). Transactions of the Royal Society of South Australia, 61, 187–190.

Madigan, C.T., 1940. The Boxhole meteoritic iron, central Australia. Mineralogical Magazine, 25, 481–486.

Melosh, H.J., 1989. Impact cratering — a geologic process. Oxford University Press.

Milton, D.J., 1972. Structural geology of the Henbury meteorite craters, Northern Territory, Australia. US Geological Survey Professional Paper 599–C, C1–C17.

Nininger, H.H., 1956. Arizona's meteorite crater. World Press Inc., Denver, 100–105.

Nininger, H.H. & Huss, G.I., 1960. The unique meteorite crater at Dalgaranga, Western Australia. Mineralogical Magazine, 32, 619.

Passey, Q.R. & Melosh, H.J., 1980. The effects of atmospheric breakup on crater-field formation. Icarus, 42, 211–233.

Rayner, J.M., 1939. Examination of the Henbury meteorite craters by the methods of applied geophysics. Report of the Australian and New Zealand Association for the Advancement of Science, Canberra, 24, 72–78.

Reeves, F. & Chalmers, R.O., 1949. The Wolf Creek Crater. Australian Journal of Sciences 11, 145–156.

Roddy, D.J., Pepin, R.O. & R.B. Merrill (editors), 1977. Impact and explosion cratering. Pergamon Press, New York.

Scott, E.R.D., Wasson, J.T. & Buchwald, V.F., 1973. The chemical classification of iron meteorites, VII: A re–investigation of irons with Ge concentrations between 25 and 80 ppm. Geochimica et Cosmochimica Acta, 37, 1957–1983.

Shoemaker, E.M., 1960. Penetration mechanics of high velocity meteorites, illustrated by Meteor Crater, Arizona. Proceedings of the 21st International Geological Congress, Copenhagen, Section 18, 418–434.

Shoemaker, E.M., 1962. Interpretation of lunar craters. In: Kopal, Z. (editor), Physics and astronomy of the Moon. Academic Press, New York and London, 283–359.

Shoemaker, E.M., 1963. Impact mechanics at Meteor Crater, Arizona. In: Middlehurst, B. & Kuiper, G.P. (editors), The Solar System, Volume IV: Moon, meteorites and craters. University of Chicago Press, Chicago, 301–336.

Shoemaker, E.M., Gault, D.E., Moore, H.J. & Lugn, R.V., 1963. Hypervelocity impact of steel into Coconino sandstone. American Journal of Science, 261, 668–682.

Shoemaker, E.M. & Shoemaker, C.S., 1988. Impact structures of Australia. Lunar and Planetary Science Conference, XIX, 1079–1080.

Shoemaker, E.M., Shoemaker, C.S., Nishiizumi, K., Kohl, C.P., Arnold, J.R., Klein, J., Fink, D., Middleton, R., Kubik, P.W. & Sharma, P., 1990. Ages of Australian meteorite craters — a preliminary report (abstract). Meteoritics, 25, 409.

Simpson, E.S., 1938. Some new and little-known meteorites found in Western Australia. Mineralogical Magazine, 25, 157–171.

Spencer, L.J. & Hey, M.H., 1933. Meteoritic iron and silica glass from the meteorite craters of Henbury (central Australia) and Wabar (Arabia). Mineralogical Magazine, 23, 387–404.

Stöffler, D., 1971. Progressive metamorphism and classification of shocked and brecciated crystalline rocks in impact craters. Journal of Geophysical Research, 76, 5541–5551.

Stöffler, D., 1972. Deformation and transformation of rock-forming minerals by natural and experimental shock processes. I: Behaviour of minerals under shock compression. Förtschritte der Mineralogie, 49, 50–113.

Stöffler, D., 1974. Deformation and transformation of rock-forming minerals by natural and experimental shock processes. II: Physical properties of shocked minerals. Förtschritte der Mineralogie, 51, 256–289.

Taylor, S.R., 1965. The Wolf Creek iron meteorite. Nature, 208, 944–945.

Taylor, S.R., 1967. Composition of meteorite impact glass across the Henbury strewnfield. Geochimica et Cosmochimica Acta, 31, 961–968.

Vdovykin, G.P., 1973. The Canyon Diablo meteorite. Space Science Reviews, 14, 758–731.

Wasson, J.T. & Kimberlin, J., 1967. The chemical classification of iron meteorites — II. Irons and pallasites with germanium concentrations between 8 and 100 ppm. Geochimica et Cosmochimica Acta, 31, 2065–2093.

Wasson, J.T., Schaudy, R., Bild, R.W. & Chou, C.L., 1974. Mesosiderites — I: Compositions of their metallic portions and possible relationship to other metal-rich meteorite groups. Geochimica et Cosmochimica Acta, 38, 135–149.

Wasson, J.T., Ouyang, X., Wang, J. & Jerde E., 1989. Chemical classification of iron meteorites. XI: Multi–element studies of 38 new irons and the high abundance of ungrouped irons from Antarctica. Geochimica et Cosmochimica Acta, 53, 735–744.

White, J.S., Henderson, E.P. & Mason, B., 1967. Secondary minerals produced by weathering of the Wolf Creek meteorite. American Mineralogist, 52, 1190–1197.

Wichman, R.W. & Schultz, P.H., 1994. In: Dressler, B., Grieve, R.A.F. & Sharpton, V.L (editors), Large meteorite impacts and planetary evolution. Geological Society of America, Special Publication 293, 61–72.

Yang, W. & Ahrens, T.J., 1995. Impact jetting of geological materials. Icarus, 116, 269–274.

Yeates, A.N., Crowe, R.W.A. & Towner, R.R., 1976. The Veevers Crater: a possible meteoritic feature. BMR Journal of Australian Geology & Geophysics, 1, 77–78.

AGSO Journal of Australian Geology & Geophysics, 16 (4), 431–442

Magnetic signature and morphology of the Acraman impact structure, South Australia

G.E. Williams[1], P.W. Schmidt[2] & D.M. Boyd[1]

Acraman is a major complex impact structure located in the Mesoproterozoic Gawler Range Volcanics of the Gawler Craton, South Australia, and has parts of its distal ejecta preserved in late Neoproterozoic (~590 Ma) strata of adjacent basins. Geomorphology and satellite images reveal a severely degraded structure comprising a near-circular central topographic depression 30 km across and arcuate features at 85–90 and ~150 km diameter. Disrupted bedrock of Yardea Dacite displaying shatter cones, shatter cleavage, and multiple sets of planar shock lamellae in quartz grains, and a dyke of melt rock, crop out at the centre of the structure.

High-resolution digital aeromagnetic data (400-m line-spacing, 80-m ground clearance) for Acraman reveal a conspicuous circular magnetic low, 20 km in diameter, exhibiting subdued magnetic relief and a central high-amplitude dipolar anomaly. A subdued magnetic signature in places reaches ~30 km diameter, which is at the limit of the topographic depression and disrupted dacite bedrock. Several discontinuous magnetic lineaments that roughly parallel the boundary of the circular magnetic low occur at 85–90 km diameter. The 20-km-diameter magnetic low is unrelated to topography, and its subdued character evidently reflects a measured decrease in susceptibility of the disrupted dacite relative to undisturbed dacite. The central dipolar anomaly, whose axis is deflected by remanent magnetisation with a direction similar to that of the melt rock, may indicate a concentration of impact melt material at shallow depth that was magnetised in the ambient geomagnetic field at the time of the impact.

Acraman originally was a complex crater with central peak. Suggested original diameters of major structural features are ~20 km ('peak ring' and central uplift marked by the magnetic low), ~40 km (estimated extent of transient cavity/excavated area), 85–90 km (possible final structural rim of the collapse crater), and ~150 km (possible outer limit of structural disturbance). The ratio of estimated original diameters of adjacent structural features is about 2, which is near the upper limit suggested by theoretical models and the dimensions of other terrestrial complex impact structures.

Introduction

The Acraman structure on the Gawler Craton, South Australia (Fig. 1), is a major complex impact structure (Williams 1986, 1987, 1994a, b). It is distinguished among known terrestrial impact structures in having parts of its widely dispersed distal ejecta blanket of shattered bedrock preserved, 220–470 km distant from the site of impact, in late Neoproterozoic (~590 Ma) strata of the Adelaide Geosyncline (or Adelaide 'Foldbelt') and Officer Basin (inset, Fig. 1; Gostin et al. 1986, 1989; Compston et al. 1987; Wallace et al. 1989, 1990a–c).

Acraman lies almost entirely within the Yardea Dacite of the Gawler Range Volcanics, a Mesoproterozoic continental suite of mainly acid lavas and ash flows (Giles 1988; Creaser & White 1991). U–Pb zircon geochronology indicates an age of 1592 ± 3 Ma for the Yardea Dacite and a pooled age of 1592 ± 2 Ma for extrusion of the Gawler Range Volcanics (Fanning et al. 1988). The undeformed volcanics now cover more than 25 000 km^2, and outlying remnants indicate that formerly the suite was much more extensive. Gravity modelling suggests that the volcanics have a full thickness of ~4 km. The Yardea Dacite, the uppermost and most widespread unit of the Gawler Range Volcanics, crops out continuously over 12 000 km^2. It has an exposed thickness of 250 m but probably is much thicker, and an unknown thickness has been removed by erosion. The Yardea Dacite ranks as one of the world's largest felsic volcanic units, and shows remarkable mineralogical and geochemical homogeneity over its outcrop area. No unequivocal evidence for volcanism of the 'caldera-collapse–resurgence' type is known from the Gawler Range Volcanics (Creaser & White 1991). Intrusion of the northwest–southeast-trending mafic Gairdner dyke swarm during the Neoproterozoic (Sm–Nd age of ~800 Ma; Zhao et al. 1994) was the last significant magmatic event in the Gawler Ranges region.

Intensely shattered and shock-deformed Yardea Dacite crops out in the southeastern part of Lake Acraman near the centre of the Acraman structure. Broken surfaces of disrupted dacite commonly display shatter cleavage and small (<3 cm long) shatter cones, and larger shatter cones up to 15 cm long occur locally. All the shattered rocks studied show microscopic evidence of fracturing and deformation in feldspar phenocrysts and other mineral grains, including quartz, zircon, and apatite. From 5–90 per cent of quartz grains in thin sections of shattered dacite from the central area exhibit closely spaced parallel planar lamellae decorated with cavities and finely divided material. As many as four different sets of lamellae have been observed in the same grain. Such planar features indicate type C shock deformation, and shock pressures of ~15 GPa (Robertson et al. 1968). Shock lamellae in one or more sets occur also in some feldspar grains. Unshattered fine-grained melt rock, probably a dyke below the former crater floor, also occurs in the central area. The extent of the central area of intense shattering, shock metamorphism, and melt rock is uncertain because of the sparse outcrop. Microscopic evidence of shock deformation of minerals has not been observed in bedrock outside this central area.

This paper reviews evidence from geomorphology and satellite images and presents new high-resolution digital aeromagnetic data that together reveal Acraman as a severely degraded complex impact structure.

Geomorphology and satellite images

Major geographic features of the Gawler Ranges region are shown in Figure 1, and a digital elevation image (Fig. 2) provides details of the topography. Lake Acraman is a young (Pleistocene) geographic feature eccentrically placed within a near-circular topographic depression ~30 km in diameter termed the 'Acraman depression' (Williams 1986). The surface of the Acraman depression slopes gently inward from an eleva-

[1] Department of Geology & Geophysics, University of Adelaide, Adelaide, SA 5005.
[2] CSIRO Division of Exploration & Mining, PO Box 136, North Ryde, NSW 2113.

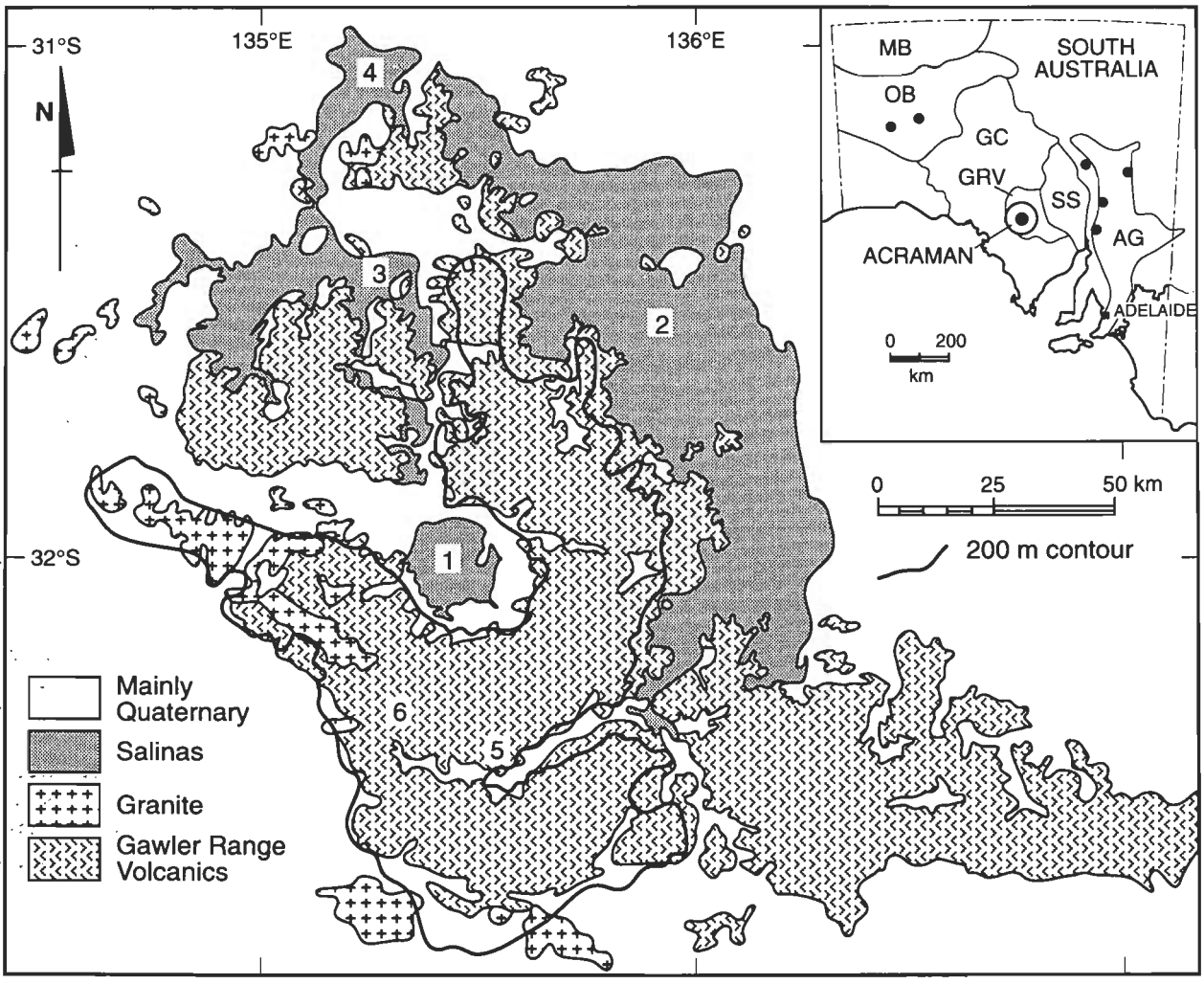

Figure 1. Geological map of the Gawler Ranges region, South Australia, showing distribution of the Mesoproterozoic Gawler Range Volcanics and coeval granites of the Hiltaba suite. 1, Lake Acraman, within the Acraman depression; 2, Lake Gairdner; 3, Lake Everard; 4, Lake Harris; 5, the Yardea corridor; 6, locality of closely jointed volcanics. The 200-m generalised contour is taken from the Port Augusta and Tarcoola 1:1 000 000 topographic sheets. Inset shows Acraman and the main localities of the late Neoproterozoic ejecta horizon (small solid dots) in the Adelaide Geosyncline and Officer Basin. AG, Adelaide Geosyncline; SS, Stuart Shelf; GRV, Gawler Range Volcanics; GC, Gawler Craton; OB, Officer Basin; MB, Musgrave Block.

tion of 180–200 m at the base of the surrounding ranges to 140 m near the edge of Lake Acraman; the lake bed is as much as 6 m below the level of the adjacent plain. Except in the northwest, the Acraman depression is ringed by the Gawler Ranges rising to 300 m above the lake bed. The Gawler Ranges are bordered to the east and north by low-lying country that contains Lake Gairdner (elevation 113–121 m) and to the northwest by Lakes Everard and Harris (121–124 m). The ranges thus form a 25–30-km-wide annulus of higher ground around the Acraman depression that is breached only in the northwest.

The Yardea corridor (Williams 1986), 30 km south of the Acraman depression, comprises several nearly straight valleys as much as 3 km wide that link up to form an arcuate feature extending for at least 70 km roughly parallel to the southern margin of the depression (Figs. 1 and 2). A fault has been mapped along the Yardea corridor for 35 km (Blissett 1987; Blissett et al. 1988).

A NOAA–AVHRR satellite infrared night image (Fig. 3) reveals the Acraman depression largely encircled at 85–90 km diameter by the Yardea corridor and other lineaments, which together produce a polygonal outline. A break in this feature occurs northwest of Lake Acraman where lineaments coincide with the outlet for Tertiary palaeodrainage to the north. An arcuate feature at ~150 m diameter includes a line that passes through Lakes Gairdner and Everard and may extend to the southern margin of the Gawler Ranges south of Lake Acraman.

A Landsat scene of most of the Acraman structure (Fig. 4) shows the Acraman depression and part of the Yardea corridor. The arcuate feature is evident at ~150 km diameter, extending 170 km from the southeastern corner of Lake Gairdner northwestward to Lake Everard. As noted by Williams (1994b), apparent changes in character of the lake deposits and salt crust across the arc through Lake Gairdner suggest that the line may mark basement structure or buried topography.

The Landsat scene shows that erosion of the Gawler Range Volcanics is strongly influenced by joints and structural lineaments. The dominant regional trend of valleys in the Yardea Dacite is northeast–southwest; other trends are between north–south and northwest–southeast. In addition, several straight structural corridors 3 to 10 km wide, marked by subdued outcrop and small

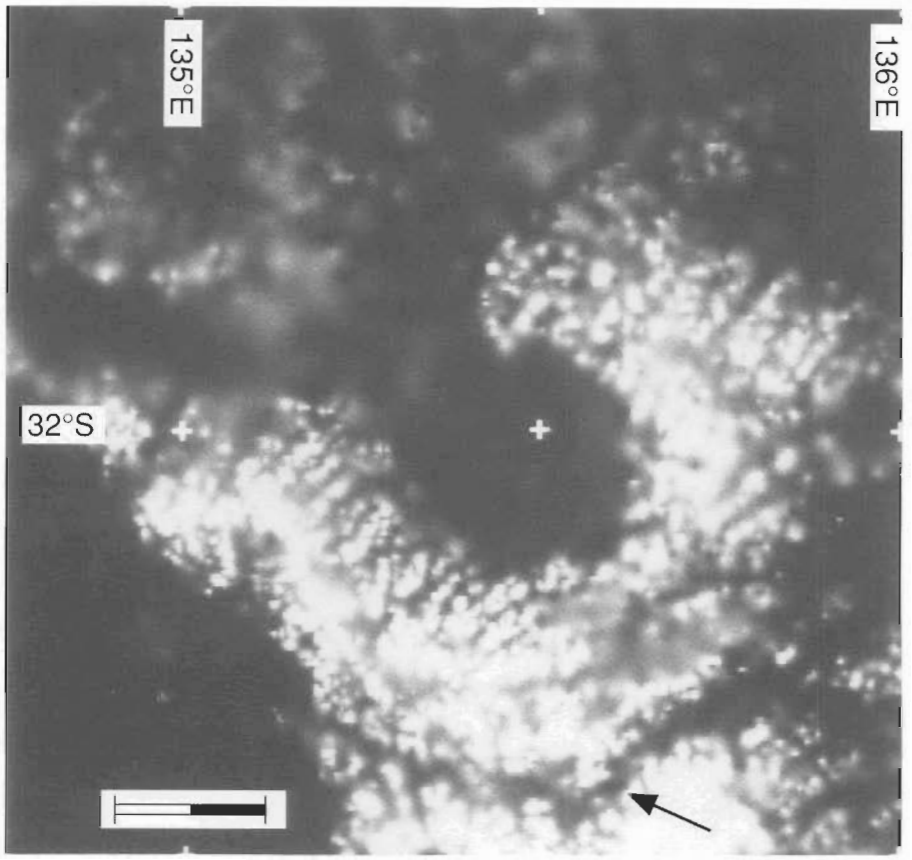

Figure 2. Digital elevation image (greyscale, light = high elevations, dark = low elevations) of the Gawler Ranges region, showing the Acraman depression surrounded by an annulus of elevated country, and the Yardea corridor (arrow). Scale bar 20 km. Image derived from data supplied by AUSLIG, Australia's national mapping agency, and reproduced by permission of the General Manager, Australian Surveying and Land Information Group, Department of Administrative Services, Canberra, ACT. Data processed by BHP Minerals, Melbourne.

depressions with salinas, traverse the Gawler Ranges region. The intersection of two lineaments and the palaeodrainage outlet northwest of Lake Acraman accounts for the paucity of outcrop in that area. The joint and fracture patterns in the volcanics evidently are of great antiquity, having influenced the form of a palaeosurface buried by Mesoproterozoic (~1400 Ma) sandstones in the eastern Gawler Ranges (Campbell & Twidale 1991).

Satellite images thus confirm geographic and topographic evidence that the main geomorphological features of the Gawler Ranges are centred on the Acraman depression. This regional arrangement of geomorphological features is unrelated to the stratigraphy of the Gawler Range Volcanics.

Magnetic signature

High-resolution digital aeromagnetic data for the Gawler Craton was released by Mines and Energy South Australia (MESA) in 1993 as part of the South Australian Exploration Initiative (Drexel et al. 1993; Preiss 1993). The surveys were flown at a constant 400-m line-spacing along designated northings and eastings; the altitude specification was 80 ± 20 m continuous ground clearance, but the typical standard deviation of ground clearance attained was ± 5 m (Tucker 1993).

Digital images

An ER Mapper image of total magnetic intensity (Fig. 5) shows that Acraman is marked by a circular low with subdued magnetic relief that is conspicuous among other geological and structural features (Fig. 6). More detailed ER Mapper images of total magnetic intensity (Fig. 7), downward continuation 1 (Fig. 8), total magnetic intensity with sun angles from the northwest and northeast (Fig. 9A, B), and high pass (Fig. 9C) show a circular feature ~20 km in diameter marked by generally subdued magnetic relief, an inner area about 12 km across that displays less subdued magnetic relief, and a central high-amplitude dipolar anomaly. An outer zone of magnetic disturbance with partly subdued relief extends from about 20 to 30 km diameter, best shown to the northeast and east. The full extent of the magnetic disturbance thus coincides with the limits of the Acraman depression and the presumed present extent of disrupted Yardea Dacite.

The central dipolar anomaly (Fig. 9D), located at latitude 32°02'26"S, longitude 135°27'54"E, comprises a high 1–2 km across and a sinuous low that trends west-northwest for 5.5 km. The dipolar anomaly occurs at the southwestern margin of a roughly circular area ~4 km across that is marked by an irregular magnetic response.

The aeromagnetic images reveal conspicuous northeast–southwest lineaments (strike ~40°) in the Yardea Dacite to the northeast of Acraman; several of these features coincide with straight valleys that evidently are controlled by structural lineaments in the Gawler Range Volcanics (Fig. 4). These magnetic lineaments are truncated by the northeastern part of the 20-km-diameter circular magnetic low, and are discernible although subdued in the southwestern part of that feature. Discontinuous north–south lineaments in the eastern part of the aeromagnetic images also appear to be truncated or subdued by the circular magnetic low. These observations suggest that the sets of northeast–southwest- and north–south-trending magnetic lineaments in the Yardea Dacite, which comprise groups of parallel (not radial) lineaments (Fig. 6), record structures predating the formation of the circular low. Arcuate lineaments just outside and parallel to the margin of the circular low, best shown in the north and southwest, suggest contemporaneity with that feature.

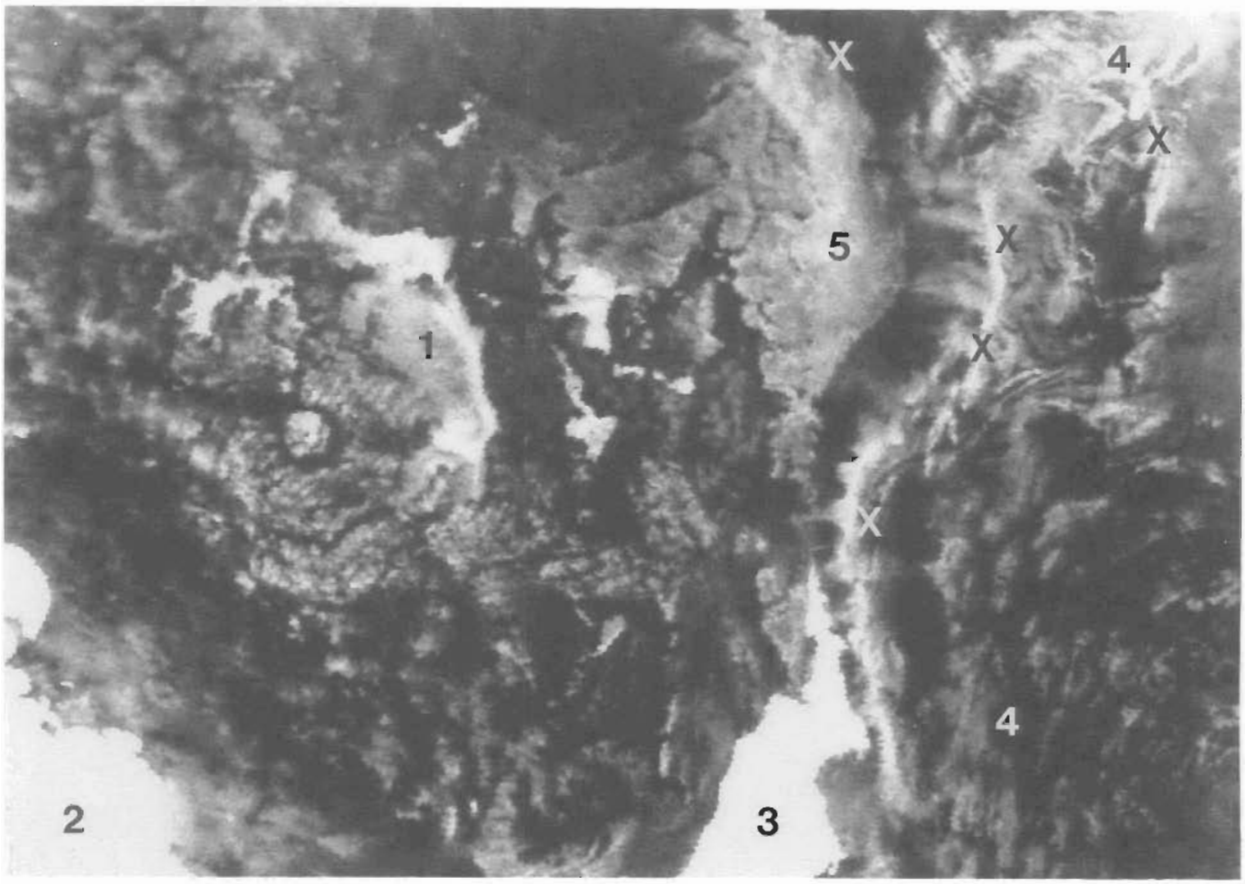

Figure 3. Thermal infrared night image of northern South Australia taken by NOAA satellite. Warm areas including the sea and some salinas appear white, cool areas dark. The Acraman structure appears as a large ringed feature in the western part of the scene, comprising a dark, circular inner area (Acraman depression) that contains Lake Acraman (paler tone) and arcuate features at 85–90 km (dark, polygonal corridor) and ~150 km diameter. The structure is breached in the northwest by northwest–southeast and north–south lineaments. Geographic features include: 1, Lake Gairdner; 2, Great Australian Bight; 3, Spencer Gulf; 4, Flinders Ranges (northern Adelaide Geosyncline); 5, Lake Torrens. Crosses mark important ejecta localities as much as 350 km from Acraman. NOAA9–AVHRR Band 3, Orbit no. 2246, 21 May 1985, 2200 hours. Image geometrically corrected, Lambert conic conformal projection; processed by BHP Minerals, Melbourne.

In addition, magnetic lineaments trending northwest–southeast and northeast–southwest coincide with the Yardea corridor to the south of the circular low, at 85–90 km diameter (Figs. 5 and 6), and confirm the presence of faults in this area. Magnetic features of uncertain origin trending west-northwest to east–west cut across basement structure at ~88 km diameter to the northeast and north of the circular low. No magnetic feature of seeming relevance to Acraman is evident at ~150 km diameter.

Modelling of the central dipolar anomaly

The central dipolar anomaly has an amplitude of about +300/–500 nT and indicates a shallow magnetic source. Schmidt & Williams (1991) noted that the magnetisation direction of the subsurface source evidently is similar to the mean direction observed in melt rock which crops out near the centre of Acraman (declination = 48.3°, inclination = 54.7°, α_{95} = 5.2°) and causes the axis of the anomaly to be deflected to the northeast (clockwise). The melt rock acquired its remanent magnetisation upon cooling immediately after the impact (thermoremanent magnetisation, with titanomagnetite carrier).

If remanent magnetisation is ignored and induced magnetisation alone is assumed to be the source of the magnetic anomaly, a dipping prismatic body is not applicable for closely modelling the magnetic profile. A prism with a moderate or steep dip produces an anomaly that is too symmetric. The form of the main part of the anomaly is clearly antisymmetric because the low to the southwest and the high to the northeast are of the same order, albeit of opposite sign. Although the main part of the anomaly can be matched by a gently dipping prism, albeit of an unrealistically large susceptibilty (required to compensate for the reduced thickness of gently dipping bodies), there is no corresponding anomaly for the bottom of the prism, which would be shallow because of the required low dip. An alternative is for the prism to extend to great depth, which would stipulate a pencil-shaped body subparallel to the surface. However, this is geologically unacceptable. Moreover, from measurements of outcrop samples, we suspect that remanent magnetisation contributes to the anomaly.

We have found that a spherical body magnetised by both induction and remanence yields a satisfactory fit to the main part of the anomaly, notwithstanding the ambiguity between ellipsoidal shapes and depths and the higher spacial frequencies present in the magnetic record, which we assume indicate shallow irregular sources in addition to the main body. This keeps the modelling as simple as possible, because we are fitting only four parameters—depth and radius of the sphere, and magnitudes of the susceptibility and remanence. The direction of

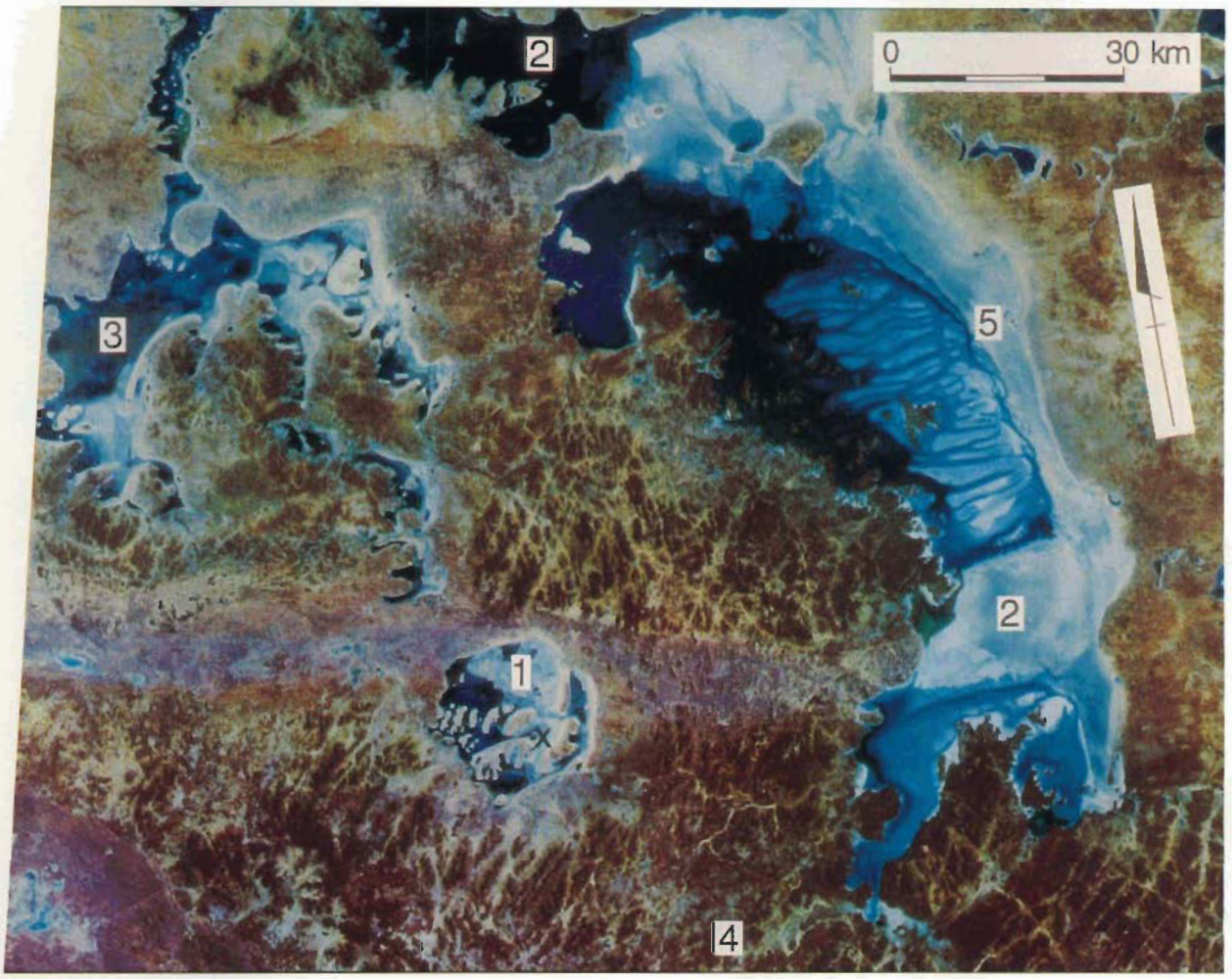

Figure 4. Landsat scene covering most of the Acraman structure, showing: 1, Lake Acraman within the Acraman depression; 2, Lake Gairdner; 3, Lake Everard; 4, the Yardea corridor at 85–90 km diameter. Surface water (darker blue) in Lake Gairdner helps define an arcuate trend (5) at ~150 km diameter that continues westward to Lake Everard. X marks the location of the central dipolar magnetic anomaly in the southeastern part of Lake Acraman (see Figs. 6–10), and shattered and shock-deformed dacite crops out in adjacent islands. The Gawler Range Volcanics are strongly jointed, and a northwest–southeast structural lineament occurs on the northern side of Lake Acraman. A Tertiary palaeodrainage course runs northward from the northwestern margin of the Acraman depression via a chain of small salinas and Lake Everard. Landsat scene 15 February 1973, scene centre S31–30 E135–51; processed by BHP Minerals, Melbourne.

the remanence is constrained by direct measurements on outcrop samples of melt rock (Schmidt & Williams 1991), although the magnetic properties estimated from measurements of the melt rock samples are too feeble to explain the observed anomaly. Remanence of outcrop samples commonly is affected by weathering and/or lightning, and whereas palaeomagnetic cleaning can isolate the original remanence direction the remanence magnitude is often irretrievable (Clark 1983).

In model 1 (Fig. 10A, B), a sphere 1167 m in diameter and centred at a depth of 1167 m was taken as the source body, together with estimated values for the following properties: susceptibility = 0.013 SI (0.001 cgs), natural remanent intensity = 0.5 A/m (500 μcgs), declination = 50°, inclination = 55°. The estimated Koenigsberger ratio is therefore 0.86. The magnetic anomaly arising from these estimated values is more than an order of magnitude smaller than that observed. Although magnetic properties an order of magnitude greater than the estimated values yield a magnetic anomaly of the required magnitude, anomalies of higher frequency in the record suggest that a sphere is a crude representation of the source body. The high-frequency anomalies superimposed on the main, deeper body may be apophyses or dykes radiating from the top of the body.

The tenfold discrepancy between the estimated values and those demanded by model 1 can be reconciled, or at least ameliorated, by increasing the volume of the body. This has been done in model 2 (Fig. 10C, D), in which the diameter has been doubled so the body just reaches the surface. The anomaly arising from the estimated values is clearly enhanced, but again is insufficient to adequately explain the observed anomaly. The form of the anomaly also is different, indicating that either a spherical source is incorrect or that the Koenigsberger ratio is incorrect. In the absence of further geological information, we explore here the implications of the latter suggestion, particularly since magnetic properties of surface samples are notoriously unrepresentative of the bulk properties at depth (Clark 1983). The best-fit values of properties are: susceptibility = 0.019 SI (0.0015 cgs), remanent intensity = 1.5 A/m (1500 μcgs), declination = 50°, inclination = 40°. This implies a Koenigsberger ratio of 1.72. If we have approximated the volume of the source body accurately, the estimated values of properties for the surface samples of melt rock are significantly smaller than values

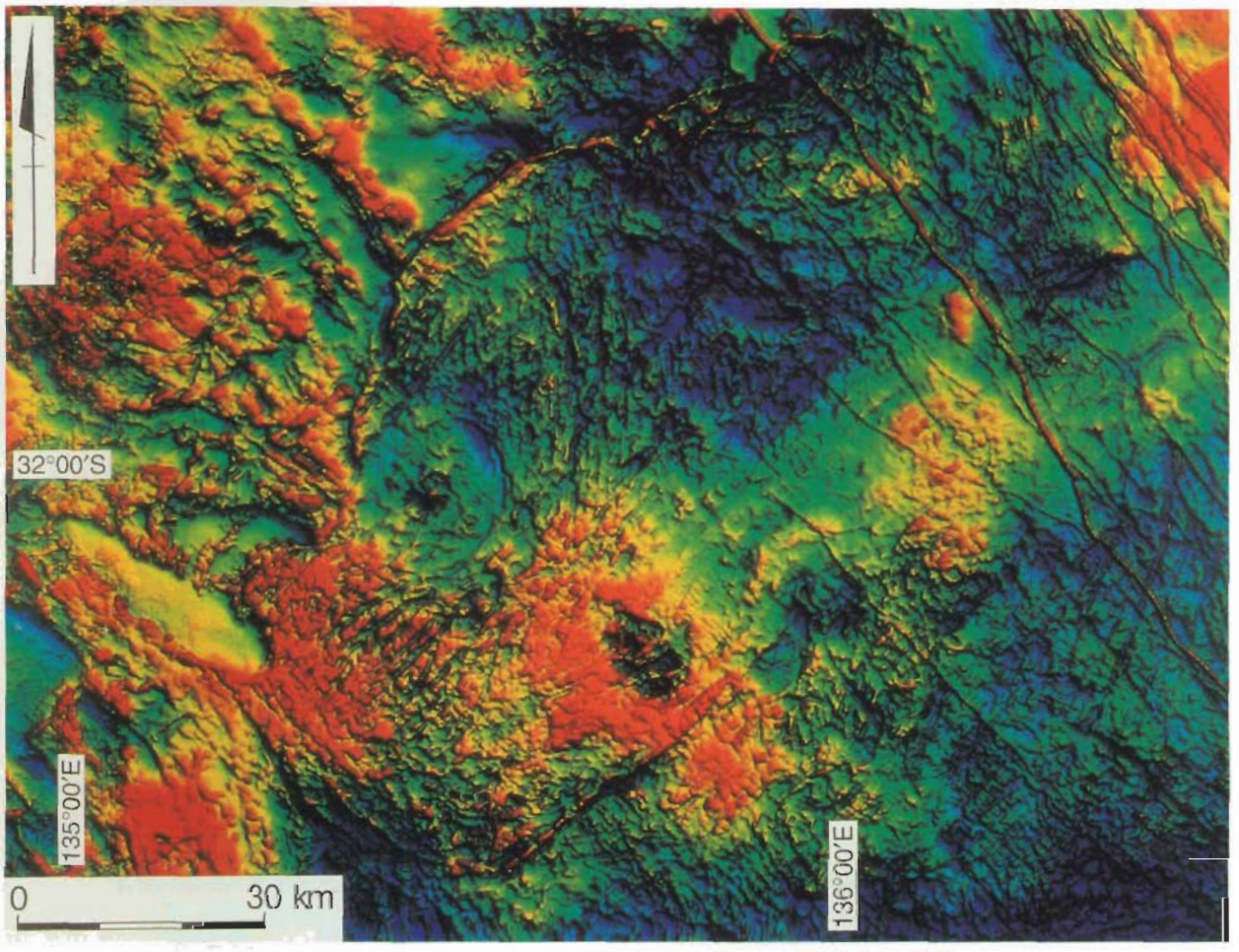

Figure 5. Aeromagnetic image of the Acraman area of the Gawler Craton (see text for details of the aeromagnetic survey), covering the area of the Landsat scene shown in Figure 4. ER Mapper file: total magnetic intensity, pseudocolor (Gaussian equalisation histogram stretch), sun angle from the northeast. Image processed by P. Freeman, MESA.

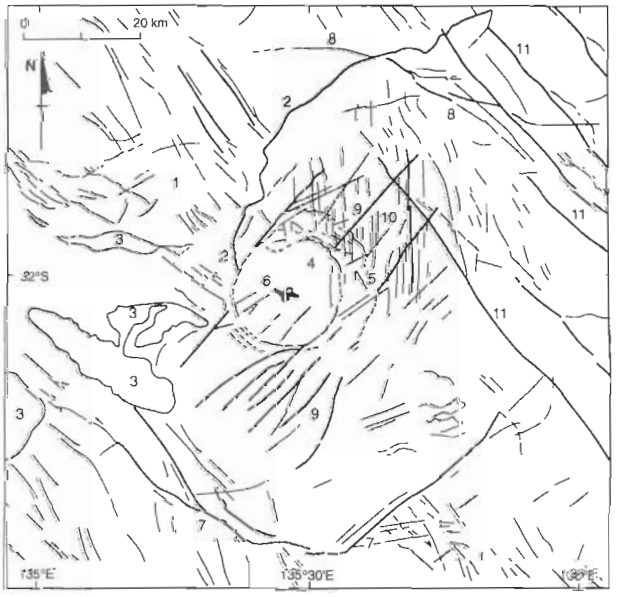

Figure 6. Prominent magnetic features of the Acraman area of the Gawler Craton indicated by several aeromagnetic images including that shown in Figure 5. 1, northwest–southeast trends in basement rocks beneath the lower Gawler Range Volcanics. 2, northwestern margin of the Yardea Dacite. 3, non-magnetic Mesoproterozoic granites of the Hiltaba suite. 4, magnetic low with subdued magnetic relief at Acraman (~20 km diameter). 5, limits of subdued magnetic signature at Acraman (~30 km diameter). 6, central dipolar anomaly. 7, faults associated with the Yardea corridor at 85–90 km diameter. 8, arcuate feature at ~88 km diameter. 9, northeast–southwest major lineaments in the Yardea Dacite. 10, north–south lineaments in the Yardea Dacite. 11, northwest–southeast mafic dykes of the Neoproterozoic Gairdner dyke swarm.

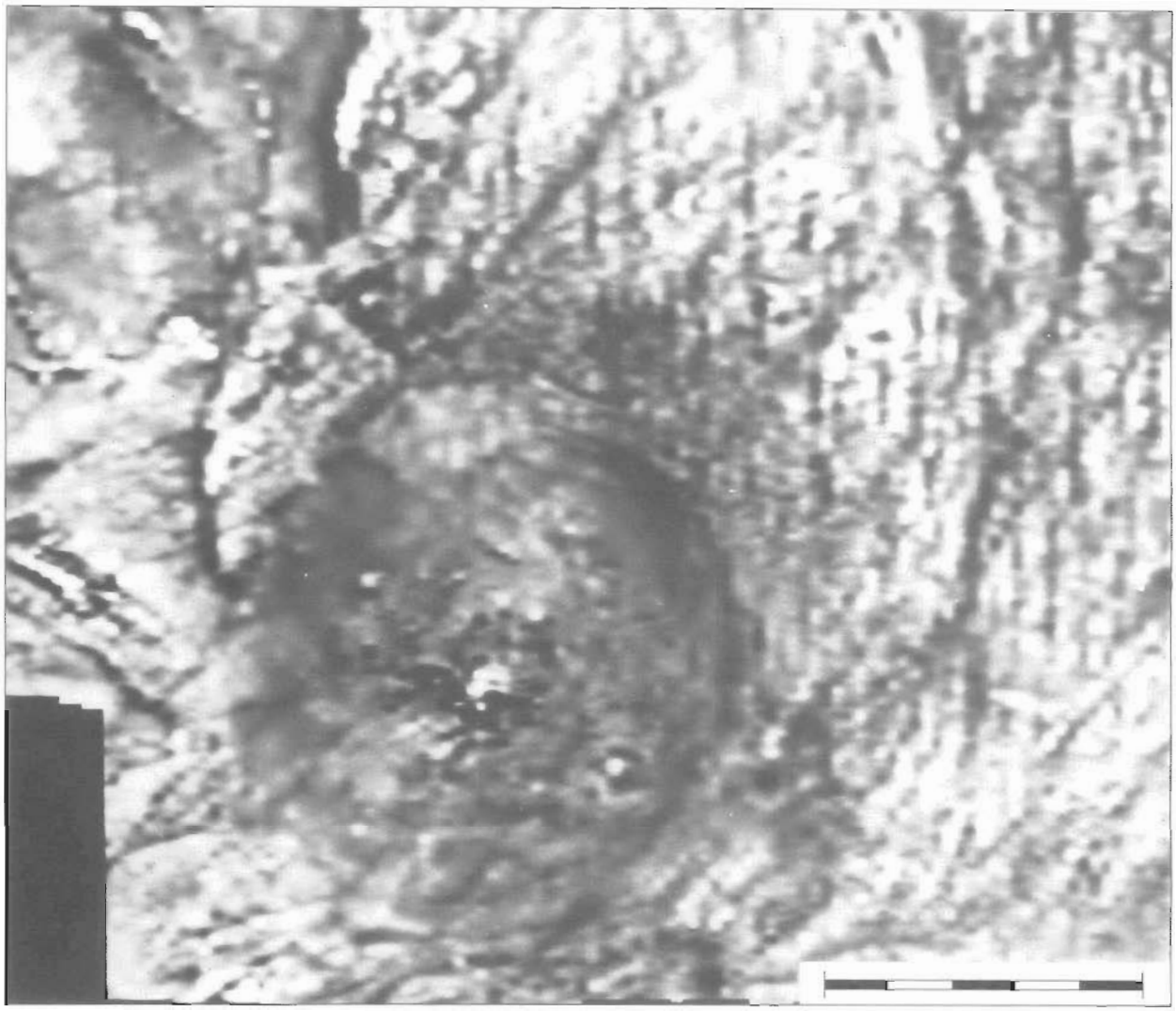

Figure 7. Aeromagnetic image of the central part of the Acraman structure (see text for details of the aeromagnetic survey). ER Mapper file: total magnetic intensity, greyscale, edges sharpen11. Scale bar 10 km; north to top of image. Aeromagnetic data provided by MESA.

for the bulk properties at depth. The susceptibility of the samples is lower by a factor of 2/3 and the remanent intensity is too low by a factor of three. Confirmation of these findings must await diamond drilling of the source body.

The results confirm that the magnetisation direction of the subsurface magnetic source is similar to that observed in the melt rock. The indicated body may be quite large, possibly about 2 km in diameter and centred about 1 km below the surface.

Origin of the magnetic signature

The magnetic field over the Gawler Range Volcanics is not influenced noticeably by regional topographic depressions like those of Lake Gairdner and Lake Everard, and the 20-km-diameter circular magnetic low is not centred on Lake Acraman (Figs. 4 and 5). Furthermore, specimens of shattered dacite from outcrops in the southeastern part of Lake Acraman show a 70 per cent decrease in magnetic susceptibility, on average, relative to values for specimens of undisturbed Yardea Dacite from outside the Acraman depression. These observations strongly suggest that the 20-km-diameter magnetic low at Acraman does not result from topography but records a decrease in susceptibility. The melt rock has a mean magnetic susceptibility nearly twice that of undisturbed Yardea Dacite.

The most common magnetic signature associated with impact structures is a magnetic low with subdued magnetic relief, caused by a reduction in susceptibility (Pilkington & Grieve 1992). The presence at Acraman of a circular magnetic low with subdued magnetic relief, and the reduced magnetic susceptibility of the shattered dacite, therefore strongly support an impact origin for the Acraman structure.

The central dipolar anomaly at Acraman equates with the central high-amplitude magnetic anomalies displayed by many impact structures, including all those >40 km in diameter (see Pilkington & Grieve 1992). The central anomaly may reflect mafic basement rocks brought from great depth by structural uplift and remagnetised by the impact (shock remanent magnetisation; Pilkington & Grieve 1992), or a concentration of impact-produced melt rock or melt-bearing breccia; in either case, the source body was magnetised in the ambient geomagnetic field at the time of the impact. Modelling of the anomaly indicates that the top of the source body may be close to the surface. However, the anomaly occurs in an area of Lake Acraman

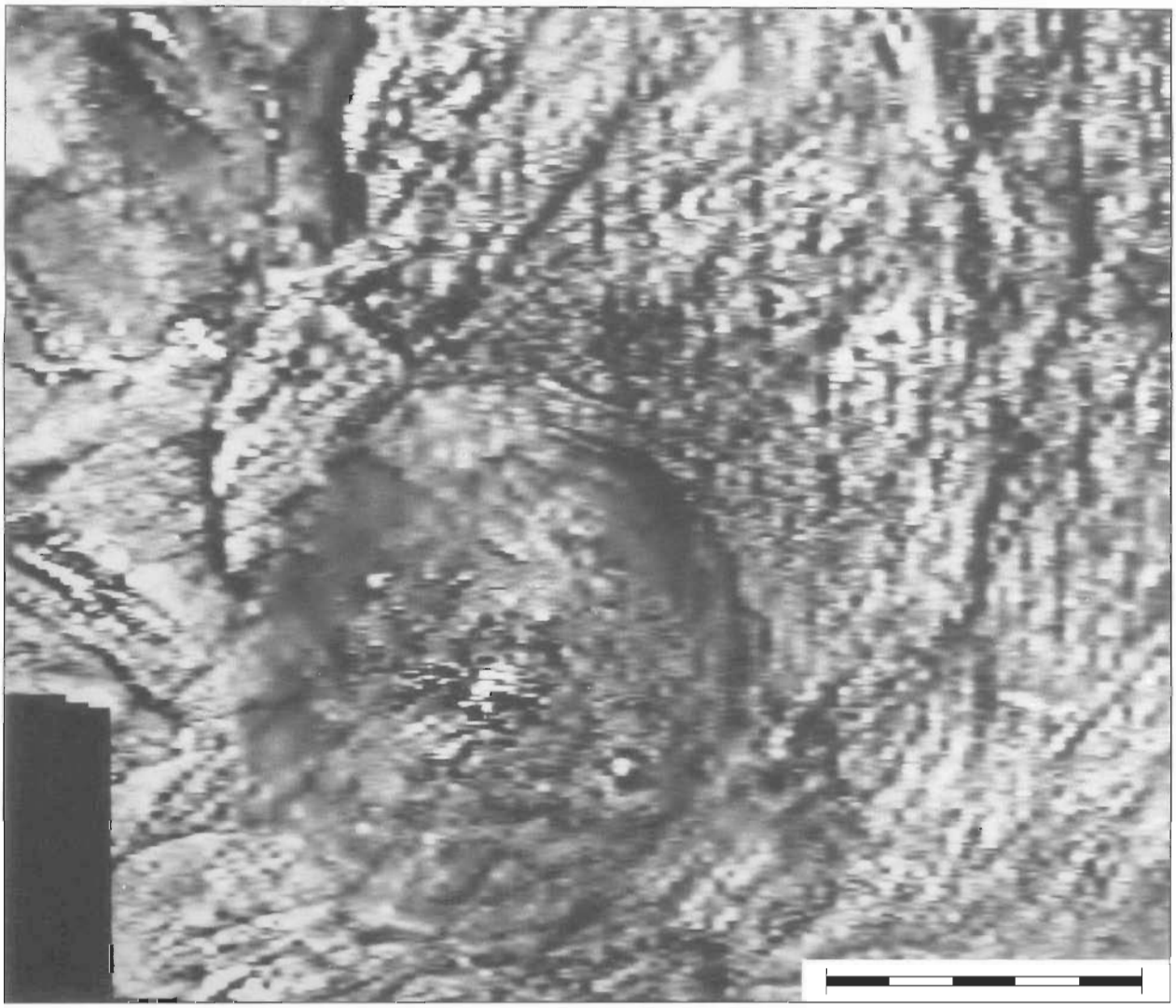

Figure 8. Aeromagnetic image of the central part of the Acraman structure (see text for details of the aeromagnetic survey). ER Mapper file: downward continuation 1, greyscale. Scale bar 10 km; north to top of image. Aeromagnetic data provided by MESA.

with no bedrock outcrop (Fig. 4), and drilling will be required to determine the nature of the magnetic source below the lake bed.

Pilkington & Grieve (1992) observed that the regional magnetic signature of impact structures is often complicated by large variations in the magnetic properties of the basement rocks. The conspicuous magnetic signature for Acraman — to our knowledge the clearest regional digital magnetic image recognised for an impact structure — is attributable to the high quality of the aeromagnetic data and the occurrence of Acraman in a thick and extensive body of flat-lying and remarkably homogeneous volcanics.

Discussion

Impact origin of the Acraman structure

Acraman displays numerous criteria for the identification of terrestrial impact structures: circular plan, concentric structure, negative gravity anomaly, magnetic low with subdued magnetic signature and central high-amplitude magnetic anomaly, shocked central area, intense brecciation and reduced magnetic susceptibility of bedrock, shatter cones in bedrock, multiple sets of planar shock lamellae in quartz grains in shattered bedrock, and presence of melt rock (Williams 1994a, b). Indeed, Acraman qualifies on virtually all criteria given by Dence (1972) for the identification of ancient terrestrial impact structures. In addition, Acraman evidently has part of its distal ejecta blanket of shattered volcanic bedrock preserved in the ~590-Ma Bunyeroo Formation of the Adelaide Geosyncline and in the correlative Rodda beds of the Officer Basin (inset, Fig. 1; Gostin et al. 1986; Compston et al. 1987; Wallace et al. 1989, 1990c). The ejecta horizon is anomalous in cosmogenic siderophile elements, including Ir, and locally contains abundant altered microtektite-like spherules and shard-like clasts (Gostin et al. 1989; Wallace et al. 1989, 1990a–c). These observations argue forcibly that the Acraman structure is of impact origin.

The ejecta horizon in the Bunyeroo Formation 220–350 km east of Acraman ranges from 0 to 40 cm in thickness, but usually is <10 cm thick, and contains clasts up to 50 cm in diameter (see Wallace et al. this issue). True thicknesses of ejecta that fell in the Adelaide Geosyncline may be less than maximum measured thicknesses in the Bunyeroo Formation because some ejecta might have been redeposited. Any development of ejecta rays also would have caused lateral variation in ejecta thickness.

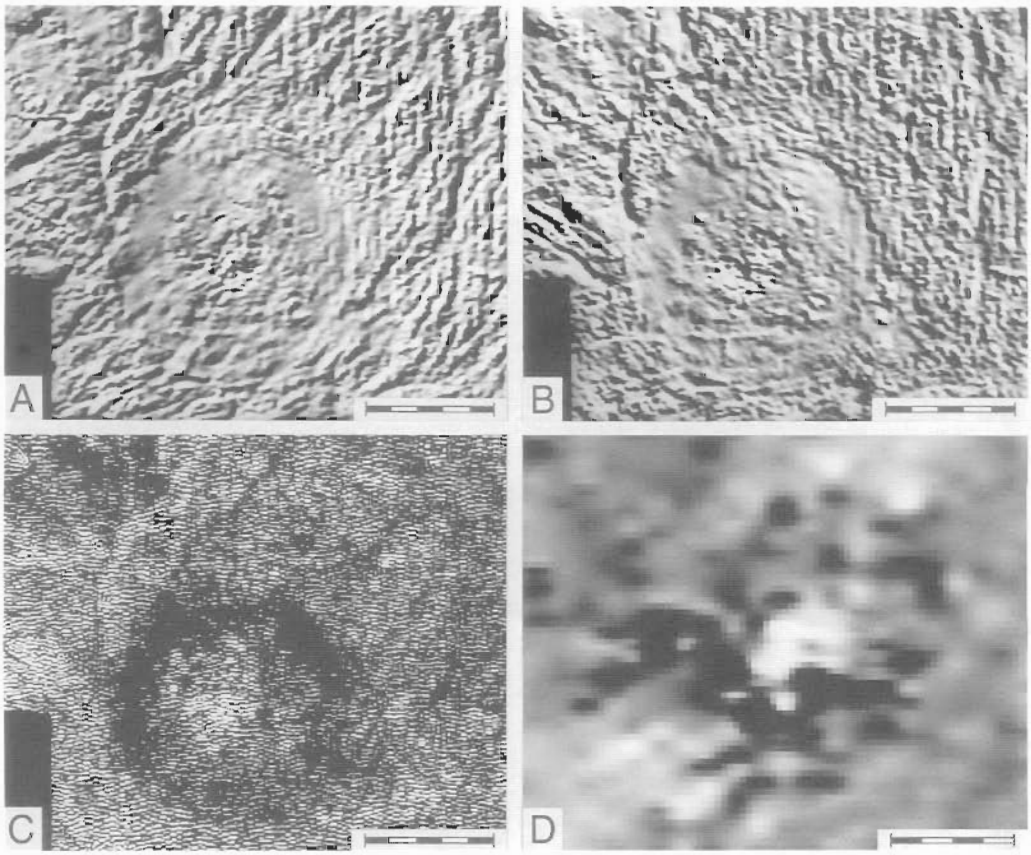

Figure 9. Aeromagnetic images of the central part of the Acraman structure (see text for details of the aeromagnetic survey). ER Mapper files. North to top of images. (A) Total magnetic intensity, greyscale, sun angle from the northwest. Scale bar 10 km. (B) Total magnetic intensity, greyscale, sun angle from the northeast. Scale bar 10 km. (C) High pass 4, greyscale, with equalised histogram. Scale bar 10 km. (D) Enlargement of the central dipolar anomaly; total magnetic intensity, greyscale, edges sharpen11. Scale bar 2 km. Aeromagnetic data provided by MESA.

Given distances from the impact site are minima for the time of impact because subsequent folding and reverse faulting within the Adelaide Geosyncline during the Cambro-Ordovician Delamerian Orogeny would have shortened the distances between Acraman and eastern ejecta sites, possibly by tens of kilometres (Gostin et al. 1986). The sandy ejecta in the Officer Basin 470 km northwest of the impact site, seen only in drillcores, is <1 mm to 7 mm thick (Wallace et al. 1989).

Palaeomagnetic data support correlation of the Acraman impact and deposition of the ejecta horizon in the Bunyeroo Formation. The cleaned remanence direction for the melt rock that crops out at Acraman (declination = 48.3°, inclination = 54.7°) and the best-fit direction determined here for the central dipolar anomaly (declination = 50°, inclination = 40°), considering their virtual geomagnetic nature, are essentially identical with the pre-folding remanence direction (declination = 54.9°, inclination = 28.2°) determined from a recent palaeomagnetic study of the Bunyeroo Formation (P.W. Schmidt, unpublished data). These new data substantiate our earlier inference (Schmidt & Williams 1991), which relied on an inconclusive palaeomagnetic fold test, that the Acraman impact and deposition of the Bunyeroo ejecta horizon were contemporaneous.

Former morphology of the Acraman structure

Acraman displays 'erosional level 7' of Grieve & Robertson (1979), defined as 'crater floor removed, substructure exposed'. Such severe degradation is consistent with a late Neoproterozoic age for the impact. The estimated rate of erosion of the Gawler Range Volcanics since 100–200 Ma, and apatite fission-track data for bedrock from the centre of Acraman, suggest that erosion has lowered the land surface at Acraman by at least 2 km since the impact at ~590 Ma (Williams 1994a, b). Acraman appears never to have been buried and may be more degraded than some other, exhumed Proterozoic impact structures in Australia. The dimensions of the former crater at Acraman therefore must be estimated, with due caution, from the extent of disrupted rocks well below the former crater floor

The geomorphological, geological, and satellite observations and aeromagnetic data suggest that, before it was deeply eroded, Acraman was a complex crater with central peak. The 30-km-diameter Acraman depression, which evidently is underlain by disrupted rocks, provides a guide to the diameter of the transient cavity and excavated area: Williams (1994a, b) estimated that the transient cavity/excavated area may have been as much as 40 km in diameter, some 30 per cent greater than that of the present central (Acraman) depression. The validity of this estimate may be tested by independent observations. *Cratering* data (obtained from small-scale laboratory experiments, nuclear and high-explosive craters, terrestrial meteorite impact craters, and estimates for lunar craters) suggest that, over a wide range of scales, ejecta blanket thickness (T) decreases with radial distance (r) from a crater centre as:

$$T = 0.14R^{0.74}(r/R)^{-3.0} \text{ for } r \geq R \qquad (1)$$

where R is the transient cavity radius and all dimensions are in metres (McGetchin et al. 1973). According to equation (1), a

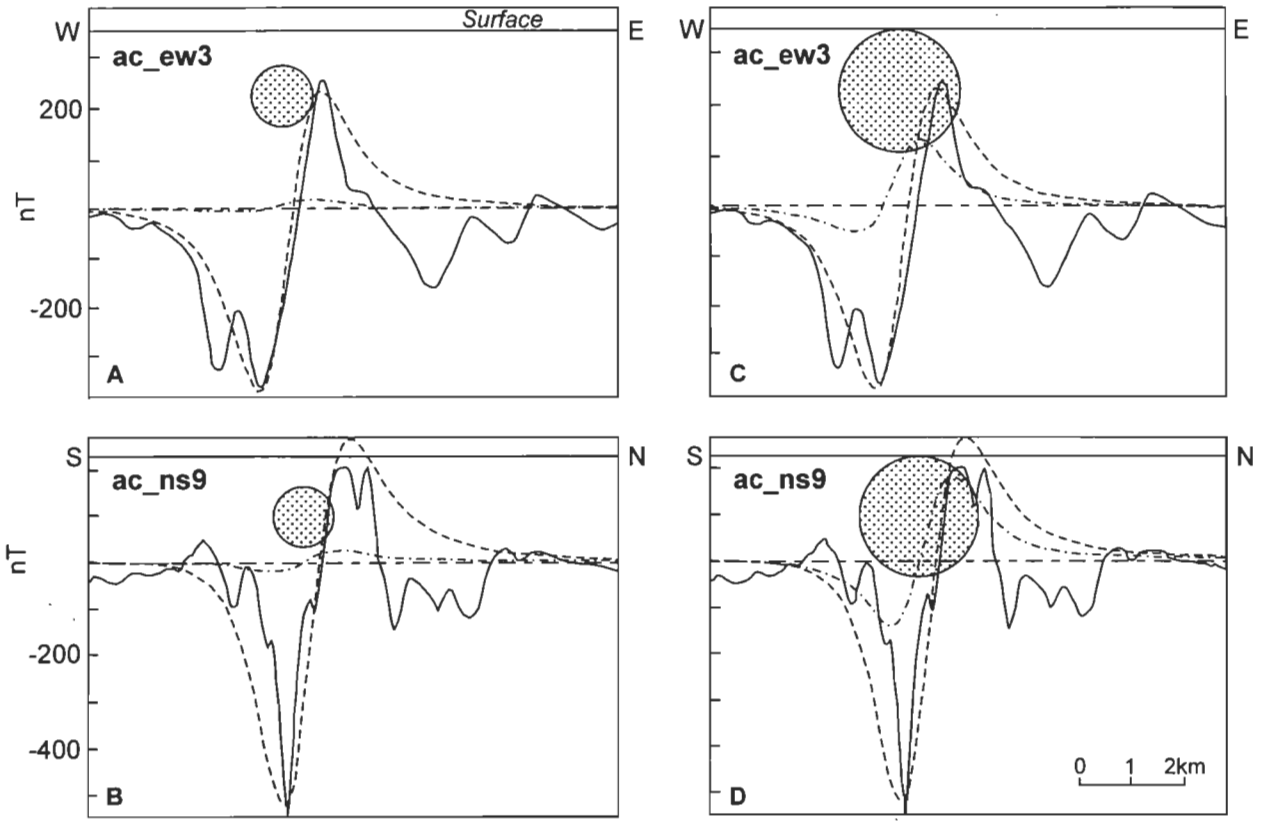

Figure 10. Two sets of modelled profiles oriented east–west and north–south and passing through the central dipolar anomaly. Continuous curves represent the observed anomalies, dashed curves represent best-fit profiles, and dot–dash curves represent profiles calculated from measured properties of surface samples of melt rock. The source bodies' centres are 1167 m deep, with diameters of 1167 m (A and B) and 2334 m (C and D). The Earth's field, taken from AGSO's Australian Geomagnetic Reference Field, has an intensity = 46 A/m (0.58 Oe), declination = 7° and inclination = –64°.

transient cavity of 20-km radius for Acraman gives a thickness for undisturbed ejecta of 16 cm at a radial distance of 220 km from the crater centre, a thickness of 4 cm at a distance of 350 km, and a thickness of 1.6 cm at a distance of 470 km. These estimated thicknesses for an undisturbed ejecta blanket at specific distances from a crater centre are of the same order as observed thicknesses for the ejecta horizons in the Bunyeroo Formation and Rodda beds at the same respective distances from the centre of Acraman. Hence the thickness distribution of the Bunyeroo–Rodda ejecta blanket is consistent with a 40-km-diameter transient cavity at Acraman.

The 20-km-diameter circular magnetic low is unlikely to mark the full extent of the transient cavity/excavated area at Acraman because the low occurs well within the present area of disrupted rocks marked by the Acraman depression. Furthermore, according to equation (1), a 20-km-diameter transient cavity provides ejecta thicknesses (1.2 cm at a radial distance of 220 km, 3.0 mm at 350 km, and 1.2 mm at 470 km) that are more than an order of magnitude smaller than those observed in the Bunyeroo Formation and Rodda beds at the same respective distances. Hence the extent of substantially reduced magnetic susceptibility of bedrock induced by the impact evidently was less than that of the transient cavity/excavated area. The form of the magnetic low (e.g., Fig. 9C) suggests it may record the extent of the 'peak ring' and highly disturbed rocks of the central uplift. Interestingly, the ~50-km-diameter circular magnetic feature at the deeply eroded 2000-Ma Vredefort impact structure in South Africa also is much smaller than the estimated original crater diameter of ~300 km (see Hart et al. 1995, and cover photograph and caption for Geology, vol. 23, no. 3, March 1995).

The original diameters of major structural features at Acraman therefore may have been ~20 km for the extent of the 'peak ring' and central uplift, ~40 km for the transient cavity/excavated area underlain by disrupted bedrock, 85–90 km for the possible final structural rim of the collapse crater, and ~150 km for arcuate lineaments possibly marking the outer limit of structural disturbance beyond the collapse crater. A transient cavity/excavated area 40 km in diameter would have been ~4 km deep, and an 85–90-km-diameter final collapse crater ~1.3 km deep (see Grieve 1991; Pilkington & Grieve 1992). The polygonal shape of the feature at 85–90-km diameter, exemplified by the fault-controlled Yardea corridor, implies that any final collapse occurred along pre-existing fractures; as discussed above, geological and aeromagnetic evidence confirms the existence of major lineaments and fractures in the Gawler Range Volcanics before the impact.

The ratio of estimated original diameters of adjacent structural features (larger:smaller) for Acraman is close to 2 (range 1.7 to 2.3). Theoretical models (Melosh & McKinnon 1978) suggest that the ratio of diameters of the final structural rim and transient cavity is between 1.2 and 2 for large craters. Grieve (1991) noted that the final crater diameter for crystalline targets (D_f) ranges from about $1.5D_e$ to $2D_e$ (where D_e is the diameter of obvious excavation of a terrestrial impact structure), and data from Lakomy (1990) give $D_f \approx (1.75 \pm 0.10)D_t$ (where Dt is the

transient cavity diameter) for seven Phanerozoic impact structures. Hence ratios for the estimated original dimensions of major structural features at Acraman approximate the upper limit suggested by theoretical models and the dimensions of other terrestrial complex impact structures. Such estimates and comparisons are tentative, however, because of the severe degradation of Acraman and the paucity of data for well-preserved large terrestrial craters.

Accurate comparison of the original dimensions of terrestrial impact structures in different geological settings and of different ages can be difficult because various degrees of degradation and exhumation usually are displayed. However, if the 85–90-km-diameter fault-controlled feature at Acraman indeed marks the position of the final structural rim of the collapse crater, Acraman would rank as the largest complex impact structure recognised in Australia. The dynamics of the Acraman impact are discussed by Williams (1994a, b) based on data in Schmidt & Holsapple (1982). A structure with a transient cavity/excavated area 40 km in diameter, as estimated for Acraman, indicates impactor kinetic energy of 6×10^{22} J, equivalent to 1.5×10^{7} megatons of explosive energy. Acraman could have resulted from impact with an Earth-crossing chondritic asteroid 4.7 km in diameter and of density 3.5 t m^{-3} moving at 25 km s^{-1} relative to the Earth.

Acknowledgments

We thank MESA for providing the digital aeromagnetic data; Prue Freeman of MESA for processing the image shown in Figure 5; John Willoughby, Irena Kivior, Mohammad Haidarian, Rick Barrett, and Dave Clark for assistance and discussion; and Shanti Rajagopalan for constructive comments on the manuscript. BHP Minerals, Melbourne, processed the Landsat, NOAA, and digital terrain data. Figure 2 is reproduced with the permission of the General Manager, Australian Surveying and Land Information Group, Department of Administrative Services, Canberra. Williams acknowledges the support of an ARC Senior Research Fellowship.

References

Blissett, A.H. (compiler), 1987. Geological setting of the Gawler Range Volcanics, Geological Atlas Special Series, 1:500 000. South Australian Department of Mines and Energy, Adelaide.

Blissett, A.H., Parker, A.J. & Crooks, A.F., 1988. Yardea map sheet, 1:250 000 Geological Series. South Australian Department of Mines and Energy, Adelaide.

Campbell, E.M. & Twidale, C.R., 1991. The evolution of bornhardts in silicic volcanic rocks in the Gawler Ranges. Australian Journal of Earth Sciences, 38, 79–93.

Clark, D.A., 1983. Comments on magnetic petrophysics. Bulletin of the Australian Society of Exploration Geophysicists, 14, 49–62.

Compston, W., Williams, I.S., Jenkins, R.J.F., Gostin, V.A. & Haines, P.W., 1987. Zircon age evidence for the late Precambrian Acraman ejecta blanket. Australian Journal of Earth Sciences, 34, 435–445.

Creaser, R.A. & White, A.J.R., 1991. Yardea Dacite — large-volume, high-temperature felsic volcanism from the Middle Proterozoic of South Australia. Geology, 19, 48–51.

Dence, M.R., 1972. The nature and significance of terrestrial impact structures. 24th International Geological Congress, Montreal, Section 15, 77–89.

Drexel, J.F., Preiss, W.V. & Parker, A.J. (editors), 1993. The geology of South Australia. Volume 1, The Precambrian. Geological Survey of South Australia, Bulletin 54.

Fanning, C.M., Flint, R.B., Parker, A.J., Ludwig, K.R. & Blissett, A.H., 1988. Refined Proterozoic evolution of the Gawler Craton, South Australia, through U–Pb zircon geochronology. Precambrian Research, 40/41, 363–386.

Giles, C.W., 1988. Petrogenesis of the Proterozoic Gawler Range Volcanics, South Australia. Precambrian Research, 40/41, 407–427.

Gostin, V.A., Haines, P.W., Jenkins, R.J.F., Compston, W. & Williams, I.S., 1986. Impact ejecta horizon within late Precambrian shales, Adelaide Geosyncline, South Australia. Science, 233, 198–200.

Gostin, V.A., Keays, R.R. & Wallace, M.W., 1989. Iridium anomaly from the Acraman impact ejecta horizon: impacts can produce sedimentary iridium peaks. Nature, 340, 542–544.

Grieve, R.A.F., 1991. Terrestrial impact: the record in the rocks. Meteoritics, 26, 175–194.

Grieve, R.A.F. & Robertson, P.B., 1979. The terrestrial cratering record. I. Current status of observations. Icarus, 38, 212–229.

Hart, R.J., Hargraves, R.B., Andreoli, M.A.G., Tredoux, M. & DoucourÈ, C.M., 1995. Magnetic anomaly near the center of the Vredefort structure: implications for impact-related magnetic signatures. Geology, 23, 277–280.

Lakomy, R., 1990. Distribution of impact induced phenomena in complex terrestrial impact structures: implications for transient cavity dimensions. Proceedings of the Lunar and Planetary Science Conference, 21, 676–677.

McGetchin, T.R., Settle, M. & Head, J.W., 1973. Radial thickness variation in impact crater ejecta: implications for lunar basin deposits. Earth and Planetary Science Letters, 20, 226–236.

Melosh, H.J. & McKinnon, W.B., 1978. The mechanics of ringed basin formation. Geophysical Research Letters, 5, 985–988.

Pilkington, M. & Grieve, R.A.F., 1992. The geophysical signature of terrestrial impact structures. Reviews of Geophysics, 30, 161–181.

Preiss, W.V. (editor), 1993. South Australian resources. Technical Sessions Abstracts, Mines and Energy South Australia, Adelaide.

Robertson, P.B., Dence, M.R. & Vos, M.A., 1968. Deformation in rock-forming minerals from Canadian craters. In: French, B.M. & Short, N.M. (editors), Shock metamorphism of natural materials. Mono Book Corporation, Baltimore, 433–452.

Schmidt, P.W. & Williams, G.E., 1991. Palaeomagnetic correlation of the Acraman impact structure and the Late Proterozoic Bunyeroo ejecta horizon, South Australia. Australian Journal of Earth Sciences, 38, 283–289.

Schmidt, R.M. & Holsapple, K.A., 1982. Estimates of crater size for large-body impact: gravity-scaling results. Geological Society of America, Special Paper 190, 93–102.

Tucker, D.H., 1993. Gawler Craton — airborne geophysics. In: Preiss, W.V. (editor), South Australian resources. Technical Sessions Abstracts, Mines and Energy South Australia, Adelaide, 6–11.

Wallace, M.W., Gostin, V.A. & Keays, R.R., 1989. Discovery of the Acraman impact ejecta blanket in the Officer Basin

and its stratigraphic significance. Australian Journal of Earth Sciences, 36, 585–587.

Wallace, M.W., Gostin, V.A. & Keays, R.R., 1990a. Acraman impact ejecta and host shales: evidence for low-temperature mobilization of iridium and other platinoids. Geology, 18, 132–135.

Wallace, M.W., Gostin, V.A. & Keays, R.R., 1990b. Spherules and shard-like clasts from the late Proterozoic Acraman impact ejecta horizon, South Australia. Meteoritics, 25, 161–165.

Wallace, M.W., Gostin, V.A. & Keays, R.R., 1996. Sedimentology of the Neoproterozoic Acraman impact-ejecta horizon, South Australia. AGSO Journal of Australian Geology & Geophysics, this issue.

Wallace, M.W., Williams, G.E., Gostin, V A. & Keays, R.R., 1990c. The Late Proterozoic Acraman impact — towards an understanding of impact events in the sedimentary record. Mines and Energy Review, South Australia, 57, 29–35.

Williams, G.E., 1986. The Acraman impact structure: source of ejecta in late Precambrian shales, South Australia. Science, 233, 200–203.

Williams, G.E., 1987. The Acraman structure — Australia's largest impact scar. Search, 18, 143–145.

Williams, G.E., 1994a. Acraman: A major impact structure from the Neoproterozoic of Australia. In: Dressler, B.O., Grieve, R.A.F. & Sharpton, V.L. (editors), Large meteorite impacts and planetary evolution. Geological Society of America, Special Paper 293, 209–224.

Williams, G.E., 1994b. Acraman, South Australia: Australia's largest meteorite impact structure. Proceedings of the Royal Society of Victoria, 106, 105–127.

Zhao, J., McCulloch, M.T. & Korsch, R.J., 1994. Characterisation of a plume-related ~800 Ma magmatic event and its implications for basin formation in central-southern Australia. Earth and Planetary Science Letters, 121, 349–367.

AGSO Journal of Australian Geology & Geophysics, 16 (4), 443–451

Sedimentology of the Neoproterozoic Acraman impact-ejecta horizon, South Australia

Malcolm W. Wallace[1], Victor A. Gostin[2] & Reid R. Keays[3]

The Acraman ejecta horizon is a thin (0–40 cm) sand/breccia unit consisting almost entirely of angular volcanic fragments. The horizon occurs within Neoproterozoic (~590 Ma) deep-water (below storm-wave-base) shales of the Adelaide Geosyncline (Bunyeroo Formation) and Officer Basin (Rodda beds). Much evidence points to the derivation of the horizon from Australia's largest meteorite impact feature, the Acraman structure, in the Gawler Ranges. The ejecta horizon contains anomalous quantities of Ir, Au, Pt, Pd, Ru, and Cr, consistent with a meteoritic source for the horizon. Other evidence for an impact-related origin is the presence of shattered mineral grains, multiple sets of planar shock lamellae within quartz phenocrysts, the occurrence of small shatter cones on clasts, and the presence of altered melt particles.

Two major sedimentological styles of ejecta occur in the Adelaide Geosyncline: type 1 ejecta sequences are characterised by a distinctive lonestone/breccia–sandy mudstone–graded-sandstone sequence whose clasts are almost perfectly sorted and normally graded; and type 2 sequences are characterised by weak normal grading, poor sorting, and common cross-lamination. Type 1 ejecta sequences are widespread in the central and eastern portions of the Adelaide Geosyncline, while type 2 sequences are more common in the western part of the Geosyncline. In the Officer Basin, the ejecta horizon consists of thin (0–0.7 cm) layers of sand-size angular volcanic clasts. We interpret type 1 sequences as primary fallout deposits whose perfect sorting and normal grading reflects suspension settling; and type 2 sequences as ejecta that have been completely reworked by impact-induced tsunamis.

When treated as a single sediment sample, the grainsize distribution in the type 1 ejecta sequences displays two quite distinct populations: the basal breccia forms a very poorly sorted population ($\sigma \approx 5\ \Phi$); and the graded sand constitutes a moderately well sorted population ($\sigma \approx 0.75\ \Phi$). These two grainsize populations might represent different transport modes: the breccia by fireball processes or ejecta flows, and the sand by atmospheric processes such as impact-induced air-blasts.

Introduction

Although the remnants of large meteorite impacts are fairly common features of the Earth's crust, preserved ejecta blankets from such impacts have rarely been identified in the sedimentary record. Thus the environmental and sedimentological effects of major meteoroid impacts are poorly constrained. The discovery of well-preserved and widely dispersed ejecta in Neoproterozoic sedimentary rocks in South Australia, linked to the Acraman impact structure, has provided a rare opportunity to analyse the sequence of sedimentary events that occurred immediately after a major impact. Here we report on the sedimentological and petrological characteristics of the Acraman ejecta, mainly from the Adelaide Geosyncline.

Geological setting

The Acraman impact structure (Fig. 1), situated in the Gawler Ranges, is the largest complex impact structure recognised in Australia (Williams 1986, 1987, 1994). It is centred on the Acraman depression (~30 km diameter), which is surrounded by a ring-shaped corridor 85–90 km in diameter and a possible outer ring feature about 160 km in diameter. The final collapse crater may have been 85–90 km in diameter, but the great age of the impact (~590 Ma) has resulted in several kilometres of erosion and removal of the former crater, so that only a multi-ring scar remains (Williams 1986, 1987, 1994).

The major rock type at the impact site is the Yardea Dacite, a unit of the mid-Proterozoic Gawler Range Volcanics. Outcrops of dacite within the Acraman depression are intensely fractured, and shatter cones are locally present. Evidence for an impact origin includes:

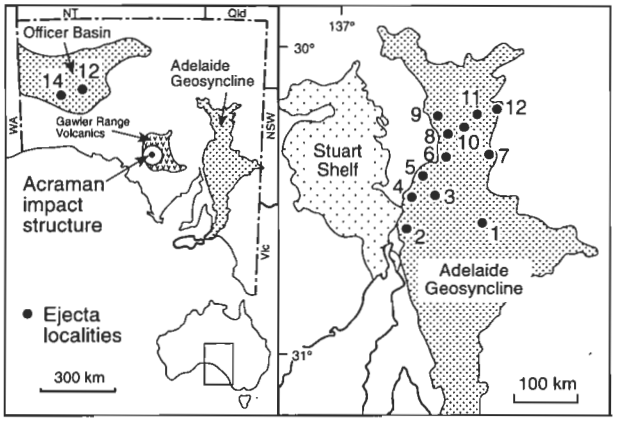

Figure 1. Location of Acraman impact site, and ejecta localities referred to in text. Localities are: 1, Bagalowie; 2, Pichi Richi Pass; 3, Yappala; 4, Warakimbo; 5, Merna Mora; 6, Bunyeroo Gorge–Brachina Gorge; 7, Reaphook Hill; 8, Parachilna Gorge; 9, Trebilcock Gap; 10, Donkey Valley; 11, Jubilee Mines; 12, Wearing Hills; 13, DDH Observatory Hill No. 1; 14, DDH Lake Maurice West.

- an abundance of shattered mineral grains (Gostin et al. 1986; Compston et al. 1987);
- the presence of multiple sets of shock lamellae within quartz phenocrysts (Gostin et al. 1986);
- the occurrence of small shatter cones on volcanic clasts;
- the presence of an Ir anomaly at the ejecta horizon (Gostin et al. 1989); and
- the presence of devitrified melt particles (Wallace et al. 1990b).

Several observations indicate that the Acraman impact structure is the source of coarse ejecta in the Adelaide Geosyncline and Officer Basin:

[1] School of Earth Sciences, University of Melbourne, Parkville, Vic. 3052 Australia.
[2] Department of Geology and Geophysics, Adelaide University, Adelaide, SA 5005.
[3] Department of Earth Sciences, Laurentian University, Sudbury, Ontario, Canada P3E 2C6.

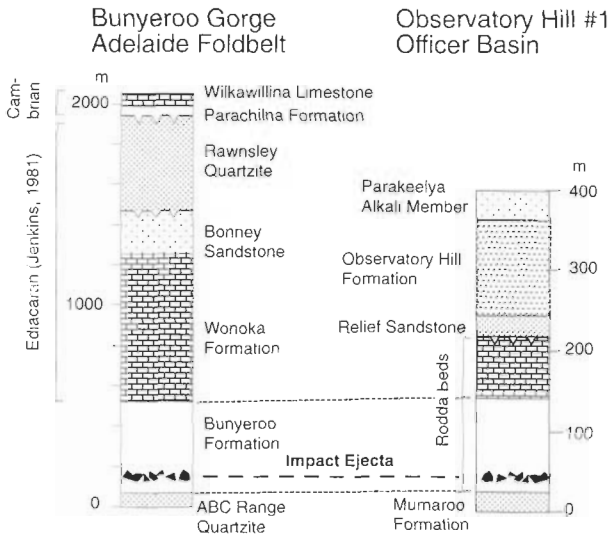

Figure 2. Stratigraphic position of the ejecta horizon within the Adelaide Geosyncline and the Officer Basin (modified from Wallace et al. 1989).

Figure 3. Ejecta horizon in outcrop (arrow), Donkey Valley. The prominent bed below the ejecta is a diagenetic carbonate horizon.

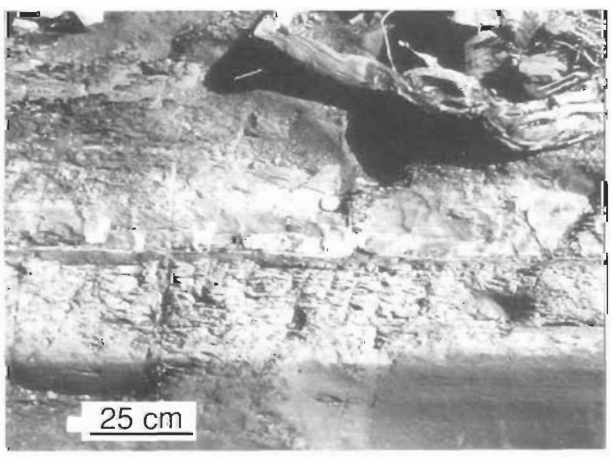

Figure 4. Ejecta horizon (arrow) surrounded by halo of reduced green shales, Bunyeroo Gorge.

- the acid volcanic clasts within the ejecta closely resemble the Yardea Dacite at the impact site;
- similar shock deformation is apparent within the ejecta clasts and within the Yardea Dacite at the impact site (Williams 1994);
- the isotopic age obtained from zircons within the ejecta (1575 ± 11 Ma) is similar to that obtained from the Gawler Range Volcanics (1592 ± 2 Ma; Compston et al. 1987; Fanning et al. 1988);
- the deep erosion of the Acraman impact structure accords with a Neoproterozoic age (Williams 1994); and
- palaeomagnetic data support correlation of the Acraman impact and deposition of the ejecta horizon in the Bunyeroo Formation (Schmidt & Williams 1991).

The Acraman impact-ejecta horizon is located within the Neoproterozoic (~590 Ma) Bunyeroo Formation (Figs. 2 and 3) in the Adelaide Geosyncline (Gostin et al. 1986), and in the contemporaneous Rodda beds in the Officer Basin (Wallace et al. 1989). Virtually all the clasts consist of pink–red porphyritic volcanic fragments that are commonly highly fractured.

The impact-ejecta horizon occurs from 40 to 80 m stratigraphically above the base of the Bunyeroo Formation (Fig. 2). Selected localities where the ejecta have been located are listed in Figure 1. The ejecta horizon has been located wherever the basal Bunyeroo shale is well exposed, and is laterally continuous over a wide area. However, the ejecta horizon is generally difficult to locate in the field because the host Bunyeroo shale commonly is poorly exposed.

The Bunyeroo Formation consists of a monotonous sequence of greyish red and greenish grey shale overlying the ABC Range Quartzite and its equivalents. It is extremely uniform; lithologies other than shale are rare. Thin (typically <0.5 cm thick) siltstone laminae occur locally in the shale. Thin bedding-parallel lamination is the most common sedimentary structure. The lowermost 30 m of the Bunyeroo Formation commonly contains dolomite concretions, particularly where the shale is greyish red. The ejecta horizon is readily identified in the field where it occurs in the greyish red shale, as it is almost invariably enveloped by green shale varying in thickness from a few millimetres to several metres (Fig. 4). Wallace et al. (1990a) interpreted these green shale envelopes to be a product of diagenesis and basinal fluid flow along the permeable ejecta horizon. The ejecta horizon is much less easily identified in the greenish grey shale, in which it lacks a green shale envelope.

The environment of deposition of the shale is unclear because it lacks sedimentary structures. Mawson & Segnit (1949) suggested that it was a loess because of its great thickness (~400 m in the western Adelaide Geosyncline) and homogeneity. Gostin & Jenkins (1983), however, regarded it as a deep-water marine deposit. Sandy horizons in the lower part of the overlying Wonoka Formation (the subdivision of Gostin & Jenkins 1983) have been interpreted as turbidites by Haines (1988). This indicates a moderately deep-water (below storm-wave-base) origin for this part of the succession. It appears likely that the lower part of the Bunyeroo Formation was deposited in a moderately deep-water shelf environment, as suggested by Preiss (1987).

The ejecta horizon in the Rodda beds of the Officer Basin (Fig. 2) was intersected in two diamond drillholes, Observa-

tory Hill No. 1 and Lake Maurice West (Fig. 1). In both drillholes, the ejecta horizon consists of sand laminae (1–7 mm thick) mainly composed of medium to coarse angular clasts of acid volcanic rock. It occurs in a mostly red shale unit of the Rodda beds, and is surrounded by a thin (~1 cm) green shale envelope similar to that in the Bunyeroo Formation of the Adelaide Geosyncline.

The Officer Basin ejecta horizon was identified in hand specimen by the distinctive red colour of the clasts, and is interpreted to be a correlative of the Acraman ejecta blanket on the basis of:

- the predominance of angular fragments of red acid volcanic rock;
- the presence of planar shock lamellae within the quartz phenocrysts in the acid volcanic fragments; and
- the presence of anomalously high concentrations of Ir and other precious metals similar to those found in the ejecta horizon in the Adelaide Geosyncline.

Although the Rodda beds contain numerous other fine sand and silt laminae, none of them apparently consist of sand-size angular acid volcanic fragments (Wallace et al. 1989).

Geochemistry

The ejecta horizon is strongly enriched in Ir, Au, Pt, Pd, Ru, and Cr. Iridium reaches a peak of 1.25 ppb at the ejecta horizon, which is over 50 times greater than the average red shale background of 0.02 ppb (Gostin et al. 1989). However, the acid volcanic target rock at the Acraman impact site has very low Ir, Au, Pt, Pd, and Cr values (Ir <0.005 ppb; Gostin et al. 1989). Since both the host red shale and the target rocks at the impact site are low in platinum metals, the most likely source of these elements within the ejecta horizon appears to be the impactor itself. The anomalously high Cr levels within the ejecta horizon are enigmatic, and the Cr may be enriched by some other process.

Analysis of individual layers within the ejecta horizon indicates that the highest concentrations of elements such as Ir and Cr occur within the coarser (boulder to medium sand-grade) ejecta (Gostin et al. 1989). Even coarse ejecta which have been reworked by traction currents are high in these elements. This finding suggests that most of the Ir and Cr is carried by the ejected clasts, and analysis of individual volcanic clasts reveals that these are also enriched in Ir. In contrast, the fine silt and shale layers directly overlying the ejecta horizon are Ir and Cr poor.

Samples from the ejecta horizon that have been least affected by diagenesis (small green shale envelopes of low Cu content) have platinum-metal inter-elemental ratios similar to chondrites (Gostin et al. 1989). In addition, these elemental ratios overlap those of the Cretaceous/Tertiary (KT) boundary samples (Gostin et al. 1989). This again is consistent with the platinum metals having been derived from the impacting meteorite. Had these elements been derived from a crustal source, it is more likely that elements like Au would be much more strongly enriched than Ir (Wallace et al. 1990a).

Ejecta horizon lithofacies

The Acraman ejecta horizon most commonly consists of a thin (2–5 cm), normally graded unit (type 1; Figs. 5–8). Less commonly, the ejecta horizon consists of poorly sorted, weakly, normally graded breccia and sand that may be cross-laminated (type 2; Fig. 5, 6, and 9). The two most common ejecta sequences are described below.

Normally graded sequence: type 1 ejecta sequences

This is the most widespread ejecta sequence present in the Adelaide Geosyncline. In its idealised form, it comprises, from base to top:

- basal breccia and/or lonestones;
- sandy mudstone (mudstone with floating sand-size clasts);
- graded sand; and
- cross-laminated siltstone and sandstone (commonly overlying the graded sand, Figs. 5–8).

The most characteristic feature of the sequence is the virtually perfect normal grading of clasts (Fig. 8), although the sequence usually differs to some extent from the idealised form outlined above. The normally graded ejecta sequence or variants of it occur at Bunyeroo Gorge, Brachina Gorge, Donkey Valley, Bagalowie, Yappala, Jubilee Mines, Reaphook Hill, and the Wearing Hills (Fig. 1). The units of the normally graded sequence are described below.

When treated as a single sediment sample (excluding the mudstone matrix), the whole of the normally graded ejecta sequence has a grainsize distribution made up of at least two distinct populations (Fig. 10). The lonestones and breccia form a population that is extremely poorly sorted ($\sigma \approx 5\ \Phi$), and the graded sand forms a second population which is moderately well sorted ($\sigma \approx 0.75\ \Phi$). These two grainsize populations are so distinct as to be observable in the field. The lonestones and breccia typically account for less than 20 per cent by volume of the ejecta horizon, but contain a clast size range of around 10 cm to 0.5 mm (> 5 phi units). In contrast, the graded sand accounts for around 60 to 90 per cent by volume of the ejecta horizon (depending on locality), but has a grainsize variation of only 0.5 to 0.12 mm (2 phi units). The sandy mudstone unit of the normally graded ejecta sequence separates these two grainsize populations. The mud-size fraction of the ejecta horizon could not be quantitatively analysed in terms of its grainsize parameters.

Breccia and lonestones. Lenticular breccia and lonestones occur at the base of the ejecta horizon at most localities (Figs. 7 and 8). The basal breccia ranges from zero to 4 cm thick

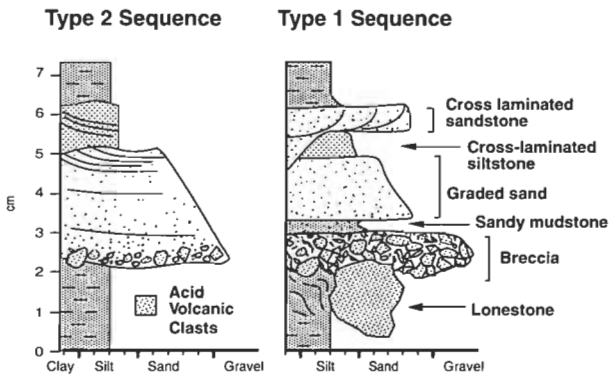

Figure 5. The two major styles of ejecta sequence found in the Adelaide Geosyncline. The type 1 sequence displayed here is a composite section similar to that found in the Bunyeroo and Brachina Gorges areas. Note that the cross-laminated siltstone and sandstone in the upper portion of the ejecta are not always present. The type 2 sequence is that found at Merna Mora.

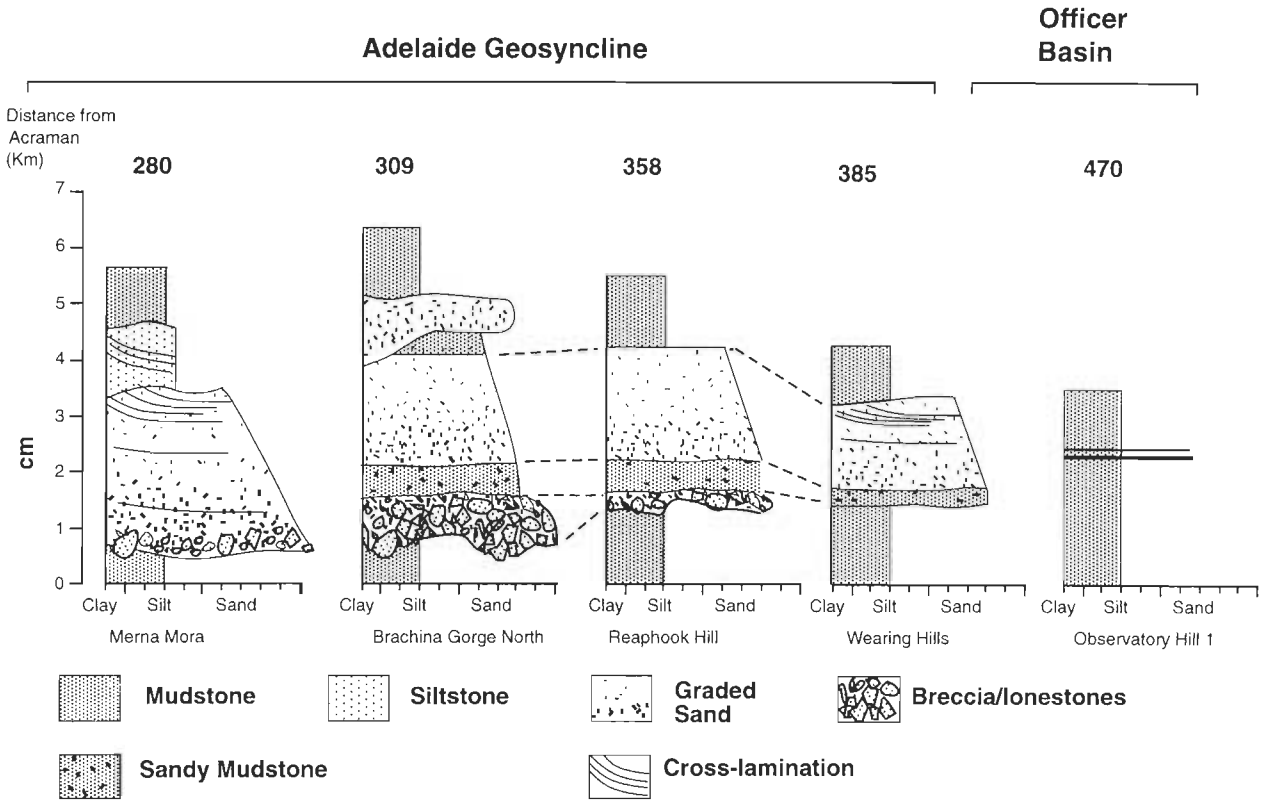

Figure 6. Representative ejecta sequences ranging from proximal to distal from the Adelaide Geosyncline and the Officer Basin.

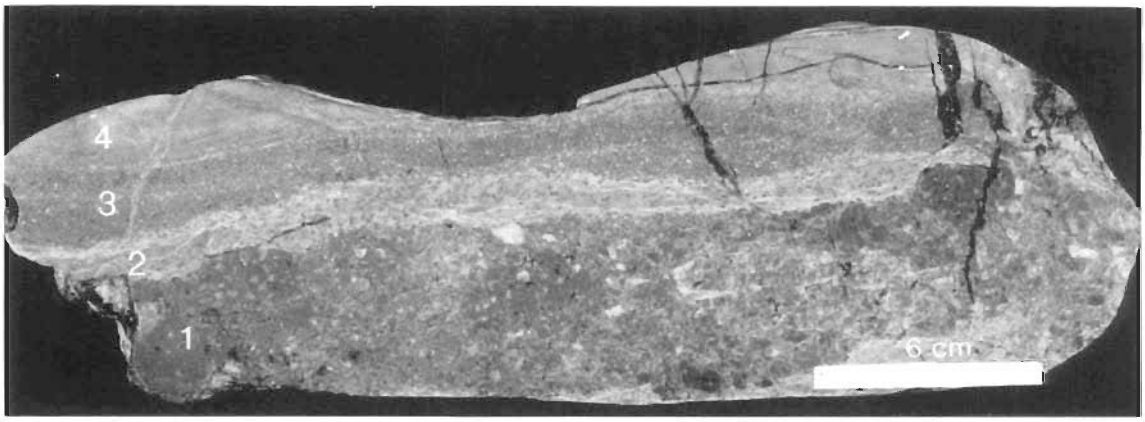

Figure 7. Hand specimen of normally graded ejecta from Bunyeroo Gorge. The breccia unit is unusually thick in this sample. 1, breccia; 2, sandy mudstone; 3, graded sand; 4, cross-laminated siltstone.

(excluding large lonestones), is clast-supported and well to moderately sorted, and consists entirely of angular to subrounded acid volcanic fragments. Although the clast diameter in the breccia/lonestones ranges from 50 cm to 0.5 mm, the more common size range is 5 cm to 0.5 mm. There appears to be little correlation between maximum clast size and breccia volume, because isolated large blocks commonly occur where little or no breccia is present. The average clast size within the breccia varies across the Adelaide Geosyncline, but a marked decrease in clast size is apparent from west to east.

The breccia generally displays normal grading and has a matrix, less commonly, it displays reverse (or no) grading and has no matrix. The matrix is mudstone of similar composition to that of the host Bunyeroo Formation. Large acid volcanic clasts commonly appear to 'float' on finer breccia material in the reverse-graded breccia, which is lenticular over distances of tens of centimetres or metres. Where the breccia lacks a matrix, it is cemented by a variety of phases, including calcite, barite, pyrite, feldspar, and chlorite.

The grain shape and surface texture of larger clasts (>4 cm in diameter) are quite distinctive. Large clasts typically have an overall subrounded shape, but an extremely irregular surface texture. The surface irregularity takes the form of multiple high-angle fracture surfaces, and gives the clasts the appearance of having been pulverised.

Sandy mudstone. Directly overlying the breccia, this unit provides one of the most characteristic features of the normally graded ejecta sequence (Figs. 7 and 8). Its thickness ranges from 2 to 20 mm, but is more commonly around 6 mm. It consists of angular to subangular acid volcanic fragments floating

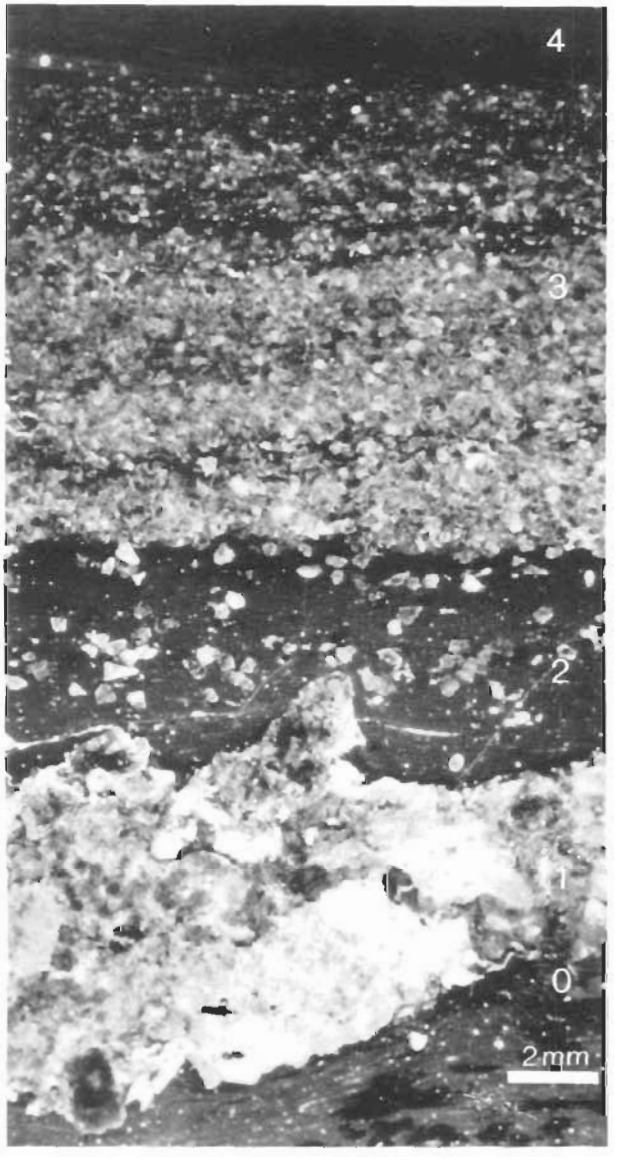

Figure 8. Plane-polarised-light photomicrograph of type 1 normally graded sequence, Bunyeroo Gorge. 0, host Bunyeroo shale; 1, breccia; 2, sandy mudstone; 3, graded sand; 4, cross-laminated siltstone.

Figure 9. Hand specimen of type 2 sequence from Merna Mora.

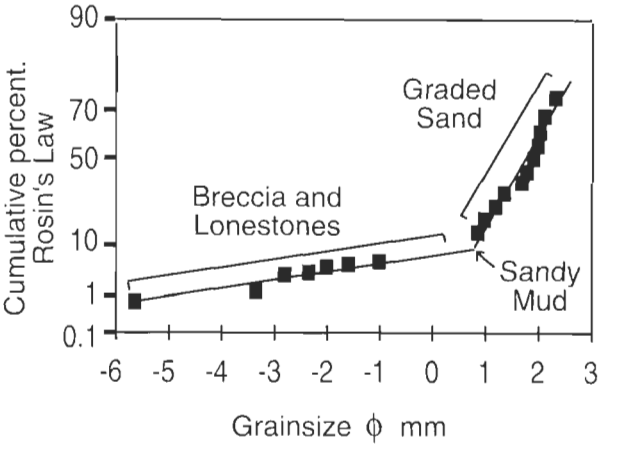

Figure 10. Cumulative grainsize distribution in type 1 ejecta sequence, Brachina Gorge.

in a matrix of mudstone. The clasts typically constitute around 10 to 20 per cent by volume of the lithology. The clast size is almost invariably around 500 to 600 μm, is very well sorted (<0.35 Φ), and shows little or no recognisable size variation from the base to the top of the unit. The basal contact with the breccia is typically abrupt, whereas the upper contact may be gradational over a few millimetres. Lobes of ejecta sandstone (similar to the overlying graded sand) commonly occur within the sandy mudstone, either completely isolated from or forming irregular extensions of the overlying graded sandstone.

The mudstone matrix consists of unlaminated clay minerals with dispersed silt-size quartz grains, and is virtually identical to that of the host shale (Fig. 8). A greater proportion of quartz silt is apparent locally within the mudstone at the base of the unit.

Graded sand. This unit consists of normally graded, clast-supported sand, and is very well sorted (<0.35 Φ). It overlies the sandy mudstone and ranges from 1.5 to 3.5 cm thick. The basal contact may be abrupt or transitional (from matrix-supported to grain-supported over a 1–2 mm stratigraphic thickness). The basal portion of the sand has a uniform grainsize of 450 to 550 μm over a wide geographic area in the Adelaide Geosyncline. The grainsize decreases to around 120–200 μm in the uppermost portion of the unit. At one locality (Bagalowie), this unit grades up into a very fine quartz-rich sand with a grainsize around 70 μm. Masses of dispersed clay minerals are generally present between clasts, and this may indicate the former presence of a matrix.

In the lower portion of the unit, the clasts consist entirely of angular to subangular acid volcanic fragments. However, in the upper portion, subangular to rounded quartz and feldspar clasts make up to ~5 per cent of the total clasts. The more rounded quartz and feldspar clasts typically have a grainsize of <300 μm.

The graded sand is generally massive but may be weakly laminated or may display low-angle cross-lamination. The lamination is typically defined by thin (<1 mm) clay-rich zones, in which a matrix-supported texture is present. Where there is no matrix, the pore spaces have been filled by a number of cement phases, including calcite, barite, pyrite, feldspar, and chlorite

Cross-laminated siltstone and sandstone. A siltstone commonly overlies the graded sand unit. It has a clast size of 10–50 μm, and typically consists of quartz (60–70%), feldspar (0–10%),

and muscovite (10–20%). Angular–subangular volcanic fragments (clast size ~ 120–150 μm) are commonly dispersed throughout the siltstone. At some localities, the siltstone displays normal grading, ranging in grainsize from a basal 50 μm up to 20 μm. At many localities, it displays a prominent low-angle unidirectional trough cross-lamination. Individual troughs are typically around 10–20 cm wide and, where measured, have cross-lamination orientations indicating transport from the west.

At other localities, the upper portion of the ejecta horizon consists of a matrix-free cross-laminated sandstone that is commonly separated from the underlying normally graded ejecta by a sharp erosional surface. The cross-laminated sandstone generally has a similar composition to the normally graded ejecta, consisting almost entirely of angular volcanic clasts. However, it is only moderately sorted, unlike the normally graded ejecta. Small-scale (5 cm) hummocky rippled surfaces are locally superimposed on it. The cross-laminated sandstone varies from 0 to 40 cm thick, and may be present where there is no normally graded ejecta sequence.

Poorly sorted and normally graded ejecta sequences: type 2 ejecta sequences

At many localities in the western Adelaide Geosyncline (e.g., Pichi Richi Pass, Warakimbo, Merna Mora, Parachilna Gorge; Fig. 1), the ejecta horizon occurs as a weakly graded unit comprising a basal breccia grading up to a fine sand (Figs. 5 and 9). As in the normally graded ejecta sequence, the clasts are dominated by angular acid volcanic fragments. However, these occurrences differ from the more widespread normally graded sequence by:

- being only moderately to poorly sorted;
- being more weakly graded;
- containing no sandy mudstone unit;
- commonly displaying cross-lamination throughout; and
- commonly containing rounded quartz.

These weakly graded ejecta-breccia/sand sequences are commonly capped by a green siltstone with low-angle cross-lamination, very similar to the siltstone in the type 1 ejecta sequences. They range in thickness from 4 to 40 cm.

Lateral variation in the ejecta blanket

The character of the ejecta horizon (thickness, sequence, etc.) is moderately uniform on a lateral scale of 5 to 10 m. However, on a larger scale (tens of metres), there is commonly a substantial variation in thickness and ejecta type. At Bunyeroo Gorge, for example, the ejecta horizon is a cross-laminated type 2 sequence whose thickness varies from 40 cm to 0 m over a distance of 100 m. The normally graded ejecta sequence, however, is more uniform in thickness on a local scale.

On a regional scale, systematic changes occur from west to east in the Adelaide Geosyncline (Fig. 6). In the west (about 300 km east of Acraman), large blocks up to 50 cm in diameter are present and the ejecta horizon is up to 40 cm thick. By contrast, in the east (around 400 km east of Acraman), the ejecta horizon is only a few centimetres thick and clasts greater than coarse sand-size have rarely been found (only one gravel-size clast has been found which measured 2 cm in diameter). In the Officer Basin (450–500 km west-northwest of Acraman), the ejecta horizon is only 0.7 cm thick and consists entirely of sand-size particles. There is thus a correlation between ejecta thickness and distance from the Acraman impact structure.

Environment of deposition

Type 1 sequences: breccia, lonestones, and graded sand

The perfect normal grading and sorting of clasts within the typical ejecta sequence are consistent with deposition of the ejecta from suspension. Suspension settling through a large water column (where sorting and grading reflect the differential settling velocities of the various clast sizes) is one of the few sedimentological processes which could explain the perfect sorting and normal grading. Other sedimentological processes — like turbidity flows, debris flows, and tempestite formation — can produce normal grading, but the sorting in these deposits is generally poor.

The reverse-graded matrix-free breccias, which are less commonly present within type 1 ejecta sequences, are likely to be the product of grainflow within the ejecta before deposition of the overlying sandy mudstone. The lenticular nature of these breccia types is also consistent with deposition from grainflows.

Type 1 sequences: sandy mudstone

Because of its argillaceous matrix, the sandy mudstone lithofacies of the ejecta horizon is anomalous in the graded sequence. However, this unit is widespread, and contains clasts with grainsizes precisely matching the normally graded parts of the sequence above and below it. These features indicate that the sandy mudstone is an integral part of the graded sequence. Mineralogically and geochemically, the matrix appears to be identical with the mudstone of the host Bunyeroo Formation. Gostin et al. (1989) found that the sandy mudstone contains moderately low abundances of meteoritic components. It therefore appears probable that the matrix of the sandy mudstone unit is derived from the Bunyeroo Formation, and is not allochthonous material derived from the impact.

The simplest explanation for the origin of the matrix within the sandy mudstone is that it is reworked Bunyeroo mud. Disturbance of uncompacted mud at the sediment–water interface would be expected during a post-impact seismic disturbance, and possibly during ejecta deposition. Post-impact seismic events could produce turbidity currents, or simply resuspend unconsolidated surface sediments. The presence of sand-size clasts within the mudstone indicates that the disturbed Bunyeroo mud and impact ejecta were deposited contemporaneously.

Type 2 poorly graded ejecta and type 1 cross-laminated rippled sandstone and siltstone

Several factors indicate that the cross-laminated siltstone and sandstone in the upper parts of type 1 ejecta sequences are products of ejecta reworking— for example, the sharp and erosional base, and the clast composition of the sandstone, which is similar to that of the normally graded ejecta. The energy required to extensively rework sand-size sediments appears anomalous in view of the very fine grainsize of the host shale. The host shale is totally devoid of other sandstone layers for hundreds of metres of stratigraphic thickness. The reworking therefore

might have been a consequence of the impact. Impact-induced tsunamis are likely candidates to explain such reworking of the ejecta. The relative timing of the reworking (post-dating most ejecta deposition) is also consistent with the hypothesis of an impact-induced tsunami.

Similarly, the type 2 poorly graded ejecta sequences, comprising completely reworked primary ejecta which are so common in the western Adelaide Geosyncline, may be tsunamigenic deposits. The moderate sorting, crude grading, and abundant cross-laminae are all consistent with reworking by a tsunami. Similarly, the greater abundance of rounded quartz may be explained by tsunamigenic transport from the shallower portions of the shelf, as has been suggested to occur during storms in other settings (Brenchley 1985). The graded sequences interpreted as tsunamigenic deposits at the KT boundary in Texas (Bourgeois et al. 1988) appear to share many of the characteristics of the type 2 ejecta sequences. The abundance of such reworked tsunamigenic deposits in the western Adelaide Geosyncline may be explained by a combination of shallower water depths and more proximal location.

Tsunamis are considered to be capable of reworking sand-size (medium and coarse) sediments to a water depth of 200 m (Pickering et al. 1991). In deeper water, the velocity is probably insufficient to move sediment coarser than fine sand or coarse silt. In theory, the wavelength of bedforms associated with tsunamigenic reworking should be in the order of 50–100 m (Pickering et al. 1991). The scale of thickness variation for the cross-laminated ejecta sand is of this order. Pickering et al. (1991) also pointed out that associated processes like the back-surge of water could produce unidirectional flow and other sedimentary structures; this may account for the unidirectional trough cross-lamination observed in the siltstone of the ejecta horizon.

The above considerations suggest that impact-generated tsunamis and related processes are the cause of extensive reworking observed in the Acraman ejecta. It is difficult to envisage other processes which could cause such high-energy sedimentary structures in the moderately deep-water (below storm-wave-base) low-energy setting of the host shale.

Ejecta-transport mechanisms

Because the terrestrial record of distal impact ejecta is poor, distal-transport mechanisms for ejecta resulting from terrestrial impacts are not well understood. Furthermore, the extensive studies of lunar impact ejecta are not necessarily directly applicable to terrestrial impacts because of the atmosphere-free and water-free lunar environment. The ejecta-transport mechanisms on Mars and Venus may be of more relevance to terrestrial impacts because of atmospheric factors. The major processes of distal ejecta transport suggested for martian and venusian

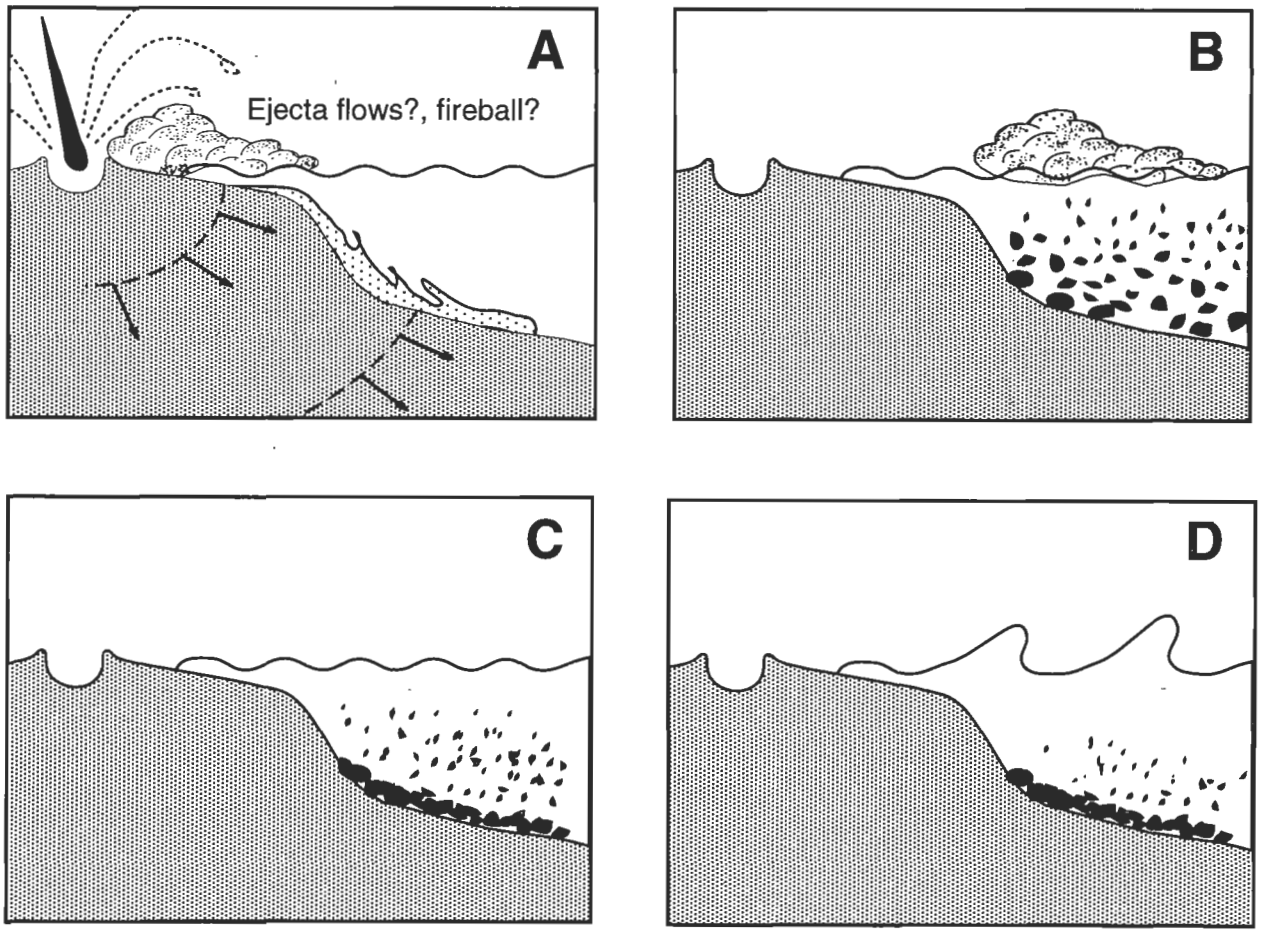

Figure 11. Schematic diagram depicting the sequence of events leading to deposition of the ejecta horizon in the Adelaide Geosyncline: (A) initial impact — massive seismic event causes disruption and slumping of Bunyeroo mud; (B) settling, sorting, and deposition of ejecta simultaneously with resettling of disturbed Bunyeroo mud; some mass flow of ejecta by grainflows; (C) disturbed Bunyeroo mud has resettled, but deposition of ejecta sand fraction continues; (D) arrival of tsunami at site of deposition causes reworking of ejecta during final stages of ejecta deposition.

impacts include impact-generated air-blasts, ballistic ejection from crater, non-ballistic basal ejecta flows, ejection by recovery winds, and distal ejecta flows from down-range fireballs (Schultz 1992a, b). These atmosphere-induced processes lead to a more complex array of ejecta types and ejecta distribution than in atmosphere-free conditions. In addition, impact angle can have a major effect on ejecta types and distribution.

The only direct evidence for the transport mechanisms of the Acraman impact ejecta is the grainsize distribution of the sediment. As discussed above, the ejecta horizon consists of two distinct grainsize populations: the lonestones and breccia; and the graded sand. The lonestone–breccia population is poorly sorted, similar to tills, explosion breccias, and pyroclastic flows (see Friedman & Sanders 1978; Bond & Sparks 1976). In contrast, the graded sand is moderately well sorted, having a sorting similar to most inland dune systems, some marine-shelf and river sediments, and many other depositional settings (see Friedman 1962; Visher 1969). The two grainsize populations also have different distributions: the coarse breccia is restricted to more proximal areas, whereas the sand is spread over the entire study area. According to the rationale of Visher (1969), these two grainsize populations suggest two different transport mechanisms. The sandy mud unit which separates the two populations may indicate a short time gap between their arrival. Clasts within the sandy mudstone may be derived from either of the two populations.

Schultz (1992a) suggested that for Venus, impact-induced air-blast processes appear to produce small quantities of widely dispersed ejecta, whereas the various ejecta-flow and fireball processes produce larger volumes of less widely dispersed ejecta. Perhaps, the graded sand and lonestone–breccia grainsize populations within the ejecta represent impact-induced air-blast transport, and ejecta-flow and/or fireball transport, respectively. This would be consistent with the sorting characteristics of the two populations; the moderately good sorting of the widely dispersed sand population is typical of atmospheric/aeolian transport, and the poor sorting of the geographically restricted lonestone–breccia population is typical of pyroclastic and presumably ejecta flows.

Sequence of post-impact events

From the above constraints on ejecta processes, we suggest that the following sequence of events occurred at a locality around 300 km distant from the impact in the marine basin that is now the Adelaide Geosyncline (Fig. 11):

- impact: seismic shock, reworking, and suspension of unconsolidated marine muds;
- transport of lonestones and breccia by fireball or ejecta flows followed by suspension settling and deposition; some mass flow of breccia;
- deposition of sandy mudstone by resettling of Bunyeroo mud; minor sand-size ejecta deposited contemporaneously;
- transport of sand-grade ejecta by impact-induced air-blast processes; deposition of graded sand from suspension settling, producing type 1 ejecta sequences;
- impact-generated tsunami causes variable reworking of ejecta; deposition of type 2 ejecta sequences, and some reworking of type 1 ejecta sequences;
- waning tsunamigenic influences; deposition of cross-laminated siltstone; and
- return to deposition of host mud.

Conclusions

The Acraman ejecta horizon provides a classic example of subaqueous distal impact-ejecta blanket deposition. The ejecta sedimentology is more complicated than might be intuitively expected, but can be explained in terms of three major depositional processes:

- impact-induced seismic shock and disturbance of host sediments;
- suspension settling of impact ejecta and disturbed host sediments; and
- impact-induced tsunamis reworking ejecta deposits.

These three major processes should apply to some extent in all impact-ejecta blankets where subaqueous deposition occurs. Major factors which control the importance of each of these processes at different localities are many and varied, but must include magnitude of impact, nature of impact site (marine or non-marine), distance from impact site, and depth of depositional environment. The last of these is probably most important in a preservational sense — only in deep-water environments (below storm-wave base) will impact-generated facies be preserved from normal sedimentological reworking.

Finally, it is interesting to note the overall effect of such a major meteorite impact on the surrounding environment. After the Acraman impact, when the short-term impact-generated processes like seismic and tsunamigenic events had subsided, the environment returned to its pre-impact state (i.e., to deposition of red mud). This finding indicates that on a long timescale, such deep-shelf depositional systems are little affected by major meteorite impact.

Acknowledgments

This contribution is part of a continuing research project into the sedimentology, geochemistry, and diagenetic history of the Acraman ejecta horizon, funded by the Australian Research Council, the Australian Institute for Nuclear Science and Engineering, and the Mark Mitchell Research Foundation. We are grateful to G.E. Williams, J.A. Webb, and P.W. Haines for their careful reviews of the manuscript. We especially thank G.E. Williams for his continued enthusiasm and support over the life of the project.

References

Bond, A. & Sparks, R.S.J., 1976. The Minoan eruption of Santorini, Greece. Journal of the Geological Society of London, 132, 1–16.

Bourgeois, J., Hansen, T.A., Wiberg, P.L. & Kauffman, E.G., 1988. A tsunami deposit at the Cretaceous–Tertiary boundary in Texas. Science, 241, 567–570.

Brenchley, P.J., 1985. Storm influenced sandstone beds. Modern Geology, 9, 369–396.

Compston, W., Williams, I.S., Jenkins, R.J.F., Gostin, V.A. & Haines, P.W., 1987. Zircon age evidence for the late Precambrian Acraman ejecta blanket. Australian Journal of Earth Sciences, 34, 435–445.

Fanning, C.M., Flint, R.B., Parker, A.J., Ludwig, K.R. & Blissett, A.H., 1988. Refined Proterozoic evolution of the Gawler Craton, South Australia, through U–Pb zircon geochronology. Precambrian Research, 40/41, 363–386.

Friedman, G.M., 1962. On sorting, sorting coefficients and the lognormality of the grain-size distribution of sandstones. Journal of Geology, 70, 737–753.

Friedman, G.M. & Sanders, J.E., 1978. Principles of sedimentology. John Wiley and Sons, New York.

Gostin, V.A., Haines, P.W., Jenkins, R.J.F., Compston, W. & Williams, I.S., 1986. Impact ejecta horizon within late Precambrian shales, Adelaide Geosyncline, South Australia. Science, 233, 198–200.

Gostin, V.A. & Jenkins, R.J.F., 1983. Sedimentation of the early Ediacaran, Flinders Ranges, South Australia. 6th Australian Geological Convention, Abstracts, Canberra, 196–197.

Gostin, V.A., Keays, R.R. & Wallace, M.W., 1989. Iridium anomaly from the Acraman impact ejecta horizon: impacts can produce sedimentary iridium peaks. Nature, 340, 542–544.

Haines, P.W., 1988. Storm-dominated mixed carbonate/siliciclastic shelf sequence displaying cycles of hummocky cross-stratification, Late Proterozoic Wonoka Formation, South Australia. Sedimentary Geology, 58, 237–254.

Mawson, D. & Segnit, E.R., 1949. Purple slates of the Adelaide System. Transactions of the Royal Society of South Australia, 72, 276–280.

Pickering, K.T., Soh, W. & Taira, A., 1991. Scale of tsunami-generated sedimentary structures in deep water. Journal of the Geological Society of London, 148, 211–214.

Preiss, W.V., 1987. The Adelaide Geosyncline: Late Proterozoic stratigraphy, sedimentation, palaeontology and tectonics. Geological Survey of South Australia, Bulletin, 53.

Schmidt, P.W. & Williams, G.E., 1991. Paleomagnetic correlation of the Acraman impact structure and the Late Proterozoic Bunyeroo ejecta horizon, South Australia. Australian Journal of Earth Sciences, 38, 283–289.

Schultz, P.H., 1992a. Atmospheric effects on ejecta emplacement. Journal of Geophysical Research, 97, 11623–11662.

Schultz, P.H., 1992b. Atmospheric effects on ejecta emplacement and crater formation on Venus from Magellan. Journal of Geophysical Research, 97, 16183–16248.

Visher, G.S., 1969. Grain size distributions and depositional processes. Journal of Sedimentary Petrology, 39, 1074–1106.

Wallace, M.W., Gostin, V.A. & Keays, R.R., 1989. Discovery of the Acraman impact ejecta blanket in the Officer Basin and its stratigraphic significance. Australian Journal of Earth Sciences, 36, 585–587.

Wallace, M.W., Gostin, V.A. & Keays, R.R., 1990a. Acraman impact ejecta and host shales — evidence for low-temperature mobilization of iridium and other platinoids. Geology, 18, 132–135.

Wallace, M.W., Gostin, V.A. & Keays, R.R., 1990b. Spherules and shard-like clasts from the Late Proterozoic Acraman impact ejecta horizon, South Australia. Meteoritics, 25, 161–165.

Williams, G.E., 1986. The Acraman impact structure: source of ejecta in late Precambrian shales, South Australia. Science, 233, 200–203.

Williams, G.E., 1987. The Acraman structure — Australia's largest impact scar. Search, 18, 143–145.

Williams, G.E., 1994. Acraman, South Australia: Australia's largest meteorite impact structure. Proceedings of the Royal Society of Victoria, 106, 105–127.

AGSO Journal of Australian Geology & Geophysics, 16 (4), 453–486

Gosses Bluff — a latest Jurassic impact structure, central Australia. Part 1: geological structure, stratigraphy, and origin

D.J. Milton[1], A.Y. Glikson[2], & R. Brett[1]

Gosses Bluff consists of a prominent circular ridge, 4.5 km in diameter, surrounded by a less well-exposed deformed outer ring, 24 km in diameter, which incorporates annular breccia troughs. The circular ridge, which forms part of an eroded central uplift, is composed of fractured and brecciated Ordovician to Devonian sandstone and shale, capped in places by overturned megabreccia. The structure was formed by the impact of an asteroid or comet.

Evidence for an extraterrestrial impact origin includes: (1) the circular symmetry of the disturbed zone, which comprises outcrops of vertical to overturned strata whose original stratigraphic position would be at depths of <3–4 km; (2) the presence of shatter cones and rhomboidal fracture patterns diagnostic of intense shock; (3) shatter-cone axes that define a structurally central focus at shallow depth beneath the palaeosurface when reconstructed to their pre-impact orientation; (4) outward ejection of large blocks; (5) melting of sandstone and siltstone to form melt breccia; (6) a gradation with increasing depth from shock-melted breccia into recrystallised and unheated breccia, suggesting a high central heat source; (7) a depth limit of the structural disturbance defined by continuous seismic reflectors below about 3500 m; (8) the absence of gravity anomalies which would provide evidence for deep-seated mass excess or deficiency.

Mineralogical and microstructural features diagnostic of instantaneously applied shock pressures abound. Quartz in both breccia and bedrock shows shock-induced fractures and planar deformation features. The melt breccia at Mount Pyroclast records higher shock levels: quartz has been transformed to glass, partly recrystallised into tridymite, and subsequently converted to solid-state diaplectic quartz. The fusion of shale resulted in potassium-enriched hot solutions circulating below the crater floor, and recrystallisation into pumiceous aggregates of sanidine accompanied by zeolites and hematite. Ar–Ar plateau ages of this sanidine-rich material suggest recrystallisation at 142.5 ± 0.8 Ma, which — along with the orientation and reverse nature of the geomagnetic field at the time of the event — points to a latest Jurassic age.

Calculations indicate that a crater the diameter of the Gosses Bluff structure reflects the release of energy in the order of 10^5–10^6 Mt, which could have been generated by an asteroid or comet estimated to have been about 2 km in diameter.

Introduction

Gosses Bluff (lat. 23°49'S, long. 132°18.5'E) represents one of the most completely preserved and best-exposed impact structures worldwide — thanks to its occurrence within a succession of nearly flat-lying strata, and the excellent preservation of a central uplift, annular breccia troughs, and lower sections of the original breccia-filled crater (Figs. 1–5). Located 50 km west of Hermannsburg Aboriginal settlement and 160 km west of Alice Springs, the structure lies on the Missionary Plain — a flat-floored syncline between a near-vertical dipping north limb which delimits the Macdonnell Ranges and a south limb which dips gently in the Krichauff Ranges. The Missionary Plain occurs in the northwestern part of the Amadeus Basin — a latitudinal intracratonic depression 800 km long in central Australia (Wells et al. 1970; Lindsay 1993). The basin contains a Late Proterozoic to Devonian sedimentary succession 8–10 km thick (Fig. 6).

Gosses Bluff, or Tnorula in the Aboriginal Aranda language, consists morphologically of an isolated circular ridge (or topographic bluff) 4.5 km in average diameter, and an outer ring 24 km in diameter (Tingate et al. this issue; Fig. 1). The circular ridge rises 180 m above the Missionary Plain (Figs. 1–5; 1:7500 map[3], in the back pocket). It is breached on its east side where a creek drains the central pound. It is the physiographic expression of the central ring of a larger structural disturbance which appears on satellite imagery as a circular area — the outer ring.

Outcrops at Gosses Bluff consist of steep to vertically dipping intensely deformed sandstone, siltstone, and shale (Figs. 6–9). In places, they are affected by unique intersecting rhombohedral cleavage and striated shatter-cone fracture patterns, and include annular troughs of megabreccia, breccia, and melt breccia (Figs. 10 and 11). The exposed sedimentary units, correlated with strata found in deep drilling, form a section about 3000 m thick. They extend from the Stairway Sandstone (Ordovician) in the central ring to the Brewer Conglomerate (Devonian) at the outer limits of the disturbed zone, which is surrounded by nearly flat-lying sedimentary rocks of the Missionary Syncline. Breccias occur at high elevations in the circular ridge and in the less well-exposed outer ring. A prominent hill, Mount Pyroclast, a few kilometres south of the ridge, consists largely of melt breccia and partly fused rock.

This paper forms the first part of a two-paper series accompanying the release of a geological map of Gosses Bluff (1:7500 map, in the back pocket; Milton et al. 1978); the second paper addresses geophysical studies of the structure (Milton et al. 1996). Both are based on the results of a study of the Gosses Bluff structure by the Bureau of Mineral Resources, Geology and Geophysics (BMR; now the Australian Geological Survey Organisation, AGSO), and the United States Geological Survey (USGS) on behalf of the National Aeronautics and Space Administration (NASA). Geological mapping of the central and outer rings (Milton et al. 1972; Glikson 1969), and extensive shallow drilling (39 holes; Appendix 1) were accompanied by geophysical surveys — including seismic (Moss 1964; Brown 1973), aeromagnetic (Young 1972), ground magnetic and palaeomagnetic (Sedmik 1983; Manwaring 1983), and gravity (Barlow 1979) investigations.

Previous investigations

The European discovery of Gosses Bluff was made on 8 September 1872 by Ernest Giles, who named it Gosse's Range '...after Mr. Harry Gosse, who had been out from the Alice Springs Telegraph-Station, but where his travels took him to I

[1] United States Geological Survey, Reston, Virginia 22092.
[2] Australian Geological Survey Organisation (formerly Bureau of Mineral Resources, Geology and Geophysics), GPO Box 378, Canberra, ACT 2601.
[3] Bibliographic reference: Milton, D.J., 1978. Geology of the central uplift, Gosses Bluff impact structure, Northern Territory. Bureau of Mineral Resources, Australia, 1:7500 map.

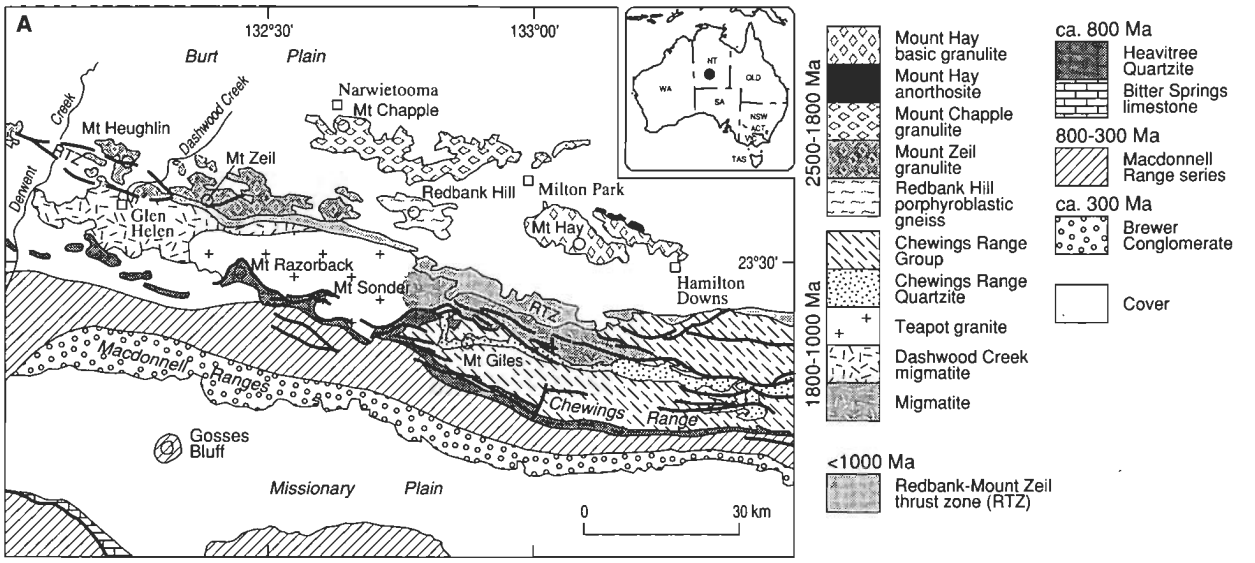

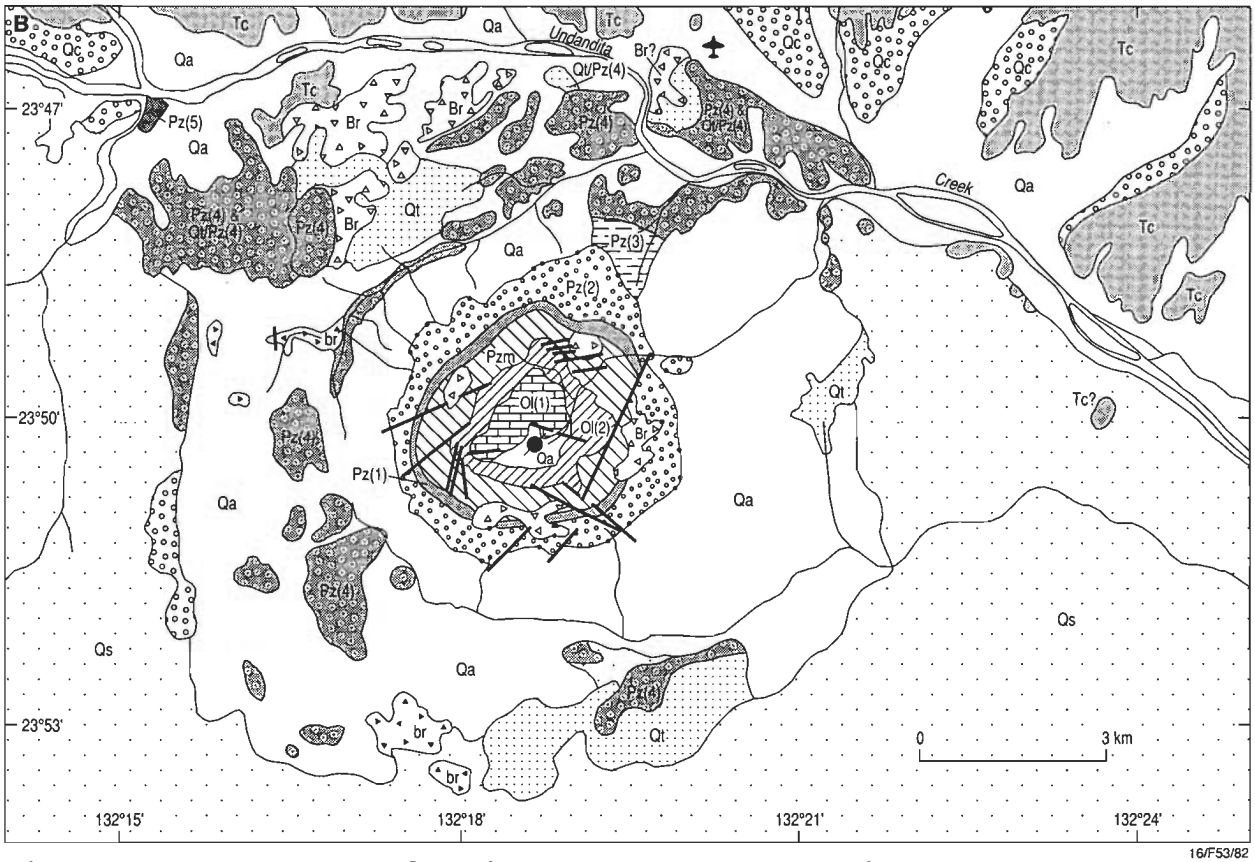

QUATERNARY

- Qa — *Alluvium*
- Qs — *Aeolian sand*
- Qt — *Travertine*
- Qc — *Conglomerate*

TERTIARY

- Tc — *Conglomerate and conglomeratic sandstone-poorly consolidated*

Breccia

- Br — *Breccia; massive clasts; some finer breccia associated*
- br — *Breccia clasts of arenite and lutite in a sandy matrix*

Pertnjara Group (upper)

- Pz(5) — *Red-brown conglomeratic sandstone*
- Pz(4) — *Red-brown poorly sorted sandstone-pebbly in places*
- Pz(3) — *Red-brown and green micaceous siltstone; minor thin sandstone*

Pertnjara Group (lower)

- Pz(2) — *Brown or red-brown sandstone and silty sandstone*
- Pz(1) — *Red siltstone and sandy siltstone*

Mereenie Sandstone

- Pzm — *White or pale brown, cross-bedded sandstone*

Larapinta Group

- Ol(2) — *Red-brown siltstone and silty sandstone (equivalent in part to Carmichael Sandstone and Stokes Formation)*
- Ol(1) — *Sandstone, siltstone, limestone (equivalent in part to Stokes Formation and Stairway Sandstone)*

Geological boundary

Fault

Gosses Bluff 1 (abandoned oil well)

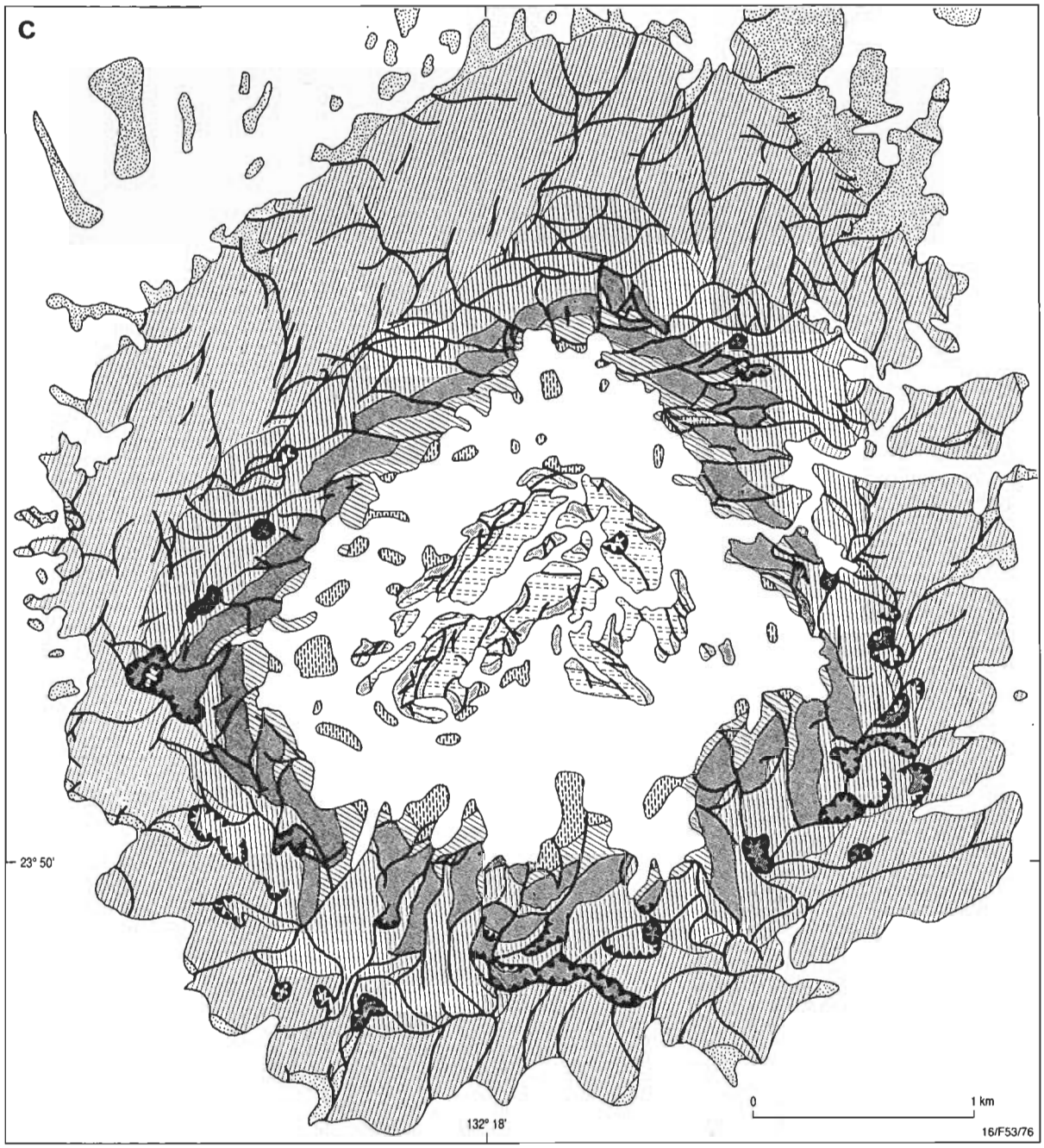

Figure 1. (a, facing page) Geological sketch map of the Amadeus Basin; (b, facing page) geological sketch map of the Gosses Bluff structure; (c, above) geological sketch map of the central ring of Gosses Bluff.

did not hear' (Giles 1875, p. 19). Gosses Bluff could have been observed only from the distance by pioneer geologists (Chewings 1928; Madigan 1932), who did not note its circular physiographic and structural features. It was first recognised as a geological anomaly during the 1956 regional reconnaissance of Prichard & Quinlan (1962), who suggested the structure was a diapir produced by mobilisation of incompetent carbonate and evaporites in the Precambrian Bitter Springs Formation. Brunnschweiler et al. (1959) regarded the structure as basically diapiric, but revised this view in favour of igneous intrusion after discovering fused rock at Mount Pyroclast (Brunnschweiler 1959). The hypothesis of a salt diapir led to the siting — in the centre of the central pound — of Gosses Bluff No. 1 well (McNaughton et al. 1968), abandoned dry at a depth of 1383 m (Pemberton & Planalp 1965). Acceptance of an impact origin led to a reassessment of the petroleum potential, and to the drilling of Gosses Bluff No. 2 well to a depth of 2652 m, 580 m northeast of Gosses Bluff No. 1.

The current understanding of Gosses Bluff dates from 1965, when the discovery of shatter cones led to its identification as a cryptoexplosion structure (Crook & Cook 1966) formed either by an extraterrestrial impact (favoured by K.A.W. Crook) or a violent intraterrestrial event (favoured by P.J. Cook). After further geologic mapping and shallow drilling, Cook (1968) revised his opinion to favour the impact hypothesis. An interpretation in terms of a mud volcano overlying a salt dome was advanced by Ranneft (1970). Earlier geophysical studies included a BMR seismic reflection traverse that crossed Gosses Bluff (Moss 1964), and an extensive seismic survey of the Missionary Plain by Geophysical Associates Pty Ltd (1965) for Magellan Petroleum (NT) Pty Ltd, of which the results were summarised by Froelich & Krieg (1969).

Stratigraphy

Interpretations of the Amadeus Basin succession and of the Palaeozoic section in the Gosses Bluff surrounds are presented in Figures 6 and 7 respectively. Correlations of well-log units with exposed units in the bluff (column 3, Fig. 7) were used in the compilation of geological maps at scales of 1:50 000 (Milton et al. 1978) and 1:7500 (in the back pocket) for the entire structure and the central ring respectively.

The Mereenie Sandstone, originally thought to be a mainly Devonian unit, is now assigned to the Late Ordovician–Early Devonian. Detailed studies of the Carmichael Sandstone and Mereenie Sandstone throughout the Amadeus Basin suggest that the contact between them is conformable, and that the upper unit of the Carmichael Sandstone is best classified as the lower unit of the Mereenie Sandstone (M.J. Owen, formerly BMR, personal communication 1989; column 6, Fig. 7).

Subsurface stratigraphy

Metamorphic/igneous basement and Late Proterozoic formations

Amphibolite- to granulite-facies paragneiss, orthogneiss, mafic granulite, and intrusive granitoids are thrust southward over the Amadeus Basin sequence north of the Macdonnell Ranges (Fig. 1a; Quinlan & Forman 1968; Glikson 1987a, b). The Amadeus Basin succession (Fig. 6) commences with the Heavitree Quartzite, a unit dominated by silicified sandstone ~500 m thick that overlies the basement unconformably. The overlying Bitter

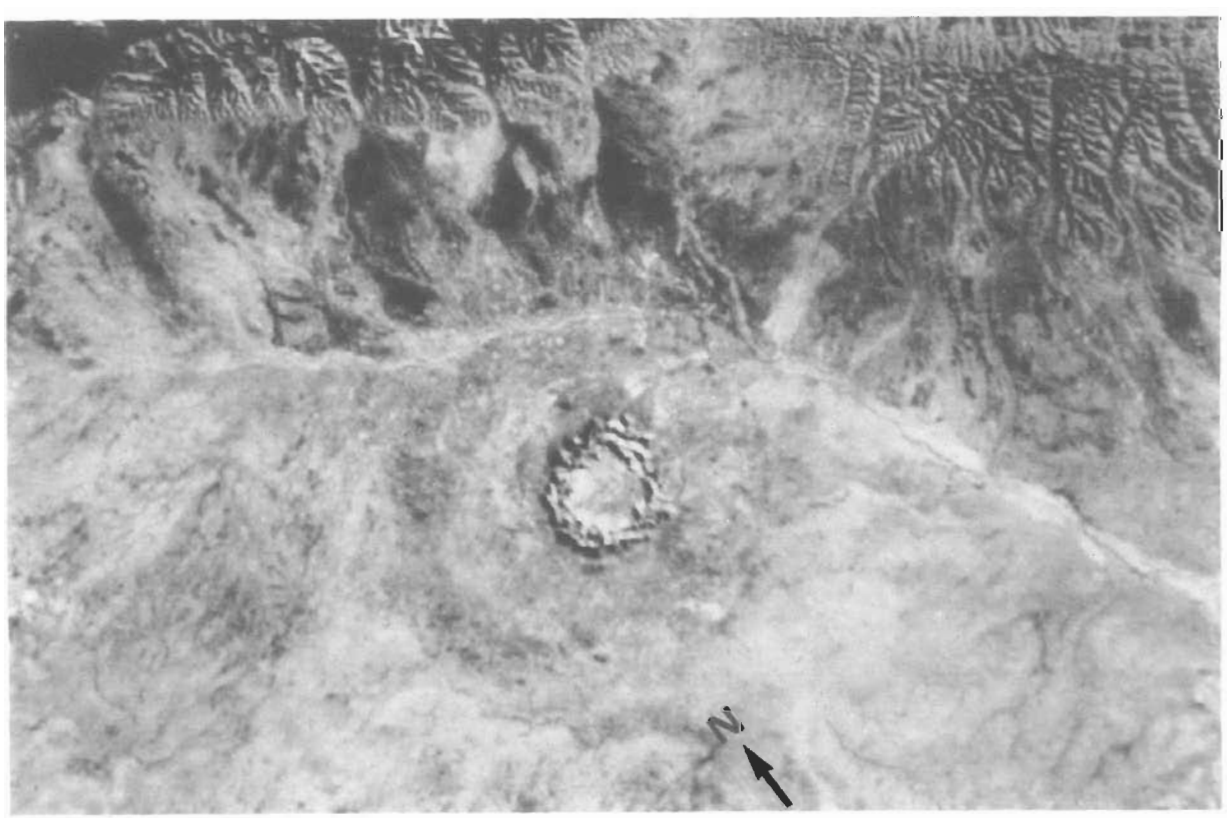

Figure 2. Gemini IV photo of a part of the northern margin of the Amadeus Basin, showing Gosses Bluff at the centre of the Missionary Plain between the Macdonnell Ranges to the north and the James Ranges to the south (area ~80 × 60 km).

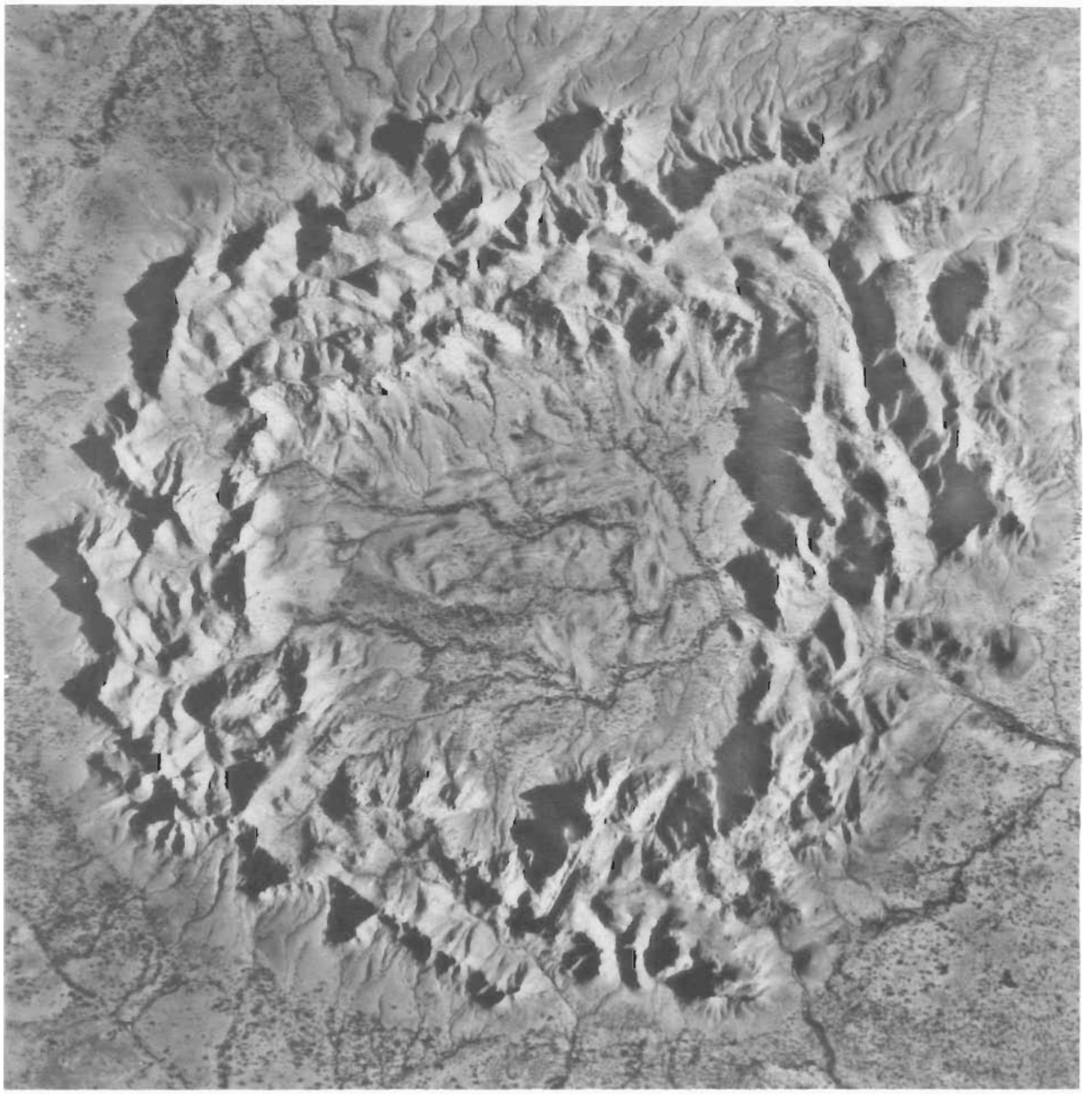

Figure 3. Vertical aerial view of Gosses Bluff.

Springs Formation — consisting of dolomite and cherty limestone, minor siltstone, and locally gypsum and salt beds — is ~750 m thick 75 km east of Gosses Bluff. The possible existence of evaporites beneath Gosses Bluff may have had an important role in the structural development of this structure. The overlying Areyonga Formation, ~120 m thick, comprises conglomerate, poorly sorted siltstone, and greywacke, and incorporates striated and faceted clasts that suggest a marine glacial environment of sedimentation. The overlying Pertatataka Formation consists of a succession of siltstone and lesser sandstone and limestone ~750 m thick.

Pertaoorta Group (Cambrian)

The Pertaoorta Group conformably overlies the Pertatataka Formation, and is estimated as about 1400 m thick near Gosses Bluff, where the bottom third of this unit is correlated with the Arumbera Sandstone in the Macdonnell Ranges or its equivalent — the Eninta Sandstone — in the Gardiner Ranges. The middle third is correlated with beds transitional between the Hugh River Shale and Jay Creek Limestone of the Macdonnell Ranges, and the coarser clastic beds of the Tempe Formation, Illara Sandstone, Deception Formation, and Petermann Sandstone of the Gardiner Range. The top third is the Goyder Formation, a unit of sandstone, siltstone, dolomite, and limestone.

Lower to upper Larapinta Group (Cambro-Ordovician)

The Larapinta Group includes the stratigraphically oldest units exposed in the core of the Gosses Bluff structure. The lower part of the group, the Pacoota Sandstone (~700 m thick) and Horn Valley Siltstone (~200 m thick), were penetrated in Gosses Bluff No. 2 well. The upper unit of the Pacoota Sandstone comprises interbedded very fine- to fine-grained sandstone and siltstone. The Horn Valley Siltstone consists of siltstone with interbedded limestone and sandstone, including a marker horizon of buff-grey limestone and pale grey fine-grained locally glauconitic sandstone. Cuttings examined by G. Playford (personal communication) contain a poorly preserved assemblage of acritarchs, rare chitinozoans, and a few indeterminate scolecodont

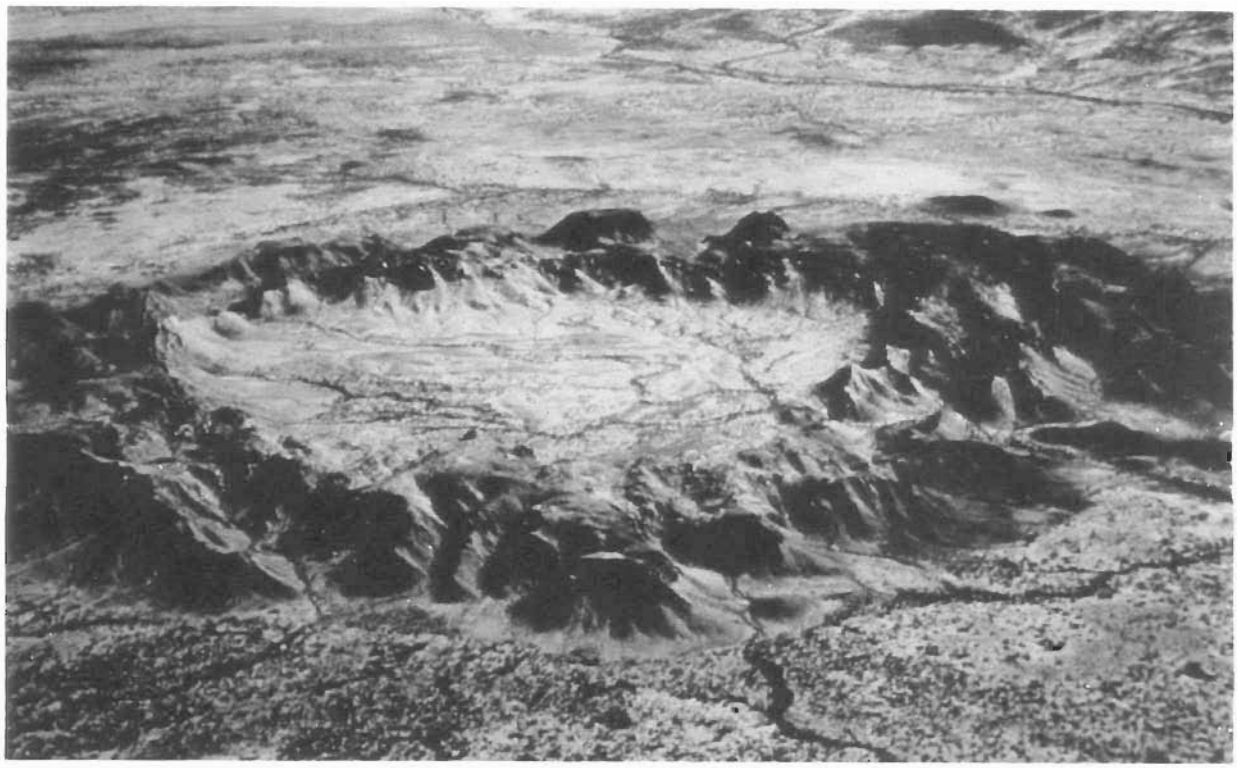

Figure 4. Oblique aerial view of Gosses Bluff taken from the southwest.

fragments that indicate an Early to Middle Ordovician age. The Stairway Sandstone (part of the upper Larapinta Group) exposed in the Macdonnell Ranges consists of a lower sandstone unit (~60 m thick), a middle unit of siltstone and sandstone (~100 m thick), and an upper unit of sandstone with minor siltstone and thin bands of phosphorite (~175 m thick).

Bedrock units exposed at and around Gosses Bluff

Exposed bedrock at Gosses Bluff belongs to the upper part of the Ordovician Larapinta Group, the Late Ordovician–Early Devonian Mereenie Sandstone, and the Devonian Pertnjara Group.

Upper Larapinta Group (Ordovician)

Stairway Sandstone (Ordovician). The oldest exposed unit is lithologically transitional between typical Stairway Sandstone and Stokes Siltstone of the Larapinta Group, and is somewhat arbitrarily assigned to the upper part of the former. It consists of fine- to very fine-grained sandstone, in part calcareous, forming beds 3–20 cm and in places up to 50 cm thick. Phosphate pellets 1–2 mm in diameter occur sporadically, but coarse sand grains are absent. A section 123 m thick was measured in the northeast part of the central pound.

Stokes Siltstone (Middle to Late Ordovician): lower unit. A unit of limestone, calcareous sandstone, and poorly exposed siltstone, 67 m thick, exposed in the central pound is assigned to the lower Stokes Siltstone. Much of the sandstone is texturally bimodal: it has well-rounded quartz grains 0.4–0.8 mm in diameter set in a matrix of much smaller subangular grains. Shock deformation gives the large quartz grains a conspicuous milky appearance.

Upper unit. A broad zone of poor exposure separates the central pound from the circular ridge. The few outcrops consist of shale and siltstone, generally green and grey in the lower part and red-brown above, and some beds of fossiliferous limestone near the base. The intervals in the northwest and northeast parts of the central pound suggest about 375 m of section, which matches an interval of shale 403 m thick assigned to the upper Stokes Siltstone encountered in Tyler No. 1 well, 15 km northeast of the centre of Gosses Bluff.

Carmichael Sandstone (Late Ordovician). The Carmichael Sandstone (Wells et al. 1970) underlies the gentler slopes at the base of the inner wall of the circular ridge; its base is defined as the lowest exposed sandstone. It consists of interbedded, mainly red sandstone and siltstone, and is 98 m thick on the west side of the bluff. It is thicker than the 30 m thickness estimated by Wells et al. (1970), and is tentatively correlated with a similar unit 32 m thick in Tyler No. 1 well between depths of 3027 and 3059 m. Fish plates found in the Carmichael Sandstone suggest a Caradoc age (M.J. Owen, personal communication 1989).

Mereenie Sandstone (Late Ordovician–Early Devonian)

Lower unit. The light-coloured quartzitic sandstone that forms the inner part of the circular ridge, mapped as the upper unit of the Carmichael Sandstone (1:7500 map, in the back pocket; and Fig. 1b, c) is now assigned to the lower part of the Mereenie Sandstone, defined as Siluro-Devonian by Cook (1968) and as latest Ordovician to Early Devonian by M.J. Owen (formerly BMR, unpublished data). The sandstone is aeolian, in contrast to the deltaic Carmichael Sandstone. It consists of clean white sandstone in beds ranging from a few centimetres to 3 m thick, and is evenly bedded or evinces low-angle cross-bedding. Much of the unit is intensely silicified, especially near the top. Its base is marked by the disappearance of the red colour of the underlying unit, abruptly or within an interval of a few decimetres, without any noticeable change in the sand grains themselves. Unlike the overlying unit, *Scolithos* tubes are absent.

Figure 5. Gosses Bluff viewed from the east along seismic traverse 2-E.

This unit, which occurs in the Macdonnell Ranges, thickens westward. It is 116 m thick in a measured section on the west side of Gosses Bluff. Exposures of it were recognised as far east as Glen Helen Gorge (lat. 23°42.4'S, long. 132°40.3'E). It is 15–25 m thick between Goyder Pass (lat. 23°38.0'S, long. 132°32.9'E) and Tyler Pass (lat. 23°39.4'S, long. 132°25.0'E), and about 180 m thick at Harajica Pass (lat. 23°34.8'S, long. 132°34.8'E). It appears to occupy a 60-m interval from a depth of 2967 to 3027 m in Tyler No. 1 well.

Upper unit. The bulk of the Mereenie Sandstone at Gosses Bluff is a clean, well-sorted light-coloured sandstone, mostly medium- or fine-grained. Bedding thickness is variable, and cross-bedding at low or moderate angles is common. 'Pipe rock' with *Scolithos* tubes up to 60 cm long is abundant, especially in the lower half of the unit. Below the clean well-sorted sandstone is a zone 15–25 m thick (but locally thinner or absent) of poorly sorted red sandstone and siltstone. Coarse sandstone and gritstone are abundant in this interval; small quartz pebbles occur at one locality in the southeast corner of the circular ridge. In the Macdonnell Ranges, to the north, pebble and even cobble conglomerates occur at an equivalent level, and a 42-m interval of pebbly siltstone and sandstone was intersected in Tyler No. 1 between 2925 and 2967 m.

The poorly sorted red sandstone is regarded as part of a lobe of fluvial sedimentation which extended from the north and east into an arid environment in mid-Mereenie times, and is restricted to the central north of the Amadeus Basin. Similar but distinct lobes are known in the Alice Springs area and in the southeast of the basin, and appear to have resulted from tectonic events which occurred northeast of the basin.

The upper part of the Mereenie Sandstone in a measured section on the northeast side of Gosses Bluff is 286 m thick, which is consistent with the 309 m encountered in Tyler No. 1 well between 2658 and 2967 m. These sections are thinner than those measured in the western Macdonnell and Gardiner Ranges, even if beds apparently equivalent to the lower unit are subtracted from the measured sections. Magellan geologists interpreted the thickness variations as due to thinning over a pre-existing structure. Mapping suggests that thinning of the Carmichael Sandstone and basal Mereenie Sandstone from west to east along the Macdonnell Ranges is due to progressive onlap onto an eastern 'high' formed during the Stokes Siltstone–Carmichael Sandstone transition by the Rodingan Movement (M.J. Owen, personal communication 1989).

Pertnjara Group (Devonian)

The Pertnjara Group, which forms the outer part of the circular ridge and underlies the outer zone of the structure and the surrounding country, comprises three formations (Wells et al. 1970) and several members (Jones 1972). Placoderm fish plates and spores found elsewhere suggest an Upper Devonian age (Playford et al. 1976).

Parke Siltstone. This unit is exposed over a belt about 1.6 km wide that includes the outer part of the circular ridge and the inner part of the surrounding plain. It consists of interbedded sandstone, siltstone, and shale; pelitic rocks constitute about a third of the unit. In thin section, the quartz grains are subrounded and densely packed, and have an argillaceous matrix or calcareous cement. The siltstone and shale beds range from a few centimetres to some metres in thickness. The shale is usually green, but oxidised brown shale occurring along the boundaries of green shale horizons, or as independent layers, is common. The transitions from sandstone to shale are abrupt, and little grading is apparent.

Cook (1966) discovered fragmentary arthrodiran fish plates identified as Early Devonian (Young 1985, 1988) in displaced blocks of red sandstone which he assigned to the Parke Siltstone (lowest Pertnjara Group). D.J. Milton, on the other hand, assigns these rocks to the basal Mereenie Sandstone adjacent to similar red Pertnjara sandstone; this implies a Devonian age for the entire Mereenie Sandstone (see also Young 1985). If the fossils are in the Pertnjara Group, the Mereenie Sandstone must be pre-Middle Devonian.

Young et al. (1987) reported a new Devonian fish fossil from the N'Dahla Member in the Ross River Syncline, about 220 km east of Gosses Bluff. This member was previously supposed to belong to the Ordovician Pacoota Sandstone. However, calcareous beds containing an equivalent fish fauna collected by M.J. Owen from the Cleland Hills, about 160 km west of Gosses Bluff, overlie the Mereenie Sandstone, and were assigned to the Deering Siltstone Member of the lowest Parke Siltstone (Wells et al. 1970; Jones 1972). It follows that the N'Dahla Member is roughly equivalent to the lowest Pertnjara Group. Stratigraphic revision suggests that the Mereenie Sandstone was misidentified in the Ross River Syncline, and that the view of Cook (1966) — that the fossils at Gosses Bluff are derived from the Parke Siltstone — is correct. This view is confirmed by further studies of Devonian fish fossils, allowing correlation of the displaced blocks of arthrodiran-fish-bearing sandstone with the basal beds of the Pertnjara Group (Young 1988).

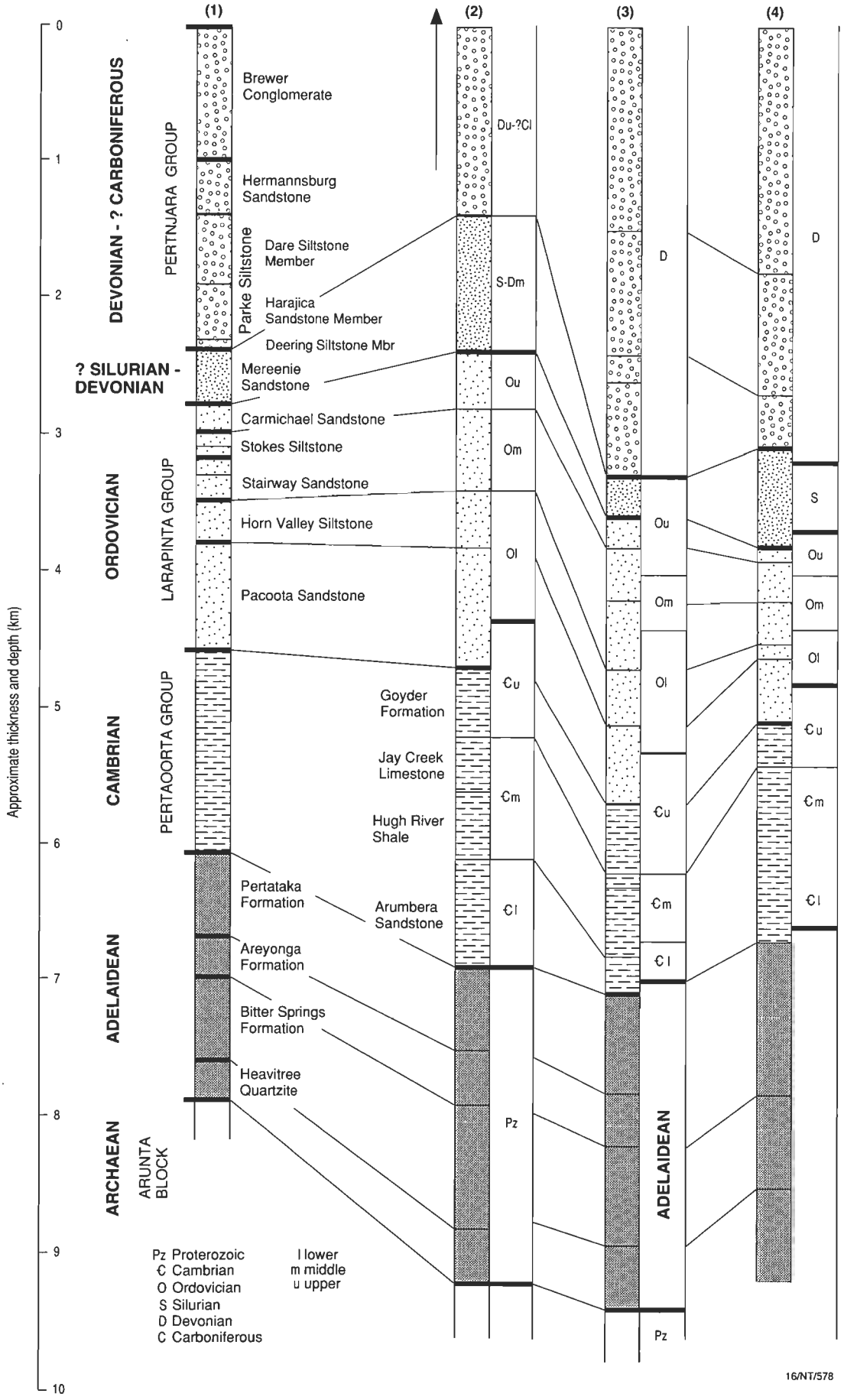

Figure 6. Stratigraphic sections of the northwestern Amadeus Basin as proposed by various authors: (1) Cook (1966, 1968); Glikson (1969); (2) Wells et al. (1970); (3) as proposed by D.J. Milton and adopted by Brown (1973) and Barlow (1979); (4) seismically determined depths to formations (Goleby et al. 1988; Wright et al. 1989), stratigraphy in accord with M.J. Owen (formerly BMR, personal communication 1989).

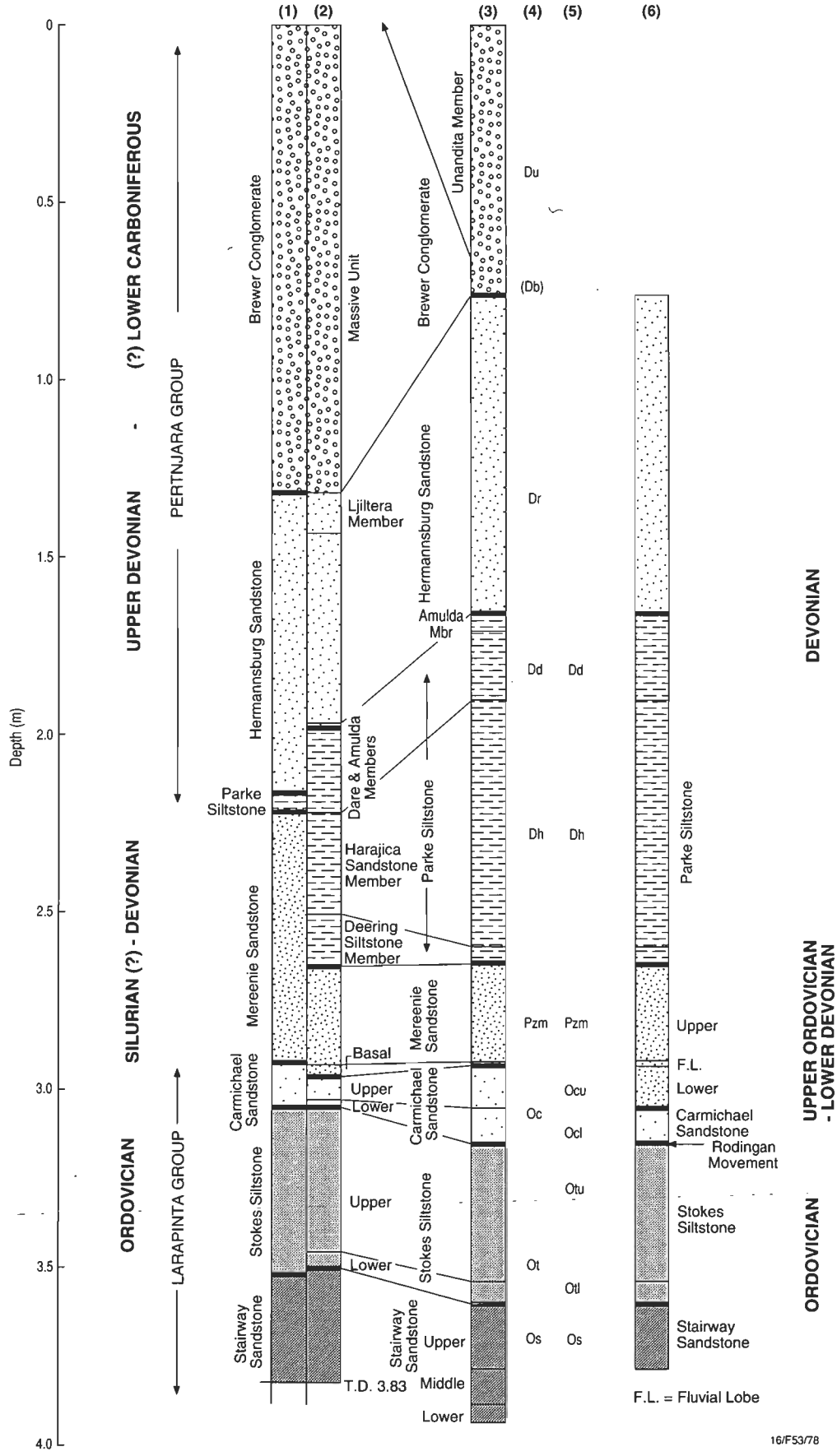

Figure 7. Stratigraphic divisions and interpretations at Gosses Bluff and its vicinity: (1) formations penetrated in Tyler No. 1 well as interpreted by Huckaba & Magee (1969); (2) revised interpretation of Tyler No. 1 well according to Milton et al. (1972); (3) Milton et al. (1972) interpretation of correlation between Tyler No. 1 well and outcropping formations in Gosses Bluff structure; (4) stratigraphic symbols used by Milton et al. 1978; (5) stratigraphic symbols used on the 1:7500 map (in the back pocket); (6) reinterpretation of outcropping stratigraphy based on M.J. Owen (personal communication 1989).

Deering Siltstone Member of the Parke Siltstone. The base of the Parke Siltstone, defined as the Deering Siltstone Member, is marked by the appearance of siltstone above light-coloured Mereenie Sandstone. Local thin siltstone beds, mud flakes in sandstone, and red sandstone beds in the uppermost Mereenie Sandstone suggest a transitional conformable relation.

Harajica Sandstone Member of the Parke Siltstone. A section that B.G. Jones and D.J. Milton measured east of the northern edge of the circular ridge includes 40 m of interbedded red sandstone and siltstone, 170 m of sandstone with minor siltstone beds, and 526 m of massive and cross-bedded fine- to medium-grained red-brown sandstone. Jones considers this

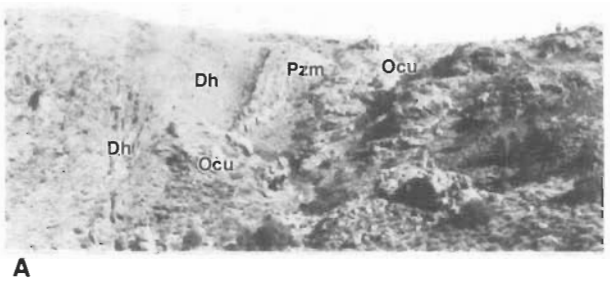

A

B

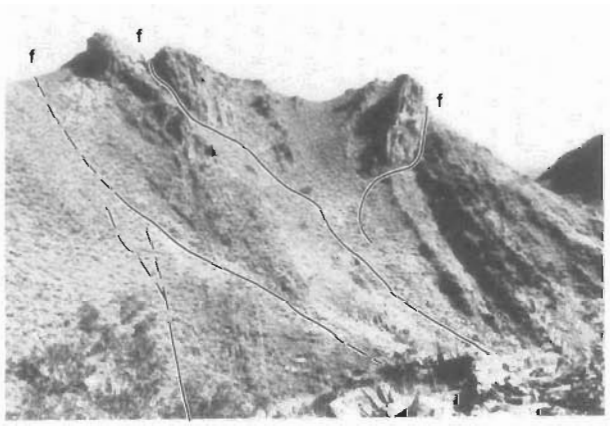

C

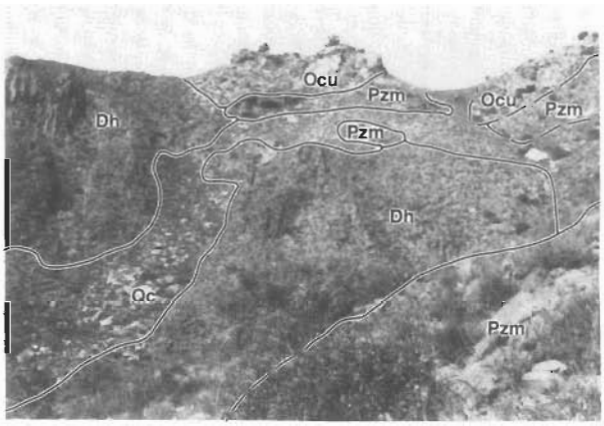

D

E

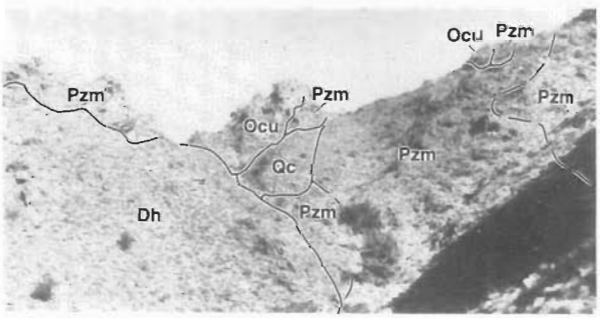

F

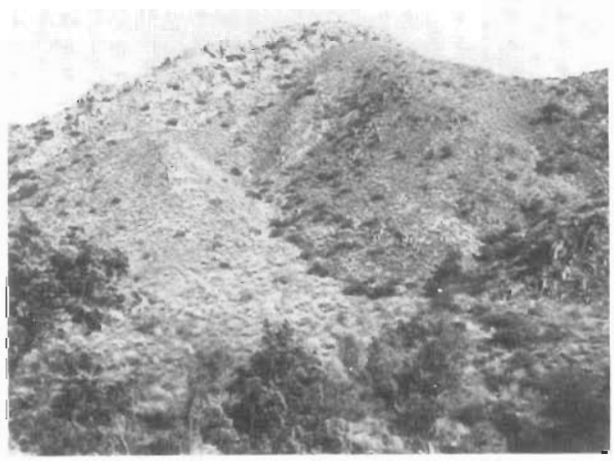

G

H

16/F53/79

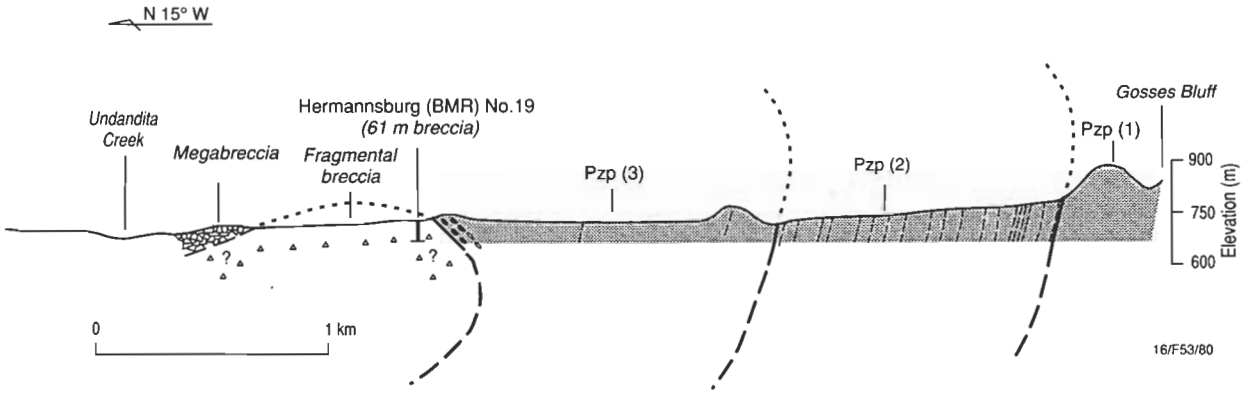

Figure 9. Diagrammatic cross-section through the northern part of the outer deformed zone of Gosses Bluff, showing a major breccia trough originally overlain by overturned plates of Hermannsburg Sandstone [Pzp(3)]. Pzp(1) and Pzp(2) are the Harajica Sandsone Member and Dare Siltstone Member, respectively, of the Parke Siltstone.

entire 736 m succession to represent the Harajica Sandstone Member, although the basal silty zone may correlate with the upper part of the Deering Siltstone Member. This zone was susceptible to fragmentation and ejection during cratering and later erosion, and forms valleys that divide the circular ridge into inner and outer rings.

Dare Siltstone Member of the Parke Siltstone. The outer walls of the circular ridge are marked by an abrupt contact between the Harajica Sandstone Member and the overlying Dare Siltstone Member, in which shale or siltstone predominate near the base and mostly grey fine-grained sandstone is more common higher up. A section measured near the northern edge of the circular ridge is 226 m thick, including — at the top — a 46-m sandstone-rich zone which B.G. Jones (University of Wollongong, personal communication) placed in the Amulda Member of the Parke Siltstone.

Hermannsburg Sandstone. This is the principal unit underlying the outer zone, and is exposed as isolated low hills surrounding and lying between 1.6 and 3.2 km from the outer walls of the circular ridge. Its thickness is uncertain, but estimated to be about 900 m (B.G. Jones, personal communication 1989). Its contact with the underlying Parke Siltstone is transitional. The unit typically comprises medium- or coarse-grained rather than fine-grained sandstones, and includes gritstones and conglomeratic beds. The sandstone is generally well indurated and brown in outcrop; in drillholes, white, grey, green, and red sandstones have also been observed. Pebble beds are abundant in the upper part north of the circular ridge, but are absent to the south, apparently corresponding to the southward thinning of its Ljiltera Member. A prominent hill 1 km northwest of the circular ridge (GR 244659) may represent a channel deposit within or at the base of the Hermannsburg Sandstone. In thin section, the sandstone displays subangular to subrounded quartz grains cemented by argillaceous and calcareous matrices. Feldspar grains, lithic clasts, and weathered detrital mica are common. Hematite staining is common in rocks collected from immediately below the weathering zone.

Brewer Conglomerate (Late Devonian)

Massive unit. The Brewer Conglomerate is a piedmont deposit formed in coalescing alluvial fans at the foot of a Late Devonian escarpment to the north. The transition from the underlying Hermannsburg Sandstone is marked by a gradual increase in the abundance of conglomeratic horizons and pebbly sandstones. The facies changes abruptly from north to south. At the edge of the Macdonnell Ranges, the Brewer Conglomerate comprises a massive boulder conglomerate which erodes to steep rounded hills with a dense network of short steep gullies. The unit was penetrated from the surface to a depth of 1325 m in Tyler No. 1 well, but wedges out over a short distance to the south so that it does not crop out within the limits of the Gosses Bluff structure itself.

Figure 8 (facing page). Folded, faulted, overturned, and megabrecciated structures in the central uplift of Gosses Bluff. Stratigraphic symbols: Dh — Harajica Sandstone Member; Pzm — Mereenie Sandstone; Ocu — Carmichael Sandstone; Qc — Quaternary colluvium; f — faults (see 1:7500 map, in the back pocket): (A) steeply dipping Harajica Sandstone Member overlying Mereenie Sandstone and overlain by breccia of lower Mereenie Sandstone and of upper Carmichael Sandstone, southeast part of Gosses Bluff; view to southeast; (B) valley above waterholes on the west side of Gosses Bluff; lower Mereenie Sandstone at right, upper Mereenie Sandstone at centre distance, and Harajica Sandstone Member at left; prominent allochthonous blocks in alluvium-filled valley consist of lower Mereenie Sandstone, but Carmichael Sandstone and upper Mereenie Sandstone blocks are also represented; the notch at left is the lowest in the western rim, and may mark the course of a former drainage channel developed during the dissection of the upper peneplain erosional surface; (C) telescoped structures in interbedded sandstone and siltstone of the lower Harajica Sandstone Member, northwestern part of Gosses Bluff; crowding tangential to the structure has been accomplished by faulting at low angles to the strike of plates; (D) allochthonous block of upper Carmichael Sandstone and lower Mereenie Sandstone overturned above vertically dipping sandstones of the Harajica Sandstone Member, eastern part of Gosses Bluff; (E) Carmichael Sandstone (centre) and lower Mereenie Sandstone (right) in faulted contact with lower Mereenie Sandstone (left), central depression; (F) allochthonous breccia and blocks in interval at base of Harajica Sandstone Member, centre of eastern side of Gosses Bluff; view to south; autochthonous upper Mereenie Sandstone at right, mostly brecciated Harajica Sandstone Member at left; allochthonous blocks and breccia of upper Mereenie Sandstone at centre and left skyline; at centre skyline, a block of lower Mereenie Sandstone dips vertically but faces inward after rotating; a similar smaller block is at right skyline; (G) silicified lower Mereenie Sandstone forming a ridge in contact with less durable upper Mereenie Sandstone, southern side; (H) the westernmost plate of upper Mereenie Sandstone in the south wall of Gosses Bluff viewed from the north; to the left are breccia and overturned plates of lower Mereenie Sandstone.

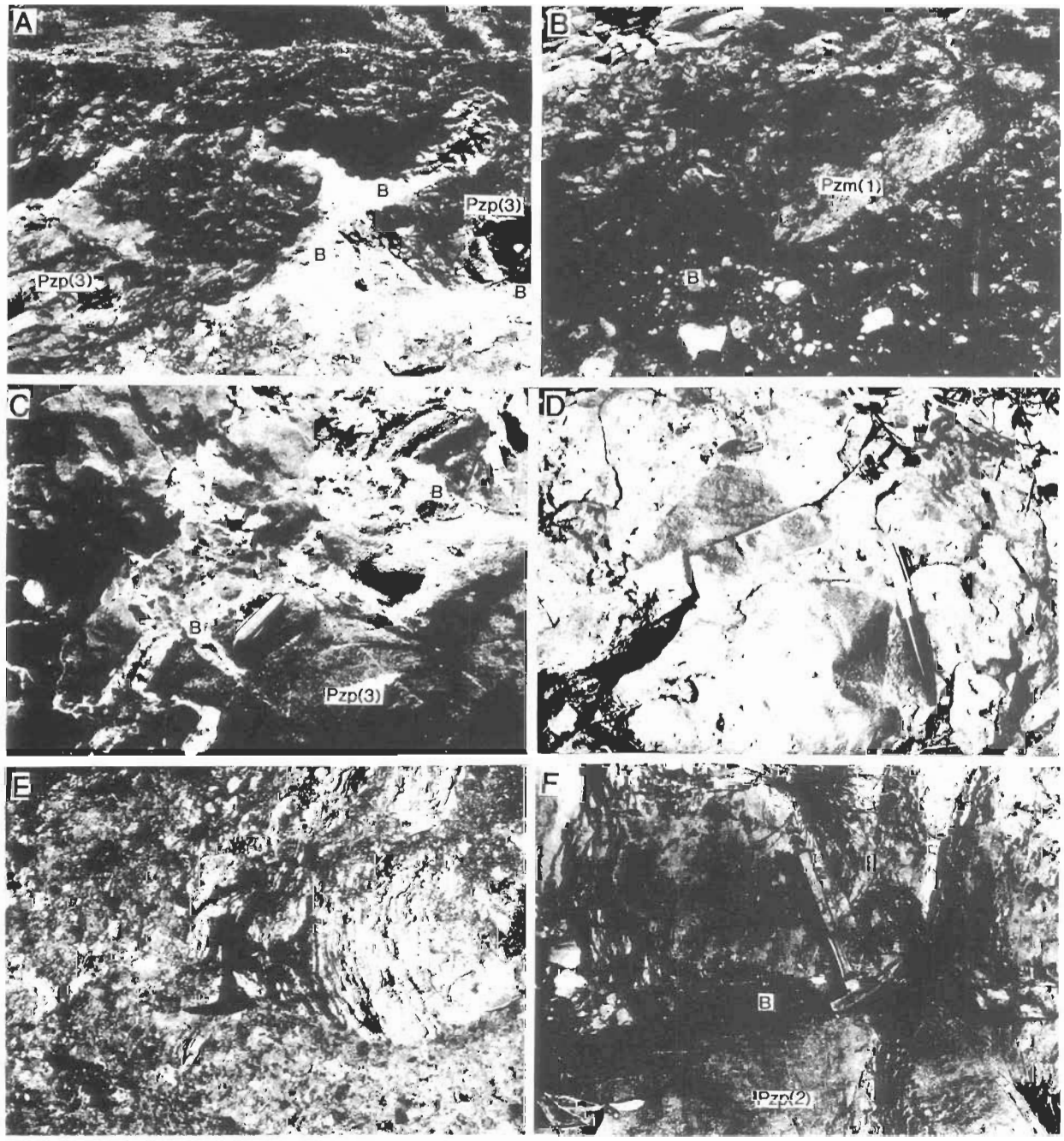

Figure 10 (A–F, above; G–L, on facing page). Breccia outcrops on the circular ridge and the outer ring of Gosses Bluff. The breccias are shown in the vertical succession in which they occur within circular troughs in the outer ring of Gosses Bluff (i.e., from unrecrystallised breccia at the base, to recrystallised quartzitic breccia above, to flow-structured fused breccia, or suevite): (A) comminuted pulverised fragmental breccia (B) injected into overturned blocks of Hermannsburg Sandstone [Pzp(3)] in the northern breccia trough of the outer zone of Gosses Bluff; (B) fragmental breccia overlain by an overturned block of the lower Mereenie Sandstone [Pzm(1)], which has a wedge of intrusive breccia (B) at its base; (C) veins of pulverised breccia (B) injected into fractures in the Hermannsburg Sandstone in the northern breccia trough of the outer zone of Gosses Bluff; (D) recrystallised breccia containing angular fragments of quartzitic sandstone set in an indurated microbrecciated matrix near Mount Pyroclast; (E) boulders of banded siltstone set in finer fragmental breccia in the northern breccia trough of the outer zone of Gosses Bluff; (F) dyke of microbreccia (B) intruded into sandstone of the Harajica Sandtone Member [Pzp(2)] of the Parke Siltstone north of the central ring of Gosses Bluff; (G) flow structures in shock-melted breccia at Mount Pyroclast; (H) flow structures in shock-melted breccia at Mount Pyroclast; (I) ptygmatically folded flow in melted sandstone at Mount Pyroclast; (J) shock-melted breccia at Mount Pyroclast; note the vertical flow in the left part of the photograph; (K) drillcore section of melt breccia with mudstone fragments (black) and sandstone fragments (light) in a microbrecciated matrix of devitrified silica glass, Mount Pyroclast; (L) drillcore section of melt breccia with banded flows of devitrified silica glass interspersed with brecciated matrix consisting of mudstone fragments, sandstone fragments, and devitrified glass, Mount Pyroclast.

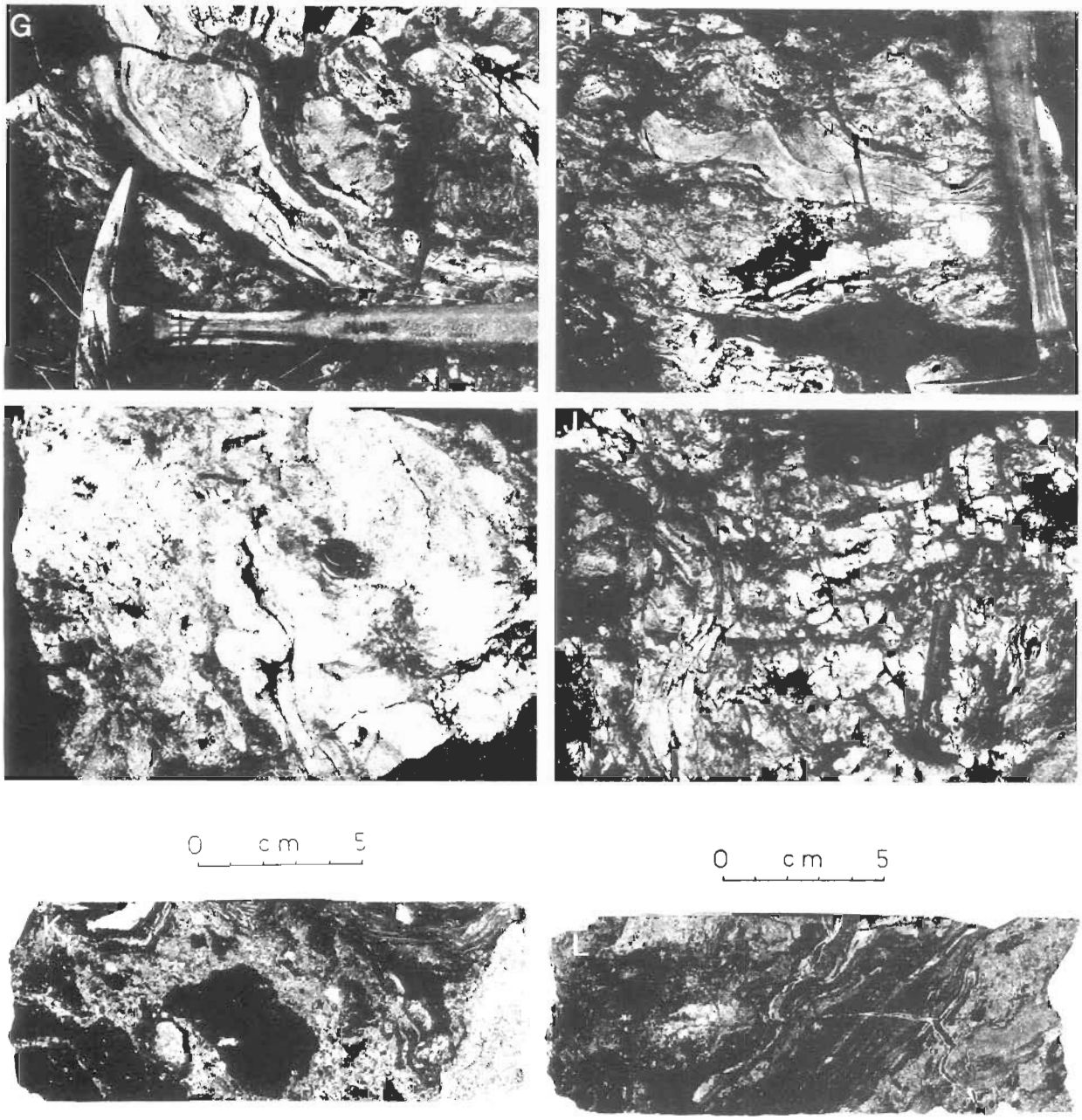

Undandita Member. This member is a conglomeratic sandstone dominated by coarse sandstone beds, in places cross-bedded, in which foreset beds dip at angles of up to 35° and pebbles are commonly concentrated near the base of 1 to 3-m-thick beds and cross-bed sets. The pebbles consist of a wide range of rock types — including variegated quartzite, gneiss, amphibolite, limestone, stromatolitic limestone, and sandstone with *Scolithos*. Conglomerate beds up to a few metres thick also occur, particularly to the north. The Undandita Member characteristically erodes to gravel-covered terraces that contrast sharply with the steep-sided hills of the massive unit of the Brewer Conglomerate. At the southern margin of exposures, the Undandita Member is in contact with the Ljiltera Member of the Hermannsburg Sandstone, and may be distinguished by its friability and grey and pink colours, in contrast to the better lithified brown pebbly sandstone of the Hermannsburg Sandstone. Jones (1972) estimated the thickness of the Undandita Member to be up to 1000 m.

Impact breccias

Fragmental breccia

Fragmental deposits comprising clasts that have lost their original relative orientation are defined as breccia (clasts 2 mm to <0.5 m) or megabreccia (clasts >0.5 m). Breccia and megabreccia zones overlying the circular ridge are, with rare exceptions, monomictic. Where polymictic breccias derived from different stratigraphic units are juxtaposed, the contact either is abrupt or evinces partial mixing (Fig. 10A).

Breccia in the central uplift consists of white quartzitic sandstone derived from the lower unit of the Mereenie Sandstone (Fig. 8A, D, F, H), and less commonly from the Stairway Sand-

stone. In the outer zone, the breccia in the northwest commonly occurs in troughs between steeply dipping beds (Fig. 1b; Milton et al. 1978). Around locality H1 (GR 215644), breccia abounds in green and brown shale fragments that are petrographically identical with the shale of the Parke Siltstone which forms the walls of the troughs. Breccia at locality H19 (GR 238674) is likewise composed of fragments of sandstone, gritstone, and conglomerate derived from the Hermannsburg Sandstone exposed along the southern walls of the breccia zone, clearly suggesting subautochthonous derivation.

Breccia generally consists of unsorted angular clasts whose sizes range from powdered submicroscopic microbreccia to fault blocks hundreds of metres across, but they commonly display an upper size limit; blocks >0.5 m are scarce. Patches of finer and coarser breccia may be segregated in places. In general, clasts are randomly oriented (Fig. 10B, D) or may show relict orientation parallel to adjacent less disturbed beds transitional to fault blocks. Parallel orientations, apparently unrelated to surrounding structure, are locally apparent. Flow-deformation texture is developed in places in shale-rich breccias. Clasts do not show rounding or slickensides. Shatter-fracturing within clasts and entire shatter-cone fragments are common. Veining of large clasts by the fine-matrix breccia is a distinct phenomenon (Fig. 10A, C, F).

Breccia is generally massive, and mostly well lithified; fractures generally cut through clasts rather than pass around them. Fractures tend to be irregular, and a generally subhorizontal irregular cleavage occurs in some, particularly the finer-grained breccia. A clear example occurs on the northwest side of the circular ridge, where fine-grained breccia derived from the Mereenie Sandstone and consisting of mostly rock powder containing scattered clasts up to several centimetres shows a subhorizontal cleavage with spacing as close as 1 cm (Fig. 10B). The bedrock wall of the breccia is steeply dipping. Quartz grains in this material evince severe shock damage, suggesting heating to several hundred degrees. The cleavage may be a result of thermal stresses, and its good expression may be due to a lesser overburden in the central uplift during cooling relative to buried breccia of the outer zone.

Broken rock

Zones distinguished on the 1:7500 map (in the back pocket) as broken rock are those in which severe fracturing and displacement has occurred, but the attitudes of at least the larger clasts retain a general consistency, in contrast to breccia, which generally has lost all trace of the original relative orientation of the clasts. Although gradations do occur, broken rock and breccia are usually distinguishable. They are, however, commonly intimately associated, and the symbol on the 1:7500 map indicates the more abundant component.

Megabreccia

As recognised by Cook (1968), the Hermannsburg Sandstone in some localities north of the circular ridge is overlain by chaotically oriented large blocks up to 100 m which may be separated by narrow zones of breccia of smaller clasts. The megabreccia is probably equivalent to zones of overturned blocks and plates of Mereenie Sandstone at the higher levels of the ridge (Fig. 8A, D, F, H). Many of the blocks are overturned, and overlie fragmental breccia (Fig. 10B).

Quartzitic (recrystallised) breccia

Quartzitic breccia occurs beneath the Mount Pyroclast melt breccia (described below), and as isolated outcrops at several localities around the bluff (e.g., GRs 212653, 202660, 219622, 230680, 258680, 278685, 293677). It is texturally similar to fragmental breccia, but is recrystallised and shows conchoidal fracture along intersecting surfaces (Fig. 10D). It is equivalent in character and occurrence to the ball-fracture breccia of the Manicouagan (Quebec) impact structure (Currie 1972). The matrix and sandstone clasts are generally red–brown, while shale fragments are black or grey, and are usually weathered out on exposed surfaces.

The quartzitic nature of the breccia is not an effect of secondary silicification; such a process should equally affect bedrock, which is generally not so affected. The occurrence of the quartzitic breccia beneath and as inclusions within melt breccia at Mount Pyroclast, similar to the occurrence of ball-fracture breccia beneath melt rocks at Manicouagan, points to heating-induced recrystallisation as a cause of induration. This process was enhanced by solution and recrystallisation of shocked and comminuted quartz, and to a lesser extent by recrystallisation of clay minerals. Shock damage in the clasts is variable and generally moderate, indicating that shock heating was less important than heat conducted from overlying fused breccia.

Breccia dykes

Breccia dykes a few centimetres to one or two metres thick cut bedrock plates and large blocks on Gosses Bluff itself and in the outer zone — for example, near Mount Pyroclast (GR 243573; GR 228670; GR 225647). Most dykes consist of 'powder breccia' containing a few large clasts (Fig. 10A, C, F), and some are composed largely of clasts of several centimetres. Large clasts may be slightly rounded, and are commonly oriented parallel to the dyke walls and concentrated in the centre of the dyke. This axial concentration suggests injection as an essentially fluid aggregate into joints and fractures in the adjacent and overlying breccia and megabreccia during the impact-rebound stage.

Melt breccia

Prominent outcrops of melt breccia occur at Mount Pyroclast, and similar rocks occur on hills northeast and northwest of this locality. Three holes drilled into melt breccia (H13, GR 229580; H14, GR 243574; H31, GR 261595) provide continuous cores of it. Melt breccia invariably overlies recrystallised quartzitic breccia. The contact between the two occurs between 12 and 25 m above the base of Mount Pyroclast. Drilling at the saddle between the two peaks of Mount Pyroclast (H14) encountered 14 m of melt breccia — roughly to the base of the hill, indicating an irregular contact. The melt breccia in outcrop near Mount Pyroclast (Fig. 10G–J) and in drillcores (Fig. 10K, L) consists of partly melted fragments of recrystallised sandstone, baked mudstone, and lumps of devitrified silica glass embedded in a flow-banded matrix of devitrified silica glass. The quartzitic fragments are white to grey, and may retain primary bedding features. The typical brown and red sandstones of the Pertnjara Group are absent, indicating reduction of iron from the ferric to ferrous state during heating.

Melt breccia on the upper slopes of Mount Pyroclast consists of fragments up to 2–3 cm, many of which have flowed into twisted ropy folds or are vesicular and pumiceous. Microscopic study reveals textural and mineralogical features that suggest partial fusion, devitrification, and the growth of silica minerals — zeolite and feldspar. Lower in the Mount Pyroclast section, clasts have retained their original shapes, although the microscopic appearance of the breccia is similar. Macroscopic flow characterises only the most intensely disturbed zones. A continuous transition occurs between these rocks and unconsolidated breccia, particularly where the breccias have a high proportion of siltstone, which is more easily shock-deformed into flow

structure. The melt breccia is commonly strongly magnetised, indicating heating and cooling through the Curie point.

The devitrified glass flows are heterogeneously structured; they comprise vesicular spongy masses alternating with ptygmatic flows of porcellaneous rock. In outcrop the porous silica exhibits soft bulbous surfaces and poorly developed flow banding. The porcellaneous silica constitutes a dense compact light-coloured rock, in which well-developed flow structures exhibit dark and light bands, which presumably testify to compositional segregation associated with the melting (Fig. 10G–I). Individual flows range up to a few metres long. The prevalent orientation of the flow structures varies, but is usually steep to vertical. The melt breccia is cut by joints, many of which pass smoothly through clasts and matrix. Most joints are steeply dipping; a minor set is subhorizontal, but there is no well-defined pattern. These joints presumably originated by contraction during cooling.

Units younger than the Gosses Bluff structure

Gravels of the high terraces. North of Rudalls Creek (GR 300670 to 420570) and Undandita Creek (GR 120690 to 270680), the Brewer Conglomerate is largely concealed under terraces capped by gravel a few metres thick. The gravel is derived from the coarser clasts of the Brewer Conglomerate, although there could be a contribution of clasts derived directly from the Macdonnell Ranges. The gravel is only weakly consolidated by a calcareous or ferruginous cement, and the pebbles themselves show a yellow weathering crust. These terraces have a complex pattern of levels not clearly related to the present drainage system, and appear to be older dissected piedmont fans. They probably correspond in general to the middle terrace of Mabbutt (1967). Their age is considered to be Tertiary (Wells et al. 1970) or Quaternary (Condon, *in* Prichard & Quinlan 1962). Quaternary gravel may include unconsolidated and unweathered gravel on surfaces a few metres above present flood plains.

Calcrete. Many exposures in the outer zone of the structurally disturbed aureole of Gosses Bluff, especially of siltstone and of breccia, are partly to extensively carbonated, which has resulted in places in the obliteration of the original character of the rocks. Near Undandita Creek, calcrete 1 to 2 m thick comprising calcite, dolomite, and magnesite is dissected by drainage; the magnesite forms hard porcellaneous 5–10-cm concretions (Wells 1977).

Alluvium and colluvium. Alluvium occurs along watercourses and on the broader plains inside and outside the circular ridge. Colluvium forms a dissected apron on moderately steep slopes. It covers the Dare Siltstone Member at the foot of the outer wall of the ridge, and less noticeably occurs above the Carmichael Sandstone inside the ridge. This colluvium is uncemented or only slightly cemented, and could correlate with the lower terrace gravels on the north flank of the Missionary Plain. Younger colluvium associated with the current erosional cycle occupies patches on the ridge, and grades into alluvium, both inside and outside it. Red aeolian sand covers much of the plain, especially south of Gosses Bluff, and mostly forms a sheet no more than 1 or 2 m thick stabilised by vegetation. Low dunes occur to the southeast.

Structure

Regional setting

Regional dips of the Missionary Plain sequence where the Gosses Bluff structure is located are low, at most 10–15°. The thickness of the sedimentary section, as indicated by the depth to magnetic basement and by seismic reflections, is about 10 000 to 11 000 m (Milton et al. this issue). To the east of the Gosses Bluff structure is the east–west trending Missionary Syncline, complicated by thrust-faulting on its north flank (Fig. 1A). To the west, a corresponding syncline has the Deering fault on its north flank. The axes of these synclines curve to the southeast and northwest of Gosses Bluff (Froelich & Krieg 1969), and flank a northeast-trending anticline — the Gardiner–Tyler anticline — which includes three structural highs: the Gardiner, Gosses Bluff, and Tyler structures. Faulting seems to be of minor significance in the Missionary Syncline in the vicinity of Gosses Bluff.

Erosion has completely destroyed the original crater-wall and -rim zones, and has removed nearly all the crater-floor debris, so that the present ground surface approximates the boundary surface between the zones of coherent deformation and closely faulted blocks in the crater floor. The central uplift, a structural ring–dome feature, consists of coherently displaced rock that originally pierced the now mostly eroded crater-fill breccia.

Zones of coherent deformation

Concentric zones of coherent displacement at Gosses Bluff consist of nearly vertically dipping strata facing outward. Consecutive inward rings comprise increasingly older strata — from the Brewer Conglomerate or Hermannsburg Sandstone, ordinarily at the surface in the Missionary Plain, to the Stairway Sandstone, which normally lies at a depth of about 3000 m, at the core of the structure. The topography is largely an expression of this structure, and of the differential resistance of strata to disintegration by either the original disturbance or subsequent erosion. The circular ridge is composed of the resistant Mereenie Sandstone and Harajica Sandstone Member; the low hills within the central pound are the topographic expression of the Stairway Sandstone and lower Stokes Siltstone; and those outside the circular ridge represent the Hermannsburg Sandstone (Figs. 1B, C). These rocks have been displaced inwardly and upwardly, and the structural pattern is determined by the necessity of fit to a contracted perimeter.

Centripetal displacement has been recognised at other impact structures — examples being Vredefort, South Africa (Manton 1965; Lilly 1980); Sierra Madera, Texas (Wilshire & Howard 1968; Wilshire et al. 1972); and Wells Creek, Tennessee (Wilson & Stearns 1968). Each one of these reflects a similar mechanism and an individual structural style according to the mechanical properties of the rock section. For example, the central area of Sierra Madera, consisting of uniform carbonate rocks, is characterised by steeply plunging radial folds. Gosses Bluff, with a more pronounced alternation of competent and incompetent strata, consists of a mosaic of displaced plates, each a few hundred metres long, separated by faults or breccia zones. Plates of competent rock acted as rigid structural units during deformation, typically showing only minor faulting or open folding internally. The structural disposition of the less competent units is concealed by poor exposure, but appears to be similar, although the Dare Siltstone Member around the

periphery of the circular ridge shows more folding, and thin slivers have been squeezed between plates of the Harajica Sandstone Member.

The central uplift has a highly systematic structural pattern with bilateral symmetry about a north–south axis. The circular ridge is roughly pentagonal; the Stairway–Stokes ridges in the interior describe a V-shape open to the south (Fig. 1C). The assembly of plates was controlled by their geometric fit; thus the structural core of the uplift does not match the axis of symmetry but is a tight anticline that lies along the inside of the northwest leg of the V-shaped structure. The plates at either end of the V trend east–west, but have opposing structural facings: southward at the southwest end and northward at the southeast end.

The Mereenie Sandstone plates in the northern part of the ridge have an *en echelon* pattern symmetrical on the northwest and northeast sides; in its southern part, they tend to be stacked with north–south trends (Milton et al. 1978). The Carmichael Sandstone trends more nearly east–west. Toward the western end of the southern wall, a broken steeply south-plunging anticline has, on its southeast limb, beds facing outward separated by a fault from beds with opposite facing — another example of the tendency towards parallel stacking of plates, regardless of their original structural position. Similarly, west-facing Mereenie Sandstone in the long plate in the centre of the south wall abuts east-facing Harajica Sandstone Member near the outer ridge wall.

The pattern of plates is less obvious in the Harajica Sandstone Member, a more massive unit with fewer marker horizons. In general, there are long successions of northeasterly strikes on the northwest and southeast sides of the ridge, and shorter successions of northwesterly strikes on the other two sides. These trends commonly do not match those of the lower units, as in the southeast, where the northeasterly trending plates of the Harajica Sandstone Member and part of the Mereenie Sandstone contrast with the northerly trending plates in the Larapinta Group and most of the Mereenie Sandstone. In the north of the ridge, where strikes are roughly parallel, a different pattern of displacement is shown by faults, which in the Carmichael and Mereenie Sandstones tend to trend east–west, and in the Harajica Sandstone Member trend north–south, suggesting decollement in the siltstone beds at the base of the Pertnjara Group.

The north–south line of symmetry of the central uplift as a whole does not appear to reflect any structural predisposition, and may be due to directional factors in the dynamic process responsible for the disturbance.

Knowledge of the subsurface structure of the central ring comes largely from logging of Gosses Bluff No. 2 well, located about 500 m east-northeast of the centre, and drilled to a depth of 2652 m. The hole deviated from the vertical to the west-southwest so that the bottom was at a lesser true depth below the ground of the centre of the structure.

The pattern of the surface structure continues at depth — i.e., plates with steeply dipping beds are bounded by steeply dipping faults. Bedding dips average 70–80° in a northeasterly and easterly direction through the upper part of the hole, and are moderately consistent between zones of disturbance or faults, of which some coincide with lithological changes at formation boundaries. The single section of core recovered — Stairway Sandstone at 1400 m — shows an overturned dip of about 82°. From about 1530 to 2135 m, dipmeter data are poor, but the sonic log indicates continued zones of disturbance and faulting. Below this depth there is a normal stratigraphic succession; dipmeter data indicate bedding dips to the east or northeast at about 45°, which decreases to about 35° near the bottom (2652 m). Faults, however, remain steep; four were recorded.

Zones of block-faulting

The faults that separate the plates and blocks in the zones of coherent displacement coincide with occurrences of breccia, which mark the zones of block-faulting. In general, however, the pattern of brecciation and breaking is not obviously related to the structural pattern of bedrock deformation, and much of the brecciation might have occurred after emplacement of bedrock plates. Most breccia shows no evidence of gross transport after brecciation, and is autochthonous with respect to the bedrock plates. Breccia and broken rock are most abundant in the Mereenie Sandstone (Fig. 8D, E), somewhat less abundant in the Harajica Sandstone Member, and notably scarce in the ridges of the Stairway Sandstone and Stokes Siltstone. In each stratigraphic unit, breccia is more abundant at higher topographic elevations. The limiting elevation of fragmentation is a function of rock competence, and is highest in the intensely silicified and boldly outcropping lower Mereenie Sandstone, which forms cliffs on the inner wall that reaches some of the highest elevations of the bluff.

Overturned but still steep dips are fairly common in bedrock plates; more extreme turning is apparent near the summit surface. The upper ends of plates in the harder strata, notably the lower Mereenie Sandstone, and also beds in the upper Mereenie Sandstone and Harajica Sandstone Member, have been inverted to recumbent attitudes, and in some instances to overturned outward-dipping inward-facing attitudes. Inverted plates and patches of breccia with large blocks lie on breccia of stratigraphically higher beds, or directly on the bevelled edges of bedrock plates (Fig. 8F).

Much of this material is contiguous with, and even continuous with, plates of the unit in its autochthonous structural position, as if it had merely tumbled from lack of support, but some lies at a distance that indicates more dynamic transport. One such detached plate of lower Mereenie Sandstone lies upside down astride the Mereenie Sandstone–Pertnjara Group contact 285 m from its normal structural position. Another spectacular example lies on edge in the valley at the base of the Pertnjara Group; it faces inward after rotation of 270° from its pre-event horizontal attitude, and lies at a distance of 235 m outward and at least 40 m downward from the edge of the normally positioned plate. Such plates and blocks must have been thrown on essentially ballistic trajectories and needed a free path. In places, fractures in overturned blocks are injected from below with a breccia of mixed clasts from underlying autochthonous breccia and from the fractured base of the block itself, indicating forceful emplacement. The small thickness or complete absence of breccia beneath many overturned blocks suggests there was a separation between bedrock with pockets of autochthonous breccia, on the one hand, from debris lofted to settle as allochthonous breccia, on the other. The profile of the surface of separation must have been close to that of the present morphology of the bluff.

An occurrence of melt breccia at the foot of the south wall indicates that the outer wall is an original structural feature, rather than merely a product of erosion, and the exotic blocks at the

base of the Pertnjara Group suggest a similar interpretation for the median valley. No evidence remains for the original contact between bedrock, megabreccia, and breccia above the central pound area. Brecciation in the less competent Larapinta Group units might have extended down close to the present ground level.

In a remarkable allochthonous outlier, blocks of the lowermost beds of the upper Stokes Siltstone lie in a broad low alluviated valley at the base of the Pertnjara Group in the east rim of the Bluff (GR 267631; lat. 23°49.15'S, long. 132°19.22'E). The only other material displaced across the inner part of the circular ridge of Mereenie Sandstone is a block of Carmichael Sandstone in an alluviated valley above the waterholes in the west rim (Fig. 8B; GR 236625). The similar rock relations at these two localities on either side of the circular ridge, in 'corners' of the structure, suggest a mechanism other than ballistic transport. The faults leading from the interior to these valleys may have gaped open momentarily, allowing the injection of these blocks or megabreccia of which only the largest clasts are exposed.

Outer zones of the Gosses Bluff structure

Although the deformed zone of the Gosses Bluff structure outside the circular ridge is poorly exposed, surface mapping and shallow drilling (Appendix 1) facilitate the identification of a series of bedrock plates with tangential strikes and steep outward-facing or overturned strata; these alternate with concentric zones of breccia (Glikson 1969). This structural pattern persists to at least as far as a ring of shallow outcrops of Hermannsburg Sandstone at a radius of about 6.75 km from the centre of the structure and probably 1 or 1.5 km beyond. Faulting appears to be the dominant mode of deformation of bedrock. Large-scale flexuring is evident only near GR 245675, where beds of Hermannsburg Sandstone curve northward along a meridional axis of symmetry which may represent a major fault line striking in a continuation of the north–south symmetry axis of the structure.

Fragmental breccia is most abundantly exposed northwest of the circular ridge, where it occupies a series of troughs in which H1 (GR 215644) and H19 (GR 238674) were drilled through 150 m and 60 m, respectively, without reaching unbrecciated rock. A cross-section from GR 233695 to 248639 across the northern part of the northwestern breccia trough in the outer zone is shown in Figure 9. The fragmental breccia in the trough is bordered to the south by overturned bedrock dipping toward the circular ridge, and by megabreccia to the north. Both the bedrock and the megabreccia consist of gritstone and conglomerate. The breccia is polymictic, in contrast to the breccia in the circular ridge, and the clasts show greater local variability in the intensity of shock (Fig. 10A, C, E). Cook (1968) reported that clasts and bentonite bands in H1 cores tend to be oriented with dips of 35–45°, and noted a possible example of graded bedding.

The megabreccia apparently corresponds structurally to the recumbent beds in the circular ridge, and consists of the disintegrated fronts of overturned bedrock plates whose roots are represented by the bedrock ridges to the south of the breccia trough (Fig. 9). The megabreccia is locally underlain by fragmental breccia, and is in places intruded by comminuted breccia, as at GR 228670 (Fig. 10C).

The applicability of the above structural interpretation for the northwestern breccia trough (Milton et al. 1978) as a whole is indicated by the consistently different nature of the southern and northern boundaries along the troughs. The southern boundary, wherever it has been observed, is characterised by a sharp transition between bedrock and fragmental breccia (e.g., near GR 220640 and between GRs 240675 and 260680). The northern boundary, on the other hand, shows a gradual transition from fragmental breccia into megabreccia and densely faulted bedrock (e.g., near GR 225667). The more polymictic breccia is perhaps best regarded as part of the basal crater fill.

Quartzitic (recrystallised) breccia is found mostly, and melt breccia entirely, south of the central bluff. The melt breccia and quartzitic breccia which crop out at Mount Pyroclast and several other localities south of the circular ridge appear to represent a more-or-less continuous breccia zone (from about GR 230575 to 265597) whose minimum dimensions are about 5 × 2.5 km. Drilling within this zone penetrated 48 and 14 m of breccia at H13 (GR 229580) and H14 (GR 243574), respectively, without reaching bedrock. At H31 (GR 261595), on the other hand, bedrock lies at a depth of 10 m. Wherever the relations between the various breccia types could be assessed, the melt breccia lies with an irregular contact over the quartzitic breccia, which in turn overlies fragmental breccia (Glikson 1969).

At Mount Pyroclast, determining the provenances of clasts in the melt breccia is complicated by metamorphic change, but they appear to be derived from the Dare Siltstone Member or Hermannsburg Sandstone. Restricted vertical mixing is indicated by a gradually increasing intensity of shock registered in clasts from the base to the top of Mount Pyroclast. Large individual flow-distorted clasts usually have steep dips. Strikes are less consistent, but there is some preference for northeast–southwest elongations. None of the clasts in the melt breccia show aerodynamic shaping. The material was apparently emplaced by mainly horizontal transport over short distances, possibly packed against the crater wall, which probably lay 1 or 2 km farther out. The Mount Pyroclast material does not constitute fallback breccia like the bulk of the suevite within the Ries crater, Germany, but is analogous in terms of its fabric, structural position, and petrography to material at Polsingen and Amerbach in the Ries crater (von Engelhardt & Stöffler 1968; Stöffler 1971, 1972).

Limits of the Gosses Bluff structure

Only scattered outcrops occur beyond the ring of outcrops of Hermannsburg Sandstone. Steeply dipping beds of the Brewer Conglomerate crop out 8 km northwest of the centre (GRs 196677 and 208677), and steeply dipping beds of sandstone were cored in H4 (GR 181650), 7.9 km west-northwest of the centre, and in H26 (GR 290692), 7.5 km northeast of the centre. Moderately dipping (<45°) tangential attitudes affect scattered outcrops to at least 8.2 km to the east and northeast (GR 306694, GR 325663), and moderately dipping sandstone and shale were cored at H17 (GR 146566), 12 km southwest of the centre. Drillhole H12 (GR 136552), drilled 1.6 km due southwest of H17, penetrated horizontal beds. The most distant disturbed beds recognised dip 5–10° eastward 12.5 km east of the centre (GR 373611).

On the other hand, flat-lying beds occur at least as close in as 7.5 km to the north (GR 241699). Beyond 7.5 km, for about 1.5 km in a radial direction, beds show mainly low outward dips, interrupted by local faults, minor breccia zones, and folds with local steep dips. In one small anticline with less than a metre amplitude, a shale bed dips vertically and intrudes the

overlying sandstone bed. This indicates compressional stress, which is consistent with the structure in this area.

The basic structural pattern in the zone between about 7.5 and 12.5 km from the centre is a gentle outward tilt of strata, perhaps with some radial compression. More intense disturbances are local and probably shallow, as suggested by the abruptness of contacts with less disturbed rocks and the smoothness of the residual gravity field. The resulting breccia (e.g., south of Gosse Dam, GR 363615) appears to be autochthonous.

The above evidence suggests that the limits of the deformed zone lie between about 9.5 and 12.5 km from the centre of the structure, and that the east–west diameter is longer than the north–south diameter. The disturbed layer is apparently very thin, so that small differences in the elevation of its base and of younger erosional levels have resulted in considerable horizontal shift of the recognised limits of the original deformed aureole. On the other hand, the gravity evidence strongly suggests that the aureole is a nearly perfect circle with a radius of 10.8 ± 0.3 km (Milton et al. this issue). There appears to be no gradual change from the steeply dipping strata of the Gosses Bluff structure to the nearly horizontal strata of the Missionary Plain. This is consistent with the gravity model of a disc with a vertical boundary for the disturbed zone, although the gravity anomaly can also be modelled with a graduated density change (see Milton et al. this issue). Perhaps the best figure to adopt for the nominal radius of the structure is 12 km (Tingate et al. this issue), according to the seismic survey by inscription within unpicked shallow reflections apparent on the records, and by the subweathering velocity profile.

The uneroded Gosses Bluff structure is thought to have constituted a crater with a rim of upturned bedrock surmounted by crater ejecta. The location of the crater rim crest cannot be closely specified from the structure at a lower level, but an estimate of its diameter as 24 km seems reasonable. The height of the rim is problematical. The peripheral structural depression of the original crater was limited by a raised rim composed mostly of debris. The Ries crater, after settling of debris and before deposition of lake sediments, appears to have been a shallow saucer with walls perhaps 100–200 m high, and the crater floor sloping gradually to perhaps 300 m greater depth at the centre. Gosses Bluff, with its central uplift, may have had even lower walls.

In a typical lunar crater of this diameter, the floor would be 1–1.5 km lower than the original ground level and the rim crest 0.5 km higher, but terrestrial craters may be shallower. With a few exceptions, the central peaks of lunar craters do not attain the original ground level (Wilhelms 1987), so the summit of Gosses Bluff may be taken as the minimum pre-event ground level. The central uplift of Gosses Bluff originally may have been buried beneath breccia, but it may well have had a ring of bedrock rising above the floor debris of the newly formed crater.

Shatter-cone fracturing

Shatter-fracturing is nearly ubiquitous in sandstone of the circular ridge, is found in the outer zone to at least 6.5 km from the centre, and was intersected in cores from Gosses Bluff No. 1 well to at least 950 m. The diagnostic feature is the presence of diverging striations on the fracture surface. Most commonly the surfaces are segments of cones, but, where the segments are flat and parallel to one another, shatter-coning is transitional with shatter cleavage.

Shatter cones

Shatter cones were first described (as *strahlenkalk*) from Steinheim — the type impact structure in Germany (Branco & Fraas 1905). Bucher (1936), who coined the present name, realised the significance of shatter cones as diagnostic of impact structures and of shock origin. Dietz (1947) showed that the shallow foci to which the axes of shatter cones point constitute definitive evidence of extraterrestrial impact. Gosses Bluff offers one of the most diverse displays of shatter cones.

When examined in detail, each cone segment may be divided into vicinal ('parasitic') segments with a lesser radius of curvature. These in turn are composed of vicinal segments with a still smaller radius of curvature. Striations initiate at the apices of the vicinal segments, giving the cone surface its characteristic 'horsetail' appearance. The striations, which may be regarded as the intersections of the ultimate vicinal segments, may be as small as about 0.1 mm in depth and width. Cone segments rarely if ever intersect. Either one terminates against the other or, especially with vicinal segments or segments at a low angle to one another, both terminate at the junction. No particular order of termination prevails; for example, imbrication in the same sense around the cone is not maintained. Cones are never really nested, although imbricate vicinal segments may define shells with nearly concentric inner and outer surfaces.

Shatter cones at Gosses Bluff are developed in sandstone (e.g., Fig. 11B–G), limestone, mudstone, gritstone, conglomerate, and shale. They are common in breccia clasts, but do not extend into the matrix of the breccia nor do they pass from one clast to another. They are characteristically 20–30 cm long, although 2-m-long segments occur in the more massive sandstone such as the Harajica Sandstone Member and the upper unit of the Mereenie Sandstone (Fig. 11B; GR 261621), and well-defined cones of a few centimetres can be found. Single cones complete through 360° are rare, although examples may be found, particularly in the Stairway Sandstone and the Mereenie Sandstone 'pipe rock'. At most outcrops, the first impression gained is of cone segments in several apparently unrelated directions. Nevertheless, all the cone segments at a locality commonly belong to a single spatial cone, or full cone (Manton 1965), a geometrical abstraction defining orientation but not position. Rarely are all parts of the spatial cone equally developed, but equally rarely are parts completely unrepresented.

Figure 11 (facing page). Fracture patterns and shatter cones at Gosses Bluff: (A) rhombic shatter cleavage in silicified lower Mereenie Sandstone; (B) shatter cones developed in upper Mereenie Sandstone; (C) shatter cones developed in the lower sandstone unit of the Pertnjara Group; (D) shatter cones pervasively developed in the Harajica Sandstone Member, consisting of heterogeneous mudflake sandstone; (E) measurement of shatter-cone striations in the Mereenie Sandstone; the cone segments near the instrument define about two-thirds of the cone; (F) differential partial development of shatter cones in ripple-marked Harajica Sandstone Member; incomplete cones are preferentially developed in finer-grained ripple-crest intervals between wider ripple troughs; (G) detached shatter cone viewed from its apex; (H) alternative methods used to restore shatter cones to their original orientation in presumed originally horizontal beds, and illustrated by three sites in steeply dipping Mereenie Sandstone near the southeast corner of the circular ridge of Gosses Bluff; see text for an outline of these methods, referred to as A, B, and C.

A

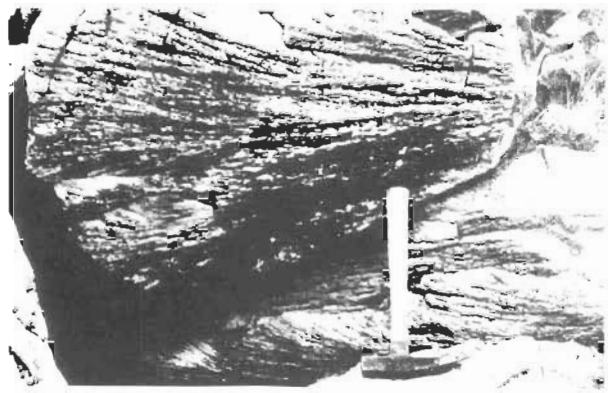

B

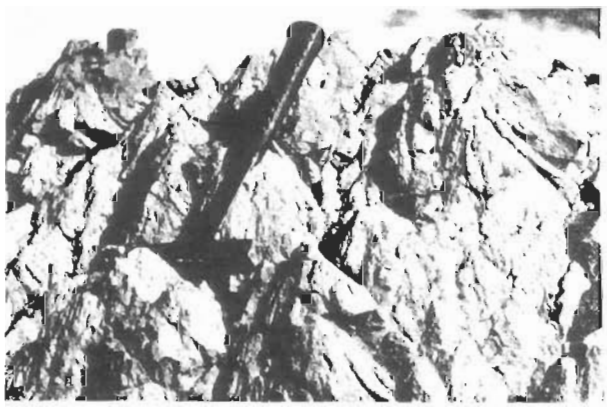

C

D

E

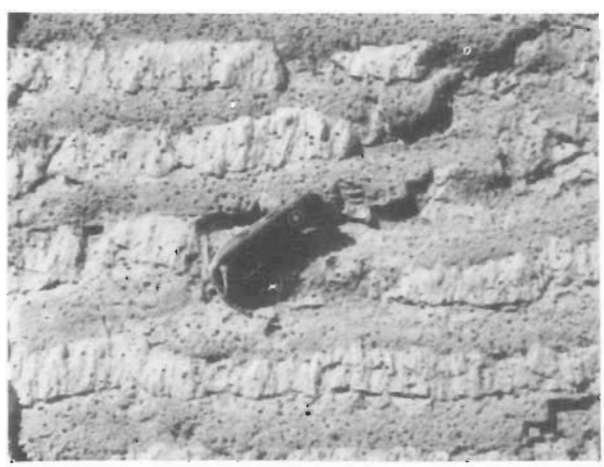

F

G

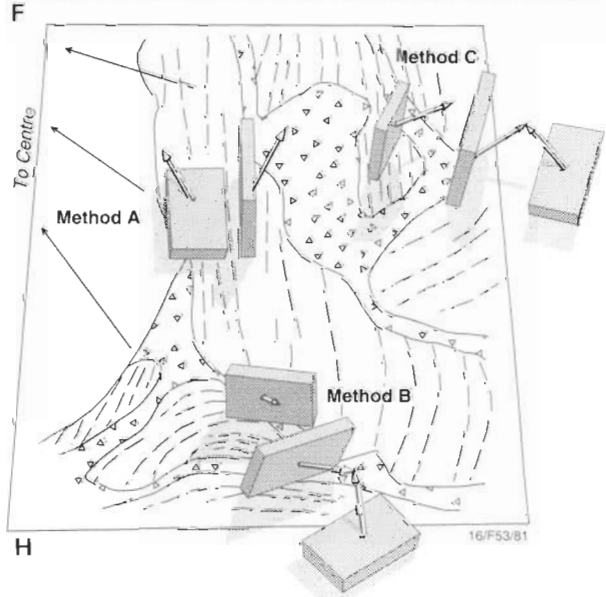

H

At Vredefort, Manton (1965) and Nicolaysen & Reimold (1987) found preferential development of the cone segment below the bedding horizon of the apex. This might apply locally at Gosses Bluff, where, however, no pattern for the preferential development of segments is generally apparent. Finding segments to complete the last 60° or 90° of the spatial cone commonly required careful search, but in any locality with abundant cone segments this search was mostly successful. Accordingly, a few stations of shatter-cone measurement consist of a single physical cone; most, however, comprise several separate segments from within a metre or at most two or three metres, but never from opposite sides of an open joint.

Shatter cleavage

In many outcrops, especially of thinner-bedded units, casual inspection reveals no shatter cones. Instead, the rock is seen to be cut by several sets of cleavage whose planes are in the order of 1–5 cm or as close as 1 mm apart. The cleavage planes may be composed of curved segments or, especially where close-set, appear straight. Planes of different sets cross one another, although one plane may terminate on reaching the plane of another set or be continued on the far side by a slightly offset plane. Plane surfaces are finely striated in the same way as shatter cones. In the wider spaced sets, the planes are composed of distinct cone segments in roughly parallel orientation. Indeed, at most localities with good cones, cone segments tend to lie parallel, and the flattish arcs of different cones lie in the same plane, so that there is a continuous gradation from shatter-coning to shatter cleavage. At one extreme, close-set cleavage planes may have nearly parallel fine striations, so that individual cone segments are barely distinguishable.

Shatter-cleaved rock characteristically has three directions of cleavage, so the rock breaks into rhomboidal units (Fig. 11A). One set generally approximates bedding or cross-bedding. On a bedding plane viewed from the basal side, the other two sets intersect in a diamond pattern. The top surface, on which the apices of downward-opening cones are exposed, has a more irregular pattern. This difference was useful, as a supplement to cross-bedding, for determining the facing of isolated plates of Mereenie Sandstone.

The striations are undoubtedly a shatter phenomenon, but the planes along which they lie could be controlled by pre-impact surfaces, as it certainly is for the bedding-plane cleavage. Close-set cleavage planes, however, are not apparent in outcrops of the same units away from the Gosses Bluff structure, nor is the pattern of three cleavages cutting the rock into rhomboidal units known beyond the structure. The shatter-cleavage planes are therefore likely to have originated at the time of impact, and their orientation probably reflects the stress pattern resulting from the shock pulse. A systematic study of the orientation of shatter-cleavage planes was not carried out, but, where definite cones could be distinguished, the cleavage planes were tangential to them.

In addition to shatter cones and shatter cleavage, isolated or widely spaced surfaces may show shatter striations. These commonly do not belong to the local cone, and may be strongly influenced by pre-existing joints.

Initiation of shatter-fracturing

The nature of shatter-fracturing depends on lithology. However, the nature of this control is not understood in detail, and apparently similar units may have contrasting shatter-fracture patterns. The abundance of cones appears to be related directly, and their sizes inversely, to the abundance of generating points, which are usually discontinuities between beds. The largest cone segments, up to 2 m long, occur in hard massive sandstone beds (Fig. 11B), particularly in the lower part of the Mereenie Sandstone. Thinner-bedded sandstone units tend to have smaller, more closely spaced cone segments. The segments tend to be flat and regularly spaced, so that the pattern is transitional to shatter cleavage, of which excellent examples occur in the upper Harajica Sandstone Member.

Some units, notably silicified parts of the lower Mereenie Sandstone, display shatter cleavage but only rare large individual cone segments. This unit has thin alternations of coarse- and fine-grained sandstone but poor bedding fissility, so coning apparently initiated at discontinuities in solid rock rather than at free surfaces. Shatter-fracturing is uncommon but occurs locally in siltstone or in the few limestone beds of the Stokes Siltstone.

The only obvious regional pattern to the shatter-fracturing is its diminution in intensity toward the margins of the structure. Within any stratigraphic unit, the intensity, and to a lesser degree the character, of shatter-fracturing may vary from place to place around the bluff. The determining factors are seldom obvious; exceptions include the lower Mereenie Sandstone, where shatter cleavage is best developed in more strongly cemented zones.

Cones are presumably initiated at inhomogeneities or discontinuities in the rock. Apices generally lie on favoured bedding planes, but the initiating feature that presumably lies at the apex of each cone can only rarely be detected. The most spectacular example of coning control is found in the 'pipe rock' of the Mereenie Sandstone, where each *Scolithos* tube may serve as the locus of a family of cone segments whose striations horsetail away from the tube.

An interesting occurrence is in a ripple-marked bed in the Harajica Sandstone Member, in which a shatter-fracture surface initiated at each ripple, cut off the sharp crest, and extended no farther than the next broad trough (Fig. 11F). The result is a parting surface more nearly planar than the original bedding.

Table 1. Apical angles of high-quality shatter cones (standard deviation of striations from the geometric cone < 7°)

Unit	*Number*	*Mean*	*Standard deviation*
Hermannsburg Sandstone	7	78.1°	4°
Harajica Sandstone Member	34	78.4°	5.9°
Mereenie Sandstone	27	82.3°	5.4°
Carmichael Sandstone	5	80.5°	9.3°
Stairway Sandstone & Stokes Siltstone	5	85.2°	2.9°
All units	78	80.3°	6.1°

Table 2. Foci of restored shatter-cone axes after rotation by alternative methods (Fig. 11H), measured from a point about 300 m north-northeast of Gosses Bluff No. 1 well at the level of the lowermost exposed bed (distances in metres)

Unit	*Number*	*Simple rotation*				*Tangential rotation*			
		North	*East*	*Up*	*RMS dev.*	*North*	*East*	*Up*	*RMS dev*
Hermannsburg Sandstone	5	3032	556	2464	3356	3082	–561	2535	1478
Harajica Sandstone Member	35	–339	–54	2505	917	–417	152	2460	1100
Mereenie Sandstone	29	–372	199	1775	877	286	198	1712	918
Carmichael Sandstone	8	–9	–50	1967	617	–5	–97	2168	455
Stairway Sandstone–Stokes Siltstone	5	–6	–280	1840	238	62	12	1304	301
Stairway Sandstone–Harajica Sandstone Member	77	0	0	2192	925	–56	96	2139	1013

Shatter-fracturing developed only where the ripple crest did not provide a parting surface near this plane, but the shattering may have been initiated at the locus in each ripple where the bedding surface and the shock front were at some critical angle.

The occurrence of shatter-fracturing in impact structures, and its absence in other tectonic environments, indicate that it is a shock phenomenon. It occurs in the zone of weak or moderate shock, where peak pressures were in the range of perhaps 2–10 GPa. At Gosses Bluff and at other impact structures, shatter cones occur in rock in which the mineral grains show no obvious or only mild shock damage. Cone fragments are common as clasts in fragmental breccia, but apparently not in the lower grades of melt breccia in which they would still be recognisable. In ordinary rock-blasting, peak pressures decay too rapidly away from the charge for shatter cones to form, but good shatter cones have been produced in granite by the detonation of multi-tonne charges of TNT at peak pressures of 3 ± 0.5 GPa (Roddy & Davis 1977) and by nuclear-cratering experiments (Bunch & Quaide 1968). Shatter-fracturing occurs early in a natural and nuclear event, obviously preceding brecciation and, as demonstrated in the following section, before any bulk displacement of rock. Shatter-coning has not received adequate theoretical and experimental modelling, which this remarkable mode of material failure deserves: none of the theoretical explanations appear satisfactory (Milton 1977). It does appear to be a phenomenon at the advancing shock front, or immediately behind it as the shock wave decays. Identification of the direction of cone axes with the local wave normal, essential to the treatment given below, is a reasonable assumption corroborated by the results of this analysis.

Measurement of shatter-cone orientations

Striations were measured to determine cone orientation and apical angle according to methods adapted from those developed by Manton (1965) at the Vredefort structure, South Africa. An average of 19 striations was measured for each of 95 stations. Measuring the pitch of a striation in an arbitrary plane, and the strike and dip of that plane with a specially designed instrument (Fig. 11E), was found to be more efficient and accurate than measuring the plunge and direction of plunge with a hand-held Brunton compass.

Although cone axes could be estimated closely from inspecting hand-plotted stereograms, final values for the orientation of an axis and the apical angle of the cone of best fit to the striations, and the standard deviation of the striations from that cone, were computed by a program based on the least-squares method of Ramsay (1967). In addition, the computer printed out stereographic projections of the striations in true orientation with the vertical as the pole, and as rotated to put the best-fit cone axis at the pole (Fig. 11E).

Cones at eight stations, all but one with standard deviations of the striations from the cone of best fit exceeding 11°, were discarded, leaving 87 for consideration in cone-axis reorientation studies. Seventy-eight cones with standard deviations of the striations less than 7° are of high enough quality for study of the apical angles; of these nearly half have standard deviations less than 4°. The apical angles range from 66–96°, and have a mean of 80.3°.

Small but statistically significant differences in apical angle are apparent in different stratigraphic units (Table 1). There appears to be a trend that might be interpreted as an increase in apical angle downward from the surface, or as a decrease in its size outward from the centre; these differences may be related to lithological variations. The apical angles at Gosses Bluff clearly differ from those at Sierra Madera (75–108°; Howard & Offield 1968) or Vredefort (90–122°; Manton 1965).

Even in a single physical cone, the apical angle is not constant, as the striated surface may curve toward or away from the axis. Most commonly the cone toes in distally; bell-like flaring is less common. For curved surfaces, an attempt was made either to measure all striations at a corresponding distance from the apex, or to take care that apical and distal striations were equally represented in each quadrant. Some cones are elliptical rather than circular; in a few, striations seem to define a triangle with curved sides rather than a circle. A significant variance of the striations from a perfect cone thus need not indicate a corresponding uncertainty in the orientation of the axis.

Some cone segments correspond to both the positive and negative branches of the spatial cone, opening away from and toward the focus respectively, but positive segments predominate by ten or twenty to one. Normally, the negative segments are perfectly coaxial, and have the same apical angle as the positive segments, indicating that they formed by the same mechanism from a point of initiation. Some cone surfaces curve through a somewhat broadened apex from a positive to a negative segment.

An exception to the rule of equivalence of positive and negative cones is apparent in a zone near the middle of the Mereenie Sandstone. Good spatial cones were difficult to obtain in these beds, which account for several of the rejected stations. Two stations appear to yield ill-defined and incomplete spatial cones of different apical angle, intersecting on the stereogram with axes somewhat less than 180° apart. The coning here might have been initiated by both direct and reflected shock waves, whose interference has prevented normal development of either cone.

Table 3. Elevation above the lowermost exposed bed of foci of restored shatter-cone axes on a vertical line through the focus of each unit (i.e., simple rotation of the values in Table 2), and through the focus of the entire range from the Stairway Sandstone (Os) to the lower Pertnjara Group (Pzp1).

Unit	*Number*	*Unit focus*		*Group focus*	
		Elevation	*RMS dev.*	*Elevation*	*RMS dev.*
Hermannsburg Sandstone	9	3867	1263	3862	1287
Harajica Sandstone Member	35	3152	1782	3092	1665
Mereenie Sandstone	29	2457	987	2732	1329
Carmichael Sandstone	9	2567	725	2563	751
Stairway Sandstone–Stokes Siltstone	5	1904	298	1965	762
Stairway Sandstone–Harajica Sandstone Member	78			2801	1477

Shatter-cone reorientation

We assume that shatter cones form during a shock event, and that their axes point in the direction from which the shock wave advances. Moreover, only after the passage of the shock wave, during the decompressional phase, does any gross displacement occur. Thus the form of the shock front may be reconstructed if cone stations are restored to their pre-impact location and orientation. Cones show a somewhat symmetrical orientation pattern of outward- and upward-pointing axes, but this merely indicates transformation by more or less regular displacements from the original pattern.

For the orientation studies, the data include computed cone-axis orientations, the attitude of the bedding at the station, the grid coordinates of the station, and the elevation in the stratigraphic section measured from the lowest exposed horizon. For almost every data set, more confidence can be placed on the cone-axis orientation than on the bedding attitude, because most of the sandstones are more or less cross-stratified. Only the Mereenie 'pipe rock', where the *Scolithos* tubes could be assumed to indicate the original vertical unambiguously, presented no problem in this regard.

In the initial reconstruction of the pattern of shatter-coning at the time of formation, the stations were restored to positions vertically below their actual positions, at elevations corresponding to their place in the stratigraphic column, and were rotated to make bedding horizontal. The bearing of a restored cone axis depends on the path of rotation chosen. Three methods are indicated (Fig. 11H):

- The simplest is a one-step rotation about the line of strike from the present dip to the horizontal (method A).
- A two-step rotation of the bed — first about a vertical axis until the strike is tangential to the structure, and then about the line of strike (method B); this was the method used by Manton (1965) to reorient the shatter cones at Vredefort.
- A third method is to rotate the bedding, first in its own plane until the cone axis and the bedding-plane normal lie in a vertical plane, and then about the line of strike (method C).

These methods approximate a reversal of the rotation to which the stations were subjected. Rotation of a station about a vertical axis according to method B is controlled by corrections related to movements along adjacent faults. Method C was applicable to stations in isolated areas of breccia and broken rock where rotation in the plane of bedding might be accommodated. Methods A and B delivered satisfactory reorientations for many stations; method C, for fewer. Accordingly, reorientations were carried out and foci computed according to methods A ('simple') and B ('tangential').

The focus is defined as the point closest to the extended lines of the cone axes, as found by a least-squares method. The root-mean-square distance of the lines from the focus serves as a measure of the variance of the solution. Foci were calculated for the stations in each unit, and were combined in the Stairway Sandstone through Harajica Sandstone Member for manipulation by the simple and tangential programs. For the tangential rotation, the adopted centre was the hypocentre of the simple focus for the combined units. Measurements were available for 82 stations (after omitting low-quality cones; one station inadvertently measured in a slump block; and those Hermannsburg Sandstone stations in megabreccia in which displacement involved tumbling rather than a reconstructable rotation). The results are shown in Table 2.

Except for the Hermannsburg Sandstone, for which the sample population may be insufficient to compensate for its large sample area, the foci group fairly well, having hypocentres close to the geometric centre of the structure. The foci determined separately by the simple and tangential programs are remarkably close. Clockwise and anticlockwise rotations closely balance. The average rotation about a vertical axis is 37°, and the average standard deviation is less than 1°. Standard deviations indicate that the simple program yields slightly better-defined foci for all units except the Hermannsburg Sandstone.

The locations of the foci determined by the two methods closely overlap the centres of symmetry determined from the gravity field. The centres of circles corresponding to the outer gradient and inner annular gravity low are very close to the hypocentres of foci of energy release determined from shatter cones.

Method A applied to stations which had not undergone a rotation about a vertical axis introduces an error in the tangential program, and method B applied to stations which had undergone a rotation introduces an error in the simple program, even if these errors are cancelled by balancing errors in other stations. In a further program, bedding at all stations was rotated so that the azimuths of the cone axes pointed directly to the centre. This program in effect considers only the angle between the bedding and the cone axis, for which the measured bedding attitude is structurally insignificant. It yields no information about the north–south and east–west coordinates of the focus, but yields improved data on the vertical coordinate. The central vertical lines were assumed to pass through the foci found by the simple rotation program for the individual and for the combined units. The mean intercepts on these verticals, and the root-mean-square departure from the means, are presented in Table 3. The mean intercepts are considerably higher than the vertical coordinates of the foci in Table 2. Moreover, a definite progression emerges of higher foci from higher units.

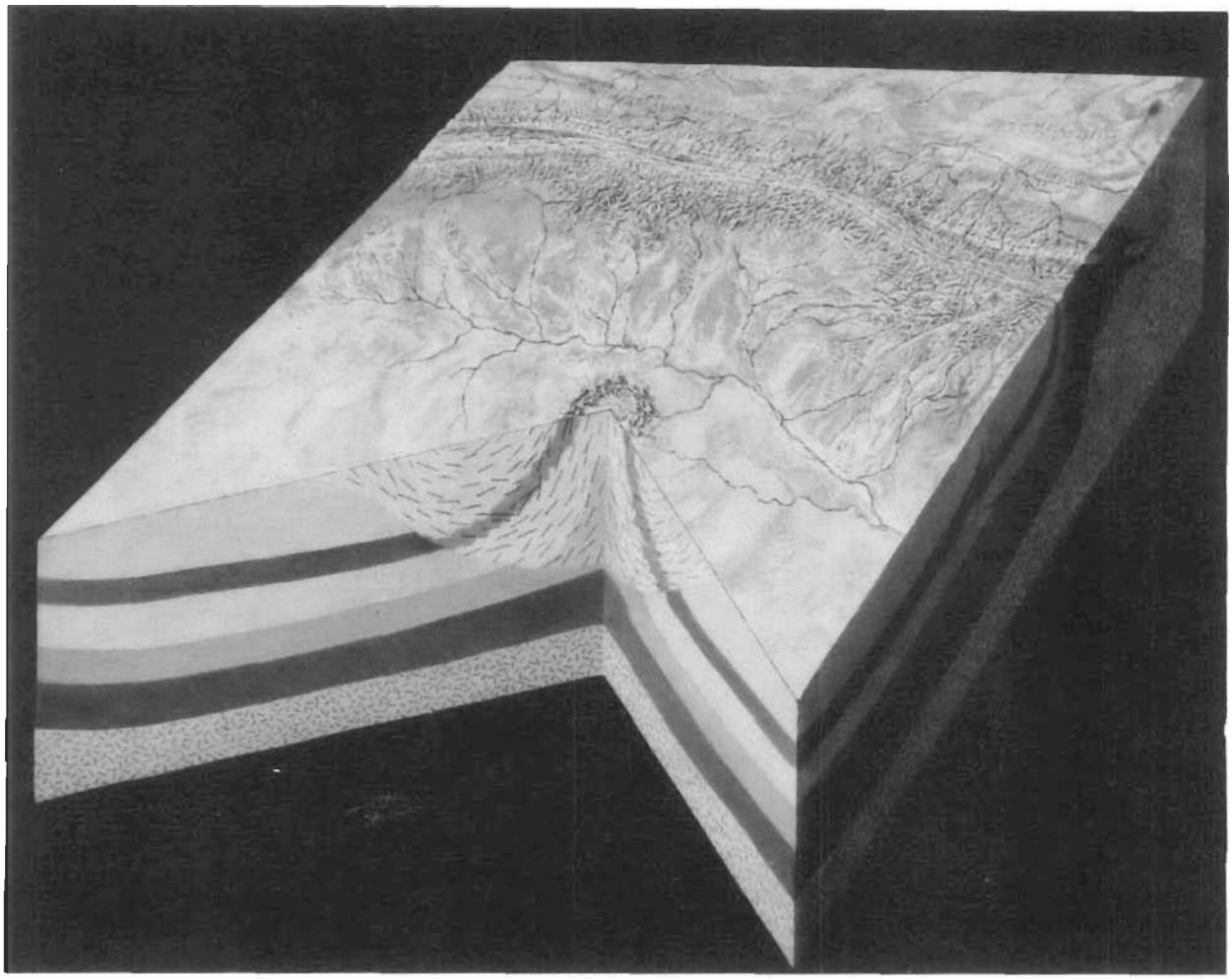

Figure 12. A three-dimensional structural model of Gosses Bluff based on the synthesis of geological and geophysical evidence (drawn by D. Davis).

The assumptions that the shock wave emanated from a point, despite its source from an extended object that penetrated some distance (Milton et al. this issue), and that it propagated as a spherical front, are clearly simplifications, but no logical modifications would yield the observed pattern. An explanation by *ad hoc* changes to the assumption of original horizontality of the strata or by grossly reducing the estimated thickness of the stratigraphic section seems equally unlikely. The error is almost certainly a result of the assumption of solely vertical displacement of the stations, despite the ample evidence for inward displacement in the central uplift. Indeed, the best measure of this displacement is given by the shatter-cone data. An assumption that the Hermannsburg Sandstone stations, at somewhat over half the radius of the structure, have not moved horizontally brings the foci for the lower units into coincidence with the Hermannsburg Sandstone focus if the mean horizontal radii to the stations have decreased from their pre-impact radii by: Harajica, 30 per cent; Mereenie, 37 per cent; Carmichael, 38 per cent; Stairway, 52 per cent.

As portrayed in the structural model of Gosses Bluff (Fig. 12), the features observed at cryptoexplosion structures are consistent with an origin by impact. The Gosses Bluff study has a special importance in supplying a degree of rigour to the qualitative observation that the focus of energy in these structures lies within or above the disturbed zone rather than below, clearly indicating an extraterrestrial origin for this event.

Petrology of disrupted rocks

Rocks associated with impact structures display a wide range of features that define a distinct type of metamorphism arising from instantaneously applied extreme pressures or shock (French & Short 1968; Roddy & Davies 1977; Stöffler 1971, 1972). Whereas the shock lasts only for fractions of a second, the cratering process might persist for seconds (R.A.F. Grieve, Geological Survey of Canada, personal communication 1995). The shock features at Gosses Bluff reflect the peak pressure. Post-shock thermal effects, however, are particularly important in the melt breccia, where heat conducted from masses of shocked rock above has produced stronger thermal effects than local shock-induced thermal effects. The nature of shock deformation in quartz and other materials is discussed below.

Quartz

The greatest variety of shock metamorphic effects is found in framework silicate minerals, especially quartz, which displays two types of phenomena: development of planar deformation features, and phase change to glass or to high-pressure crystalline polymorphs. Planar features have been referred to diverse classifications and nomenclature; the most important varieties

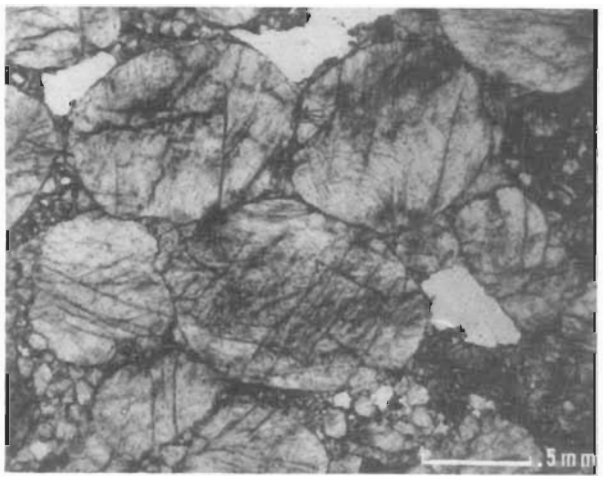

Figure 13. Sand grains showing mainly omega-type rhombohedral and basal planar elements; bimodal sandstone from the base of the Stokes Siltstone at the centre of Gosses Bluff. Phosphate pellets (dark) including small angular quartz grains appear on the right.

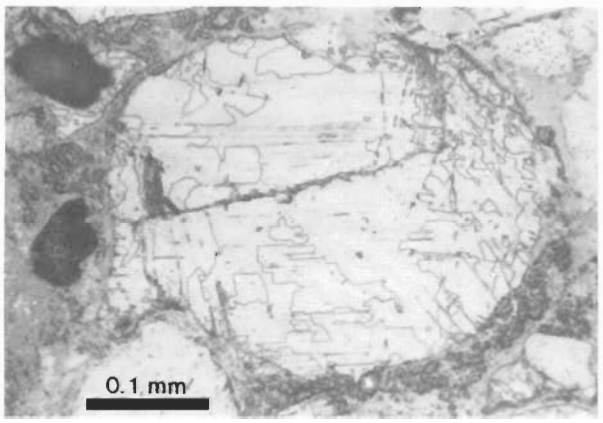

Figure 14. A twinned quartz grain showing Dauphiné twinning, polished and etched in hydrofluoric acid; from the basal Stokes Siltstone. Omega-type planar elements are developed almost exclusively in a single individual twin.

are cleavage (referred to as microfaults of some workers) and planar elements (referred to as lamellae by some workers). Cleavage planes are broad and widely spaced, whereas planar elements are narrow (1 or 2 mm), and occur in sets of closely spaced individuals; both can generally be assigned to rational crystallographic planes.

Polished thin sections of Gosses Bluff sandstone etched in hydrofluoric acid reveal several penetrative planar fracture patterns (Fig. 13). They also show that twin boundaries are often parallel to planar elements (Fig. 14), and that the pattern of these elements differs in the individual twins.

The main direction of cleavage in quartz from Gosses Bluff is r,z{1011}. The main direction of planar elements is w{1013}, often with all six planes developed in a single grain. The second most abundant set is p{1012}, and planar elements on the base c{0001} on higher rhombohedra, and perhaps on prisms, are also evident.

In a series of experiments on shock loading of single crystals, Hörz (1968) produced cleavage at 5 GPa, the lowermost pressure level investigated, where cleavage is sparse compared with that developed under higher pressures. Omega elements appear at a threshold pressure between 10 and 12 GPa. Planar elements in other orientations appear at higher shock levels; pi elements first appear between 16 and 20 GPa, and are almost as abundant as omega elements at higher pressures. Hörz (1968) found the breakdown of the quartz lattice, as indicated by reduction of refractive indices and birefringence, to begin at about 20 GPa and extend to at least 30 GPa.

Some rocks in the central uplift of Gosses Bluff show only randomly oriented fractures, and probably received shock of less than 5 GPa. Probably more abundant is rock with well developed cleavage and planar elements, mostly omega, which experimentally correspond to the 12–20 GPa range. In clasts in the sheeted breccia, pi and high-angle elements, perhaps {2241}, are well developed, indicating shock over 20 GPa.

Higher shock pressures destroy the crystalline structure of quartz, transforming it to a dense disordered phase that may crystallise to one of the two high-density silica polymorphs — coesite and stishovite — or may remain as a glass after pressure relaxation. No coesite or stishovite, and — at most — very minor quantities of silica glass, were identified at Gosses Bluff, although devitrified and recrystallised derivatives of glass abound in the melt breccia.

At Meteor Crater, Kieffer (1971) found that porosity in sandstone was eliminated at about 3 GPa, and that at about 5 GPa some grain boundaries develop yellow to gold-coloured linings that are exceedingly complex mixtures of quartz, glass, and coesite, barely resolvable under the microscope. At higher pressures, linings are opaque, probably because of vesicularity in the glass. In the initially less porous sandstones at Gosses Bluff, these grain boundary effects are less marked. Dark brown linings between grains do occur in some material from the central uplift, and may also indicate local phase changes, though if coesite were formed it no longer remains in detectable quantities.

More intensely shocked quartz is apparent in the melt breccia. Many of the clasts and grains retain the original quartz lattice; planar elements are usually abundant and often have a dusty brown appearance due to inclusions or optical anomalies that are too small to resolve. However, much of the quartz was thoroughly recrystallised, obliterating its original post-shock state.

A variety of shocked sandstone that is more common in exposures southwest of the circular ridge, where flow texture is barely developed, has a finely crystalline texture resembling chalcedony in which the original sand grains cannot be recognised, or are indicated by a vague patchiness. In hand specimen, clasts of this material commonly preserve the original bedding (indicating that the silica was never liquid), and show a well-developed cleavage with open vugs along the planes at a high angle to the bedding, abundant enough to give a puffed appearance and a low density. The cleavage in this material is very similar to that of 'variety A' sandstone from Meteor Crater (Barringer 1905). The thorough recrystallisation suggests that quartz was disordered by a solid-state shock transformation to a glass — 'diaplectic' glass of von Engelhardt & Stöffler (1968) — which subsequently devitrified. This would occur at shock pressures above about 30 or 35 GPa, and a post-shock temperature that could be as low as 300°C for a dense rock (Stöffler 1971), but would be considerably higher for an originally porous rock. The rock cleavage is most easily explained as a

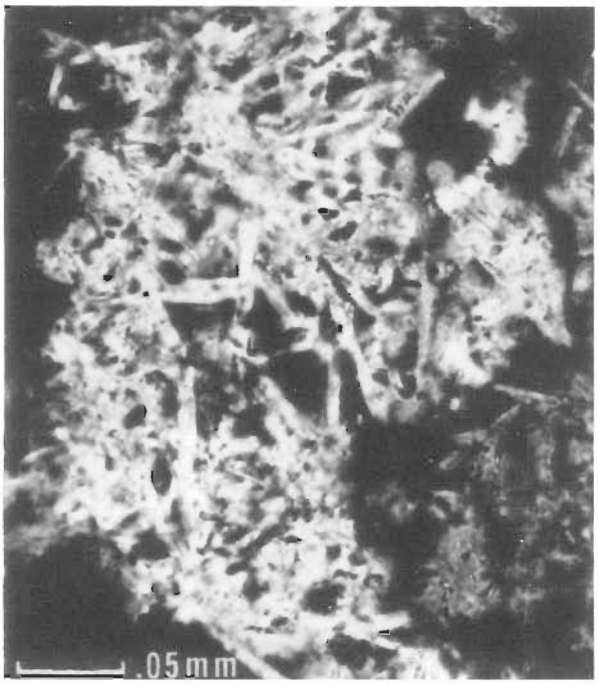

Figure 15. Paramorphs of quartz after tridymite (under crossed nicols) in melt breccia from Mount Pyroclast.

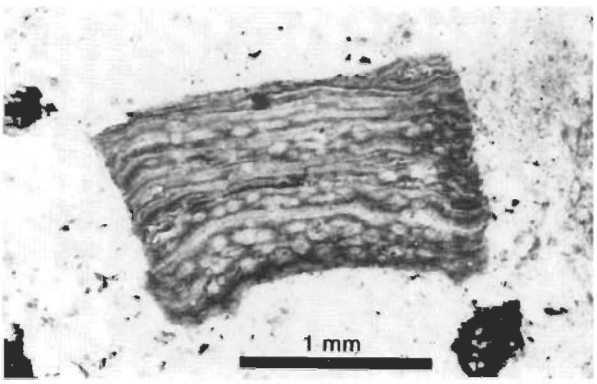

Figure 16. Microclast, with fluidal texture, composed mostly of cristobalite. The matrix consists of recrystallised quartz with minor sanidine and zeolites.

result of thermal contraction on cooling, which would imply higher maximum temperature.

In large clasts in the Mount Pyroclast melt breccia (GR 243573), which are deformed into twisted ropy folds (Fig. 10I), much or all of the quartz when viewed microscopically shows decussate aggregates of randomly oriented small-bladed and triangular crystals whose morphology is characteristic of tridymite — the high-temperature polymorph of silica stable between 867 and 1470°C at low pressure — although the optics and X-ray diffraction show it has all inverted to quartz. Paramorphs of quartz after tridymite have also been described from the Sudbury (Stevenson 1963) and Clearwater Lake (McIntyre 1962) cryptoexplosion structures in Canada. Where shocked relicts of the original quartz grains remain, their optical orientation has controlled that of the quartz in the adjacent paramorphs.

Other material with no relict quartz shows a banding expressed by the abundance and size of the voids or inclusions between tridymite blades. This banding suggests flow before the tridymite crystallised, and one might visualise the material to have been fused silica, possibly vesicular. However, the quartz produced by the inversion of tridymite is in optical continuity in patches remarkably suggestive of relict sand grains (Fig. 15). If tridymite crystallised during the cooling of diaplectic rather than fused silica glass, sufficient remnants of the quartz lattices (either as spots of untransformed quartz or an incompletely disordered glass) may have survived to orient the regrowth of quartz by the inversion of the tridymite and devitrification of whatever glass remained. These two interpretations may not be mutually exclusive if flow banding can develop with only slight relative movement, perhaps just at the softening point of silica glass.

Some small clasts and shreds at Mount Pyroclast show a well-developed flow banding in which small and greatly elongate quartz grains have wavy extinction, commonly corresponding to the tight folds of the flow banding (Fig. 16). It is not clear whether at least partly crystalline quartz was deformed plastically, or whether diaplectic glass or fused silica has recrystallised. Bands of opaque material are common in many of these clasts, suggesting that they are derived from siltstone with fine quartz grains rather than sandstone. Some shreds with similar flow texture are isotropic or nearly so, and show vaguely defined patches transecting the banding. X-ray diffraction shows that these are composed largely of cristobalite, which unlike tridymite has survived without inversion. In the pure silica system, cristobalite is stable at higher temperatures than tridymite, but cristobalite of lower crystallinity can form at much lower temperatures.

Thus the melt breccia preserved at Gosses Bluff contains abundant material representing sandstone transformed to glass. It is not clear if any of this, or at least any bulk quantities, were melted to a true liquid. There is no evidence of gross vesiculation, which is abundant at Meteor Crater or Ries Crater — for example.

The melt breccia in drillcores from troughs west of the circular ridge is composed mainly of only moderately shocked clasts, but has a minor component of intensely shocked clasts, which accordingly were quenched and preserve some shock features not seen at Mount Pyroclast. Apparently unrecrystallised glass occurs on a microscopic scale as irregular veins and patches within individual quartz grains in some rare, intensely shocked sandstone clasts in cores from H1 (GR 215644).

Since their discovery in shocked sandstone from Meteor Crater (Chao et al. 1960, 1962), the high-pressure silica polymorphs, coesite and stishovite, offer particularly convincing evidence for impact-shock events, since their formation requires pressures reached statically only deep in the mantle. According to methods essentially those of Fahey (1964, 1971), coesite and stishovite in Gosses Bluff material were sought by solution in either concentrated or dilute hydrofluoric acid and X-ray diffraction analysis of the residue at successive stages. The limits of detection according to Stöffler (1971) are between 0.05 and 0.1 per cent for coesite, and about 0.001 per cent for stishovite; the difference is due to the slight solubility of coesite, and the absolute insolubility of stishovite, in hydrofluoric acid. Neither polymorph was detected.

The occurrence of coesite and stishovite depends not only on their formation in the shock pulse, but on their stability at the high temperatures persisting after relaxation of pressure. Coesite can survive heating up to 1100°C, while stishovite inverts in a

minute at 850°C, and in a few days at 500°C (Skinner & Fahey 1963; Dachille et al. 1963). In addition, natural submicron-size grains of stishovite are highly soluble in water (Bohn & Stöber 1966).

Coesite occurs in quantities up to about 30 per cent or 40 per cent of the original quartz, and stishovite generally in quantities less than 1 per cent, at both Meteor Crater (Kieffer 1971) and Ries (Stöffler 1971), but the two localities differ significantly. In the porous Coconino Sandstone of Meteor Crater, where residual post-shock temperatures would have been high, stishovite is never found without coesite, and both are associated with glass along quartz grain boundaries. In the dense crystalline rocks at Ries, both minerals are embedded in quartz and in diaplectic glass, and stishovite without coesite is included within planar elements of quartz grains. Here detectable stishovite is an index of a lower shock range than coesite — about 12–45 GPa for stishovite, and 30–55 GPa for coesite.

Using either Meteor Crater or Ries as a model, we might expect significant quantities of coesite in the melt breccia at Gosses Bluff. If the heating of this breccia was due only to its residual post-shock heat, it is surprising that coesite has not survived. If, however, Mount Pyroclast and the other remnants lay below still hotter material, the temperature may have been high enough to destroy any coesite. It may be significant that Stöffler (1971) did not find coesite or stishovite in suevite from Amerbach, or from depth in the Wörnitzostheim borehole, two localities at Ries that are closely analogous with Mount Pyroclast. If post-shock annealing is responsible for the absence of coesite at Mount Pyroclast, selected clasts from the western breccia troughs may be more favourable, although they have not been systematically treated. Coesite in small quantities might also occur in those shocked sandstones that show dark linings between grains, although none was detected.

The Meteor Crater model offers little expectation of finding stishovite at Gosses Bluff. If however, the more silicified sandstone behaved like the crystalline rocks at Ries, traces of stishovite might occur in fragmental breccia or even in shocked bedrock. A particular effort was made to find it in the sheeted Mereenie breccia, but without success.

Other shocked materials

Sandstone in the Parke Siltstone, the parent rock of the melt breccia, is more commonly arkosic and micaceous than purely quartzose. Accordingly, zeolites and sanidine crystallised in the metamorphosed sandstones at Mount Pyroclast (GR 243573). Heulandite–clinoptilolite is the most abundant zeolite; stilbite and chabazite also occur. Crystals are rather small, usually a few millimetres. Some occupy vugs, but often zeolites form a matrix for quartz (after tridymite), suggesting that they formed by devitrification or alteration of solid material, probably glassy. Euhedral crystals in open cavities, like those characteristic of zeolites formed during the hydrothermal stage of basaltic volcanism, are rare.

An uncommon but striking variety of metamorphosed sandstone at Mount Pyroclast shows concentric bands marked particularly by abundant opaques, mainly goethite. Although all the mineral grains (including the subhedral opaque crystals) are products of recrystallisation, the banding is apparently a relict feature. Similarly, banded ironstone concretions are found in unmetamorphosed Parke Siltstone and Hermannsburg Sandstone.

Sanidine occurs as a minor constituent in metamorphosed sandstone. In addition, at Mount Pyroclast, it composes the bulk of some grey pumiceous phenoclasts that resemble the suevite of Ries crater (Milton & Sutter 1987). This rock is highly vesicular, and the most probable of any at Gosses Bluff to have been truly liquefied. In the phenoclast specimen used for radio-isotope dating, vesicles average about 0.15 mm in diameter and occupy about 35 per cent of the volume. The high potash content clearly rules out an origin by isochemical melting of any pre-impact rock; the clast is probably melted shale whose composition was altered by hot fluids circulating in the melt breccia during cooling. Potash metasomatism of analogous material is known from other impact craters.

X-ray diffractograms indicate an end-member composition and a structurally high state for the sanidine. The petrographic microscope shows an extremely fine-grained material clouded with dusty particles. Patches in optical continuity (presumably sanidine) are at most 4–5 μm across. Grains of titanian hematite, mostly less than 50 mm, pepper the material and appear as lustrous black euhedral crystals where they emerge from the matrix at vesicle walls. Although the bulk of the material is sanidine, clean sanidine was never found at the resolution of the electron-microprobe beam. Spot analyses were closer to the wet chemical analysis of the bulk material than to pure sanidine, but revealed some deficiency of the elements which reside in the hematite. Some of the vesicles are lined with thin crusts of fine-grained quartz and contain heulandite–clinoptilolite crystals.

Microclasts with a marked flow structure and a very fine-grained texture are probably metamorphosed shales. At Mount Pyroclast, these consist of phyllosilicates, sanidine, and zeolites, and silica as quartz and cryptocrystalline cristobalite. Phyllosilicates, aside from relict minerals, are a minor component at Mount Pyroclast, but bands and lenses of montmorillonite are abundant in the breccia near H1 (GR 215644), and form bentonite (Cook & Duff, *in* Cook 1966). This may be an alteration product of shock-melted shale quenched to a glass, while corresponding material at Mount Pyroclast recrystallised during slower cooling. Some isotropic microclasts in cores from this borehole may indeed preserve untransformed glass from shock-melted shale.

Scattered fragments of scoria-like material totalling about 1 kg and collected northeast of Gosses Bluff are composed of clear glass containing abundant unmelted rock inclusions and quench crystals of diopside. The glass shows no fission tracks on etching; it is therefore geologically young, and cannot have originated from the Gosses Bluff impact. Similar material has been described from other localities — for example, Tempe Downs, about 75 km south of Gosses Bluff (Baker 1953), and the Champ de Mars area of the Tomkinson Ranges, western Musgrave Block. Trendall (1964) has shown that such material represents fused soil associated with the roots of trees affected by lightning strikes, and termed accordingly 'fulgurite slag'.

Age of the Gosses Bluff impact

Stratigraphic control allows a wide range of possible ages for the Gosses Bluff impact. The youngest strata involved are Late Devonian (Playford et al. 1976); the erosion surface that cuts the summit of the circular ridge is rather vaguely dated as pre-Tertiary.

The shock effects on bedrock and fragmental breccia were not intense enough to have reset geochronological clocks (Deutsch et al. 1989). However, melt breccia at Mount Pyroclast and the heated breccia underneath supplied material suitable for fission-track, K–Ar, and $^{40}Ar/^{39}Ar$ dating. A fission-track date of 130 ± 3 Ma (which should be corrected to 134 Ma according to more recent decay constants) for zircon grains extracted from sandstone breccia clasts from drillcores at Mount Pyroclast, and a K–Ar date of 133 ± 3 Ma (to be corrected to 136.5 Ma) on the sanidine-rich material described in the preceding section, were determined by USGS and reported earlier (Milton et al. 1972).

A specimen from the clast of pumiceous melt breccia described above, and previously used for K–Ar dating, was selected for $^{39}Ar/^{40}Ar$ dating; its component high-potassium, structurally high sanidine is known to be retentive of argon under natural conditions, particularly in coarse grains. Material was irradiated in a nuclear reactor by fast neutrons, together with standard specimens, and the argon was extracted by stepwise radiofrequency heating and analysed in a rare-gas mass spectrometer. The total-gas age obtained was 137.8 Ma, which compares satisfactorily with the K–Ar age. The age spectrum produced by stepwise heating did not give a plateau in the strict sense, but gave low ages for the lower-temperature steps in a pattern characteristic of a sample that has lost a few per cent of its radiogenic argon by diffusion since crystallisation. Three higher-temperature steps, however, have apparent ages that are indistinguishable from one another analytically and together yield an age of 142.5 ± 0.8 (1s) Ma (Milton & Sutter 1987). We believe that this is the best currently available age for the Gosses Bluff impact.

The age of the Jurassic–Cretaceous boundary has been defined as 144 ± 5 Ma (Kent & Gradstein 1985), and more recently as 141 Ma (J. Claoué-Long, AGSO, personal communication 1995). During the interval 144.5 to 141 Ma (on Kent & Gradstein's correlation), chrons of reversed polarity M16, M17, and M18 occupy 80 per cent of the time, whereas — for several million years before and after this interval — polarity was normal. As the melt breccia shows a reversed remanent magnetic polarity, the Gosses Bluff impact probably occurred during one of these chrons. The impact can accordingly be assigned to the latest Jurassic.

Material ejected by the Gosses Bluff impact might have been incorporated in contemporaneous sites of sedimentation, and may in due course be detected. Ejection from the Acraman impact structure has been shown to be the source of shocked rock fragments up to 50 cm in the Bunyeroo ejecta in Late Proterozoic strata in the Flinders Range, South Australia (Gostin et al. 1986; Wallace et al. this issue), and of sand-size grains in the Officer Basin (Wallace et al. 1989); the depositional sites of these ejecta are respectively 300 and 470 km from the Acraman impact structure. Late Jurassic and Early Cretaceous strata crop out at similar distances from Gosses Bluff in the Eromanga Basin to the east and the Canning Basin to the northwest (Bradshaw & Yeung 1992).

Origin of Gosses Bluff

The concept that we espouse regarding the sequence of events involved in the formation of Gosses Bluff is illustrated in Figure 17.

The Gosses Bluff structure is a member of the class of impact structures known as astroblemes, which in the widest sense includes meteorite craters (mostly young and small) and large and old structures. Astroblemes are the deeply eroded root zones of craters (cf. Grieve & Pesonen 1992; Rondot 1994). At small craters (up to about 1 km in diameter) the presence of meteoritic fragments makes the origin self-evident. The origin of the larger, deeply eroded structures, however, is less obvious. The hypothesis of an impact origin extrapolated from meteorite craters was supported largely by the argument that no intraterrestrial process could account for the large pressures indicated by such features as shatter-coning, shock deformation, and melting. Direct evidence for the impact origin of several cryptoexplosion structures has become available from the discovery of siderophile trace-element patterns in melt breccia that indicate contamination by extraterrestrial material, some of it correlated with specific meteorite types (Palme 1982). At Gosses Bluff, analysis of material from Mount Pyroclast may prove rewarding.

Crook (1967) made a bold suggestion that gases which blew from seismic shot-holes in the Pertnjara Group around the periphery of the structure during the Magellan survey may contain a component of cometary origin. A combination of air, terrestrial hydrocarbons, and reaction products from the explosive charge would, however, seem to fit the reported compositions. Nevertheless, at Crook's suggestion, we endeavoured to collect gases from shot-holes during the BMR survey, but gas-blowing failed to recur.

On the basis of astronomical observations and orbital calculations, Shoemaker et al. (1990) concluded that a crater the size of Gosses Bluff is more likely, by a factor of 3 or 4, to have been produced by an asteroid than a comet. According to their empirical formulae (7) and (8), a crater of diameter about the size of Gosses Bluff produced in rock with a density of 2.6 t m^{-3} by an asteroid with an impact velocity of 17.9 km s^{-1} and an impact angle of 45° would involve a kinetic energy of about 300 Gt TNT equivalent (1 Gt TNT = 4.185 x 10^{25} ergs), which could be generated by an asteroid of ~2-km diameter. Such an event on the surface of a continent is estimated to occur about once in 10^6 years.

An understanding of the impact process has developed from geological observations, from laboratory-scale experiments in hypervelocity impact, from large-scale cratering experiments, particularly with nuclear devices, and from basic physical theory (Melosh 1989). Unlike most geological processes, impact events are almost instantaneous, so the laws of conservation of mass and energy place powerful constraints on them. The physical behaviour of various rock types recorded experimentally can be applied to model the course of an impact event millisecond by millisecond. The release of impact energy within a limited volume of rock may be compared with the detonation of a high-explosive charge of an order of magnitude similar to a nuclear device.

The initial stage of an impact can be treated simply as a one-dimensional event. One shock wave moves forward into the ground and another backward into the bolide. The shock-wave velocities and the particle velocities in the bolide and in the ground, and the pressure between the shock fronts (uniform in both media), can be calculated if the behaviour of the materials under shock conditions is known. These have been determined for a variety of natural and artificial materials by so-called Hugoniot experiments. Pressure during the compressional stage generated by the impact of a bolide at cosmic velocities falls in the range of 300–3000 GPa. As the shock front continues to expand into the ground, the pressure behind it

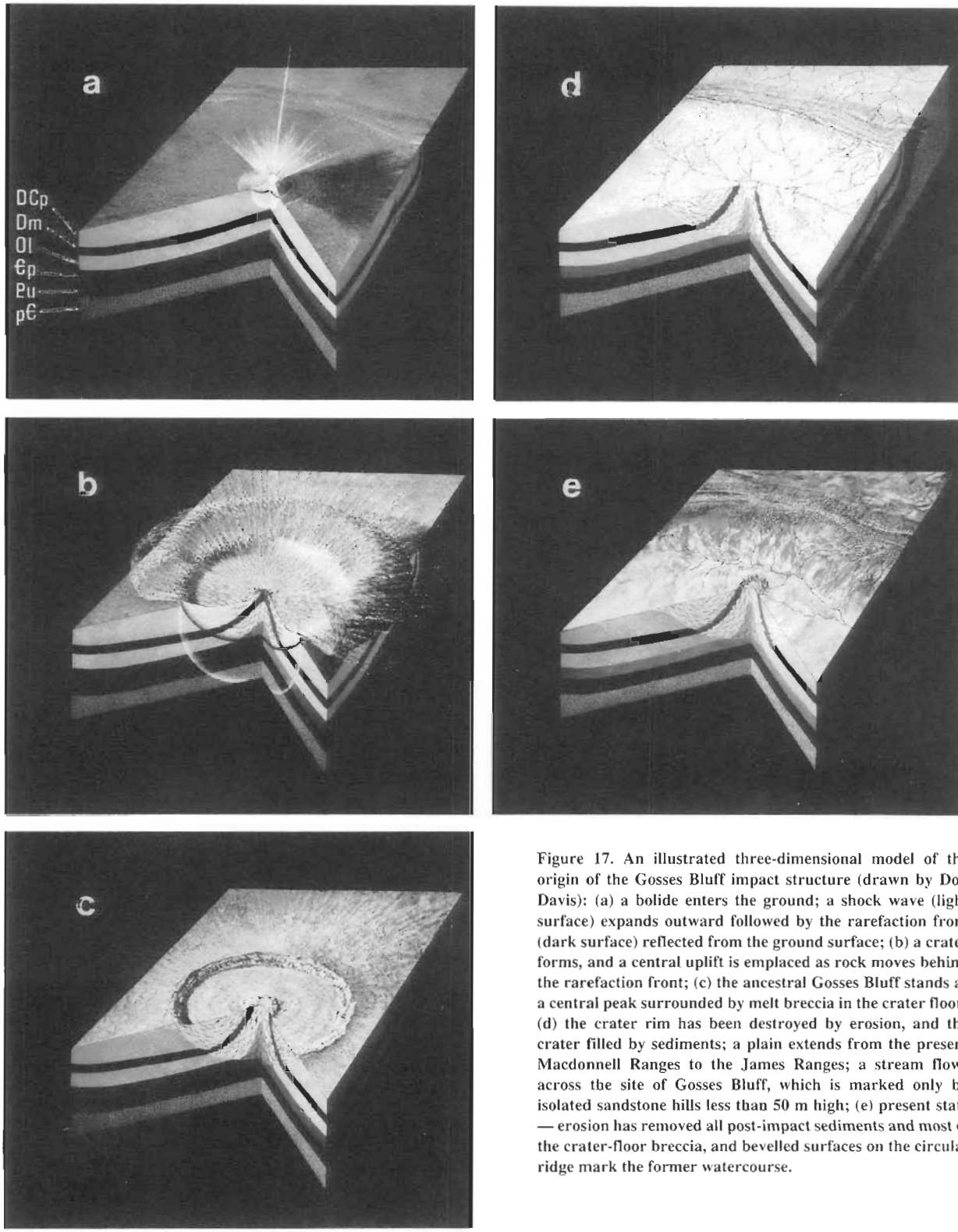

Figure 17. An illustrated three-dimensional model of the origin of the Gosses Bluff impact structure (drawn by Don Davis): (a) a bolide enters the ground; a shock wave (light surface) expands outward followed by the rarefaction front (dark surface) reflected from the ground surface; (b) a crater forms, and a central uplift is emplaced as rock moves behind the rarefaction front; (c) the ancestral Gosses Bluff stands as a central peak surrounded by melt breccia in the crater floor; (d) the crater rim has been destroyed by erosion, and the crater filled by sediments; a plain extends from the present Macdonnell Ranges to the James Ranges; a stream flows across the site of Gosses Bluff, which is marked only by isolated sandstone hills less than 50 m high; (e) present state — erosion has removed all post-impact sediments and most of the crater-floor breccia, and bevelled surfaces on the circular ridge mark the former watercourse.

decreases roughly in proportion to the volume of material engulfed. At the centre, the internal energy of the material after relaxation is far in excess of that necessary to vaporise any bolide and rock material. At greater distances it is sufficient to melt rock, and still further out to produce shock damage and fracturing. Eventually, the pressure and velocity of the shock decreases until it decays to an ordinary elastic wave.

The compressional stage nominally continues until the shock wave reaches the back of the bolide, after a few tens of milliseconds for an event of the magnitude of interest. Wherever the compressional wave intersects a free surface, it is reflected as a rarefaction. Even during the compressional stage, rarefactions originating at the sides of the bolide lead to decay of the shock waves. The succeeding excavational stage, lasting a half to one minute, involves gross displacement of material, as pressure gradients with downward acceleration — established by rarefactions generated as the shock wave intersects the ground surface — produce velocities that add vectorially to the initial particle velocities behind the shock front.

Computation of such high-speed and complex flow fields yields a general pattern of upward and outward displacements near the ground surface at radial distances that correspond to the outer part of the nascent crater, and upward and inward motion at greater depth nearer the focus of the disturbance. A calculation for Sierra Madera (Maxwell & Moises 1971) indicates inward and upward motion near the axis beginning as early as 5.5 s after impact, and dominating at 15 s, by which time ejection near the nascent crater rim has been succeeded by a downward motion. The overall flow field through the cratering event is toroidal, including a final outward sector at the upper end of the axial column of inwardly displaced material.

The similarity of this pattern to the displacements exhibited at Gosses Bluff is evident. During impact, rocks behave hydrodynamically, whereas only at a late stage of the cratering mechanism does rock strength assume some importance. Since the hydrodynamic process assumes no rock strength, the computation forms an approximation which becomes less relevant to mechanical displacements at peripheral regions where rock strength is significant. However, the hydrodynamic model is consistent with field evidence, which suggests close relationships between excavation of the crater and formation of a central uplift (Melosh, 1989). Although it is difficult to distinguish cause and effect in such complex flow fields, displacements in the axial region appear not to be coupled with gravity-induced displacements near the rim.

Post-impact morphological evolution

Little is known about the geological history of the Missionary Plain between the formation of the Late Devonian Brewer Conglomerate and the deposition of Tertiary terrace gravels, both piedmont deposits. As the central peaks of lunar craters do not generally attain the original ground level, the original summit surface of Gosses Bluff may have been the same as the minimum pre-event ground level. A Tertiary ground surface at the present erosion level at the top of Gosses Bluff accords with peneplain surfaces which cap the Macdonnell and James Ranges.

The near-surface material occupying the site of the Missionary Plain at the time of impact is unknown. It might have been equivalent to the Permian deposits mapped at the eastern and western extremities of the Amadeus Basin and encountered in a bore north of the Macdonnell Ranges (Wells et al. 1970).

If the Gosses Bluff crater was excavated largely in unconsolidated sediments, restoration of the pre-event surface by erosion of the rim and filling of the crater bowl could have been accomplished in a geologically short time. We envisage that a broad plain developed at the level of the summit of Gosses Bluff, and that the site of the central uplift was possibly marked by isolated ridges and tors of lower Mereenie Sandstone rising 30 or 40 m, or perhaps completely buried.

In the absence of stratified rocks younger than the Brewer Conglomerate at Gosses Bluff, erosion surfaces and surface deposits constitute the only evidence at hand for the study of its post-impact evolution. Three erosion surfaces have been recognised in the area, as follows:

- a relict plateau surface truncating the central uplift at an elevation of about 250 m above the level of the Missionary Plain;
- a circular pediment sloping from the base of the circular ridge, and extensively coated by travertine crusts; and
- a pediment which slopes gently southward from the foothills of the Macdonnell Ranges and comes into contact with the Gosses Bluff pediment along Rudalls Creek.

The surface deposits in the Gosses Bluff area include: travertine crusts, older alluvial terraces, younger alluvial terraces, scree slopes (colluvium), alluvial flats, and aeolian deposits.

The exhumation of Gosses Bluff appears to have parallelled that of the Macdonnell Ranges, for which a period of cliff formation and gorge incision followed the valley stage of the upland surface. The relict erosion surface at the top of the circular ridge correlates with a similar surface occurring at a similar level in the Macdonnell Ranges (Mabbutt 1966, 1967). Evidence for an early, antecedent drainage system is afforded by the creek which drains the central pound, and which originated on the western rim of the circular ridge.

Further erosion accentuated the circular ridge morphology by removing the soft shale of the Stokes Siltstone, and possibly overlying breccia, from the centre, and resulted in the formation of the circular pediment around the ridge. The drainage would have flowed over the structure as it was being unroofed, and incision would have kept pace with the gradual erosion. These developments were conceivably contemporaneous with the formation of the Macdonnell Ranges pediment, which north of Gosses Bluff is developed mainly through the truncation of flat-lying beds of the Brewer Conglomerate. The pediment is covered by higher relict alluvial terraces and by pebble drift, and is eroded by southward-flowing streams which open into narrow valleys occupied by lower-level alluvial terraces. The bulk of the pebbles of both the upper and lower terraces represent retransported pebbles of the Brewer Conglomerate, and are characterised, therefore, by a similar range of composition. The pebbles of the upper terrace commonly display yellowish weathering crusts, and are cemented by travertine. Neither feature was observed in the lower terrace.

The circular ridge is surrounded by scree slopes into which the radial gullies that drain it are entrenched. The colluvium contains sandstone pebbles derived exclusively from the Pertnjara Group and Mereenie Sandstone, and therefore can be distinguished from the upper and lower terraces of the Macdonnell Ranges pediment. Pebble drift from the Macdonnell Ranges pediment may cover portions of the Gosses Bluff pediment; the two pediments might have been continuous before the present drainage system developed. At present, dissection of these slopes and of calcrete near Undandita Creek suggests a period of increased erosion of the circular ridge.

The post-impact morphological evolution of the Gosses Bluff area may be summarised as follows:

- development of a regional peneplain;
- regional elevation, erosion, and the formation of pediments and of the upper terraces;
- a dry period, formation of the travertine, and development of dunes; and
- rejuvenated erosion associated with regional uplift and with the onset of a more humid climate, resulting in the present drainage system and the lower terraces.

Acknowledgments

The investigation reported here is based on a joint project by BMR (now AGSO), and the USGS working on behalf of the National Aeronautics and Space Administration. Geological work benefited from the interest of P.J. Cook, who spent several weeks in the field; B.G. Jones, I. Faulkes, and other staff of the Resident Geologist's office, Alice Springs; and geologists of Magellan Petroleum Corporation, and associated companies — especially L.G.G. Pearce, R.A. Magee, R.M. Hopkins, C.W. Siller, and D.A. McNaughton. Detailed mapping was assisted by aerial photographs supplied by Exoil NL. G. Berryman and P. Fisher provided excellent field assistance for the geological party. We thank R.A.F. Grieve, A. Therriault, A.T. Wells, and G.E. Williams for their constructive comments on this manuscript, and J.C. Dooley, A.N. Yeates, and G.M. Bladon for their editorial contributions.

References

Baker, G., 1953. Natural sinters from Mt. Remarkable and Tempe Downs. Transactions of the Royal Society of South Australia, 73, 23–33.

Barlow, B.C., 1979. Gravity investigations of the Gosses Bluff impact structure, central Australia. BMR Journal of Australian Geology & Geophysics, 4, 323–339.

Barringer, D.M., 1905. Coon Mountain and its crater. Proceedings of the Academy of Natural Science, Philadelphia, 57, 861–886.

Bohn, E. & Stöber, W., 1966. Coesit und Stischowit als isolierte natürliche Mineralien. Neues Jahrbuch für Mineralogie, Monatschafte, 89–96.

Bradshaw, M.T. & Yeung, M., 1992. Palaeogeographic atlas of Australia, volume 8 — Jurassic. Bureau of Mineral Resources, Canberra.

Branco, W. & Fraas, E., 1905. Das kryptovulkanische Becken von Steinheim. Abhandlungen der Preussischen Akademie der Wissenschaften, Physikalisch Klasse, 1–64.

Brown, A.R., 1973. A detailed seismic study of Gosses Bluff. Bureau of Mineral Resources, Australia, Report 163.

Brunnschweiler, R.O., 1959. Geology of Gosses Bluff (N.T.) and vicinity. Report to Enterprise Exploration Co. Pty Ltd 22 (unpublished).

Brunnschweiler, R.O., Leslie, R.B. & Richards, K.A., 1959. Review of geological and geophysical information, Gosses Bluff, Northern Territory. Frome–Broken Hill Co. Pty Ltd & Enterprise Exploration Co. Pty Ltd (unpublished).

Bucher, W.H., 1936. Cryptovolcanic structures in the United States. Report of the 16th International Geological Congress, 2, 1055–1084.

Bunch, T.E. & Quaide, W.L., 1968. Shatter cones in the Danny Bay nuclear crater. In: French, B.M. & Short, N.M. (editors), 1968, 285.

Chao, E.C.T., Shoemaker, E.M. & Marsden, B.M., 1960. First natural occurrence of coesite. Science, 132, 220–222.

Chao, E.C.T., Fahey, J.J., Litter, J. & Milton, D.J., 1962. Stishovite, SiO_2, a very high pressure new mineral for Meteor Crater, Arizona. Journal of Geophysical Research, 67, 419–421.

Chewings, C., 1928. Further notes on the stratigraphy of central Australia. Transactions of the Royal Society of South Australia, 52, 68–81.

Cook, P.J., 1966. The Gosses crypto-explosion structure. Bureau of Mineral Resources, Australia, Record 1966/132.

Cook, P.J., 1968. The Gosses Bluff crypto-explosion structure. Journal of Geology, 76, 123–139.

Crook, K.A.W. & Crook, P.J., 1966. Gosses Bluff — diapir, cryptovolcanic-volcanic structure, or astrobleme? Journal of the Geological Society of Australia, 13, 493–516.

Crook, K.A.W., 1967. Cosmic ice residuum associated with an astrobleme? Nature, 213 (5080), 999–1000.

Currie, K.L., 1972. Geology and petrology of the Manicouagan resurgent caldera. Geological Survey of Canada, Bulletin 198.

Dachille, F., Zeto, R.J. & Roy, R., 1963. Coesite and stishovite: stepwise reversal transformation. Science, 140, 991–993.

Deutsch, A., Lakomy, R. & Buhl, D., 1989. Strontium and neodymium isotopic characteristics of a heterolithic breccia in the basement of the Sudbury impact structure. Earth & Planetary Science Letters, 93, 359–370.

Dietz, R.S., 1947. Meteorite impact suggested by the orientation of shatter cones at the Kentland, Indiana, disturbance. Science, 105, 42–43.

Fahey, J.J., 1964. Recovery of coesite and stishovite from Coconino Sandstone of Meteor Crater, Arizona. American Mineralogist, 49, 1643–1647.

Fahey, J.J., 1971. The removal of potassium silicofluoride formed in the determination of coesite and stishovite. American Mineralogist, 56, 2145–2146.

French, B.M. & Short, N.M. (editors), 1968. Shock metamorphism of natural materials. Mono Book Corp., Baltimore.

Froelich, A.J. & Krieg, E.A., 1969. Geophysical–geologic study of northern Amadeus trough, Australia. American Association of Petroleum Geologists, Bulletin 53, 1978–2064.

Geophysical Associates Pty Ltd, 1965. Missionary Plain seismic and gravity survey, Oil Permits 43 & 56, Northern Territory, for Magellan Petroleum (N.T.) Pty Ltd. Bureau of Mineral Resources, Australia, Petroleum Search Subsidy Acts Report.

Giles, E., 1875. Geographic travels in central Australia from 1872–1874. Printed for the author by McCarron, Bird & Co., Melbourne.

Glikson, A.Y., 1969. Geology of the outer zone of the Gosses Bluff crypto-explosion structure. Bureau of Mineral Resources, Australia, Record 1969/42.

Glikson, A.Y. 1987a. Regional structure and evolution of the Redbank–Mt Zeil thrust zone: a major lineament in the Arunta Inlier, central Australia. BMR Journal of Australian Geology & Geophysics, 10, 89–107.

Glikson, A.Y., 1987b. An upthrusted Early Proterozoic basic granulite–anorthosite suite and anatectic gneisses, southwestern Arunta Block, central Australia: evidence on the nature of the lower crust. Transactions of the Geological Society of South Africa, 89, 263–283.

Goleby, B.R., Wright, C., Collins, C.D.N. & Kennett, B.L.N., 1988. Seismic reflection and refraction profiling across the Arunta Block and the Ngalia and Amadeus Basins. Australian Journal of Earth Sciences, 35, 275–294.

Gostin, V.A., Haines, P.W., Jenkins, R.J.F., Compston, W. & Williams, I.S., 1986. Impact ejecta horizon within late Precambrian shales, Adelaide Geosyncline, South Australia. Science, 233, 198–200.

Grieve, R.A.F. & Pesonen, L.J., 1992. The terrestrial impact cratering record. Tectonophysics, 216, 1–30.

Hörz, F., 1968. Statistical measurements of deformation structures and refractive indices in experimentally shock loaded

quartz. In: French, R.M. & Short, N.M. (editors), 1968, 243–254.

Howard, K.A. & Offield, T.W., 1968. Shatter cones at Sierra Madera, Texas. Science, 162, 724–725.

Huckaba, W.A. & Magee, R.A., 1969. Tyler No. 1, Northern Territory, final well report. Magellan Petroleum (NT) Pty Ltd (unpublished).

Jones, B.G., 1972. Upper Devonian to Lower Carboniferous stratigraphy of the Pertnjara Group, Amadeus Basin, central Australia. Journal of the Geological Society of Australia, 19, 229–249.

Kent, D.V. & Gradstein, F.M., 1985. A Cretaceous and Jurassic geochronology. Geological Society of America, Bulletin 96, 1419–1427.

Kieffer, S.W., 1971. Shock metamorphism of the Coconino Sandstone at Meteor Crater, Arizona. Journal of Geophysical Research, 76, 5449–5473.

Lilly, P.A., 1980. Faulting mechanics in the collar rocks of the Vredefort ring structure. Tectonophysics, 67, 45–60.

Lindsay, J.F., 1993. Geologic atlas of the Amadeus Basin. Australian Geological Survey Organisation, Canberra.

Mabbutt, J.A., 1966. Landforms of the western Macdonnell Ranges. In: Dury, G.H. (editor), 1966. Essays in geomorphology. Heinemann, London, 83–120.

Mabbutt, J.A., 1967. Denudation chronology in central Australia. In: Jennings, J.N. & Mabbutt, J.A. (editors), 1967 (reprinted 1971). Landform studies from Australia and New Guinea. Australian National University, Canberra, 144–181.

Madigan, C.T., 1932. The geology of the western Macdonnell Ranges, central Australia. Quarterly Journal of the Geological Society, London, 88, 672–711.

Manton, W.I., 1965. The orientation and origin of shatter-cones in the Vredefort Ring. Annals of the New York Academy of Science, 123, 1017–1072.

Manwaring, E.A., 1983. Palaeomagnetic studies. Appendix in: Sedmik, E.C.E., 1983.

Maxwell, D.E. & Moises, H., 1971. Hypervelocity impact calculations. Physics International Company, San Leandro, California, PIRF-190 (unpublished).

McIntyre, D.B., 1962. Impact metamorphism at Clearwater Lake, Quebec. Journal of Geophysical Research, 67, 1647. (Also in French, B.M. & Short, N.M. (editors), 1968, 363–366).

McNaughton, D.A., Quinlan, T., Hopkins, R.M. & Wells, A.T., 1968. Evolution of salt anticlines and salt domes in the Amadeus Basin, central Australia. Geological Society of America, Special Paper 88, 229–247.

Melosh, H.J., 1989. Impact cratering : a geologic process. Oxford University Press.

Milton, D.J., 1977. Shatter cones — an outstanding problem in shock mechanics. In Roddy, D.J., Pepin, R.O. & Merrill, R.B. (editors). Impact and explosion cratering. Pergamon Press, New York, 703–714.

Milton, D.J., Barlow, B.C., Brett, R., Brown, A.R., Glikson, A.Y., Manwaring, E.A., Moss, F.J., Sedmik, E.C.E., Van Son, J. & Young, G.A., 1972. Gosses Bluff impact structure, Australia. Science, 175, 1199–1207.

Milton, D.J., Barlow, B.C., Brown, A.R., Moss, F.J., Manwaring, E.A., Sedmik, E.C.E., Young, G.A. & Van Son, J., 1996. Gosses Bluff — an end-Jurassic impact structure, central Australia. Part 2: Seismic, magnetic, and gravity studies. AGSO Journal of Australian Geology & Geophysics (this issue).

Milton, D.J., Moss, F.J., & Barlow, B.C. (compilers), 1978. Regional geology, Gosses Bluff impact structure, Northern Territory, 1978. Bureau of Mineral Resources, Australia, 1:50 000 map.

Milton, D.J. & Sutter, J.F., 1987. Revised age for the Gosses Bluff impact structure, Northern Territory, Australia, based on $^{40}Ar/^{39}Ar$ dating. Meteoritics, 22, 281–289.

Moss, F.J., 1964. Gosses Bluff seismic survey, Amadeus Basin, Northern Territory, 1962. Bureau of Mineral Resources, Australia, Record 1964/66.

Nicolaysen, L. & Reimold W.U., 1987. Contribution to workshop on catastrophies in the geological record. University of Witwatersrand, Johannesburg (unpublished).

Palme, H., 1982. Identification of projectiles of large terrestrial impact craters. In: Silver, L.T., Geological implications of large asteroid & comet impact on the Earth. Geological Society of America, Special Paper 190, 223–233.

Pemberton, R.L. & Planalp, R.N., 1965. Well completion report, Gosses Bluff No. 1 well. Exoil (NT) Pty Ltd (unpublished).

Playford, G., Jones, B.G. & Kemp, E.M., 1976. Palynological evidence for the age of the synorogenic Brewer Conglomerate, Amadeus Basin, central Australia. Alcheringa, 1, 235–243.

Prichard, C.E. & Quinlan, T., 1962. The geology of the southern part of the Hermannsburg 1:250 000 Sheet area. Bureau of Mineral Resources, Australia, Report 61.

Quinlan, T. & Forman, D.J., 1968. Hermannsburg, NT — 1:250 000 Geological Series. Bureau of Mineral Resources, Australia, Explanatory Notes SF/53–13.

Ramsay, J.G., 1967. Folding and fracturing of rocks. McGraw-Hill, New York.

Ranneft, T.S.M., 1970. Gosses Bluff, central Australia, as a fossil mud volcano. American Association of Petroleum Geologists, Bulletin 54, 417–427.

Roddy, D.J. & Davies, L.K., 1977. Shatter cones formed in large-scale experimental explosion craters. In: Roddy, D.J., Pepin, R.O. & Merrill, R.B. (editors). Impact and explosion cratering. Pergamon Press, New York, 715–750.

Rondot, J., 1994. Recognition of eroded astroblemes. Earth Science Reviews, 35, 331–365.

Sedmik, E.C.E., 1983. Gosses Bluff ground magnetic survey. Bureau of Mineral Resources, Australia, Record 1983/28.

Shoemaker, E.M., Wolfe, R.F., & Shoemaker, C.S., 1990. Asteroid and comet flux in the neighborhood of the Earth. In Sharpton, V.L. & Ward, P.D. (editors). Global catastrophes in Earth history. Geological Society of America, Special Paper 247, 155–170.

Skinner, B.J. & Fahey, J.J., 1963. Observations on the inversion of stishovite to silica glass. Journal of Geophysical Research, 68, 5595–5604.

Stevenson, J.S., 1963. The upper contact phase of the Sudbury micropegmatite. Canadian Mineralogist, 7, 413–419.

Stöffler, D., 1971. Coesite and stishovite in shocked crystalline rocks. Journal of Geophysical Research, 76, 5474–5488.

Stöffler, D., 1972. Deformation and transformation of rock-forming minerals by natural and experimental shock processes: I. Behaviour of minerals under shock compression. Fortschritte der Mineralalogie, 49, 50–113.

Tingate, P.R., Lindsay, J.F. & Marshallsea, S.J., 1996. Impact structures as potential petroleum exploration targets: Gosses Bluff, a Late Jurassic example from central Australia. AGSO Journal of Australian Geology & Geophysics, this issue.

Trendall, A.F., 1964. Slaggy siliceous glass occurring naturally on the surface at various localities in the southern part of Western Australia. Geological Survey of Western Australia, Report 1964/12.

von Engelhardt, W. & Stöffler, D., 1968. Stages of shock metamorphism in the crystalline rocks of the Ries basin, Germany. In: French, B.M. & Short, N.M. (editors), 1968, 159–168.

Wallace, M.W., Gostin, V.A. & Keays, R.R., 1989. Discovery of the Acraman impact ejecta blanket in the Officer Basin and its stratigraphic significance. Australian Journal of Earth Sciences, 36, 585–587.

Wallace, M.W., Gostin, V.A. & Keays, R.R., 1996. Sedimentology of the Neoproterozoic Acraman impact ejecta horizon, South Australia. AGSO Journal of Australian Geology & Geophysics (this issue).

Wells, A.T., 1977. Magnesite-bearing calcrete near Gosses Bluff, Northern Territory. BMR Journal of Australian Geology & Geophysics, 2, 62–66.

Wells, A.T., Forman, D.J., Ranford, L.C. & Cook, P.J., 1970. Geology of the Amadeus Basin, central Australia. Bureau of Mineral Resources, Australia, Buletin 100.

Wilhelms, D.E., 1987. The geological history of the Moon. United States Geological Survey, Professional Paper 1348.

Williams, G.E., Schmidt, P.W. & Boyd, D.M., 1996. Magnetic signature and morphology of the Acraman impact structure, South Australia. AGSO Journal of Australian Geology & Geophysics (this issue).

Wilshire, H.G. & Howard, K.A., 1968. Structural pattern in central uplifts of cryptoexplosion structures as typified by Sierra Madera. Science, 162, 258–261.

Wilshire, H.G., Offield, T.W., Howard, K.A., & Cummings, D., 1972. Geology of the Sierra Madera cryptoexplosion structure, Pecos County, Texas. United States Geological Survey, Professional Paper 599-H.

Wilson, C.W. & Stearns, R.G., 1968. Geology of the Wells Creek structure, Tennessee. Tennessee Division of Geology, Bulletin 68.

Wright, C., Barton, T., Goleby, B.R. & Taylor, F.J., 1989. Seismic velocity variations in the northern Amadeus Basin, central Australia, from an expanding spread reflection profile. Exploration Geophysics, 20, 435–444.

Young, G.A., 1972. Gosses Bluff airborne magnetic survey. Geophysical Prospector, 20, 83–91.

Young, G.C., 1985. New discoveries of Devonian vertebrates from the Amadeus Basin, central Australia. BMR Journal of Australian Geology & Geophysics, 9, 235–254.

Young, G.C., 1988. New occurrences of phyllolepid placoderms from the Devonian of central Australia. BMR Journal of Australian Geology & Geophysics, 10, 363–376.

Young, G.C., Turner, S., Owen, M., Nicoll, R.S., Laurie, J.R. & Gorter, J.D., 1987. A new Devonian fish fauna, and revision of post-Ordovician stratigraphy in the Ross River Syncline, Amadeus Basin, central Australia. BMR Journal of Australian Geology & Geophysics, 10, 233–242.

Appendix I. Summary information from shallow drilling in the outer ring of the Gosses Bluff structure

For map location of drillholes refer to Milton et al. (1978).

Hole	*Location (Grid ref.)*	*Total depth (m)*	*Depth range (m)*	*Lithology*
H1	215644	152.4	0–6.1	Siltstone, some travertine chips
			–11.3	Siltstone
			–13.1	Breccia
			–27.4	Sandy siltstone, claystone, mostly calcareous
			–44.2	Sandy siltstone with some breccia, angular clasts of arenite and lutite
			–47.2	Breccia, large clasts in sandstone matrix; shatter cones. Dips 30–47°
			–62.5	Mostly friable sandstone
			–64.3	Apparently a large block with shatter cones common
			–65.2	Breccia
			–80.7	Sandstone and siltstone, friable
			–83.5	Breccia, sandstone with shatter cones, some mudstone & siltstone
			86.9–91.4	Hard laminated mudstone and lutite
			–105.5	Friable silty sandstone
			–106.7	Breccia, large clasts
			–126.5	Sandstone, siltstone, arenite, lutite. Some breccia near 122 m
			–129.4	Breccia, clasts up to 15 cm
			–151.2	Sandstone with some mudstone and siltstone; calcite crystals ca 143 m. Shatter cones common, 149–151 m

Hole	*Location (Grid ref.)*	*Total depth (m)*	*Depth range (m)*	*Lithology*
H2	209643	8.5	0–8.5	Fractured sandstone, some shatter cones
H3	195645	9.1	0–9.1	Poorly sorted sandstone, clay pellets. Steep dips
H4	181650	9.1	0–1.5	Gravel
			–7.3	Travertinous, friable sandstone
			–9.1	Poorly sorted feldspathic sandstone
H5	218642	8.2	0–4.0	Hard siltstone
			–8.2	Soft friable sandstone
H6	219612	9.4	0–3.0	Gravel
			–8.8	Sandstone
			–9.4	Angular clasts of arenite and lutite
H7	230609	9.1	0–7.6	Sandstone and mudstone
			–9.1	As above with vugs; shatter cones very common
H8	216583	6.4	0–3.7	Sandstone with inclusions
			–6.4	Fractured; shatter cones common.
H9	190603	14.6	0–14.6	Sandstone; some grit and quartzite below 11.6 m
H10	170595	17.7	0–17.7	Sandstone, largely argillaceous .
H11	159578	20.7	0–20.7	Sandstone
H12	136552	17.7	0–3.0	Red soil
			–17.7	Sandstone; some shale chips; horizontal beds
H13	229580	48.4	0–17.4	Flow breccia; steep flows
			–30.5	Quartz breccia and blocks
			–48.4	Sandstone; breccia zones near base; fragments may be shatter-coned.
H14	243574	14.3	0–14.0	Flow breccia, sub- to vertical banding
			–14.3	Quartz breccia
H15	242598	20.4	0–20.4	Sandstone; shatter cones and small faults
H16	231558	30.0	0–3.0	Red soil
			–30.0	Sandstone, weakly calcareous
H17	146566	17.5	0–3.0	Red soil
			–17.5	Sandstone & shale, weakly calcareous; moderate dips
H18	242672	6.7	0–6.7	Sandstone; abundant shatter cones
H19	238674	63.7	0–3.0	Exposed breccia
			–6.1	Sandstone, mudstone, gritstone
			–7.9	Fragmental breccia, <3 cm; may be shatter-coned.
			–16.5	Sandstone, mudstone, gritstone
			–18.0	Fragmental breccia
			–32.6	Sandstone, mudstone, gritstone
			–34.1	Fragmental breccia
			–44.2	Sandstone, mudstone, gritstone
			–63.7	Fragmental breccia
H20	239673	36.6	0–36.6	Sandstone, gritstone, conglomerate chips
H21	253691	21.8	0–2.7	Soil, travertine, sandstone chips
			–21.8	Sandstone and gritstone; gentle dips. Poorly defined shatter cones
H22	253708	21.6	0–21.6	Sandstone, siltstone; gritstone; gentle dips
H23	285620	15.2	0–2.7	Red soil
			–15.2	Sandstone; abundant shatter cones
H24	299621	27.6	0–27.6	Sandstone and siltstone
H25	291706	19.5	0–2.1	Terrace conglomerate
			–18.3	Clay and clayey sandstone; grit and conglomerate layers
			–19.5	Massive soft sandstone
H26	290692	15.4	0–2.7	Gravel
			–5.4	Pebbly grit
			–12.5	Sandstone; steep dips
			–15.4	Coarse sandstone and gritstone
H27	296694	18.4	0–2.7	Soil and gravel
			–18.4	Sandstone, with gritstone and shale bands below 15 m

Hole	*Location (Grid ref.)*	*Total depth (m)*	*Depth range (m)*	*Lithology*
H28	320661	6.1	0–3.0	Alluvium and gravel
			–6.1	Sandstone, travertine chips
H29	208638	21.5	0–2.7	Soil and travertine
			–18.6	Sandstone, some shale chips
			–21.5	Fragmental breccia; may be shatter-coned
H30	214645	18.3	0–2.4	Sand, soil, travertine
			–15.4	Sandstone, some shale
			–18.3	Fragmental breccia, shatter cones
H31	261595	13.5	0–2.7	Devitrified silica glass fragments
			–5.8	Fragmental breccia
			–10.4	Quartz breccia
			–13.5	Sandstone and shale

The following holes were drilled in connection with the ground magnetic survey at Mount Pyroclast. Local coordinates are given relative to the origin of the grid for the survey; the coordinates of the origin are: lat. 23°51.06'S, long. 132°17.69'E (GR 245596).

H32	792mN 113mW	?		Shale-breccia, unmetamorphosed
H33	850mN 128mW	?	0–3.5	Baked breccia; at 3.5 m thermal effect slight
H34	881mN 165mW	?		Shale or shale-breccia, no apparent thermal effect
H38	869mN 122mW	24.5	0–24.5	Shock-melted breccia; samples for palaeomagnetic measurements
H39	814mN 29mW	24.5	0–24.5	Shock-melted breccia; samples for palaeomagnetic measurements

AGSO Journal of Australian Geology & Geophysics, 16 (4), 487–527

Gosses Bluff — a latest Jurassic impact structure, central Australia. Part 2: seismic, magnetic, and gravity studies

D.J. Milton[1], B.C. Barlow[2], A.R. Brown[2], F.J. Moss[2], E.A. Manwaring[2], E.C.E. Sedmik[2], G.A. Young[2], & J. Van Son[2]

Geophysical studies of Gosses Bluff facilitate the resolution of its three-dimensional structure, which includes a broadly hemispherical low-velocity zone with a radius of about 4 km centred at the present ground level. This zone correlates with a deformed ring dominated by block-faulting, megabreccia, and annular breccia troughs. Seismic data show a drop in shallow seismic velocities from 4.6 km s^{-1} over bedrock to 2.2 km s^{-1} over breccia outcrop. The base of the structure is defined by continuous reflectors at a maximum depth of 3450 m beneath the surface. The subsurface geology was deduced by fitting the extrapolated stratigraphy into the sequence of migrated seismic horizons. The uppermost little-disturbed reflectors are correlated with the tops of the Pertatataka Formation and Bitter Springs Formation of the Late Proterozoic–early Palaeozoic Amadeus Basin sequence. Seismic data for the Bitter Springs Formation define a domal structure and local thickening under Gosses Bluff.

The gravity field associated with Gosses Bluff outlines a remarkably symmetrical circular gravity low of 440 μm s^{-2} with a radius of about 10.8 km. An annular gravity low bounded by steep gradients is associated with the central uplift. The outer limit of the near-surface gravity structure is nearly vertical. The symmetrical gravity features can be modelled by shallow density variations, and no net mass excess or deficiency is defined several thousand metres centrally under the bluff. Likewise, no gravity expression of a deep-seated Gardiner–Tyler anticline, suggested by the seismic reflection data, is apparent. Several anticlines around the bluff are shown by gravity to have low-density cores.

Total magnetic intensity (TMI) contours suggest a depth to magnetic basement of about 10 km under the bluff. A negative anomaly of 4 nT occurs between the central ring and an outcrop of flow breccia at Mount Pyroclast. Similar short-wavelength airborne magnetic anomalies of shallow sources over the eastern, southern, and western flanks of the bluff within 6 km of the centre correspond to flow breccia. The anomaly sources represent both remanent primary components of magnetisation, and remagnetisation formed during cooling, as confirmed by ground magnetic surveys in the Mount Pyroclast area. The pole position is consistent with a Jurassic–Cretaceous-boundary age.

Introduction

This paper is the second part of a two-paper series on the Gosses Bluff impact structure. Both are based on a joint study by the Bureau of Mineral Resources, Geology and Geophysics (BMR; now the Australian Geological Survey Organisation, AGSO) and the United States Geological Survey (USGS). For the geological setting of Gosses Bluff, the reader is referred to Milton et al. (this issue), whose terminology of the structure is followed here — viz., a central ring comprising a circular ridge surrounding a central pound, and a less well-exposed outer ring with a diameter of 24 km (Tingate et al. this issue; Figs. 1 and 2). This paper reports on and interprets seismic refraction and reflection surveys whose objectives were to investigate the continuity or disturbance of the deeper horizons below the structure, and to determine:

- the depth to which the disruptive effects of the impact penetrated, and the geometry of the disrupted strata;
- if the core of the structure has any intrusive material;
- whether a peripheral syncline surrounds the disrupted region;
- whether the strata are folded into an anticline at depth below the centre of the structure;
- the attitude of the strata within the disrupted region, and the dips and throws of the larger faults;
- whether folds have been induced in the strata outside the region of disruption;
- the thickness of breccia present in the disrupted region outside the circular ridge at Gosses Bluff; and
- the relation of the structure to other structural features in the Amadeus Basin.

[1] United States Geological Survey, Reston, Virginia 22092.
[2] Formerly of the Bureau of Mineral Resources, Geology and Geophysics.

A detailed aeromagnetic survey flown 90 m above ground level was specifically designed to investigate any concentric or symmetrical distribution of near-surface magnetic anomalies. Detailed ground magnetic measurements accurately located the sources of the two anomalies mapped by the airborne survey, and defined drilling targets to obtain samples for palaeomagnetic study. Palaeomagnetic measurements have been made on samples from drillcores and exposed flow breccia.

A detailed gravity survey established the degree of symmetry of the Gosses Bluff structure, the extent of the disturbance, mass excesses and deficiencies at various depths, and the relation between Gosses Bluff and other regional structures.

Seismic investigations

Early regional seismic surveys in the neighbourhood of Gosses Bluff include those by BMR, to determine the structure of the southern margin of the Amadeus Basin (Moss 1962), and to investigate the structure of the Palm Valley/Hermannsburg area (Turpie & Moss 1963). In 1962, BMR surveyed a regional traverse across the Missionary Plain, from the Macdonnell Ranges in the north, through Gosses Bluff to the Gardiner Range in the south (Moss 1964); Figure 3 shows the locations of this and other traverses through and close to Gosses Bluff . (The corners of Figs. 3, 4, and 5 coincide with GRs 056788, 446792, 062436, and 451442 on the regional map compilation of Milton et al. 1978.) The results indicate a thickness of at least 10 000 m of sedimentary rock under Missionary Plain to the north of Gosses Bluff. The quality of the data and the continuity of reflections near Gosses Bluff were poor.

Seismic surveys that Geophysical Associates (1965, 1967) carried out for Magellan Petroleum (NT) Pty Ltd during 1965 and 1966 provided extensive coverage of the northern Amadeus Basin (Fig. 3). They recorded generally good-quality data away from the bluff, and consistent reflections but poor-quality

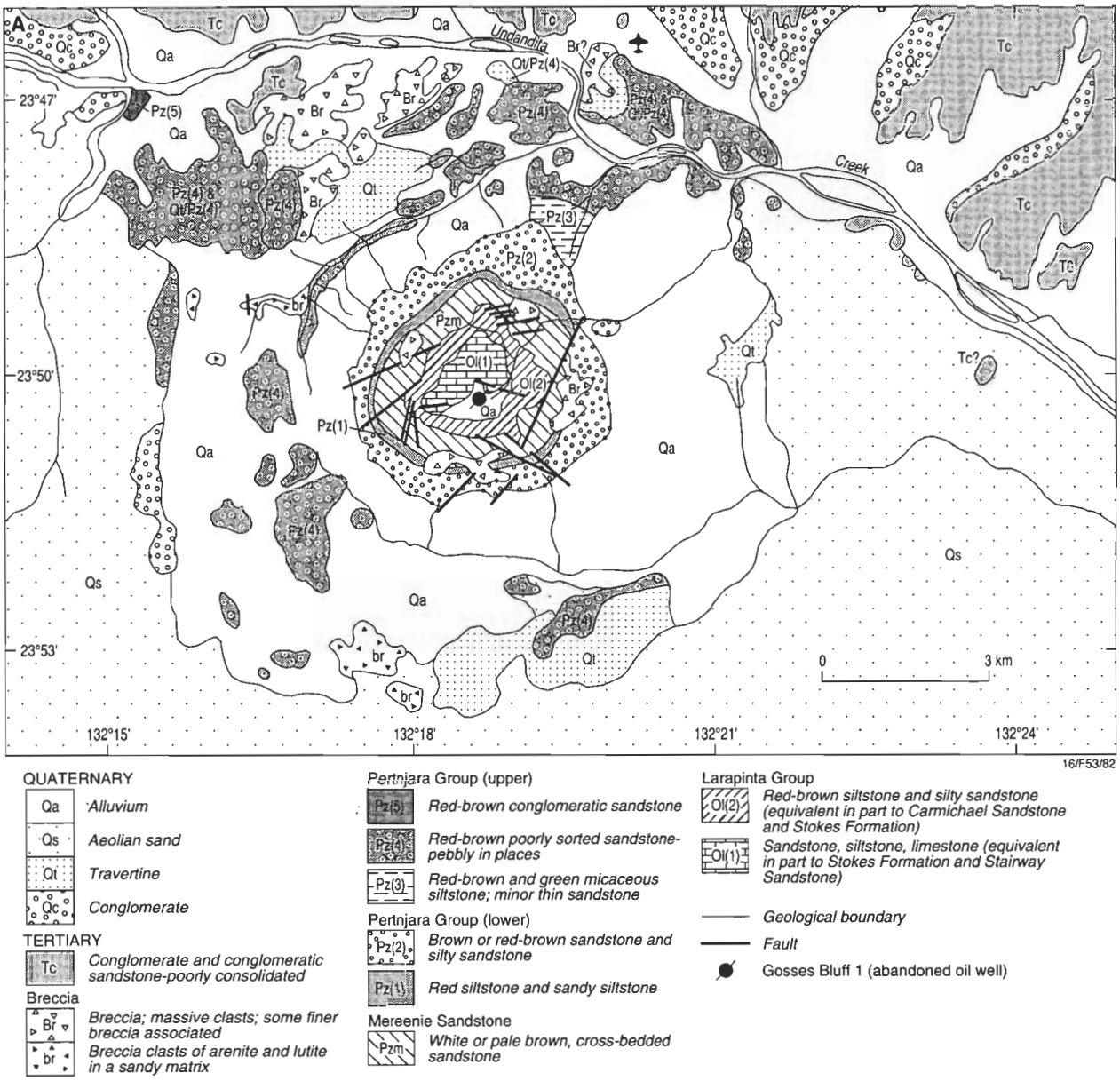

Figure 1A. Geological sketch map of the Gosses Bluff impact structure; B. (*facing page*) Geological sketch map of the central ring of Gosses Bluff.

data near the bluff, though the deeper reflections generally were more continuous towards the centre of the structure. The reason for the poor quality was shot-generated random noise, as shown by BMR's laser-scan optical-processing device. A marked improvement was shown on traverse 2-G, which applied four-fold CDP multiple coverage. Formation thicknesses, determined regionally from the results of these surveys, suggest that Gosses Bluff lies on an ancestral arcuate uplift termed the Gardiner–Tyler anticline, which extends northeast from the Gardiner Fault, through the Tyler Anticline, and possibly under the Macdonnell Ranges. Froelich & Krieg (1969) proposed that this anticline, perhaps initiated by the formation of a salt pillow, is an ancient structure whose growth ended in the early Palaeozoic.

Seismic information obtained before 1969 was considered to be consistent with a diapiric structure of the salt-dome type, though none of the data could discriminate between the various theories of the origin of the structure.

BMR undertook further seismic surveys in 1969. They comprised two main traverses, GB/A and GB/B (Figs. 3–6), and several shorter traverses, including expanding spreads for velocity information. Traverse GB/A, 24 km long, was oriented roughly parallel to the axis of the supposed subsurface Gardiner–Tyler anticline; traverse GB/B, 28 km long, was oriented at right-angles to it. Large patterns of shot-holes and geophones were used to attenuate random and coherent noise, and multiple coverage was applied where necessary. Offset shooting facilitated the recording of oblique reflections from beneath the inaccessible bluff walls.

Both traverses intersected Magellan traverses, so that the reflections could be correlated with those surrounding the bluff. One of the short traverses (GB/2-C) was shot to close a gap between Magellan traverses 2-C and 2-D. Expanding spreads were shot as traverses GB/AA, GB/AB, and GB/BA, in regions of good reflection quality, in order to obtain detailed information on the variation of velocity with depth. Traverse 81/82 was a shallow

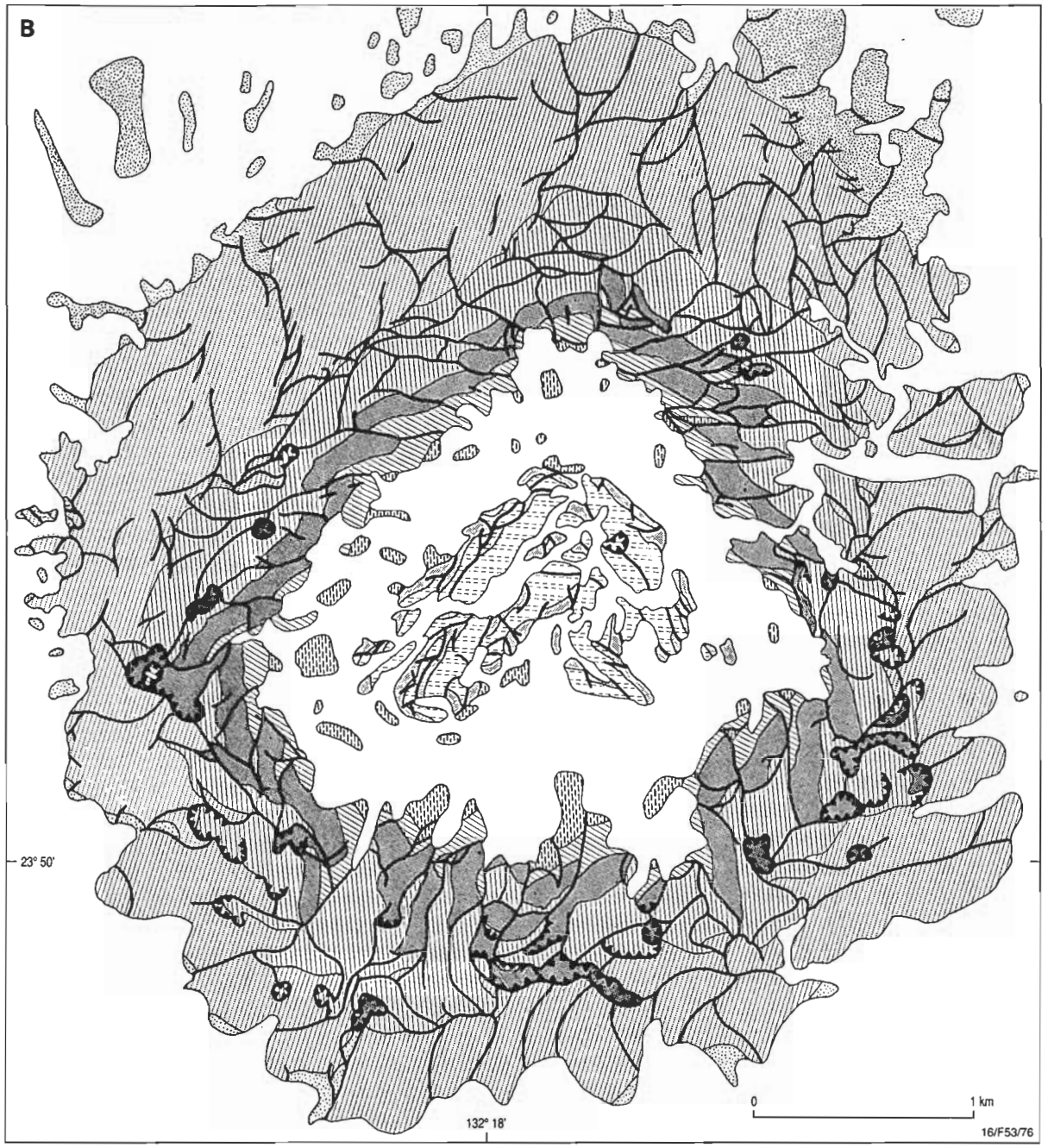

Quaternary
Alluvium

Devonian
Lower part of Pertnjara Group
Parke Siltstone
Siltstone
Sandstone

Late Ordovician to Early Devonian
Ordovician
Mereenie Sandstone
Upper
Lower

Ordovician
Upper part of Larapinta Group
Stokes Siltstone
Carmichael Sandstone
Siltstone
Sandstone
Stairway Sandstone

Contact
Fault
Base of overturned plate

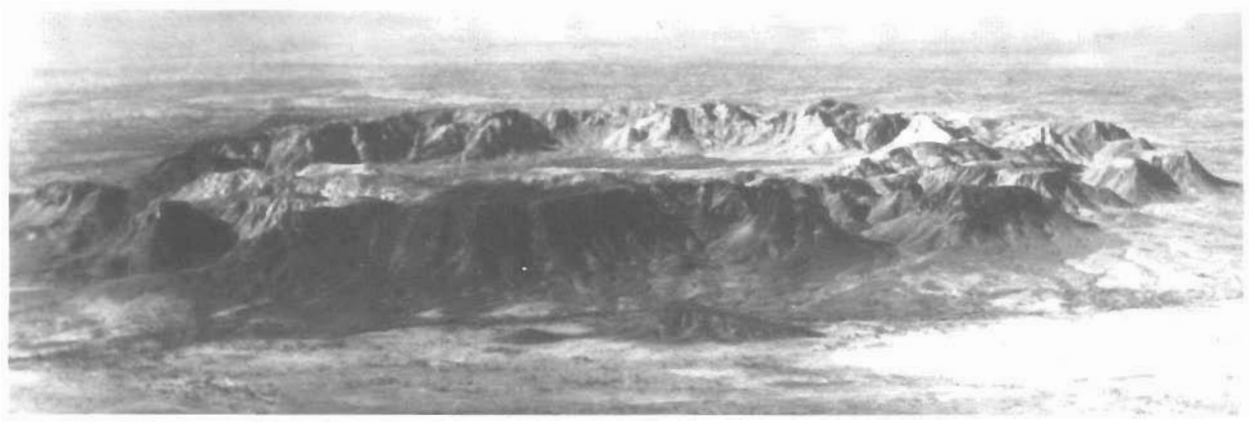

Figure 2. Oblique aerial photograph of Gosses Bluff.

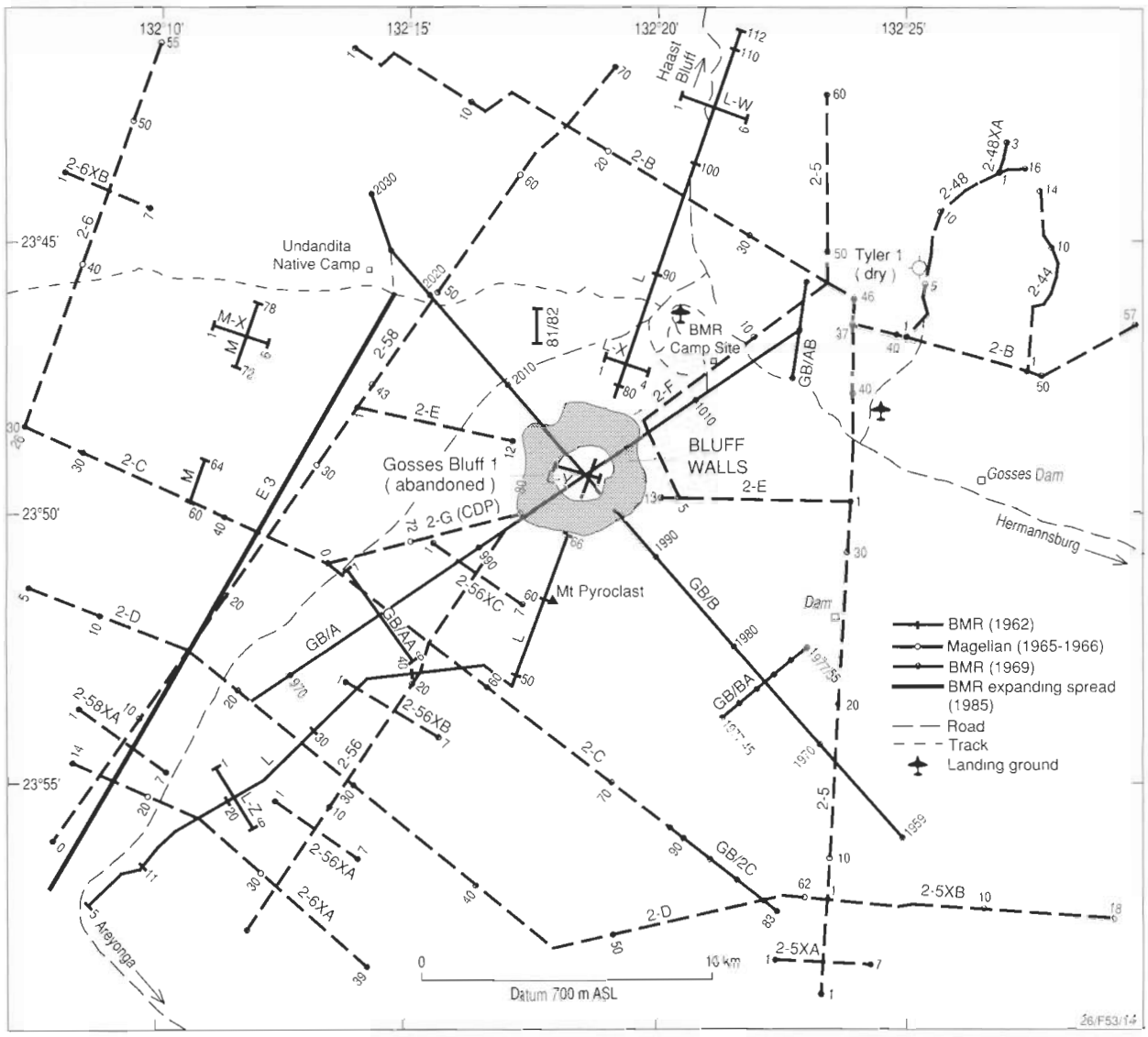

Figure 3. Locality map, seismic traverses.

refraction profile designed to determine the difference in seismic velocity between bedrock and different kinds of breccia mapped in the outer zone by Glikson (1969). Details of the field procedures and processing techniques used in analysing the 1969 survey results are presented by Brown (1973). These include noise tests, to determine the best shot and geophone patterns, and velocity analysis using information from the expanding spreads and move-out times on normal records. Single coverage was used for shooting at distances greater than 7 km from the centre of the bluff, and three-fold coverage at closer

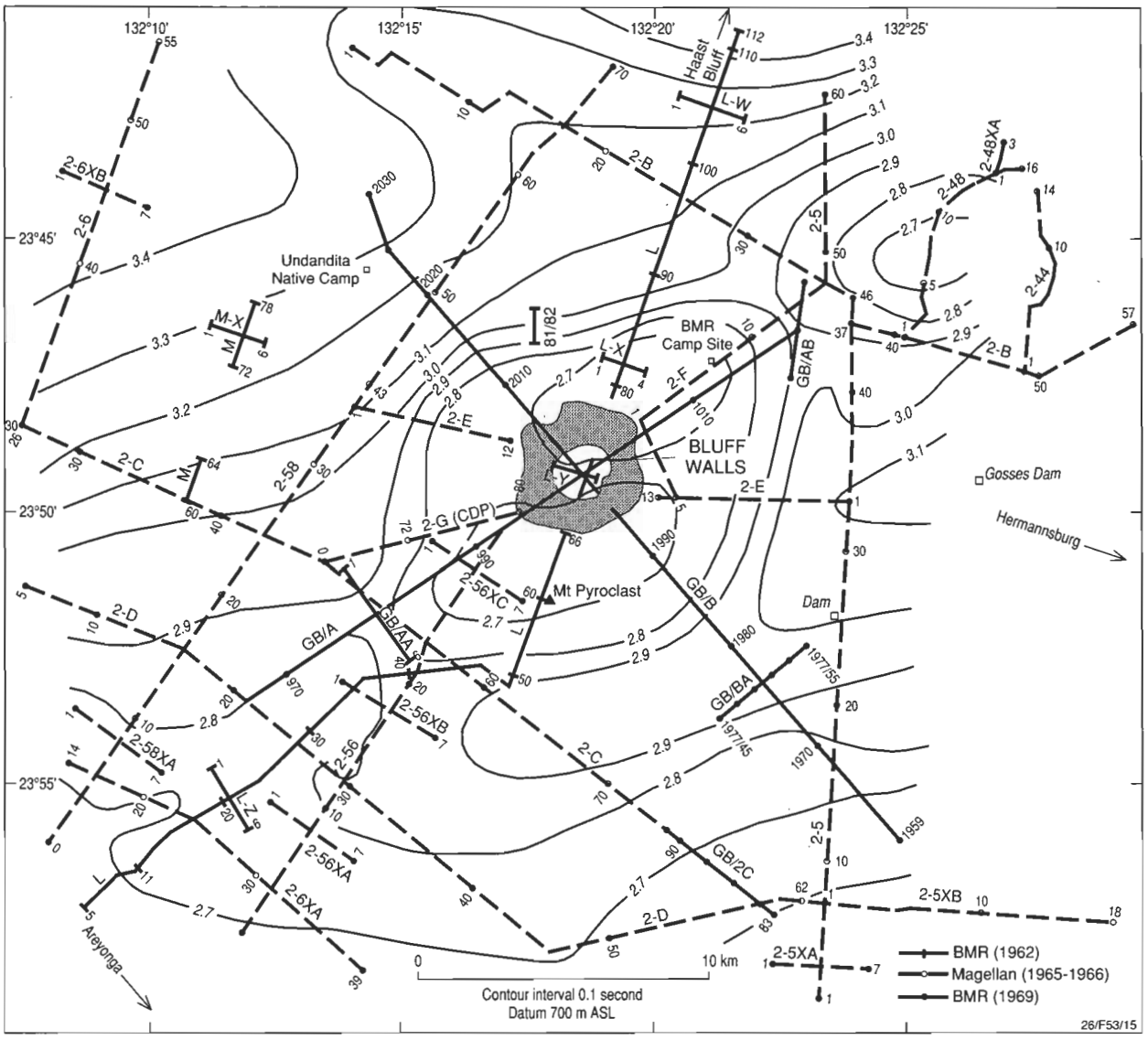

Figure 4. Reflection time to horizon E (near top of Bitter Springs Formation).

distances. Later, 24-fold CDP coverage was used inside the bluff in order to determine the shallowest reflectors maintaining continuity under the bluff. Initial analogue processing was done in BMR, followed by digital processing of data close to and under the bluff by Geophysical Service International.

A major combined reflection and refraction seismic survey was carried out in the area by BMR in 1985, mainly to study deep-crustal structure in the Arunta Block, beneath the Amadeus Basin (Goleby et al. 1988; Wright et al. 1989). Part of the seismic line passes close to Magellan traverse 2-58 (Fig. 3). An expanding spread in this part of the traverse helped improve velocity–depth determinations.

The principal reflecting horizons interpreted by Geophysical Associates (1965, 1967) have been identified on traverses GB/A (Fig. 7) and GB/B (Fig. 8), and have been correlated with the geological formations penetrated by Palm Valley No. 1, Tyler No 1, and other wells as follows:

- A — near the base of the Mereenie Sandstone;
- B — within the Horn Valley Siltstone;
- C — near the middle of the Pacoota Sandstone;
- D — near the base of the Hugh River Shale; and
- E — near the top of the Bitter Springs Formation.

Several other seismic reflection events have been interpreted on traverses GB/A and GB/B. Horizons P and Q have been correlated around the bluff, and are tentatively identified as follows:

- P — near the top of the Pertatataka Formation; and
- Q — near the top of the Heavitree Quartzite.

Other reflections earlier than horizon A have been picked independently, but could not be correlated around the bluff along the network of earlier traverses.

In the Amadeus Basin, horizon E is generally the deepest reflector. Events below this at the southeastern end of traverse GB/B are considered to be multiples. However, closer to the bluff, particularly between shot points (SPs) 1986 and 1991, horizon Q is distinct, and interpreted as originating close to the basement. This horizon also can be distinguished close to Gosses Bluff on most of the earlier seismic traverses.

A contour map of reflection time to horizon E (Bitter Springs Formation; Fig. 4) illustrates the structure at depth. It extends a similar map presented by Geophysical Associates (1967), but on a different datum, and incorporates data from the earlier surveys. The reflection-time interval between horizons E and Q over the area in which horizon Q can be identified is also presented as a contour map (Fig. 5).

Results of the BMR 1985 survey presented by Goleby et al. (1988) and Wright et al. (1989, 1990) show a similar pattern of sedimentary reflections under the Missionary Plain, and reflection horizons can be correlated with those of the earlier surveys.

Seismic velocity analysis

A knowledge of the seismic velocities and their three-dimensional variations is essential for converting reflection-time sections to depth sections. The means of determining velocities include refraction surveying, statistical analysis of move-out times on normal records, and expanding spreads in which the distance between shot and receiver is progressively increased so as to give more accurate move-out times beneath a fixed point. A velocity–depth relation (Fig. 9; Moss 1964), based partly on an expanding spread on traverse L (Fig. 3), shows the relationships between velocity, depth, and reflection; the deduced interval velocities; the conversion from reflection time to depth; and a velocity reversal centred at about 1.5 s below a 'lid' at about 1 s.

RMS velocity profiles determined from move-out analysis along traverse GB/A for record times from 1.5 to 3.0 s (Fig. 10) show a significant reduction in velocity centred on Gosses Bluff, which suggests that the rocks there are disrupted on a large scale. However, if these velocities are applied to time–depth conversion for certain seismic reflections shown in Figures 7 and 8, a major upwarp is generated on all horizons in the resulting depth sections for both traverses GB/A and GB/B (Fig. 10, lower part). As the deepest of these horizons is believed to originate very close to basement, the upwarp would imply a large dome with about 3000 m relief in metamorphic/igneous basement directly under the bluff. However, the time section along traverse GB/A, along the supposed Gardiner–Tyler anticline shows relatively minor relief — about 0.12 s (or about 0.35 km) on the deepest horizon. No corre-

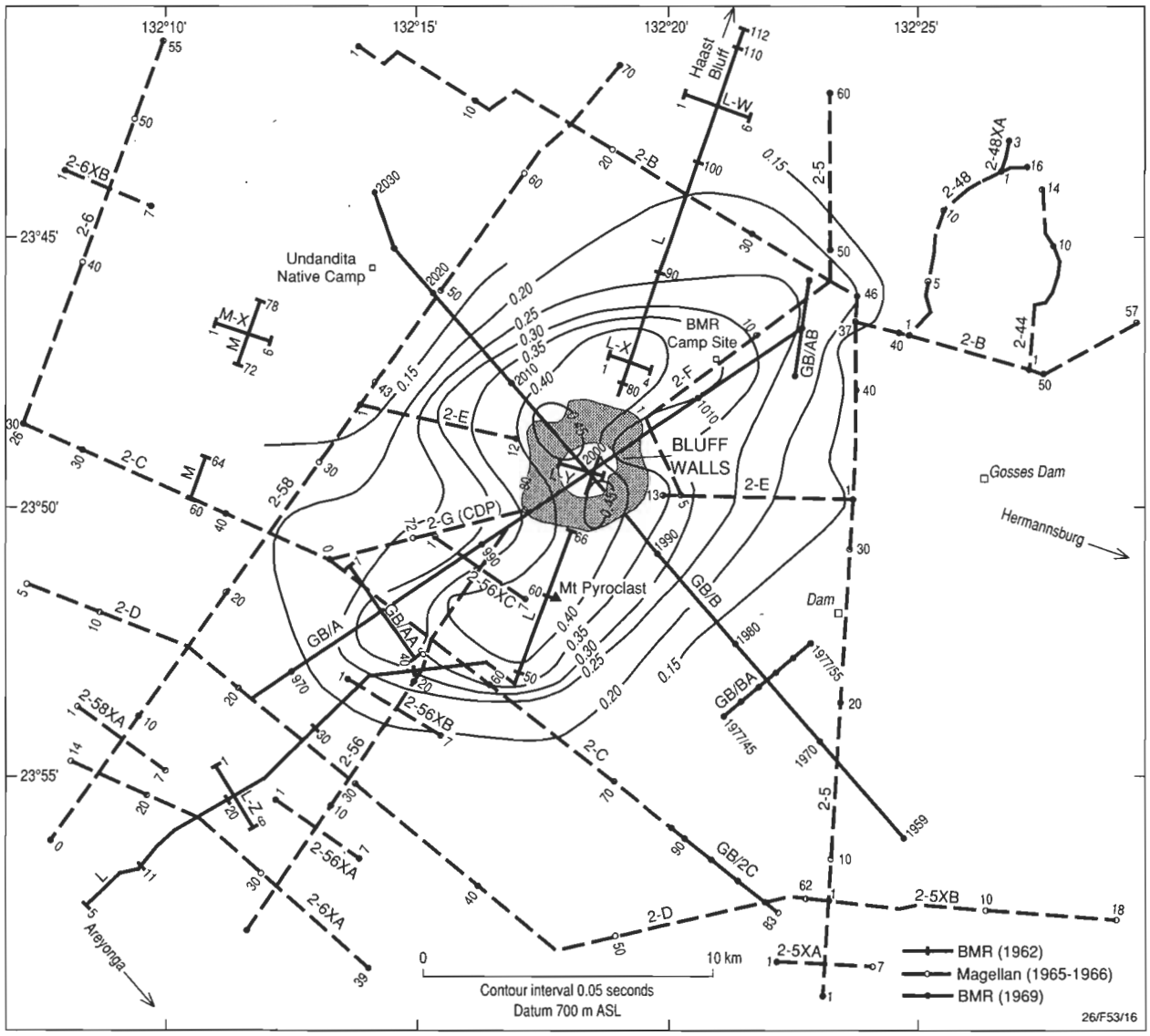

Figure 5. Reflection-time interval between horizons E (near top of Bitter Springs Formation) and Q (near top of Heavitree Quartzite).

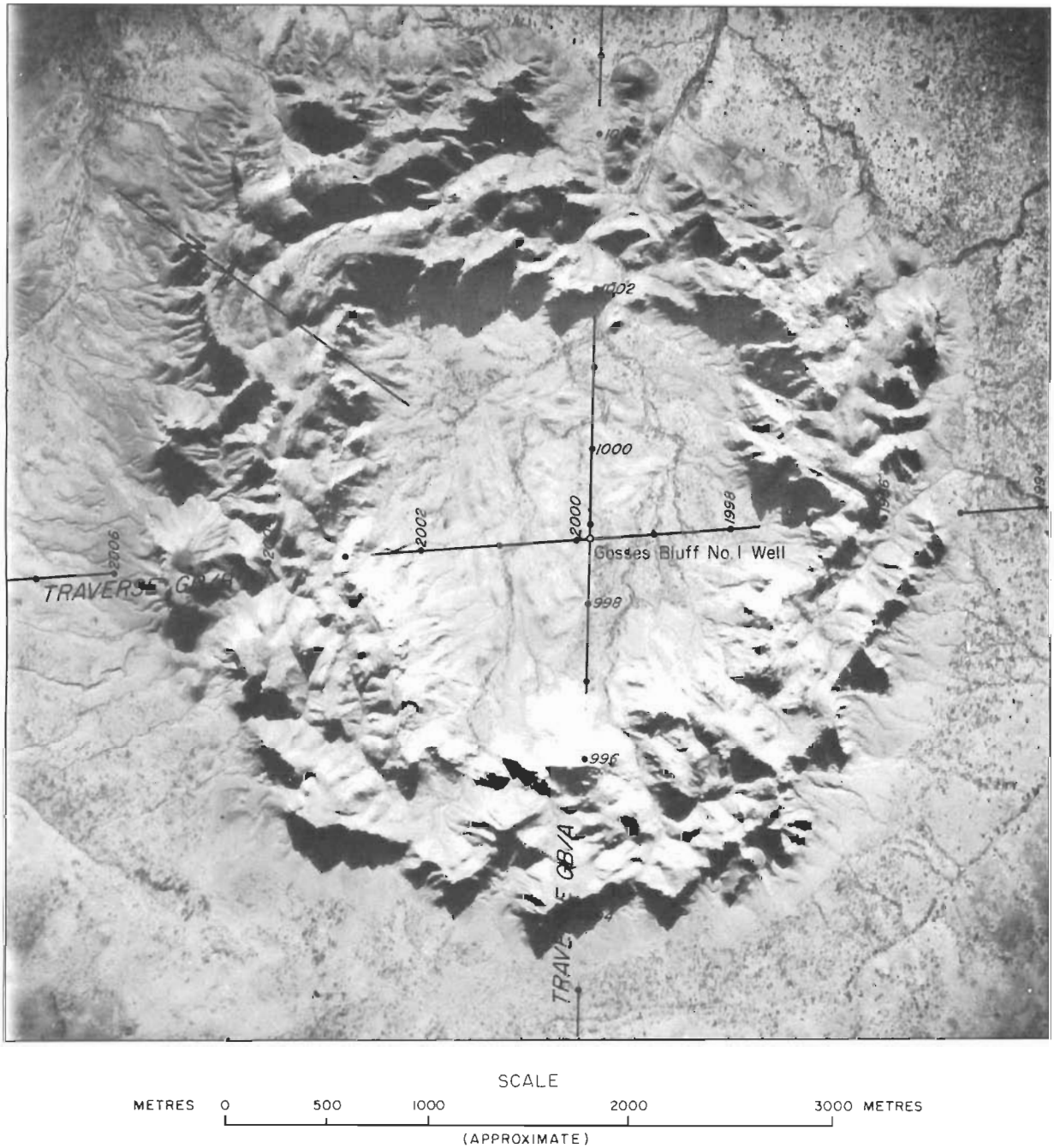

Figure 6. Aerial view of Gosses Bluff showing positions of seismic traverses GB/A and GB/B.

sponding anomaly was found in the gravity or aeromagnetic surveys (Fig. 11; Barlow 1979; Young 1972).

The determination of velocities from move-out scans is inappropriate — a conclusion that accords with the findings of Taner et al. (1970), who showed that velocity determinations depend critically on the assumption of local linearity of subsurface interfaces and, in areas of complex geology, could be too low by as much as 30 per cent.

The RMS velocities obtained by digital processing of the expanding-spread records on traverses GB/AA (Fig. 12a), AB, and BA (Brown 1973, plates 7–9) are shown in Figure 12b for horizons A, B, C, D, P, E, and Q. The velocities for GB/AB are considerably higher than those for GB/AA and GB/BA. This may be partly the effect of true higher velocities in the northern part of the area, but the large error bars and interference which can be seen on the records must cast some doubt on the very high velocities. Attempts to calculate interval velocities from the RMS velocities led to improbable and even negative values for some.

Subweathering velocities were determined from the first breaks for all shots along traverses GB/A and GB/B, and are presented as smoothed profiles in Figure 13. Areas of disruption and brec-

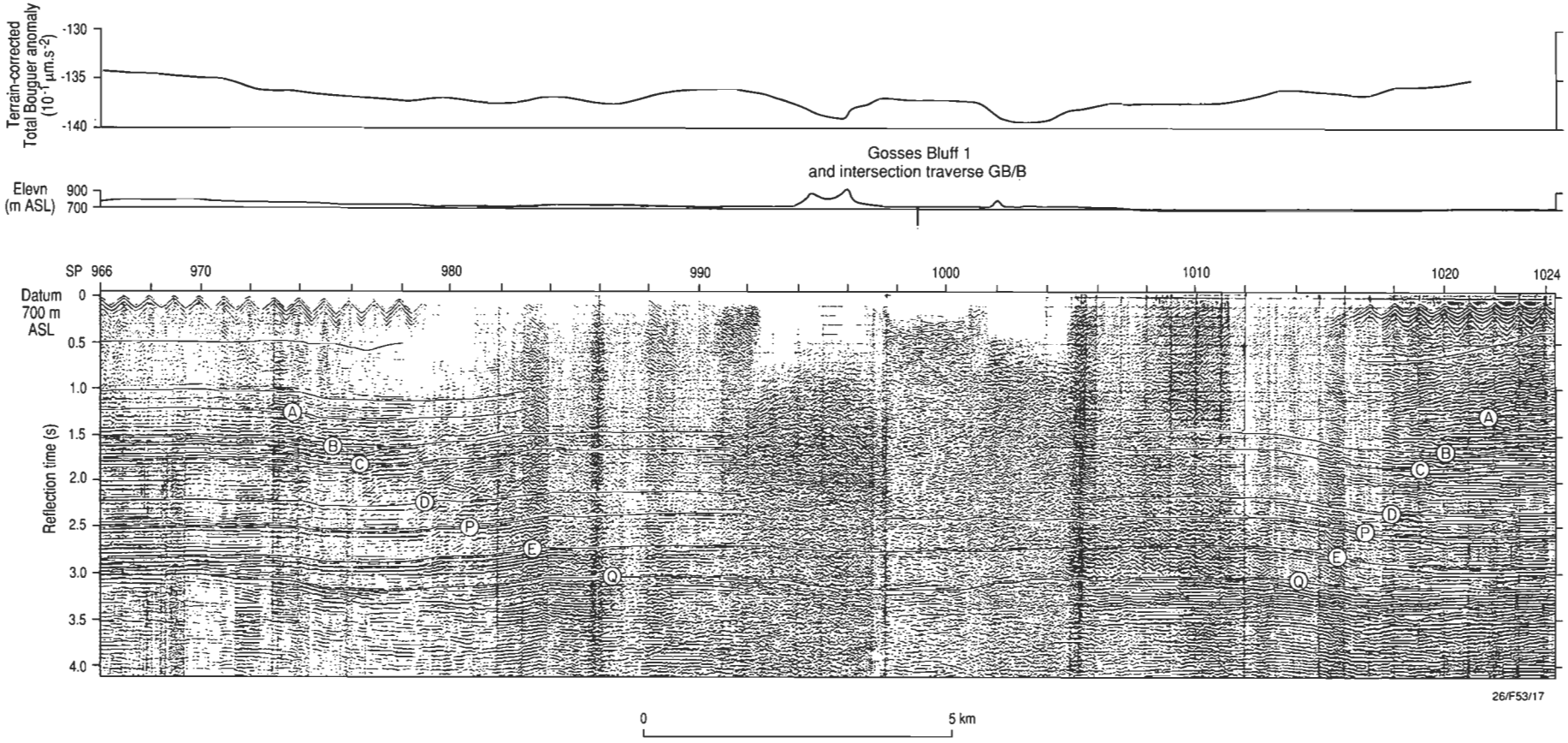

Figure 7. Interpreted record section and Bouguer anomaly profile, traverse GB/A.

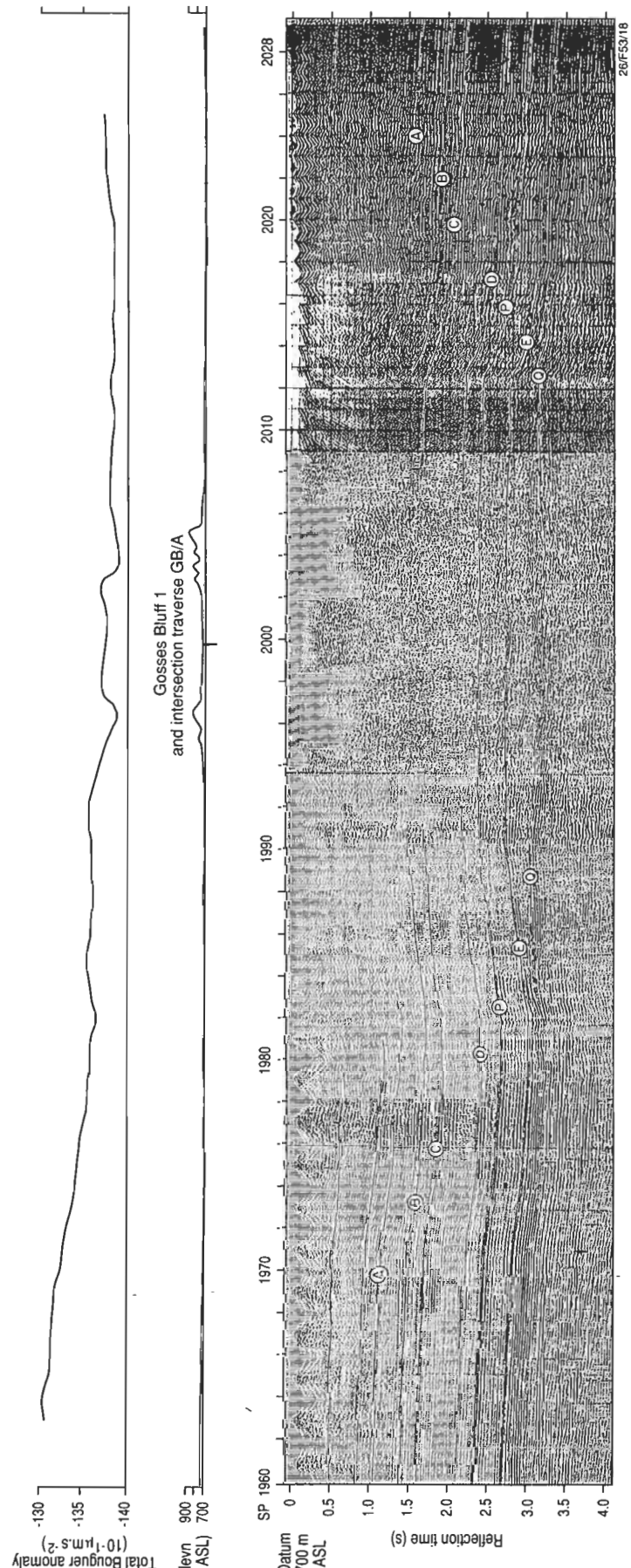

Figure 8. Interpreted record section and Bouguer anomaly profile, traverse GB/B.

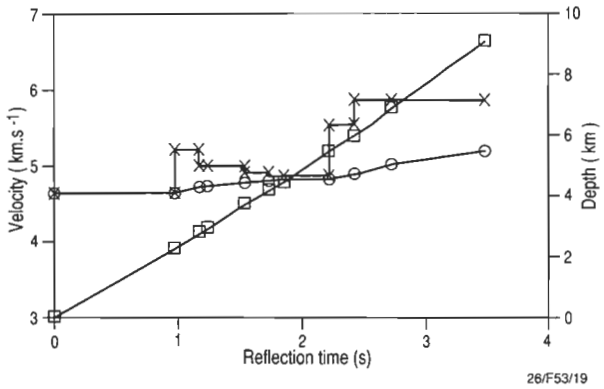

Figure 9. Time–velocity–depth relations according to Moss (1964); circles — RMS average velocity; crosses — interval velocities; squares — depths.

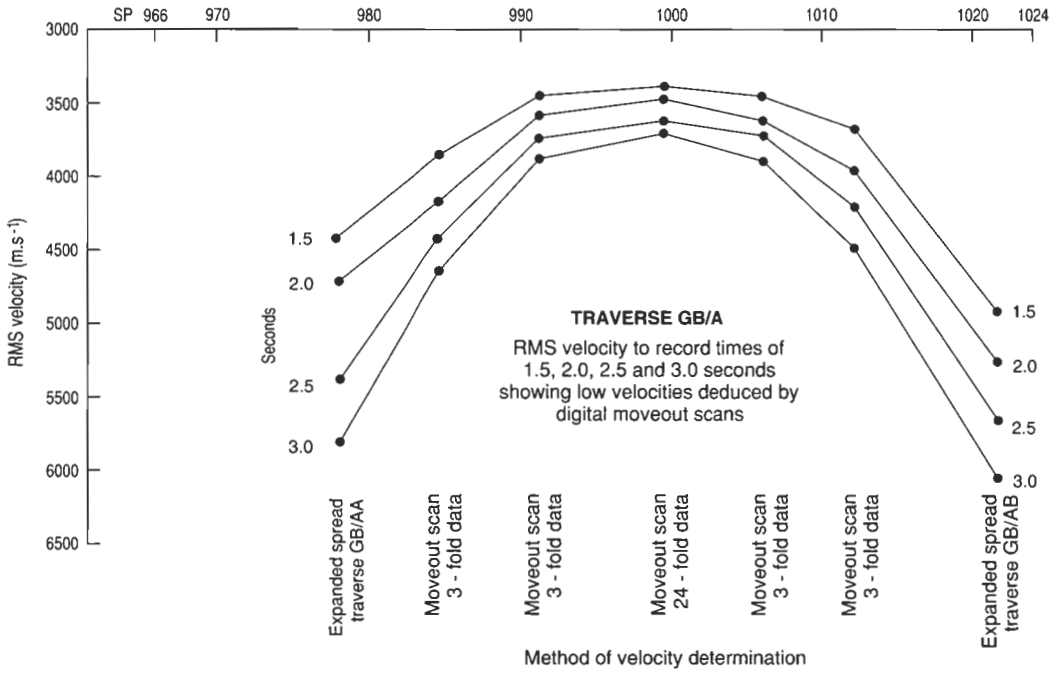

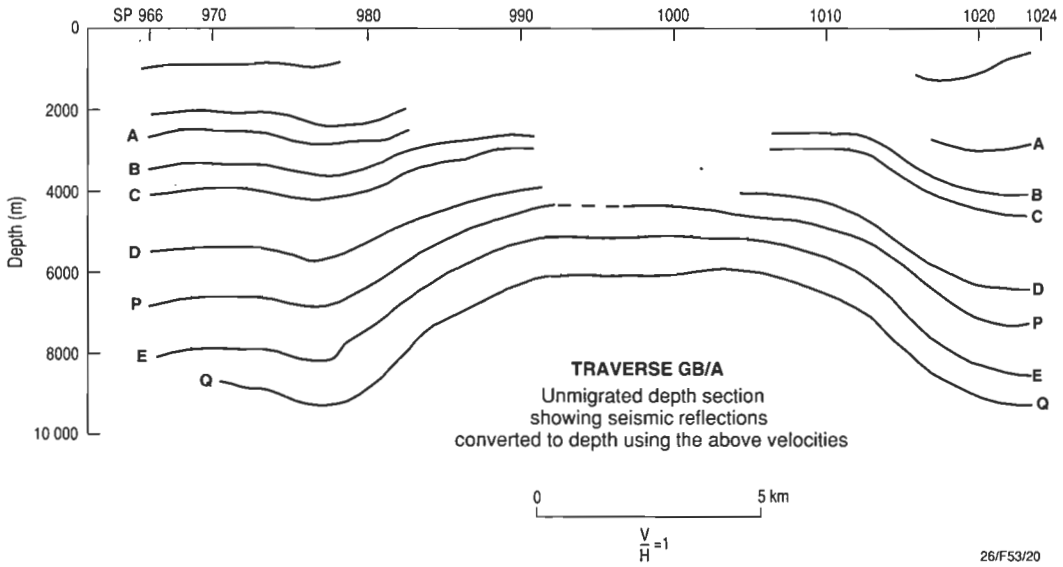

Figure 10. RMS velocity deduced by normal move-out scans and corresponding depth section for traverse GB/A.

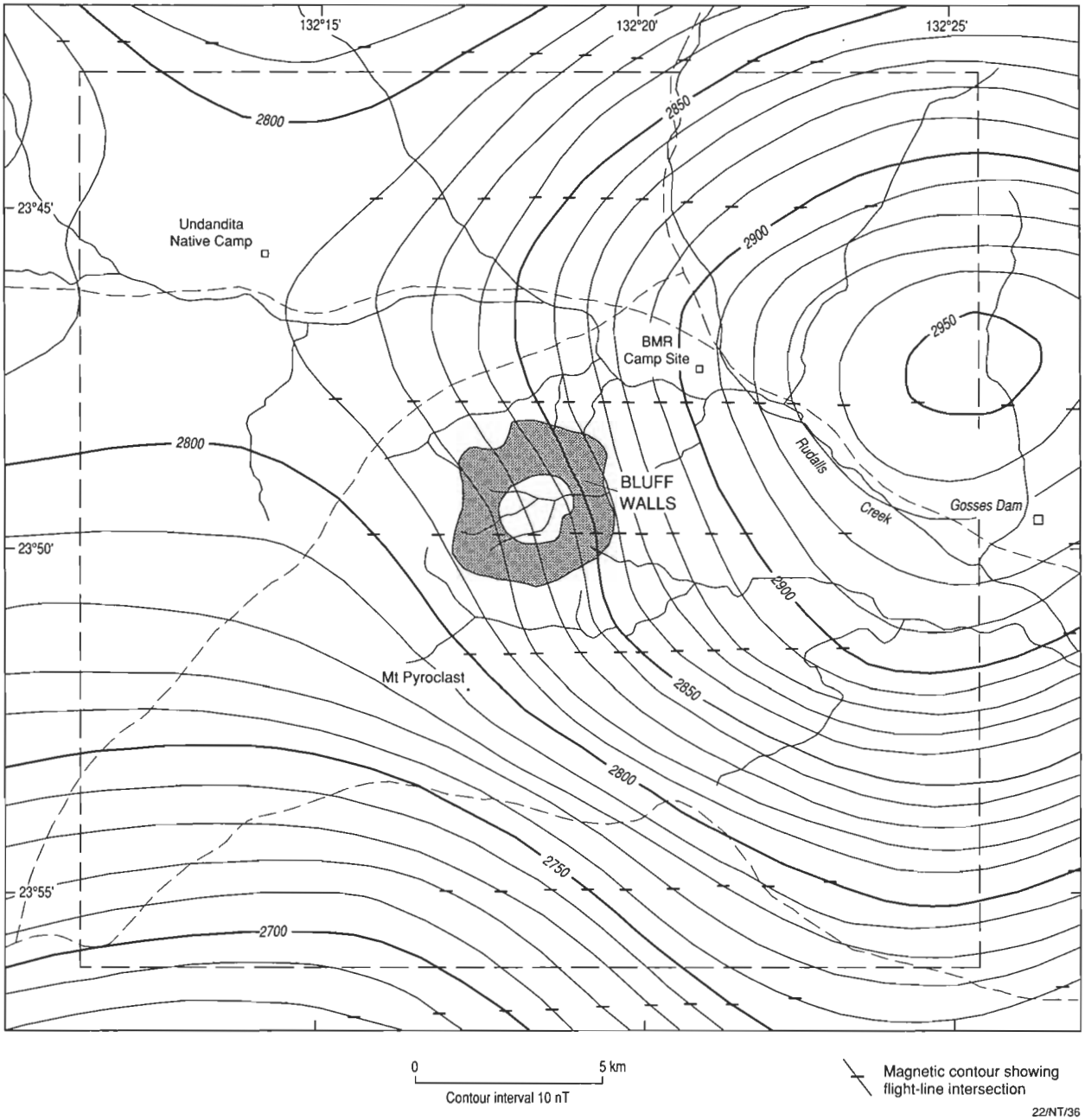

Figure 11. Contours of total magnetic intensity derived from the BMR aeromagnetic survey of the Amadeus Basin.

ciation correlate roughly with low velocities along the profiles. On traverse GB/B but not on traverse GB/A, velocities appear to drop under the outer parts of the traverses, rise as the bluff walls are approached, and drop under the centre of the bluff.

The inaccuracies and difficulties of detailed velocity determinations urged Brown (1973) to apply a simple linear velocity function — $V_{RMS} = 3350 + 590\ t$ m s^{-1} (t = two-way travel time in seconds) — to all the seismic data, except in the centre of the area, where the second term was replaced by 520 t in order to eliminate small time-troughs in the deeper horizons; these linear functions are plotted in Figure 12. The first function is also plotted in Figure 14, together with interval velocities and depths to the main horizons derived from it. The function derives a reasonable value of $V_{RMS} \sim 5200$ m s^{-1} near the basement, but the *interval* velocity at this depth is calculated as about 7000 m s^{-1}, which seems far too high by comparison with other velocity–depth profiles in this area and with crustal velocities in this depth range elsewhere.

Tyler No. 1 well, which was drilled close to the Macdonnell Ranges near the northeastern end of traverse GB/A, penetrated formations with velocities (Fig. 15) much higher than predicted from drilling and seismic work farther south (Huckaba & Magee 1969). This is thought to be a consequence of secondary silica filling most of the pore spaces in the rocks at Tyler No. 1. An increase in silicification near the Macdonnell Ranges may also be the reason for the higher velocities north of Gosses Bluff. The formations penetrated by the well are similar to those cropping out in the Gosses Bluff structure, but the velocities determined from the seismic log do not necessarily correspond

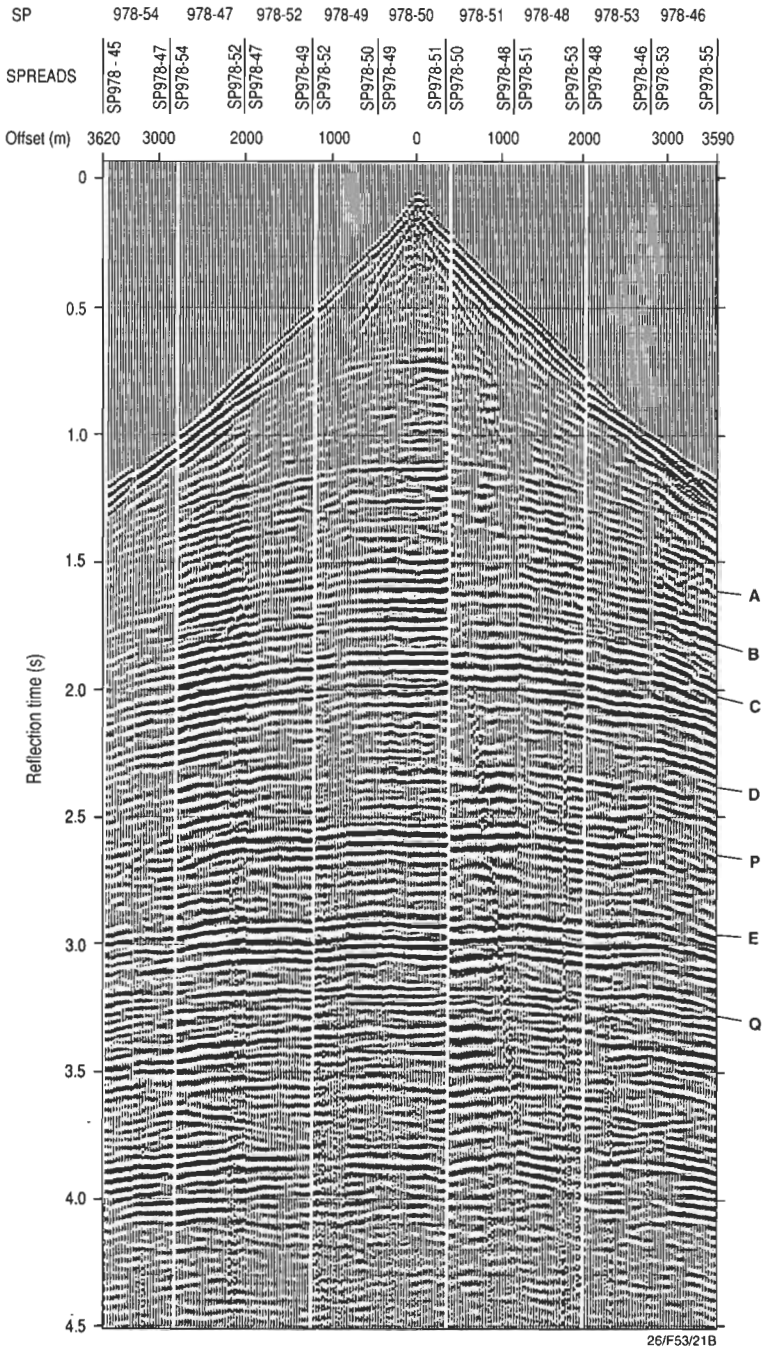

RECORD SECTION

RECORDING INFORMATION

Magnetic recorder: PMR-20
Amplifiers : PT-700
Prefilters : Out
Filters : L16 - KK135
Programmed gain :
Function : A
Geophones : HS-J, 14 Hz
Geophone station interval : 33.5 m
Geophone pattern :
32/trace in 4 rows of 8 in line
Rows 9 m apart, geophones 6 m apart
Shot hole pattern :
3 holes, 15 m apart in line
Depth 19 - 26 m
Commonest charge 3 x 36 kg

PLAYBACK INFORMATION

Filters : LL20 - KK60
AGC : SS
Compositing : Nil

VELOCITY INFORMATION

Nil

HORIZONTAL SCALE

As indicated

to velocities of formations within the structure which may evince the effects of disruption.

P.L. Harrison (formerly BMR, unpublished data) re-examined the shallow velocities near Gosses Bluff. He made a detailed analysis of shallow information, including refractor velocities based on first breaks on reflection records and expanding spreads, and measured normal move-out times on reflection records. His revised shallow velocities along traverses GB/A and GB/B (Figs. 16 and 17) confirm the general pattern of sub-weathering velocities (Fig. 13), and show more detail of variations beneath these.

Harrison also reviewed velocities within the deeper section based on the expanding spreads along traverses GB/AA, GB/AB, and GB/BA. He used the information to construct revised depth sections along traverses GB/A and GB/B. The velocity logs of Tyler No. 1 well are higher than those derived for the Gosses Bluff area, in agreement with Brown's (1973) suggestion that velocities are higher to the north near the Macdonnell Ranges. The velocities adopted are shown in Figures 18 and 19. Harrison's RMS and interval velocities (as scaled from Fig. 18 at the site of traverse GB/AA) are the source of the revised depths to the main horizons (Fig. 20).

Wright et al. (1989) presented the results of an expanding spread which lies roughly along traverse 2-58, centred at about SP 20 on that traverse (Fig. 3). The centre of this spread is only about 5 km from Brown's (1973) expanding-spread traverse GB/AA, and its four reflectors (Fig. 21) can be readily correlated with Brown's. Horizon A is slightly below Brown's (1973) horizon A, and horizons B, C, and D correspond to Brown's

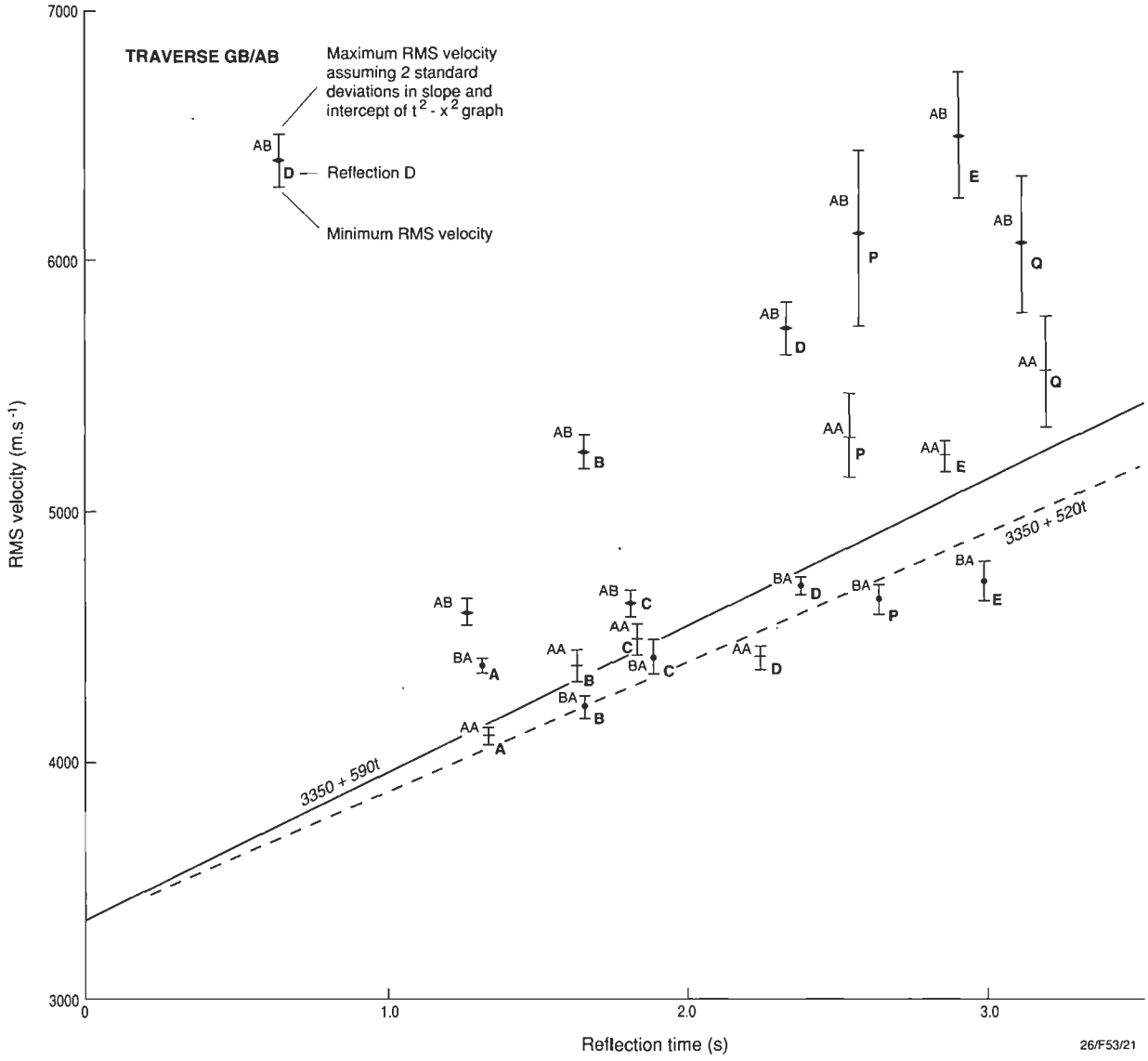

Figure 12A (*facing page*). Expanded seismic spread GB/AA centred on traverse GB/A SP978; B (*above*). RMS velocity versus reflection time from expanding-spread traverses GB/AA, GB/AB, and GB/BA.

(1973) C, P, and E. Although the 13 shots were recorded over a distance of about 25 km, only up to five shots were used in the analysis, as lateral variations destroyed consistency of the reflecting horizons; nevertheless, the offset distances up to 9 km, compared with the 3.6-km maximum of Brown (1973), provided more accuracy and detail in velocity determinations. The velocities to a depth of 1.32 km (about 6 s) were derived from a refraction survey (Fig. 22).

Velocities from the data of Wright et al. (1989; Fig. 23) were calculated first for the intervals between the main horizons; the method applied allows for the dip of boundaries. These velocities were used to derive corrections to the initial RMS velocities for 20 reflectors. A cubic spline function fitted to the RMS velocities applied weights based on the standard errors, and the interval velocities were derived from this smoothed curve. Wright et al. (1989) interpreted two marked low-velocity layers centred at about 1.5 s (Mereenie Sandstone) and 3.0 s (top of Bitter Springs Formation); the upper one agrees more or less with that of Moss (1964). The deepest interval velocities of Wright et al. are more in agreement with those of P.L. Harrison (unpublished data) and Moss (1964) than with Brown (1973), although no previous workers were able to resolve a low-velocity layer near the basement. Thus, the earlier depth–velocity determinations of Brown (1973) are superseded by the work of Wright et al. (1989; D.M. Boyd, University of Adelaide, personal communication 1995).

A comparison between the various velocity models (Fig. 24) shows that the thicknesses which Brown (1973) derived from his excessively high interval velocities for the deeper layers are greater than those derived from the other velocity functions.

Interpretation of seismic data

Using his velocity–depth relation given above, Brown (1973) converted times to depths, and migrated the reflections to their true positions. He acquired a reasonable value for the total thickness of the sedimentary section, but overestimated the thickness of the deeper layers, and the relief on their boundaries.

The migrated depth sections resulting from Harrison's (unpublished data) velocity analysis are shown in Figures 25 and 26. They differ from Brown's interpretation in their application of a

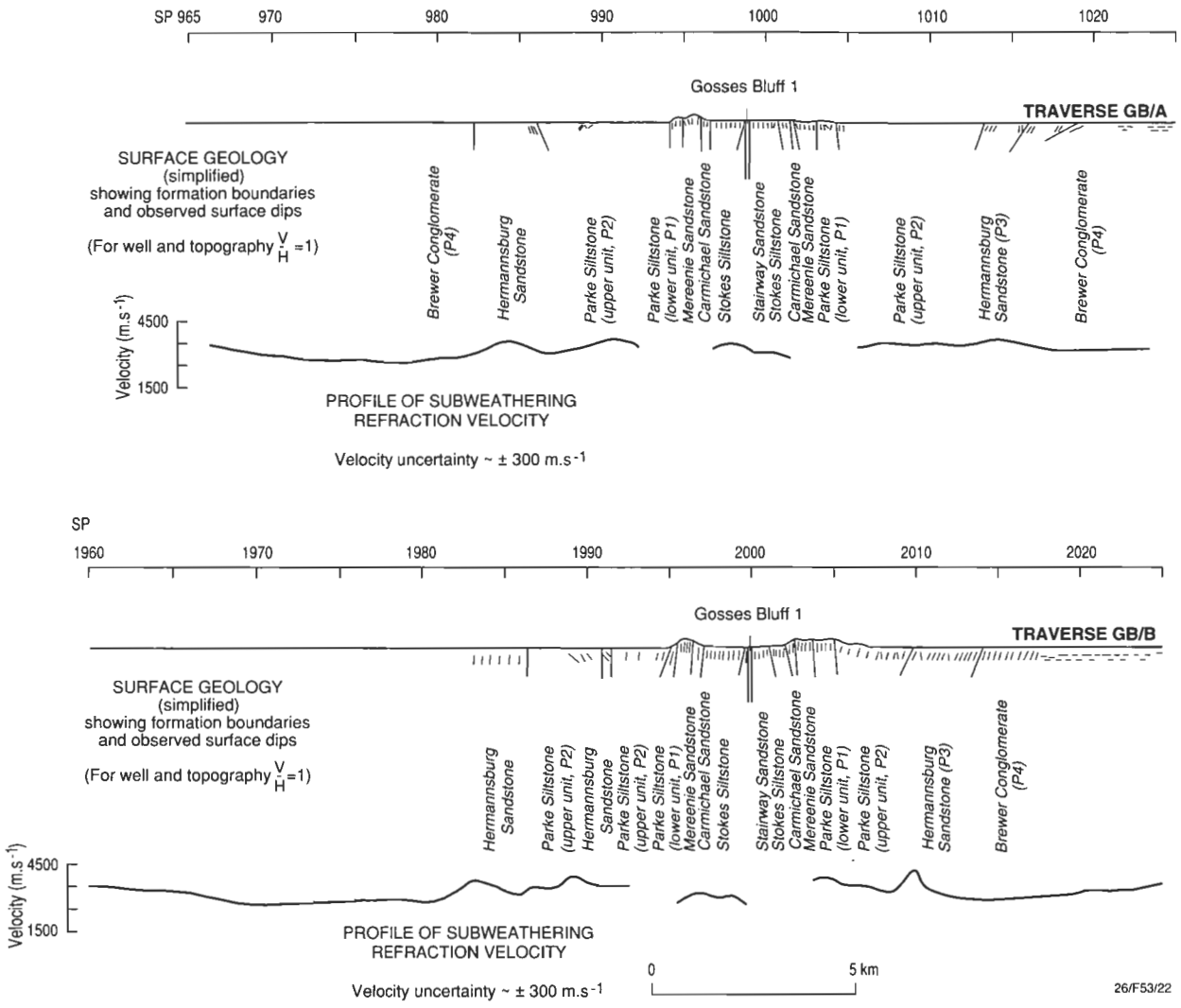

Figure 13. Surface geology and subweathering refraction velocity for traverses GB/A and GB/B.

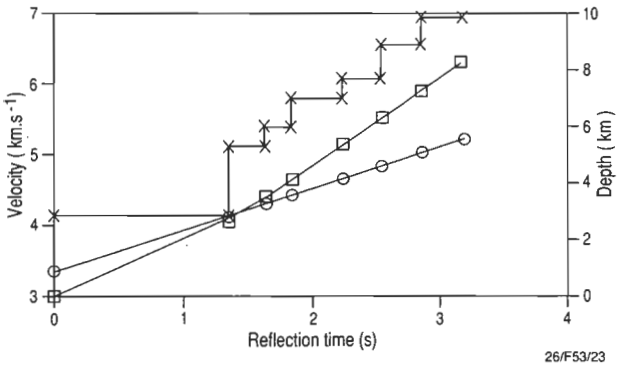

Figure 14. Time–velocity–depth relations according to Brown (1973); circles — RMS average velocity; crosses — interval velocities; squares — depths.

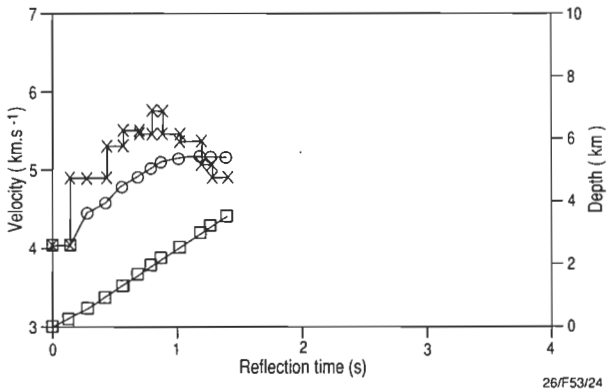

Figure 15. Time–velocity–depth relations from velocity logging of Tyler No. 1 well; circles — RMS average velocity; crosses — interval velocities; squares — depths.

variable shallow velocity, different interval velocities towards the base of the sedimentary section, and the assumption that velocity is constant within layers; by contrast, Brown assumed a constant velocity at a constant depth. Converting the time intervals of Figure 5 to depths depends on the interval velocity; the velocity function of Brown (1973) would give thicknesses about 40–50 per cent greater than that of Wright et al. (1989).

One feature of Harrison's (unpublished data) depth section along traverse GB/B (Fig. 26) is that the relief on the Gardiner–Tyler anticline is about half of that interpreted by Brown (1973). As before, there is less structural relief along traverse GB/A than along traverse GB/B, and again the amplitude is lower than that of Brown (1973). For part of horizon Q, a slightly deeper reflection was picked than that of Brown (1973); it provided 200 m more relief.

Harrison picked a shallower event with continuity under the bluff, indicating undisturbed layers at a depth of about 3450 m (Fig. 26), rather than 4550 m, as deduced by Brown (1973).

Thin near-surface low-velocity layers at SPs 974–984 on traverse GB/A (Fig. 18), and SPs 1966–1988 on traverse GB/B, may correspond to breccia layers. These differ from Brown's (1973) supposed breccia layers based on subweathering velocities.

Wright et al. (1989) seismically determined the depths to and thicknesses of the various stratigraphic layers (column 4, Fig. 27), which should represent the most accurate determination of the stratigraphic column at the site of their expanding spread but provides no information on the lateral variation of thickness or depth. Application of a velocity function to the times recorded along the seismic traverses should give the most reliable determination of thicknesses beneath the disturbed zone; however, velocity variations within the disturbed zone would affect the depths calculated to all boundaries beneath it.

The principal results of the seismic studies are summarised as follows:

1. The deeper seismic horizons beneath Gosses Bluff, although somewhat variable in character, are continuous (Figs. 25 and 26), which demonstrates that there is a bottom to the disturbance. This continuity commences about 3450 m below the present ground surface. The continuity of horizons P and E, considered to originate from near the tops of the Pertatataka Formation and Bitter Springs Formation respectively, indicates the lack of significant disturbance immediately below the Pertatataka Formation level.

2. A distinct region devoid of seismic reflections in the centre of both traverses indicates the approximate extent of the deeper part of the zone of disruption. The shape of the disturbed zone appears to be roughly hemispherical, has a radius of about 4 km, and is centred at the present ground level.

3. The subsurface geology was deduced by fitting the probable stratigraphy (Fig. 27) into the sequence of migrated seismic horizons. A cross-section along traverse GB/B showing the probable gross structure (Fig. 28) was then drawn schematically; it connects the formation boundaries interpolated at depth with the boundaries mapped at the surface. Within the zone of disruption, formations are probably largely faulted into blocks estimated to be of the order of 300 × 300 × 100 m. Unpicked shallow seismic reflections apparent on the record sections surround an area devoid of clear reflections, which presumably represents the shallower part of the disrupted zone. The diameter of the disruption at the surface is indicated as about 11.5 km by the subweathering velocity profile. This closely agrees with the 10.8-km radius of the gravity feature (Fig. 44).

4. The continuity of the deeper horizons demonstrates no large intrusive core underlying the structure.

5. The seismic sections show no direct evidence of a peripheral syncline, or folds induced in strata outside the zone of disruption.

6. Within the zone of no reflections associated with the disrupted region, structural information cannot be resolved. Neither the attitude of the strata within the disrupted zone, nor the dip or throw of the larger faults could be mapped. Thus, there is no indication that the strata were folded into an anticline at depth in the centre of the structure as a result of the impact. However, there is evidence of anticlinal doming at the level of the Bitter Springs Formation.

7. The regions of lower subweathering velocity may indicate areas of brecciation and disruption along the seismic traverses, although this would be only a rough guide. A separate shallow seismic survey — along traverse 81/82, which showed a drop in seismic velocity from 4.6 km s^{-1} over bedrock to 2.2 km s^{-1} over a breccia outcrop — may provide accurate locations and thicknesses for the breccia zones.

8. According to Figure 26, the Gosses Bluff structure is located above an anticline at the Bitter Springs level. The contours in Figure 5 indicate local thickening of the Bitter Springs Formation elongated along the axis of the anticline, and located symmetrically under Gosses Bluff.

Deep crustal seismic reflections

In view of the large negative gravity anomalies at Gosses Bluff, and as customary during BMR seismic field surveys, reflections from the deep crust in the Gosses Bluff area were recorded along shallower-level responses (Moss & Dooley 1988; Brown 1970). Records from the 1962 seismic survey (Moss 1964) indicated that the area near SP 110 on traverse L (Fig. 3) is favourable for deep energy transmission. The layout of deep-reflection shots in 1968, on traverses GB/L and GB/LA, is shown in Figure 29; SP 3110 on traverse GB/L coincides with SP 110 on traverse L of the 1962 survey. Traverse GB/LA intersects traverse GB/L at right-angles at SP 3106.

Continuous-reflection coverage was recorded between SPs 3110 and 3100. Excellent sedimentary reflections with a prominent northerly dip were obtained to about 3.6 s (Fig. 30). Coherent energy was recorded to 30 s. Events recorded at 8.5 and about 11.9 s were continuous on both the section and the cross-spread. The dominant frequency of the events is 25–30 Hz. The 8.5-s event shows little or no dip; the deeper one dips to the south, contrasting with the dip of the sedimentary formations.

One shot was recorded on traverse GB/LA at SP 3106–50; this shows a similar pattern of events to that on GB/L. The events at 8.5 and 11.9 s are synchronous, proving that the energy was returned at nearly vertical incidence. An attempt was made to record an expanding spread, but owing to limited time only the extreme shots were recorded. It is difficult to correlate the main events from the central and outer records; however, correlation

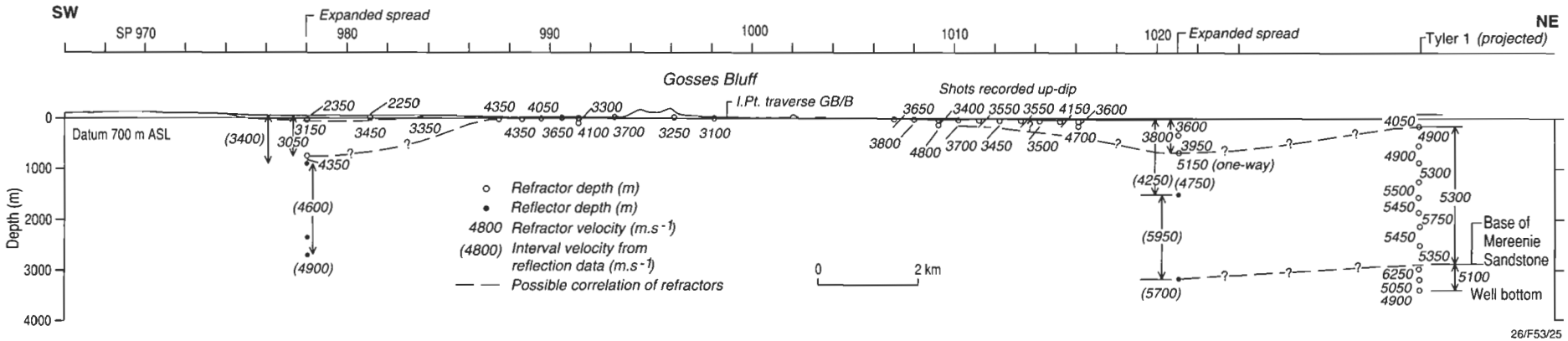

Figure 16. Shallow seismic information for traverse GB/A; velocities from P.L. Harrison (unpublished data).

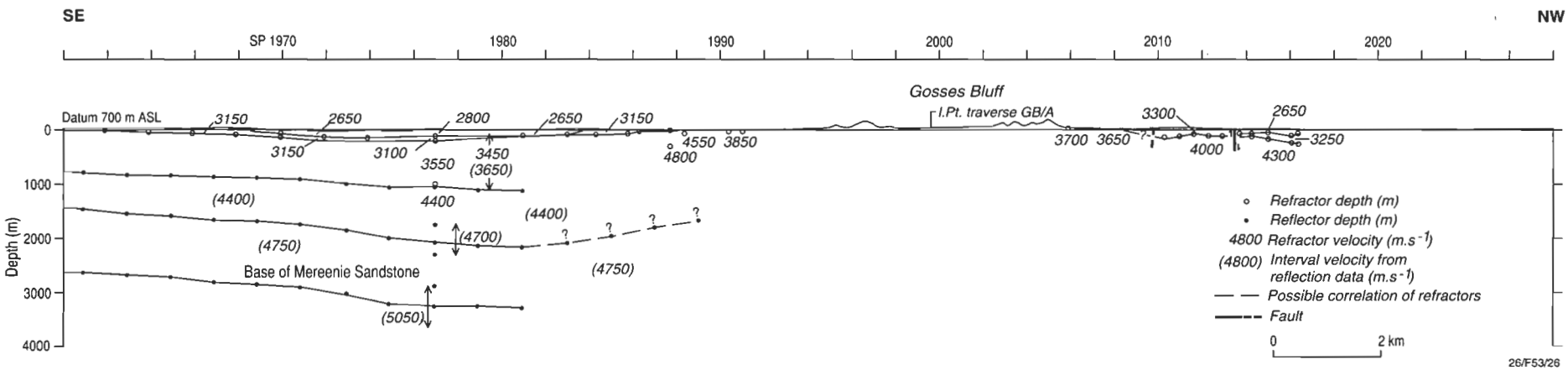

Figure 17. Shallow seismic information, traverse GB/B; velocities from P.L. Harrison (unpublished data).

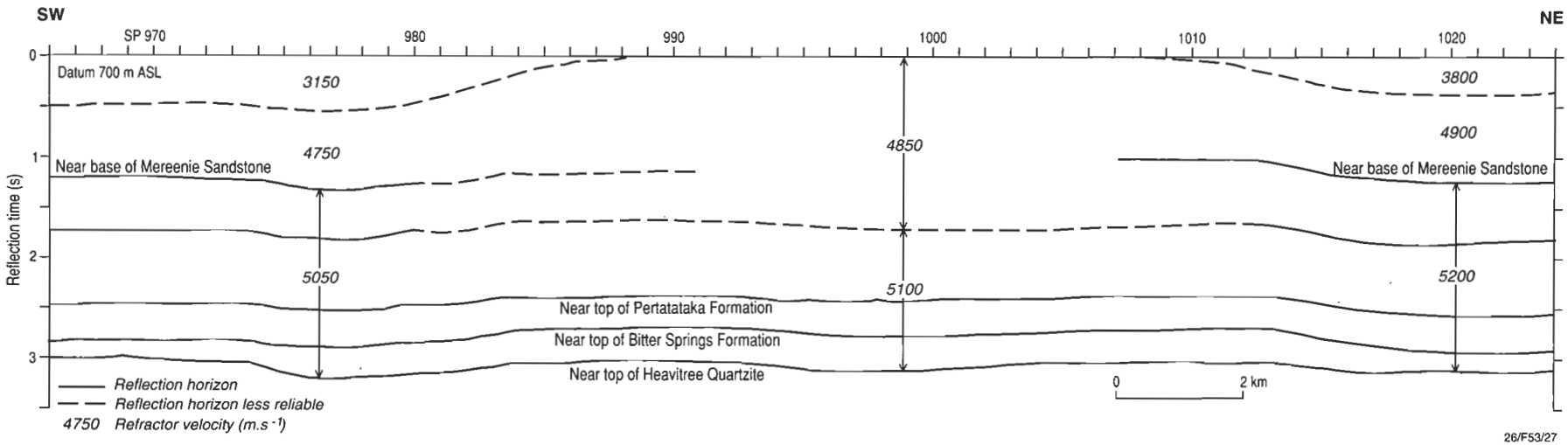

Figure 18. Reflections used for depth section, traverse GB/A; after P.L. Harrison (unpublished data).

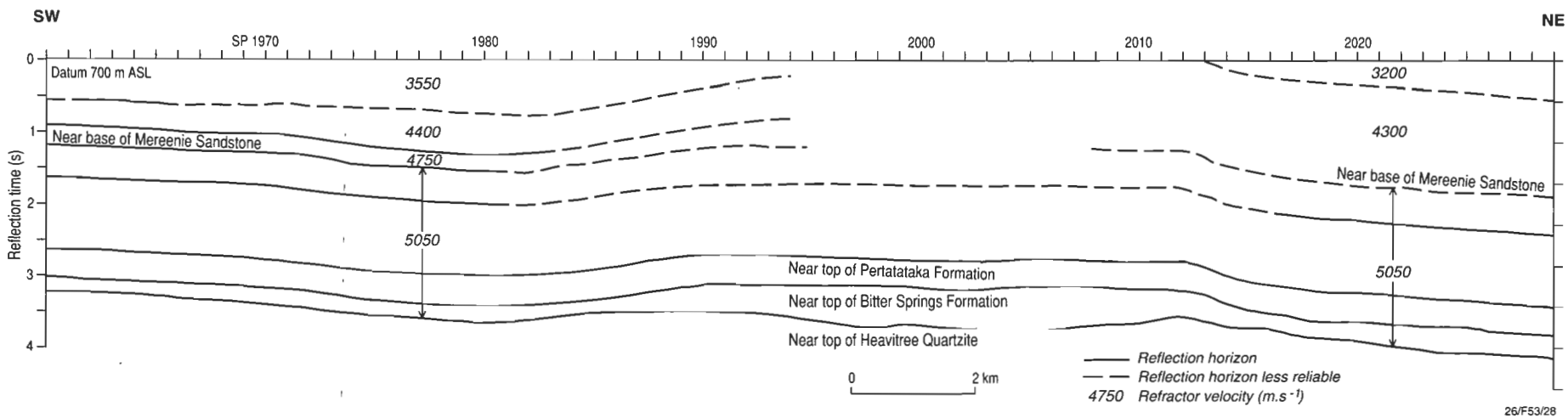

Figure 19. Reflections used for depth section, traverse GB/B; after P.L. Harrison (unpublished data).

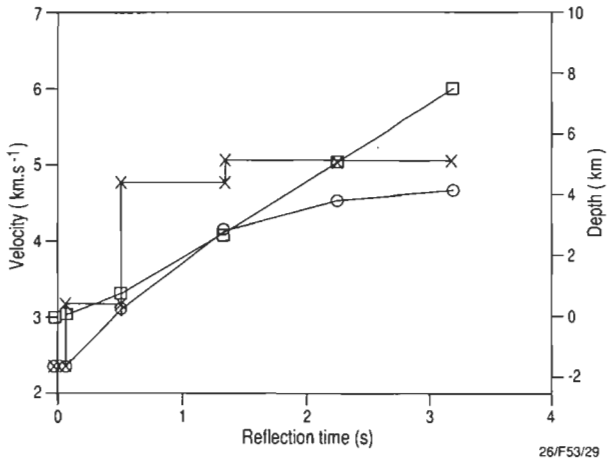

Figure 20. Time–velocity–depth relations according to P.L. Harrison (unpublished data); circles — RMS average velocity; crosses — interval velocities; squares — depths.

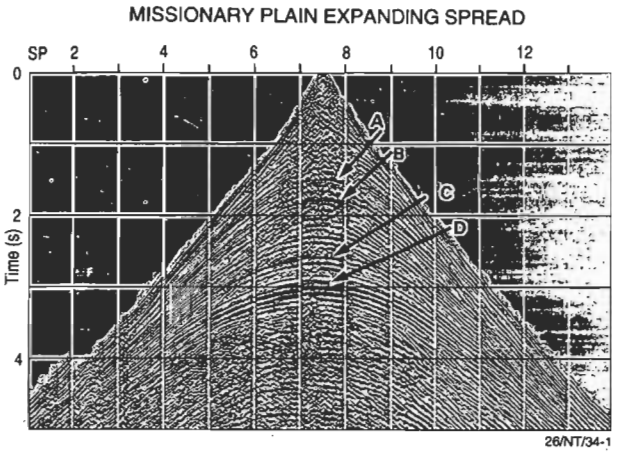

Figure 21. Seismogram from the expanding spread recorded in the Amadeus Basin; prominent reflecting boundaries A–D are marked.

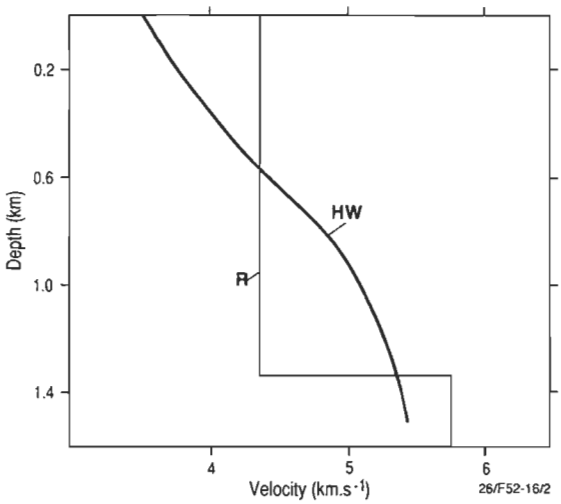

Figure 22. Velocity model derived from refracted arrivals from the Missionary Plain expanding spread. R represents the RMS velocity to the first reflector at about 1.32-km depth; HW is the first-interval-velocity model.

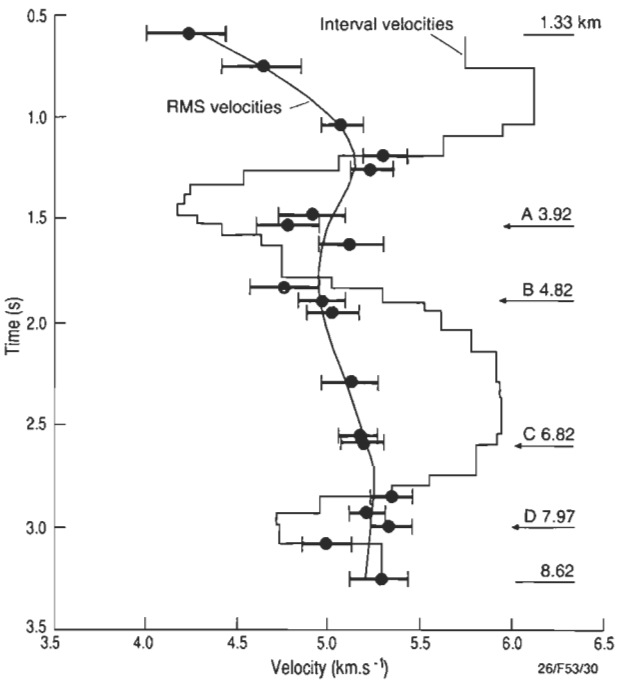

Figure 23. Time–velocity relations derived from expanding spread of Wright et al. (1989). RMS velocities are shown with error bars. The smooth curve is a cubic spline. Depths (in kilometres) to the prominent reflecting horizons A–D are shown on the right.

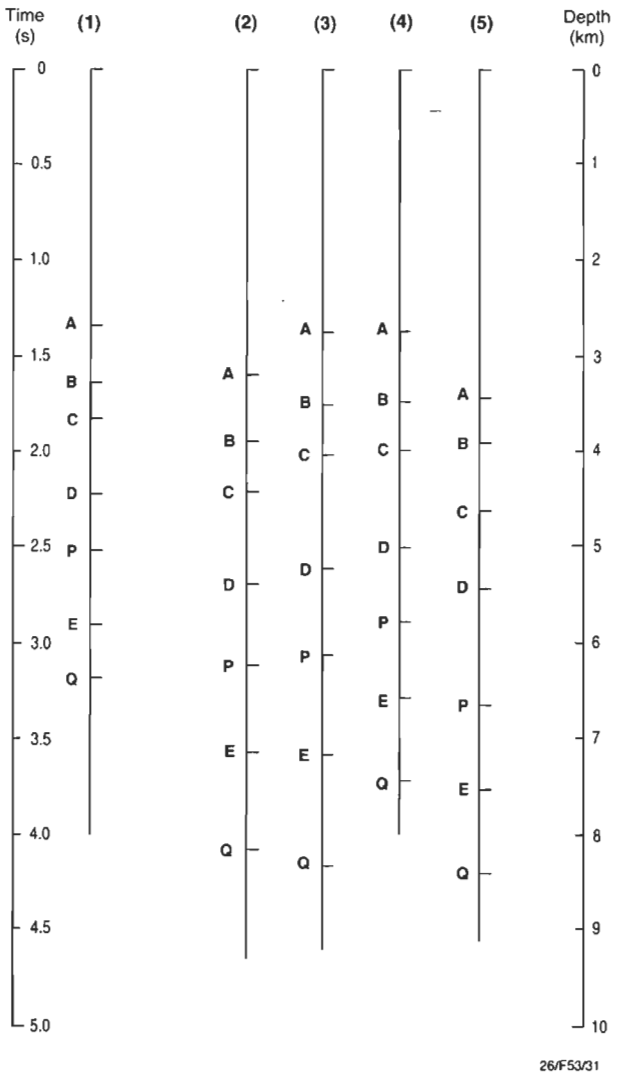

Figure 24. Depths to horizons A, B, C, D, P, E, and Q. (1) Two-way reflection times of Brown (1973) at the site of his expanding-spread traverse GB/AA. (2) to (5) Depths (in km) calculated from velocity–depth relations: (2) Moss (1964); (3) Brown (1973); (4) P.L. Harrison (unpublished data); (5) Wright et al. (1989).

of many phases showed a velocity variation with depth close to that expected for deep primary reflectors.

Depths to the 8.5- and 11.9-s reflectors are estimated as 24 and 36 km. Although the deeper one might be the Moho, Dooley & Moss (1988) — after taking into account isostasy, and crustal structure in other areas — suggested that the Moho could be substantially deeper than 36 km, and that both reflectors represent intracrustal boundaries. Goleby et al. (1988) showed a few events at times greater than the basement reflectors, but no sub-basement reflectors have been positively identified; some of them may be due to multiple reflections from the sedimentary rocks.

Magnetic surveys around Gosses Bluff

Airborne magnetic surveys

A regional airborne magnetic and radiometric survey that BMR flew over the Amadeus Basin in 1965 (Young & Shelley 1966) was designed to investigate the overall structure of the basin, in particular to assist in the assessment of its petroleum potential. East–west lines were flown with a spacing of 3 km, at an altitude of 300 m above ground level. Total magnetic intensity (TMI) contours derived from this survey are shown in Figure 11 for the region around Gosses Bluff. Depth to magnetic basement deduced from the survey over a wider area (Fig. 31) is about 10 km under the bluff. A test flight over the structure at a lower level showed a negative anomaly of 4 nT between Gosses Bluff and Mount Pyroclast.

A detailed aeromagnetic survey of an area of 580 km^2 flown in 1968 (Young 1972) had a flight-line pattern specifically designed to investigate any concentric or symmetrical distribution of near-surface magnetic anomalies (Fig. 32). Its altitude was nominally 90 m above ground level.

The residual magnetic field in areas where it exceeds ±1 nT (Fig. 33) evinces anomalies over the eastern, southern, and western flanks of the bluff within 6 km of the centre. These anomalies have short wavelengths, and reduce the intensity of the field; this indicates that they have very shallow sources whose main component of magnetisation is remanent and opposed to the Earth's present field.

The magnetic anomaly recorded on line 5 over Mount Pyroclast (negative peak at GR 241574; Fig. 34) compares with model anomalies calculated for a magnetic dipole inclined at 80° or 90°. This leads to the interpretation of the anomaly source as a magnetised, roughly spherical mass, presumably of shock-melted breccia, whose centre is 100 m below ground level. This body would have been magnetised by the Earth's field at the time of cooling.

The anomaly recorded on line 14 over the rim of the bluff (negative peak at GR 244605; Fig. 35), compared with the calculated effect of a thin sheet with width less than 105 m, extends from a depth of 90 to 270 m below ground level. The strike of this anomaly based on magnetic data is N100°E, whereas its dip is assumed to be 80°S, as indicated by geological information.

Ground magnetic surveys

Detailed magnetic measurements were made on the ground in two areas (Fig. 33) during August 1969, to locate more accurately the source of the two anomalies mapped by the airborne survey, and to define drilling targets to obtain samples for palaeomagnetic study (Sedmik 1983). The two areas were at Mount Pyroclast, to cover the anomaly on line 5, and immediately south of the south wall of Gosses Bluff, to cover the anomaly on line 14.

Mount Pyroclast: Two traverses totalling about 4300 m were surveyed with a vertical-component magnetometer. The origin of the grid of traverses is at GR 241568. Traverse 00 showed magnetic anomalies (Fig. 36) over quartzitic or flow breccia outcrops, similar to the aeromagnetic anomalies, but more irregular owing to the proximity of magnetised material. Traverse 700W showed an anomaly over impact breccia at 3500N. This could be modelled by a spherical magnetised body with centre at a depth of 44 m beneath the traverse at 3536N.

Southern end of Gosses Bluff: A grid extending over an area of about 280 × 180 m was surveyed in detail with both vertical- and horizontal-component magnetometers. The origin of the grid of traverses is at GR 245596. The results (Figs. 37 and 38) delineate four pronounced local anomalies between traverses 500W and 100E. These suggest the existence of at least two, and possibly four, magnetic bodies. The anomalies on traverses 100W and 400W have been modelled by curves calculated for magnetised spheres (Figs. 39 and 40); both vertical- and horizontal-component profiles could be fitted by spherical bodies with centres at depths of 20 to 24 m, magnetised at an inclination of +80°. Intensely heated but not quite melted breccia crops out over several square metres about 3 m north of drillhole H33 between line 400W and 450W (Fig. 37), and a similar outcrop of quartzitic breccia occurs near drillhole H39 on line 100W.

Drilling results

Holes H33, 34, and 35 (appendix I in Milton et al. this issue) were drilled before the magnetic survey. Apart from the first 3 m of H33, the penetrated rocks showed little or no thermal effects.

Holes H38 and 39 were recommended on the basis of the magnetic results. They were drilled to a depth of about 24.5 m in shock-melted breccia throughout, from which oriented cores were removed for palaeomagnetic studies.

Palaeomagnetic measurements

Nine specimens were cut from the drillcores from H38 and 39 at depths ranging from about 10 to 23 m. Manwaring (1983) has presented details of the measurements. The specimens evince consistent values of inclination between 71 and 74°, indicating stable magnetisation, but declinations were widely scattered, suggesting that the cores probably rotated in the barrel before the azimuth was marked. Demagnetisation of one specimen in increasing AC fields showed no significant change in direction of magnetisation until it became unstable at 60 nT.

Eight oriented hand samples were collected from Mount Pyroclast. One was intensely weathered, and was discarded. Two others gave similar magnetic directions, but were different in magnetisation and lithology from the other samples; they appeared to be sandstone and not breccia, and therefore would probably not have been remagnetised by the Gosses Bluff impact. The mean direction of magnetisation of the other specimens was I = 71°, D = 100°, signifying a pole position at latitude 25°S, longitude 170°E. The polar-wander curve apparently reflects some rapid movements during the Mesozoic (Idnurm et al. 1984), when pole positions were as follows:

age	*pole at*	*polar distance*	*inclination*
180 Ma	50°S, 181°E	43°	65°
140 Ma	32°S, 162°E	25°	77°
100 Ma	52°S, 157°E	73°	2°

Thus the pole position is consistent with a Jurassic–Cretaceous date of magnetisation of the rocks at Gosses Bluff. The rapid cooling of the flow breccia would have registered any displacement of the magnetic pole from the geographic pole, which is otherwise statistically cancelled in measurements from a series of lava flows or a plutonic intrusion.

The ratio of remanent to induced magnetisation of the rocks is about 3.3. If the magnetism induced by the Earth's present inclination of –55° and declination of 5°W is combined with the remanent magnetisation, the resultant inclination in the vertical plane through the traverse line is 89 ± 6°, in good agreement with the findings of the ground survey.

Gravity surveys

Regional surveys conducted by BMR and petroleum exploration companies have shown that the Amadeus Basin is characterised by a large negative gravity anomaly, of about –16 000 μm s^{-2}. This is too much to be explained solely by the known sedimentary section, and various theories involving deep crustal structure have been advanced to account for this feature.

By 1967, gravity surveys along roads and seismic lines had shown that a roughly circular gravity low about 25 km in diameter and with a maximum amplitude of only a few hundreds of micrometres per second per second is associated with Gosses Bluff. A detailed gravity survey designed to provide specific data on the structure was carried out by BMR in 1967–69 (Barlow 1979). A 0.8 × 0.8-km grid of stations (Fig. 42) over an area of 24 × 24 km centred on the bluff was measured and marked on the ground by the Division of National Mapping; the station interval was reduced to 0.4 km over the inner 6.4 × 6.4-km square. Grid stations were spirit-levelled and positioned by theodolite; the accuracy of anomalies is estimated as better than 5 μm s^{-2}. Further stations were observed at 80-m intervals along four radial profiles between 7.2 and 12.0 km from the centre to study the outer gradient. Gravity observations were also made at shot points along BMR seismic traverses GB/A and GB/B (Fig. 3). Locations of stations on and near the bluff walls were selected to minimise terrain effects, and were surveyed by stereophotogrammetry; their accuracy is somewhat lower, up to about 10 μm s^{-2} after application of terrain corrections. A rock density of 2.42 t m^3 was used for calculating Bouguer anomalies.

Bouguer anomalies

A regional field, defined by a two-dimensional polynomial surface representing a smoothed version of the field in part of the area covered by Figure 41, was subtracted from the observed field to produce the residual anomaly maps shown in Figures 43, 44, and 45.

Residual map of the Hermannsburg 1:250 000 Sheet area. The circular gravity low centred on Gosses Bluff (marked A in Fig. 43) covers the same area as Figure 44. Other closed features of similar size occur in the surrounding area. Anomalies C, E, and G (Fig. 43) mark gravity highs; G is associated with the Gardiner Range Anticline, and E is near Tyler No. 1 well, which was sited on an east–west seismic structure. Anomalies B, D, F, and H mark gravity lows. Anomaly D is near the Goyder Pass Diapir, and salt may be the cause of some of the lows. An alternative explanation is that some lows may be associated with thrusting, as suggested — for example — by the asymmetric shape of anomaly B, near the Deering Anticline. There is no evidence from gravity for the Gardiner–Tyler anticline, postulated on the basis of seismic evidence.

Residual map of the survey area. The remarkably circular shape of the outer gravity gradient (Milton et al. 1972) is confirmed in the improved residual map (Fig. 44). Residual gravity values inside the gradient zone are nearly uniform, except for the annular gravity low near the bluff walls. The average value, both inside and outside the walls, is –360 μm s^{-2}, about 440 μm s^{-2} lower than the field at large distances from the bluff. Arcuate features of short wavelength disturb the uniform field locally. The total mass deficiency can be calculated by integrating the gravity anomaly over the area it occupies; Barlow (1979) computed 17 mm s^{-2} km^2 for this integral, denoting a mass deficiency of about 3.6 x 10^{10} t less than 3 km below the central uplift. The density contrast associated with the outer gradient should lie roughly under the maximum gradient, which closely follows the –140 μm s^{-2} contour. This does not deviate by more than 0.3 km from a circle of radius 10.8 km, whose centre is marked in Figure 44.

Residual map of the inner area. A well-defined annular gravity low occurs over the centre of the Gosses Bluff structure (Fig. 45). It is bounded by a steep gradient at the inner edge of the circular ridge, along the nearly vertical beds of the Carmichael Sandstone, and by a less steep gradient at the outer edge, along the steep contact between the Dare Siltstone and Harajica Sandstone Members of the Parke Siltstone. The circular ridge consists mainly of steeply dipping sandstones (Mereenie Sandstone and Pertnjara Group), which clearly continue in a near-vertical attitude below the surface. The low gravity values reflect low rock densities. The locus of the minimum of the annular low, and the maximum of the inner gradient, which closely follows the –420 μm s^{-2} contour, are nearly circular, but have a tendency towards a pentagonal shape, corresponding to the exposed structure. Best-fitting circles have radii of 1.6 and 1.2 km, and deviations of less than 200 m. They have a common centre, determined within 100 m (Fig. 45). The marked circular symmetry and near coincidence of the centres are important factors in considering theories of the origin of the disturbance.

Radial profiles. Residual anomalies for eight radial profiles at 45° intervals of azimuth were scaled from a point midway between the two gravity centres (and marked as 5 in Fig. 45). They are plotted in Figure 46a. The inner and outer parts of the profiles have been individually shifted to bring the inner and outer maximum gradients into coincidence (Fig. 46b); the profiles have been stretched or contracted in the flat part at about 7 km from the centre to enable both gradients to fit. A representative profile (Fig. 46c) was then derived as the mean of the profiles in Figure 46b.

Using a method of Skeels (1963), Barlow (1979) interpreted the main circular gravity low by matching the profile (Fig. 46c) with the effect of a disk or flat cylinder with a vertical axis, a diameter of 10.2 km, between depths of 0.8 and 1.6 km, and a density lower than the surrounding rocks by 0.2 t m^3. The thickness of the disk would vary in inverse proportion to the density assumed, but the depth to the bottom would not change much.

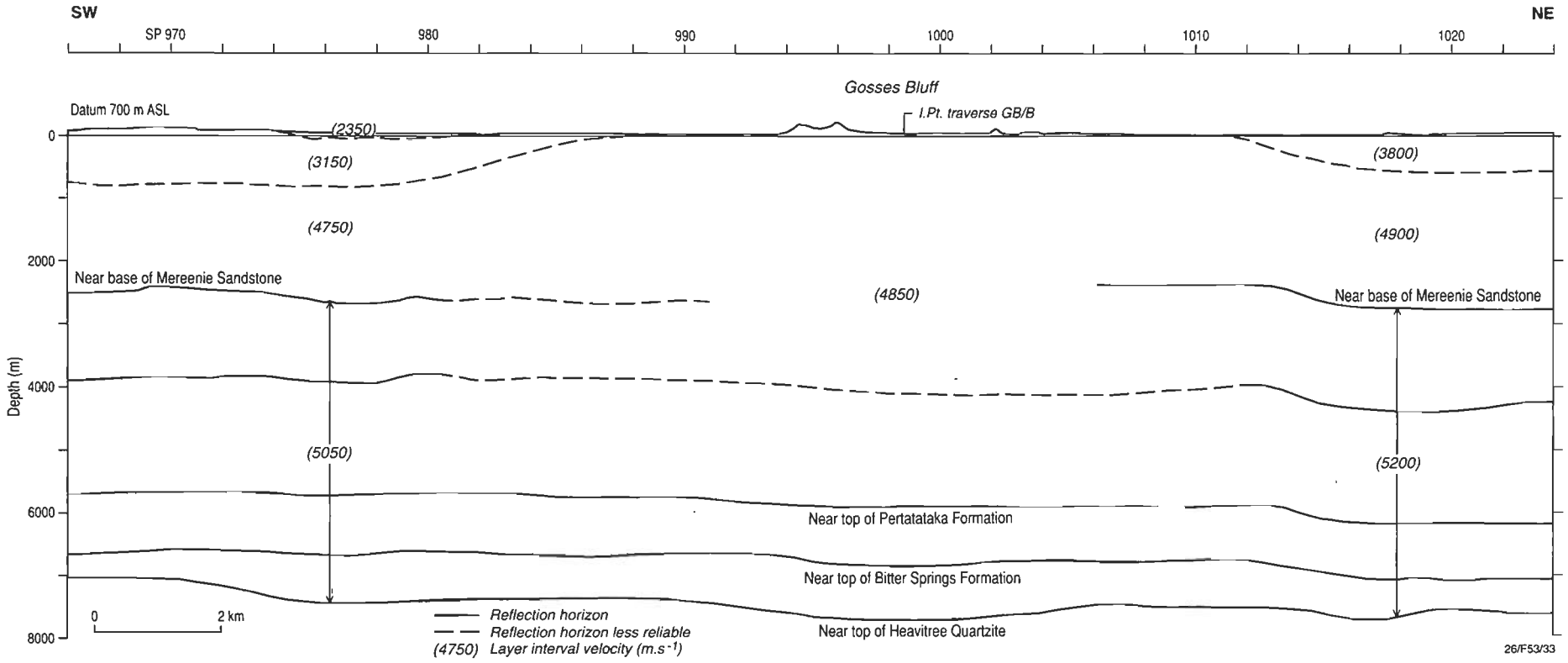

Figure 25. Migrated depth section, traverse GB/A; after P.L. Harrison (unpublished data).

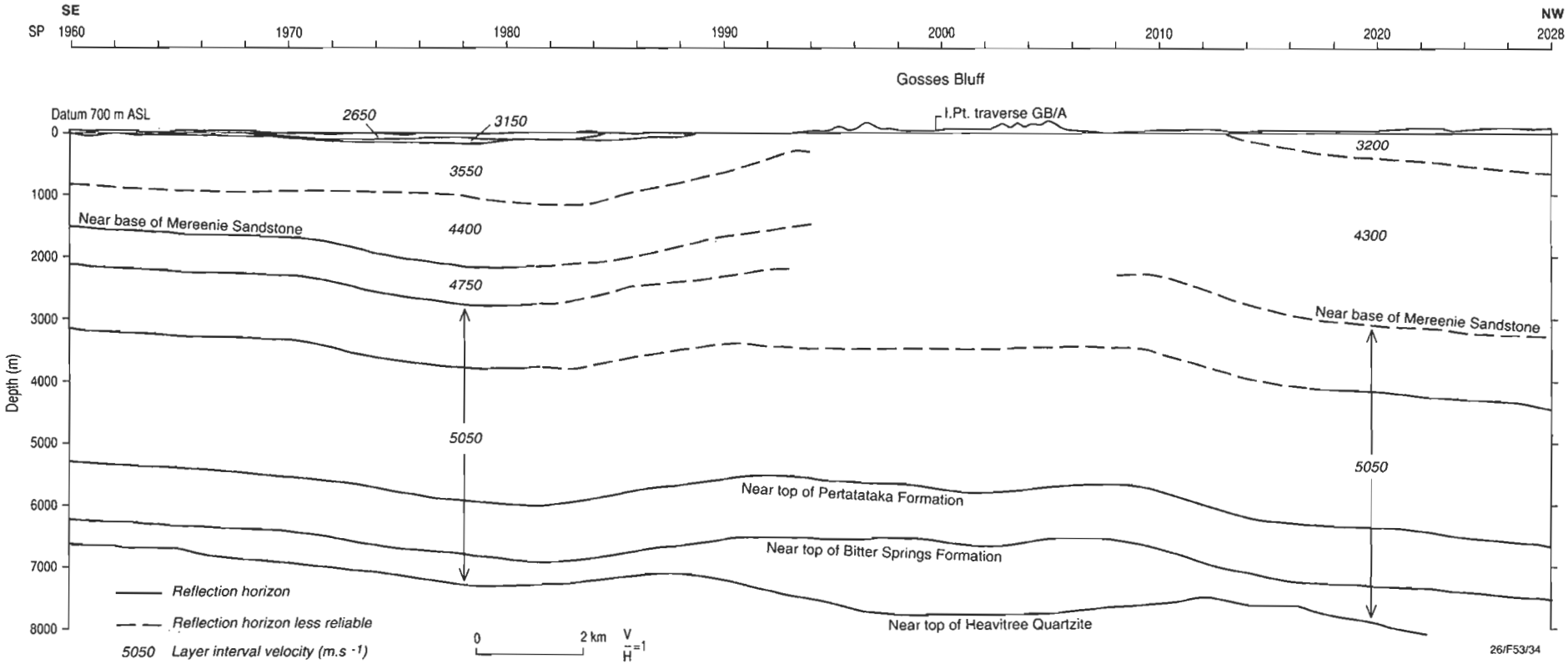

Figure 26. H6 migrated depth section, traverse GB/B; after P.L. Harrison (unpublished data).

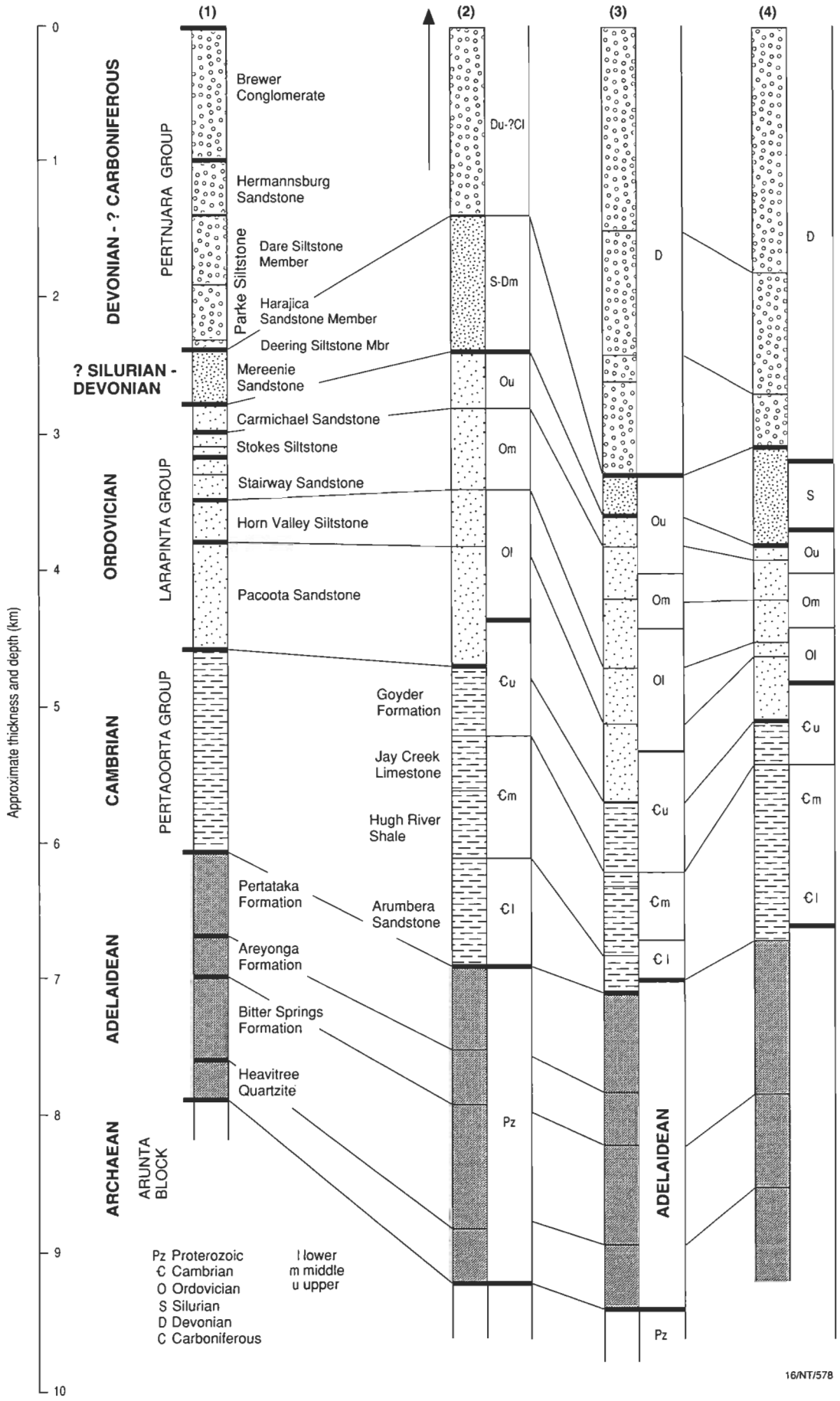

Figure 27. Stratigraphic sections of the northwest Amadeus Basin as proposed by various authors: (1) Cook (1966, 1968); Glikson (1969); (2) Wells et al. (1970); (3) D.J. Milton, adopted by Brown (1973) and Barlow (1979); (4) seismically determined depths to formations (Wright et al. 1989).

For the annular low, interpretation was based on the assumption of an infinitely long body tangential to the circle. Skeels's (1963) method computes a maximum depth for the cross-section of the anomalous body as 0.5 km, with its top at a depth of 0.13 km and thickness along the profile as 0.9 km.

Density of rocks in bluff walls. The density of elevated features is required for calculating elevation and terrain corrections. The conventional method of estimating the density (Nettleton 1939) is by correlating the gravity values with elevation along profiles crossing the elevated features; choice of the correct density should give zero correlation. However, as the principal variation in elevation occurs in the walls of Gosses Bluff, which coincide with an annular low gravity feature, there exists a correlation that will not be removed by any reasonable choice of density along the radial profiles.

Barlow (1979) used a modification of Nettleton's method to overcome this problem. The elevation of the gravity stations varies substantially around the circular ridge, so correlating between Bouguer anomalies around the annulus — rather than along profiles at right-angles to it — should give an estimate of the density of the rocks that constitute the ridge.

Bouguer anomalies calculated according to the standard density applied to the Gosses Bluff area (i.e., 2.42 t m^3) showed practically no correlation with elevation. At first sight, this might imply that 2.42 t m^3 is the correct density for the rocks. However, Barlow (1979) pointed out that there should be a correlation, because the gravitational effect of the anomalous rocks should decrease with elevation of the station, as the elevation corresponds to an increase in the distance from the bulk of the anomalous rocks; this effect is called the upward-continuation effect. Thus, the zero correlation implies that the upward-continuation effect is balanced by the use of an incorrect choice of density. By calculating the correlation to be expected from the upward-continuation effect, Barlow (1979) estimated the error in density as 0.05 t m^3 — that is, the correct density should be 2.37 t m^3. This may be assigned to the Mereenie Sandstone, which forms the bulk of the rocks in and under the circular ridge.

Calculations show that there is a small but insignificant positive correlation with elevation shown in Figure 47, modified after Barlow (1979), of about half the estimated upward-continuation effect, so that the best estimate of the density correction would be –0.03 rather than –0.05 t m^3. However, the regression coefficient estimated for the upward-continuation effect is not significantly different from zero, in view of the scatter of the data shown in Figure 47, so the estimates of density change cannot be taken as accurate.

Estimates of depth to features causing steep gradients. Model shapes and density contrasts between successive formations which crop out in the inner area can be determined with unusual reliability, because of the steep dip of the beds. Although the gravity effects are small in amplitude (maximum 300 μm s^{-2}), gradients as steep as 70 nm s^{-2} m^{-1} were reliably measured by stations at 67-m intervals along radial seismic lines.

Gravity values were calculated for subsurface models along sections ABC and BD (Fig. 45), which pass through the creek outlet from the pound and have no significant elevation variation along them. The gravity models showing density departures from standard, and the corresponding geological cross-sections, are shown in Figure 48. The density interfaces agree generally but not exactly with the formation boundaries and their dips as mapped at the surface.

Significant density variations deeper than 0.5 km are incompatible with the gravity profiles. This is in conflict with the evidence of the seismic survey, which shows that the steeply dipping beds persist to much greater depths, and of Gosses Bluff No. 1 well, which remained in steeply dipping rocks to its maximum depth of 1383 m (Pemberton & Planalp 1965). The apparent lack of lateral density variations below 0.5 km depth may conceivably arise from recementation of crushed and fractured material uplifted from various depths and/or the dominance of megabreccia with few discontinuities (rather than smaller-scale fragmental breccia). The calculated gradients, particularly along line A–B, are significantly greater than the observed gradients; this suggests that the assumed density contrast is too great, and that a lower density contrast would give a greater depth to the bottom (D.M. Boyd, personal communication 1995).

We used the density of 2.37 t m^3 determined above for the Mereenie Sandstone to help us determine the *in situ* densities of the sandstones in the gravity profiles. These densities are for rocks after they have been fractured and uplifted, and may be higher for undisturbed rocks of the same formations at depth. Froelich & Krieg (1969, fig. 4) reported average surface and core densities for formations elsewhere in the Amadeus Basin. Their core densities are about the same as Barlow's (1979) estimates, except for the Parke Siltstone and Stokes Siltstone, which are somewhat higher than those of Barlow (1979).

Minor residual field after removal of symmetrical features. Removal from the residual gravity field of its symmetrical portion leaves a 'minor' residual field consisting of short-wavelength features caused by near-surface effects. This field (contoured in Fig. 49) shows east–west (not north–south) symmetry, as in the magnetic survey.

Low values in the northern part of the disturbed zone are believed to be associated with low-density breccia, seen in scattered outcrops and encountered in several shallow bores. Breccia is probably widespread under a cover of superficial alluvium, colluvium, and calcrete. H1 (GR 215644) encountered at least 152 m of breccia where the minor residual is –50 μm s^{-2}; thus the minor residual anomaly of –140 μm s^{-2} north of the bluff suggests a considerable thickness of breccia and severely fractured rock.

Detailed gravity measurements were made along seismic traverse 81/82 (Fig. 3, GR 241676). This traverse is 1160 m long, about 5 km north of the bluff centre, and crosses outcrops of bedrock, megabreccia, and fragmental breccia from south to north. The minor residual decreases by about 120 μm s^{-2}, indicating a decrease in density of about 0.5 t m^3 in the near-surface material; the seismic velocity decreases from 4.6 to 2.2 km s^{-1}.

The results of the gravity studies may be summarised as follows:

- The main part of the gravity field associated with Gosses Bluff is a remarkably symmetrical circular gravity low of 440 μm s^{-2} and radius about 10.8 km.
- An annular gravity low, bounded by steep gradients, reflects the low density of the Mereenie and Pertnjara sandstones of

the central uplift (D.M. Boyd, personal communication 1995).

- The symmetrical gravity features (Fig. 45) can be modelled only by shallow density variations; these are consistent with geological data from outcrops and shallow drillholes, and indicate shallow troughs of breccia.
- The net mass deficiency of 3.6×10^{10} t occurs at a depth of less than 3 km centrally under the bluff.
- The extent of breccia troughs is indicated in the gravity field.
- There is no gravity expression of a deep-seated Gardiner–Tyler anticline, hypothesised from seismic reflection data.
- Several structures in the region around the bluff are known to be anticlines which are shown by gravity to have low-density cores.

Acknowledgments

The investigation reported on here was a joint project of the BMR (now AGSO), and the United States Geological Survey, which operated on behalf of the National Aeronautics and Space Administration under contract R-66. It benefited from the interest of P.J. Cook, who spent several weeks in the field at the start of the first season; B.G. Jones, I. Faulkes, and other staff of the Resident Geologist's office, Alice Springs; and geologists of Magellan Petroleum Corporation, and associated companies, especially L.G.G. Pearce, R.A. Magee, R.M. Hopkins, C.W. Siller, and D.A. McNaughton. Detailed mapping was assisted by aerial photography supplied by Exoil NL. G. Berryman and P. Fisher provided excellent field assistance for the geological party. Grateful acknowledgments are due to J.C. Dooley, who edited the original manuscript on which this paper is based; and to D.M. Boyd, J. Leven, and M. Pilkington for their comprehensive reviews.

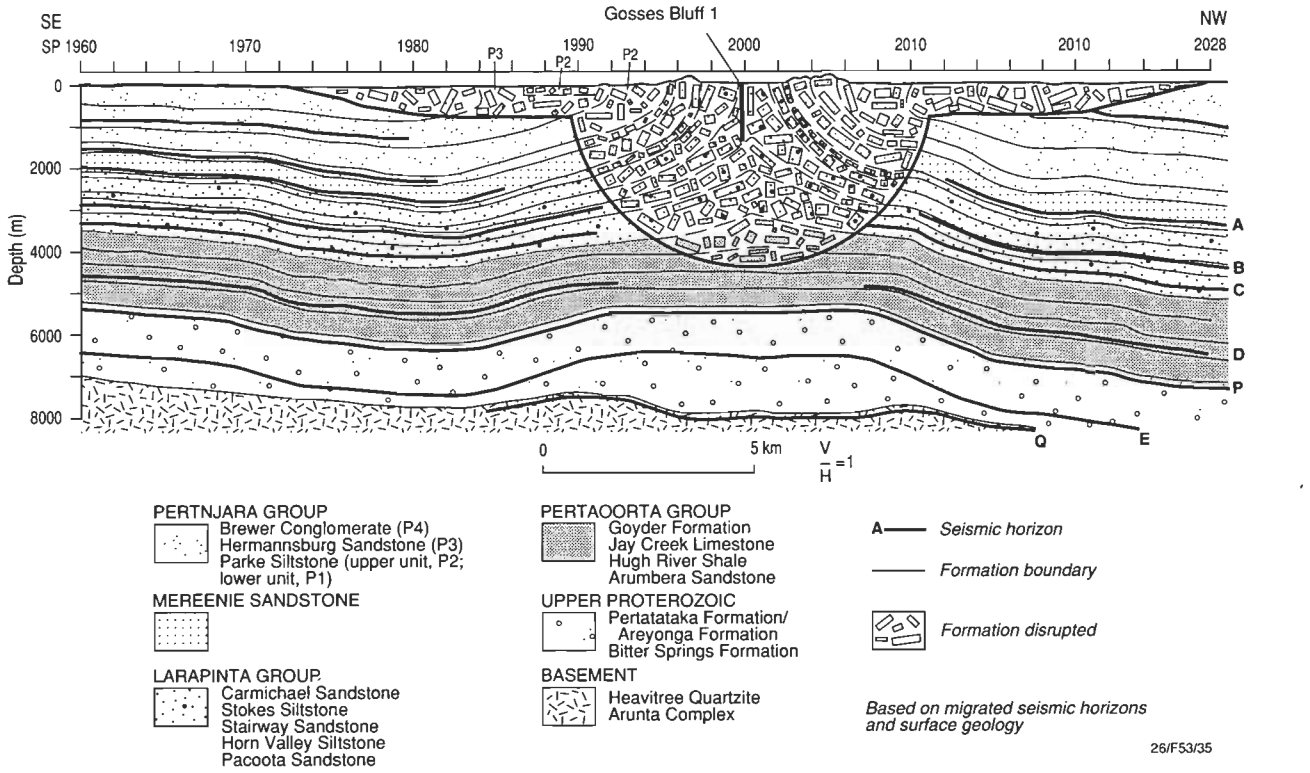

Figure 28. Schematic geological cross-section through Gosses Bluff based on seismic traverse GB/B.

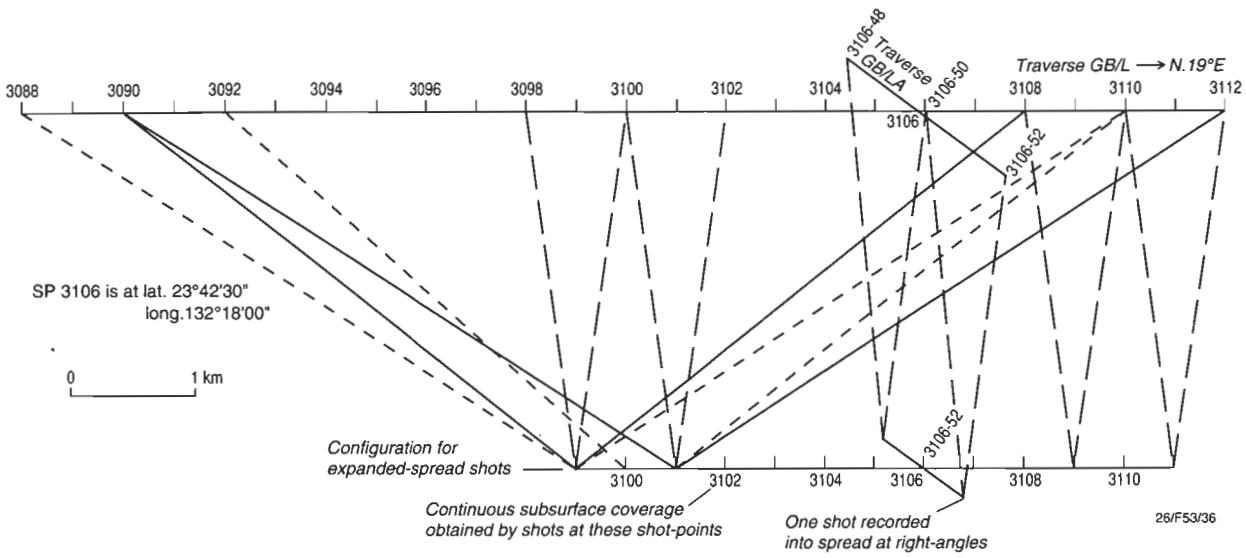

Figure 29. Shooting diagram, deep reflections.

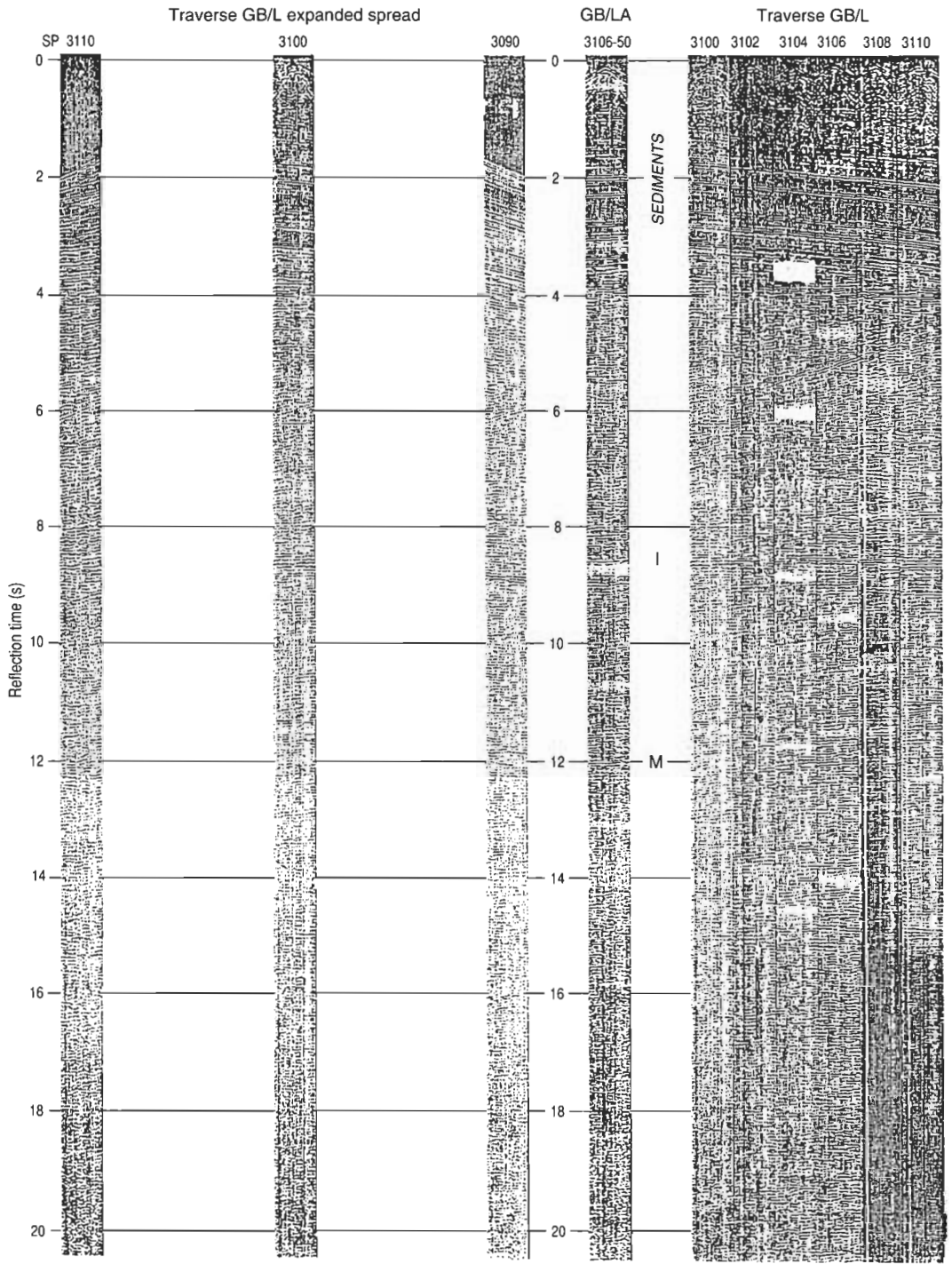

RECORDING INFORMATION

Magnetic recorder : PMR-20
Amplifiers : PT-700
Prefilters : Nil
Filters : L/16 - KK/60
AGC : SS
Gain initial : -70/-60dB
Final : FULL (except 3108,3110: -10dB)
Geophones : Hs-J, 14 Hz
Geophone station interval : 67 m

Geophone pattern :

32/trace in 2 lines of 16
spacing in line 6.1 m
spacing between lines 9.1 m

Shot hole pattern :

3 in line, spacing 23 m
Depth: 30 m
Charge: 470 kg Geophex per shot

PLAYBACK INFORMATION

Note: These are reductions of monitor records. The data were not recorded on magnetic tape and thus no playback was possible

I=Intermediate reflection
M=Moho reflection

HORIZONTAL SCALE

0 5 km

26/F53/37

Figure 30. Record section, traverses GB/L and GB/LA.

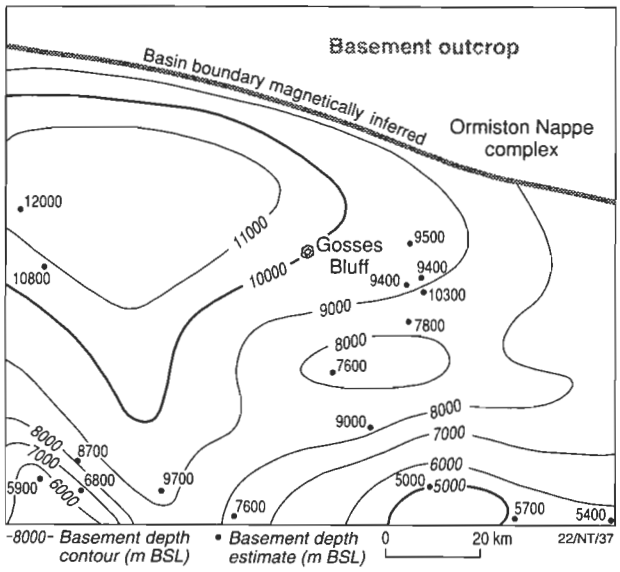

Figure 31. (*left*) **Magnetic basement contours (metres below sea level) of the region about Gosses Bluff. Data obtained from the BMR aeromagnetic survey of the Amadeus Basin.**

Figure 32. (*below*) **Flight lines of the 1968 Gosses Bluff detailed aeromagnetic survey.**

Figure 33. (*facing page*) **Contours of residual magnetic anomalies, selected flight lines of the 1968 detailed airborne survey, ground-magnetic-survey traverses, and gravity stations superimposed on generalised geology of Gosses Bluff.**

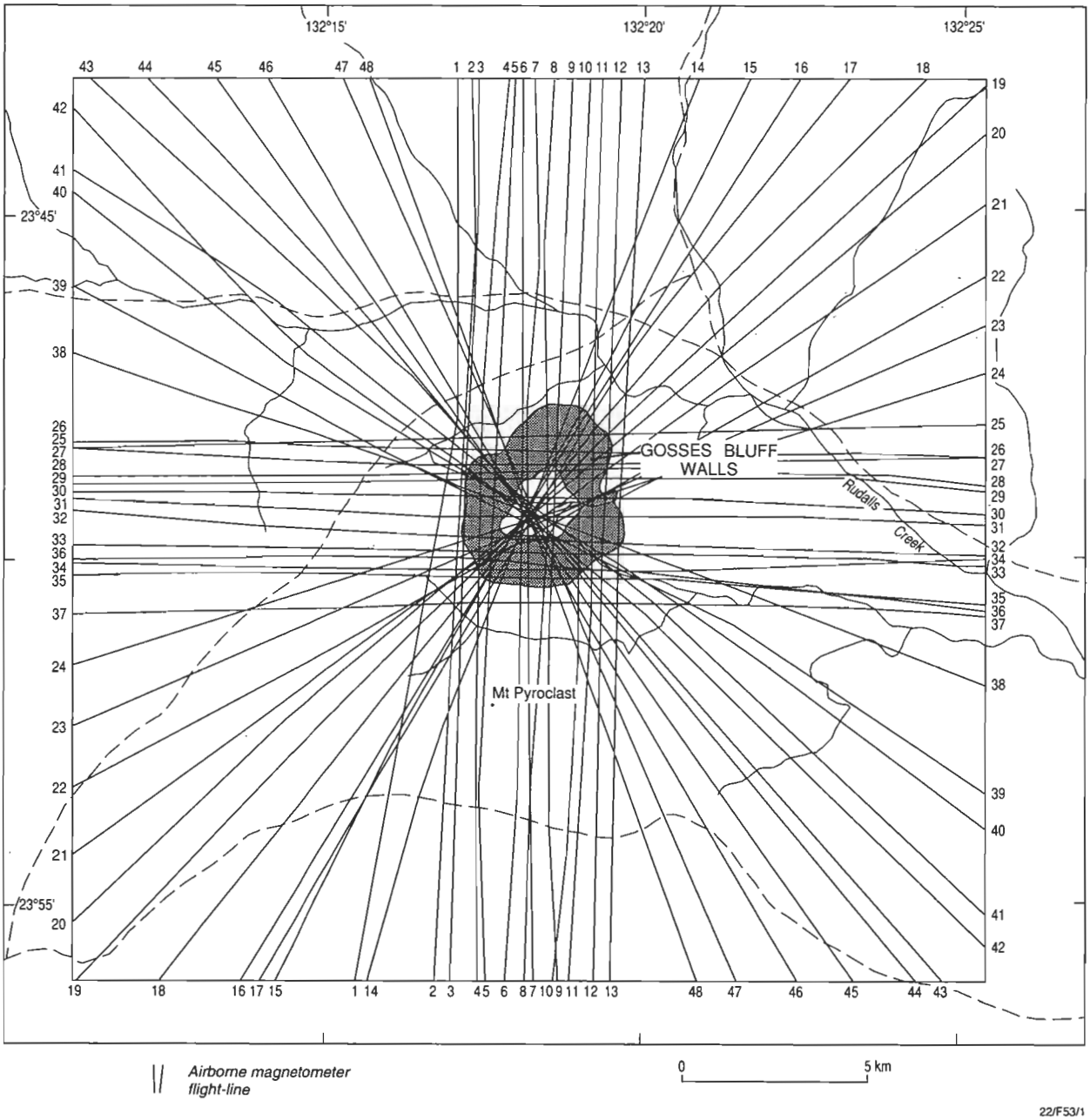

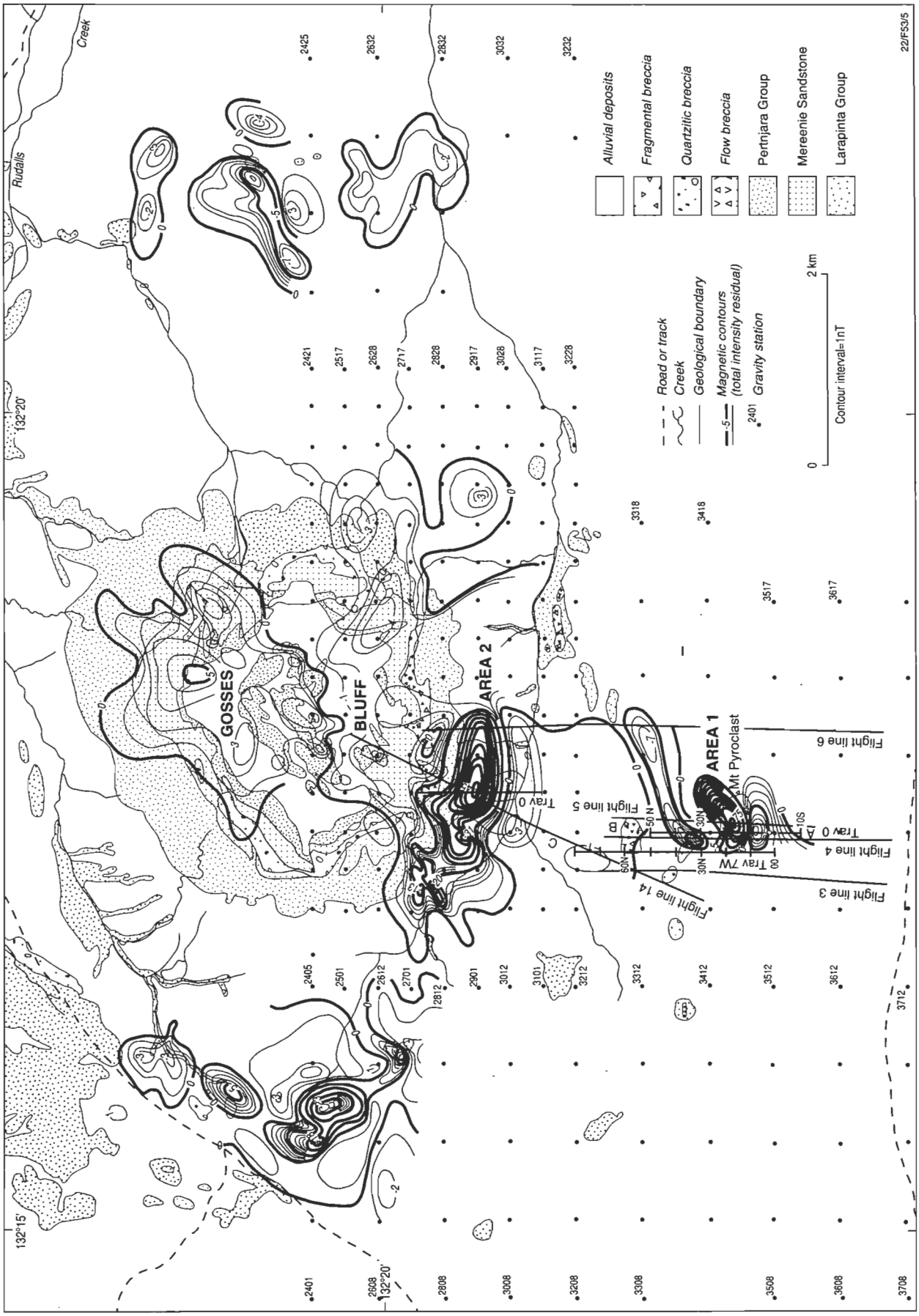
Rudalls Creek
132°20'
132°15'
22°20'
GOSSES BLUFF
AREA 2
AREA 1
Mt Pyroclast
Flight line 6
Flight line 5
Flight line 4
Flight line 3
Flight line 14
Trav 0
Trav 7W
Trav 10S
Alluvial deposits
Fragmental breccia
Quartzitic breccia
Flow breccia
Pertnjara Group
Mereenie Sandstone
Larapinta Group
Road or track
Creek
Geological boundary
Magnetic contours (total intensity residual)
Gravity station
0
2 km
Contour interval=1nT
22/F53/5

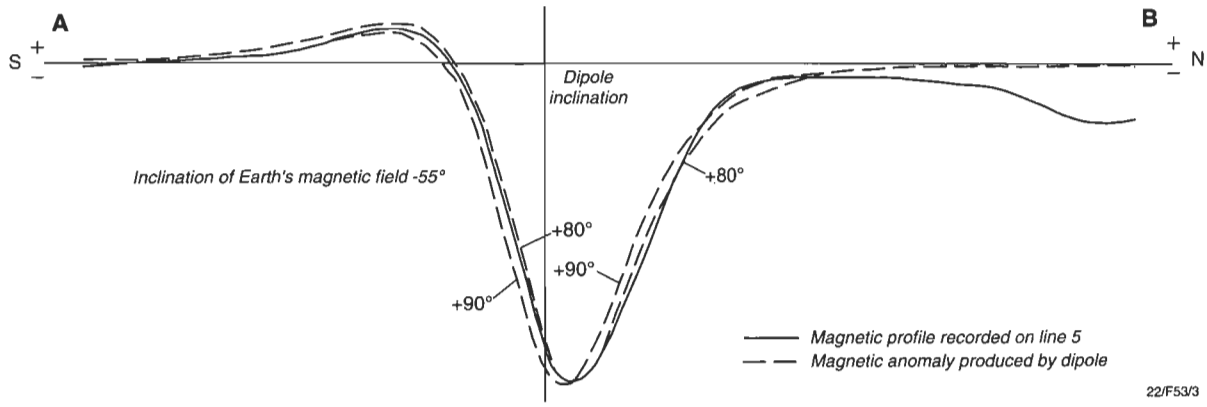

Figure 34. Comparison between the magnetic anomaly recorded on line 5 over Mount Pyroclast, and the theoretical anomaly due to dipoles inclined at +80° and +90°.

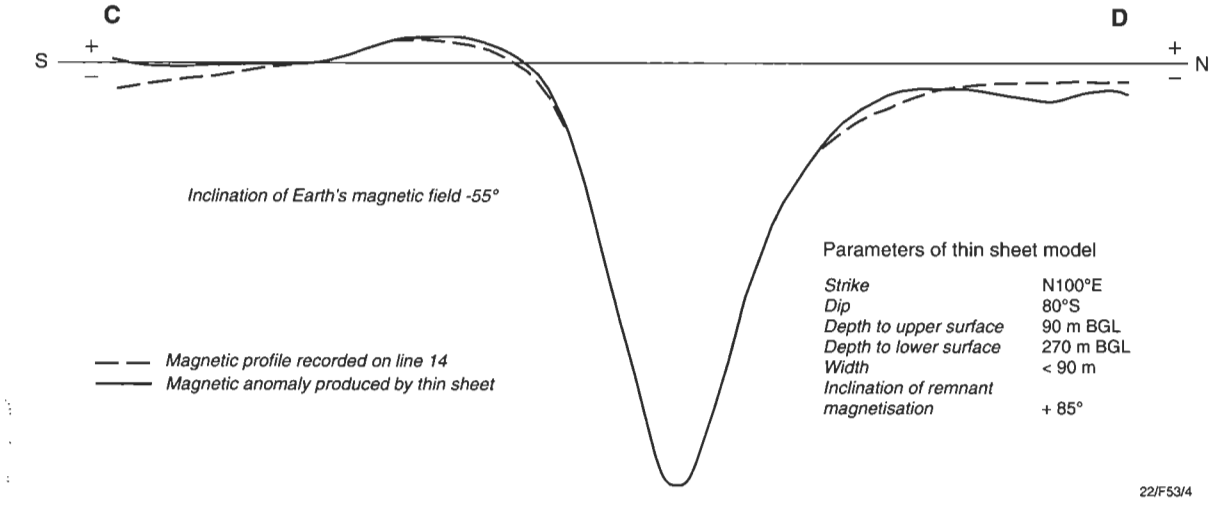

Figure 35. Comparison between the magnetic anomaly recorded on line 14 over the southwest rim of Gosses Bluff, and the theoretical anomaly due to a sheet-like body.

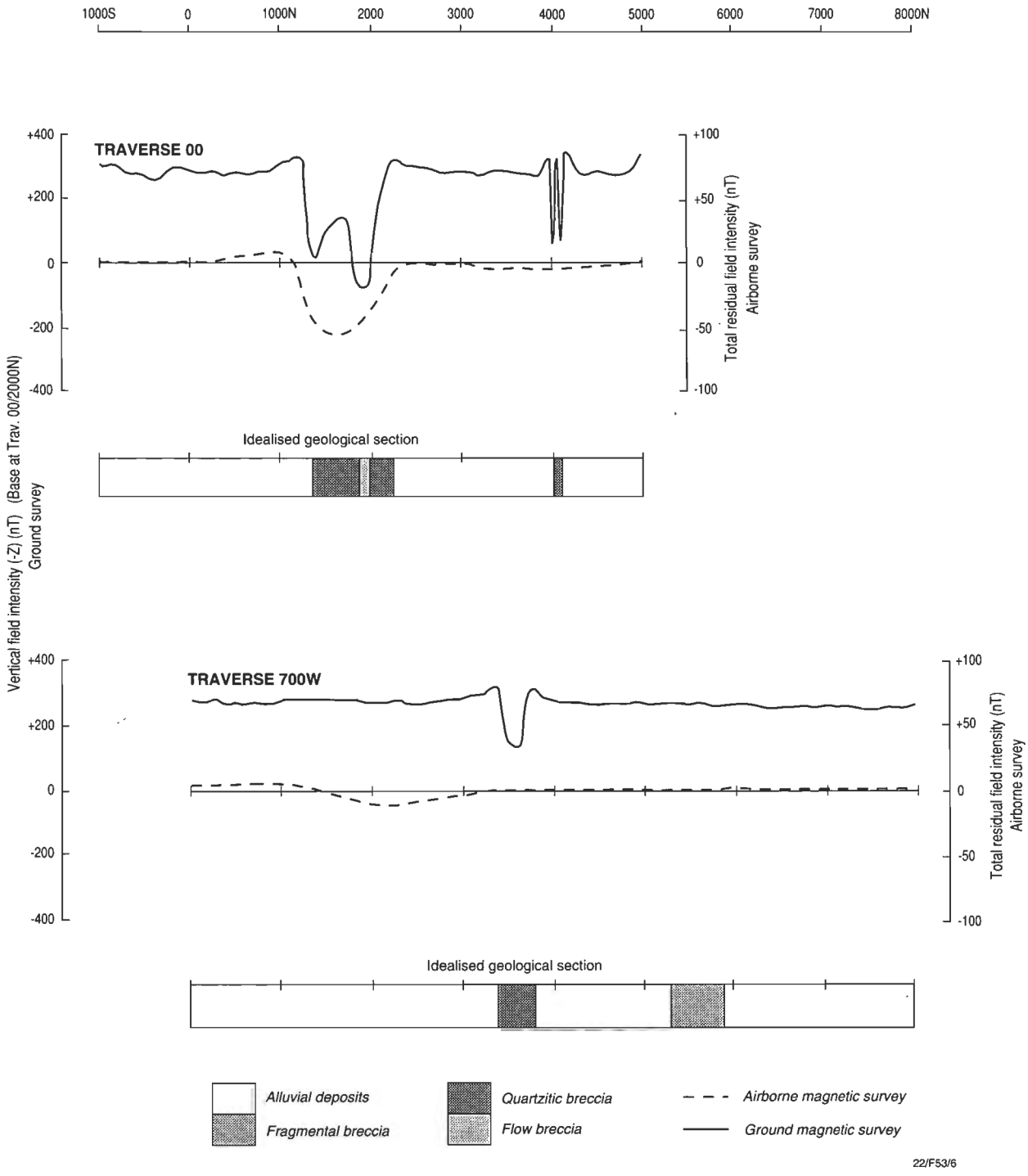

Figure 36. Ground magnetic survey at Mount Pyroclast, traverses 00 and 700W (213 m W): magnetic profiles. Residual TMI profiles from the airborne contour map are also shown for comparison.

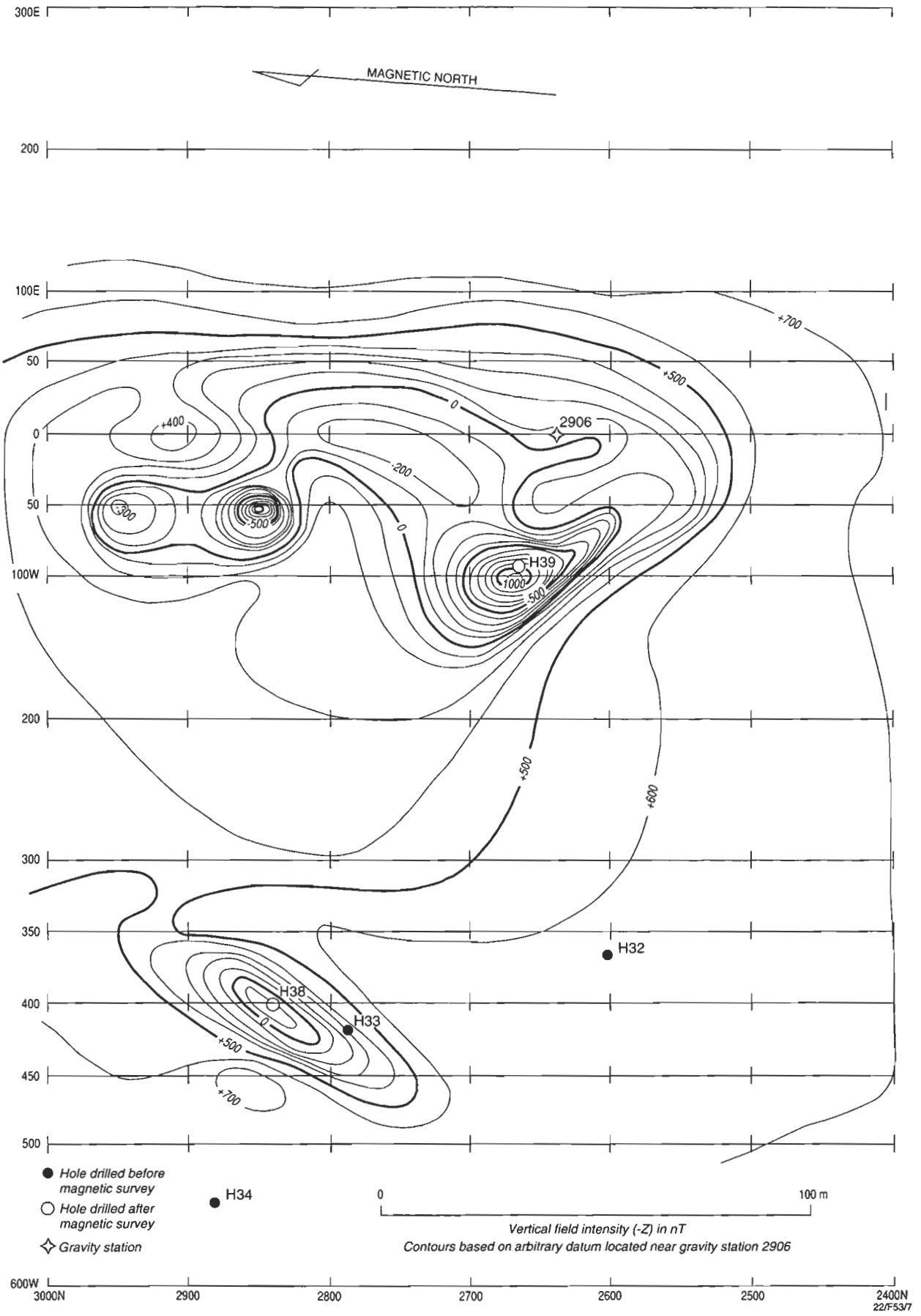

Figure 37. Ground magnetic survey south of the south wall of Gosses Bluff: vertical magnetic intensity contours and positions of drillholes.

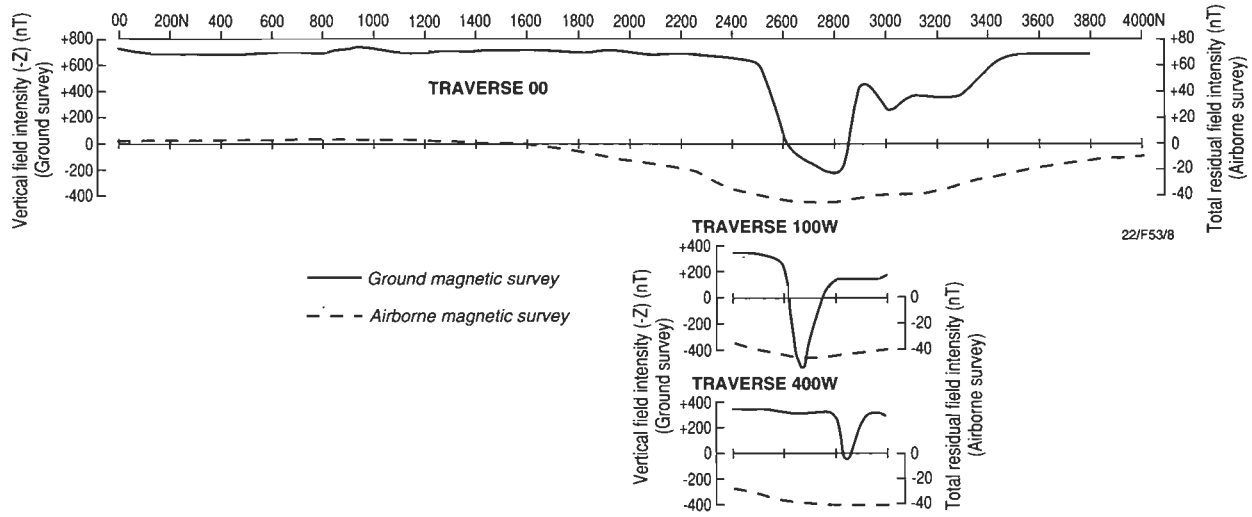

Figure 38. Ground magnetic survey south of the south wall of Gosses Bluff, traverses 00, 100W (30 m W), and 400W (122 m W): magnetic profiles. Residual TMI profiles from the airborne contour map are also shown for comparison.

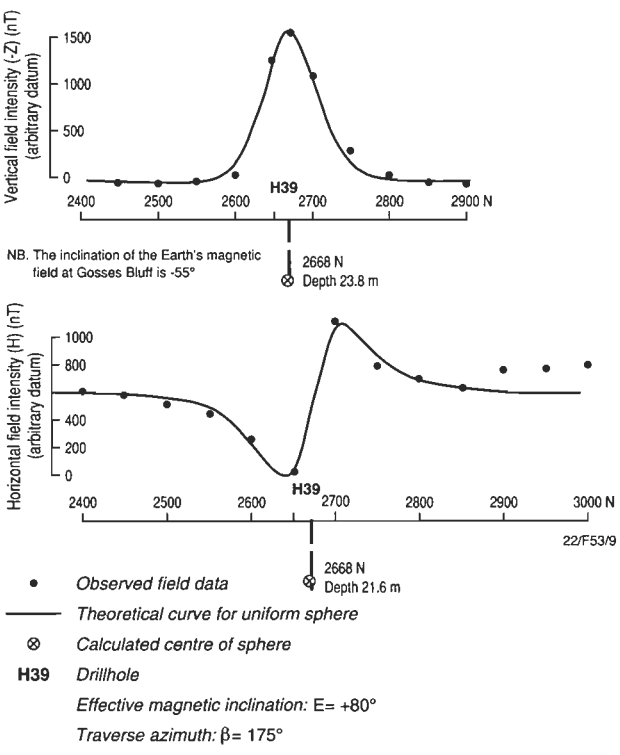

Figure 39. Ground magnetic survey south of the south wall of Gosses Bluff, traverse 30 m W: magnetic interpretation and drilling recommendations.

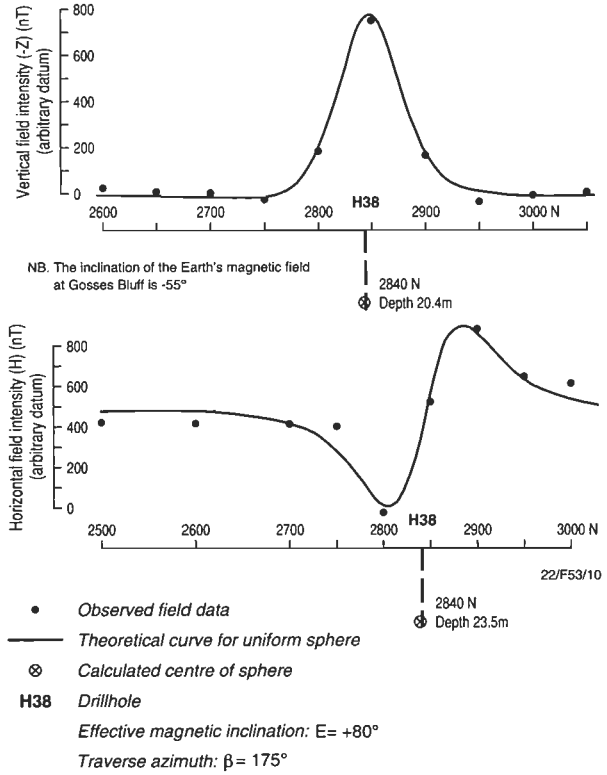

Figure 40. Ground magnetic survey south of the south wall of Gosses Bluff, traverse 122 m W: magnetic interpretation and drilling recommendations.

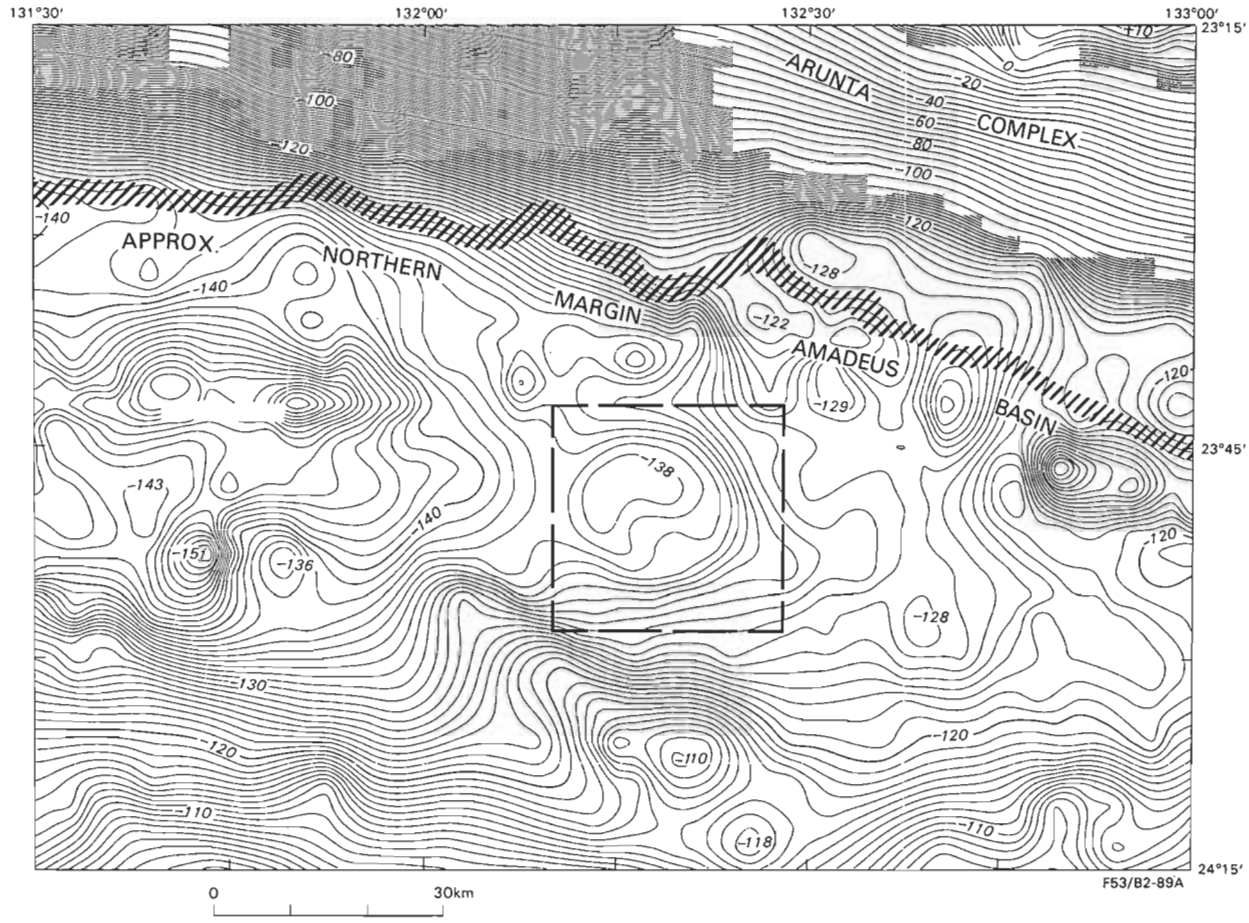
131°30′
132°00′
132°30′
133°00′
23°15′
23°45′
24°15′
ARUNTA
COMPLEX
APPROX.
NORTHERN
MARGIN
AMADEUS
BASIN
-80
-100
-120
-140
-0
-20
-40
-60
-80
-100
-120
-128
-122
-129
-138
-143
-140
-151
-136
-130
-120
-110
-118
F53/B2-89A
0
30km

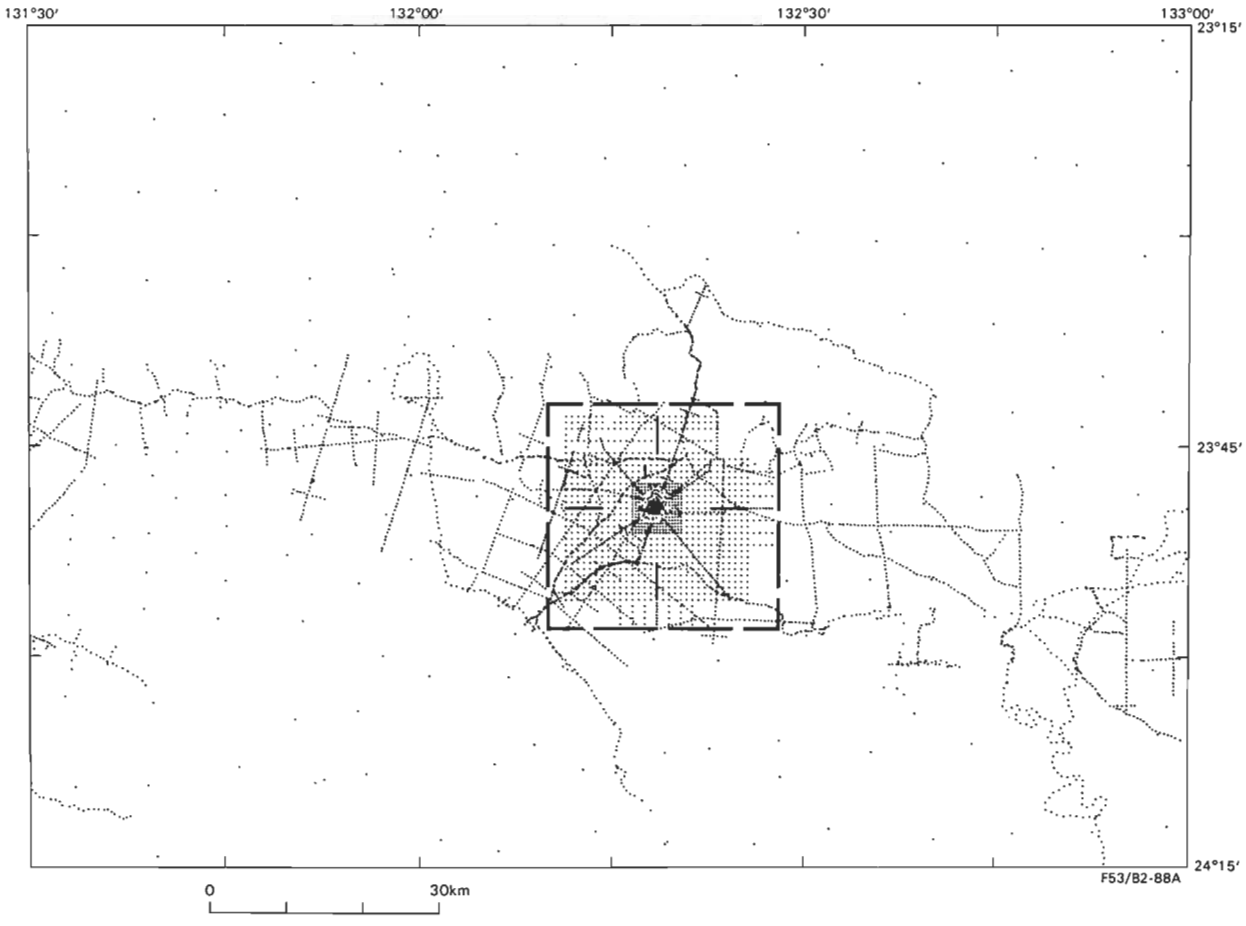
131°30′
132°00′
132°30′
133°00′
23°15′
23°45′
24°15′
F53/B2-88A
0
30km

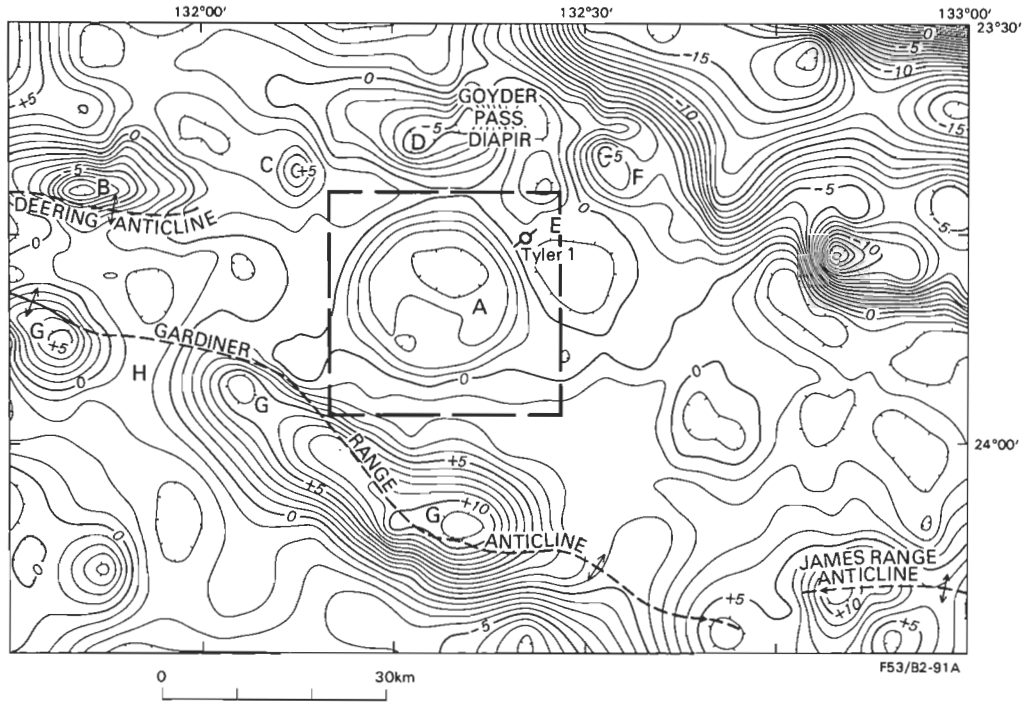

Figure 43. Residual gravity anomaly map of the Gosses Bluff area (regional values removed). Features A–H are discussed in the text. Original scale 1:250 000; contour units in 10 μm s^{-2}.

Figure 41. (*facing page, top*) **Observed Bouguer anomaly map of the western Missionary Plain area. Original scale 1:250 000; contour units in 10 μm s^{-2}.**

Figure 42. (*facing page, bottom*) **Distribution of gravity stations within the limits of the regional Bouguer anomaly map (Fig. 41).**

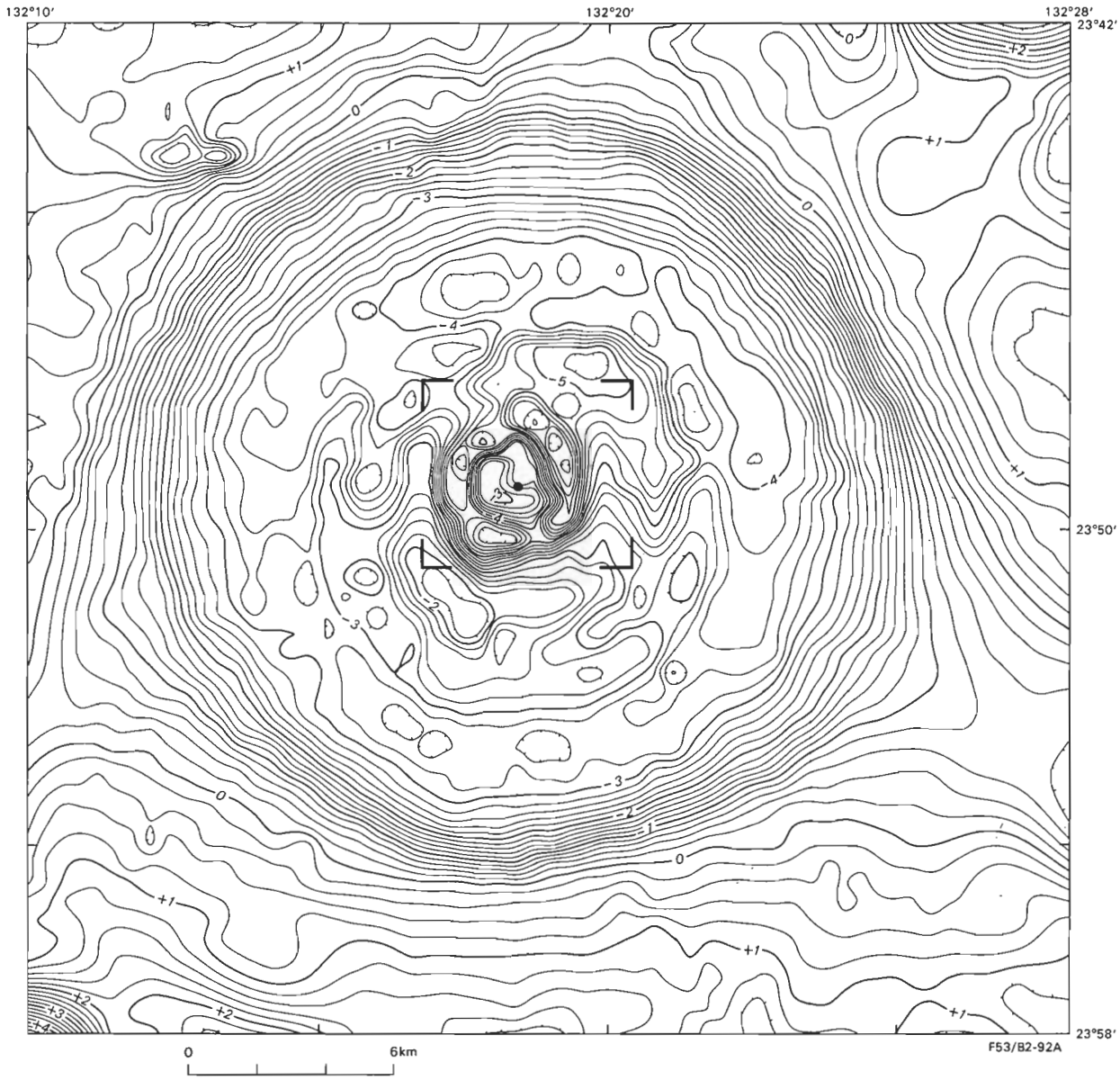

Figure 44. Residual gravity anomaly map of the Gosses Bluff structure (regional values removed). The circular ridge corresponds with the annular gravity low (diameter 3 km). The outer gravity gradient and its circular symmetry are clearly shown on this map, but have no topographic expression. The centre of the circle of best fit to the outer gradient is shown. Contour units in 10 μm s^{-2}. The area covered by Figure 45 is indicated by corner ticks.

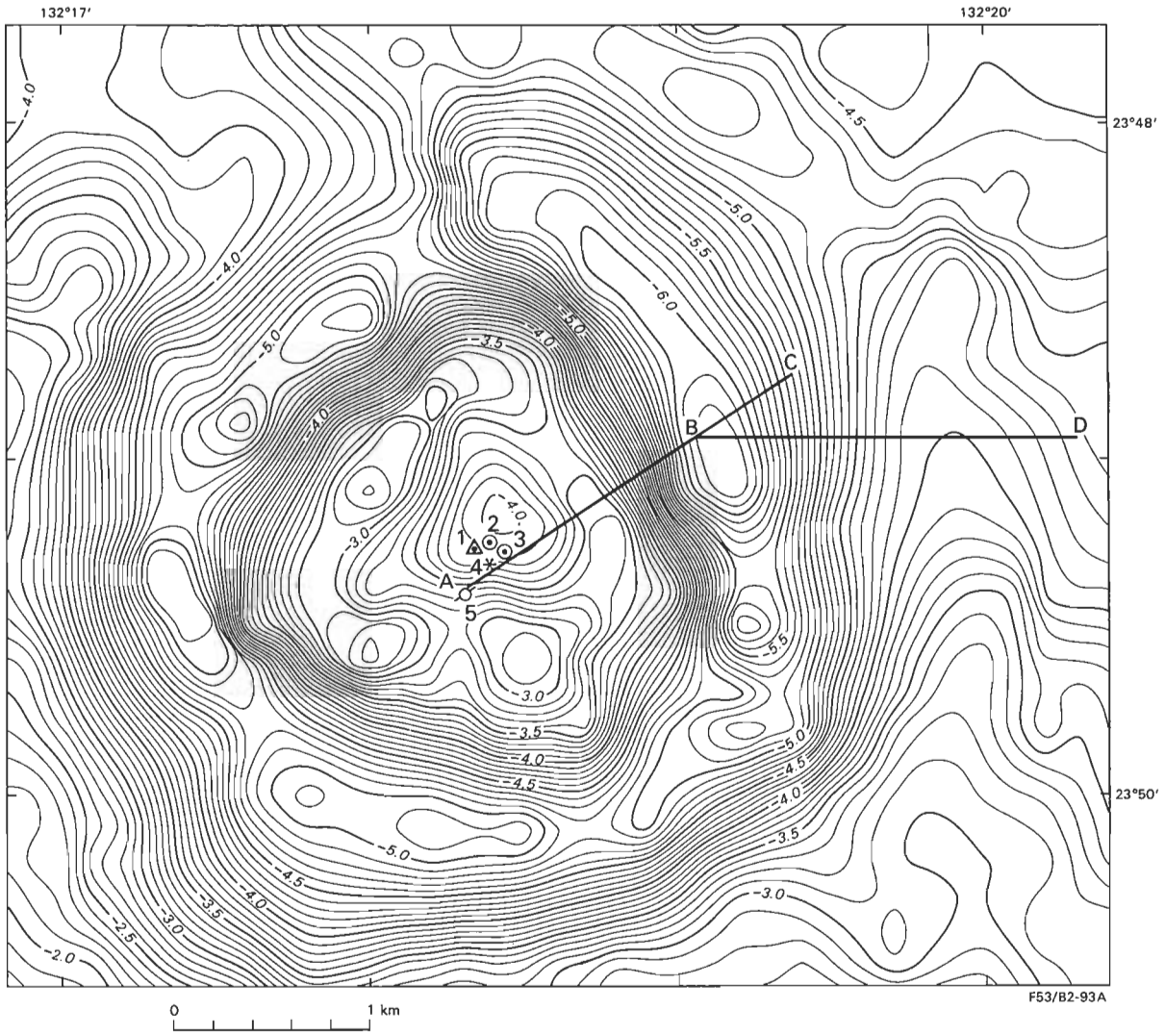

Figure 45. Residual gravity anomaly map of the circular ridge and central depression. These features coincide with the annular gravity low (diameter 3 km). Section lines ABC and BD are modelled in Figure 48. The centre determined from the annular low and the innermost gradient (1), the hypocentres of foci determined by shatter-cone reorientation studies (2 and 3), and the centre (4) used for scaling of eight radial profiles (Fig. 46) are all shown. All are within 240 m of one another, and are 250 m northeast of Gosses Bluff No. 1 well (5). Original scale 1:7500; contour units in 10 μm s^{-2}.

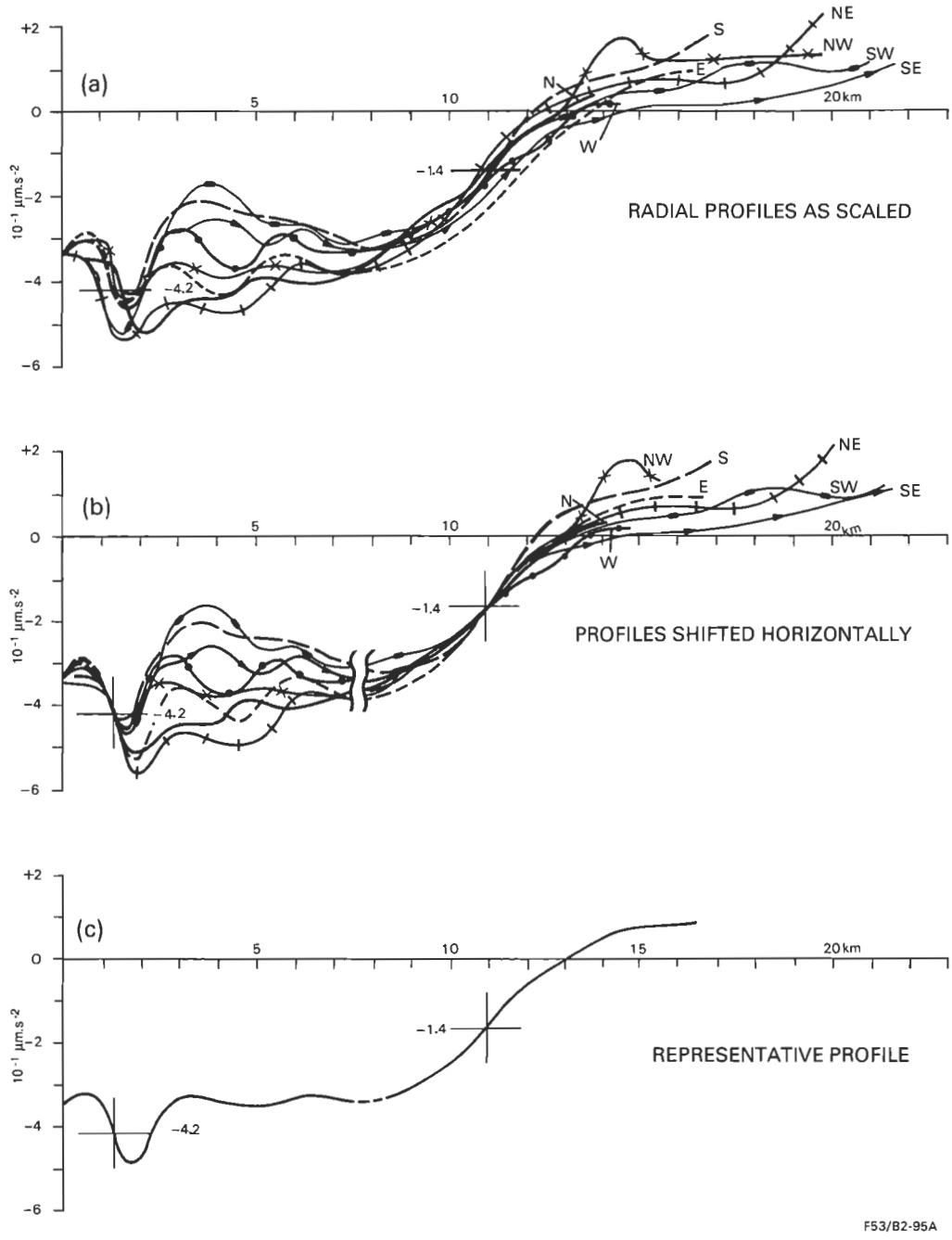

Figure 46. Determination of representative radial gravity profile: (a) Radial profiles as scaled from 1:50 000 map; (b) Inner and outer portions separately merged horizontally; (c) Representative profile, mean of those shown in (b).

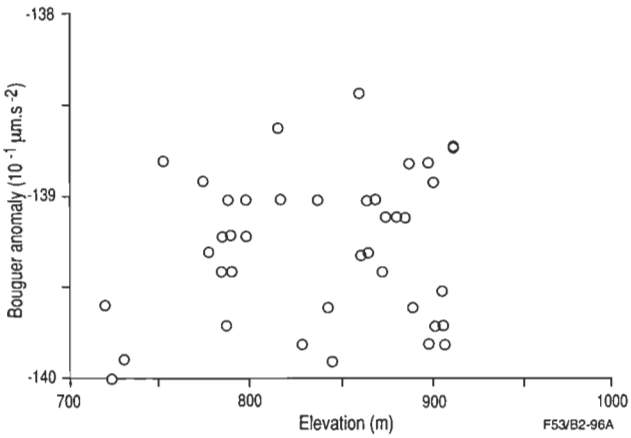

Figure 47. Regression plot showing lack of significant correlation of Bouguer anomaly against height for stations in annular gravity low over the Gosses Bluff circular ridge.

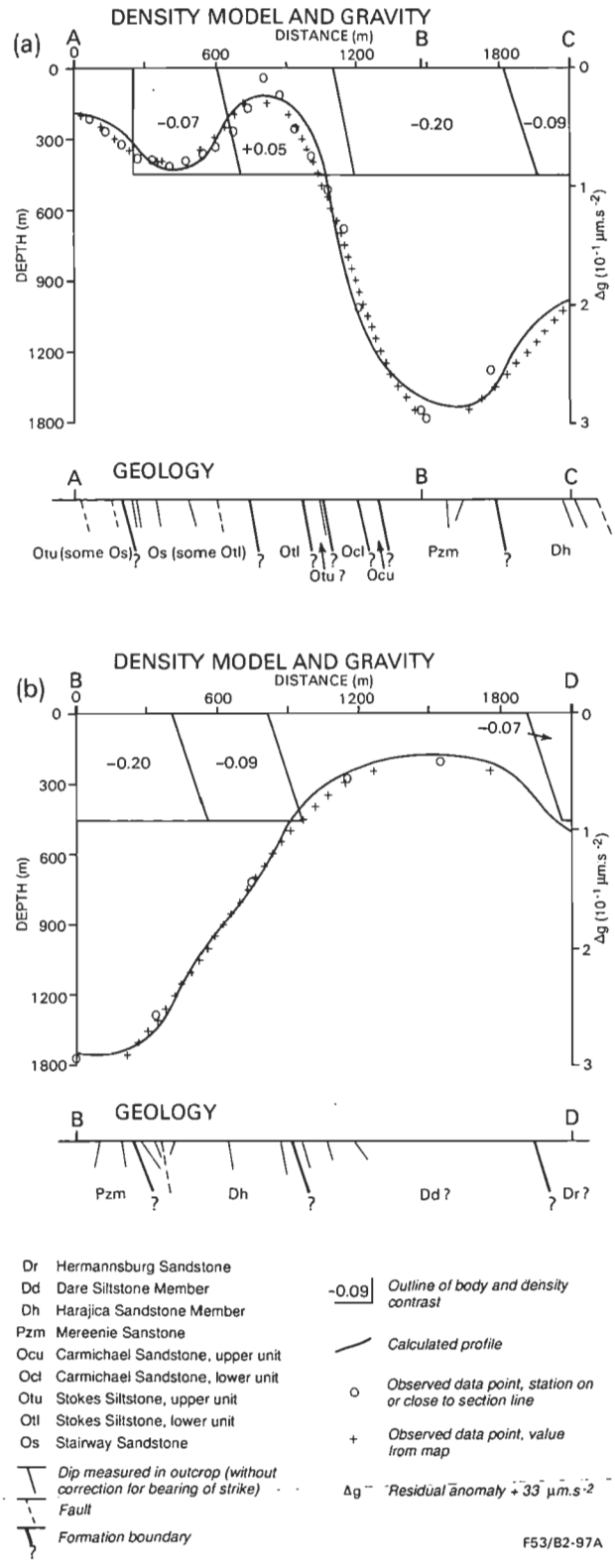

Figure 48. Two-dimensional modelling of sections ABC and BD (Fig. 45). Sharp and steep density interfaces continuing to the surface are needed to model the steep gravity gradients. The small amplitudes of the anomalies limit the depth of the density contrasts (460 m in these models).

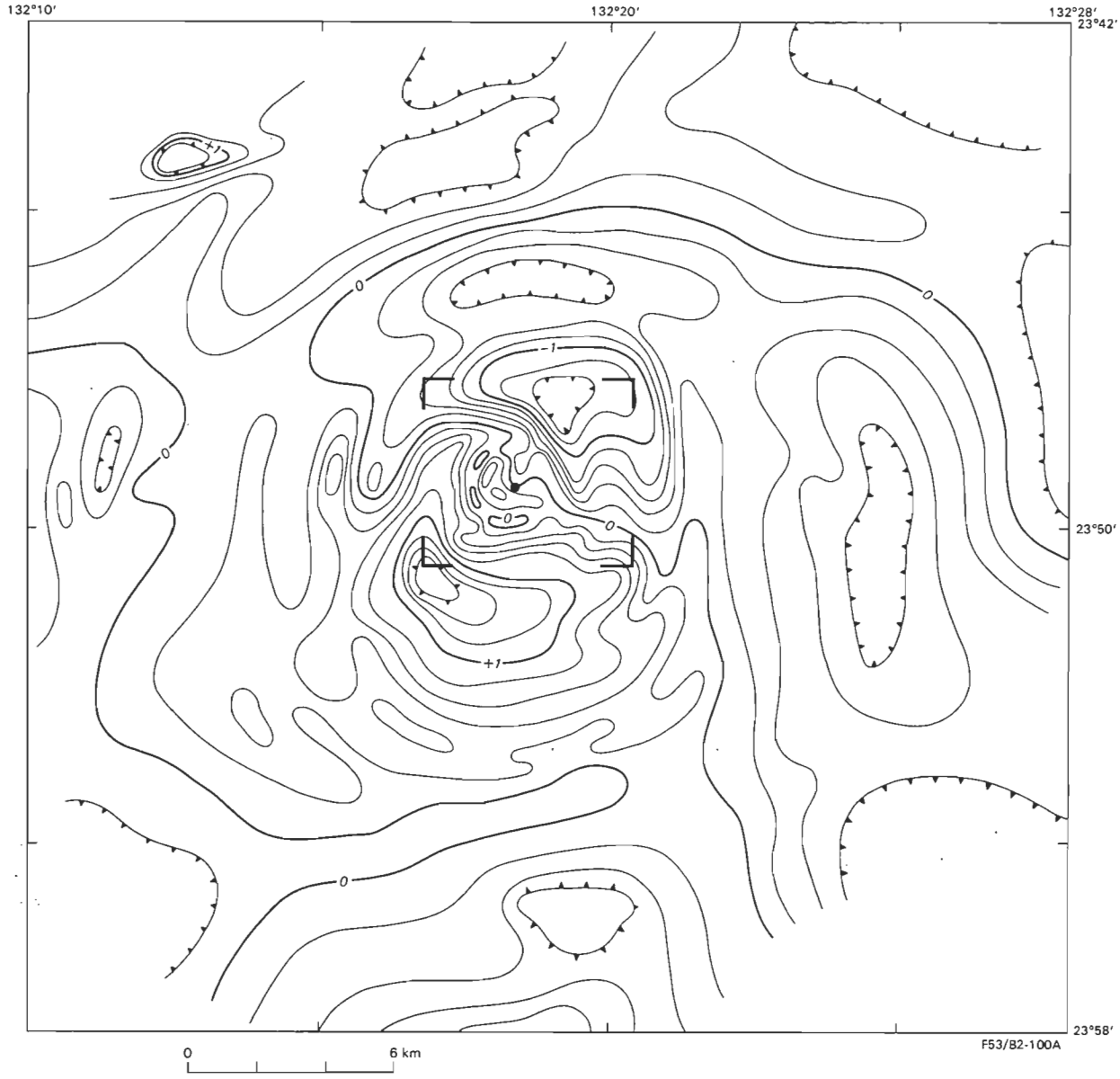

Figure 49. Minor residual gravity map constructed after removal of the symmetrical part of the residual field from the residual anomaly field (Fig. 44). Original scale 1:50 000; contour units in 10 μm s^{-2}.

References

Barlow, B.C., 1979. Gravity investigations of the Gosses Bluff impact structure, central Australia. BMR Journal of Australian Geology & Geophysics, 4, 323–339.

Brown, A.R., 1970. Deep crustal reflection studies, Amadeus and Ngalia Basins, N.T. 1969. Bureau of Mineral Resources, Australia, Record 1970/94.

Brown, A.R., 1973. A detailed seismic study of Gosses Bluff. Bureau of Mineral Resources, Australia, Report 163.

Cook, P.J., 1966. The Gosses Bluff crypto-explosion structure. Bureau of Mineral Resources, Australia, Record 1966/132.

Cook, P.J., 1968. The Gosses Bluff crypto-explosion structure. Journal of Geology, 76, 123–139.

Dooley, J.C. & Moss, F.J., 1988. Deep crustal reflection recordings in Australia 1957–1973: II. Crustal models. Geophysical Journal, 93, 239–249.

Froelich, A.J. & Krieg, E.A., 1969. Geophysical–geologic study of northern Amadeus trough, Australia. American Association of Petroleum Geologists, Bulletin 53, 1978–2064.

Geophysical Associates Pty Ltd, 1965. Missionary Plain seismic and gravity survey, Oil Permits 43 and 56, Northern Territory, for Magellan Petroleum (N.T.) Pty Ltd. Bureau of Mineral Resources, Australia, Petroleum Search Subsidy Acts Report.

Geophysical Associates Pty Ltd, 1967. Mount Rennie—Ooraminna seismic and gravity survey 1966, Oil Permits 43 and 56, Northern Territory, for Magellan Petroleum (N.T.) Pty Ltd. Bureau of Mineral Resources, Australia, Petroleum Search Subsidy Acts Report.

Glikson, A.Y., 1969. Geology of the outer zone of the Gosses Bluff crypto-explosion structure. Bureau of Mineral Resources, Australia, Record 1969/42.

Goleby, B.R., Wright, C., Collins, C.D.N. & Kennett, B.L.N., 1988. Seismic reflection and refraction profiling across the Arunta Block and the Ngalia and Amadeus Basins. Australian Journal of Earth Sciences, 35, 275–294.

Huckaba, W.A. & Magee, R.A., 1969. Tyler No. 1, Northern Territory, final well report. Magellan Petroleum (NT) Pty Ltd (unpublished).

Idnurm, M., Giddings, J.W. & Klootwijk, C.T., 1984. Palaeomagnetism. In: BMR Earth Science Atlas of Australia. Bureau of Mineral Resources, Canberra.

Manwaring, E.A., 1983. Gosses Bluff palaeomagnetic studies. Appendix in: Sedmik, E.C.E., 1983.

Milton, D.J., Barlow, B.C., Brett, R., Brown, A.R., Glikson, A.Y., Manwaring, E.A., Moss, F.J., Sedmik, E.C.E., Van Son, J. & Young, G.A., 1972. Gosses Bluff impact structure, Australia. Science, 175, 1199–1207.

Milton, D.J., Glikson, A.Y. & Brett, P.R., 1996. Gosses Bluff — a latest Jurassic impact structure, central Australia. Part 1: geological structure, stratigraphy, and origin. AGSO Journal of Australian Geology & Geophysics (this issue).

Milton, D.J., Moss, F.J., & Barlow, B.C. (compilers), 1978. Regional geology, Gosses Bluff impact structure, Northern Territory, 1978. Bureau of Mineral Resources, Australia, 1:50 000 map.

Moss, F.J., 1962. Amadeus Basin (southern margin) seismic survey, Northern Territory, 1961. Bureau of Mineral Resources, Australia, Record 1962/167.

Moss, F.J., 1964. Gosses Bluff seismic survey, Amadeus Basin, Northern Territory, 1962. Bureau of Mineral Resources, Australia, Record 1964/66.

Moss, F.J. & Dooley, J.C., 1988. Deep crustal reflection recordings in Australia 1957–1973: I. Data acquisition and presentation. Geophysical Journal, 93, 229–237.

Nettleton, L.L., 1939. Determination of density for the reduction of gravity meter observations. Geophysics, 4, 176–183.

Pemberton, R.L. & Planalp, R.N., 1965. Well completion report, Gosses Bluff No. 1 well. Exoil (NT) Pty Ltd (unpublished).

Sedmik, E.C.E., 1983. Gosses Bluff ground magnetic survey NT, 1969. Bureau of Mineral Resources, Australia, Record 1983/28.

Skeels, D.C., 1963. An approximate solution of the problem of maximum depth in gravity interpretation. Geophysics, 28, 724–735.

Taner, M.T., Cook, E.E. & Neidell, N.S., 1970. Limitations of the reflection method; lessons from computer simulations. Geophysics, 35, 551–573.

Tingate, P.R., Lindsay, J.F. & Marshallsea, S.J., 1996. Impact structures as potential petroleum exploration targets: Gosses Bluff, a Late Jurassic example from central Australia. AGSO Journal of Australian Geology & Geophysics, this issue.

Turpie, A. & Moss, F.J., 1963. Palm Valley–Hermannsburg seismic survey, N.T., 1961. Bureau of Mineral Resources, Australia, Record 1963/5.

Wells, A.T., Forman, D.J., Ranford, L.C. & Cook, P.J., 1970. Geology of the Amadeus Basin, central Australia. Bureau of Mineral Resources, Australia, Bulletin 100.

Wright, C., Barton, T., Goleby, B.R., Spence, A.G. & Pfister, D., 1990. The interpretation of expanding spread reflection profiles from central and eastern Australia. Tectonophysics, 117, 73–82.

Wright, C., Barton, T., Goleby, B.R. & Taylor, F.J., 1989. Seismic velocity variations in the northern Amadeus Basin, central Australia, from an expanding-spread reflection profile. Exploration Geophysics, 20, 435–444.

Young, G.A., 1972. Gosses Bluff airborne magnetic survey. Geophysical Prospecting, 20, 83–91.

Young, G.A. & Shelley, E.P., 1966. Amadeus Basin airborne magnetic and radiometric survey, N.T., 1965. Bureau of Mineral Resources, Australia, Record 1966/64.

AGSO Journal of Australian Geology & Geophysics, 16 (4), 529–552

Impact structures as potential petroleum exploration targets: Gosses Bluff, a Late Jurassic example in central Australia

Peter R. Tingate[1], John F. Lindsay[2], & Susan J. Marshallsea[3]

Gosses Bluff, a prominent complex annular structure in central Australia, was produced by hypervelocity impact during the Late Jurassic. The impact occurred in the thick sedimentary succession close to the centre of a major sub-basin within the Amadeus Basin. The structure is well exposed and has good subsurface control as a consequence of earlier unsuccessful hydrocarbon exploration programs. It provides an opportunity to study the effects of impact on a sedimentary succession without basement involvement, and to evaluate the potential of such structures as hydrocarbon plays.

Seismic data across the structure show that the original crater was 24 km in diameter, suggesting that originally a major ejecta blanket extended for at least 60 km beyond the rim. The underlying Neoproterozoic and Palaeozoic sedimentary rocks of the Amadeus Basin have been deformed to depths of several kilometres. Uplift at the centre of the Gosses Bluff structure is especially pronounced owing to rebound of the primary shock wave from the upper surface of the evaporites of the Bitter Springs Formation.

The thermal effects of impact on outcrop and core samples have been studied from apatite fission-track analysis (AFTA). Samples from the crater floor and remnant crater fill indicate that no significant fission-track annealing has occurred in response to the impact. All samples preserve tracks that were formed before the impact (~140 Ma) and are consistent with the regional thermal history. AFTA data from central uplift samples indicate that the main thermal effect of impact was not heating, but cooling related to exhumation.

Results have shown that, whereas shock-related fracturing enhanced porosity and permeability of underlying reservoir units to some extent, quartz cementation associated with impact reduced overall reservoir quality. The only potential hydrocarbon play, as yet untested, is the rim anticline formed beneath the crater rim as a response to post-impact salt migration.

Ultimately, the major factor that limits the petroleum potential of the Gosses Bluff structure is the timing of events. The impact occurred too late in basin evolution for an effective seal to be deposited over the structure. Further, the structure formed at about 140 Ma, whereas petroleum was probably generated before 200 Ma. Thus, any hydrocarbons trapped in the structure probably represent migration from pre-impact accumulations. In spite of the limited petroleum potential at Gosses Bluff, it does provide an important analogue for buried impact structures with more favourable thermal histories.

Introduction

Hypervelocity impact structures are ubiquitous on the surface of smaller planetary bodies such as the Moon and Mercury, which lack atmospheres. On the Earth's surface, such structures are rare and considerably less obvious. The reasons for this disparity are twofold. Firstly, a planetary body the size of the Earth can retain a significant atmosphere which shields the planet's surface from the effects of the vast bulk of the meteorite flux. Secondly, on larger planets such as the Earth, the planetary surface is renewed by endogenic processes that destroy much of the evidence of hypervelocity impact (i.e., plate tectonics; Lindsay 1976; 1992).

In spite of these effects, some evidence of hypervelocity impact does exist on the Earth's surface. Two major structures of presumed impact origin were recently identified seismically within the sedimentary succession of a major Australian sedimentary basin, the Eromanga Basin, and it has been suggested that they may be potential hydrocarbon traps (Gorter et al. 1989; Longley 1989). In assessing the petroleum potential of impact structures, it is useful to consider Gosses Bluff, which is a well-exposed structure that has been tested for hydrocarbon prospectivity (Pemberton & Planalp 1965; Berry et al. 1989).

In this paper, we look at the petroleum prospectivity of the Gosses Bluff impact structure (Figs. 1 and 2), and the implications for other impact-related petroleum targets. Gosses Bluff is a particularly suitable structure for study as it formed in a thick sedimentary succession with a well-documented stratigraphy supported by subsurface information from petroleum wells and geophysical data. A nearby deep well (Tyler No. 1, Fig. 3) also provides information on the undisturbed section outside the impact structure. Using this database, we have investigated the structure, reservoir quality, and thermal history associated with the impact. The structural study is based largely on seismic data acquired more recently than the original studies of Gosses Bluff (e.g., Milton et al. 1972). Fission-track dating has proved useful for dating impact structures (e.g., Miller & Wagner 1979; Omar et al. 1987; Kohn et al. 1995), and has been used at Gosses Bluff to help constrain the timing of impact (Milton et al. 1972; Milton & Sutter 1987). Milton & Sutter (1987) reported total annealing of fission tracks in zircon associated with conductive heating within and below melt breccia at Gosses Bluff. The apatite fission-track analysis (AFTA) study presented in this paper was carried out to assess the thermal effects of the impact at Gosses Bluff, and to investigate whether these effects influenced the petroleum potential of the structure.

Geological setting of Gosses Bluff

Gosses Bluff (Fig. 1) lies in the centre of the Missionary Plain, a broad open plain in central Australia, and is 160 km west of Alice Springs (Fig. 1). It was named (originally Gosses Range) by Ernest Giles in 1872 after Harry Gosse, one of the earliest officers attached to the Alice Springs telegraph station. The bluff, a unique prominent topographic feature of the area, consists of an almost completely enclosed circular ridge or rim of sedimentary rocks 4.5 km in diameter that projects 180 to 240 m above the local topography.

Because of its unique geology and topographic form (Figs. 1 and 4), the origin of the structure was debated for some time. It received some attention during the early phases of regional mapping in the 1950s and 1960s (Wells et al. 1970). In 1962, the Bureau of Mineral Resources, Geology and Geophysics gathered the first seismic reflection and refraction data across the structure (Moss 1964). The petroleum potential of the struc-

[1] National Centre for Petroleum Geology and Geophysics, Thebarton Campus, University of Adelaide, South Australia 5005.
[2] Division of Marine, Petroleum & Sedimentary Resources, Australian Geological Survey Organisation, GPO Box 378, Canberra, ACT 2601.
[3] Geotrack International Pty Ltd, PO Box 4120, University of Melbourne, Victoria 3052.

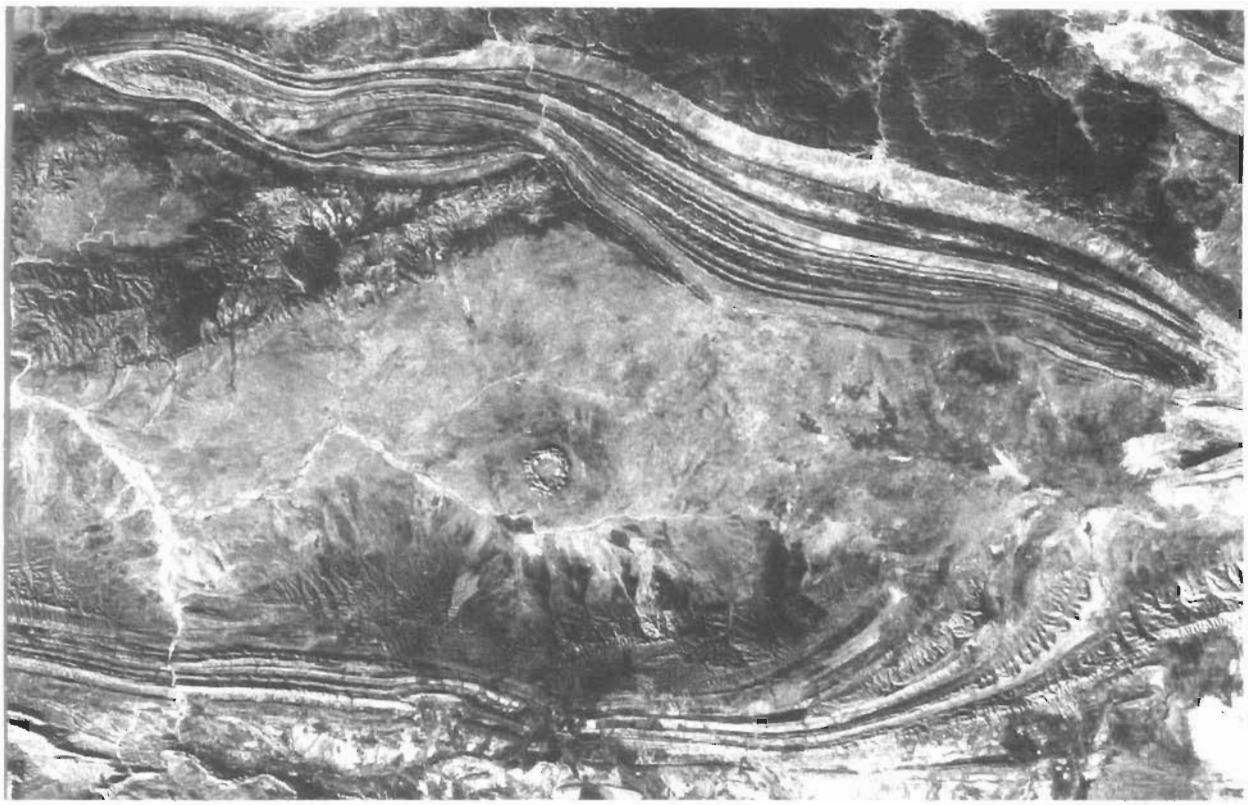

Figure 1. Landsat image of Gosses Bluff and the surrounding Missionary Plain. The circular structure of the bluff is readily apparent, and so is the more subtle, deeply eroded crater whose outline surrounds the bluff.

ture was tested in 1965 when Exoil (NT) Pty Ltd drilled one of the earliest wildcat wells, Gosses Bluff No. 1, at the centre of the structure (Pemberton & Planalp 1965). At this stage, the structure was thought to be the result of either endogenic processes (and compared with salt structures along the Gulf Coast of the United States) or explosive volcanism (Brunnschweiler et al. 1959; Pemberton & Planalp 1965). Crook & Cook (1966) and Cook (1968) suggested an origin due to explosive volcanism or meteorite impact. Dietz (1967) and Milton et al. (1972, 1978) used geophysical and shock-metamorphic evidence to show that an impact origin was the only explanation consistent with both the large- and small-scale features at Gosses Bluff.

The impact at Gosses Bluff affected sedimentary rocks within the Late Proterozoic–Devonian Amadeus Basin, a broad shallow intracratonic basin that underlies much of central Australia (Wells et al. 1970; Lindsay & Korsch 1989, 1991). The best estimate for the timing of this event is Late Jurassic (142.5 ± 0.8 Ma; Milton & Sutter 1987). The basin, a complex polyphase structure, was initiated during the Neoproterozoic at about 800 Ma, and continued to subside until the mid-late Palaeozoic when the Alice Springs Orogeny effectively brought sedimentation to an end (Lindsay & Korsch 1989, 1991). Three deep sub-basins developed along the northern margin of the Amadeus Basin, and locally accumulated up to 14 km of sediments; the deepest of them (Figs. 2 and 3) underlies the Missionary Plain (Lindsay 1993). The Gosses Bluff structure lies close to the centre of the sub-basin and is underlain by about 11 km of sedimentary rocks. With the exception of the Bitter Springs Formation, the succession preserved in this part of the basin is largely clastic, and contains a high proportion of arkosic sandstone. In contrast, the Bitter Springs Formation consists of two non-clastic members, a lower evaporitic member (Gillen Member) and an upper carbonate member (Loves Creek Member). As discussed below, the distinctive lithologies of these two units are central to understanding the unique structural style of Gosses Bluff.

The crater-like form of Gosses Bluff is deceptive because its physiographic form is the product of post-impact differential erosion. The original crater formed by the impact has been almost obliterated by post-impact erosion, although relics of the crater floor remain. Breccia remnants of the original crater fill form a semicircle extending up to 5 km south, west, and north from the centre of Gosses Bluff (Milton et al. 1978). Sandstone breccia occurs at the base of Mount Pyroclast, a hill 4 km south of the centre of Gosses Bluff (Fig. 7). A gradual increase in the proportion of highly shocked and melted clasts occurs from the base of this hill to the top, where melt breccia crops out. These breccias are presumably a remnant of a more extensive crater fill, such as those in craters of similar size (e.g., the Ries crater, Miller & Wagner 1979; and Haughton astrobleme, Omar et al. 1987). No evidence of the ejecta blanket that formed beyond the crater rim has been found.

Gosses Bluff is an annular structure formed in Amadeus Basin strata. Outcropping Late Devonian Brewer Conglomerate at its outer extremes gradually gives way to successively older units, derived from greater depth, towards the centre of the structure. The resistant rim of Gosses Bluff consists of steeply dipping to partly overturned fault-bounded plates or slabs of the lower Pertnjara Group and Mereenie and Carmichael Sandstones that

originally formed the central uplift of the impact crater. The enclosed pound at the core of the bluff consists of less resistant units of the Ordovician Stairway Sandstone and Stokes Siltstone (Milton et al. 1978). The impact caused the upper Stairway Sandstone exposed in the core of the structure to rise about 3.5 km from its present depth according to seismic and well (Tyler No. 1) data at the margins of the structure. This amount of uplift is considerably more than might have been expected from earlier empirical studies (Grieve & Pesonen 1992).

Subsurface structure

Several seismic surveys have investigated the Amadeus Basin structure since the 1960s. Details of these early surveys are outlined by Lindsay (1993). The most recent seismic data, the basis for the following descriptions, were gathered across the structure in 1982, during the interval between the drilling of two petroleum wells in the pound close to the centre of the structure (Fig. 3): Gosses Bluff No. 1 (in 1965; Pemberton & Planalp 1965) and Gosses Bluff No. 2 (in 1989; Berry et al. 1989). Mil-

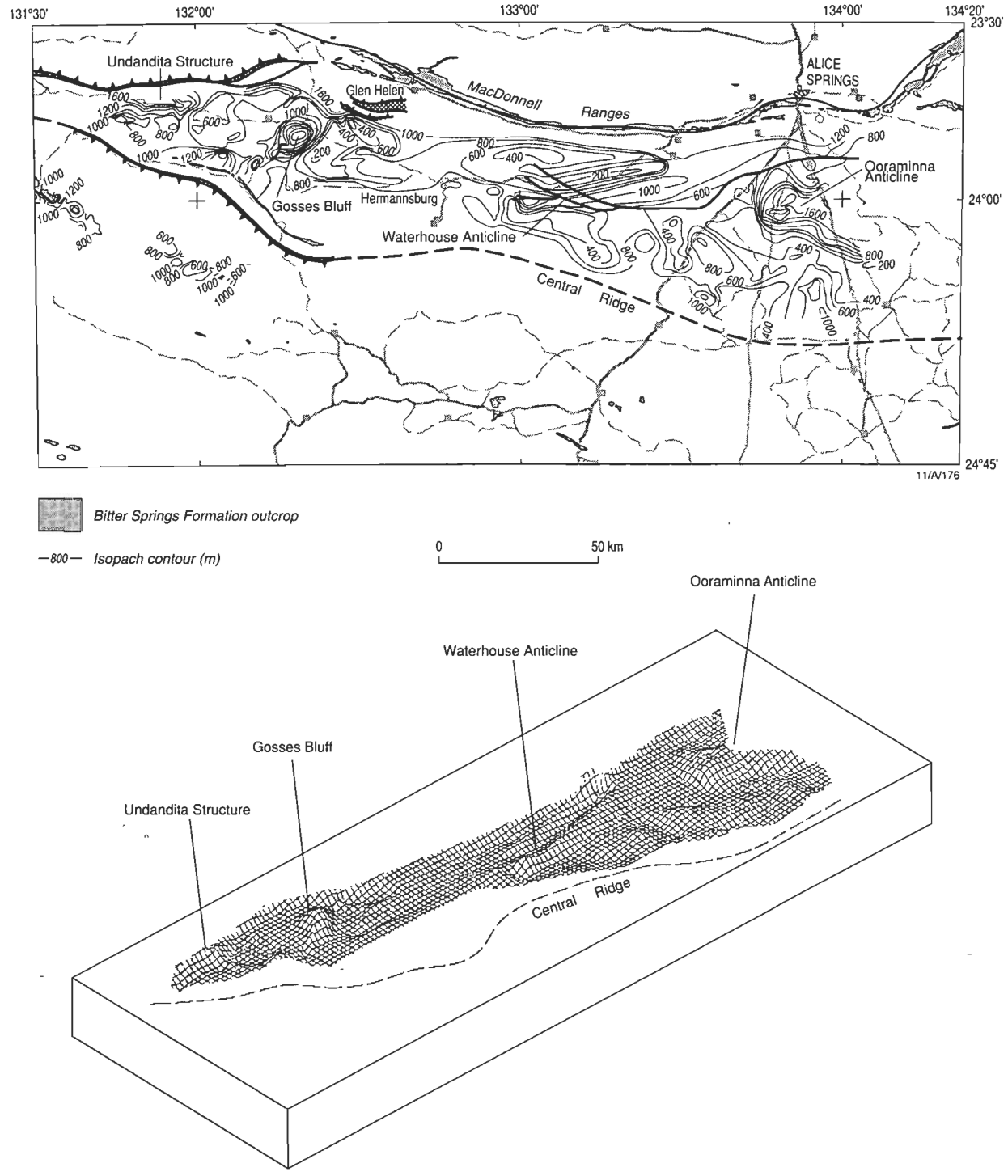

Figure 2. Isopach map and perspective net diagram of the Gillen Member of the Bitter Springs Formation (zone 3). Note that the salt units increase markedly in thickness beneath Gosses Bluff.

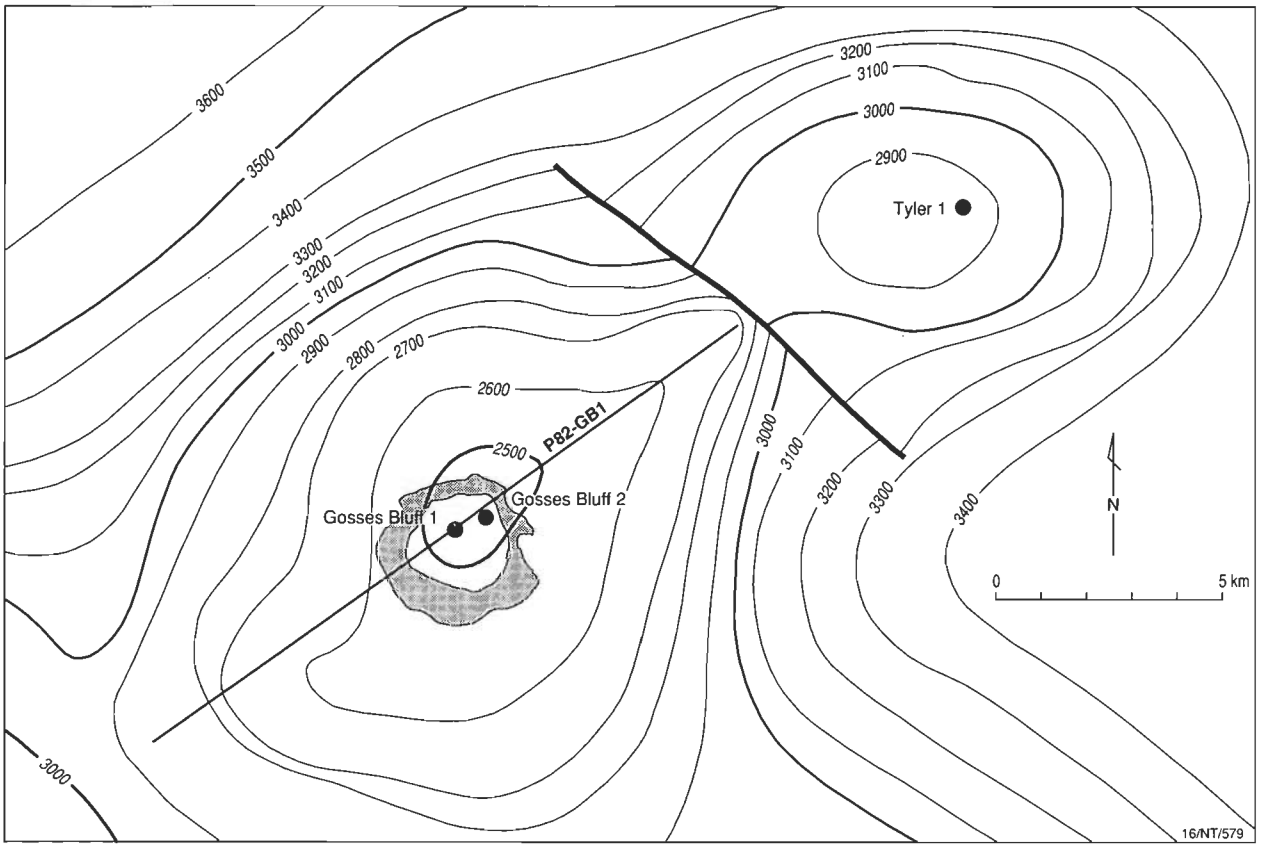

Figure 3. Structure contours on the sequence boundary at the top of the Pacoota Sandstone show the doming of the stratal surface beneath Gosses Bluff at the top of zone 2. Note the ridge of the Gardiner-Tyler anticline extending northeast from the uplifted region, and the locations of Tyler No. 1 well and seismic line P82-GB1.

ton et al. (1972) made an early attempt to interpret the subsurface structure of Gosses Bluff from seismic data, but had limited success. Improvements in data-gathering and, more importantly, processing techniques have provided much more detailed images of the subsurface.

Despite the erosion of the surface form of the crater, seismic reflection profiles (Figs. 4 and 5) show the subsurface structure of Gosses Bluff in some detail. Directly beneath the bluff, the sedimentary rocks of the Amadeus Basin have been deformed by the impact, but, as might be expected, the degree of deformation gradually decreases with depth. For convenience, the rocks can be considered to constitute four deformational zones.

Zone 1 (0–2300 m): fractured and uplifted strata

The Amadeus Basin sedimentary succession has been totally disrupted, and the sedimentary rocks faulted and fractured, to a depth of 2300 m directly beneath Gosses Bluff (Figs. 4 and 5). The zone is dish- or lens-shaped, and gradually decreases in thickness laterally until the first continuous reflections indicate the eroded remnants of the original overturned crater rim, the start of the bulk ejecta, about 12 km from the centre of the structure.

Gosses Bluff Nos. 1 and 2 were drilled largely within this fractured and faulted zone (to total depths of 1383 m and 2652 m respectively; Fig. 5). By design, Gosses Bluff No. 2 reached the top of zone 2. The stratigraphic succession intersected by these two wells shows that zone 1 consists of steeply dipping, overturned, and repeated beds of Stokes Siltstone and Stairway Sandstone (Fig. 6) extending downward to a more moderately dipping Ordovician succession at the top of zone 2. In Gosses Bluff No. 2, part of the succession at a depth of about 1400 m is overturned. Anomalies in sonic-log data suggest that the signal attenuates over complex fracture zones, which are especially noticeable at formation contacts. Anomalies are also evident on the caliper logs, suggesting that the whole succession consists of faulted blocks of sedimentary rock that have been completely fractured by the impact. Further indication of the degree of deformation in zone 1 can be gained from the randomness of bedding dips (Fig. 6).

Shatter cones in association with steeply dipping strata, zones of brecciation, and small-scale faults occur in surface exposures to a distance of more than 6 km from the centre of the structure, and imply pressures of at least 2 to 8 GPa (20 to 80 kb; Dietz 1967). Shatter cones are also present in cores from Gosses Bluff No. 1 well to a depth of at least 1200 m, and provide an indication of the degree of deformation when the plunges of shatter-cone axes are compared with the dips of bedding (Fig. 6a). The apices of shatter cones point towards the impressed shock-wave front. Before impact, the sedimentary units of the Amadeus Basin were essentially horizontal, so that the shatter cones directly beneath the centre of the crater would have formed normal to the bedding surfaces during passage of the primary shock wave. The fact that they have not retained that relationship suggests that either the faulted blocks are small, or that deformed material has been drawn in from regions where the shock wave intersected the bedding surfaces at angles < 90° at some distance away from the centre of the structure.

Petrographic data (Berry et al. 1989) for the brecciated rocks of zone 1 are limited. An analysis of core from a depth of 1400 m

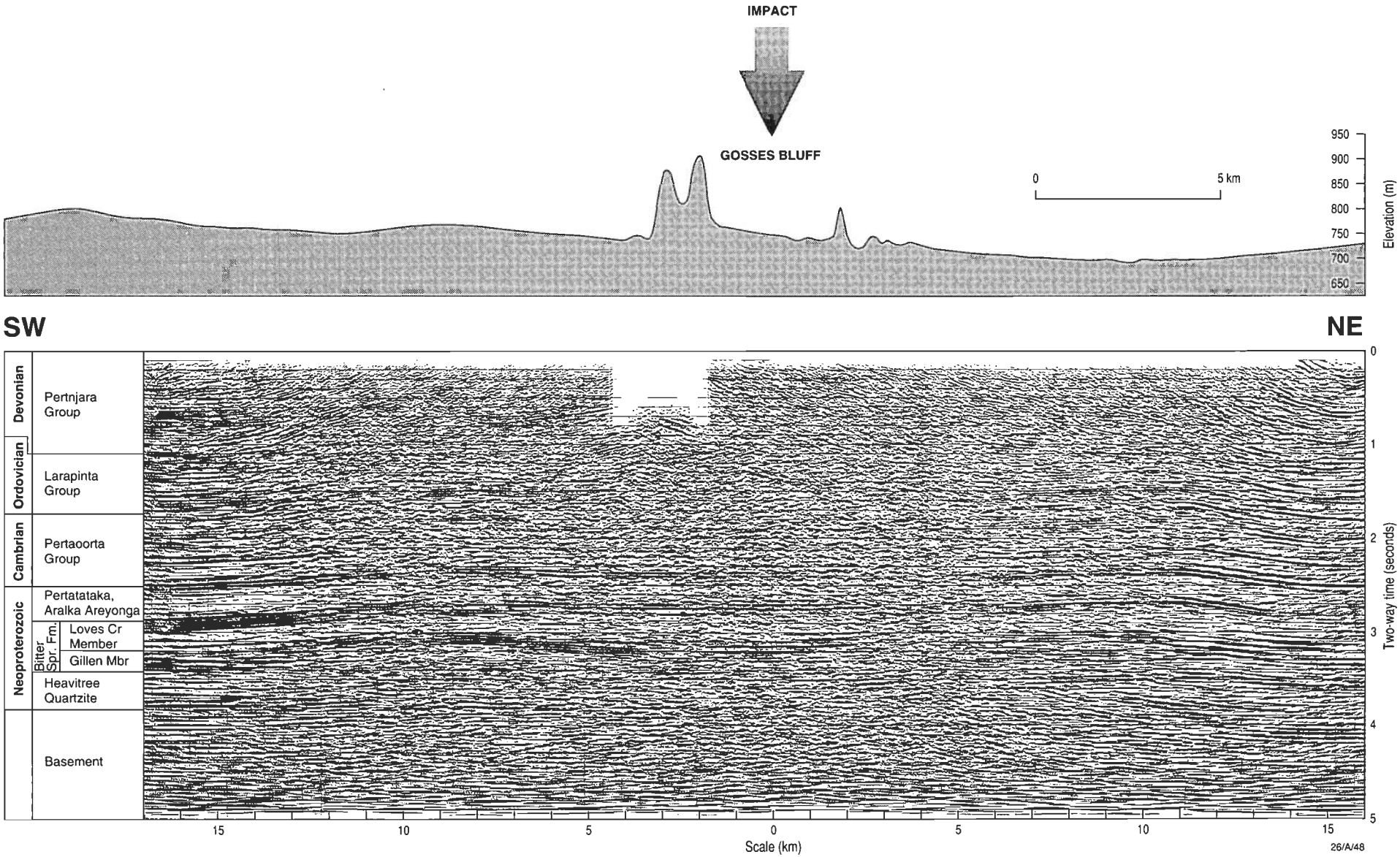

Figure 4. Seismic section P82-GB1 (see Fig. 5 for interpretation; Fig. 3 for location).

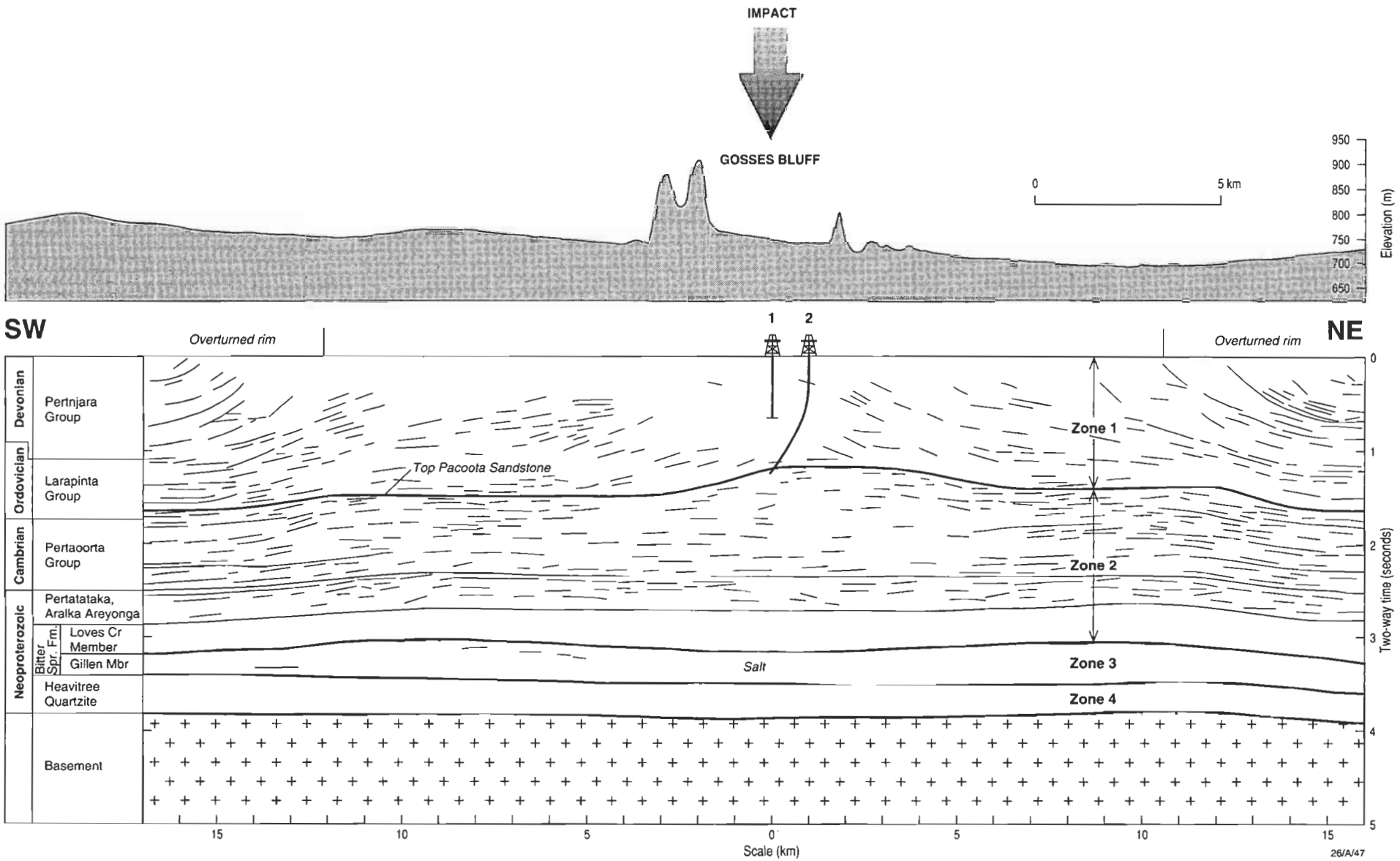

Figure 5. Line drawing based on seismic section P82-GB1 (see Fig. 4). Note the position of the overturned rocks at the crater rim, and the evaporites of the Bitter Springs Formation. The original crater has been almost entirely removed by erosion such that only the roots of the crater rim are preserved.

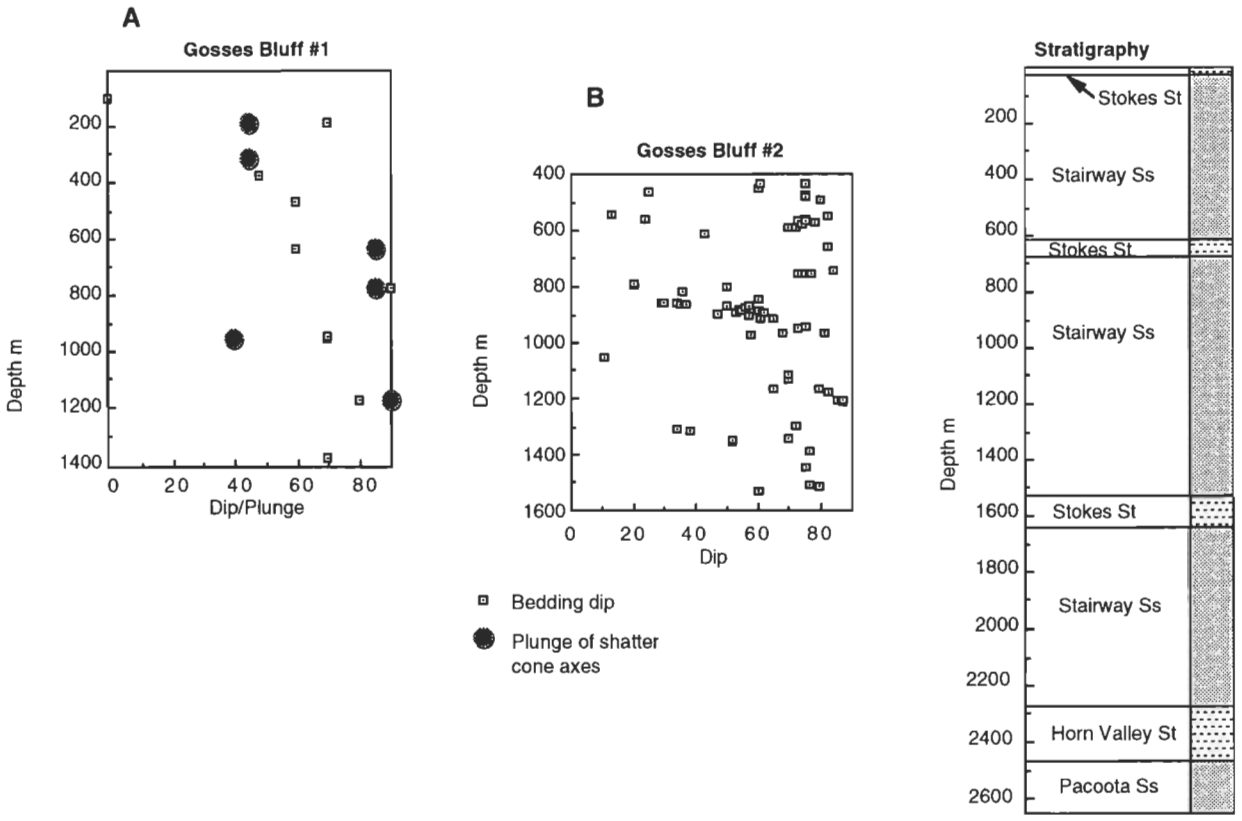

Figure 6. Dip of bedding surfaces intersected in Gosses Bluff Nos. 1 and 2. The plunge of shatter-cone axes is also shown for Gosses Bluff No. 1. Note that bedding dips are generally chaotic, and there appears to be no obvious relationship between the orientation of shatter cones and bedding surfaces, suggesting that the interval intersected by the wells is completely brecciated.

in Gosses Bluff No. 2 shows that the Stairway Sandstone is pervaded by an anastomosing complex of fractures. The fractures are typically less than 1 mm wide, and consist of crushed quartz grains produced by compression during the passage of the primary shock wave induced by the impact. The crushed quartz is well-cemented and chert-like in appearance, but shows no evidence of fusion. A study of thin sections of cuttings from a range of depths in Gosses Bluff No. 2 well suggests that in general fewer than 5 per cent of the cuttings show evidence of shock-induced crushing of the quartz grains.

Zone 2 (2300–6300 m): fractured and domed strata

The sequence boundary at the top of the Pacoota Sandstone is the first apparently continuous reflector beneath zone 1 (Fig. 5). Even the Stairway Sandstone, which lies a short distance above the Pacoota Sandstone in zone 1, is faulted and fractured, and blocks of the unit appear in exposures at the centre of the bluff. Directly beneath the bluff the upper surface of the Pacoota Sandstone has been uplifted by about 680 m. Beneath this reflection, successively deeper reflections indicate doming of the stratal surfaces. The doming of these stratal surfaces gradually becomes less severe with depth down to the top of the Gillen Member of the Bitter Springs Formation.

Zone 3 (6300–7000 m): salt

The Gillen Member of the Bitter Springs Formation consists of at least two, and possibly more, thick halite units (Lindsay 1987). The degree of deformation changes abruptly across these units, which assimilated the strain of the shock wave generated by the impact such that the rock units below the evaporites are largely undeformed. The upper surface of the Gillen Member is domed, but its lower surface is essentially planar (Figs. 2 and 5). Salt has been drawn in from some distance beyond the impact to form a large domal structure, whose edge extends out to 12 km from the point of impact and lies beneath the upturned edge of the original crater rim. The dome is not a simple feature but has a raised rim or rim anticline. The centre of the dome is thus generally depressed below the rim but has a slightly uplifted centre. The salt thickens from 400 m beyond the limits of deformation to more than 1000 m beneath the uplifted region. A structural high referred to as the Gardiner–Tyler anticline (Fig. 3) extends to the northeast from beneath the Gosses Bluff uplift and appears to be an earlier structure, probably produced in large part by salt migration during the Palaeozoic Alice Springs Orogeny (Lindsay 1987).

Zone 4 (7000+ m): undisturbed strata

Beneath the lower contact of the Bitter Springs Formation there are few signs of deformation. The Heavitree Quartzite, a well-cemented quartzose sandstone, produces clearly defined, largely uninterrupted parallel seismic reflections. Minor cross-cutting reflections associated with the boundary between the Heavitree Quartzite and the underlying crystalline basement at a depth of about 10 800 m may relate to small-scale out-of-plane faulting or perhaps to topography on the basal surface. In terms of deformation, the energy released by impact had been completely dissipated before it could reach zone 4.

AFTA, and the thermal history of Gosses Bluff

Samples were collected for AFTA in order to help constrain the age of impact and the thermal history of the impact structure. One aim was to examine the relative importance of the two main thermal effects associated with the Gosses Bluff impact structure. The first effect was heating associated with the blanket of highly shocked and melted clasts that probably covered much of the present structure. The second effect was cooling due to the kilometre-scale exhumation of the rocks in the centre of the structure. Transient heating as the shock wave penetrated the present crater floor was probably negligible. Most of the crater floor was subjected to peak shock pressures <10 Gpa (<100 kb; Milton et al. 1972) which would have heated but not vaporised pore waters (Kieffer et al. 1976). The present topographic surface of the Gosses Bluff impact structure is close to the original crater floor. Even though the bulk of the crater fill has been removed by erosion, Mount Pyroclast and nearby areas evince remnants of melt breccia composed of clasts of fused and highly shocked Parke Siltstone (Milton et al. 1972). Many of the clasts in these deposits were heated to temperatures sufficient to totally anneal fission tracks in zircon and apatite (Milton & Sutter 1987).

An additional aim of the study was to examine annealing of fission tracks due to shock. Although annealing of fission tracks is typically related to thermal conditions, shock pressures of ~10 GPa (~100 kb) have been reported to cause near-total fission-track annealing in apatites and sphene (Fleischer et al. 1974). Pressures of this order or higher have affected rocks in the core of Gosses Bluff and individual clasts at Mount Pyroclast.

Accordingly, our sampling strategy focused on three data sets:

- subsurface control samples from Tyler No. 1 well, which is located beyond the Gosses Bluff aureole and penetrated the original, pre-impact horizontal stratigraphic succession;
- the impact aureole of Gosses Bluff; and
- the impact breccias (Mount Pyroclast).

Sampling and methods

Twenty-six outcrop and borehole samples ranging from 0.5 to 10 kg were collected for analysis from most formations across the structure, and apatite grains were separated by conventional heavy-liquid and magnetic techniques (Green 1986). Fourteen samples contained sufficient apatite for analysis. Details of the other samples are presented by Tingate (1990). More recently, six cuttings samples were also collected from Gosses Bluff No. 2, but no apatite suitable for analysis was recovered from them. Most of the apatites separated from the Mereenie Sandstone and Larapinta Group are highly fractured, reflecting shock levels of 5–10 GPa (50–100 kb; Milton et al. 1972), and could not be analysed. However, the least fractured parts of some grains could still be counted. The density of fracturing within the apatites decreases away from the centre of Gosses Bluff, excluding samples from Mount Pyroclast, which are also highly fractured.

All analytical data come from detrital apatites. The apatites were analysed by the external detector method (Gleadow 1981; Green 1981), and their ages calculated by the zeta calibration technique (Fleischer & Hart 1972; Hurford & Green 1982, 1983). A zeta calibration value of 356 ± 7, produced by counting standard age material, was used (Hurford & Green 1983). Irradiations were carried out at the X–7 facility of the Hifar Reactor, Lucas Heights, New South Wales. Apatite fission-track ages were calculated from pooling single grain-track counts, unless the $P(\chi^2)$ value was less than 5 per cent, in which case the central age was used (Galbraith 1981, 1992). Confined track lengths were measured as described in Kamp & Green (1990). Further details concerning sample preparation and zeta calibration are presented by Tingate (1990).

Principles of interpretation

Interpretation of the thermal history of Gosses Bluff from AFTA data is based on the annealing behaviour of spontaneous fission tracks in geological environments (Gleadow et al. 1983; Green et al. 1989a), and length data from geological samples (Gleadow et al. 1986), together with descriptions of induced fission-track annealing in laboratory experiments (Green et al. 1986; Laslett et al. 1987; Duddy et al. 1988) that have been extended to geological situations (Green et al. 1989b). These laboratory annealing studies have concentrated on fission-track-length measurements, and their relation to fission-track density (and hence age) has been described by Laslett et al. (1984) and Green (1988). Considerations of the effect of apatite chemical composition on track annealing come from Tingate (1990) and Green et al. (1985, 1986). Apatites from the Amadeus Basin are fluorine-rich, and have a mean chlorine content of 0.1 weight per cent; the typical range of chlorine in a sample is 0 to 0.5 weight per cent (Tingate 1990, 1991).

A key result from annealing studies is that the length of individual fission tracks is primarily controlled by the maximum temperature that the track has experienced, and that changes in the order of magnitude of the heating duration cause differences in annealing equivalent to temperature changes of ~10°C (Duddy et al. 1988; Green et al. 1989b). Samples that cool rapidly from temperatures greater than 110°C to less than 50°C, and are not subsequently heated above 50°C, have mean track lengths of 14–15 μm with standard deviations of ~1 μm. The track-length distributions of such samples are identical with the age standards used for calibration, and so the fission-track age records the time of initial cooling and track retention.

Progressive heating to present maximum temperatures maintained for ~10 Ma has caused borehole samples with typical Amadeus Basin apatite compositions to exhibit a decrease in mean track length from ~14 μm at ~50°C to zero at ~110°C (Green et al. 1989a; Tingate 1990). Over the same temperature range, the fission-track age has also decreased to zero.

If a sample containing apatites with a range of chlorine contents reaches maximum temperatures of 90 to 110°C before it cools, the ages recorded by a single grain can be quite disparate. Before they cool, chlorine-poor grains will have been strongly or totally annealed, yet chlorine-rich grains will still contain partly annealed tracks and so give older ages.

For a sedimentary rock that has been heated sufficiently to have all tracks totally annealed, and then cooled below ~110°C so that it starts to accumulate tracks again, the fission-track age and mean track length will reflect the thermal history since it cooled. If the sample has cooled rapidly to temperatures below 50°C, then the fission-track age will approximate the time of cooling. If the sample has annealed at temperatures >50°C since the initial track was retained, the time of cooling below ~110°C

Table 1. Tyler No. 1 sample details and apatite fission-track data

Sample no.	*N*[a]	ρ_s[a] $x10^6$ cm^{-2} (N_s)	ρ_i[a] $x10^6$ cm^{-2}(N_i)	ρ_d[a] $x10^6$ cm^{-2} (N_d)	$P(\chi^2)$[b] (%)	*Fission -track age (Ma)*	*Mean track length (μm)*	*No. of tracks*	*Stand. devn*	*'Corrected'*[c] *age (Ma)*	*Present tempera-ture (°C)*
Brewer Conglomerate (outcrop)											
8451-89	14	2.087 (1496)	2.216 (1588)	1.624 (4582)	94	267 ± 10	12.55 ± 0.16	100	1.58	308	25
Brewer Conglomerate (856–857 m)											
8351-31	8	2.032 (669)	3.696 (1217)	1.827 (4334)	4	176 ± 9 180 ± 13*	12.81 ± 0.15	100	1.50	203	41
Mereenie Sandstone (2784 m)											
8351-32	13	1.371 (239)	3.390 (591)	1.827 (4334)	90	130 ± 10	10.79 ± 0.37	18	1.57	180	78
Stairway Sandstone (3563–3566 m)											
8351-33	10	0.0887 (115)	0.5329 (691)	1.827 (4334)	<1	54 ± 6 49 ± 12*	9.71 ± 0.50	21	2.28	86	93

[a] Ages have been obtained by the external detector method (Gleadow 1981); N = number of grains counted, ρ_S = fossil track density in apatite, ρ_i = induced track density counted in external (muscovite) detector, and ρ_d = standard glass SRM612 track density (measured in mica external detector). Numbers in brackets refer to number of tracks counted in track-density measurements. Ages are calculated from a zeta calibration of 356 as outlined in Hurford & Green (1983). All ages quoted at ± 1 σ.
[b] Probability given by chi-squared statistic as described by Galbraith (1981). *Central age (Galbraith 1992) used when $P(\chi^2)$ <5%.
[c] Corrected age calculated from fission-track age and mean length according to the length/density relation of Green (1988).

can be estimated by calculating a 'corrected age' from the track-length/track-density-reduction relationship of Green (1988). The corrected age is strictly valid only for samples in which all tracks have effectively experienced the same maximum temperature. For samples that have had more complex histories since their initial tracks were retained, the corrected age will be a minimum estimate of the time the sample cooled below ~110°C.

Once limits on the timing and style of the thermal history for samples had been made from the AFTA data and geological constraints, forward computer modelling was undertaken to check and refine possible thermal histories. Software used for modelling is based on the mathematical description of induced track annealing in monocompositional Durango apatite (Laslett et al. 1987; Duddy et al. 1988; Green et al. 1989b).

Subsurface control samples (Tyler No. 1)

Samples from Tyler No. 1 well (Figs. 3 and 7) provide useful data for comparing with data from within the impact structure. The well and Gosses Bluff share a similar stratigraphy, and their pre-impact burial and thermal histories were probably similar too. Figure 8 shows the variation in fission-track age and mean track length with present temperature in Tyler No. 1. Sample information and analytical data are presented in Table 1.

Sample 8451-89 is from a Brewer Conglomerate outcrop at the Tyler No. 1 well site. Its fission-track age (267 ± 10 Ma) being younger than its stratigraphic age (ca 370 Ma; Playford et al. 1976) indicates that it has undergone significant annealing since deposition. It has a mean length of 12.55 ± 0.16 μm, suggesting that it has been heated to temperatures greater than 70°C since deposition. Its length histogram (Fig. 9) shows that it has a low proportion of tracks which formed at temperatures <50°C, suggesting that it started cooling from temperatures of ~60°C in the last 100 Ma. The age and length parameters of sample 8451-89 are typical of Brewer Conglomerate samples analysed from the Missionary Plain, and reflect a regional pattern of elevated palaeotemperatures (Tingate 1990).

The age and length parameters of the three samples recovered at depth in Tyler No. 1 (Fig. 8) also indicate that each sample has experienced higher temperatures than at present. Corrected ages for the samples in Tyler No. 1 are given in Table 1. The outcrop sample (8451-89) has a corrected age moderately close to its stratigraphic age (~370 Ma). Although it has undergone significant annealing, it has not been totally annealed since deposition. This conclusion is supported by other Pertnjara Group data from in and around the impact structure, and is discussed below. Samples 8351-31 and 32 have similar corrected ages, close to 200 Ma, much younger than their stratigraphic ages. This suggests that 8351-32 has been totally annealed at palaeotemperatures >110°C, and that 8351-31 was almost totally annealed at palaeotemperatures of ~110°C before it cooled at about 200 Ma. Sample 8351-33 has a corrected age of 86 Ma, probably reflecting more recent cooling in the last 100 Ma.

The fission-track parameters and modelling of thermal histories suggest that the Tyler No. 1 samples started cooling from elevated palaeotemperatures some time between 240 and 180 Ma and again between 100 and 40 Ma. Maximum palaeotemperature estimates for these times are presented in Table 2. Schematic thermal histories are shown for sample 8451-89 in Figure 10. The AFTA thermal history constraints are consistent with progressive cooling or cycles of burial followed by uplift and erosion.

An important aspect of the thermal history data from Tyler No. 1 is that the samples appear to have cooled from maximum temperatures after the main structural event affecting the basin, the Alice Springs Orogeny. The structure on which Tyler No. 1 is drilled probably finished growing some time after Brewer Conglomerate deposition (~360 Ma) and before major crustal shortening ceased at 320–300 Ma (Shaw et al. 1992). Temperature constraints for this time period are also shown in Figure 10.

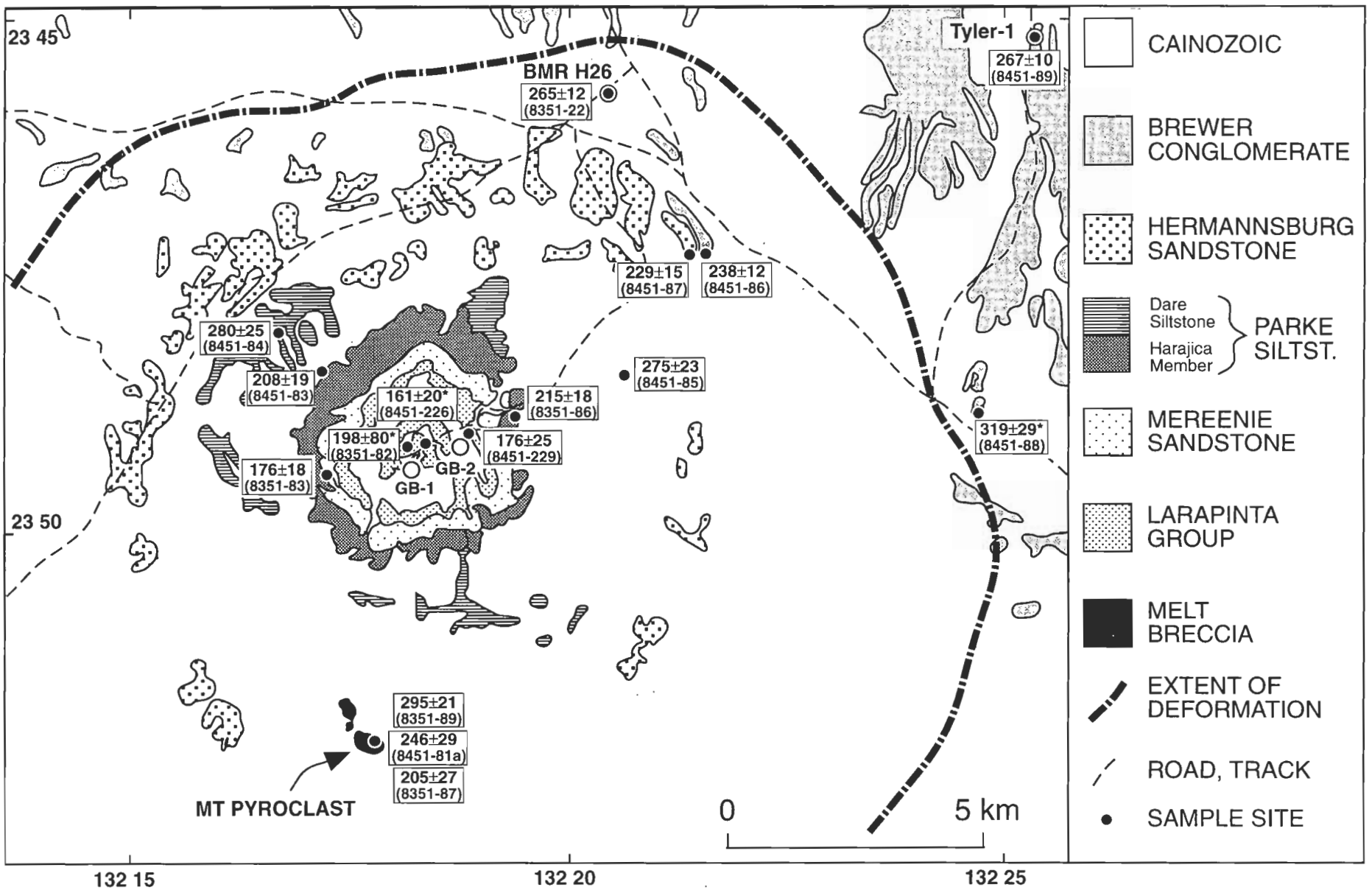

Figure 7. Apatite fission-track ages (± 1 σ) for outcrop and shallow (<20 m) borehole samples (Tables 1 and 3) from Gosses Bluff impact structure and surrounds (geology after Milton et al. 1978). Asterisks denote central ages for which $P(\chi^2)$ <5 per cent.

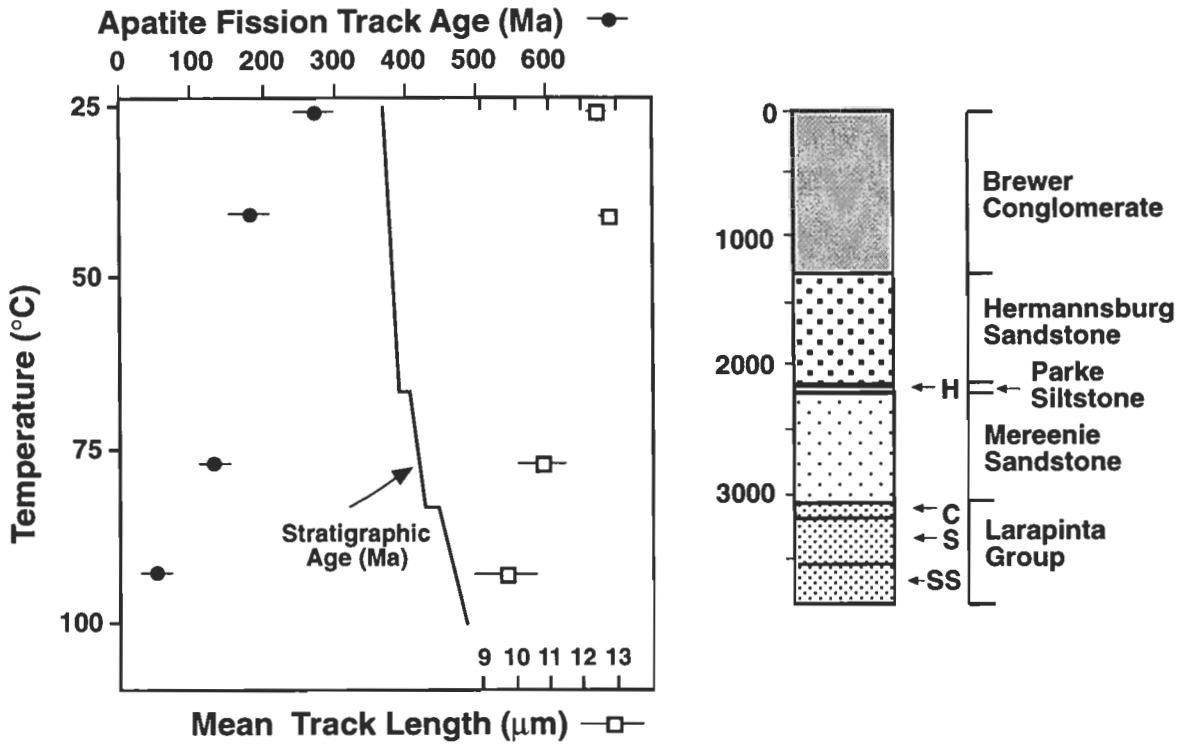

Figure 8. Tyler No. 1 apatite fission-track age (± 2 σ) and mean length (± 2 σ) plotted against present temperature (Table 1). Present geothermal gradient is 19°C km^{-1}. Well stratigraphy is also shown (H = Harajica Sandstone Member, C = Carmichael Sandstone, S = Stokes Siltstone, and SS = Stairway Sandstone).

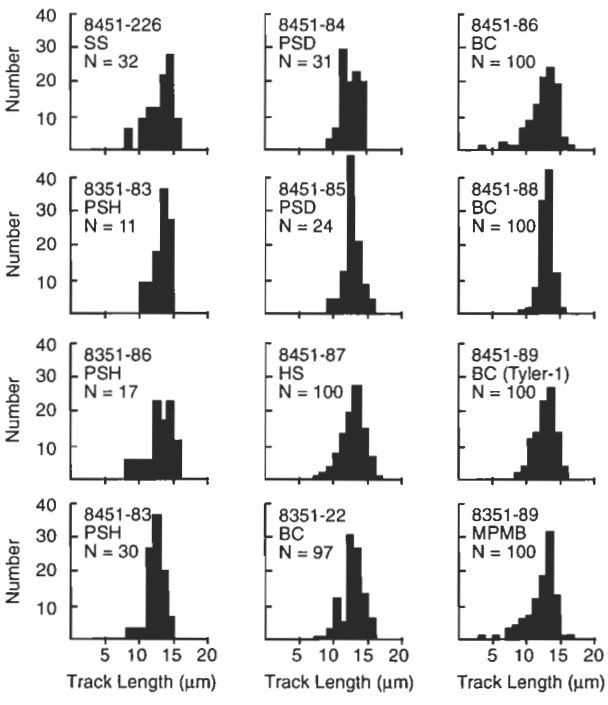

Figure 9. Confined track-length histograms for samples from the Gosses Bluff impact structure and surrounds (further details in Tables 1 and 3). All histograms are normalised to 100 tracks (N = number of track lengths measured). Stratigraphic abbreviations are: SS = Stairway Sandstone, PSH = Parke Siltstone (Harajica Sandstone Member), PSD = Parke Siltstone (Dare Siltstone Member), HS = Hermannsburg Sandstone, BC = Brewer Conglomerate, and MPMB = Mount Pyroclast melt breccia.

The impact structure (Gosses Bluff and environs)

AFTA data from outcrop samples collected near Gosses Bluff show a general trend of decreasing fission-track age towards the centre of the impact structure (Figs. 7 and 11; Table 3). All the formations sampled give ages younger than their stratigraphic ages, and most are older than Milton & Sutters' (1987) best estimate of the timing of impact, 142.5 ± 0.8 Ma. If we ignore the imprecise age determination from sample 8351-82, three samples from near the centre of the structure, 8451-226, 8451-229, and 8351-83, have ages within two standard deviations of the Milton & Sutter (1987) estimate. These samples are from the Stairway Sandstone, Carmichael Sandstone, and Harajica Sandstone Member of the Parke Siltstone, and have ages between 160 and 176 Ma. Other Harajica sample ages are close to 210 Ma. The fission-track ages from the upper part of the Parke Siltstone — the Dare Siltstone Member — increase to around 280 Ma. The apatite ages decrease in the samples from the top of the Hermannsburg Sandstone and the base of the Brewer Conglomerate (8451-87 and 8451-86) to a range of 230–240 Ma. The outermost Brewer Conglomerate sample from within the deformed zone, 8351-22, has an age of 265 ± 12 Ma. It has an age similar to sample 8451-89, the Brewer Conglomerate outcrop sample at Tyler No. 1 well site. Another Brewer Conglomerate sample from outside the impact structure, sample 8451-88, has an even older age.

Samples 8451-88, 8351-82, and 8451-226 have single-grain age variations inconsistent with a single age population ($P(\chi^2) < 5\%$). Examination of the single-grain age distribution for sample 8451-88 (Tingate 1990) shows that it has some grains older than its stratigraphic age (>370 Ma) and also a younger grain (~150 Ma) that fall outside the quoted central age. The

Table 2. Tyler No. 1 palaeotemperature data

Sample no.	*Depth (m)*	*Maximum palaeotemperatures[a] (°C) at different times*			
		360–300[b] Ma	*240–180 Ma*	*100–40 Ma*	*Present*
8451-89	outcrop	<90	90	60	25
8351-31	856–857	<110	~110	70	41
8351-32	2784		>110	95	78
8351-33	3563–3566		>110	100–110+	93

[a] Temperatures based on heating duration of ~10 Ma, precision of ±10°C unless stated otherwise.
[b] Timing constraint taken from Tingate (1990).

presence of the older grains indicates that fission tracks in the sample have not been totally annealed since deposition, whereas the younger grain reflects a higher degree of annealing which is probably compositionally related. Samples 8351-82 and 8451-226 also have significant variation in single-grain age. Both samples have one or two young grains (~70 Ma) which are the main cause of the low $P(\chi^2)$ statistic. Further age determinations are planned, to confirm whether a consistently young single-grain population is present in the Larapinta Group. The number of grains found is inconclusive, but suggests that the Larapinta Group in the centre of Gosses Bluff could have cooled from palaeotemperatures of ~90°C at some time since 140 Ma.

The mean track-length measurements from samples within the impact structure vary between 12.2 and 13.2 μm (Fig. 11). The mean track-length measurements indicate that none of the fission-track ages from the samples can be interpreted in terms of rapid cooling from palaeotemperatures >110°C, followed by residence at temperatures less than 50°C. Since all mean track lengths are <14 μm, the fission-track ages for all samples indicate that initial tracks were maintained before the measured fission-track age. A minimum estimate for when track retention started is provided by the corrected ages shown in Table 3. The corrected ages tend to fall into two groups: between 180 and 250 Ma for samples from the Harajica Sandstone Member and older formations, and between 260 and 360 Ma for samples from the upper Pertnjara Group. As all the corrected ages are greater than the time of impact (142.5 Ma; Milton & Sutter 1987), none of the samples were totally annealed before or during this event. The corrected ages from formations within the impact structure are similar to those derived from the three shallowest samples in Tyler No. 1 (Table 1), and reflect the regional cooling pattern rather than exhibiting evidence of significant annealing associated with the impact.

The confined track lengths for sample 8451-226 (Stairway Sandstone) are mostly between 13 and 16 μm (Fig. 9); shorter tracks, <11 μm, experienced palaeotemperatures >80°C. For an impact age of 142.5 Ma, the shorter lengths also indicate that the sample was not totally annealed immediately before or during the impact. Sample 8451-83, the only one with lengths determined from more than 30 track measurements from the Harajica Sandstone, has a narrow track-length distribution, and fewer short tracks than 8451-226.

All the Dare Siltstone Member and younger Pertnjara Group outcrop samples from within and outside the impact structure have essentially similar broad track-length distributions with track length modes of 12 or 13 μm and a small but significant number of short tracks less than 10 μm long (Fig. 9). The short tracks indicate that the samples contain early-formed tracks that have been heated to temperatures greater than 80°C since deposition. Sample 8451-88 has a slightly narrower distribution and a lower proportion of short lengths than the other samples, suggesting slightly less annealing since deposition. The difference between its length distribution and the other Brewer Conglomerate outcrop sample (8451-89) outside the impact structure is ascribed to a regional variation rather than any effect of the impact.

All the confined track distributions from the impact structure and surrounds (Fig. 9) consistently exhibit a small proportion of long tracks >14 μm. This feature indicates that they have spent a small part of the time represented by their fission-track ages at temperatures <50°C. None of the samples reflect cooling to present temperatures before 100 Ma.

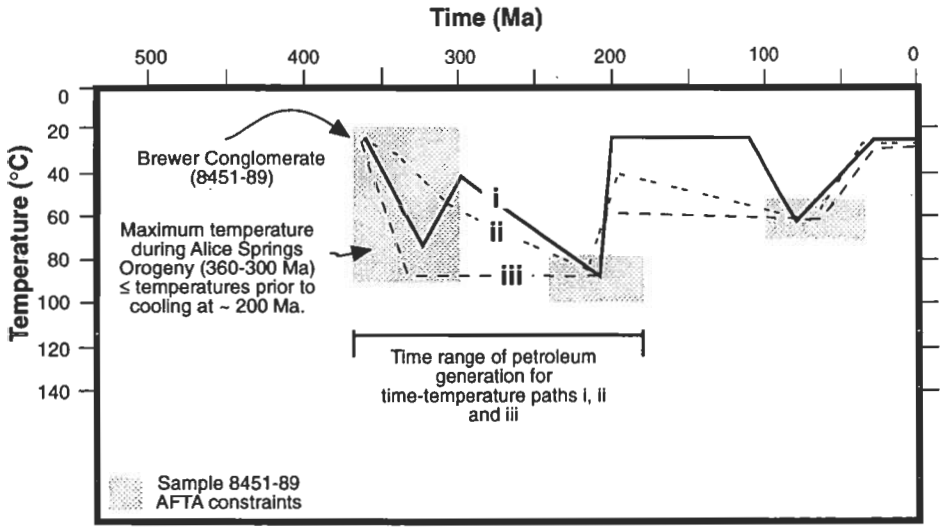

Figure 10. AFTA constraints and possible thermal history paths for the top of the Brewer Conglomerate (sample 8451-89) at Tyler No. 1. Likely timing of petroleum generation within the Larapinta Group is also shown.

Mount Pyroclast breccias

The most highly shocked rocks are the melt breccias of Mount Pyroclast (Fig. 7), an erosional remnant of the original crater fill. Melted clasts, thought to be originally from the Parke Siltstone, represent exposure to shock pressures of about 50 GPa (500 kb; Milton et al. 1972). Samples 8351-87 and 8451-81a were taken from breccia at the base of Mount Pyroclast, and 8351-89 is from the melt breccia at the top of the hill (Table 3). All were samples of 6–10-kg weight and contained many clasts. Most of the apatite grains from them were intensely shocked, and most of these were uncountable after etching. Although 8351-89 had the highest proportion of highly shocked and melted clasts, it yielded more countable grains, which contributed to the greater precision of its age determination — 295 ± 21 Ma. All three samples have fission-track ages between 200 and 300 Ma, older than the $^{40}Ar/^{39}Ar$ age determination of 142.5 ± 0.8 Ma from a sanidine-rich clast near the top of Mount Pyroclast (Milton & Sutter 1987). The three fission-track ages are within two standard deviations of one another, and are similar to the age determinations from the Dare Siltstone Member (e.g., 8451-84), from which most of the clasts in the melt breccia at Mount Pyroclast were originally derived (Milton et al. 1972).

Sample 8351-89 has a mean length of 12.2 μm and a standard deviation of 2.17 μm. The mean length and the high standard deviation are related to the presence of short tracks less than 10 μm in the length distribution (Fig. 9). Minor annealing of tracks due to heating during melt breccia formation cannot be ruled out, but the fission-track age and length data are not significantly different from the upper Parke Siltstone samples within the impact structure. Although the melt breccia undoubtedly contains clasts that were highly shocked and melted, the age and length data indicate that the apatites dated from the melt breccia were not strongly annealed either by shock or heat.

The presence of non-reset apatites at the top and the base of the melt breccia in this study differs from the fission-track results presented by Milton & Sutter (1987). They presented single-crystal-zircon fission-track ages from unmelted clasts within the melt breccia and from underlying sandstone breccia that are close to 140 Ma. These zircon fission-track ages represent total annealing of pre-existing tracks at the time of impact. A sandstone-breccia sample from about 14 m below the base of the melt breccia yielded zircon single-grain fission-track ages greater than 500 Ma (Milton & Sutter 1987), which probably represent the provenance age. Two apatite single-grain ages from the same sample are within two standard deviations of age determinations from the sandstone-breccia in this study (200–250 Ma). Milton & Sutter (1987) suggested that direct shock heating of the upper samples was probably insufficient to cause the zircon fission-track annealing observed, and that conductive heating associated with the melt breccia was more likely.

The results of our study indicate that conductive heating within the melt breccia was not sufficient to totally anneal fission tracks in apatite, and would have been incapable of significantly annealing fission tracks in zircon, which are more resistant to thermal annealing. Apatite fission tracks are totally annealed at temperatures of about 370°C for 1 hour, 240°C for 1 year, and 190°C for 1000 year (Laslett et al. 1987). These temperatures place maximum limits on the temperature of the melt breccia for different heating durations.

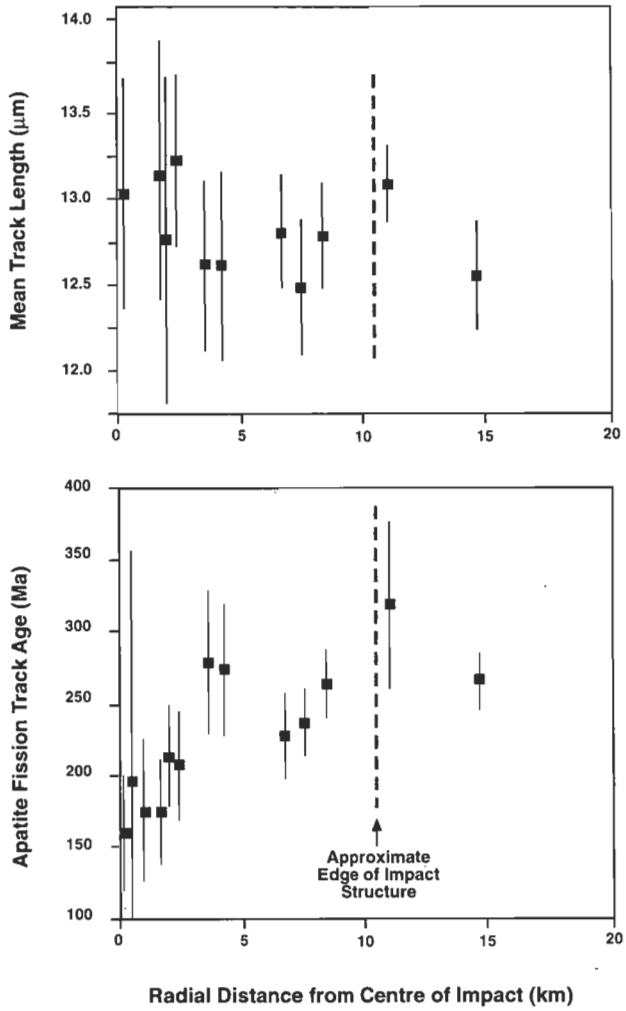

Figure 11. Plot of apatite fission-track age (±2 σ) and mean length (±2 σ) versus radial distance from the centre of Gosses Bluff (excluding data from Mount Pyroclast). Sample positions are shown in Figure 7.

An explanation consistent with fission-track data from both studies is that the young zircon fission-track ages reflect total annealing caused by the passage of the initial shock wave rather than conductive heating within the melt breccia. An important factor to consider is that fission tracks in sphene, which have broadly similar thermal track-annealing behaviour to zircon, have been reported to be totally annealed by shock pressures of ~10 GPa (~100 kb) in nuclear explosions (Fleischer et al. 1974). Fleischer et al. (1974) further demonstrated that the annealing was attributable only to shock, as the associated increase in temperature was negligible (in terms of thermal annealing of fission tracks in sphene).

Part of the reason for the lack of totally overprinted single apatite grains with ages of ~140 Ma in the samples collected at Mount Pyroclast in this study appears to be associated with the mechanical response of apatite to shock. The apatites from the Stairway Sandstone in the centre of the bluff have probably experienced shock pressures of ~10 GPa (~100 kb; Milton et al. 1972), which caused dense fracturing in all grains and rendered nearly all of them uncountable after etching. Most of the clasts in the breccias at Mount Pyroclast have experienced pressures >10 GPa (100 kb; Milton et al. 1972), so nearly all the apatite grains were too shattered to be counted or had been melted into glass. Thus the apatites dated from the breccias in this study are

Table 3. Gosses Bluff apatite fission-track data

Sample no.	*N*[a]	ρ_s[a] $x10^6$ cm^{-2} (N_s)	ρ_i[a] $x10^6$ cm^{-2}(N_i)	ρ_d[a] $x10^6$ cm^{-2} (N_d)	$P(\chi^2)$[b] (%)	*Fission -track age (Ma)*	*Mean track length (μm)*	*No. of tracks*	*Stand. devn*	*'Corrected'*[c] *age (Ma)*
Outside structure										
Brewer Conglomerate										
8451-88	12	1.491 (742)	1.911 (951)	2.317 (4060)	<1	314 ± 16 319 ± 29*	13.09 ± 0.11	100	1.05	354
Inside structure										
Brewer Conglomerate										
BMR Hermannsburg 26 (14 m depth; Fig. 7)										
8351-22	8	2.733 (1008)	3.284 (1211)	1.827 (8771)	70	265 ± 12	12.79 ± 0.16	100	1.61	300
8451-86	17	1.773 (710)	3.227 (1292)	2.475 (5203)	7	238 ± 12	12.48 ± 0.20	100	2.03	276
Hermannsburg Sandstone										
8451-87	9	3.805 (400)	6.744 (709)	2.317 (4060)	20	229 ± 15	12.81 ± 0.17	100	1.68	259
Parke Siltstone (Dare Siltstone Member)										
8451-85	13	4.646 (232)	7.289 (364)	2.475 (5203)	15	275 ± 23	12.61 ± 0.28	24	1.35	316
8451-84	17	3.113 (210)	4.788 (323)	2.475 (5203)	50	280 ± 25	12.61 ± 0.25	31	1.41	322
Parke Siltstone (Harajica Sandstone Member)										
8451-83	16	3.044 (184)	6.336 (383)	2.475 (5203)	25	208 ± 19	13.22 ±. 0.25	30	1.37	228
8351-86	3	3.192 (316)	3.051 (302)	1.171 (4124)	30	215 ± 18	12.77 ± 0.48	17	1.97	244
8351-83	9	2.757 (193)	3.214 (225)	1.171 (4124)	40	176 ± 18	13.14 ± 0.40	11	1.33	194
Carmichael Sandstone										
8451-229	3	0.901 (75)	2.079 (173)	2.317 (4060)	85	176 ± 25				
Stairway Sandstone										
8351-82	4	1.051 (83)	0.835 (66)	1.171 (4124)	<1	257 ± 43 198 ± 80*				
8451-226	18	2.408 (270)	6.536 (733)	2.475 (5203)	<1	160 ± 12 161 ± 20*	13.03 ± 0.34	32	1.90	180
Mount Pyroclast										
Melt Breccia at top										
8351-89	14	3.083 (522)	2.132 (361)	1.171 (4124)	60	295 ± 21	12.20 ± 0.22	100	2.17	350
Breccia at base										
8351-87	3	3.683 (116)	3.683 (116)	1.171 (4124)	30	205 ± 27				
Breccia at base										
8451-81a	15	0.662 (112)	1.165 (197)	2.475 (5203)	20	246 ± 29				

[a] Ages have been obtained by the external detector method (Gleadow 1981); N = number of grains counted, ρ_S = fossil track density in apatite, ρ_i = induced track density counted in external (muscovite) detector, and ρ_d = standard glass SRM612 track density (measured in mica external detector). Numbers in brackets refer to number of tracks counted in track-density measurements. Ages are calculated from a zeta calibration of 356 as outlined in Hurford & Green (1983). All ages quoted at ± 1 σ.

[b] Probability given by chi-squared statistic as described by Galbraith (1981). *Central age (Galbraith 1992) used when $P(\chi^2)$ <5%.

[c] Corrected age calculated from fission-track age and mean length according to the length/density relation of Green (1988).

not representative of most of the clasts in these deposits, and probably represent a minor fraction of less shocked fragments incorporated into the breccia. Zircon appears to be more resistant to fracturing at high shock pressures than apatite (Milton & Sutter 1987), and grains of it can be dated from totally annealed tracks associated with shock pressures >10 Gpa (>100 kb).

Relation of AFTA results to pre-impact geometry

The sample data from the Gosses Bluff structure have been plotted at their corresponding depths before impact and relative to the present land surface (Fig. 12). Formation thicknesses are derived from isopach maps in Wells et al. (1970) and Jones (1972). Although the Larapinta Group appears to have been at essentially the same depth at Gosses Bluff and in Tyler No. 1, the Parke Siltstone is considerably thicker at Gosses Bluff than in Tyler No. 1. A corresponding decrease in thickness in the Brewer Conglomerate at Gosses Bluff compensates for the greater thickness of the siltstone there.

As some of the samples within the structure come from near the tops or bottoms of formations, their pre-impact depths are moderately easy to estimate. The depths of other samples, located farther from formation boundaries, were more difficult to estimate owing to the faulting within the structure. Any inaccuracy in a depth estimate is limited by the thickness of the formation or member itself. Samples from Mount Pyroclast have been plotted as part of the Dare Siltstone Member from which it was derived. AFTA sample data from Tyler No. 1 have also been plotted in Figure 12; as these are plotted at the depths shown in Figure 8, the sampled formation will not necessarily correspond with the reconstructed Gosses Bluff stratigraphy, particularly within the Pertnjara Group.

The effect of the Gosses Bluff impact on the apatite fission-track data relative to the undisturbed samples from Tyler No. 1 can be judged from Figure 12. The three deepest AFTA samples from Tyler No. 1, derived from environments currently at higher temperatures than the Gosses Bluff outcrop samples, yield age and length data that reflect this difference, which becomes more accentuated with increasing depth and present temperature (Fig. 12a and b). The plot of corrected age versus reconstructed depth (Fig. 12c) helps take into account differences in annealing due to variations in present temperature, and offers a more valid comparison of the two data sets. The uncorrected and corrected fission-track ages (Fig. 12a and c) in Tyler No. 1 decrease considerably from the surface to 850 m, and show little change between 850 and 2800 m, which is interpreted to reflect moderately rapid regional cooling between 240 and 180 Ma. The young age of the lowermost sample in Tyler No. 1 reflects annealing at palaeotemperatures between 90 and 110°C in the last 100 Ma.

The Gosses Bluff fission-track age data from the upper 1000 m are similar to the data from Tyler No. 1, reflecting a similar thermal history. However, the fission-track ages for the Dare Siltstone Member, below 1000 m, increase, deviating from the Tyler No. 1 trend. The corrected ages for these samples range from 300 to 350 Ma, and approach their stratigraphic age (~380 Ma). The local increases in fission-track age in the Dare Siltstone Member relative to the Hermannsburg Sandstone and Brewer Conglomerate samples resemble those in the Pertnjara Group in Alice No. 1 (Tingate 1990). They record differences in the provenance fission-track ages, and reflect progressive unroofing of the source regions of the Pertnjara Group. During deposition of the upper part of the Pertnjara Group, most apatites had few fission tracks because the detrital grains were derived from source regions that had recently cooled from temperatures greater than 110°C. The preservation of the inherited age pattern in the Pertnjara Group indicates that outcrop samples from the Dare Siltstone Member and younger formations around Gosses Bluff have not been totally annealed since deposition. Gosses Bluff outcrop samples with reconstructed depths below 1.5 km show little variation in corrected age, and are considered to have been totally annealed at palaeotemperatures ≥110°C before cooling at ~200 Ma.

A minimum estimate of ~3.5 km for the pre-impact depth of the Stairway Sandstone can be derived from the preserved stratigraphy at Gosses Bluff. According to the geothermal gradient of 19°C km^{-1} (measured in Tyler No. 1), the top of the Stairway Sandstone would have been at a minimum temperature of ~90°C before impact. The track-length histogram of sample 8451-226 (Fig. 9) contains some short tracks which are consistent with residence at temperatures between 90 and 110°C before impact. The observed short tracks can be explained purely by the depth of burial before impact, and no annealing due either to shock or heating associated with the impact needs to be invoked. The presence of these more highly annealed tracks indicates that the heating and/or shock associated with the impact was not sufficient to totally anneal pre-existing tracks.

The plot of fission-track age and mean length (Fig. 12) emphasises how the variation across Gosses Bluff follows the stratigraphy. In terms of thermal effect, it is no different from a plot across a post-depositional structure, such as an anticline or uplifted fault block. Citing the results of conodont colour alteration index (CAI) studies, Gorter et al. (this issue) report a CAI value of 4 for samples from the Stokes Siltstone exposed in the core of Gosses Bluff. This, as discussed by Gorter et al., is compatible with the thermal levels of the Stokes Siltstone at a depth of 4.5 to 5 km adjacent to the Gosses Bluff structure (Milton et al. this issue). The net effect of the impact appears to have been to uplift and cool rocks from different palaeotemperature levels related to their burial depth before impact.

Age of the impact

The near-vertical beds at Gosses Bluff have been bevelled about 200 m above the present level of the plain, similar to other features in the region (Mabbutt 1965). The age of this surface is uncertain, but is probably older than, or of similar age to, the Eocene–Oligocene Cordillo Surface (Wopfner 1978) developed on Cretaceous and early Tertiary units further east in the basin. The youngest formation affected by the impact is the Brewer Conglomerate (Frasnian–Famennian; Playford et al. 1976), so the age limits for the impact are Late Devonian to early Tertiary.

A further constraint on the timing of the impact comes from the cooling data derived from the Larapinta Group in the centre of Gosses Bluff. A component of old short tracks in Stairway Sandstone sample 8451-226 indicates that it cooled later than its corrected fission track age of ~180 Ma. The Stairway Sandstone samples also contain a few younger grains, which suggest that they might have experienced palaeotemperatures of about 90°C before cooling to lower temperatures as late as ~70 Ma. However, more sampling is required to determine if a significant young population occurs in the Larapinta Group.

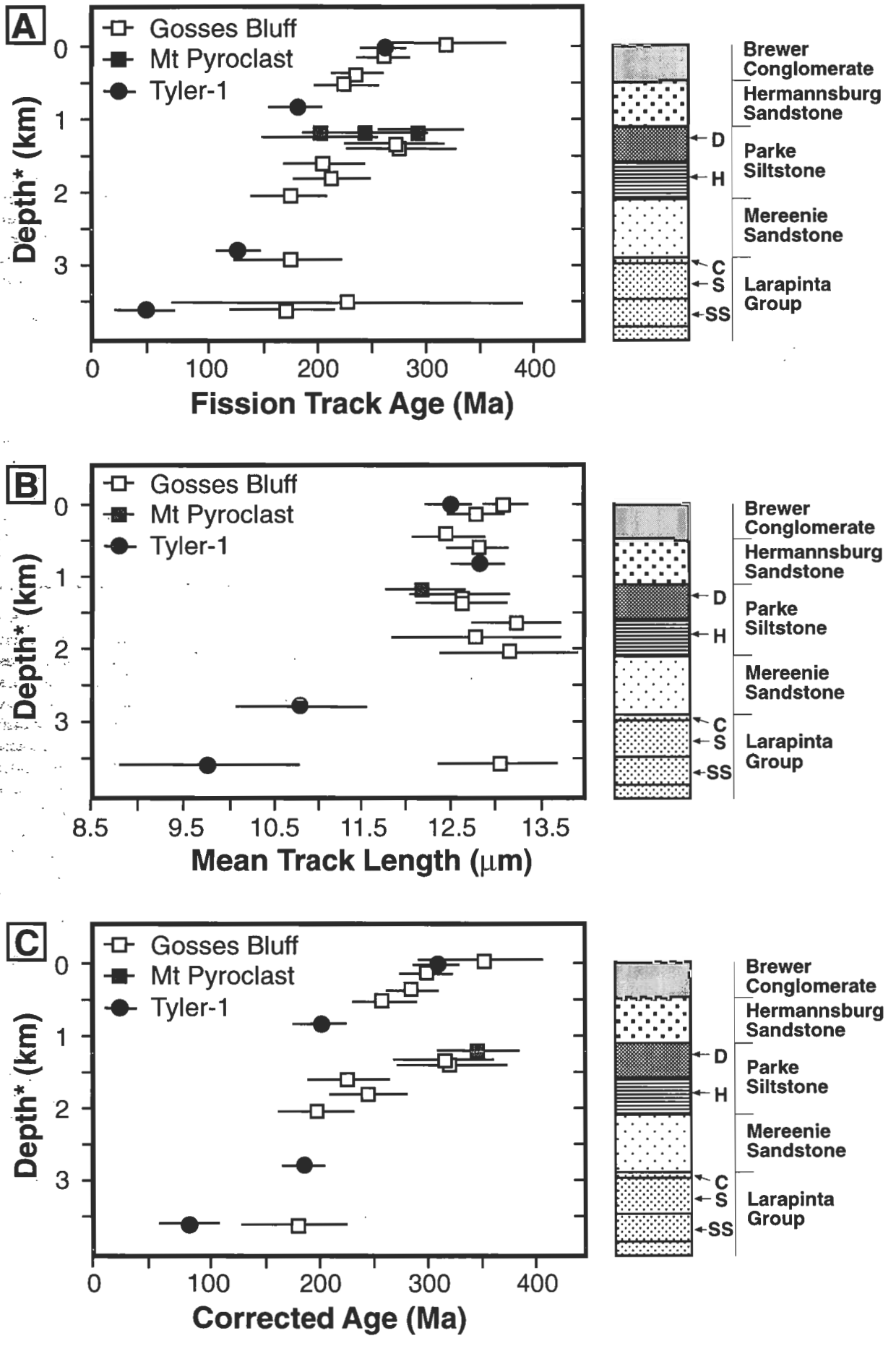
A
Gosses Bluff
Mt Pyroclast
Tyler-1
Depth* (km)
0
1
2
3
0
100
200
300
400
Fission Track Age (Ma)
Brewer Conglomerate
Hermannsburg Sandstone
Parke Siltstone
Mereenie Sandstone
Larapinta Group
D
H
C
S
SS
B
Gosses Bluff
Mt Pyroclast
Tyler-1
Depth* (km)
8.5
9.5
10.5
11.5
12.5
13.5
Mean Track Length (μm)
Brewer Conglomerate
Hermannsburg Sandstone
Parke Siltstone
Mereenie Sandstone
Larapinta Group
D
H
C
S
SS
C
Gosses Bluff
Mt Pyroclast
Tyler-1
Depth* (km)
0
100
200
300
400
Corrected Age (Ma)
Brewer Conglomerate
Hermannsburg Sandstone
Parke Siltstone
Mereenie Sandstone
Larapinta Group
D
H
C
S
SS

Table 4. Gosses Bluff palaeotemperature data

Sample number	*Maximum palaeoemperatures[a] (°C) at different times*				
	360–300[b] Ma	*240–180 Ma*	*142.5 Ma[c]*	*100–40 Ma*	*Present*
Outside structure					
Brewer Conglomerate					
8451-88	≤80	80		60	25
Within structure					
Brewer Conglomerate					
8351-22	≤90	90	<80	60	25
8451-86	≤100	100	<80	60	25
Hermannsburg Sandstone					
8451-87	≤100	100	<80	60	25
Parke Siltstone					
Dare Siltstone Member					
8451-85	≤100	100	<80	60	25
8451-84	≤100	100	<80	60	25
Harajica Sandstone Member					
8451-83		≥110	<80	60	25
8351-86		≥110	<110	60	25
8351-83		≥110	<110	60	25
Carmichael Sandstone					
8451-229		>110	<110		25
Stairway Sandstone					
8351-82		>110	<110		25
8451-226		>110	90	60	25
Melt breccia					
8351-89	≤100	100	≤80	60	25

[a] Temperatures based on heating duration of ~10 Ma, precision of ±10°C unless stated otherwise.
[b] Timing taken from Tingate (1990); [c] Timing of impact from Milton & Sutter (1987).

Apart from the single-grain-age data, computer modelling of the AFTA parameters are consistent with Milton & Sutter's (1987) $^{40}Ar/^{39}Ar$ age determination of 142.5 ± 0.8 Ma, the estimate that is applied to the discussion of the AFTA palaeotemperature data.

AFTA palaeotemperature estimates for Gosses Bluff

The variation of apatite fission-track parameters across Amadeus Basin strata within the Gosses Bluff impact structure reflects the pre-impact vertical annealing pattern. Palaeotemperature estimates for samples at various times are listed in Table 4. The corrected age variation observed in the structure is similar to that observed in Tyler No. 1. Samples from below the upper part of the Parke Siltstone and older formations are interpreted to have cooled rapidly below 110°C between 240 and 180 Ma, and were then uplifted at ~142 Ma to palaeotemperatures of 60°C or less. Maximum palaeotemperature estimates immediately before impact are shown in Table 4.

No samples from Gosses Bluff or the surrounding areas have track-length distributions consistent with residence at present temperatures for ~140 Ma. Modelling of age and length parameters suggests that all samples started cooling from ~60°C between 100 and 40 Ma.

According to a geothermal gradient of 19°C km^{-1} and a surface temperature of 25°C, the present surface at Gosses Bluff was about 1.8 km deeper between 100 and 40 Ma. The overlying material could have been crater fill or younger sediments that buried the crater. Increasing the palaeogeothermal gradient to 40°C km^{-1} would reduce to about 1 km the thickness of cover required to satisfy the AFTA data; however, no significant increase in palaeogeothermal gradient is indicated by the AFTA data in Tyler No. 1. It should be stressed that cooling from temperatures of ~60°C between 100 and 40 Ma is not limited to the vicinity of Gosses Bluff, but is part of a regional cooling pattern affecting much of central Australia (Tingate 1990), including areas to the east where Cretaceous rocks overlie the Amadeus Basin sequence. Tingate (1990) has proposed that much of central Australia was covered by Cretaceous sedimentary rocks before uplift and erosion in the Late Cretaceous and early Tertiary.

An interesting feature of the Gosses Bluff AFTA data is that they support sedimentary burial followed by erosion of the impact structure. An assumption that the present surface at Gosses Bluff was buried by thick crater-fill deposits rather than later sediments leads to inaccurate palaeotemperature predictions. Accordingly, the top of the Stairway Sandstone presently exposed in the core of the structure would have been uplifted

Figure 12 (facing page). Plots of (a) apatite fission-track age, (b) mean track length, and (c) corrected age from Gosses Bluff impact structure and surrounding region plotted against reconstructed pre-impact depth. All AFTA data are plotted at ± 2 σ; although no depth error bars are shown, the position of a Gosses Bluff sample within a given formation is only approximate. *Note that the depths are minimum estimates based on preserved stratigraphy. Tyler No. 1 AFTA data are also plotted according to the depth of recovery in the well, and show similar trends to the data derived from within the impact structure. Stratigraphic abbreviations are: D = Dare Siltstone Member, H = Harajica Sandstone Member, C = Carmichael Sandstone, S = Stokes Siltstone, and SS = Stairway Sandstone.

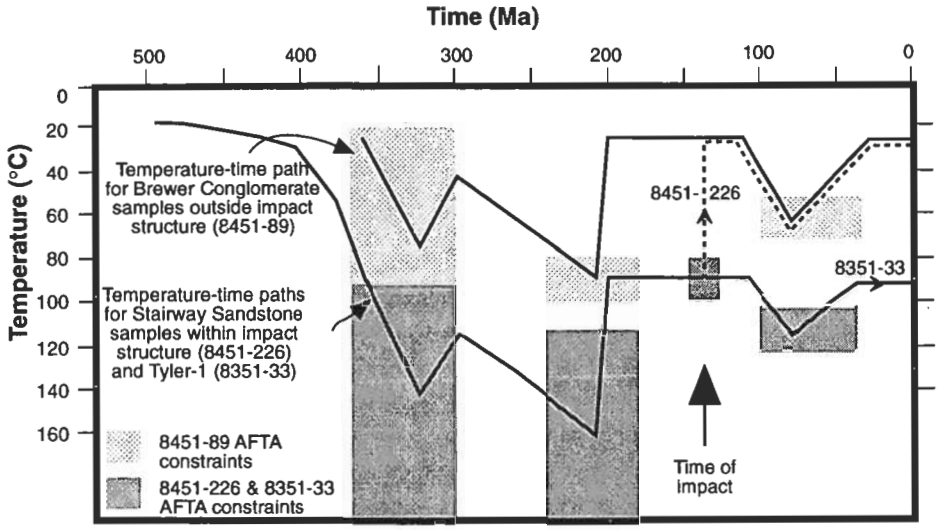

Figure 13. Thermal histories compiled from palaeotemperature information (Tables 2 and 4) for samples within and outside the Gosses Bluff impact structure. The thermal history style for samples 8451-89, 8351-33, and 8451-226 is based on type (i) in Figure 10.

from a depth of 5.3 km (1.8 km greater than its present reconstructed depth). The present geothermal gradient of 19°C km^{-1} implies that its pre-impact temperature would have been 130°C, at which all fission tracks effectively would have been totally annealed. However, fission-track data from the Stairway Sandstone in the centre of Gosses Bluff indicate that a significant proportion of tracks existed before impact at 142.5 Ma, and suggest that the present land surface in the Missionary Plain was probably at a depth of < 500 m immediately after impact.

A similar argument can be made for sample 8451-83 (Harajica Sandstone Member of the Parke Siltstone). The reconstructed stratigraphy suggests that this sample was at a minimum depth of 1.6 km (55°C) before impact. If the current surface then had been 1.8 km deeper than now, it would have been at temperatures of ~90°C before impact (according to a geothermal gradient of 19°C km^{-1}). However, modelling of age and length parameters suggest that it was <80°C at that time.

The foregoing data suggest that much of the cover over Gosses Bluff was Cretaceous sediment which was eroded away in the Late Cretaceous to early Tertiary. The depth of the original crater at Gosses Bluff was probably much less than 1.8 km. This estimate is consistent with other craters of similar size (e.g., the Ries crater, Miller & Wagner 1979; and Haughton astrobleme, Omar et al. 1987). Schematic thermal histories for samples within and outside the Gosses Bluff structure are shown in Figure 13.

Shock annealing of fission tracks

Fleischer et al. (1974) and Ahrens et al. (1970) have studied the effects of shock on track stability in apatite. Fleischer et al. (1974) investigated samples from an underground nuclear explosion, and Ahrens et al. (1970) studied high-velocity bodies colliding with large single crystals of apatite from Durango, Mexico. Different annealing behaviour was noted in the two studies, as well as different mechanical effects on the apatites. In the nuclear explosion study, annealing was significant at pressures of 3 GPa (30 kb), and the original track density had decreased to less than 10 per cent of its original value at pressures of 10 GPa (100 kb) or higher. In contrast, the laboratory experiments on the single crystals of Durango apatite showed no significant annealing for pressures of 4 GPa (40 kb); for pressures of 8 GPa (80 kb) or greater, the apatite was too shattered to measure the track density. Fleischer et al. (1974) suggested some possible explanations for the discrepancy: (a) errors in the calculation of stress in complicated natural materials; (b) a longer load duration in the nuclear explosion; (c) the microstress in a grain is different for a polymineralic aggregate and a single crystal; (d) a difference in the apatites used in the two experiments; and (e) other unidentified effects.

Apatite from samples near the centre of Gosses Bluff and Mount Pyroclast are dominated by apatites that are too fractured to determine fission-track ages. This indicates that the apatites in this study are acting more like the Durango apatite described by Ahrens et al. (1970). In fission-track dating studies involving shocked granitic rocks, highly shocked apatites appear to be less severely fractured (Miller & Wagner 1979; Omar et al. 1987). The rock type bearing the apatite apparently has an effect on the mechanical response of the apatite to shock, and might also affect its track-annealing response.

Apart from the breccias, the centre of the Gosses Bluff structure experienced maximum shock, and the shock features indicate decreasing peak pressures away from it. Here too, the rocks have been brought from the greatest depths, where they experienced higher palaeotemperatures due to burial. The maximum shock experienced by rocks here is thought to have been 10 GPa (100 kb) or more according to shock-induced planar deformation fractures (PDFs) in quartz of the Stairway Sandstone (Milton et al. 1972). PDFs in quartz elsewhere around Gosses Bluff indicate peak pressures of around 5 Gpa (50 kb; Hörz 1968), which is consistent with the distribution of shatter cones.

These pressure estimates and the Fleischer et al. (1974) relationship between pressure and annealing imply that apatites from the centre of Gosses Bluff (i.e., Stairway Sandstone) should have had their pre-impact track densities decreased by 95 per cent as a result of the shock. Samples near the edge of the bluff should have recorded a 50 per cent decrease in track densities as a result of a shock ≥5 GPa (≥50 kb). The high degree of annealing predicted by Fleischer et al. (1974) is not apparent in samples from Gosses Bluff, suggesting that the Ahrens et al. (1970) study on single crystals of apatite might be more applicable to the impact-induced response of apatite contained in the Gosses Bluff sandstones.

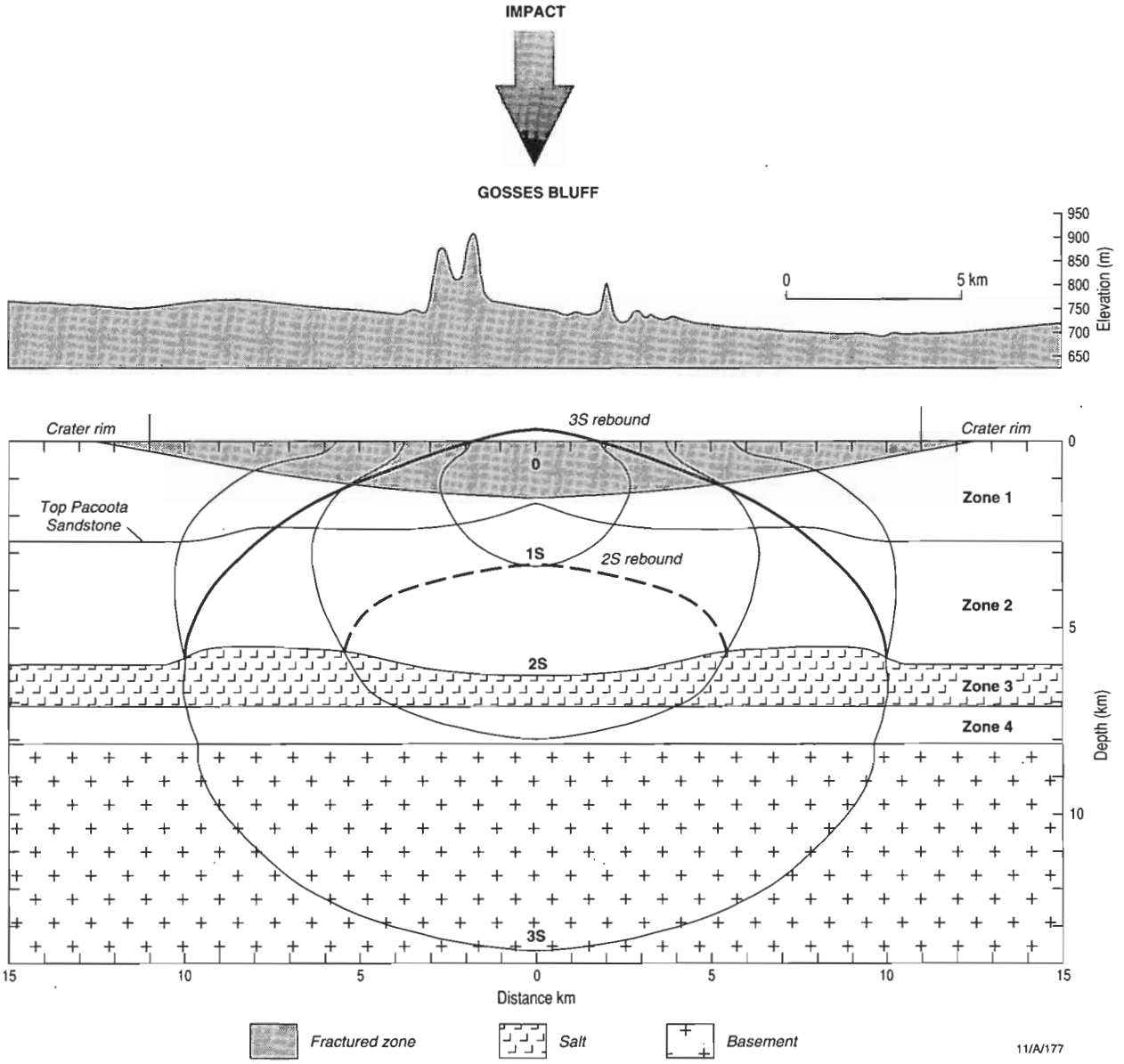

Figure 14. Idealised cross-section of Gosses Bluff shows the progress of the shock front through the Amadeus Basin strata. Much of the acoustic energy would have been reflected from the interface at the top of the Bitter Springs evaporitic interval, and this would have resulted in the formation of the central uplift within three seconds of impact.

Formation of Gosses Bluff impact structure and implications for petroleum exploration

Gosses Bluff consists of an erosional remnant of a structural uplift formed at the centre of a large impact crater. From seismic data, the original crater was 24 km in diameter, and had a large overturned rim covered by base-surge deposits which probably extended to a distance of 60 km from the point of impact. Median orbital velocities for terrestrial impacts are of the order of 20 km s^{-1} (RMS velocity; see Gault et al. 1972), suggesting that the impacting body had a mass of the order of 10^{15} g (Lindsay 1976). To provide some insight into the variables with the potential to affect the petroleum potential of an impact structure, it is necessary to understand something of the broad processes involved in cratering mechanics.

Cratering mechanics

Following impact, crater development progresses in three stages (Gault et al. 1968):

- a compressional stage;
- an excavation stage; and
- a modification stage.

During this process, the kinetic energy of the impact is expended in heating, fragmenting, and ejecting the projectile and target materials to form the crater and its associated ejecta blanket.

The compressional stage begins at the instant of impact, when two shock fronts are generated — one moving upwards into the projectile, the second moving downwards into the substrate.

During this stage, pressures and deformational stresses generated are three to four orders of magnitude greater than the material strength of the substrate. The compressional stage comes to an end when terminal engulfment occurs — that is, when the first shock wave reflects from the back of the projectile and stress relaxation can begin. In an event of the magnitude of Gosses Bluff, this stage was probably completed in as little as 100 ms.

During the excavation stage, the shock-wave geometry is roughly hemispherical. Compressed material expands radially, distributing kinetic energy over an ever-increasing volume of target material (Gault et al. 1968). Crater growth is a well-regulated process during which the enlarging cavity takes on the same form as the final crater, while ejecta move up and shear out from its walls in a steady flow. Ejecta formation is complex, but three broad categories of sediment are produced: bulk ejecta, ballistic ejecta, and ground-flow ejecta. Bulk ejecta form near the crater rim, where tangential flow causes the substrate to move upwards and outwards, folding and completely overturning the moderately coherent rock. The eroded remnants of the bulk ejecta have been imaged seismically at Gosses Bluff 12 km from the centre of the structure (Figs. 4 and 5). Ballistic ejecta are individual fragments of target material that are ejected completely from the crater and fall back to Earth to be incorporated into the ground-flow ejecta, or to form an ejecta blanket within or beyond the crater rim. Ground-flow ejecta result from the formation of base surges — large-scale gravity flows which flow outward at high velocity from the crater to form a hot gaseous blanket over the surrounding area. The base surge is a density current formed by expanding gases moving laterally from the centre of the impact, and picking up solid particulate material as it proceeds.

The modification stage may involve a number of factors depending on the scale of the event — including slumping of the crater rim, formation of a central dome due to isostatic readjustment, flooding by lava, and erosion of the crater.

Reservoir geometry

Dietz (1967) noted the apparently anomalously large dimensions of the central uplift of Gosses Bluff, and suggested that the crater was the product of a very high-velocity object, which implied that it was a cometary impact. Milton et al. (1972) suggested that the unique central uplift of the Gosses Bluff structure was a response to upward acceleration due to the zone of rarefaction following passage of the primary shock wave. Such an origin is unlikely, as zones of central uplift in craters are generally an indication of a shallow, more consolidated substrate beneath the structure. Whatever origin is ascribed to the crater, the central uplift is considerably greater than might be predicted from empirical studies (Grieve & Pesonen 1992), suggesting the involvement of another set of variables.

Oberbeck & Quaide (1967) and Quaide & Oberbeck (1968) made detailed empirical studies of crater morphology resulting from hypervelocity impacts into unconsolidated soils overlying bedrock. Although the results of their work are not strictly applicable to the Gosses Bluff setting, they do offer insights into the morphology of Gosses Bluff (Lindsay 1976). Oberbeck & Quaide (1967) and Quaide & Oberbeck (1968) found that, when a hypervelocity body penetrates a layer of unconsolidated materials overlying bedrock, the morphology of the resulting crater is determined by the ratio of the crater-rim diameter to the thickness of the unconsolidated layer. When the ratio is small, normal crater development occurs because the thickness of the unconsolidated layer is close to normal crater depth. However, as the ratio increases, the bedrock substrate interferes with normal crater development. Initially, flat-bottomed craters develop and, in the extreme, complex concentric craters characterised by a double annular or arcuate structure are formed. These complex structures are essentially craters within craters resulting from the interaction of the expanding shock wave with the interface between the unconsolidated and consolidated materials.

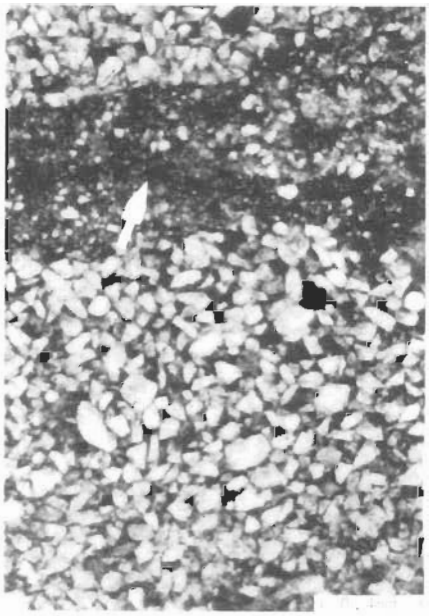

Figure 15. Photomicrograph of a thin section from the Stairway Sandstone from a depth of 1400 m in Gosses Bluff No. 2 well (after Berry et al. 1989). The photograph shows a thin zone of crushed quartz grains (arrow) produced by compression during the passage of the primary impact shock wave. The crushed quartz is well cemented, probably a product of post-impact precipitation of silica.

The Amadeus Basin provides an analogue because the high-velocity evaporites of the Bitter Springs Formation form an acoustic substrate. The Gosses Bluff central uplift was formed when the primary shock wave, radiating downward from the point of impact, reached the clastic/evaporite interface at the top of the Gillen Member of the Neoproterozoic Bitter Springs Formation (Fig. 14). In response to the high-impedance contrast across this interface, much of the energy of the shock wave was reflected back towards the surface. As it approached the unconstrained rocks nearer the surface, the rapidly decelerating shock wave thrust the centre of the impact structure upward, and in the process completely brecciated a zone of material to a depth of 2300 m beneath the structure and displaced large volumes of well-consolidated clastic rock. This displaced volume was taken up by lateral movement of salt within the Gillen Member. Beneath the structure, the salt forms a 2000-m-thick dome which has roughly the same diameter as the crater. The suggestion that the apparently earlier Gardiner–Tyler anticlinal high (Fig. 3) is a salt-generated structure insinuates that salt was unstable in the area, and might have migrated rapidly into the strained region beneath the impact.

Reservoir quality

The Ordovician Pacoota Sandstone, the main reservoir interval in the Amadeus Basin, lies at the base of the Larapinta Group. It is a highly cyclical unit composed of many thin sequences or

parasequences deposited in a shallow-marine to fluvial setting. In general, it has poor reservoir quality, and a maximum porosity of 10 per cent (Lindsay & Gorter 1992), except where its potential is enhanced by another mechanism such as fracturing. The key to the survival and creation of porosity has been a balance between mechanical sorting of the detrital materials and later diagenetic alteration. Sands that were well-sorted at the tops of the major cycles became quartz-rich as their feldspar was removed. This resulted in massive quartz cementation. In less well-sorted sands, primary porosity was poor and was reduced even further by clay minerals. Lower in the formation, reservoir units at the top of shallowing-upward cycles are well sorted, and provide primary porosity without the extremes of either quartz cementation or clay minerals. Feldspar was abundant, allowing the development of a secondary porosity. However, even arkosic sandstones may be impermeable owing to dolomite cementation.

The potential effects of hypervelocity cratering on reservoir quality are difficult to evaluate fully. Fracturing of bedrock beneath impact structures can be extensive, but the effect fades in all directions away from the point of impact as the fractures became more widely spaced. The thickness of the 'brecciated' lens or dish-shaped zone (B) was found to be $B = 0.624D_t^{1.2658}$, where D_t is the depth of the crater in metres (Baldwin 1963). This relationship is moderately consistent with observed fracturing in zone 1 beneath the Gosses Bluff structure.

The Pacoota Sandstone lies just below the 'brecciated' lens (zone 1) beneath Gosses Bluff. Even though extensively fractured, the fractures do not enhance permeability or porosity to any great extent. In large part, the fractures are filled by recrystallised fine-grained quartz. This is consistent with observations made by Kieffer et al. (1976) on weakly shocked (<10 GPa; <100 kb) porous quartzites, which showed that a shock wave had a tendency to collapse pores by shearing grains past each other on fracture surfaces. They also found that small amounts of high-pressure phases, thetomorphic glass, and melt can form. Extension fractures develop and pore water is heated but not vaporised after passage of the shock wave. At Gosses Bluff, heated pore waters might have partly dissolved glass and other unstable phases, and precipitated them as fine-grained quartz. Other potential reservoir units above the Pacoota Sandstone, such as the Stairway Sandstone in zone 1, have been highly fractured, and their reservoir properties enhanced to some degree. However, even at these higher levels, diagenesis has significantly reduced the potential improvements in reservoir quality by the remobilisation of quartz as discussed above (Fig. 15).

The effects of brecciation and fracturing due to impact on the creation of a suitable petroleum habitat are potentially very large. However, without an effective seal a major impact does little more than provide a conduit for the escape of hydrocarbons into the atmosphere. Two major structures recently identified seismically in the Eromanga Basin appear to be of impact origin. Since they were formed during the main period of basin subsidence, effective seals have been deposited over the structures, and raise the possibility that they may have potential as hydrocarbon traps (Gorter et al. 1989; Longley 1989).

Thermal effects

Energy partitioning during a hypervelocity impact is complex, and determined by a number of variables — such as the velocity and density of the projectile, the magnitude of the event, and the nature of the substrate, among others. The kinetic energy of an impact is dispersed in compressing, comminuting, and ejecting the projectile and substrate from the crater, but much of it is irreversibly lost as heat.

Heat energy may be released by vaporising or fusing the projectile and target, or lost by radiation or conduction. Most of the phase changes occur early in the impact process during the compressional stage shortly before terminal engulfment. In impacts developed in crystalline rock, much of the melt produced during this stage remains on the crater floor (Dence 1965, 1968; French 1970). The Gosses Bluff impact produced ejecta, probably of the order of 10^{18}g, of which about 5 per cent would have been fused or vaporised (e.g., Dence 1965). The fused and glassy clasts at Mount Pyroclast probably represent disrupted crater floor deposits which have undergone some lateral transport (Milton et al. 1972). However, the high fluid content of the sedimentary rocks of the Amadeus Basin would have contributed to the generation of large volumes of volatiles and to the dispersal of most of the early-formed melt (Kieffer & Simonds 1980), which was probably associated with a well-developed base-surge phase of cratering. This large-scale high-temperature base surge probably produced deposits that blanketed the countryside for 60 km or more beyond the impact site (Moore 1967; Rohrer 1965). How effective both this blanket and the crater-floor deposits were in heating the underlying bedrock is debatable.

The apatite fission-track data from at or below the crater floor in the Gosses Bluff impact structure do not show evidence of significant annealing associated with the impact, either from the shock wave or overlying crater fill (now eroded). Rather, the main effect of the event appears to have been to uplift and cool strata from deeper levels to a shallower level. The data vary with the stratigraphy across the structure and reflect the pre-impact thermal history.

Although many individual clasts in the melt breccia at Gosses Bluff were heated to high temperatures (>500°C) from the initial shock wave resulting from impact, thermal conditions due to heat transfer were not sufficient to cause significant annealing in apatite within the breccia. The AFTA data from Mount Pyroclast suggest that hot clasts were rapidly quenched during and after deposition of the breccias, probably concurrent with the early introduction of water.

Petroleum generation

AFTA results from Tyler No. 1 and outcrop samples at Gosses Bluff place constraints on the thermal history of the main source rocks in the Cambro-Ordovician and Neoproterozoic formations. AFTA results from Tyler No. 1 indicate that sedimentary rocks deposited between 450 and 350 Ma cooled from maximum temperatures at approximately 200 Ma (Fig. 10). Samples from Gosses Bluff show evidence of cooling at the same time (Fig. 13).

Petroleum may be generated when sedimentary rocks are first heated to temperatures greater than ~60°C. Apatite fission-track data indicate that this was likely to have happened in Tyler No. 1 and at Gosses Bluff before 200 Ma, when the rocks cooled from their maximum palaeotemperatures. The timing of impact at Gosses Bluff (~140 Ma) postdates the timing of maximum temperature in the potential source rocks, and therefore — irrespective of sealing problems — was unfavourable for the structure to receive a large petroleum charge from regional heating of source rocks. The most likely source of hydrocarbons within

the impact structure is migration from neighbouring pre-existing hydrocarbon accumulations.

The AFTA results from Gosses Bluff indicate that the principal thermal effect of impact on the sedimentary rocks in the central uplift was cooling related to exhumation. Heat generated during the impact had no significant effect on the underlying strata, and would have been unlikely to cause any thermal maturation of source rocks.

Relation to other impact sites

Australian impact structures with petroleum potential include buried Early Cretaceous impact structures in the Eromanga Basin (Flynn 1989; Gorter et al. 1989; Longley 1989). These structures, which are ~1 km deep, formed during basin subsidence, and consequently have some seal development and favourable timing with respect to petroleum generation. In North America, oil is associated with the central uplift and rim in impact craters in the Williston Basin and at a number of other sites (Donofrio 1981; Grieve & Masaitis 1994).

Gosses Bluff has a number of factors that minimise its potential as a petroleum play (e.g., lack of seal, unfavourable timing of impact), but it does provide a useful model for further exploration of impact sites in sedimentary basins. In particular, it shows that, if sealed, structural closure can vary with depth. Low-porosity lithologies can produce fracture-dominated reservoirs. In upper levels of the structure, the reservoir lithologies can be expected to be intensely deformed and block-faulted. Gosses Bluff demonstrates that impact structures developed within thick sedimentary sequences are unlikely to evince significant thermal effects beneath the crater. It also shows that the lithologic variation within the target sedimentary sequence influences the shape of the impact structure and the resulting geometry of potential reservoirs.

Conclusions

A Late Jurassic hypervelocity impact into the thickest part of the Amadeus Basin produced a crater 24 km in diameter with a well-developed central uplift. The central uplift was a consequence of a rebound of energy from the surface of the Neoproterozoic evaporites of the Bitter Springs Formation 6300 m beneath the structure. The impact-related brecciation of the sedimentary units beneath the Gosses Bluff structure increased both porosity and permeability of potential reservoir units. The effectiveness of the fracturing mechanism was, however, reduced by the remobilisation of silica following impact.

Without an effective seal, hydrocarbons were at best unlikely to be retained in the Gosses Bluff structure. Hydrocarbon potential was reduced even further by the timing of hydrocarbon generation. AFTA results indicate that peak hydrocarbon generation preceded the earliest Mesozoic, well before the Gosses Bluff impact. Heat generated by the impact had little effect on the underlying strata, and did not contribute to hydrocarbon generation. The structure is considered to have limited potential for hydrocarbon accumulation, but the major ring anticline generated at depth beneath the crater rim remains untested.

Acknowledgments

We thank Magellan Petroleum Australia Ltd, in Brisbane, for providing access to data and facilities; Geotrack International for their support of our study; and Drs Dennis Arne, George Williams, and Andrew Glikson for their reviews of the manuscript. Peter Tingate acknowledges the financial and logistic support from the University of Melbourne; AGSO's support of the fission-track component of the study; Prof. A.J. Gleadow and Dr O.P. Singleton for their supervision of his PhD study; and the financial support from the National Centre for Petroleum Geology & Geophysics and the Australian Petroleum Cooperative Research Centre while he prepared his contribution to the manuscript.

References

Ahrens, T.H., Fleischer, R.L., Price, P.B. & Woods, R.T., 1970. Erasure of fission tracks in glasses and silicates by shock waves. Earth and Planetary Science Letters, 8, 420–426.

Baldwin, R.B., 1963. The measure of the Moon. University of Chicago Press, Chicago.

Berry, M.D., Milne, N.A. & Roe, L.E., 1989. Gosses Bluff No. 2, O.P. 175 Northern Territory, well completion report. Magellan Petroleum Australia Ltd (unpublished).

Brunnschweiler, R.O., Leslie, R.B. & Richards, K.A., 1959. Review of geological and geophysical information, Gosses Bluff, N.T. Broken Hill Co. Pty. Ltd., Report 4300–G–30 (unpublished); AGSO open-file report 62/416.

Cook, P.J., 1968. The Gosses Bluff cryptoexplosion structure. Journal of Geology, 76(2), 123–139.

Crook, K.A.W. & Cook, P.J., 1966. Gosses Bluff — diapir, crypto-volcanic structure, or astrobleme? Journal of the Geological Society of Australia, 14, 495–516.

Dence, M.R., 1965. The extraterrestrial origin of Canadian craters. Annals of the New York Academy of Science, 123, 941–969.

Dence, M.R., 1968. Shock zoning at Canadian craters. In: French, B.M. & Short, N.M (Editors), Shock metamorphism of natural materials. Mono Book Corp., Baltimore 339–362.

Dietz, R.S., 1967. Shatter cone orientation at Gosses Bluff astrobleme. Nature, 216, 1082–1084.

Donofrio, R.R., 1981. Impact craters: implications for basement hydrocarbon production. Journal of Petroleum Geology, 3, 279–302.

Duddy, I.R., Green, P.F. & Laslett, G.M., 1988. Thermal annealing of fission–tracks in apatite: III. Variable temperature behaviour. Chemical Geology (Isotope Geoscience Section), 73, 25–38.

Fleischer, R.L. & Hart, H.R., 1972. Fission track dating: techniques and problems. In: Bishop, W.W., Miller, D.A. & Cole, S. (Editors), Calibration of hominid evolution. Scottish Academic Press, Edinburgh, 135–170.

Fleischer, R.L., Woods, R.T., Hart, H.R. Jr, Price, P.B. & Short, P.B., 1974. Effect of shock on fission track dating of apatite and sphene crystals from the Hardhat and Sedan underground nuclear explosions. Journal of Geophysical Research, 79, 339–342.

Flynn, M., 1989. The Mulkarra structure: a possible buried impact crater in the western Eromanga Basin, Australia. In: O'Neil, B.J. (Editor), The Cooper and Eromanga Basins, Australia. Proceedings of the Petroleum Exploration Society of Australia, the Society of Petroleum Engineers, and the Australian Society of Exploration Geophysicists (SA Branches), Adelaide, 431–439.

French, B.M., 1970. Possible relations between meteorite impact and petrogenesis, as indicated by the Sudbury structure, Ontario, Canada. Bulletin of Volcanology, 34–2, 466–517.

Galbraith, R.F., 1981. Graphical display of estimates having different standard error. Technometrics, 30, 271–281.

Galbraith, R.F., 1992. Statistical models for mixed ages. Abstracts with programs, 7th International Workshop on Thermochronology Philadelphia, July 13–17, 7.

Gault, D.E., Quaide, W.L. & Oberbeck, V.R., 1968. Impact cratering mechanics and structures. In: French, B.M. & Short, N.M. (Editors), Shock metamorphism of natural materials. Mono Book Corp., Baltimore, 87–100.

Gault, D.E., Hörz, F. & Hartung, J., 1972. Effects of microcratering on the lunar surface. Proceedings of the Third Lunar Science Conference, Supplement 3. Geochimica et Cosmochimica Acta, 3, 2713–2734.

Gleadow, A.J.W., 1981. Fission-track dating: what are the real alternatives? Nuclear Tracks, 5(1/2), 3–14.

Gleadow, A.J.W., Duddy, I.R. & Lovering, J.F., 1983. Fission track analysis: a new tool for the evaluation of thermal histories and hydrocarbon potential. APEA Journal, 23, 93–102.

Gleadow, A.J.W., Duddy, I.R., Green, P.F. & Lovering, J.F., 1986. Confined fission track lengths in apatite — a diagnostic tool for thermal history analysis. Contributions to Mineralogy and Petrology, 94, 405–415.

Gorter, J.D., 1984. Source potential of the Horn Valley Siltstone, Amadeus Basin. APEA Journal, 24, 66–90.

Gorter, J.D., Gostin, V.A. & Plummer, V.S., 1989. The enigmatic sub-surface Tookoonooka Complex in south-west Queensland: its impact origin and implications for hydrocarbon accumulations. In: O'Neill, B.J. (Editor), The Cooper and Eromanga Basins, Australia. Proceedings of the Petroleum Exploration Society of Australia, the Society of Petroleum Engineers, and the Australian Society of Exploration Geophysicists (SA Branches), Adelaide, 441–456.

Gorter, J.D., Korsch, R.J., Nicoll, R.S. & Summons, R.E., 1996. Thermal history of the Gosses Bluff impact structure, central Australia, from conodont colour-alteration indices: implications for hydrocarbon prospectivity and erosional history. AGSO Journal of Australian Geology & Geophysics, this issue.

Green, P.F., 1981. A new look at statistics in fission-track dating. Nuclear Tracks, 5, 77–86.

Green, P.F., 1986. On the thermo-tectonic evolution of northern England: evidence from fission track analysis. Geological Magazine, 123, 493–506.

Green, P.F., 1988. The relationship between track shortening and fission track age reduction in apatite: combined influences of inherited instability, annealing anisotropy, length bias and system calibration. Earth and Planetary Science Letters, 89, 323–328.

Green, P.F., Duddy, I.R., Gleadow, A.J.W., Tingate, P.R. & Laslett, G.M., 1985. Fission-track annealing in apatite: track length measurements and the form of the Arrhenius Plot. Nuclear Tracks, 10(3), 323–328.

Green, P.F., Duddy, I.R., Gleadow, A.J.W., Tingate, P.R. & Laslett, G.M., 1986. Thermal annealing of fission tracks in apatite. 1: A qualitative description. Chemical Geology (Isotope Geoscience Section), 59, 237–253.

Green, P.F., Duddy, I.R., Gleadow, A.J.W & Lovering J.F., 1989a. Apatite fission track analysis as a paleotemperature indicator for hydrocarbon exploration. In: Naeser, N.D. & McCulloch, T. (Editors), Thermal history of sedimentary basins — methods and case histories. Springer-Verlag, New York.

Green, P.F., Duddy, I.R., Laslett, G.M. & Gleadow, A.J.W., 1989b. Thermal annealing of fission tracks in apatite. 4: Quantitative modelling techniques and extension to geological timescales. Chemical Geology (Isotope Geoscience Section), 79, 155–182.

Grieve, R.A.F. & Masaitis, V.L., 1994. The economic potential of terrestrial impacts. International Geology Review, 36, 105–151.

Grieve, R.A.F. & Pesonen, L.J., 1992. The terrestrial impact cratering record. Tectonophysics, 216, 1–30.

Hörz, F., 1968. Statistical measurements of deformation structures and refractive indices in experimentally shock loaded quartz. In: French, B.M. & Short, N.M. (Editors), Shock metamorphism of natural materials. Mono Book Corp., Baltimore, 243–254.

Hurford, A.J. & Green, P.F., 1982. A users' guide to fission track dating calibration. Earth and Planetary Science Letters, 59, 343–354.

Hurford, A.J. & Green, P.F., 1983. The zeta age calibration of fission track dating. Chemical Geology (Isotope Geoscience Section), 1, 285–317.

Jones, B.G., 1972. Upper Devonian to Lower Carboniferous stratigraphy of the Pertnjara Group, Amadeus Basin, central Australia. Journal of the Geological Society of Australia, 19, 229–249.

Kamp, P.J.J. & Green, P.F., 1990. Thermal and tectonic history of selected Taranaki Basin (New Zealand) wells assessed by apatite fission track analysis. American Association of Petroleum Geology, Bulletin 74, 1401–1419.

Kieffer, S.W., Phakey, P.P. & Christie, 1976. Shock processes in porous quartzite: transmission electron microscope observations and theory. Contributions to Mineralogy and Petrology, 59, 41–93.

Kieffer, S.W. & Simonds, C.H., 1980. Role of volatiles and lithology in impact cratering process. Reviews of Geophysics and Space Physics, 18(1), 143–181.

Kohn, B.P., Osadetz, K.G. & Bezys, R.K., 1995. Apatite fission track dating of two crater structures in the Canadian Williston Basin. Bulletin of Canadian Petroleum Geology, 43, 54–64.

Laslett, G.M., Gleadow, A.J.W. & Duddy, I.R., 1984. The relationship between fission track length and density in apatite. Nuclear Tracks, 9, 29–38.

Laslett, G.M., Green, P.F., Duddy, I.R. & Gleadow, A.J.W., 1987. Thermal annealing of fission-tracks in apatite. 2: A quantitative analysis. Chemical Geology (Isotope Geoscience Section), 65, 1–13.

Lindsay, J.F., 1976. Lunar stratigraphy and sedimentology. Elsevier, Amsterdam.

Lindsay, J.F., 1987. Late Proterozoic evaporites in the Amadeus Basin, central Australia and their role in basin tectonics. Geological Society of America, Bulletin 99, 852–865.

Lindsay, J.F., 1992. Extraterrestrial soils — the lunar experience. In: Martini, I.P. & Chesworth, W. (Editors), Weathering, soils & paleosols. Elsevier, Amsterdam, 41–70.

Lindsay, J.F. (Editor), 1993. Geological atlas of the Amadeus Basin (25 plates). Australian Geological Survey Organisation.

Lindsay, J.F. & Korsch, R. J., 1989. Interplay of tectonics and sea-level changes in basin evolution: an example from the intracratonic Amadeus Basin, central Australia. Basin Research, 2, 3–25.

Lindsay, J.F. & Korsch, R.J., 1991. The evolution of the Amadeus Basin, central Australia. In: Korsch, R.J. & Kennard, J.M. (editors), Geological and geophysical studies in the Amadeus Basin, central Australia. Bureau of Mineral Resources, Australia, Bulletin, 236, 7–32.

Lindsay, J.F. & Gorter J.D., 1992. Clastic petroleum reservoirs of the Late Proterozoic and early Paleozoic Amadeus Basin, central Australia. Chapter 3 in: Rhodes, E.G. & Moslow, T.F. (Editors), Marine clastic reservoirs: examples and analogs. Springer-Verlag, New York, 39–74.

Longley, I.M., 1989. The Talundilly anomaly and its implications for hydrocarbon exploration of Eromanga astroblemes. In: O'Neill, B.J. (Editor), The Cooper and Eromanga Basins, Australia. Proceedings of the Petroleum Exploration Society of Australia, the Society of Petroleum Engineers, and the Australian Society of Exploration Geophysicists (SA Branches), Adelaide, 473–490.

Mabbutt, J.A., 1965. The weathered land surface in central Australia. Zeitschrift fur Geomorphologie, 9, 82–114.

Miller, D.S. & Wagner, G.A., 1979. Age and intensity of thermal events by fission track analysis: the Ries impact crater. Earth and Planetary Science Letters, 43, 351–358.

Milton, D.F. & Sutter, J.F., 1987. Revised age for the Gosses Bluff impact structure, Northern Territory, Australia, based on $^{40}Ar/^{39}Ar$ dating. Meteoritics, 22, 281–287.

Milton, D.J., Barlow, B.C., Brett, R., Brown, A.R., Glikson, A.Y., Manwaring, E.A., Moss, F.J., Sedmik, E.C.E., van Son, J. & Young, G.A., 1972. Gosses Bluff impact structure, Australia: geological and geophysical techniques establish the origin of an analog of lunar craters. Science, 175, 1199–1207.

Milton, D.J., Glikson, A.Y., & Brett, P.R., 1996. Gosses Bluff — a latest Jurassic impact structure, central Australia. Part 1: geological structure, stratigraphy, and origin. AGSO Journal of Australian Geology & Geophysics, this issue.

Milton, D.J., Moss, F.J. & Barlow, 1978. Regional geology, Gosses Bluff impact structure, Northern Territory, 1:50 000 geologic map. Bureau of Mineral Resources, Australia.

Moore, J.G., 1967. Base surge in recent volcanic eruptions. Bulletin of Volcanology, 30, 337–363.

Moss, F.J., 1964. Gosses Bluff seismic survey, Amadeus Basin, Northern Territory, 1962. Bureau of Mineral Resources, Australia, Record 1964/66.

Oberbeck, V.R. & Quaide, W.L., 1967. Estimated thickness of a fragmental surface layer of Oceanus Procellarum. Journal of Geophysical Research, 72, 4697–4704.

Omar, G., Johnson, K.R., Hickey, L.J., Robertson, P.B., Dawson, M.R. & Barnosky, C.W, 1987. Fission-track dating of Haughton astrobleme and included biota, Devon Island, Canada. Science, 237, 1603–1605.

Pemberton, R.L. & Planalp, R.N., 1965. Well completion report, Gosses Bluff No. 1 well. Exoil (NT) Pty Ltd, Petroleum Search Subsidy Act, Report 65/4132 (unpublished).

Playford, G., Jones, B.G. & Kemp, E.M., 1976. Palynological evidence for the age of the synorogenic Brewer Conglomerate, Amadeus Basin, central Australia. Alcheringa, 1, 235–243.

Quaide, W.L. & Oberbeck, V.R., 1968. Genetic implications of lunar regolith thickness variations. Icarus, 9, 446–465.

Rohrer, R., 1965. Base surge and cloud formation — Project pre–Schooner. University of California, Lawrence Radiation Laboratory, PNE–503F.

Shaw, R.D., Zeitler, P., McDougall, I. & Tingate, P.R., 1992. The Palaeozoic history of an unusual intracratonic thrust belt in central Australia based on $^{40/39}Ar$, K/Ar and fission track dating. Journal of the Geological Society of London, 149, 937–954.

Tingate, P., 1990. Apatite fission track studies from the Amadeus Basin, central Australia. PhD Thesis, University of Melbourne (unpublished).

Tingate, P.R., 1991. Apatite fission track analysis of the Pacoota and Stairway Sandstones, Amadeus Basin, central Australia. In: Korsch, R.J & Kennard, J.N. (Editors), Geological and geophysical studies in the Amadeus Basin, central Australia. Bureau of Mineral Resources, Australia, Bulletin 236, 525–540.

Wells, A.T., Forman, D.J., Ranford, L.C. & Cook, P.J., 1970. Geology of the Amadeus Basin. Bureau of Mineral Resources, Australia, Bulletin 100.

Wopfer, H., 1978. Silcretes of northern South Australia and adjacent regions. In: Langford-Smith, T. (Editor), Silcrete in Australia. Department of Geography, University of New England, Armidale.

AGSO Journal of Australian Geology & Geophysics, 16 (4), 553–560

Thermal history of the Gosses Bluff impact structure, central Australia, from conodont colour-alteration indices: implications for hydrocarbon prospectivity and erosional history

John D. Gorter[1], Russell J. Korsch[2], & Robert S. Nicoll[2]

Gosses Bluff is the remnant of a latest Jurassic asteroid or comet impact structure in the Amadeus Basin, central Australia. Conodonts have been successfully extracted from rocks exposed at the central uplift core of the impact structure, as well as from samples in petroleum exploration wells drilled into the structure. Maximum maturation of the source beds in the Early Ordovician Horn Valley Siltstone is reflected by the conodont colour-alteration index (CAI) value of 4 in Gosses Bluff No. 2 well. A similar maturation level was attained by late Early Ordovician carbonates of the Stokes Siltstone, both in outcrop and drilled at shallow levels in Gosses Bluff No. 1 well. A value of CAI 4 at the present surface indicates that these rocks were uplifted at least 4500 m as a result of the impact.

Combined with the CAI values from conodonts recovered from petroleum exploration wells to the northeast (Tyler No. 1) and southeast (Palm Valley No. 1 and West Waterhouse No. 1), the conodont CAI values derived from Gosses Bluff allow the construction of a palaeodepth trend, similar to the CAI–depth trend of the Appalachians and the Kidson Sub-basin of the Canning Basin. This indicates that about 500 m of rock has been eroded from above the Gosses Bluff and Tyler No. 1 well area, and that about 1700–2800 m has been eroded from the Palm Valley and Waterhouse Range Anticlines. The CAI 4 value for the Horn Valley Siltstone, the primary rich hydrocarbon source rock in the basin, indicates that the organic matter in this formation in the Missionary Plain had reached a level of maturity equivalent to that for production of dry gas before about 140 Ma.

Introduction

Gosses Bluff, a prominent circular feature in the Missionary Plain, is 160 km west-southwest of Alice Springs, Northern Territory, in the Amadeus Basin (Fig. 1). It has a deformed outer ring about 24 km in diameter, and is interpreted to be a complex impact structure caused by a comet or asteroid impact (Crook & Cook 1966; Cook 1968; Milton et al. 1972, 1996a, 1996b). Milton & Sutter (1987) determined a $^{40}Ar/^{39}Ar$ age of 142.5 ± 0.8 Ma for a clast consisting essentially of sanidine from melt breccia at Mount Pyroclast, about 6 km to the south of Gosses Bluff No. 1 well, and interpreted this as the time of the impact. This indicates a latest Jurassic age for the impact according to the recent assessment of the age control for the Jurassic–Cretaceous boundary (Jones 1996).

[1] Hardy Petroleum Ltd, PO Box 1265, West Perth, WA 6872.
[2] Division of Marine, Petroleum & Sedimentary Resources, Australian Geological Survey Organisation, GPO Box 378, Canberra, ACT 2601.

Detailed geological mapping of the Gosses Bluff area by Milton et al. (1972, 1996a, 1996b) and Glikson et al. (1969) shows that Ordovician strata, including limestone of the Stokes Siltstone, are exposed at the surface. Seismic profiles tied to well control outside the Gosses Bluff structure show that the Stokes Siltstone is deeply buried adjacent to the impact structure (Milton et al. 1996a, figs. 6, 7, and 28). Gosses Bluff provides a suitable structure for the investigation of the maturation level, through the study of conodonts (Fig. 2), of the late Early Ordovician Stokes Siltstone and the Early Ordovician Horn Valley Siltstone, which are otherwise buried by over 3 km of the Late Devonian Pertnjara Group in the Missionary Plain. The Horn Valley Siltstone contains the most important hydrocarbon source rocks in the Amadeus Basin (Gorter 1984), and was the source of the hydrocarbons in the Palm Valley Gas Field and the Mereenie Oil and Gas Field, the two commercial fields in the basin (Fig. 1).

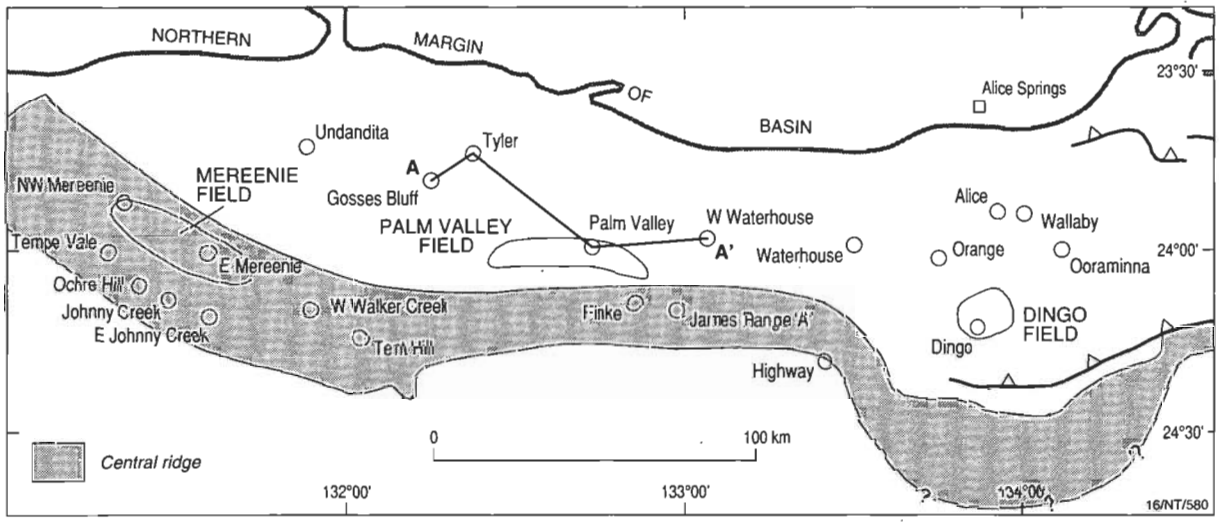

Figure 1. Locality map showing the locations of Gosses Bluff, wells mentioned in the text, the northern boundary of the Amadeus Basin, and the line of section shown in Figure 5.

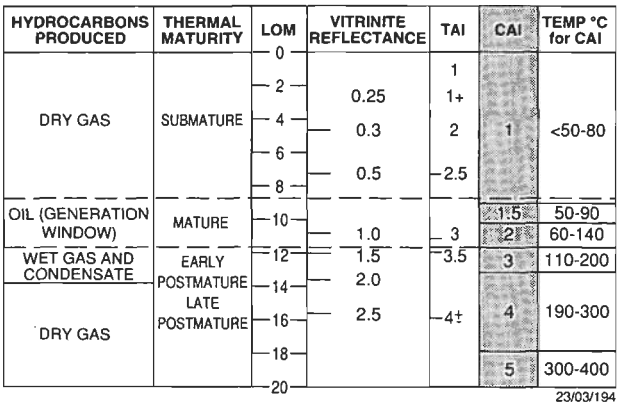

Figure 2. Comparison of hydrocarbon-maturity-indicator ranges (after Perry et al. 1983; Epstein et al. 1977): LOM, level of organic maturity; CAI, conodont colour alteration index; TAI, thermal alteration index.

In the Amadeus Basin, conodonts have been found in the marine interval from low in the Pacoota Sandstone (Fig. 3) through to the lower part of the Stokes Siltstone (Cooper 1981; Nicoll, in Shergold et al. 1991). They range in age from the Late Cambrian to the late Early Ordovician, and are especially abundant in limestone and shale of the Horn Valley and Stokes Siltstones (Nicoll, in Shergold et al. 1991). The progressive darkening of these phosphatic microfossils, quantified as the conodont colour-alteration index (CAI), has been used to determine thermal maturation levels and organic maturity profiles in marine sedimentary rocks, and was first applied in the Appalachians (Epstein et al. 1977). Conodonts from many localities in the Amadeus Basin have been used previously in the study of the potential maturation of hydrocarbons (Gorter & Nicoll 1983; Gorter 1984), although a depth-related maturation profile had not been previously constructed, principally because less than 1000 m of the sedimentary succession contains conodonts. The thick Neoproterozoic and Early Cambrian succession in the basin predates the appearance of conodonts in the sedimentary record. Further, the Late Ordovician to Devonian rocks in the Amadeus Basin are non-marine, and contain only scattered recycled Ordovician conodonts (Young et al. 1987).

The establishment of a maturation profile for a sedimentary basin is critical for an understanding of the timing of oil and gas generation. This paper aims to:

- establish the CAI values of conodonts in the impact structure, to determine whether the CAI is related to the thermal effects of impact or to regional geotherms;
- construct, with the aid of conodonts, a depth-related maturation profile, to determine the maturity of the Ordovician succession in the Gosses Bluff structure; and
- compare the above with CAI data from wells outside the Gosses Bluff structure, including Tyler No. 1, Palm Valley No. 1, and West Waterhouse No. 1 (Fig. 1).

Gosses Bluff petroleum exploration wells

Two petroleum exploration wells have been drilled into the central core of the Gosses Bluff structure (Fig. 4). In 1965, Exoil drilled Gosses Bluff No. 1 in the centre of the crater to a depth of 1383 m. The well terminated in vertically dipping Stairway Sandstone (Pemberton & Planalp 1965) without penetrating the

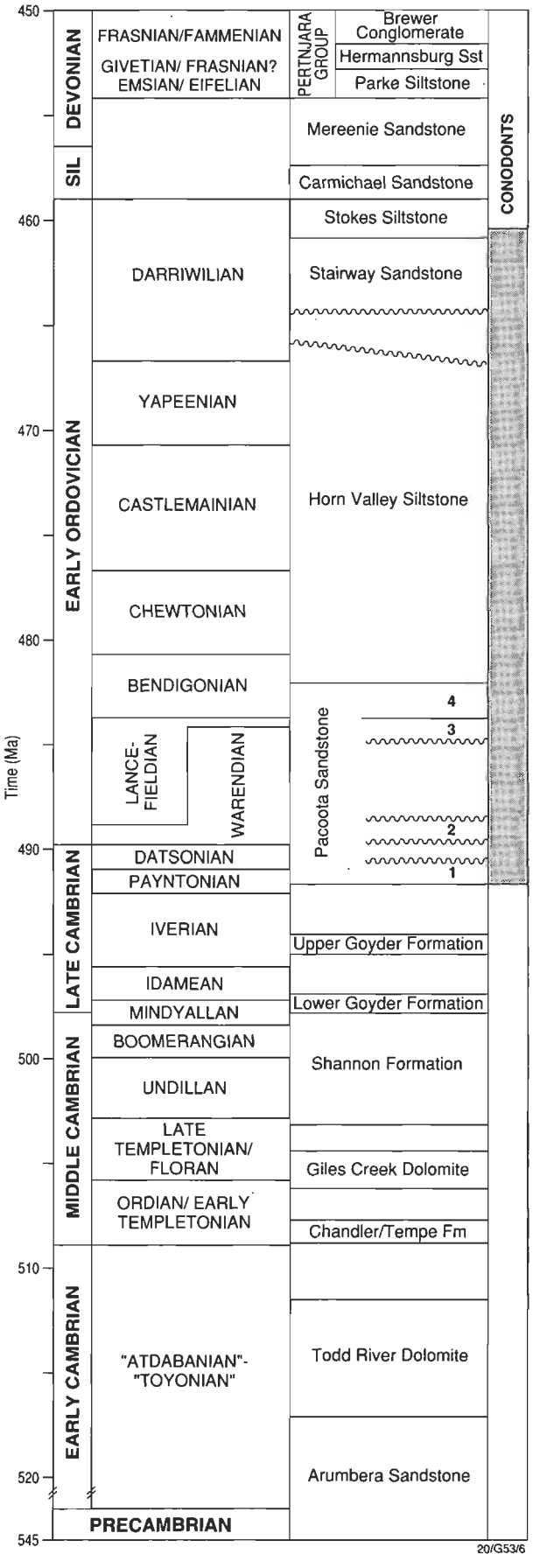

Figure 3. Stratigraphic column of the Amadeus Basin showing the ranges of conodonts in the basin.

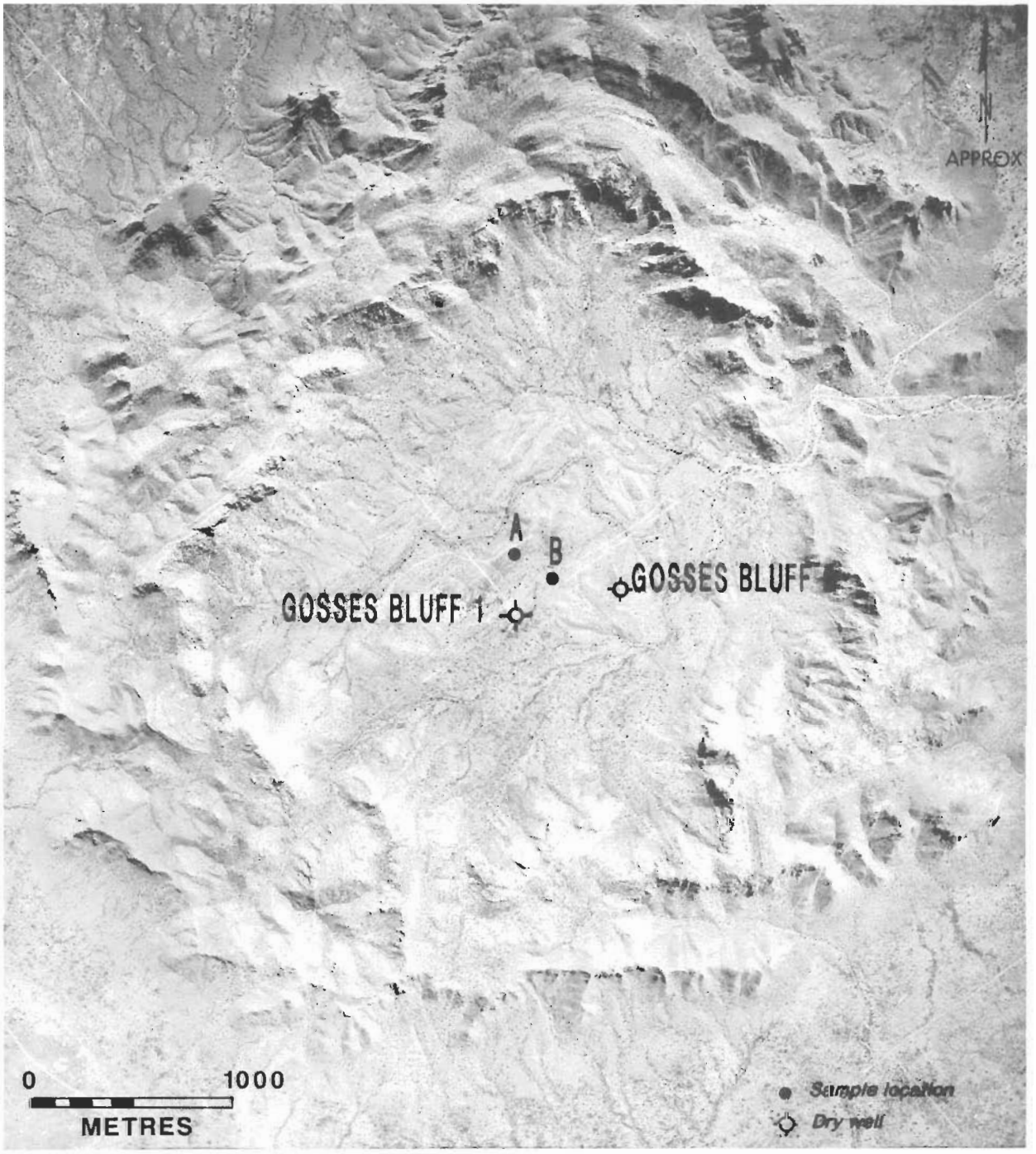

Figure 4. Vertical aerial photograph of Gosses Bluff showing the locations of Gosses Bluff Nos. 1 and 2, and the surface samples that yielded conodonts.

Horn Valley Siltstone or the target reservoir, the Pacoota Sandstone. In its uppermost part, the well encountered carbonate rocks in the Stokes Siltstone, which also crop out near the well site. Gosses Bluff No. 2 was drilled by Magellan Petroleum Australia Limited in 1988–89 (Roe 1991) to a total depth of 2652 m. The well penetrated the Pacoota Sandstone objective, but, despite minor gas shows, adequate porosity and permeability were lacking, and the well was plugged and abandoned. Gosses Bluff No. 2 confirmed the structural complications associated with a complex impact structure. It encountered steeply dipping, overturned, and intensely faulted strata in the upper, disturbed zone, but the beds are less disturbed — having gentler dips and no extensive fractures — at depth (Roe 1991).

Cores and cuttings of limestone from Gosses Bluff No. 1, and rock from surface exposures in the Gosses Bluff structure, were sampled for conodont biostratigraphic study and to determine the thermal maturity according to the CAI method of Epstein et al. (1977). Initial results were reported by Gorter & Nicoll (1983) and Gorter (1984). Cuttings from a depth of 2438 m (8000 ft) in Gosses Bluff No. 2 were later sampled for source-rock characterisation, and the contained conodonts recovered from limestones in the cuttings assessed for CAI (Table 1).

Table 1. Conodont faunas and CAI values for wells and outcrop samples in and near Gosses Bluff

Locality/well + depth	*Conodont fauna*	*Formation*	*CAI*
Gosses Bluff outcrop sample A	15 elements ?*Phragmodus* sp. indet	Stokes Siltstone	4
Gosses Bluff outcrop sample B	8 elements indet. fragments	Stokes Siltstone	3–4
Gosses Bluff 1 core 1 319–329 ft 97–100 m)	23 elements *Phragmodus* sp. indet.	Stokes Siltstone	4
Gosses Bluff 1 cuttings 880-1020 ft (268–311m)	1 element indet. fragment	Stokes Siltstone	4
Gosses Bluff 2 cuttings 2438 m	18 elements *Drepanoistodus* sp. indet *Oepikodus communis*	Horn Valley Siltstone	4
Palm Valley 1 core 14 1697 m	158 elements *Bergstroemognathus extensus* *Oepikodus communis* *Oepikodus* n. sp. A *Protopanderodus nyinti*	Horn Valley Siltstone	3
Tyler 1 cuttings 3429–3520 m	3 elements *Phragmodus* sp. indet.	Stokes Siltstone	3
West Waterhouse 1 cuttings 1762–1790 m	47 elements *Prioniodus amadeus* *Protoprioniodus aranda*	Horn Valley Siltstone	3

Sample preparation

Conodonts. The conodont samples were processed by standard techniques for conodont preparation (Lindström 1964) at the AGSO acid laboratory, and the CAI values (Table 1) were determined by optical microscopic examination from a standard CAI set supplied by A.G. Harris of the United States Geological Survey.

Source rocks. Shale and limestone cuttings from the lower to middle part of the Horn Valley Siltstone in Gosses Bluff No. 2 well were analysed at AGSO by the Rock-Eval pyrolysis technique. The results are summarised in Table 2.

Table 2. Rock-Eval data determined by the AGSO Organic Geochemistry Laboratory for a cutting from a depth of 2438 m in Gosses Bluff 2

Tmax	*S1*	*S2*	*S3*	*S1+S2*	*PI*	*TOC*	*HI*	*OI*
384	1.01	0.08	1.08	1.09	0.92	0.62	13	174

CAI observations

Conodonts were recovered from two outcrop samples — one (sample A) near the centre of the structure, the other (sample B) just northeast of the Gosses Bluff No. 1 drill site (Fig. 4) — both probably from the Stokes Siltstone. From the wells, conodonts were recovered from the Stokes Siltstone in Gosses Bluff No. 1 and from the Horn Valley Siltstone in Gosses Bluff No. 2 (Table 1). The Stokes Siltstone was not sampled in Gosses Bluff No. 2.

Conodont samples from Gosses Bluff No. 1, Palm Valley No. 1, Tyler No. 1, and West Waterhouse No. 1 (Fig. 1; Gorter 1984) were re-examined and combined with the new observations from Gosses Bluff No. 2 and the outcrop samples. The CAI results provide control for the interpretation of thermal gradients in the Amadeus Basin.

Surface sample A has a CAI value of 4, and surface sample B has a CAI value of 3–4 (Table 1). These samples contain conodont faunas that are representative of the Stokes Siltstone. CAI values from the Stokes Siltstone in Gosses Bluff No. 1 (97 to 311 m) were originally reported by Gorter (1984) to be 2–3. Our re-examination of the material determined a CAI value of 4. The fauna is typical of that found in the Stokes Siltstone at other localities in the Amadeus Basin. At Gosses Bluff No. 2, 18 conodont elements or element fragments were recovered from the sample at 2438 m. All have a CAI value of 4, the same as that in the stratigraphically younger material from Gosses Bluff No. 1. The fauna includes *Oepikodus communis* and *Drepanoistodus* sp. indet. In the Amadeus Basin, *O. communis* is restricted to the lower part of the Horn Valley Siltstone (Nicoll, in Shergold et al. 1991).

Source-rock maturity levels based on CAI

The conodonts with a CAI value of 4 indicate an equivalent vitrinite reflectance level from 1.8 to at least 3 per cent (Fig. 2). According to the CAI data, the organic matter in the sample from the lower part of the Horn Valley Siltstone in Gosses Bluff No. 2 has passed well beyond the stage of wet gas and condensate generation, and is within the zone of dry gas generation (190–300°C, Fig. 2). However, this sample has a low organic content, and very low Tmax value (Table 2), probably owing to the bitumen component (high S1 compared to S2). It is from an organic-poor part of the Horn Valley Siltstone, in which rich organic matter is confined to thin beds — particularly near the middle of the formation (Gorter 1984, 1991; Elphinstone & Gorter 1991).

The CAI 4 value for all the Gosses Bluff surface and subsurface samples (Figs. 5 and 6) contrasts with the CAI 3 value for the Stokes Siltstone at depths of 3429–3520 m in Tyler No. 1, 15 km to the northeast, and in the Horn Valley Siltstone at shallower depths in Palm Valley No. 1 (40 km to the southeast; 1697 m) and West Waterhouse No. 1 (90 km to the east-southeast; 1762–1790 m; Table 1; see also Gorter 1984). A CAI value of 3 is consistent with wet gas and condensate generation from any source rocks at this stratigraphic level (Fig. 2).

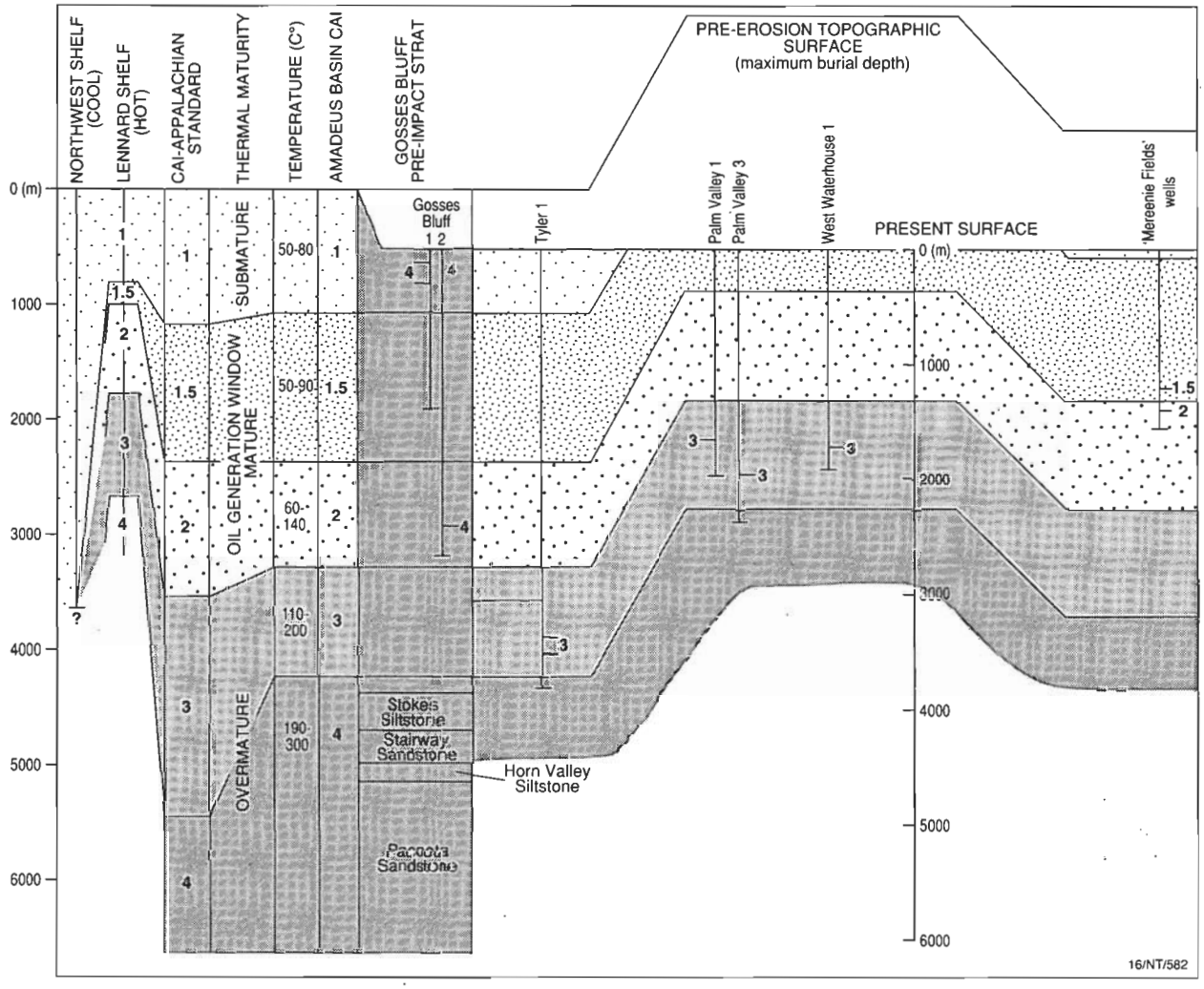

Figure 5 . Cross-section showing the conodont CAI values in wells from Gosses Bluff No. 1 to West Waterhouse No. 1 and conodont CAI values. The CAI maturation gradient of the standard Appalachian scheme is applied to the Amadeus Basin and compared with gradients in the Canning Basin (Nicoll & Gorter 1984a, 1984b).

Discussion

CAI data from conodonts are derived from sedimentary successions that are two or three thousand metres thick in several Australian basins of Cambrian to Triassic age — for example, the Canning Basin (Nicoll & Gorter 1984a, 1984b). In the Amadeus Basin, however, similar CAI information is restricted to a stratigraphic interval of less than 1000 m, and well control points are widely scattered. Thus, a CAI-based regional thermal gradient has not been previously established. The conodonts recovered from different depth ranges in Gosses Bluff Nos. 1 and 2 and Tyler No. 1, 15 km apart, constitute the first good vertical control for a conodont maturation profile in this basin (Fig. 5).

The different present-day depths from which the conodonts were recovered in Gosses Bluff No. 1 (97–311 m) and 2 (2438 m) reflect the near-vertical structural attitudes in the central uplift of Gosses Bluff. Rebound following impact elevated the Ordovician conodont-bearing rocks from their original burial depths to their present locations. In their pre-impact relationship, however, they were stratigraphically separated by no more than 500 m.

The Stokes Siltstone and Stairway Sandstone are exposed in the central uplift of Gosses Bluff, and are overlain by younger rocks of the Carmichael Sandstone, Mereenie Sandstone, and Pertnjara Group (Fig. 3). In Tyler No. 1, the Stokes Siltstone occurs at 3200–3600 m below the surface. Conodonts with a CAI 3 value were recovered from a depth of 3429 to 3520 m in Tyler No. 1, suggesting that the samples of Stokes Siltstone from Gosses Bluff — which have a CAI 4 value — were originally more deeply buried than the Stokes Siltstone in Tyler No. 1.

Analysis of seismic velocities from an expanding spread associated with the deep seismic reflection line BMR85.1B, 8 km to the west of Gosses Bluff in the Missionary Plain, indicates that the Stokes Siltstone occurs at about 3890–4190 m, the Stairway Sandstone at about 4190–4500 m, and the Horn Valley Siltstone at about 4500–4630 m (Wright et al. 1991). Thus, within Gosses Bluff, the Stokes Siltstone was uplifted by up to 4200 m. The Horn Valley Siltstone samples taken from Gosses Bluff No. 2 at a depth of 2438 m were uplifted during the impact by at least 2000 m to their present position.

CAI due to regional geothermal effects

CAI data from the Siljan astrobleme in Sweden (Bergström 1980), and from similar structures in North America (Votaw 1980), show that CAI values reflect burial trends rather than the

amount of heat generated by impact. At Gosses Bluff, elevated temperatures melted the country rock to produce an aureole of melt breccia and recrystallised breccia. The melt breccia is now mainly preserved at Mount Pyroclast, about 6 km south of the centre of the impact. It was evidently produced by heat generated on impact (Milton et al. 1972). The heat generated by the impacting body is mostly dissipated through the melting of impacted rocks and of the bolide itself. The dissipated, high-temperature fall-back debris and plume contribute heat to the atmosphere. At depth, however, the thermal effect of the impact was apparently insufficient or too brief to have significantly altered the colour of the conodonts that were originally over 4000 m below the impact site. We suggest that the CAI of the samples recovered from Gosses Bluff Nos. 1 and 2 and outcrops are the result of elevated temperatures that reflect the original depth of burial and the regional geothermal gradient. Because the impact provided no significant heating influence, the CAI value should relate to the maximum temperature reached at present-day depths of around 4000 to 4500 m in this part of the basin.

The conodonts recovered from both the Gosses Bluff wells and surface samples within the bluff contain abundant microfractures. This fracturing is attributed to disruption of the rocks by the primary impact shock wave, and by the rebound of the central uplift. Microfractures are not apparent in conodonts recovered from Tyler No. 1, Palm Valley No. 1, and West Waterhouse No. 1 — all outside the deformed aureole of Gosses Bluff. In an apatite fission-track analysis of Gosses Bluff, Tingate (1990) and Tingate & others (1996) reported intense fracturing of most of the apatite grains in their samples.

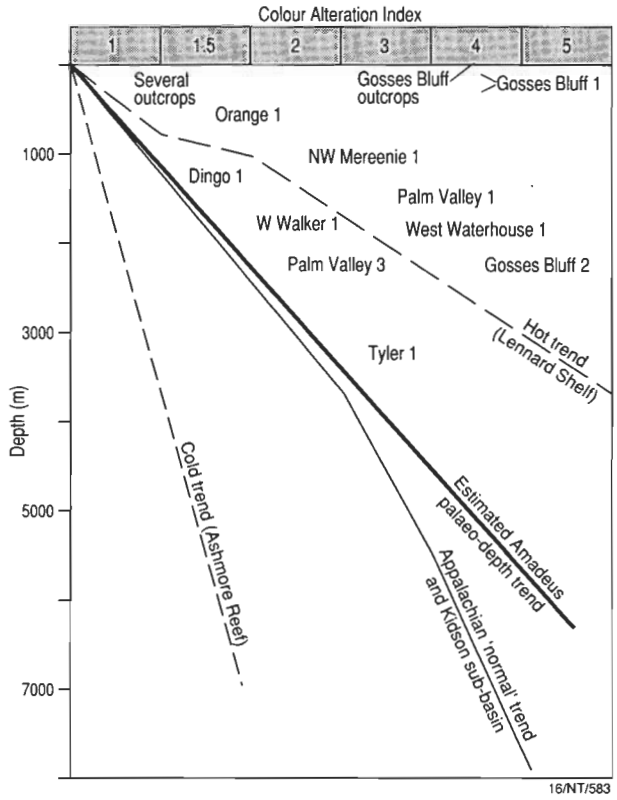

Figure 6. Graph of CAI values versus depth, comparing selected Amadeus Basin samples with the Appalachian 'normal' trend of Epstein et al. (1977) and 'hot' and 'cold' trends from other Australian basins.

Depth-related maturation profile

The CAI trend developed for the Appalachian fold belt (Figs. 5 and 6) has been taken as a standard against which to compare conodont thermal maturation. The study of conodont colour alteration in various Australian basins is instructive because it demonstrates the extent of variation in local or regional geothermal gradients, even within a single basin (Nicoll & Gorter 1984a, 1984b; Gorter 1984; Nicoll & Foster 1994). For example, Nicoll & Gorter (1984a, 1984b) published maturation information based on CAI for the Canning Basin, but only in a few wells were CAI values of over 3 recognised. The Willara No. 1 well shows CAI values of 3–4 at about 3020 m, and Kidson No. 1 has a CAI value of 3 at 3070 m. In the Amadeus Basin, for comparison, Palm Valley No. 1 and West Waterhouse No. 1 have a CAI value of 3 at depths of less than 1800 m (Fig. 5, Table 1). In the Appalachians, a CAI 3 value reflects burial between 3660 to 5500 m (Epstein et al. 1977).

The differences in these depths for the same CAI value may be explained by differences in regional thermal gradients, by erosion of large thicknesses of strata from the preserved stratigraphic section, or by local heat sources such as igneous intrusions. There are no igneous intrusions in this part of the Amadeus Basin, and the close proximity of all of these localities (Fig. 1) suggests that former thicker sediment loading, probably by the Pertnjara Group clastic rocks, produced a more deeply buried structure and thus a higher apparent thermal gradient.

A comparison can be made between the CAI–depth pairs from the Amadeus Basin and the CAI–depth trends from other basins (Fig. 6). The standard Appalachian trend is shown along with a 'hot' trend based on the Lennard Shelf in the Canning Basin (Nicoll & Gorter 1984a, 1984b), and a 'cold' trend based on the Ashmore Platform in the western Timor Sea (according to data from Nicoll & Foster 1994, and unpublished data of J.D. Gorter and R.S. Nicoll).

The Amadeus Basin CAI values mostly plot near the Lennard Shelf trend, with the exception of the sample from Tyler No. 1 (Fig. 6). Depths to the Ordovician formations in Tyler No. 1, and depths determined from seismic data on the Missionary Plain nearby (Wright et al. 1991), indicate that the maximum depths for the CAI zones based on the Appalachian trend are possibly too deep, and that the Amadeus Basin trend would be slightly hotter than the Appalachian one, particularly for CAI zones 3 and 4. The Amadeus Basin trend, however, was not as hot as the trend for the Lennard Shelf, because most of the CAI values are from structures that have experienced post-burial uplift and do not reflect the palaeoburial trend. Hence the Amadeus Basin trend must be cooler than the trend for the Lennard Shelf. According to apatite fission-track data, Tingate et al. (1996) concluded that palaeogeothermal gradients were very similar to those of the present day, and that the present surface of the Missionary Plain is within 500 m of the land surface at the time of impact. Thus, if we assume that the sample in Tyler No. 1 was 500 m deeper at the time of impact, then the palaeoburial trend for the Amadeus Basin would be slightly hotter than the Appalachian trend (Fig. 6).

Estimates of the possible amounts of uplift for Gosses Bluff can be made by comparing present-day depths with the predicted palaeodepths based on an Amadeus Basin trend that was slightly hotter than the standard Appalachian trend (Fig. 6 and Table 3). The CAI 4 value at the surface at Gosses Bluff and near the surface in Gosses Bluff No. 1 could reflect burial depths of 4500 to

Table 3. Estimates of possible amounts of uplift determined by comparing present-day depths with the predicted palaeodepths based on an Amadeus Basin trend that was slightly hotter than the standard Appalachian trend (see Fig. 6)

Location/well	*CAI*	*Sample depth (m)*	*Range of estimated uplift (m)*
Sundry surface samples	1	surface	0–1100
Orange 1	1.5	ca 735	400–1500
Dingo 1	1.5	ca 1030	100–1200
North West Mereenie 1	2	ca 1200	1000–2250
West Walker 1	2	ca 1350	900–2100
Palm Valley 1	3	ca 1697	1750–2800
West Waterhouse 1	3	ca 1775	1675–2725
Palm Valley 3	3	ca 2000	1450–2500
Tyler 1	3	ca 3475	ca 500
Gosses Bluff outcrops	4	surface	4500–5600
Gosses Bluff 1	4	100 & 300	4200–5500
Gosses Bluff 2	4	2438	2000–3150

5600 m, and the Horn Valley Siltstone in Gosses Bluff No. 2 would have been uplifted at least 2000 m during the impact (Table 3). These burial depths are consistent with current depths to the Ordovician formations estimated from nearby seismic data on the Missionary Plain (Wright et al. 1991).

Regional implications

Jackson et al. (1984) and Tingate (1991) have suggested that up to 2 km of section has been stripped from the Mereenie Anticline (Fig. 1), where CAI values of 1.5 to 2 have been derived for the Horn Valley Siltstone at current depths of about 1050–1250 m (Gorter 1984). From Figure 6 it can be inferred that the sample from North West Mereenie No. 1 well was buried 1000 to 2250 m deeper in the past (Table 3). Similarly, a CAI 3 value derived for the Horn Valley Siltstone in Palm Valley No. 3 (1981–2039 m) and in West Waterhouse No. 1 (1762–1789 m) indicates deeper burial in the past of about 1700–2800 m (Table 3). The Palm Valley and Waterhouse Range Anticlines reflect considerable uplift and erosion during the late Palaeozoic Alice Springs Orogeny (Nicoll et al. 1991). Lesser amounts of burial, in the order of 100–1500 m, are predicted for Orange No. 1 and Dingo No. 1 (Table 3). Most outcrop samples with a value of CAI 1 could have been buried by up to 1100 m in the past.

As CAI values reflect the maximum level of maturation attained by the rocks as a result of their burial, the CAI 4 value for outcrops at Gosses Bluff is an indicator of the maturity level of the organic matter in the Stokes and Horn Valley Siltstones at the time of impact — that is, about 140 million years ago — provided that these units were not more deeply buried thereafter or exposed to magmatic processes at any time. By then, the organic matter in the rocks had already passed beyond the wet gas and condensate production field into that of dry gas (Fig. 2). This result confirms the very high thermal maturity of Palaeozoic and older source rocks in the Missionary Plain (Gorter 1984; Jackson et al. 1984), and indicates that these areas have only dry gas potential.

Conclusions

In the Amadeus Basin, the maximum maturation of organic matter in the source beds in the Early Ordovician Horn Valley Siltstone is reflected by a value of CAI 4 derived from samples from Gosses Bluff No. 2. Similar depths of burial were attained by the late Early Ordovician carbonates in the Stokes Siltstone, now exposed and at shallow levels in Gosses Bluff No. 1. This CAI value is best explained by a regional palaeogeotherm, and is not related to the effects of the impact.

The conodont CAI values in the Gosses Bluff area allow the construction of a regional palaeodepth trend (or maturation profile), and show that it would have a slightly higher geothermal gradient than both the standard Appalachian CAI–depth trend of Epstein et al. (1977) and the trend for the Kidson Sub-basin of the Canning Basin (Nicoll & Gorter 1984a, 1984b). This gradient is to be expected in an intracratonic basin setting where the last major event was rapid sedimentation due to foreland loading.

The amount of former burial and/or uplift can be estimated from this regional palaeodepth trend. Thus the maximum thickness of the sedimentary succession of the Missionary Plain before impact was no more than about the present thickness plus 500 m, subsequently eroded from above the Gosses Bluff and Tyler No. 1 area. However, in the Palm Valley and Waterhouse Range areas, the succession had an additional 1700–2800 m of sediment. A value of CAI 4 at the present surface at Gosses Bluff, however, indicates that these rocks were elevated by at least 4500 m, during the impact of the asteroid or comet.

The regional palaeodepth trend for the Gosses Bluff area places the Horn Valley Siltstone source rock in the dry gas zone. Thus exploration targets in the Missionary Plain area could expect only gas from Ordovician or older targets.

Acknowledgments

We thank Roger Summons for the Rock-Eval pyrolysis analyses of cuttings and for an explanation of their significance; Andrew Glikson and John Laurie for their thoughtful reviews of this paper; and Lana Murray of AGSO's Cartographic Services Unit for drafting the figures.

References

Bergström, S.M., 1980. Conodonts as paleotemperature tools in Ordovician rocks of the Caledonides and adjacent areas in Scandinavia and the British Isles. Geologiska Föreningens i Stockholm Förhandlingar, 102, 377–392.

Cook, P.J., 1968. The Gosses Bluff cryptoexplosion structure. Journal of Geology, 76, 123–139.

Cooper, B.J., 1981. Early Ordovician conodonts from the Horn Valley Siltstone, central Australia. Palaeontology, 24, 147–183.

Crook, K.A.W. & Cook, P.J., 1966. Gosses Bluff — diapir, crypto-volcanic structure or astrobleme? Journal of the Geological Society of Australia, 13, 495–516.

Elphinstone, R. & Gorter, J.D., 1991. As the worm turns: implications of bioturbation on source rocks of the Horn Valley Siltstone. In: Korsch, R.J. & Kennard, J.M. (editors), Geological and geophysical studies in the Amadeus Basin, central Australia. Bureau of Mineral Resources, Australia, Bulletin, 236, 317–332.

Epstein, A.C., Epstein, J.B. & Harris, L.D., 1977. Conodont color alteration, an index to organic metamorphism. United States Geological Survey, Professional Paper 995, 1–27.

Glikson, A.Y., 1969. Geology of the outer zone of the Gosses Bluff crypto-explosion structure. Bureau of Mineral Resources, Australia, Record 1969/42.

Gorter, J.D., 1984. Source potential of the Horn Valley Siltstone, Amadeus Basin. APEA Journal, 24, 66–90.

Gorter, J.D., 1991. Palaeogeography of Late Cambrian to Early Ordovician sediments in the Amadeus Basin, central Australia. In: Korsch, R.J. & Kennard, J.M. (editors), Geological and geophysical studies in the Amadeus Basin, central Australia. Bureau of Mineral Resources, Australia, Bulletin, 236, 253–275.

Gorter, J.D. & Nicoll, R.S., 1983. Interpretation of conodont color alteration and thermal maturation in Amadeus Basin, central Australia. American Association of Petroleum Geologists, Bulletin, 67, 473.

Jackson, K.S., McKirdy, D.M. & Deckelman, J.A., 1984. Hydrocarbon generation in the Amadeus Basin, central Australia. APEA Journal, 24, 42–65.

Jones, P.J., 1996. AGSO Phanerozoic timescale 1995: wallchart and explanatory notes. Oxford University Press, Melbourne.

Lindström, M., 1964. Conodonts. Elsevier, Amsterdam.

Milton, D.J., Barlow, B.C., Brett, R., Brown, A.R., Glikson, A.Y., Manwaring, E.A., Moss, F.J., Sedmik, E.C.E., Van Son, J. & Young, G.A., 1972. Gosses Bluff impact structure, Australia. Science, 175, 1199–1207.

Milton, D.J., Barlow, B.C., Brown, A.R., Moss, F.J., Manwaring, E.A., Sedmik, E.C.E., Young, G.A., & Van Son, J., 1996a. Gosses Bluff — a latest Jurassic impact structure, central Australia. Part 2: seismic, magnetic, and gravity studies. AGSO Journal of Australian Geology & Geophysics, this issue.

Milton, D.J., Glikson, A.Y., & Brett, P.R., 1996b. Gosses Bluff — a latest Jurassic impact structure, central Australia. Part 1: geological structure, stratigraphy, and origin. AGSO Journal of Australian Geology & Geophysics, this issue.

Milton, D.J. & Sutter, J.F., 1987. Revised age for the Gosses Bluff impact structure, Northern Territory, Australia, based on $^{40}Ar/^{39}Ar$ dating. Meteoritics, 22, 281–289.

Nicoll, R.S. & Foster, C.B., 1994. Late Triassic conodont and palynomorph biostratigraphy and conodont thermal maturation, North West Shelf, Australia. AGSO Journal of Australian Geology & Geophysics, 15, 101–118.

Nicoll, R.S. & Gorter, J.D., 1984a. Conodont colour alteration, thermal maturation and geothermal history of the Canning Basin, Western Australia. APEA Journal, 24, 414–429.

Nicoll, R.S. & Gorter, J.D., 1984b. Interpretation of additional conodont colour alteration data and the thermal maturation and geothermal history of the Canning Basin, Western Australia. In: Purcell, P.G. (editor), The Canning Basin, W.A. Proceedings of the Geological Society of Australia/Petroleum Exploration Society of Australia Symposium, Perth, 411–425.

Nicoll, R.S., Gorter, J.D. & Owen, M., 1991. Ordovician sediments in the Waterhouse Range Anticline, Amadeus Basin, central Australia: their interpretation and tectonic implications. In: Korsch, R.J. & Kennard, J.M. (editors), Geological and geophysical studies in the Amadeus Basin, central Australia. Bureau of Mineral Resources, Australia, Bulletin, 236, 277–284.

Pemberton, R.L. & Planalp, R.N., 1965. Well completion report Gosses Bluff No. 1 well. Exoil NL (unpublished).

Perry, W.J., Jr., Wardlaw, B.R., Bostick, N.H. & Maughan, E.K., 1983. Structure, burial history, and petroleum potential of frontal thrust belt and adjacent foreland, southwest Montana. American Association of Petroleum Geologists, Bulletin, 67, 725–743.

Roe, L.E., 1991. Petroleum exploration in the Amadeus Basin. In: Korsch, R.J. & Kennard, J.M. (editors), Geological and geophysical studies in the Amadeus Basin, central Australia. Bureau of Mineral Resources, Australia, Bulletin, 236, 463–476.

Shergold, J.H., Elphinstone, R., Laurie, J.R., Nicoll, R.S., Walter, M.R., Young, G.C. & Zang, W., 1991. Late Proterozoic and early Palaeozoic palaeontology and biostratigraphy of the Amadeus Basin. In: Korsch, R.J. & Kennard, J.M. (editors), Geological and geophysical studies in the Amadeus Basin, central Australia. Bureau of Mineral Resources, Australia, Bulletin, 236, 97–111.

Tingate, P.R., 1990. Apatite fission track studies from the Amadeus Basin, central Australia. PhD Thesis, University of Melbourne (unpublished).

Tingate, P.R., 1991. Apatite fission track analysis of the Pacoota and Stairway Sandstones, Amadeus Basin, central Australia. In: Korsch, R.J. & Kennard, J.M. (editors), Geological and geophysical studies in the Amadeus Basin, central Australia. Bureau of Mineral Resources, Australia, Bulletin, 236, 525–540.

Tingate, P.R., Lindsay, J.F. & Marshallsea, S.J., 1996. Impact structures as potential petroleum exploration targets: Gosses Bluff, a Late Jurassic example from central Australia. AGSO Journal of Australian Geology & Geophysics, this issue.

Votaw, R.B., 1980. Middle Ordovician conodonts from the Kentland structure, Indiana. Geological Society of America, Abstracts with Programs, 12, 259.

Wright, C., Barton, T., Goleby, B.R. & Taylor, F.J., 1991. Seismic velocities in the Missionary Plain region: an aid to stratigraphic studies. In: Korsch, R.J. & Kennard, J.M. (editors), Geological and geophysical studies in the Amadeus Basin, central Australia. Bureau of Mineral Resources, Australia, Bulletin, 236, 67–72.

Young, G.C., Turner, S., Owen, M., Nicoll, R.S., Laurie, J.R. & Gorter, J.D., 1987. A new Devonian fish fauna, and revision of post-Ordovician stratigraphy in the Ross River Syncline, Amadeus Basin, central Australia. BMR Journal of Australian Geology & Geophysics. 10, 233–242.

AGSO Journal of Australian Geology & Geophysics, 16 (4), 561–566

Goyder impact structure, Arnhem Land, Northern Territory

Peter W. Haines[1]

A circular structural uplift of 3 km diameter in sandstone and mudstone of the Abner Sandstone crops out within the McArthur Basin of central Arnhem Land, Northern Territory, Australia. The surrounding area contains little outcrop, but the strata are believed to be flat-lying to gently dipping. An outer annulus of sand (disintegrated sandstone) contains scattered outcrops of fractured and brecciated sandstone generally striking tangentially to the structure and dipping outwards. Silicified sandstone bearing shatter cones crops out in the radially faulted core of the structure. Petrographic analysis of sandstone and breccia from the central area reveals abundant fracturing, and single and multiple sets of closely spaced parallel planar deformation features in quartz. The orientation of these planar deformation features is consistent with impact-produced shock metamorphism.

The structure is interpreted as the remnant of the central uplift of a deeply eroded complex impact crater. The crater rim and floor have been removed by erosion, and considerable uncertainty surrounds the original rim dimensions. Comparisons with other terrestrial impact structures allow for a diameter in the range of 7–25 km. The age of the structure is probably pre-Cretaceous, but it could be as old as the Mesoproterozoic (~1400 Ma) age of the target rocks.

Introduction

The impact of large meteorites and comets with the planets of our solar system is a common event by the standards of geological time, and one which has had profound effects on the evolution of life on Earth. The number of confirmed terrestrial craters and eroded impact scars increases every year, and now numbers over 130 authenticated sites worldwide (Grieve & Pesonen 1992). Most of the currently identified large impact sites are situated in the older cratonic areas of North America, Europe, and Australia. The geological stability and slow rate of erosion of these regions over long periods of time is an essential factor for the preservation of such structures.

One of such terrains in Australia is the McArthur Basin, whose moderately simple geology — including extensive areas of flat-lying to gently dipping strata — and stability since the Proterozoic suit it to the preservation and recognition of impact structures. Two impact structures have been previously recognised in the McArthur Basin: Liverpool and Strangways (Guppy et al. 1971). Liverpool is a fairly well-preserved simple bowl-shaped crater 1.6 km in diameter, whereas Strangways is a complex crater, 25 km in diameter, with preserved impact melt. A number of other ancient and deeply eroded impact structures have been recognised within contemporaneous or older Proterozoic terrains elsewhere in Australia, including the Acraman, Kelly West, Lawn Hill, Spider, and Teague structures (Shoemaker & Shoemaker 1990, this issue).

Discovery and location

The discovery of impact structures commonly follows from the investigation of anomalous circular features initially identified on aerial photographs, images, or geological maps. During preparations for geological mapping in Arnhem Land, northern Australia, I identified a circular structural anomaly of 3 km diameter on aerial photographs. This feature is located at latitude 13°28.5'S, longitude 135°02.5'E, 80 km east-northeast of Bulman and about 40 km east of the nearest road; it is 120 km southeast of Liverpool, and 250 km northeast of Strangways (Fig. 1). Its structural pattern is distinct from the essentially flat-lying outcrops of Mesoproterozoic strata in the surrounding area, and it was targeted for ground investigation.

I visited the site by helicopter in August 1991 while participating in joint regional geological mapping by the Northern Territory Geological Survey and the Australian Geological Survey Organisation (then the Bureau of Mineral Resources, Geology and Geophysics). Fracturing and brecciation are ubiquitous features, and shatter cones occur in the central part of the structure. Subsequent petrographic studies, as detailed in this paper, confirm a probable impact origin for the structure. The site is named the Goyder structure, as it lies within the catchment area of the Goyder River.

[1] Department of Applied Geology, University of South Australia, The Levels, SA 5095.

Geological setting

Regional

The Palaeo- to Mesoproterozoic McArthur Basin contains an unmetamorphosed succession of sedimentary rocks and minor volcanics locally up to 12 km thick (Jackson et al. 1987). The rocks are mostly only weakly deformed, except locally in major fault zones. The succession crops out over about 200 000 km^2 of northern Australia, and is divided into a number of groups separated by regional unconformities. The youngest of these, the Roper Group, constitutes the host rocks for the Goyder structure. The Roper Group is a cyclic package of shallow-marine sandstone and mudstone up to several thousand metres thick, though notably thinner in the area of interest.

The best estimate of the age of the Roper Group is provided by an Rb–Sr illite date of 1429 ± 31 Ma from the McMinn Formation near the top of the group (Kralik 1982). This represents a minimum estimate for the age of diagenesis of this formation. A maximum age is provided by the 1599 ± 11 Ma U–Pb zircon date from tuffaceous rocks at the top of the Balma Group (Pietsch et al. 1994), which lies stratigraphically lower in the basin succession. After deposition of the Roper Group, the McArthur Basin sequence was intruded by extensive thick dolerite sills, and subsequently faulted and locally folded by a regional tectonic event at some time before renewed deposition in the late Neoproterozoic and Cambrian. Apart from a brief depositional episode during the Cretaceous, the area has undergone very slow erosion, continuing to the present day.

Local stratigraphy

The outcrop of the Goyder structure consists entirely of the Abner Sandstone, a formation within the Roper Group. The Abner Sandstone is divided into the Arnold Sandstone, Jalboi, and Hodgson Sandstone Members in ascending order. The Arnold and Hodgson Sandstone Members consist of medium-grained cross-bedded sandstone; the intervening Jalboi

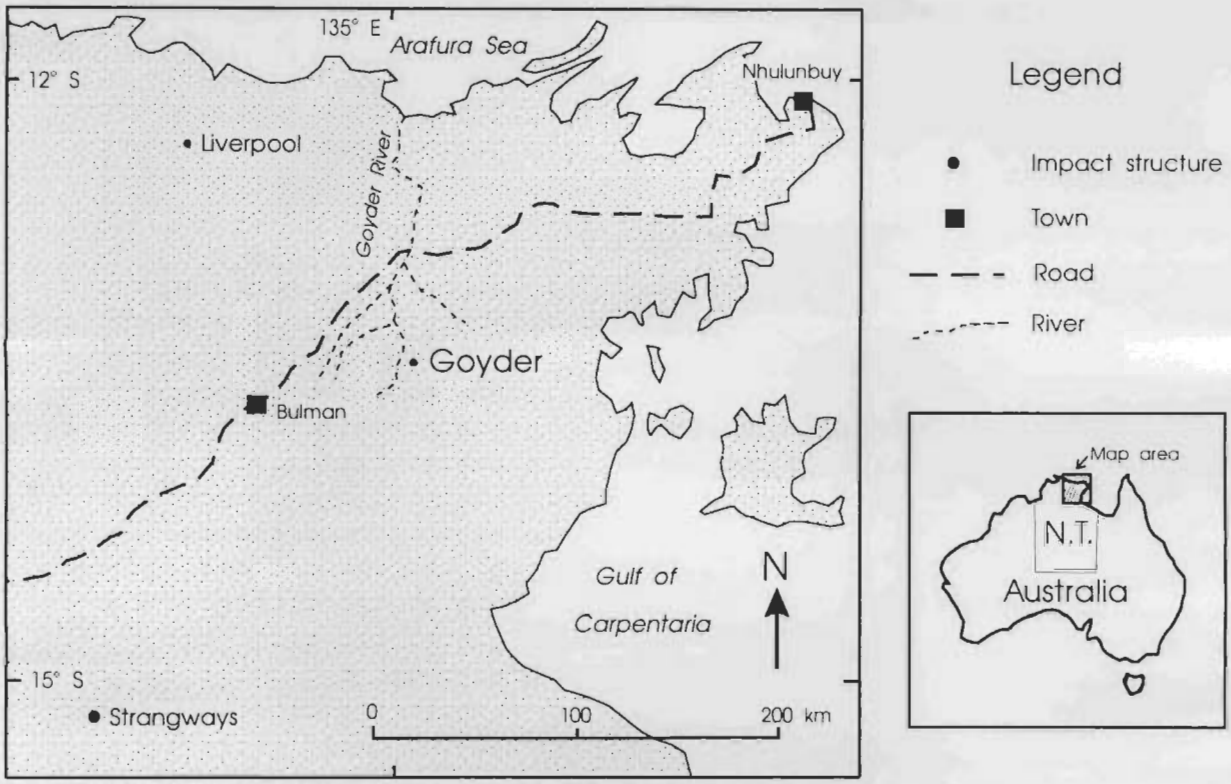

Figure 1. Location of Goyder and other nearby impact structures (Liverpool and Strangways) in the northeastern part of the Northern Territory.

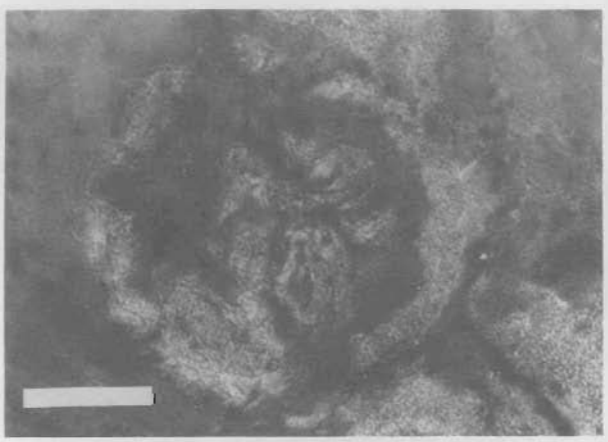

Figure 2. Vertical aerial photograph of the eroded central uplift of the Goyder impact structure. Scale bar = 1 km.

Member is composed of recessive interbedded sandstone and mudstone. The Abner Sandstone is underlain by fine-grained glauconitic sandstone and interbedded mudstone of the Crawford Formation. Although no outcrops of the Crawford Formation have been positively identified within the Goyder structure, this unit is presumed to be present in the near subsurface of the central area of the structure.

The Abner Sandstone is overlain sharply by the Corcoran Formation, a recessive unit of mudstone and interbedded sandstone. The formation is poorly exposed immediately south of the Goyder structure. It has a gradational contact with the overlying Bessie Creek Sandstone, comprising cross-bedded clean quartz sandstones similar to the Hodgson Sandstone Member. In the area of interest (Fig. 3), the Bessie Creek Sandstone has almost entirely disintegrated, leaving a low white sand plateau with minor outcrop to the southeast of the Goyder structure.

The thicknesses of the Abner Sandstone and its individual members are not accurately known near the Goyder structure owing to poor exposure, incomplete outcrop, and generally low attitude. Though no drilling has been undertaken in the area, the Abner Sandstone is between 200 and 300 m thick in a number of stratigraphic drillholes in the Roper River area about 150 km to the south and southwest, and over 600 m thick farther south (Jackson et al. 1988). The amount of deformation, including the potential for structural repetition, precludes the measurement of reliable thickness data within the Goyder structure itself.

Description

Morphology

The circular feature constituting the Goyder structure is a structural uplift which can be divided into three elements according to airphoto expression (Fig. 2). These are:

- a pale-coloured central hilly region;
- a pale-coloured outer annulus, in part a low ridge; and
- an intervening dark area with largely no exposure on the western side and poor exposure on the eastern side.

These divisions relate to lithological variations and their differential resistance to weathering, and correspond closely to the outcrop distributions of the three members of the Abner Sandstone (Fig. 3). The maximum relief in the area is only about 30 m. The regional slope is towards the northwest, and small ephemeral streams drain to the north and northwest from the centre of the uplift and from around the outside of its margins.

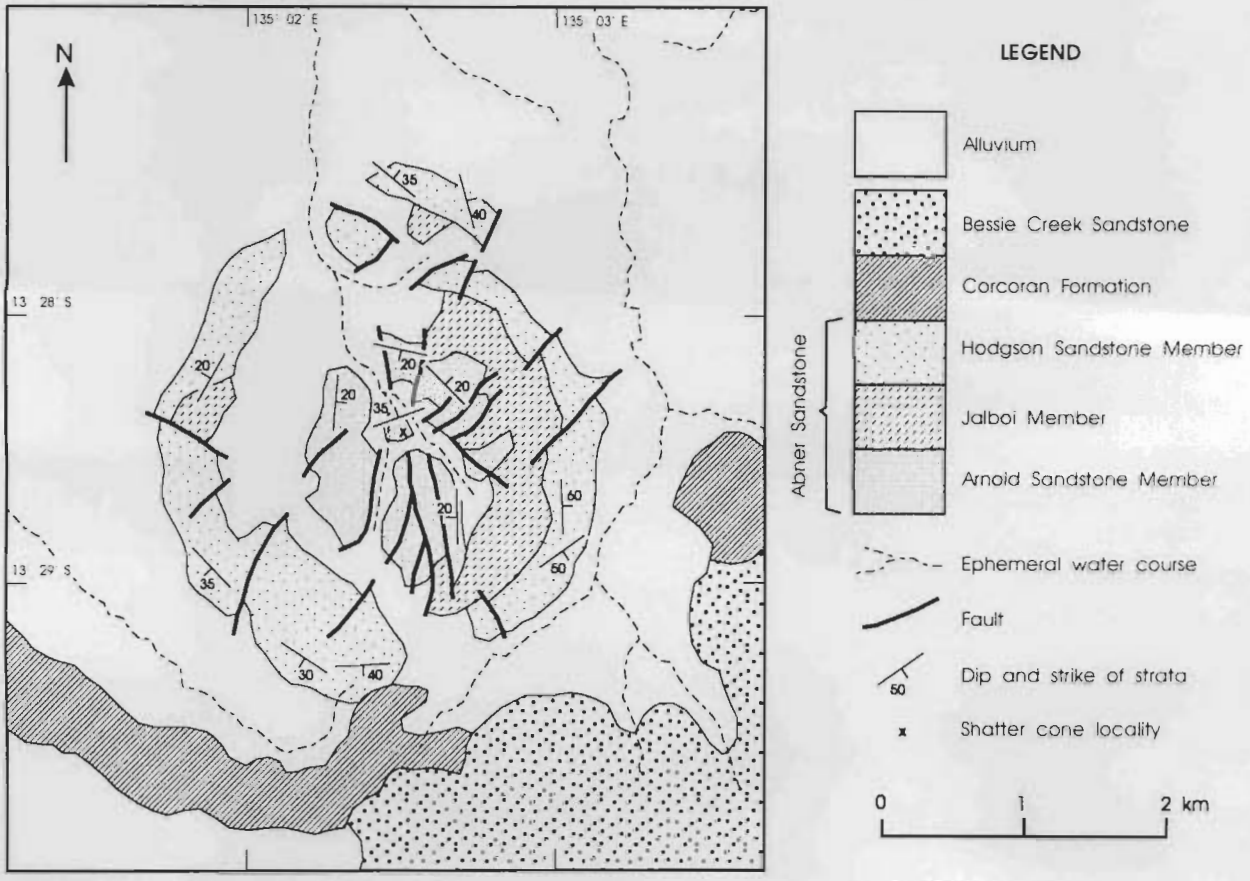

Figure 3. Geology of the central uplift of the Goyder impact structure.

The central hilly region is clearly distinguishable in Figure 2 by its pale colouration and essentially radial trends. It has an average diameter of about 1.5 km, though it is slightly elongate in the north–south direction. Outcrops consist entirely of the Arnold Sandstone Member, composed of fairly massive white to pale pink medium-grained quartz sandstone. The rocks are generally more silicified than those of the outer annulus. The region is intensely faulted; most of the faults are arranged in a roughly radial pattern, although the larger and more prominent faults have a slight north–south bias (Fig. 3). Several narrow alluvium-filled radial corridors separate the hills. Bedding orientation may be moderately consistent for several hundred metres along strike, but generally contrasts with that of the next fault block. Beds tend to dip at moderately low angles, averaging 20–30°, but there is no consistent pattern to dip directions. The sandstone is generally fractured to varying degrees, and microfaulting (seen as a stepped effect on bedding surfaces) is also common. Striated fracture surfaces occur sparsely throughout the area, but well-developed shatter cones are apparent at only one locality (Fig. 3). Though close to the overall centre of the structure, this locality is displaced a short distance north of the centre of the central hilly region. Many of the faults, and the corridors of alluvium, seem to radiate away from this locality. Individual shatter cones are about 50 cm long (Fig. 4). Most in-situ examples seem to be oriented roughly parallel to the bedding, but there are too few of them to make regionally significant conclusions regarding orientation. The sandstone is intensely brecciated near the shatter-cone locality.

The outer annulus is clearly distinguishable on aerial photographs by its pale colour contrasting with darker surrounding

Figure 4. Field photograph of large in situ shatter cones from the locality indicated in Figure 3. The cone axes are roughly horizontal. Hammer head (bottom centre) is 18 cm across.

areas. Its outer diameter is about 3 km, and its average width is of the order of 300–400 m, though it appears considerably wider in the southwest. In the west, the annulus has low topographic relief (a few metres) above surrounding areas. In the east, it has little or no topographic expression, and lies within a gentle regional gradient from the central hilly region to the plain farther east. Most of the outer annulus is composed of clean white quartz sand. The sand has been derived by the weathering of an underlying unit of sandstone, as evidenced by isolated to scattered small outcrops of white medium-grained cross-bedded quartz sandstone assigned to the Hodgson Sandstone Member. The sandstone displays thin surface silicification, but, when broken, it is generally very friable and easily

disintegrates to sand. Such disintegration is locally common in Roper Group sandstone formations, and relates to dissolution of the silica cement by surface processes in the tropical weathering climate. In the Goyder structure, shock-fracturing might have accentuated the tendency of the rock to disintegrate. Bedding is commonly contorted and offset by abundant microfaults, locally increasing in intensity until the rock is brecciated. Microfaults and clast boundaries in the breccias are generally highlighted by thin quartz veins. No shatter cones were observed in the outer annulus. Outcropping strata tend to dip outwards with a roughly tangential strike, although local deviations are common. Measured dip angles vary widely but average around 30–40°. The annulus is slightly offset by a number of minor faults, most of which are oriented roughly normal to the local strike. The annulus is more intensely disrupted at its northern and southern ends.

The gap between the outer annulus and the central hilly region is almost devoid of exposed rock in the west. In the east, it contains scattered rubbly exposures of the Jalboi Member: brown to purple fine- to medium-grained thin-bedded micaceous and ferruginous sandstone and interbedded ferruginous shale. Exposure is generally too poor for the structure to be observed; faults clearly visible in the sandstone units are not easily traced through this member.

Overall, the structure is nearly circular, but displays a weak bilateral symmetry about a roughly north–south axis. This is most clearly seen in the central hilly region of the structure. The shatter-cone locality lies on this axis, but is displaced a little north of centre.

Petrography

Thin sections of medium-grained sandstone of the Arnold Sandstone Member from the central hilly region, including samples of shatter cones and breccias, were examined for evidence of shock deformation. In all thin sections, most quartz grains display planar and curved sets of fractures. Some contain shear planes resulting in offsets of grain boundaries. Additionally, about 10 per cent of the grains display sets of planar deformation features (Fig. 5). These sets are defined by the presence of fine lamellae which are sharp, straight, parallel, and closely spaced, thus conforming to the characteristics specified by Alexopoulos et al. (1988), as discussed further below. Most sets have lamellae spaced 1–5 mm apart. They are generally decorated with minute inclusions or bubbles. The lamellae sets cover varying proportions of grains, and originate from the grain margin or from internal fractures and shears (Fig. 5b). Individual grains may contain one or, less commonly, multiple sets of planar deformation features with different orientations; the maximum number of sets observed per grain was three.

In one sample, the crystallographic orientations of 21 sets of planar deformation features in 15 quartz grains were determined on a universal stage. The angle between poles to the lamellae and the quartz c-axis are plotted as a histogram (Fig. 6). The poles correspond to specific crystallographic orientations of the quartz lattice (allowing for ± 5% error due to the degree of deformation and undulose extinction): 42.9 per cent plotted at c{0001}, and other sets corresponded to m,a ($\{10\bar{1}0\}$, $\{11\bar{2}0\}$), π$\{10\bar{1}2\}$, s$\{11\bar{2}1\}$, and ξ$\{11\bar{2}2\}$ in decreasing order of abundance.

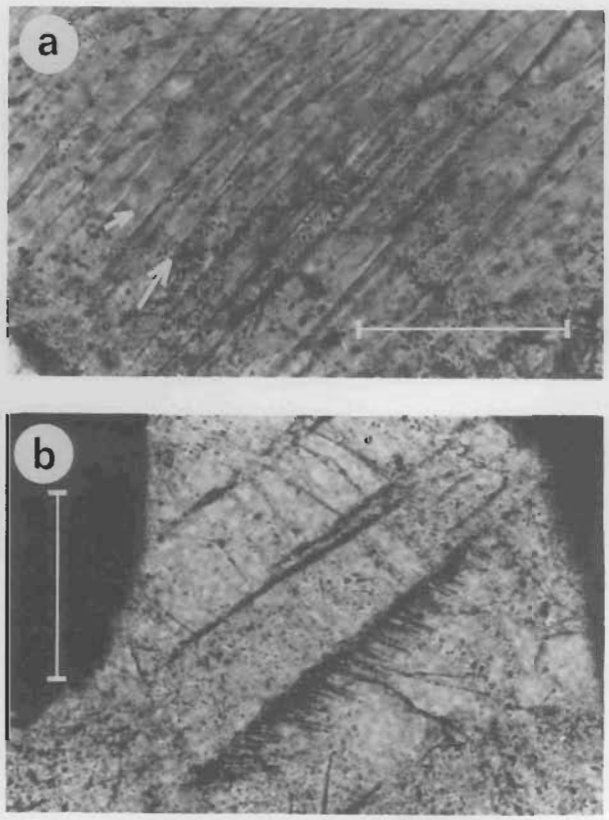

Figure 5. Photomicrographs of quartz grains in sandstone from the centre of the Goyder impact structure. (a) Two sets of planar deformation features intersecting at about 20°. The directions of the dominant and a weaker set are indicated by large and small arrows respectively. Scale bar = 50 μm. (b) Localised set of planar deformation features initialised at a shear fracture. Orthogonal fractures are apparent in the upper half of the photograph. Scale bar = 100 μm.

Discussion and conclusions

Impact origin

The planar deformation features petrographically observed in quartz grains are of the form observed from confidently identified impact sites and produced experimentally by high shock pressures (Alexopoulos et al. 1988). The orientations of planar deformation feature sets are similar to those determined at a number of impact structures involving sedimentary target rocks (A. Therriault and R.A.F. Grieve, personal communication, August 1995). Shock produces planar features with orientations strongly biased towards certain crystallographic directions, whereas planar features generated by tectonic or other processes display more random orientations (Alexopoulos et al. 1988). The majority view of workers in this field is that the physical form and orientation of planar deformation features can be used to discriminate between an origin involving impact, as opposed to other natural deformational processes (Alexopoulos et al. 1988; Grieve & Pesonen 1992). A minority view (e.g., Officer & Carter 1991) contends that volcanic explosions or high-strain-rate tectonic processes may be capable of similar effects to those of impact-induced shock.

Robertson et al. (1968) and Stöffler & Langenhorst (1994) have suggested progressive schemes for determining the intensity of shock from the character and orientation of planar deformation features. For the samples from the Goyder structure, the predominance of fractures over planar deformation features, the dominance of planar-deformation-feature poles parallel to c{0001}, and the prevalence of single sets of planar deformation features per grain, suggest moderately weak shock effects. Weak shock is consistent with the suggestion that the structure is deeply eroded, and that more highly shocked material that occurred near the original surface has been removed, as discussed below.

Shatter cones are also widely considered to result from conditions of shock pressure, such as those that are known to occur naturally only during hypervelocity impact (e.g., Dietz 1968). Once again, a minority view contends that these features could be produced by internal explosions such as those associated with diatremes (Officer & Carter 1991).

A number of other observations are consistent with an impact origin for the Goyder structure. These observations include:

- a circular feature younging and dipping radially outward, and having its central portion uplifted relative to the surrounding terrain;
- the roughly radial fault pattern; and
- an abundance of macroscopic fracturing, microfaulting, brecciation, and quartz veins within an area surrounded by essentially flat-lying and largely undeformed sedimentary rocks.

Other modes of origin seem unlikely, as no igneous rocks were found in or around the structure and no sedimentary diapirism has been reported from the McArthur Basin. Small structural domes mapped elsewhere in the McArthur Basin are clearly associated with major faults which bisect and displace the halves of the dome. Such domes are generally more elongate and less regular than the Goyder structure.

Original form and size

The outcropping structure is interpreted as the erosional remnant of the central uplift of a complex impact crater. Erosion has probably reached a level well below the original crater floor. No obvious indicators of the original crater rim are preserved. If such features as ring faults are present, they are not exposed.

From studies of well-preserved terrestrial craters, general empirical relationships have been established between crater diameter and the dimensions and amount of uplift of the central peak (Pike 1985; Grieve 1991; Grieve & Pesonen 1992). Thus, the original diameters of complex craters can be estimated if the original statistics of the central peak can be determined. However, Grieve (1991) cautions that only the most general relationships can be inferred from the spread of data provided by terrestrial impact structures.

For the Goyder structure, there is some doubt about the original size of the central peak. The preservation of the outer annulus is due to the existence of a moderately resistant stratigraphic horizon, the Hodgson Sandstone Member, between more recessive mudstone-bearing units. Thus, this feature does not necessarily represent the outer limit of the structural uplift, although no significant uplift is evident in the few outcrops of Corcoran Formation observed south of the annulus. The apparent diameter of the structural uplift is affected by the depth of subsequent erosion, another uncertain parameter at the Goyder structure. The amount of structural uplift is also difficult to calculate because the original surface position is unknown, and because the thicknesses of the stratigraphic units involved could not be accurately determined. If the outer diameter of the annulus is assumed to be not substantially different from the diameter of

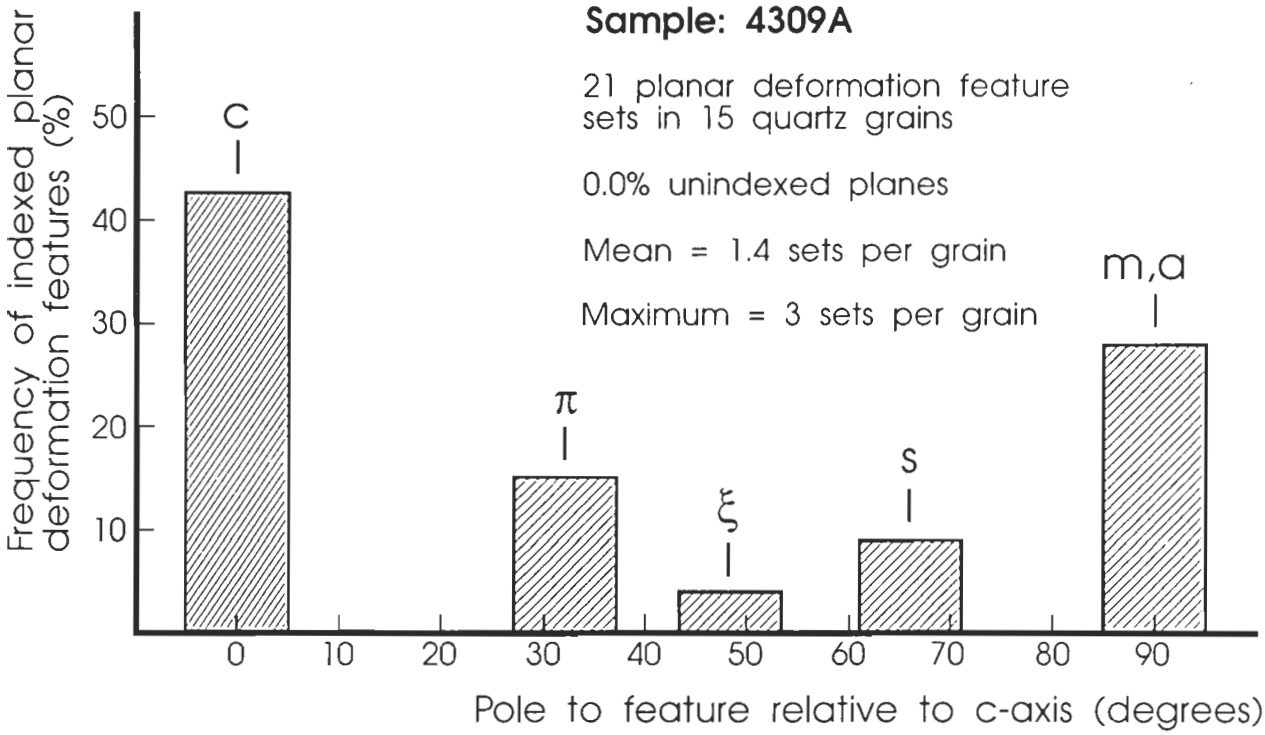

Figure 6. Frequency-distribution histogram depicting orientations of poles to sets of planar deformation features relative to the c-axis in quartz grains for a sample from the central shatter-cone locality. The positions of quartz crystallographic indices are indicated by their symbols. Measurements were determined by Ann Therriault at the Geological Survey of Canada.

the original central peak, then broad comparisons can be made with the data from other terrestrial impact structures presented graphically by Grieve (1991). To fit within the wide spread of these data, a crater with a central peak of 3 km diameter could have a diameter of between about 7 and 25 km.

The slight bilateral symmetry of the structure might indicate that the impact was somewhat oblique, considering that the pre-impact geology was probably fairly uniform. The weak axis of symmetry is oriented roughly north–south, suggesting a northerly or southerly trajectory.

Age

The time of impact that produced the Goyder structure is poorly constrained. No melt rocks or pseudotachylites that could be amenable to isotopic dating have been found at the site. A maximum possible age is given by the Mesoproterozoic (~1400 Ma) age of the target rocks. Outcrops younger than the Roper Group are not exposed close enough to the Goyder structure to have been significantly affected by the impact.

As the impact structure is believed to be deeply eroded, some idea of its antiquity may be gained from the erosional history of the McArthur Basin. Thin Early to Middle Cretaceous deposits once blanketed much of the basin, but erosion has reduced them to scattered relict flat-lying outcrops. The basal unconformity of these deposits generally lies close to the modern land surface. The deposits fill valleys, and cap and abut low ranges. The modern topography is therefore at a late stage of being exhumed, and apparently is little different from the pre-Cretaceous topography (Haines et al. 1993).

Scattered thin flat-lying outcrops of Cretaceous rocks are present across the low-relief terrain in which the Goyder structure is situated, and their basal unconformities essentially coincide with, or lie a little above the modern land surface, as observed on a regional scale. The nearest Cretaceous outcrop is about 7 km to the east of the Goyder structure. These observations suggest that the area surrounding the Goyder structure has had a similar erosional history to other parts of the McArthur Basin, and that the Proterozoic terrain has not been lowered significantly by erosion since the Cretaceous. The erosional history before the Cretaceous is unknown. The degree of inferred erosion since the impact event is thus more consistent with a pre-Cretaceous age for the Goyder structure.

Relationships with Cretaceous rocks also have been used to infer the age of the neighbouring Liverpool crater. At its centre, this crater contains undeformed sandstones which Guppy et al. (1971) have interpreted as Cretaceous in age. Consequently, these authors contend that the Liverpool crater is Cretaceous or older and has been recently exhumed. They suggest that its excellent state of preservation implies that the impact occurred close to the time of burial by Cretaceous sediments. By contrast, a considerably longer period of erosion before Cretaceous burial can be inferred for the more deeply eroded Goyder structure.

Acknowledgments

Fieldwork was undertaken while I was employed by the Northern Territory Geological Survey. I am grateful to traditional Aboriginal owners and the Northern Land Council for permitting access to the area. I am also indebted to A. Therriault for performing universal-stage measurements of planar deformation features in quartz, and to A. Therriault and R.A.F. Grieve (Geological Survey of Canada) for comments on thin sections. Barry Pietsch (Northern Territory Geological Survey) is thanked for discussions on the local geology. The manuscript was substantially improved following reviews by M.W. Wallace, E.M. Shoemaker, A.J. Stewart, A.Y. Glikson, and an anonymous referee.

References

Alexopoulos, J.S., Grieve, R.A.F. & Robertson, P.B., 1988. Microscopic lamellar deformation features in quartz: discriminative characteristics of shock-generated varieties. Geology, 16, 796–799.

Dietz, R.S., 1968. Shatter cones in cryptoexplosion structures. In: French, B.M. & Short, N.M. (editors), Shock metamorphism of natural materials. Mono Book Corporation, Baltimore, 267–285.

Grieve, R.A.F., 1991. Terrestrial impact: the record in the rocks. Meteoritics, 26, 175–194.

Grieve, R.A.F. & Pesonen, L.J., 1992. The terrestrial impact cratering record. Tectonophysics, 216, 1–30.

Guppy, D.J., Brett, R. & Milton, D.J., 1971. Liverpool and Strangways craters, Northern Territory: two structures of probable impact origin. Journal of Geophysical Research, 76, 5387–5393.

Haines, P.W., Pietsch, B.A., Rawlings, D.J., Madigan, T.A. & Findhammer, T.L.R., 1993. Mount Young, Northern Territory — 1:250 000 Geological Map Series. Northern Territory Geological Survey, Explanatory Notes, SD53–15.

Jackson, M.J., Muir, M.D. & Plumb, K.A., 1987. Geology of the southern McArthur Basin, Northern Territory, Australia. Bureau of Mineral Resources, Australia, Bulletin 220.

Jackson, M.J., Sweet, I.P. & Powell, T.G., 1988. Studies on petroleum geology and geochemistry, Middle Proterozoic, McArthur Basin, northern Australia. I: Petroleum potential. The APEA Journal, 28 (1), 283–302.

Kralik, M., 1982. Rb–Sr age determinations on Precambrian carbonate rocks of the Carpentarian McArthur Basin, Northern Territory, Australia. Precambrian Research, 18, 157–170.

Officer, C.B. & Carter, N.L., 1991. A review of the structure, petrology, and dynamic deformation characteristics of some enigmatic terrestrial structures. Earth Science Reviews, 30, 1–49.

Pietsch, B.A., Plumb, K.A., Page, R.W., Haines, P.W., Rawlings, D.J. & Sweet, I.P., 1994. A revised stratigraphic framework for the McArthur Basin, NT. The AusIMM Annual Conference, Darwin 1994, 135–138.

Pike, R.J., 1985. Some morphological systematics of complex impact structures. Meteoritics, 20, 49–68.

Robertson, P.B., Dence, M.R. & Vos M.A., 1968. Deformation in rock-forming minerals from Canadian Craters. In: French, B.M. & Short, N.M. (editors), Shock metamorphism of natural materials. Mono Book Corporation, Baltimore, 433–452.

Shoemaker, E.M. & Shoemaker, C.S., 1990. Proterozoic impact record of Australia. International Workshop on Meteorite Impact on the Early Earth, Perth, Australia. Lunar and Planetary Institute Contribution 746, 47–48.

Shoemaker, E.M. & Shoemaker, C.S., 1996. The Proterozoic impact record in Australia. AGSO Journal of Australian Geology & Geophysics (this issue).

Stöffler, D. & Langenhorst, F., 1994. Shock metamorphism of quartz in nature and experiment: I. Basic observations and theory. Meteoritics, 29, 155–181.

AGSO Journal of Australian Geology & Geophysics, 16 (4), 567–585

The Cretaceous/Tertiary-boundary impact and its global effects with reference to Australia

F.L. Sutherland[1]

Considerable evidence exists for a major impact at Chicxulub, Mexico, and its effects at the Cretaceous/Tertiary boundary (KTB). It includes a buried crater, subglobal ejecta, and global fireball deposits that incorporate shocked minerals and non-terrestrial spinels. Platinum-group-element enrichments (Ir anomaly) and marked C- and O-isotope shifts at the KTB coincide with an extinction event. Australia contributes little to the KT impact story so far, but was isolated from the severest impact and extinction effects.

A Chicxulub strike (C- or L-chondrite impactor) explains many KTB features, but does not satisfy all KTB studies. Continuing KTB impact debates include the size of Chicxulub crater, the extent of tsunami deposits, the number of impacts, and the origin of heterogeneous spinels. The role of KT plume volcanism (whether impact-induced or not) and the nature of KTB extinctions (whether caused by climatic cooling or warming and whether sharp, gradual, or latitudinally reduced) are also in debate.

This synthesis suggests that the Chicxulub impact produced a crater 180 km wide and possibly induced tsunamigenic activity; that compositional differences between impact deposits might reflect more than one impact coinciding with the KTB; that the Deccan volcanism predates the KTB in India; and that several KTB sections evince gradual extinctions at high latitudes. Australia formed part of a more subdued southern extinction zone. Recent KTB studies tentatively suggest maximum impact and subordinate volcanic effects within lower latitudes. A search for fireball deposits and KTB fossil suites in Australia, which lay outside the Chicxulub ejecta apron, is needed to improve its KTB story.

Introduction

A major impact on Earth at 65 Ma (Alvarez et al. 1980) was proposed to explain unexpected platinum-group-element (PGE) enrichments (the iridium anomaly) at the Cretaceous/Tertiary boundary (KTB). This impact hypothesis produced its own enormous impact on the scientific research on, and the concepts of, the external control on extinction events in the fossil record (Glen 1994). The search for the impact site was honed by extensive geological, geophysical, and geochronological investigations, and finally focused on the Chicxulub site, Yucatan Peninsula, Gulf of Mexico (Hildebrand 1993).

A large KT impact should have coincided with other major terrestrial events (e.g., the Deccan flood-basalt volcanism), and a lively debate has ensued over their likely effects on KTB phenomena, including mass extinctions (Sutherland 1994). The demise of dinosaurs figured prominently in the mass-extinction debate (Sutherland 1993), without resolving the issue (Benton & Little 1994). This paper aims to summarise present studies on KT impacts, and to present a synthesis of the effects of impact in relation to extinction events during KT time, especially in Australia. Only a small proportion of several thousand papers of the KTB literature is cited here and mostly includes the later literature.

Australia has contributed little to KTB studies (Sutherland 1993). This largely arises from poor exposure of and failure to identify KT sections, and reflects in part the erosion of critical sequences during tectonic instability in major sedimentary basins during KT time (Otway, Bass, Gippsland, northern Tasman basins; Morrison et al. 1989; Hill 1992). However, shocked quartz, a typical KTB indicator, is recorded in the older Tasman Sea sequence off eastern Australia (Alvarez & Asaro 1990) and botanical changes across the KTB in southeast Australian basins have received preliminary studies (Macphail 1994).

In its synthesis, this paper will suggest that Australia escaped more immediate impact effects (ejecta deposits) of a northern KT impact (Hildebrand 1993), and occupied a transitional position in which the effects of mass extinctions appear less severe in the antipodes (Johnson 1993). Comparisons of the KTB boundary impact with the more restricted 0.77-Ma Australasian tektite event, which is better preserved in Australia, were made by Chao (1993). This presentation of the KT impact and its effects aims to stimulate greater attention to KTB studies in Australia.

[1] Division of Earth and Environmental Sciences, Australian Museum, 6 College Street, Sydney, NSW, 2000.

KT impacts

The most precisely dated KTB impact site is the buried crater identified at Chicxulub (65.0 Ma; Swisher et al. 1992). Other, smaller craters previously assigned to the KTB have, after more rigorous dating, proved significantly older (Manson crater; Izett et al. 1993) or younger (Kamensk crater; Izett et al. 1994). Indirect evidence has led to claims of other KT impacts — for example, near Bombay, to account for geophysical profiles across the Indian Deccan flood basalts (Negi et al. 1993); and in the northern Pacific Ocean, to explain the distribution of distinct extraterrestrial spinels in KTB sections (Robin et al. 1993). Such sites are discussed here, but the Chicxulub impact has received the greatest study, and is regarded as the instigator of the global KTB anomalies (McLaren & Goodfellow 1990).

Gulf of Mexico impact

A partly preserved multi-ring impact crater is interpreted from geophysical surveys and drilling to be buried under Tertiary limestone at Chicxulub on the Yucatan Peninsula (Fig.1). The size of the crater (165–180, 240, or 260–300 km wide) is the subject of debate (Hildebrand et al. 1991; Pope et al. 1994; Sharpton et al. 1994). However, a ring of sinkholes (cenotes) in the surface limestone has been related to the underlying crater (Perry et al. 1995), and is considered to mark its outer rim at a diameter of 180 km (Hildebrand et al. 1995).

A KT crater at Chicxulub was disputed on palaeontological dating and volcanic interpretations (Meyerhoff et al. 1994; Adatte et al. 1994). However, precise dating of glassy rocks to the KTB (65.0–65.2 ± 0.05–0.4 Ma; Swisher et al. 1992), identification of melt breccias (Schuraytz et al. 1994), and revised palaeontological dating of overlying marine beds (Marin et al. 1994) consolidate the impact view. Shocked zircons at Chicxulub trend to a 65.5 ± 3-Ma reset age, and suggest source rocks of about 418 ± 16 and 545 ± 5 Ma (Krogh et al. 1993a, b). This compares

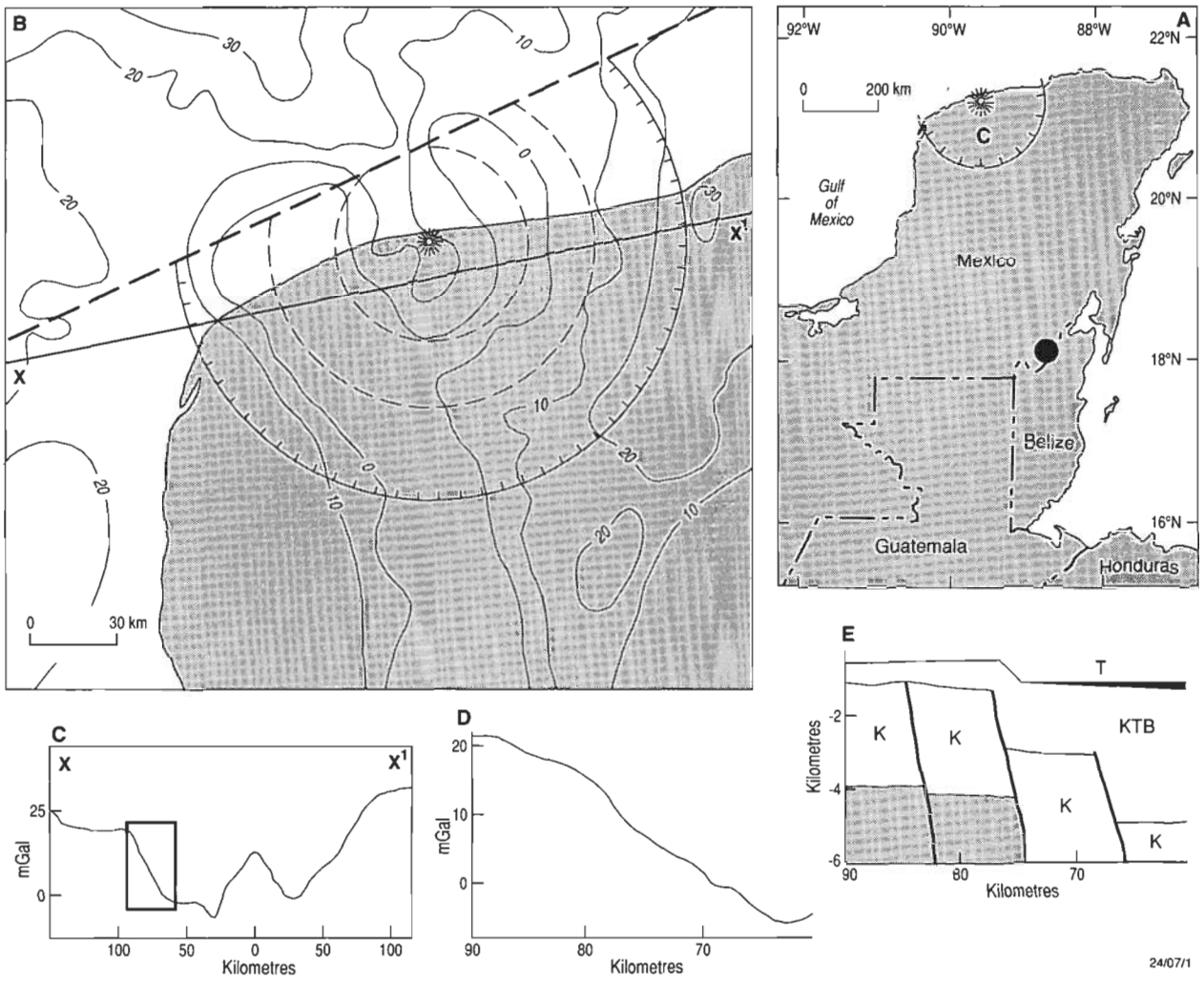

Figure 1(A). Location and structure of the Chicxulub KTB crater (C) with suspected impact site (star) and crater and cenote rim (hatched margin), in relation to the Belize proximal KTB deposit (solid circle). (B). Map of gravity anomalies associated with the Chicxulub crater. The Yucatan coast is screened; the ocean, unscreened. Gravity contours are shown at +10 mGal intervals. The central uplift area (star) is ringed by a gravity low (dashed circles) and crater rim (hatched line). The structure is truncated in the northwest by a regional lineament (heavy dashed line). (C) Bouguer gravity profile (mGal) across the Chicxulub crater along section line x-x^{1} in B. Note the central high, flanking depressions, and crater rim. (D) Part of the observed gravity profile across the Chicxulub crater, 60–90 km from centre; it was used to calculate density differences and assign structural elements within the crater. (E) Interpreted crater structure, 60–90 km from centre, based on drilling and gravity profile (compiled from Ocampo 1995; Hildebrand 1993; and Hildebrand et al. 1995). It shows Tertiary beds (T); KT ejected breccia (KTB), and a layer of overlying melt breccia (black zone); Cretaceous beds (K); and crystalline basement (grey screen).

with a 410 ± 15-Ma rhyolite drilled nearby, and with metamorphosed granitic gneiss and quartz–mica schist in Chicxulub impact breccias. Re–Os isotopes in Chicxulub melt rocks suggest a 3 per cent contribution from an impactor, within the range reported for large craters (Koeberl et al. 1994).

Impact energies calculated for stony bodies 10 km across (1.6 x 10^{12} t) travelling at 25 km s^{-1} (Alvarez et al. 1995) and 32 km across (5.5 x 10^{13} t) travelling at 20 km s^{-1} (Holsapple 1994) are computed as 5 x 10^{23} J and 2.3 x 10^{24} J respectively. These criteria provide likely limits for craters 180 and 300 km in diameter resulting from the cratering process (Melosh 1989). According to Alvarez et al. (1995), for a 180-km final crater, the impact-point shock-wave pressures would have reached about 660 GPa, but declined to under 15 GPa two seconds after the impact.

Ejecta deposits

Synsedimentary ejecta layers yielding KTB ages in Haiti (64.4–65.1 ± 0.05–0.1 Ma), the Gulf of Mexico (64.8–65.1 ± 0.06–0.1 Ma), and mid-west continental North America (65.0 ± 0.03 Ma) have been analysed and correlated with the Chicxulub impact (Izett et al. 1991; Sharpton et al. 1992; Sigurdsson et al. 1992; Alvarez et al. 1992; Swisher et al. 1992, 1993; Dalrymple et al. 1993). Some pseudomorphed ejecta appear to identify the ejecta layer, even when other KTB indicators are dispersed (Pitakpaivan et al. 1994). The ejecta layer has been found up to 4000 km from the Chicxulub target, from which it diminishes in thickness on a power-law basis (Hildebrand 1993; Bohor & Glass 1995). Proximal ejecta are recorded at the Belize KTB, 200 km south of Chicxulub, where boulders up to 8 m in the section attest to the enormous energy of the impact (Ocampo 1995). Closely studied proximal ejecta lie northeast of Chicxulub in Haiti (Kring et al. 1994; Leroux et al. 1995).

Haitian ejecta glasses are preserved as relict cores within smectite replacements (Sigurdsson et al. 1991a b; Izett et al. 1991; Kring & Boynton 1991). They are mainly dark, but some possess coatings and streaks of calcic yellow glass, and honey-yellow glass (up to 7%) forms a separate group within samples. The dark glasses resemble basaltic andesite to dacite in composition, and average a crustal andesitic composition. The yellow glasses show the lowest Si and highest Ca, and those with high Ca (up to 30 wt %) contain sulphur (up to 1 wt %).

The water contents of the glasses are more similar to those of impact glasses (Koeberl 1992) than volcanic glasses (Lyons & Officer 1992; Officer & Lyons 1993), but the matter remains in dispute (Koeberl 1994a; Robin et al. 1994a). An Haitian high-Ca, sulphide-bearing yellow glass was considered to be fused sulphate-rich evaporite (Sigurdsson et al. 1991b, 1992), but this interpretation did not match oxygen-isotope and trace-element results, which suggest <10 per cent sulphate content and a likely limestone–sandstone admixture (Blum & Chamberlain 1992; Koeberl 1993, 1994b). An Haitian-glass–Chicxulub-melt-rock mixing array, unrelated to volcanic trends, was proposed by Kring & Boynton (1992), but their plots were criticised on petrological grounds (Schuraytz & Sharpton 1993). The difficulties regarding groundmass alteration of the Chicxulub melt-rock, and the adopted petrological projections, were clarified by Kring & Boynton (1993), who showed that the main mixing-array and very high-Ca honey-coloured glasses form two distinct trends which they attributed to melt ejected from different regions of the crater. In addition, glasses within the mixing array have similar Sr, Nd, and O isotopes (Blum et al. 1993), and, although problems with precise source lithologies remain (Koeberl 1993), further glass analyses are compatible with the mixing-array compositions (Bohor & Glass 1995).

Isotopic signatures for U–Th–Pb, Rb–Sr, and Sm–Nd in dark Haitian glasses suggest continental post-mid Proterozoic (<1080 Ma) and probably post-Ordovician (<400 Ma) source rocks (Premo & Izett 1992). Oxygen isotopes of both the dark and yellow glasses follow a terrestrial fractionation line in $\delta^{16}O$–$\delta^{18}O$ plots (Hough et al. 1994). Carbon isotopes measured on the dark glasses yield one component in which $\delta^{13}C$ –0.8‰ was released between 420 and 460°C, suggesting a marine carbonate target; and another component in which $\delta^{13}C$ –19‰ was released between 350 and 600°C, matching C-isotope values and combustion temperatures found in residues containing nanodiamonds in a distal Canadian KTB layer (Hough et al. 1993, 1994). Sulphur-isotopic studies of calcic glasses showed that S and Ca vary considerably in the yellow glasses, which incorporate high-Ca components other than anhydrite according to 60 per cent of the analyses (Chaussidon et al. 1994). Thus, isotope studies indicate that continental target rocks, Ca-carbonate-dominant marine sediments, and minor anhydrite beds all contributed to melt ejected from Chicxulub crater.

The Haitian ejecta underlie other fallout materials — including abundant shocked quartz, distinct Ni-rich spinels, and an Ir anomaly (Kring et al. 1994; Bohor & Glass 1995; Leroux et al. 1995). The moderately large size (up to 1.25 mm), amount (up to 70% quartz), and enormous concentration (up to 10^4 grains cm^{-2}) of shocked quartz at the Haitian KTB compared with other KTB sites confirms its proximity to the impact target. Isotopic analysis of shocked KT zircons have yielded source ages similar to those found at Chicxulub (ca 418 and 545 Ma; Krogh et al. 1993a, b). The impact that provided Haitian KTB ejecta excavated silicate lithologies dominated by quartzite and metaquartzite, granitic to andesitic rocks, and marine carbonates — all from probably different stratigraphic levels (Kring et al. 1994). Amphiboles in Haitian KTB beds suggest formation pressures equating with depths of 9–12 km (Sigurdsson et al. 1994), but they are probably related to local volcanic sources rather than an impact source (Kring et al. 1994).

Gulf of Mexico–Caribbean KT tsunamigenic deposits

A continuing debate focuses on the extent of secondary tsunamigenic deposits generated by impact into a shallow-marine shelf at Yucatan during KT time (Smit et al. 1994b; Stinnesbeck et al. 1994). True impact-generated tsunamigenic deposits are championed by some (Florentin et al. 1991; Alvarez et al. 1992; Smit et al. 1992, 1994a), and are claimed to extend to between 2000 and 3000 km from the Chicxulub impact site. Others interpret these as sea-level low-stand deposits (Keller et al. 1993a; Stinnesbeck et al. 1993; Savrda 1993; Beeson et al. 1994). Ginsberg (1994) has summarised the two views. Further support for tsunamigenic activity in the Gulf of Mexico is claimed from studies of fossil charcoal at the KTB, which is regarded as vegetation burnt in a firestorm and washed far offshore in a tsunamigenic backwash (Kruge et al. 1994).

Resolving the debate might hinge on defining criteria for recognising the behaviour of mega-tsunamis in the complex marine embayments that would have existed during KT time (Bourgeois 1994).

Global KT fallout

The KT ejecta deposits (Fig. 2) are overlapped by a fireball layer 2–6 mm thick, and the impact couplet extends for 4000 km beyond Haiti (Bohor & Glass 1995). The fireball layer contains the bulk of shocked quartz (attributed to impact; Stöffler & Langenhorst 1994), the PGE enrichment (including the Ir anomaly; Evans et al. 1993), Ni-rich spinels (Robin et al. 1992), and high-pressure minerals (such as stishovite and impact or plasma-formed diamonds; Gilmour et al. 1992). It also includes soot (e.g., Sumbar site; Wolbach et al. 1990) — attributed to wild fires ignited by impact and ballistic re-entry heating — and traces of fullerenes attributed to the sooting process (e.g., New Zealand sites; Heymann et al. 1994). The grainsize and percentage of shocked quartz in this layer decreases north away from the Chicxulub impact site and across the globe to minimal values in New Zealand KTB sites (Kring et al. 1994). Two distinct forms of glassy fragments occur in the fireball layer (Bohor & Glass 1995): splash-form ejecta, attributed to the fusion of target rocks; and a globally distributed form of accreted, partly alkaline spheroids, formed by condensation of fireball material. In marine KTB deposits, the glassy materials were largely altered by hydration to palagonite and then smectite and smectite–illite mixtures, whereas those in terrestrial deposits commonly altered to kaolinite and sometimes gorceixite (Sigurdsson et al. 1991a; Izett 1991; Evans et al. 1994).

An asymmetric fallout distribution (size of shocked quartz; distinct Pacific spinels) may imply a northwesterly directed low-angle oblique impact at Chicxulub (Schultz & Gault 1990; Kyte & Bostwick 1995). Alternatively, Alvarez et al. (1995) have explained the size and distribution of shocked quartz by energetic high-angle launch (>65°) into the atmosphere, followed by ballistic re-entry and fall onto a rotating globe. In this

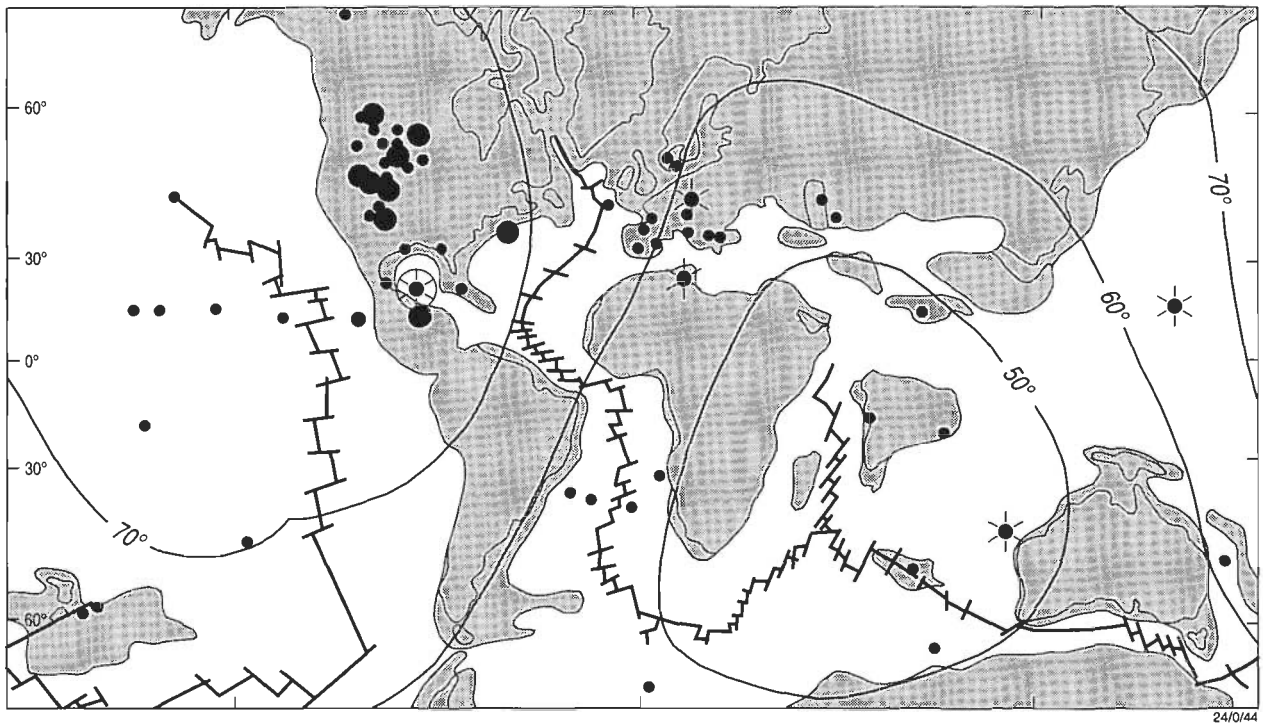

Figure 2. Global distribution of KTB impact deposits relative to the Chicxulub impact site (circle with star) and Australia (map modified from Alvarez & Asaro 1990). It shows sites containing large fragments of shocked quartz (large filled circles), sites with small shocked quartz (small filled circles), and sites at which distinctive non-terrestrial spinels have been sampled (star). The limits of the shadow zones for secondary reimpact of ballistic ejecta launched at angles of 50°, 60°, and 70° elevation from a Chicxulub impact are shown as contours (after Alvarez et al. 1995).

model, the Chicxulub impact produced a fireball 'doublet' consisting of:

- a very hot fireball of vaporised meteorite and target carbonate and silicate rocks; and
- a warm fireball of carbon dioxide and steam, which jetted shocked minerals into their steep trajectories.

Both types of fireball formed before the ejecta were expelled. However, the ejecta curtain would have arrived at distant sites first owing to its low-angle flight path (up to 45°). The warm fireball debris would have followed, and, thereafter, the fine hot fireball material would have settled more slowly. Calculated travel times for ejecta-curtain and steep-trajectory materials derive falls from minutes to tens of minutes apart for the two types of deposit across North America. The model predicts that the Ir is concentrated at the top of the final fallout. As Australia lay outside the ejecta radius and largely within the shadow zone for eastbound ballistic launches at elevation angles of 50–60° (Fig. 2), only rare fine-grained shocked quartz would be expected in KT fallout over the continent.

The PGE anomaly usually contains a background contamination of volcanic elements (Sawlowicz 1993), but a high-Ir anomaly (14 ppb) in the Pacific (DSDP site 596) is accompanied by atypical PGE/siderophile- and chalcophile-element ratios (Zhou et al. 1991). PGE/Ir ratios vary in relation to chondritic value, and northern sites approach chondritic values more closely than southern sites (Tredoux et al. 1989). Global integration of PGE concentrations produces a flat chondrite-normalised pattern, suggesting a Cl- or L-chondrite impactor (Evans et al. 1993). Increasing Ru/Ir ratios (0.6–3) with palaeodistance from Chicxulub are related to primary fractionation within the fireball cloud (Evans et al. 1995). The high Se, Sb, Co, Fe, Ag, As, and Zn that accompanies the KTB PGE anomaly has been attributed to marine processes (Gilmour & Anders 1989) or terrestrial causes (Vannucci et al. 1990). These element enrichments are present in a Deccan basalt sequence, which favours a wider fallout than just a marine process (Bhandari et al. 1995).

A sharp Ir peak was confirmed in some intensively studied KTB sections (e.g., Gubbio, Italy), and subsidiary Ir peaks are usually considered to represent reworking (Alvarez et al. 1990; Zhou et al. 1991; Habib 1994). Some Ir anomalies rise from a broad low Ir hump, which is considered to be a definitive feature (Gubbio; Rocchia et al. 1990). In the Ir anomaly in the east Indian marine KTB (Bhandari et al. 1993a, b, 1994, 1995; Fig. 3), the main peak (12 ppb) and broader basal anomaly (under 0.3 ppb) evince different Os/Ir ratios (0.4 and 1.8). An impact origin for the subsidiary Ir hump is unlikely, as it lacks a persistent Ni-rich spinel component, and it may represent a volcanic input (Rocchia et al. 1990; Bhandari et al. 1993b, 1994) or extended cometary debris infall (Bhandari et al. 1994, 1995).

The marine Ir anomaly accompanied a peak in $^{87}Sr/^{86}Sr$ ratios, ascribed to enhanced Sr stripped from continental rocks by acid rain following an impact (Martin & Macdougall 1991). According to Nelson et al. (1991), a shift in Sr-isotope ratios preceded the KTB. A slight increase in isotopic ratios below the boundary, noted in a detailed study of the Sumbar section, would argue against a single catastrophic cause, unless the underlying sediment and boundary clay had been mixed (Meisel & Pettke 1994). The maximum $^{87}Sr/^{86}Sr$ ratio in the Sumbar boundary clay coincides with a minimum $^{187}Os/^{188}Os$ ratio, favouring a combined impact/acid rain or tsunamigenic process, rather than volcanism, as the main KTB contributor (Meisel et al. 1995).

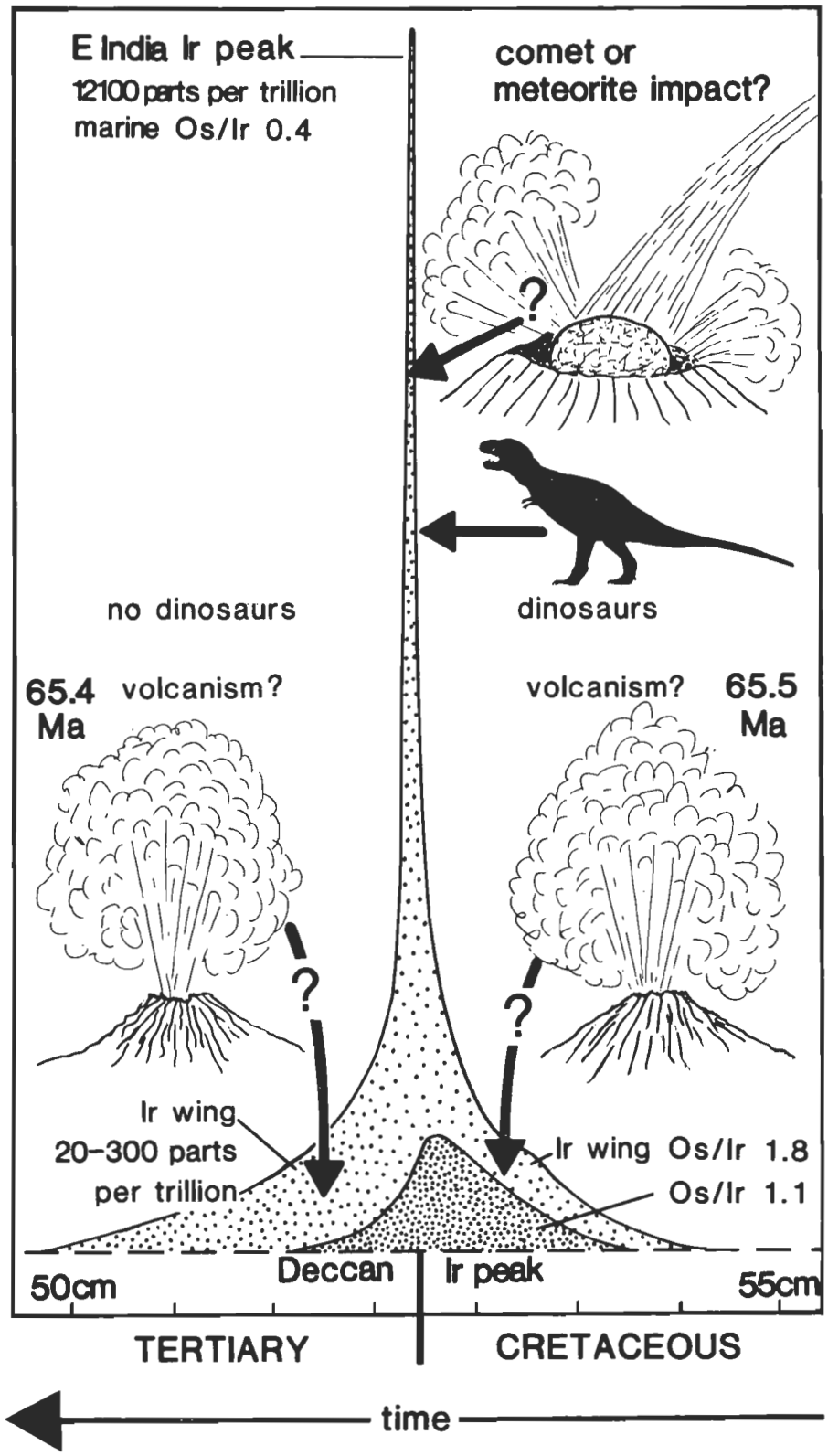

Figure 3. Summary diagram of Indian KT Ir anomalies (Meghalaya marine and Deccan terrestrial sections) in relation to KT extinction and volcanism (based on data from Bhandari et al. 1994, 1995). The horizontal scale records the thickness of the KTB layer in centimetres relative to the iridium peak. The diagram assumes contemporaneous marine and terrestrial Ir peaks, and the dinosaur represents no particular species. Adapted from Sutherland (1993).

Multiple impacts?

The impact ejecta-fireball model neatly explains dual-layered KTB deposits (Hildebrand 1993; Bohor & Glass 1995), although some discrepancies were reported in some sections. In distant North American KTB sections, these include time breaks involving growth periods of plants or significant erosion (Wolfe 1991; Shoemaker & Izett 1992; Chao 1993). The interpretation of a growth period is questioned by Alvarez et al. (1995). In their model, they considered that the plant roots were carbonised by infra-red heat from the re-entry of ejecta a few minutes before a hail of shocked quartz. At Haiti, ejecta glasses and overlying shocked quartz, Ni-rich spinel, and enriched Ir form a quasi-simultaneous deposit that is overlain by an additional horizon of shocked quartz, spinel, and high Ir, from which it is separated by 4 cm of sedimentary deposit (Leroux et al. 1995). This sequence differs from that produced by the

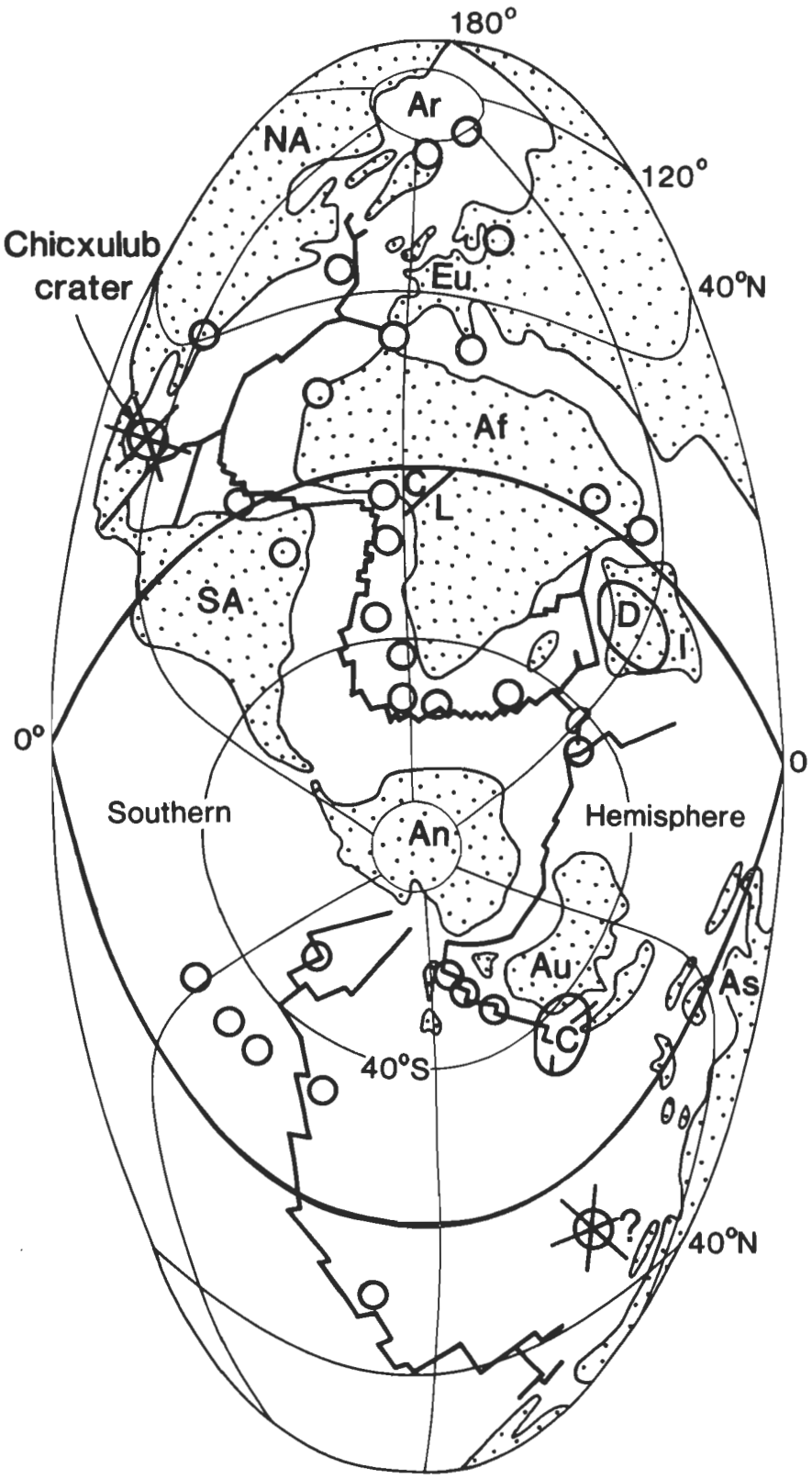

Figure 4. Distribution of proposed KT impact sites (star bursts) and hot-spot/hot-line basaltic plume volcanism (unfilled circles, and lines) based on a 65-Ma south-centred projection of continents (stippled areas) and oceans (blank areas, with spreading-ridge lines). The Chicxulub crater is labelled, and a potential Shatsky Rise Pacific impact is question-marked. The main southern volcanic features include the Cameroon Line (C/L), Deccan plume (D), and Coral Sea plume (C). Also shown: North America (NA), Arctic area (Ar), Eurasia (Eu), Africa (Af), South America (SA), India (I), Antarctica (An), Australia (Au), and Asia (As). Modified from Sutherland (1994).

doublet fireball (Alvarez et al. 1995), which is represented in the lower impact deposit, and does not equate with merely one impact. The quartz and spinel grains in the upper layer are distinct from those in the lower impact deposit (at the KTB), and suggest that a second, separate impact followed the Chicxulub impact.

Suggestions of a prior impact come from the marine sequence at Walvis Ridge, South Atlantic (Huffman et al. 1990). Here a prominent secondary peak in shocked minerals and characteristic element enrichments is recorded 1.9 m below the KTB, corresponding to some 10^5 y of intervening deposition. Multiple impacts were proposed by some workers according to distinct geochemistry of KTB spinels within discrete regions. A Pacific impact near Shatsky Rise was proposed to explain a 2×10^7 km^2 spread of homogeneous Al-rich spinels (Robin et al. 1993), and distinct inhomogeneities in European and North African spinels

compared with more oxidised, homogeneous Pacific and Indian Ocean spinels were attributed to impacts of different sizes (Robin et al. 1994b). These variations, alternatively, were related to a single impact, in which different spinel compositions reflect variations in formational temperatures within an expanding fireball (Kyte & Bostwick 1995).

KT impact and volcanism

Detailed isotopic and magnetic dating of the 500 000 km^2 Deccan basalt field suggested that major flood basalt volcanism coincided with KTB events (Courtillot et al. 1990; Baksi & Farrar 1991). However, precise relationships between the volcanism, KTB impact, and extinctions remain contentious (Sutherland 1994). Three causes of voluminous KTB volcanism have been advanced:

- mantle melting in response to a direct major impact;
- mantle melting through transmitted shock waves from an impact; and
- mantle melting caused by impingement of a deep mantle plume, unrelated to an impact.

Impact-induced volcanism

Some workers consider that the Deccan volcanism was triggered by a direct impact below the focus of flood basaltic activity, and point to abnormal structures detected in the shallow lithosphere by gravity surveys (Negi et al. 1992, 1993). These include an unwarped asthenosphere (40 km depth) and shallow Moho (18 km depth) below a dense 'magmatic' conduit (18–5 km deep). These structures were linked to the formation of fractionated tholeiitic basalts that prevail in the Deccan sequence, rather than to the activity of a deep mantle plume.

An alternative view which involves impact, but not an in-situ strike, maintains that lithospheric fracturing and flood volcanism are triggered by the transmission and focusing of shock waves from a major antipodal impact (10^{24}: Rampino & Caldeira 1992). Thus, Deccan volcanism could reflect a Chicxulub impact, although cause and effect would be offset by 120° rather than a true antipodal 180° (Fig. 4). Detailed computer simulations of axial focusing of energy from a hypervelocity impact can generate conditions for major melting at antipodal points (Boslough et al. 1995), and predict that shock waves travel around the globe in 90 minutes (see pictures in Jackson 1995). This mechanism might be feasible if the Deccan volcanism correlates closely with impact, and can be assessed with reference to a critical appraisal of the dating of the basaltic sequence.

Impact versus plume volcanism

$^{40}Ar/^{39}Ar$ dating of Deccan lavas and intrusives reported by Venkatesan et al. (1993) and Basu et al. (1993) has challenged a KTB age for rapid Deccan volcanism during Chron 29R. These studies placed isolated early Deccan alkaline activity at 68.5 Ma; major basalt eruption during 66 Ma; and an eruptive span extending to at least 65 and possibly 63 Ma. This revision of ages was disputed on experimental technicalities by Féraud & Courtillot (1994), but in reply was reaffirmed by Venkatesan et al. (1994). Further $^{40}Ar/^{39}Ar$ dating of basalt enabled Baksi (1994) to ascribe 80 per cent of the exposed Deccan sequence to eruption between 65 and 64 Ma in Chron 29R. A decisive breakthrough came with the location of the KTB Ir anomaly in sediments between basalt flows dated at 65.4 and 65.5 Ma within the Deccan sequence, proving initial volcanism was not triggered by impact (Bhandari et al. 1995).

Further support for pre-Deccan rifting, plume incubation, and basalt extrusion before the KTB comes from several other avenues. These include:

- gravity and seismic results in the Cambay rift basin, which suggest a thick basalt fill and late-Cretaceous rifting (Tewari et al. 1995);
- a deep mantle origin for the Deccan melting, according to plume studies (Campbell & Griffiths 1992; Coffin & Eldholm 1993);
- a primitive high ^3He mantle-plume signature for initial Deccan volcanism (Basu et al. 1993);
- finds of Late Cretaceous eutherian mammal remains between flows 4 and 5 in the southeast Deccan basalts (Prasad et al. 1994); and
- dating of southwest Indian dyke swarms by $^{36}Ar/^{40}Ar$-versus-$^{39}Ar/^{40}Ar$-isotope correlations combined with palaeomagnetic measurements (Radhakrishna et al. 1994); which suggest Deccan-style basalt eruptions here at 69 ± 1 Ma during Chron 31 before erosion removed the flows.

Present evidence favours deep-plume Deccan magmatism preceding any KTB impact. Rapid major later intrusion of magma into decoupled zones within the lower crust and asthenosphere (Singh & Meissner 1995) can account for both magnesian basalts (originating around 100 km depth; Murari et al. 1993) and fractionated tholeiitic basalts (in which geochemistry suggests initial incorporation of Archaean amphibolites and later considerable crustal contamination; Peng et al. 1994; Peng & Mahoney 1995).

KT impact and extinction effects

The KTB marks a mass extinction event, particularly among marine biota (47% genera, 76 ± 5% species extinction; Jabolonski 1991). These extinctions have been linked to abrupt climatic and water-temperature and -chemistry changes induced by the Chicxulub impact and its global wild fires (Sigurdsson et al. 1992; Brett 1992; Ivany & Salawitch 1993a; Pope et al. 1994; D'Hondt et al. 1994). Atmospheric effects such as dust screens, acid rains, aerosol cooling, and greenhouse warming generated by the pulverisation and volatilisation of target rocks and water-column effects have been evaluated by numerical simulation of impact cratering (Takata & Ahrens 1994). The impact would have produced as much as 5 x 10^{15} kg of partly volatilised material from its strike into submerged carbonate evaporative platform sediments (Alvarez et al. 1995). The precise balance between cooling and heating effects estimated in the calculations depends on the exact size and target lithology of the impactor and its arrival time relative to the Earth's hemispherical seasons. Some relative magnitudes of these effects are now considered.

Acid rains and global cooling represent two effects of a major impact. Maximum estimates for nitric acid produced by atmospheric entry of the impactor, and sulphuric acid generated by the Chicxulub impact, are 10^{15} and 10^{17} moles respectively, but total acid contents probably remained under 10^{15} moles, according to observed fresh- and marine-water acidification and KT

extinction patterns (D'Hondt et al. 1994). Thus, acid rains were not regarded as a probable prime cause of KT extinctions.

Instead Pope et al. (1994) favoured a decade of major aerosol cooling (impact winter). They calculated a -300 W m^{-2} cooling from sulphate aerosol reactions relative to a $+8$ W m^{-2} greenhouse warming from released carbon dioxide; final cooling would have been buffered by heat exchanges at the surface. Their sulphate-induced cooling estimate, based on an impact that produced a 180-km crater and 4×10^{17} moles of released sulphur dioxide, was less than an earlier estimate by Sigurdsson et al. (1992) for a similar-size impact releasing 2×10^{18} moles of sulphur dioxide. The higher value was based on a high anhydrite component for yellow impact glasses, which isotopic measurements later showed to be intensely heterogeneous in sulphur (Chaussidon et al. 1994). The later sulphur dioxide estimate may still be excessive, as shock-induced volatilisation reactions of calcium sulphate up to 42 GPa produce 10^{-2} less sulphur dioxide and sulphur trioxide than amounts calculated from equilibrium (Chen et al. 1994). These authors suggested that sulphate-cooling dropped global temperatures 5 to 9°K over tens of years, which they considered insufficient for a major KTB extinction mechanism.

The calculated effects of short aerosol-cooling and longer greenhouse-warming depend on the criteria applied to the model. Thus, for a large impactor forming a 300-km-diameter crater, the maximum amount of carbon dioxide added to the atmosphere would have ranged between 10^{16} and 10^{19} kg, corresponding to a calculated maximum warming effect of 4°C (Takata & Ahrens 1994; Pope et al. 1994). This is less than earlier estimates of 2–10°C (Chen et al. 1994). The likely balance of the aerosol-cooling/greenhouse-warming can be judged from oxygen-isotope records measured across the KTB (–8 to +4°C; Brett 1992). In the undisturbed KTB section at Mangyshlak, Kazakhstan (Sarkar et al. 1992), high-resolution $\delta^{18}O$ analyses across the section suggest a rapid cooling (6°C) over 10^3 years at the boundary, followed by fast warming (10°C) in the next 10^3 years. This matches a catastrophic event such as an impact, although the slow organic productivity change shown by the $\delta^{13}C$ profile at Mangyshlak seems more compatible with complex multicausal events.

Wholesale destruction of organisms and consequent disruptions to carbon productivity and carbon dioxide exchanges from the KTB impact are correlated with observed shifts in carbon-isotope records (Hollander et al. 1993). This view interprets a short-term negative anomaly in $\delta^{13}C$ and a following sharp positive anomaly (10^3–10^4 y) in terms of a period of lifeless oceans, which became invaded by algal blooms before more normal productivity resumed. This interpretation may not explain the full complexity of KT records — for example, where the production and burial of organic carbon continued in local terrestrial and shallow-marine environments (Kump 1991; Meyers 1992). Assuming a 25 per cent burning of global plant mass, Ivany & Salawitch (1993a) attributed the negative shift in $\delta^{13}C$ in marine carbonate sections to the absorption of isotopically light carbon dioxide released into the atmosphere by impact wild fires. This view was challenged (Keller & MacLeod 1993) but entered into a dispute (Ivany & Salawitch 1993b). An increase in carbon and a negative shift in $\delta^{13}C$ (–2 ‰) also appear in non-marine sections at the KTB (Gardner et al. 1994). A corresponding increase in nitrogen and a negative shift in $\delta^{15}N$ accompany the changes in carbon in non-marine KTB sections, but there is little evidence for the fixation of nitrogen from atmospheric shock-induced nitric acid rain at the KTB.

Terrestrial extinctions

Terrestrial extinctions at the KTB include significant reductions and disappearances of some faunal groups, particularly among vertebrates, and widespread changes in flora (Upchurch 1989). Among North American vertebrates, those feeding on the freshwater food chain fared best by sustaining less than 40 per cent extinction of genera (average 26%), while those feeding on the terrestrial food chain fared worst; several groups lost over 40 per cent of their genera (average 55%). Some groups, such as the dinosaurs suffered total extinction; all later appearances represent reworked remains (Sutherland 1994).

The dinosaurs were used to test catastrophic versus non-catastrophic causes for their extinction (Williams 1994a). This test showed no decline in dinosaur remains up to the KTB, but revealed a non-random distribution, not predicted by the impact-extinction model. Reasons for the lack of a high count of dinosaur remains at the KTB were discussed by Hunter (1994), but Williams (1994b) still questions the impact model. In another test for an impact hypothesis, survivors among vertebrate species in Montana (53 out of 104 species) across the KTB were matched against predicted environmental factors by Archibald (1994). He considered that habitat fragmentation from marine regressions had greater influence on the vertebrate turnovers than an impact, and that a single-cause extinction was unlikely. Such testing is disputed by Fastovsky & Sheehan (1994), who suggested that an 88 per cent land-dwelling vertebrate extinction compared with a 10 per cent aquatic vertebrate extinction is best explained by radiation loss from an impact. Among invertebrates, insects show little evidence of global changes in genera across the KTB, although some groups increased in biodiversity (Jarzembowski & Ross 1993).

Pronounced changes in flora are apparent across the North American KTB (Nichols et al. 1990), and evidence for snap-freezing of aquatic leaves in their reproductive stage was cited for an 'impact winter' within a summer season (Wolfe 1991). Detailed studies suggest that North American–Canadian KTB sections show complex regional extinctions: the floras in the boundary bed are different from those below it, and reflect recolonisation by indigenous rather than distant survivors (Sweet & Braman 1992). KT terrestrial floral collapses can be traced into marine sections through the sudden influx of environmentally resistant plant spores, such as bryophytes (Netherlands KTB; Brinkhuis & Visscher 1994). The predicted season of impact, based on limited floral evidence, has important consequences for considering extinctions in polar regions, where animals and plants had already adapted to conditions of low temperature and reduced light.

Detailed studies of vertebrate faunas in Late Cretaceous sections on the Alaskan North Slope revealed a mainly endothermic population of dinosaurs and mammals (Clemens & Nelms 1993a). There were no traces of amphibians and non-dinosaurian reptiles typical of vertebrates in North American sections of this age in middle palaeolatitudes. As the Alaskan vertebrate faunas that were adapted to cold, dark conditions did not survive the KTB, whereas faunas in warmer climates largely survived, Clemens & Nelms argued against short-term cold and darkness (impact winter) as an extinction mechanism. This particularly applies to a northern summer impact. A suggestion that

Alaskan dinosaurs expired from greenhouse-heating — due to excess water vapour after an oceanic impact — generated further discussion, without conclusive agreement (Emiliani 1993; Clemens & Nelms 1993b).

Marine extinctions

Many marine sections show abrupt extinctions of microfaunal species followed by blooms of surviving species across KTB sections (e.g., Black Sea, Bulgaria; Preisenger et al. 1993). The extinctions may reflect marked selectivity, as in the Austrian KTB section, where planktic species fell from 90 to <15 per cent of the faunal assemblage and benthic species increased from 20 to 85 per cent (Peryt et al. 1993). Differences in planktic assemblages approaching the KTB appear in some sections, such as El Kef, Tunisia. Here nannoplanktic assemblages show no change before the KTB, at which level some depth-sensitive planktic foraminifera disappear from the fauna (Pospichal 1994). A catastrophic collapse of both planktic and benthic foraminiferal faunas — apparent at the KTB in Caravaca, Spain — is followed by a rapid rebound in diversity (Coccioni & Galeotti 1994). Sharp negative shifts in carbon-isotope ratios in marine planktic algae (coccoliths) suggest massive extinction of and later redeposition of Cretaceous species (Gartner et al. 1994). In contrast, siliceous micro-organisms may show no evidence of mass extinctions across the KTB, although ratios of different groups may change abruptly — e.g., diatom/radiolarian populations at the New Zealand KTB (Hollis et al. 1995).

The macro-invertebrate marine faunas at the KTB have also received considerable study, particularly molluscan faunas, and some studies suggest that planktotrophically reproducing species were disadvantaged (northern Atlantic Coastal Plain; Gallagher 1991). A detailed study of molluscan faunas in sections above the Texas KTB suggest that a rebound in species diversity was related to a rapid catastrophic extinction (Hansen & Upshaw 1990). A wide survey of KTB molluscan bivalve faunas suggested that their extinction patterns were statistically sharp and similar in intensity on a global scale (Raup & Jablonski 1993). However, after detailed qualitative and quantitative taxonomic analysis of the Crassatellidae bivalves in eastern USA, the accuracy of the published fossil record was questioned (Wingard 1993). This study suggested that unreliable classification had biased the fossil record towards higher rates of evolution and extinction, more catastrophic faunal turnovers, higher species diversity, shorter species duration, and more restricted geographic ranges. A standardised taxonomy in contrast suggested a slower evolutionary rate and a non-catastrophic faunal change at the KTB.

Abrupt versus gradual KTB extinctions

Although abrupt massive extinctions are recorded from many KTB sections, some are claimed to be erosional truncations of more gradual extinction patterns (MacLeod & Keller 1991), particularly sections in higher latitudes (Keller et al. 1993b). These opposing views have created two schools among investigators.

The abrupt school regard anomalous Cretaceous species above the KTB as reworked (Gartner et al. 1994; Habib 1994; Liu & Olsson 1994; Pospichal 1994). The gradual school considers that faunal changes were in train before the KTB, and that Cretaceous forms include significant surviving species (Beeson et al. 1994; Donze et al. 1994; Drobne et al. 1994; Keller 1994a; Keller et al. 1994; Lopez-Oliva & Keller 1994; MacLeod 1994). Some of these conflicts may arise from studying highly disturbed areas near the Chicxulub impact site (Olsson & Liu 1994). To resolve the argument a 'blind test' on samples from the El Kef KTB section in Tunisia was organised. However, the combined results, which yielded a more abrupt picture, remained under dispute (Keller 1994b; MacLeod 1994; Kerr 1994).

Rigby et al. (1993) interpreted a gradual extinction for terrestrial dinosaurs beyond the KTB in the Nanxiong Basin, China. These dinosaur remains occur in the upper part of a section bounded by volcanic horizons dated at 62 and 67 Ma. However, full details are needed to critically appraise both the dinosaur remains as unreworked and the potential error margins in the dating.

The claims of gradual KTB extinctions at high latitudes are supported by recent studies in southern latitudes. In New Zealand KTB sections, flora show muted extinctions (Johnson 1993), and radiolarians remain profligate across the boundary (Hollis et al. 1995). In the continuous KTB sections on Seymour Island, Antarctic Peninsula, the macrofaunas, microfaunas, and floras (including abundant dinocysts) show no compelling evidence for mass extinction (Elliot et al. 1994; Zinsmeister & Griffin 1995). Nearby, in southern Patagonia, South America, studies of gastropods show no clear-cut mass extinction within their ranks (Griffin & Hünicken 1994). In northern latitudes, in the landlocked Arctic Basin, some characteristic Mesozoic shallow-marine bivalves and gastropods are claimed to survive into Paleocene deposits (Marincovich 1993), in contrast to other studies (Raup & Jablonski 1993). However, this may reflect uncertain location of the KTB boundary here (Johnson 1993), and needs further detailed appraisal.

Thus, evidence for differential KTB extinctions on a global latitudinal scale, particularly in the southern hemisphere, appears to be mounting, but it must be considered in terms of environmental changes which preceded the KTB in southern-latitude oceanic sites (36–65°S; Barrera 1994). Stable carbon-, oxygen-, and strontium-isotope data from planktic and benthic foraminifera from these sites reveal major instabilities in the chemistry of both climate and ocean 4 to 6 Ma before the KTB, which was only the last of a series of major environmental changes in the Late Cretaceous. Australia's palaeoposition around 65 Ma was 40–70°S, close to New Zealand at 50–55°S and Antarctic at 70–90°S (Veevers et al. 1991). Thus, Australia extended into the region of lesser KTB extinctions which took place in a climate of cool unsettled conditions.

Discussion

The case for a major KTB impact that formed a crater in the continental shelf at Chicxulub, radiated ejecta over distances of 5500 km, and distributed a global fallout of shocked minerals, meteoritic spinels, and PGE-enriched fine material seems to be sustained by recent investigations (Hildebrand 1993; Bohor & Glass 1995; Alvarez et al. 1995). Nevertheless, several problems concerning details of the impact remain, and require discussion.

Size and number of impacts

Fixing the exact size of the crater at Chicxulub — whether it is around 180 or 300 km in diameter (Hildebrand et al. 1995; cf. Sharpton et al. 1994) — is important for estimating the magnitudes of impact-generated effects. This also bears on potential extinction mechanisms. Upper estimates of the effects of acid

rain and temperature changes are excessive when considered in the light of a single impact event, such as Chicxulub (Takata & Ahrens 1994), but are consistent with indications for multiple KTB impacts (Leroux et al. 1995). Proposals for several small to large KTB impacts invoke compositional differences between Caribbean, European, North African, Indian Ocean, and Pacific Ocean meteoritic spinels (Robin et al. 1993, 1994b), and imply up to five impacts — a radically different concept from that of one impact to explain all KTB features. A separate KTB impact could explain the large Turkemenia soot and Ir anomaly in thick undisturbed boundary clay (lat. 38°N, long. 56°E; Wolbach et al. 1990), a feature not easily matched with an impact and thermal-pulse fall-off from Chicxulub but one closer to the distinct European–North African spinels. In addition, the PGE anomaly is missing in some KTB sections (e.g., in southeast South Africa and Spain; Tredoux et al. 1989; Galbraun et al. 1993; Colombo 1994), of which some, however, may represent reworked sections. The anomaly still awaits discovery and confirmation in some large continental areas (Australia, parts of Russia, and Asia).

Alternative mechanisms could explain the inhomogeneous distribution of spinel and PGE . Examples of such processes are asymmetric or randomly oriented ejections and chemical fractionation during vapour condensation (Kyte & Bostwick 1995), and secondary Ir concentration due to absorption processes correlated with carbon levels at the KTB. Thus, suggestions for several impacts need further substantive support, such as other impact craters dated to KTB time. Identification and study of Australian KTB horizons would help fill a large gap in regional spinel and PGE distribution.

Tsunamigenic effects

Identification of tsunamigenic deposits around the Gulf of Mexico remains a controversial topic (Keller et al. 1993a; cf. Smit et al. 1994a, b). The nature of tsunamis generated by a Chicxulub impact (Bourgeois 1994) must be resolved before disputes about sedimentation, foraminiferal zones, and the nature of extinctions at the KTB can be settled. Some studies provide indirect support for KTB tsunamigenic deposits (offshore burnt logs; Krunge et al. 1994), but others pose difficulties for tsunamigenic interpretations, such as consistent separation of impact glasses and meteoritic spinels within KTB sections (Rocchia et al. 1994).

Until the controversy is settled, the area of interpreted tsunamigenic deposits — extending 2000–3000 km from the Chicxulub crater — is best considered partial or provisional tsunamigenic territory. This marks an area of potentially severe devastation for marine faunas because it lies within the larger apron of lethal effects related to ballistic re-entry of ejecta (Hildebrand 1993).

Volcanic effects

The KTB impact coincided with a period of extensive hot-spot volcanism that created the Deccan flood basalts. The combined effects of impact and volcanism need to be evaluated in relation to KTB extinctions (Sutherland 1994). Although the number of hot spots operating at KTB time (Fig. 4) might have been no more than at the present day, the Deccan eruptions provided a significant additional discharge. The Deccan eruptive ages and rates of volcanic discharge are considered here.

Isotopic ages indicate that the Deccan plume was active before an Ir anomaly was preserved in terrestrial sediments lying between basalt flows 65.4 and 65.5 Ma old (Bhandari et al. 1995). Javoy & Michard (1990) quantified the volume of carbon dioxide released into the atmosphere by the Deccan eruptions as 10^8 moles, which they considered to have been sufficient to produce the size and isotopic composition of the KTB $\delta^{13}C$ anomaly. According to Caldeira & Rampino (1990), the total emission of carbon dioxide (both eruptive and non-eruptive) was around 10^{16} moles, which they calculated to be insufficient to have increased global temperatures by more than 1°C if the Deccan eruptions lasted a million years. However, the longer duration now ascribed to the volcanism (69 to 65 Ma; Basu et al. 1993) would have reduced the atmospheric effects of the released carbon dioxide, and only mildly influenced the KTB $\delta^{13}C$ anomaly or temperature changes. Although plume-related nephelinite–carbonatite complexes are now identified in Deccan activity, and would have discharged higher concentrations of carbon dioxide, they are few and small, and their consideration would not greatly add to the estimates of carbon dioxide emission.

A potential effect of the Deccan activity might be judged from considering the Laki hot-spot eruption of 1783–1785, which created an aerosol cooling of 1–2°C over 3 years, locally reduced livestock by 50 per cent (fluoride poisoning), and indirectly killed 22 per cent of the Icelandic human population (Thordarson & Self 1993). However, the Deccan eruptive sequence reflects periods of sedimentation during which strata up to 9 m thick accumulated, and the development of red boles on some flows, so is unlikely to have caused similar effects beyond isolated short periods. Thus, at best, Deccan volcanism probably only contributed to rather than created any abrupt climatic and environmental changes that would have been required to trigger a mass extinction.

Isotopic dating has suggested that KTB impacts did not initiate the plume-related Deccan flood volcanism through antipodal seismic focusing, although considerable post-65 Ma volcanism is reflected in the Deccan, Greenland, and Cameroon Line eruptives (Sutherland 1994). Cretaceous plumes were already present under southern India (Radhakrishna et al. 1994) and west of Greenland (Lawver & Müller 1994), so they represent neither KTB starting plumes (Campbell & Griffiths 1992) nor KTB impact-produced antipodal plumes (Rampino & Caldeira 1992). However, seismic shock waves from KTB impacts might have galvanised plume systems to generate greater Tertiary Deccan, Greenland, and Cameroon Line eruptions (Sutherland 1994).

Extinction effects

Although the Chicxulub impact correlates precisely with the KTB mass extinctions, accumulating evidence suggests that the extinctions were uneven in a global context. Claims for more gradual marine extinctions were tested and disputed in some KTB sections (El Kef, Tunisia; Keller et al. 1994; cf. Pospichal 1994), and global studies of some groups provide conflicting evidence for sharp and gradual extinctions (marine bivalve groups; Raup & Jablonski 1993; cf. Crassatellidae bivalves; Wingard 1993). Moderately convincing evidence for less severe extinctions comes from high-latitude KTB sections, particularly those in southern latitudes (southeast Australia, New Zealand, and Antarctica–Patagonia), and applies to both floras and faunas. Some organisms were already reacting to climatic and oceanic instabilities before KTB time, including planktic and benthic foraminifera (Barrera 1994; Longoria & Gamper 1995),

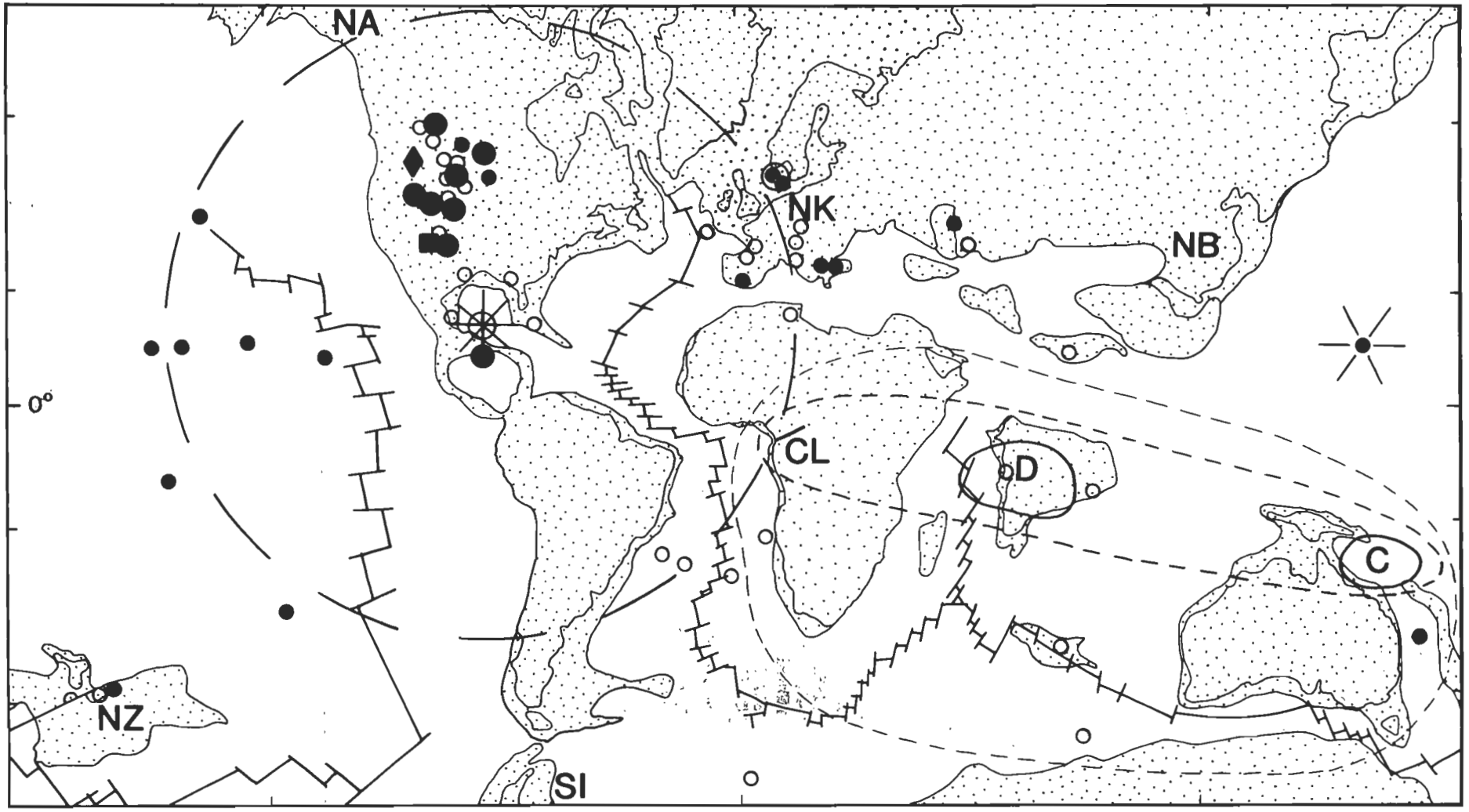

Figure 5. Global distribution of proposed KT impact and volcanic features. Chicxulub crater (circle star burst) lies within a maximum thermal aureole of 550-km radius (large dashed circle) according to Hildebrand (1993). Other related KT features include reported Ir anomalies with shocked quartz grains (filled circles: the large ones indicate grains >0.5 mm; the small ones, grains <0.55 mm), Ir anomalies unaccompanied by shocked quartz grains (unfilled circles), nanodiamond site (filled diamond), and stishovite site (filled square) according to Alvarez & Asaro (1990) and after Hildebrand (1993), Sutherland (1993), Kyte & Bostwick (1995), and Alvarez et al. (1995). A potential Shatsky Rise (Pacific) impact according to Robin et al. (1993) is indicated by a dot-centred star burst. The main KT volcanic features (Deccan plume, D; Cameroon Line, CL; and Coral Sea plume, C) are contained in a short dashed envelope, within a southern mantle plume 'swarm' (small dashed aureole). Distribution of continents (stippled areas) and oceans (blank areas with spreading ridge lines) is based on Alvarez & Asaro (1990). Sites of reported KT extinction transitions, as well as southeast Australia, include North Alaska and Arctic Basin (NA); Nye Klove, Denmark (NK); Nanxiong Basin, China (NB); New Zealand (NZ); and Seymour Island, Antarctica (SI).

radiolarians and diatoms (Hollis et al. 1995), gastropods (Zinsmeister & Griffin 1995), flora (Macphail 1994), and even dinosaurs (Le Loeuff et al. 1994), although other members in these groups were truncated at the KTB.

Considerable debate remains on the exact mechanisms for KTB mass extinction. Acid rains were considered insufficient cause (D'Hondt et al. 1994; Gardner et al. 1994), and severe cooling from sulphate aerosol reactions was promoted as a chief cause (Pope et al. 1994). The magnitude of this effect would have depended on the amount of shock-induced volatilisation and rates of disassociation reactions of sulphates in target rocks; the sulphate effect is probably overestimated in respect of carbon dioxide greenhouse-warming effects (Chen et al. 1994). However, additional sulphur-rich aerosols might have been produced by vaporisation of the impactor, as well as the target rocks (Kring et al. 1995). A Chicxulub-size impactor (10-km diameter) would have produced over 10^{15} g of sulphur, which would have induced an additional 2°C drop in temperature over 3 years. It would also have added some 9×10^{14} g of chlorine and 5×10^{12} g of bromine into the stratosphere, to further perturb the atmosphere and ozone layer. An additional source of carbon dioxide for consideration, besides that resulting from the disassociation of carbonate target rocks, is that generated from impact wild fires (Ivany & Salawitch 1993a), although the influence of this source of the gas in the water column is uncertain (Keller & MacLeod 1993). The relative climatic effects also depend on the season and hemisphere of impact (Wolfe 1991), and the roles of water-vapour warming and dark cold winters in the extinction phenomenon is also under debate (Emiliani 1993; cf. Clemens & Nelms 1993a, b). The question of multiple impacts further clouds the overall picture of KTB extinction conditions.

Synthesis

A wide spectrum of scientific endeavour has established the likely parameters for a large Chicxulub impact at the KTB that precisely correlates with a mass extinction event. Abnormal hot-spot volcanism, unsettled climates and seas, and adaptive changes in fauna and flora were already abroad before impact. The impact — including its ejected melts, debris, and vaporised materials — triggered biomass burning and imprinted a first-order climatic change on the environment. These sudden changes, and the consequent mass organic mortality, created abrupt short-term shifts in the isotopic signatures in sedimentary sequences. The impact did not cause Deccan plume volcanism, but might have increased related activity. A single impact producing a sharp, severe, global extinction is an explanation that is probably too simple to account for all the observed KTB features, and multiple impacts and gradational extinctions in some regions need serious consideration.

The Chicxulub impact site, its thermal aureole related to ballistic re-entry of ejecta, and the global distribution of shocked quartz and anomalous Ir are shown in Figure 5. Superimposed on the impact data are the Deccan plume volcanism, large basaltic volcanic lines and hot-spot spreading rifts initiated or active at KTB time, and the sites at which gradual extinctions are proposed at higher latitudes.

The KTB scenario contains at least one major impact site (Chicxulub) with a subglobal aureole of maximum lethal thermal pulse, and at least one zone of extended mantle volcanism, centred on the Deccan flood basalts. Volcanogenic sediments from 65–60 Ma in the Indian Ocean suggest that Deccan products erupted northeasterly from the plume (Sykes & Kidd 1994). Thus, regions of maximum impact and subsidiary volcanic disturbance lie across a subequatorial zone. Whether the KTB environment was further perturbed by other impacts is unclear, but the proposed regions of separate spinel types also largely fall within lower latitudes. Therefore, a tentative KTB model would favour maximum impact and mantle-volcanic effects lying at low latitudes, and would accommodate suggestions of gradual KTB extinction at high latitudes.

A major unresolved factor in the KTB impact story is the exact number of impacts involved. This factor largely rests on the significance that distinct non-terrestrial spinel compositions (over 1% Ni, and Fe^{3+}/Fe_{total} ratios of over 70%; Robin et al. 1994b; Kyte & Bostwick 1995) have for the origin of these minerals. An origin by ablation and oxidation of meteoritic debris in the atmosphere would imply several objects (Robin et al. 1992, 1994), whereas crystallisation of such spinels from silicate liquids within a fractionating vapour cloud could be constrained to a single Chicxulub impact (Kyte & Bostwick 1995). Separate spinel compositions in the Haiti section (Leroux et al. 1995) seem to favour more than one impact, and the proponents advocating several impacts would gain encouragement from the break-up and successive impacts observed during the Comet Shoemaker–Levy 9 collision with Jupiter in 1994 (Levy et al. 1995).

The KTB impact and flood volcanism scenario represents one of several periodic events which correlate statistically with geological stage boundaries and extinction events (Stothers 1993a, b). However, the precise controls of KTB impact and volcanism on extinctions need to be evaluated. The low Ir hump and associated volatile- and chalcophile-element enrichments which extend across some KTB Ir peaks have been interpreted in different ways — including inputs from volcanism, acid-rain leaching, and a cometary debris fall that accompanies the fall of a cometary nucleus (Bhandari et al. 1994, 1995). Reports of extraterrestrial amino acids found on either side of the KTB (Zahnle & Grinspoon 1990) favour at least some related cometary-fall contribution. The complexity of the story outlined here suggests that multiple working hypotheses may be relevant to studies of the KTB impact extinction event (Raup 1995). Australia, a neglected participant, has a role in future refinements of the KTB impact story.

Acknowledgments

A.R. Hildebrand (Geological Survey of Canada, Ottawa) provided literature and constructive criticisms on impact aspects, and A.R. Sweet (Geological Survey of Canada, Calgary) provided literature on floral extinctions. N. Bhandari (Physical Research Laboratory, Ahmedabad) provided valuable references on Indian KT sections, and J.G. Negi (National Geophysical Research Institute) sent literature on Deccan geophysical results. C.J. Hollis (Institute of Geological and Nuclear Sciences, Lower Hutt) and K.A. Rogers (University of Auckland) contributed information on New Zealand KT sections. M. Macphail (University of Sydney) and N. Kemp (Tasmanian Museum) assisted with further KT literature. A. Bevan (Western Australian Museum, Perth), G. Ryder (Lunar and Planetary Institute, Houston), and anonymous reviewers helped greatly to improve a draft version of the manuscript. S. Folwell, J. Howarth, and G. Webb (Australian Museum) aided preparation of the final manuscript after guidance by A.Y. Glikson (AGSO, Canberra).

References

Adatte, T., Stinnesbeck, W. & Keller, G., 1994. Mineralogical correlations of near-KT-boundary deposits in northeastern Mexico: evidence for long–term deposition and volcaniclastic influence. In: New developments regarding the KT event and other catastrophes in Earth history. LPI Contribution 825, Lunar and Planetary Institute, Houston, 1–2.

Alvarez, L.W., Alvarez, W., Asaro, F. & Michel, H.V., 1980. Extraterrestrial causes of the Cretaceous/Tertiary extinction. Science, 208, 1095–1108.

Alvarez, W. & Asaro, F., 1990. An extraterrestrial impact. Scientific American, 263, 44–52.

Alvarez, W., Asaro, F. & Martanari, A., 1990. Iridium profile for 10 million years across the Cretaceous/Tertiary boundary at Gubbio, Italy. Science, 250, 1700–1702.

Alvarez, W., Claeys, P. & Kieffer, S.W., 1995. Emplacement of Cretaceous–Tertiary boundary shocked quartz from Chicxulub crater. Science, 269, 930–935.

Alvarez, W., Smit, J., Lowrie, W., Asaro, F., Margolis, S.V., Claeys, P., Kaster, M. & Hildebrand, A.R., 1992. Proximal impact deposits at the Cretaceous–Tertiary boundary in the Gulf of Mexico: a restudy of DSDP Leg 77 Sites 536 and 540. Geology, 20, 697–700.

Archibald, J.D., 1994. Testing KT extinction hypotheses using the vertebrate fossil record. In: Developments regarding the KT event and other catastrophes in Earth history. LPI Contribution 825, Lunar and Planetary Institute, Houston, 6–7.

Baksi, A.K., 1994. Geochronological studies on whole-rock basalts, Deccan Traps, India: evaluation of the timing of volcanism relative to the K/T boundary. Earth and Planetary Science Letters, 121, 43–56.

Baksi, A.K. & Farrar, E., 1991. $^{40}Ar/^{39}Ar$ dating of the Siberian Traps, USSR: evaluation of the ages of the two major extinction events relative to episodes of flood-basalt volcanism in the USSR and the Deccan Traps, India. Geology, 19, 461–464.

Barrera, E., 1994. Global environmental changes preceding the Cretaceous–Tertiary boundary: early–late Maastrichtian transition. Geology, 22, 877–880.

Basu, A.R., Renne, P.R., Das Gupta, D.K., Teichmann, F. & Poreda, R.J., 1993. Early and late alkali igneous pulses and a high ^{3}He plume origin for the Deccan flood basalts. Science, 261, 902–906.

Beeson, D., Gartner, S., Keller, G., MacLeod, N., Medus, J., Rocchia, R. & Robin, E. 1994. The KT boundary along the Brazos River, Falls Country, Texas: multidisciplinary stratigraphy and depositional environment. In: New developments regarding the KT event and other catastrophes in Earth history. LPI Contribution 825, Lunar and Planetary Institute, Houston, 9–10.

Benton, M.J. & Little, C.T.S., 1994. Impact in the Caribbean and death of the dinosaurs. Geology Today, November–December, 222–227.

Bhandari, N., Gupta, M., & Shukla, P.N., 1993a. Deccan volcanic contribution of Ir and other trace elements near the K/T boundary. Chemical Geology, 103, 129–139.

Bhandari, N., Shukla, P.N., & Castagnoli, G.C., 1993b. Geochemistry of some K/T sections. Palaeogeography Palaeoclimatology Palaeoecology, 104, 199–211.

Bhandari, N., Gupta, M., Pandey, J. & Shukla, P.N., 1994. Chemical profiles in K/T boundary sections of Meghalaya, India: cometary, asteroidal or volcanic. Chemical Geology, 113, 45–60.

Bhandari, N., Shukla, P.N., Ghevaria, Z.G. & Sundaram, S.M., 1995. Impact did not trigger Deccan volcanism: evidence from the K/T boundary layer at Anjar. Geophysical Research Letters, 22, 433–436.

Blum, J.D. & Chamberlain, C.P., 1992. Oxygen isotope constraints on the origin of impact glasses from the Cretaceous–Tertiary boundary. Science, 257, 1104–1107.

Blum, J.D., Chamberlain, C.P., Hingston, M.P., Koeberl, C., Marin, L.E., Schuraytz, B.C. & Sharpton, V.L., 1993. Isotopic comparison of K/T boundary impact glass with melt rock from the Chicxulub and Manson impact structures. Nature, 364, 325–327.

Bohor, B.F. & Glass, B.P., 1995. Origin and diagenesis of K/T impact spherules — from Haiti to Wyoming and beyond. Meteoritics, 39, 182–198.

Boslough, M.B., Chael, E.P., Trucano, T.G., Kipp, M.E. & Crawford, D.A., 1995. Axial focusing of impact energy in the Earth's interior: proof–of–principle tests of a new hypothesis. In: New developments regarding the KT event and other catastrophes in Earth history. LPI Contribution 825, Lunar and Planetary Institute, Houston, 14–15.

Bourgeois, J., 1994. Tsunami deposits and the KT boundary: a sedimentologist's perspective. In: New developments regarding the KT event and other catastrophes in Earth history. LPI Contribution 825, Lunar and Planetary Institute, Houston, 16–17.

Brett, R., 1992. The Cretaceous–Tertiary extinction: a lethal mechanism involving anhydrite target rocks. Geochimica et Cosmochimica Acta, 56, 3603.

Brinkhuis, H. & Visscher, H., 1994. New evidence for terrestrial ecosystem collapse at the KT and Permian/Triassic boundaries. In: New developments regarding the KT event and other catastrophes in Earth history. LPI Contribution 825, Lunar and Planetary Institute, Houston, 17.

Caldeira, K. & Rampino, M.R., 1990. Carbon-dioxide emissions from Deccan volcanism and a K/T boundary greenhouse-effect. Geophysical Research Letters, 17, 1299–1302.

Campbell, I.H. & Griffiths, R.W., 1992. The changing nature of mantle hotspots through time: implications for the chemical evolution of the mantle. Journal of Geology, 82, 497–523.

Chao, E.C.T., 1993. Comparison of the Cretaceous–Tertiary boundary impact events and the 0.77 Ma Australasian tektite event: relevance to mass extinction. US Geological Survey, Bulletin 2050, 1–22.

Chaussidon, M., Sigurdsson, H. & Metrich, N., 1994. Sulfur isotope study of high-calcium impact glasses from the K/T boundary. In: New developments regarding the KT event and other catastrophes in Earth history. LPI Contribution 825, Lunar and Planetary Institute, Houston, 21–22.

Chen, G., Tyburczy, J.A. & Ahrens, T.J., 1994. Shock-induced devolatilization of calcium sulfate and implications for K–T extinctions. Earth and Planetary Science Letters, 128, 612–628.

Clemens, W.A. & Nelms, L.G., 1993a. Paleoecological implications of Alaskan terrestrial vertebrate fauna in latest Cretaceous time at high paleolatitudes. Geology, 21, 503–506.

Clemens, W.A. & Nelms, L.G., 1993b. Paleoecological implications of Alaskan terrestrial vertebrate fauna in latest Cretaceous time at high paleolatitudes: reply. Geology, 21, 1151–1152.

Coccioni, R. & Galeotti, S., 1994. K–T boundary extinction: Geologically instantaneous or gradual event? Evidence from deep-sea benthic foraminifera. Geology, 22, 779–782.

Coffin, M.F. & Eldholm, O., 1993. Scratching the surface: estimating dimensions of large igneous provinces. Geology, 21, 515–578.

Colombo, F., 1994. The KT boundary in the southeastern Pyrenees Ager Basin, northeastern Spain (Lleida Province). In: New developments regarding the KT event and other catastrophes in Earth history. LPI Contribution 825, Lunar and Planetary Institute, Houston, 25–27.

Courtillot, V., Vandamme, D., Besse, J., Jaeger J.J. & Javoy, M., 1990. Deccan volcanism at the Cretaceous/Tertiary boundary; data and inferences. Geological Society of America, Special Paper 247, 401–410.

Dalrymple, G.B., Izett, G.A., Snee, L.W. & Obradovich, J.D., 1993. $^{40}Ar/^{39}Ar$ age spectra and total-fusion ages of Ttktites from Cretaceous–Tertiary boundary sedimentary rocks in the Beloc Formation, Haiti. US Geological Survey, Bulletin 2065, 1–20.

D'Hondt, S., Pilson, M.E.Q., Sigurdsson, H., Hanson, A.K. & Carey, S., 1994. Surface-water acidification and extinction at the Cretaceous–Tertiary boundary. Geology, 22, 983–986.

Donze, P., Méon, H., Rocchia, R., Robin, E. & Froget, L., 1994. Biological changes at the KT stratotype of El Kef (Tunisia). In: New developments regarding the KT event and other catastrophes in Earth history. LPI Contribution 825, Lunar and Planetary Institute, Houston, 29–30.

Drobne, K., Ogorelic, B., Lowrie, W. & Marton, E., 1994. Shallow benthic fauna: their extinction and survival on the KT boundary, Adriatic Platform, Slovenia. In: New developments regarding the KT event and other catastrophes in Earth history. LPI Contribution 825, Lunar and Planetary Institute, Houston, 31–33.

Elliot, D.H., Askin, R.A., Kyte, F.R. & Zinsmeister, W.J., 1994. Iridium and dinocysts at the Cretaceous–Tertiary boundary on Seymour Island, Antarctica: implications for the K–T event. Geology, 22, 675–678.

Emiliani, C., 1993. Palaeoecological implications of Alaskan terrestrial vertebrate fauna in latest Cretaceous time at high palaeolatitudes: comment. Geology, 21, 1151–1152.

Evans, N.J., Ahrens, T.J. & Gregoire, D.C., 1995. Fractionation of ruthenium from iridium at the Cretaceous–Tertiary boundary. Earth and Planetary Science Letters, 134, 141–153.

Evans, N.J., Gregoire, D.C., Grieve, R.A.F., Goodfellow, W.D. & Veizer, J., 1993. Use of platinum group elements for impactor identification: terrestrial impact craters and Cretaceous–Tertiary boundary. Geochimica et Cosmochimica Acta, 57, 3737–3748.

Evans, N.J., Gregoire, D.C., Goodfellow, W.D., Miles, N. & Veizer, J., 1994. The Cretaceous–Tertiary fireball layer, ejecta layer and coal seam: platinum-group element content and mineralogy of size fractions. Meteoritics, 29, 223–235.

Fastovsky, D.E. & Sheehan, P.M., 1994. Habitat vs. asteroid fragmentation in vertebrate extinctions at the KT boundary: the good, the bad and the untested. In: New developments regarding the KT event and other catastrophes in Earth history. LPI Contribution 825, Lunar and Planetary Institute, Houston, 36–37.

Féraud, G. & Courtillot, V., 1994. Comment on 'Did Deccan volcanism pre-date the Cretaceous–Tertiary transition?' Earth and Planetary Science Letters, 122, 259–262.

Florentin, J.-M., Maurrasse, R. & Sen, G., 1991. Impacts, tsunamis and the Haitian Cretaceous–Tertiary boundary layer. Science, 252, 1690–1693.

Galbraun, B., Feist, M., Colombo, F., Rocchia, R. & Tambareau, Y., 1993. Magnetostratigraphy and biostratigraphy of Cretaceous-Tertiary continental deposits, Ager Basin Province of Lerida, Spain. Palaeogeography Palaeoclimatology Palaeoecology, 102, 41–52.

Gallagher, W.B., 1991. Selective extinction and survival across the Cretaceous/Tertiary continental deposits. Geology, 19, 967–974.

Gardner, A.F., Wright, I.P. & Gilmour, I., 1994. Organic matter changes across nonmarine KT boundary sections. In: New developments regarding the KT event and other catastrophes in Earth history. LPI Contribution 825, Lunar and Planetary Institute, Houston, 38–40.

Gartner, S., Alcala, J. & Grossman, E., 1994. Coccolith extinction at the KT boundary: gradual or abrupt. In: New developments regarding the KT event and other catastrophes in Earth history. LPI Contribution 825, Lunar and Planetary Institute, Houston, 40–41.

Gilmour, I. & Anders, E., 1989. Cretaceous–Tertiary boundary event: evidence for a short time scale. Geochimica et Cosmochimica Acta, 53, 503–511.

Gilmour, I., Russell, S.S., Arden, J.W., Lee, M.R., Franchi, I.A. & Pillinger, C., 1992. Terrestrial carbon and nitrogen isotopic ratios from Cretaceous–Tertiary boundary nanodiamonds. Science, 258, 1624–1626.

Ginsberg, R.N., 1994. MEXICO: On the trail of the KTB impact splash. Geology Today, 10, 89.

Glen, W., 1994. The mass-extinction debates: how science works in a crisis. Stanford University Press, Stanford, USA.

Griffin, M. & Hünicken, M.A., 1994. Late Cretaceous–early Tertiary gastropods from southwestern Patagonia, Argentina. Journal of Paleontology, 68, 257–274.

Habib, D., 1994. Biostratigraphical evidence for the KT boundary in the Eastern Gulf Coastal Plain, north of the Chicxulub crater. In: New developments regarding the KT event and other catastrophes in Earth history. LPI Contribution 825, Lunar and Planetary Institute, Houston, 45–46.

Hansen, T.A. & Upshaw, B., 1990. Aftermath of the Cretaceous–Tertiary extinction: rate and nature of the early Palaeocence molluscan rebound. In: Kauffman, E.G. & Walliser, O.H. (Editors), Extinction events in Earth history. Springer–Verlag, Berlin, 401–409.

Heymann, D., Chibante, L.P.F., Brooks, R.R., Wolbach, W.S. & Smalley, R.E., 1994. Fullerenes in the Cretaceous–Tertiary boundary layer. Science, 265, 645–647.

Hildebrand, A.R., 1993. The Cretaceous/Tertiary boundary impact (or the dinosaurs didn't have a chance). Journal of the Royal Astronomical Society of Canada, 87, 77–118.

Hildebrand, A.R., Penfield, G.T., Kring, D.A., Pilkington, M., Camargo, A., Jacobsen S.B. & Boynton, W.V., 1991. Chicxulub crater, a possible Cretaceous/Tertiary boundary impact cater on the Yucatán Peninsula, Mexico. Geology, 19, 867–871.

Hildebrand, A.R., Pilkington, M., Connors, M., Ortiz-Aleman, C. & Chavez, R.E., 1995. Size and structure of the Chicxulub crater revealed by horizontal gravity gradients and cenotes. Nature, 376, 415–417.

Hill, P.J., 1992. Capricorn and northern Tasman Basins: structure and depositional systems. Exploration Geophysics, 23, 153–162.

Hollis, C.J., Rodgers, K.A. & Parker, R.J., 1995. Siliceous plankton bloom in the earliest Tertiary of Marlborough, New Zealand. Geology, 23, 835–839.

Hollander, D.J., McKenzie, J.A. & Hsü, K.T., 1993. Carbon isotope evidence for unusual blooms and fluctuations of surface water CO^2 in "Strangelove Ocean" after terminal Cretaceous events. Palaeogeography Palaeoclimatology Palaeoecology, 104, 229–237.

Holsapple, K.A., 1994. Estimation of the measures of the Chicxulub cratering event. In:New developments regarding the KT event and other catastrophes in Earth history. LPI Contribution 825, Lunar and Planetary Institute, Houston, 40–52.

Hough, H., Sigurdsson, H., Franchi, I.A., Wright, I.P., Pillinger, C.T. & Gilmour, I., 1993. Carbon and oxygen isotopic measurements of K/T boundary spherules from Haiti. Meteoritics, 28, 364–365.

Hough, H., Sigurdsson, H., Franchi, I.A., Wright, I.P., Pillinger, C.T. & Gilmour, I., 1994. Carbonate derived gases in Haiti KT boundary glass spherules. In: New developments regarding the KT event and other catastrophes in Earth history. LPI Contribution 825, Lunar and Planetary Institute, Houston, 53–54.

Huffman, A.R., Crockett, J.H., Carter, N.L., Borella, P.E. & Officer, C.B., 1990. Chemistry and mineralogy across the Cretaceous/Tertiary boundary at DSPP Site 527, Walvis Ridge, south Atlantic Ocean. Geological Society of America, Special Paper 247, 319–330.

Hunter, J., 1994. Lack of a high body count at the K–T boundary. Journal of Paleontology, 68(5), 1158.

Ivany, L.C. & Salawitch, R.J., 1993a. Carbon isotope evidence for biomass burning at the K–T boundary. Geology, 21, 487–490.

Ivany, L.C. & Salawitch, R.J., 1993b. Reply to comment on 'Carbon isotopic evidence for biomass burning at the K–T boundary'. Geology, 21, 1150–1151.

Izett, G.A., 1991. Tektites in Cretaceous–Tertiary boundary rocks on Haiti and their bearing on the Alvarez extinction impact hypothesis. Journal of Geophysical Research, 96, 20879–20905.

Izett, G.A., Dalrymple, G.B. & Snee, L.W., 1991. $^{40}Ar/^{39}Ar$ age of Cretaceous–Tertiary boundary tektites from Haiti. Science, 252, 1539–1541.

Izett, G.A., Cobban, W.A., Obradovick, J.D. & Kunk, M.J., 1993. The Manson impact structure: $^{40}Ar/^{39}Ar$ age and its distal impact ejecta in the Pierre Shale in southeastern South Dakota. Science, 262, 729–732.

Izett, G.A., Masaitis, V.L., Shoemaker, E.M., Dalrymple, G.B. & Steiner, M.B., 1994. Eocene age of the Kamensk buried crater of Russia. In: New developments regarding the KT event and other catastrophes in Earth history. LPI Contribution 825, Lunar and Planetary Institute, Houston, 55–56.

Jabolonski, D., 1991. Extinctions: a palaeontological perspective. Science, 253, 745–757.

Jackson, J.A. (editor), 1995. Model links ancient impact to volcanic eruptions. Geotimes, 40, 11.

Jarzembowski, E. & Ross, A., 1993. June flies: the geological record of insects. Geology Today, 9(6), 218–223.

Javoy, M. & Michard, G., 1990. Global catastrophes and volcanic events: a comparison of volcanic and industrial outgassings under normal and catastrophic conditions. Geological Society of Australia, Abstract Series, 27, 51.

Johnson, K.R., 1993. Extinctions at the antipodes. Nature, 366, 511–512.

Keller, G., 1994a. Global biotic effects of the KT boundary event: mass extinction restricted to low latitudes? In: New developments regarding the KT event and other catastrophes in Earth history. LPI Contribution 825, Lunar and Planetary Institute, Houston, 59–60.

Keller, G., 1994b. K–T boundary issues — letters. Science, 264, 641.

Keller, G. & MacLeod, N., 1993. Comment on 'Carbon isotope evidence for biomass burning at the K–T boundary'. Geology, 21, 1149–1150.

Keller, G., Li, L. & MacLeod, N., 1994. The KT boundary stratotype section at El Kef, Tunisia: how catastrophic was the mass extinction? In: New developments regarding the KT event and other catastrophes in Earth history. LPI Contribution 825, Lunar and Planetary Institute, Houston, 59–60.

Keller, G., MacLeod, N. Lyons, J.B. & Officer, C.B., 1993a. Is there evidence for Cretaceous–Tertiary boundary-age deep-water deposits in the Caribbean and Gulf of Mexico? Geology, 21, 776–780.

Keller, G., Barrera, E., Schmitz, B. & Mattson, E., 1993b. Gradual mass extinction, species survivorship, and long-term environmental change across the Cretaceous Tertiary boundary in high latitudes. Geological Society of America, Bulletin 105, 979–997.

Kerr, R.A., 1994. K–T boundary issues — letters. Science, 264, 642.

Koeberl, C., 1992. Water content of glasses from the K/T boundary, Haiti: an indication of impact origin. Geochimica et Cosmochimica Acta, 56, 4329–4332.

Koeberl, C., 1993. Chicxulub crater, Yucatan: tektites, impact glasses, and the geochemistry of target rocks and breccias. Geology, 21, 211–214.

Koeberl, C., 1994a. Deposition of channel deposits near the Cretaceous–Tertiary boundary in northeastern Mexico: catastrophic or "normal" sedimentary deposits? Reply to comment by Stinnesbeck et al. Geology, 22, 957.

Koeberl, C., 1994b. On source and origin of Haitian KT boundary impact glasses. In: New developments regarding the KT event and other catastrophes in Earth history. LPI Contribution 825, Lunar and Planetary Institute, Houston, 60–61.

Koeberl, C., Sharpton, V.L., Schuraytz, B.C., Shirey, S.B., Blum, J.D. & Marin, L.E., 1994. Evidence for a meteoritic component in impact melt rock from the Chicxulub structure. Geochimica et Cosmochimica Acta, 58, 1679–1684.

Kring, D.A. & Boynton, W.V., 1991. Altered spherules of impact melt and associated relic glass from the K/T boundary sediment in Haiti. Geochimica et Cosmochimica Acta, 55, 1737–1742.

Kring, D.A. & Boynton, W.V., 1992. Petrogenesis of an augite-bearing melt rock in the Chicxulub structure and its relationship to K/T impact spherules in Haiti. Nature, 358, 141–144.

Kring, D.A. & Boynton, W.V., 1993. K/T melt glasses. Nature, 363, 503–504.

Kring, D.A., Hildebrand, A.R. & Boynton, W.V., 1994. Provenance of mineral phases in the Cretaceous–Tertiary boundary sediments exposed on the southern peninsula of Haiti. Earth and Planetary Science Letters, 128, 629–641.

Kring, D.A., Melosh, H.J. & Hunten, D.M., 1995. Possible climatic perturbations produced by impacting asteroids and comets. Meteoritics, 30, 530.

Krogh, T.E., Kamo, S.L. & Bohor, B.F., 1993a. Impact-shocked zircons: fingerprinting the K/T impact site and determining the time of impacts by U–Pb dating of single shocked zircons from distal ejecta. Earth and Planetary Science Letters, 119, 425–429.

Krogh, T.E., Kamo, S.L., Sharpton, V.L., Marin, L.E. & Hildebrand, A.R., 1993b. U–Pb ages of single shock zircons linking distal K/T ejecta to the Chicxulub crater. Nature, 366, 731–734.

Kruge, M.A., Stankiewicz, B.A., Crelling, J.C., Montanari, A. & Bensley, D.F., 1994. Fossil charcoal in Cretaceous–Tertiary boundary strata: evidence for catastrophic firestorm and megawave. Geochimica et Cosmochimica Acta, 58, 1393–1397.

Kump, L.R., 1991. Interpreting carbon–isotope excursions: Strangelove Oceans. Geology, 19, 299–302.

Kyte, F.T. & Bostwick, J.A., 1995. Magnesioferrite spinel in Cretaceous/Tertiary boundary sediments of the Pacific basin: remnants of hot, early ejecta from the Chicxulub impact? Earth and Planetary Science Letters, 132, 113–127.

Lawver, L.A. & MÅller, R.D., 1994. Iceland hotspot track. Geology, 22, 311–314.

Le Loeuff, J., Buffetaut, E. & Martin, M., 1994. The last stages of dinosaur faunal history in Europe: a succession of Maastrichtian dinosaur assemblages from the Corbières (southern France). Geological Magazine, 131, 625–630.

Leroux, H., Rocchia, R., Froget, L., Orue-Etxebarria, X., Doukhan, J.-C. & Robin, E., 1995. The K/T boundary at Beloc (Haiti): compared stratigraphic distributions of the boundary markets. Earth and Planetary Science Letters, 131, 255–268.

Levy, D.H., Shoemaker, E.M. & Shoemaker, C.S., 1995. Comet Shoemaker–Levy 9 meets Jupiter. Scientific American, 273, 69–75.

Liu, C. & Olsson, R.K., 1994. Patterns of planktonic foraminifera extinction at the end of Cretaceous: stepwise, gradual, foreshadowed/extended, latitudinally controlled or instantaneous? In: New developments regarding the KT event and other catastrophes in Earth history. LPI Contribution 825, Lunar and Planetary Institute, Houston, 68–69.

Longoria, L.F. & Gamper, M.A., 1995. Planktonic foraminiferal faunas across the Cretaceous–Tertiary succession of Mexico: implications for the Cretaceous–Tertiary problem. Geology, 23(4), 329–332.

Lopez–Oliva, J.G. & Keller, G., 1994. Biotic effects of the KT boundary events in northeastern Mexico. In: New developments regarding the KT event and other catastrophes in Earth history. LPI Contribution 825, Lunar and Planetary Institute, Houston, 72–73.

Lyons, J.B. & Officer, C.B., 1992. Mineralogy and petrology of the Haiti Cretaceous/Tertiary section. Earth and Planetary Science Letters, 109, 205–224.

McLaren, D.J. & Goodfellow, W.D., 1990. Geological and biological consequences of giant impacts. Annual Reviews of Earth and Planetary Science, 18, 123–171.

MacLeod, N., 1994. K–T boundary issues — letters. Science, 264, 641–642.

MacLeod, N. & Keller, G. 1991. Hiatus distribution and mass extinctions at the Cretaceous–Tertiary boundary. Geology, 19, 497–501.

Macphail, M., 1994. Impact of the K/T Event on the southeast Australian flora and vegetation: mass extinction, niche disruption or nil? Palaeoaustral, 1, 9–13.

Marin, L.E., Sharpton, V.L., Urrutia-Fucugauchi, J., Sikora, P. & Carney, C., 1994. The "Upper Cretaceous unit" in the Chicxulub multiring basin: new age based on planktic foraminiferal assemblages. In: New developments regarding the KT event and other catastrophes in Earth history. LPI Contribution 825, Lunar and Planetary Institute, Houston, 77.

Marincovich, J. Jnr., 1993. Delayed extinction of Mesozoic marine molluscs in the Palaeocene Arctic Ocean Basin. Geological Society of America, Abstracts with Progams, 25, 295.

Martin, E.E. & Macdougall, J.D., 1991. Seawater Sr isotopes at the Cretaceous/Tertiary boundary. Earth and Planetary Science Letters, 104, 166–180.

Meisel, T. & Pettke, T., 1994. Strontium isotopic composition of carbonates from the Sumbar KT boundary. Meteoritics, 29, 501–502.

Meisel, T., Krähenbühl, U. & Mazaroy, M.A., 1995. Combined osmium and strontium isotopic study of the Cretaceous–Tertiary boundary at Sumbar, Turkmenistan: a test for an impact vs. a volcanic hypothesis. Geology, 23, 313–316.

Melosh, H.J., 1989. Impact cratering. Oxford University Press.

Meyerhoff, A., Lyons, J.B. & Officer, C.B., 1994. Chicxulub structure: a volcanic sequence of Late Cretaceous age. Geology, 22, 3–4.

Meyers, P.A., 1992. Changes in organic carbon stable isotope ratios across the K/T boundary: global or local control? Chemical Geology, 101, 283–291.

Morrison, K.C., Baillie, P.W., Davidson, J.K. & Quilty, P.G., 1989. Tectonic and depositional framework. In: Burrett, C.F. & Martin, E.L. (editors), Geology and mineral resources of Tasmania. Geological Society of Australia, Special Publication 15, 339–346.

Murari, R., Krishnamurthy, P., Tikhonenko, P.I. & Goplan, K., 1993. Magnesian ilmenites in picrite basalts for Siberian and Deccan Traps — additional mineralogical evidence for primary melt compositions (?). Mineralogical Magazine, 57, 733–735.

Negi, J.G., Agrawal, P.K., Singh, A.P. & Pandey, O.P., 1992. Bombay gravity high and eruption of Deccan flood basalts (India) from a shallow secondary plume. Tectonophysics, 206, 341–350.

Negi, J.G., Agrawal, P.K., Pandey, O.P. & Singh, A.P., 1993. A possible K–T boundary bolide impact site offshore near Bombay and triggering of rapid Deccan volcanism. Physics of the Earth and Planetary Interiors, 76, 189–197.

Nelson, B.K., MacLeod, G.K. & Ward, P.D., 1991. Rapid change in strontium isotopic composition of seawater before the Cretaceous/Tertiary boundary. Nature, 351, 644–647.

Nichols, D.J., Fleming, R.F. & Frederiksen, N.O., 1990. Palynological evidence of effects of the terminal Cretaceous event on terrestrial floras in western North America. In: Kauffman, E.G. & Walliser, O.H. (Editors). Extinction events in Earth history. Springer–Verlag, Berlin, 351–364.

Ocampo, A.C., 1995. Journey to the end of the dinosaur era: a society expedition to Belize. The Planetary Report, XV(4), 10–14.

Officer, C.B. & Lyons, J.B., 1993. A short note on the origin of the yellow glasses of the Haiti Cretaceous/Tertiary section. Earth and Planetary Science Letters, 118, 349–351.

Olsson, R.K. & Liu, C., 1994. On the reality of the KT boundary. In: New developments regarding the KT event and other catastrophes in Earth history. LPI Contribution 825, Lunar and Planetary Institute, Houston, 87–85.

Peng, Z.X. & Mahoney, J.J., 1995. Drillhole lavas from the northwestern Deccan Traps, and the evolution of Réunion hotspot mantle. Earth and Planetary Science Letters, 134, 169–185.

Peng, Z.X., Mahoney, J., Hooper, P., Harris, P. & Beane, J., 1994. A role for lower continental crust in flood basalt genesis? Isotopic and incompatible element study of the lower six formations of the western Deccan Traps. Geochimica et Cosmochimica Acta, 58, 267–288.

Perry, E., Marin, L., McClain, J. & Guadalupe, V., 1995. Ring of cenotes (sinkholes), northwest Yucatan, Mexico: its hydrogeologic characteristics and possible association with the Chicxulub impact crater. Geology, 23, 17–20.

Peryt, D., Lahodynsky, R., Rocchia, R. & Boclet, D., 1993. The Cretaceous/Palaeogene boundary and planktonic foraminifera in the Flyschgosau (eastern Alps, Austria). Palaeogeography Palaeoclimatology Palaeoecology, 104, 239–252.

Pitakpaivan, K., Byerly, G.R. & Hazel, J.E., 1994. Pseudomorphs of impact spherules from a Cretaceous–Tertiary boundary section at Shell Creek, Alabama. Earth and Planetary Science Letters, 124, 49–56.

Pope, K.O., Baines, K.H., Ocampo, A.C. & Ivanov, B.A., 1994. Impact winter and the Cretaceous/Tertiary extinctions: results of a Chicxulub asteroid impact model. Earth and Planetary Science Letters, 128, 719–725.

Pospichal, J.J., 1994. Calcareous nannofossils at the K–T boundary, El Kef: no evidence for stepwise, gradual, or sequential extinctions. Geology, 22, 99–102.

Prasad, G.V.R., Jaeger, J.J., Sahni, A., Gheerbrant, E. & Khajuria, C.K., 1994. Eutherian mammals from the Upper Cretaceous (Maastrichtian) Intertrappean Beds of Naskal, Andhra Pradesh, India. Journal of Vertebrate Paleontology, 14, 260–277.

Preisenger, A., Aslanian, S., Stoykova, K., Grass, F., Muritsch, H.J. & Scholger, R., 1993. Cretaceous/Tertiary boundary sections on the coast of the Black Sea near Bjala (Bulgaria). Palaeogeography Palaeoclimatology Palaeoecology, 104, 219–228.

Premo, W.R. & Izett, G.A., 1992. Isotopic signatures of black tektites from the K–T boundary on Haiti: implications of the age and type source material. Meteoritics, 27, 413–423.

Radhakrishna, T., Dallmeyer, R.D. & Joseph, M., 1994. Palaeomagnetism and $^{40}Ar/^{39}Arvs.$ $^{40}Ar/^{39}Ar$ isotope correlation ages of dyke swarms in central Kerala, India: tectonic implications. Earth and Planetary Science Letters, 121, 213–226.

Rampino, M.R. & Caldeira, K., 1992. Antipodal hotspot pairs on the Earth. Geophysical Research Letters, 19, 2011–2014.

Raup, D.C., 1995. The method of multiple working hypotheses, by T.C. Chamberlin. Journal of Geology, 103, 349–354.

Raup, D.M. & Jablonski, D., 1993. Geography of end-Cretaceous marine bivalve extinctions. Science, 260, 971–973.

Rigby, J.K. Jnr., Snee, L.W., Unruh, D.M., Harlan, S.S., Guan, J., Li, F. & Kowalis, B.J., 1993. $^{40}Ar/^{39}Ar$ and U–Pb dates for dinosaur extinction, Nanxiong Basin, Guangdong Province, Peoples Republic of China. Geological Society of America, Abstracts with Programs, 25, 296.

Robin, E., Bonté, Ph., Froget, L., Jéhanno, C. & Rocchia, R., 1992. Formation of spinels in cosmic objects during atmospheric entry: a clue to the Cretaceous–Tertiary boundary event. Earth and Planetary Science Letters, 108, 181–190.

Robin, E., Froget, L., Jéhanno, C. & Rocchia, R., 1993. Evidence for a K/T impact event in the Pacific. Nature, 363, 615–617.

Robin, E., Rocchia, R., Lyons, J.B. & Officer, C.B., 1994a. Deposition of channel deposits near the Cretaceous–Tertiary boundary in northeastern Mexico: reply to comment by Koeberl. Geology, 22, 958.

Robin, E., Gayraud, J., Froget, L. & Rocchia, R., 1994b. On the origin of the regional variations in spinel compositions at the KT boundary. In: New developments regarding the KT event and other catastrophes in Earth history. LPI Contribution 825, Lunar and Planetary Institute, Houston, 96–97.

Rocchia, R., Boclet, D., Bonté, C., Chen, Y., Courtillot, V., Mary, C. & Wezel, F., 1990. The Cretaceous–Tertiary boundary at Gubbio revisited: vertical extent of the Ir anomaly. Earth and Planetary Science Letters, 99, 206–219.

Rocchia, R., Robin, E., Froget, L. & Gayraud, J. 1994. Ni–rich spinels (meteoric spinels) as indicators of the KT event timing. In: New developments regarding the KT event and other catastrophes in Earth history. LPI Contribution 825, Lunar and Planetary Institute, Houston, 99–100.

Sarkar, A., Bhattacharya, S.K., Shukla, P.N., Bhandari, N. & Naidin, D.P., 1992. High-resolution profile of stable isotopes and iridium across a K/T boundary section from Koshak Hill, Mangyshlak, Kazakhstan. Terra Nova, 4, 585–590.

Savrda, C.E., 1993. Ichnosedimentologic evidence for non catastrophic origin of Cretaceous–Tertiary boundary sands in Alabama. Geology, 21, 1075–1078.

Sawlowicz, A., 1993. Iridium and other platinum group elements as geochemical markers in sedimentary environments. Palaeogeography Palaeoclimatology Palaeoecology, 104, 253–270.

Schultz, P.H. & Gault D.E., 1990. Prolonged global catastrophes from oblique impacts. Geological Society of America, Special Paper 247, 239–261.

Schuraytz, B.C. & Sharpton, V.L., 1993. Chicxulub–K/T melt complexities. Nature, 362, 503–504.

Schuraytz, B.C., Sharpton, V.L. & Marin, L.E., 1994. Petrology of impact-melt rocks at the Chicxulub multiring basin, Yucatán, Mexico. Geology, 22, 868–872.

Sharpton, V.L., Dalrymple, G.B., Marin, L.E., Ryder, G., Schuraytz, B.C. & Urrutia-Fucugauchi, J., 1992. New links between the Chicxulub impact structure and the Cretaceous/Tertiary boundary. Nature, 359, 819–821.

Sharpton, V.L., Marin, L.E. & Schuraytz, B.C., 1994. The Chicxulub multiring impact basin: evaluation of geophysical data, well logs, and drill core samples. In: New developments regarding the KT event and other catastrophes in Earth history. LPI Contribution 825, Lunar and Planetary Institute, Houston, 108–110.

Shoemaker, E.M. & Izett, G.A., 1992. K/T boundary stratigraphy: evidence for multiple impacts and a possible comet stream. In: Large meteorite impacts and planetary evolution. LPI Contribution 790, Lunar and Planetary Institute, Houston, 67–68.

Sigurdsson, H., D'Hondt, S. & Carey, S., 1992. The impact of the Cretaceous/Tertiary bolide on evaporite terrane and generation of major sulphuric acid aerosol. Earth and Planetary Science Letters, 109, 543–559.

Sigurdsson, H., D'Hondt, S., Arthur, M.A., Bralower, T.J., Zachos, J.C., Van Fossen, M. & Channell, J.E.T., 1991a. Glass from the Cretaceous/Tertiary boundary in Haiti. Nature, 349, 482–487.

Sigurdsson, H., Bonté, Ph., Turpin, L., Chaussidon, M., Metrick, N., Steinberg, M., Pradel, Ph. & D'Hondt, S.D., 1991b. Geochemical constraints on source region of Cretaceous/Tertiary impact glasses. Nature, 353, 839–842.

Sigurdsson, H., Smith, S., D'Hondt, S., Carey, S. & Espindola, J.-M., 1994. Crystals, lithics, and glassy ejecta at the KT boundary: implications for lithology of the crust of the impact site. In: New developments regarding the KT event and other catastrophes in Earth history. LPI Contribution 825, Lunar and Planetary Institute, Houston, 114–115.

Singh, A.P. & Meissner, R., 1995. Crustal configuration of the Narmada–Tapti region (India) from gravity studies. Journal of Geodynamics, 20, 111–127.

Smit, J., Montanari, A., Swinburne, N.H.M., Alvarez, W., Hildebrand, A.R., Margolis, S.V., Claeys, P., Lowrie, W. & Asaro, F., 1992. Tektite-bearing, deep-water, clastic unit at the Cretaceous–Tertiary boundary in northeastern Mexico. Geology, 20, 99–103.

Smit, J., Roep, Th.B., Alvarez, W., Claeys, Ph. & Montanari, A., 1994a. Deposition of channel deposits near the Cretaceous–Tertiary boundary in northeastern Mexico: catastrophic or "Normal" sedimentary deposits? and is there evidence for Cretaceous–Tertiary boundary-age deep-water deposits in the Caribbean and Gulf of Mexico?: comment. Geology, 22, 953–954.

Smit, J., Roep, Th.B., Alvarez, W., Claeys, P., Montanari, S. & Grajales, M., 1994b. Impact–tsunami-generated clastic beds at the KT boundary of the Gulf coastal plain: a synthesis of old and new outcrops. In: New developments regarding the KT event and other catastrophes in Earth history. LPI Contribution 825, Lunar and Planetary Institute, Houston, 117–119.

Stinnesbeck, W., Barbarin, J.M., Keller, G., Lopez-Oliva, J.G., Pivnik, D.A., Lyons, J.B., Officer, C.B., Adatte, T., Graup, G., Rocchia, R. & Robin, E., 1993. Deposition of channel deposits near the Cretaceous–Tertiary boundary in northeastern Mexico: catastrophic or "normal" sedimentary deposits? Geology, 21, 707–710.

Stinnesbeck, W., Keller, G., Adatte, T. & MacLeod, N., 1994. Deposition of channel deposits near the Cretaceous–Tertiary boundary in northeastern Mexico: catastrophic or "normal" sedimentary deposits? Reply to comment by Smit et al. Geology, 22, 955–956.

Stöffler, D., & Langenhorst, F., 1994. Shock metamorphism of quartz in nature and experiment: 1. Basic observation and theory: The Barringer Award address. Meteoritics, 29, 155–181.

Stothers, R.B., 1993a. Impact cratering at geologic stage boundaries. Geophysical Research Letters, 20, 887–890.

Stothers, R.B., 1993b. Flood basalts and extinction events. Geophysical Research Letters, 20, 1399–1402.

Sutherland, F.L., 1993. Demise of the dinosaurs and other denizens: II — by combined catastrophic causes? Presidential address, 7th April 1993. Journal and Proceedings of the Royal Society of New South Wales, 126, 1–25.

Sutherland, F.L., 1994. Volcanism around K/T boundary time — its rôle in an impact scenario for the K/T extinction events. Earth-Science Reviews, 36, 1–26.

Sweet A.R. & Braman D.R., 1992. The K–T boundary and contiguous strata in western Canada: interactions between paleoenvironments and palynological assemblages. Cretaceous Research, 13, 31–79.

Swisher, C.C. III., Dingus, L. & Butler, R.F., 1993. $^{40}Ar/^{39}Ar$ dating and magnetostratigraphic consolidation of the terrestrial Cretaceous–Palaeogene boundary and Puercan mammal age, Hell Creek–Tullock formations, eastern Montana. Canadian Journal of Earth Sciences, 30, 1981–1996.

Swisher, C.C. III, Grajales-Nishimura, J.M., Montanari, A., Margolis, S.V., Claeys, P., Alvarez, W., Renne, P., Cedillo-Pardo, E., Maurasse, F.J.-M.R., Curtis, G.H., Smit, J. & McWilliams, M.O., 1992. Coeval $^{40}Ar/^{39}Ar$ ages of 65.0 million years ago from Chicxulub crater melt rock and Cretaceous–Tertiary boundary tektites. Science, 257, 954–958.

Sykes, T.J.S. & Kidd, R.B., 1994. Volcanogenic sediment distributions in the Indian Ocean through the Cretaceous and Cenozoic, and their palaeoenvironmental implications. Marine Geology, 116, 267–291.

Takata, T. & Ahrens T.J., 1994. Numerical simulation of impact cratering at Chicxulub and the possible causes of KT catastrophe. In: New developments regarding the KT event and other catastrophes in Earth history. LPI Contribution 825, Lunar and Planetary Institute, Houston, 125–126.

Tewari, H.C., Dixit, M.M. & Sarkar, D., 1995. Relationship of the Cambay Rift Basin to the Deccan volcanism. Journal of Geodynamics, 20(1), 85–95.

Thordarson, Th. & Self, S., 1993. The Laki (Skaftár Fires) and Grímsvötn eruptions in 1783–1785. Bulletin of Volcanology, 55, 233–263.

Tredoux, M., de Wit, M.T., Hart, R.J., Lindsay, N.M., Verhagen, B. & Sellschop, J.P.F., 1989. Chemostratigraphy across the Cretaceous–Tertiary boundary. Journal of Geology, 97, 585–605.

Upchurch, G.R. Jr., 1989. Terrestrial environmental changes and extinction patterns at the Cretaceous–Tertiary boundary, North America. In: Donovan, S.K. (editor), Mass extinctions — processes and evidence. Belhaven Press, London, 195–216.

Vannucci, S., Pancani, M.G., Voselli, O. & Cordossi, N., 1990. Mineralogical and geochemical features of the Cretaceous–Tertiary boundary clay in the Barrando Del Gredero section (Caravaca, SE–Spain). Chem Erde, 50, 189–202.

Veevers, J.J., Powell, C. McA. & Roots, S.R., 1991. Review of seafloor spreading around Australia. 1. Synthesis of the patterns of spreading. Australian Journal of Earth Sciences, 38, 373–389.

Venkatesan, T.R., Pande, K. & Gopalan, K., 1993. Did Deccan volcanism pre-date the Cretaceous/Tertiary transition? Earth and Planetary Science Letters, 119, 181–189.

Venkatesan, T.R., Pande, E. & Gopalan, K., 1994. Reply to comment on 'Did Deccan volcanism pre-date the Cretaceous–Tertiary transition?' Earth and Planetary Science Letters, 122, 263–265.

Williams, M.E., 1994a. Catastrophic versus noncatastrophic extinction of the dinosaurs: testing, falsifiability, and the burden of proof. Journal of Paleontology, 68, 183–190.

Williams, M.E., 1994b. Comment on: Lack of a high body count at the K–T boundary. Journal of Paleontology, 68, 1168.

Wingard, G.L., 1993. A detailed taxonomy of Upper Cretaceous and lower Tertiary Crassatellidae in the eastern United States — an example of the nature of extinction at the boundary. US Geological Survey, Professional Paper 1535, 1–131.

Wolbach, W.S., Anders, E. & Nazarov, M.A., 1990. Fires at the K/T boundary: carbon at the Sumbar, Turkemenia site. Geochimica et Cosmochimica Acta, 54, 1133–1146.

Wolfe, J.A., 1991. Palaeobotanical evidence for a June impact winter at the Cretaceous/Tertiary boundary. Nature, 348, 157–160.

Zahnle, K. & Grinspoon, D., 1990. Comet dust as a source of amino acids at the Cretaceous/Tertiary. Nature, 348, 157–160.

Zhou, L., Kyte, F.T. & Bohor, B.F., 1991. Cretaceous/Tertiary boundary at DSDP Site 596, South Pacific. Geology, 19, 694–697.

Zinsmeister, W.J. & Griffin, M., 1995. Late Cretaceous and Tertiary apporrhaid gastropods from the southern rim of the Pacific Ocean. Journal of Paleontology, 69(4), 692–702.

AGSO Journal of Australian Geology & Geophysics, 16 (4), 587–607

Mega-impacts and mantle-melting episodes: tests of possible correlations*

Andrew Yoram Glikson[1]

The criteria for recognising the effects of impacts by large-diameter extraterrestrial projectiles (D_p >>10 km) on thin, geothermally active crust must vary fundamentally from those pertaining to impacts on thick, cooler continental crust. The release of energy on the scale of $\geq 10^9$ Mt (10^9 x 10^6 t TNT) unleashed by such events triggers seismic activity orders of magnitude higher than that induced by purely endogenic movements. Faulting at both proximal and distal foci from impact sites, and associated adiabatic melting of underlying mantle, are expected consequences.

Thermal overprinting of shock-metamorphic effects (breccias, shatter cones, pseudotachylite, shock lamellae, high-pressure polymorphs) induced by both shock-induced fusion and heat transfer from impact-rebounded adiabatically melting mantle is capable of obscuring the criteria for impact. The distal effects of mega-impacts on subducted Precambrian oceanic crust are no longer preserved in the geological record. Ensuing proximal and distal phenomena may span the range between clearly recognisable extraterrestrial impact effects and endogenic igneous activity. Age correlations between Phanerozoic impacts and plateau basalts yield preliminary support for this hypothesis. Although the bulk of the terrestrial cratering record has been destroyed by both erosion of elevated terrains and plate subduction, or obscured by burial, a search for Precambrian mega-impacts is facilitated by the preservation of their likely secondary effects: mega-earthquake-triggered faults; ensuing diamictites, and the deposits of turbidity currents; microtektites; spherulitic condensates of vaporised asteroid and target materials; and distal tectonic and igneous effects.

Clues to the origin of thermal events are provided by peaks on isotopic-age histograms of precise U–Pb, Ar–Ar, and Sm–Nd mineral–whole-rock ages. These peaks, spatially corroborated by detailed mapping of Precambrian terrains, support an episodic nature of at least certain major Precambrian events and some correlations with impact events, for example: (1) formation of greenstone–granite terranes at ca 3.45 Ga; (2) rifting and clastic sedimentation, including the deposition of iridium-rich spherule units in the basal Fig Tree Group (Kaapvaal Craton, South Africa) and in the Gorge Creek Group (Pilbara Block, Western Australia) at 3.2 Ga; (3) global greenstone–granite events at ca 3.0 Ga; (4) global greenstone–granite events at ca 2.7 Ga; (5) deposition of the Hamersley spherule beds, and the emplacement of global mafic dyke swarms, at ca 2.45 Ga; (6) initiation of global Proterozoic rift networks, and possibly the emplacement of the Bushveld Complex at ca 2.05 Ga; (7) the Sudbury (Canada) and Uppland (Sweden) impacts, and peak rifting in mobile belts, at ca 1.85–1.80 Ga; (8) probable impact structures in Sweden, and the Grenville/Keweenawan global rifting and magmatic activity, at ca 1.2–1.05 Ga; and (9) the Beaverhead (Canada), Acraman (South Australia), and Janisjarvi (Karelia) impacts, and the Vendian–Early Cambrian global rifting, ocean-floor spreading (Iapetus Ocean), and igneous activity (Franklin Province, Canada), at 0.7–0.5 Ga.

Preliminary time-series analyses of Precambrian events yield values consistent with the Phanerozoic galactic rotation period (250 ± 50 Ma), and the solar system's cross-galactic-plane oscillation period (33 ± 3 Ma). Possible correlations between mega-impacts and tectonic/thermal events are capable of being tested through isotopic-age studies of diamictites and spherule units of impact origin and of potentially coeval rifting and mafic igneous events.

Introduction

Harold C. Urey, in 'Comet collisions and geological periods' (1963), suggested a link between extraterrestrial events and the termination of geological periods. Salisbury & Ronca (1966) and Ronca (1966) correlated the origin of continental nuclei with major impacts. These departures from the traditional endogenic paradigm inherent in Earth science succeeded controversies surrounding the origin of 'cryptoexplosion' structures, including small young craters (e.g., Meteor Crater, Arizona; Barringer 1905), intermediate-size structures (e.g. Gosses Bluff, central Australia; Crook & Cook 1966; Glikson 1969; Milton et al., this issue), and large circular uplifts and basins (Vredefort ring, Transvaal; Dietz 1961a, b; Nicolaysen & Ferguson 1990; Sudbury Basin, Ontario; Dietz 1964; French 1972; Peredery & Morrison 1984; Muir 1984; Bushveld Complex, Transvaal; Hamilton 1970; Rhodes 1975; French 1990; Elston 1992). More recently, this divergence has been manifested by the controversy regarding the Cretaceous–Tertiary (KT) boundary events (Alvarez et al. 1980; Alvarez 1986; Shoemaker & Wolfe 1994).

With few exceptions, concepts of the nature and evolution of the Precambrian crust are dominated by modified uniformitarian plate-tectonic models (cf. Hoffman 1989; Condie 1993a, b; Windley 1993), which take little account of the effects of large ($D_p \geq 10$ km, where D_p is the projectile diameter) Precambrian mega-impact events that postdate the Late Heavy Bombardment (LHB: 4.1–3.9 Ga; Ryder 1990). These models are based on comparisons with island-arc (Folinsbee et al. 1968; Jakes & White 1971; Anhaeusser 1973), back-arc (Tarney et al. 1976), primitive-simatic-crust (Engel 1966; Glikson 1972, 1984), oceanic-plate (Hoffmann & Ranalli 1988; de Wit & Hart 1993), and ensialic-rift (Archibald & Bettenay 1977; Blake & Groves 1987) tectonic environments, to cite just a few. Thus, despite a rapid increase in the volume of data on Precambrian terranes, notably precise isotopic ages, the diversity of models has steadily *increased instead of being constrained,* which hints at the existence of as yet unidentified factors. These models take little account of the effects of mega-impacts on the Precambrian Earth, predicted by the history of the Moon, Phanerozoic impact rates, and the observed asteroid flux.

Post-LHB terrestrial impact rates based on the lunar record (Wilhelms 1987; Baldwin 1985; Melosh 1989), Proterozoic cratering rates (Shoemaker & Shoemaker 1990, this issue), and Phanerozoic cratering rates (Grieve & Dence 1979) are estimated as $(5.4 \pm 2.7) \times 10^{-15}$ km^{-2} y^{-1} for craters of D_c >20 km (where D_c is crater diameter; Grieve & Pesonen 1992), in agreement with estimates of the asteroid flux of $(4.9 \pm 2.9) \times 10^{-15}$ km^{-2} y^{-1} (Wetherill & Shoemaker 1982). Extrapolations from the post-LHB lunar record of Wilhelms (1987), taking the Earth/Moon surface ratio (13.4) and the gravity section (1.4) into account, suggest the following impact concentrations for the Earth:

- *3.8–3.2 Ga (lunar upper Imbrian)*: ca 3200 terrestrial craters of D_c >35 km; some ≥300 km;

[1] Division of Regional Geology & Minerals, Australian Geological Survey Organisation, PO Box 378, Canberra, ACT 2601.

* In honour of Robert Sinclair Dietz [1914–1995]: pioneer of extraterrestrial impact research

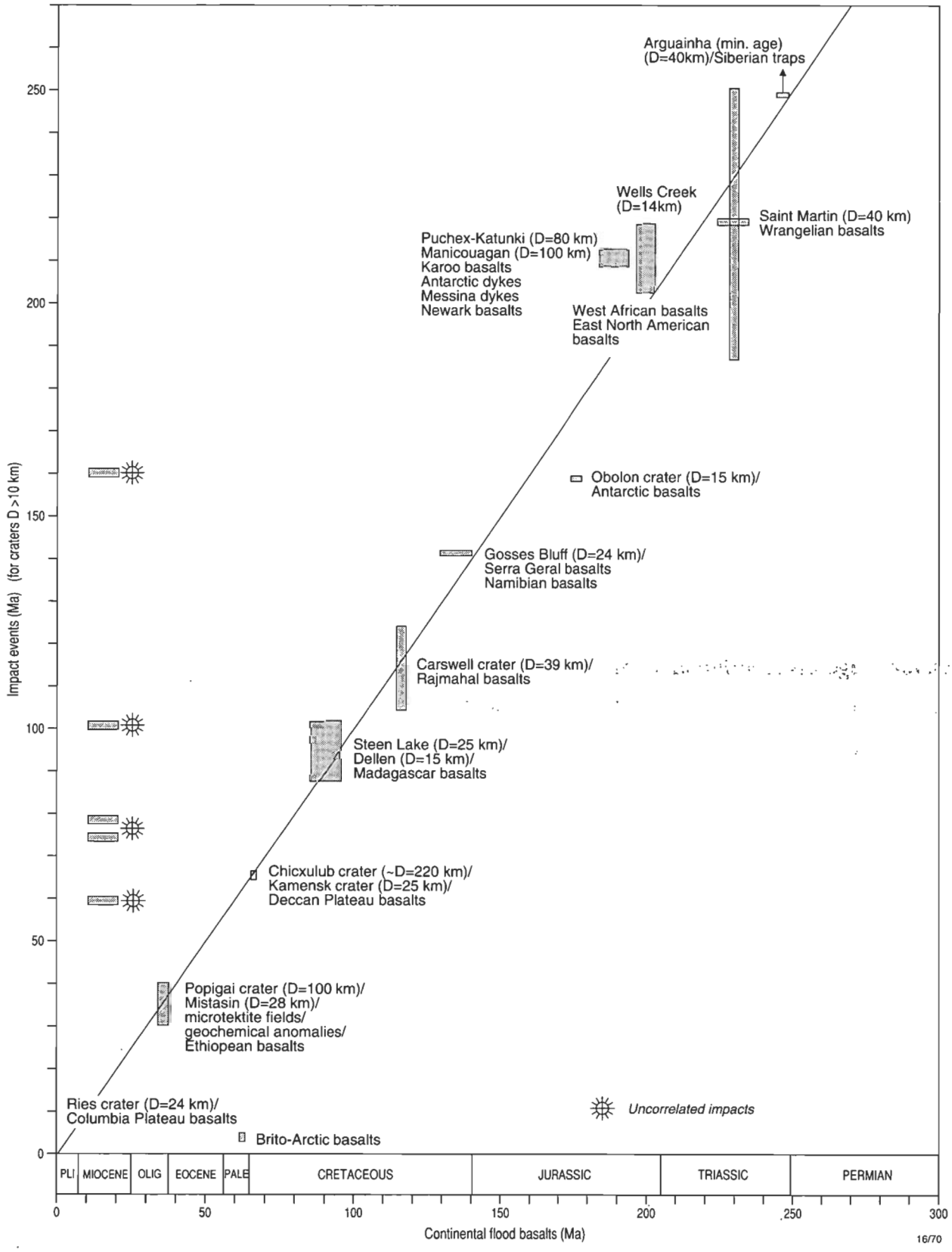

Figure 1. Plots of ages of late Phanerozoic mega-impacts (D_c >10 km) against ages of plateau basalts (based on data listed in Table 2). Stars denote impact events with which no major mafic volcanic plateau basalts are known to correlate.

- *3.2–1.1 Ga (lunar Eratosthenian)*: ca 1650 terrestrial craters of D_c >35 km; some >180 km (scaled from the lunar Hansen crater: D_c = 167 km); and
- *<1.1 Ga (lunar Copernican)*: ca 820 terrestrial craters of D_c >35 km; some >100 km.

According to these figures, ca 6000 terrestrial impact structures (D_c >35 km) postdate the LHB. The size distribution of lunar post-LHB craters and of terrestrial structures imply that about one per cent of them (ca 60 craters) would have D_c >150 km, and some would be likely to exceed the largest

recorded impact structures — e.g., Chicxulub (Mexico; D_c = >180 km) and Uppland (Sweden; D_c = 320 km).

From the post-3.8-Ga lunar-crater stratigraphy, Baldwin (1985) suggested a possible episodic distribution of asteroid impacts on the Moon, which has likely implications for correlation with the terrestrial impact history (Stothers 1992). In the following, the Precambrian impact record is examined in connection with this possibility.

Central to the debate surrounding Phanerozoic mass extinctions are possible correlations between Mesozoic–Cainozoic continental flood basalts and mega-impact events (Alt et al. 1988; Stothers & Rampino 1990; Stothers 1992; Rampino & Caldeira 1993; Stothers 1993a, b; Fig. 1). A corollary to this correlation suggests tests of potential links between Precambrian igneous events and extraterrestrial triggers. The best candidates to date are the Deccan plateau basalts which correlate precisely with the impact(s) at the 65-Ma KT boundary. Since the refraction of high-energy seismic waves through the Earth may result in allochthonous and antipodal structural disturbances, spatial juxtaposition between mega-impact scars and seismically triggered volcanism is not necessarily expected (Rampino 1993). Possible distal mechanical, thermal, and igneous consequences of large-scale impacts (Grieve 1980; Melosh 1989; Wichman & Schultz 1990a, b; Glikson 1976, 1993) can be tested by isotopic-age correlations of impact signatures and their potentially triggered igneous effects; the age studies should include a re-examination of the existing geochronological data sets.

Isotopic-age-distribution anomalies

According to a compilation of K–Ar, Rb–Sr, and U–Th–Pb ages, Gastil (1960) suggested that worldwide thermal and igneous events evince at least eight maxima (ca 2.6, 2.1, 1.8, 1.4, 1.0, 0.48, 0.35, and 0.105 Ga) that identify a cyclicity of 350–500 Ma. Further model and isochron K–Ar and Rb–Sr ages (Stockwell 1968; Dearnley 1966) emphasise peak events at ca 2.6, 1.8, 1.1, and 0.6 Ga (Fig. 2a). Rb–Sr isochron and U–Pb zircon age peaks have been documented at 3.5, 3.0, and 2.7 Ga (Moorbath 1977; Card 1990; Pidgeon & Wilde 1990, and are supported by further compilations of U–Pb zircon ages (Glikson 1993; and this paper). Such long-term episodicity is difficult to reconcile with the expectation of a *continuity or quasicontinuity* of thermal events inherent in ongoing accretion/subduction processes. The literature indicates an episodic distribution of several types of geological event, including (Figs. 2 and 3):

- several peaks in the development of intracratonic rifts (e.g., ca 3.2, 2.4, 2.1, 1.8, 1.5, 1.2–1.05, and 0.7–0.5 Ga; e.g., J.C. Green 1993);
- major periods of dyke formation (e.g., ca 3.4, 3.0–2.9, 2.5, 2.2–1.9, 1.3–1.1, 0.9–0.6, and 0.2–0 Ga; Hall & Fahrig 1987); and
- irregular crustal migration rates and directional reversals represented by apparent polar-wander paths (APWP; e.g., accelerated migration rates during certain age intervals; Irving & Park 1972; Piper 1987).

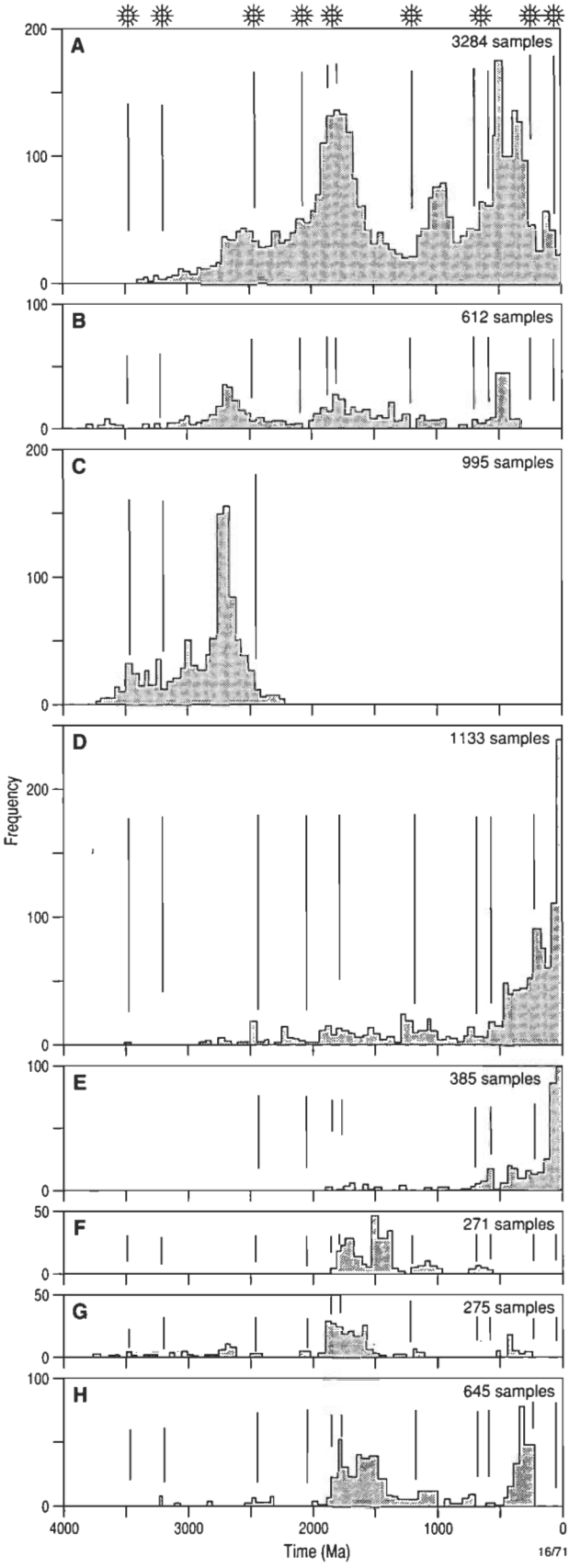

Figure 2. Frequency–distribution diagram of isotopic ages from several Precambrian terranes for 50-Ma intervals: (a) 3284 Rb–Sr, K–Ar, and U–Th–Pb ages worldwide (Dearnley 1966); (b) compilation of 612 Rb–Sr isochron ages worldwide (Glikson 1983); (c) 995 Archaean U–Pb, Rb–Sr, Sm–Nd, K–Ar, and Ar–Ar age determinations from several shields (Glikson 1993); (d) 1133 ages of basic igneous rocks worldwide from the palaeomagnetic database of Lock & McElhinny (1991); (e) 385 ages of felsic igneous rocks worldwide from the palaeomagnetic database of Lock & McElhinny (1991); (f) 271 U–Pb and Rb–Sr isochron ages from the USA (Reed et al. 1993); (g) 275 U–Pb zircon ages from Australian terranes; (h) 645 Rb–Sr isochron ages from Australian terranes. Stars and vertical lines correspond to recorded impacts or time ranges of impact clusters.

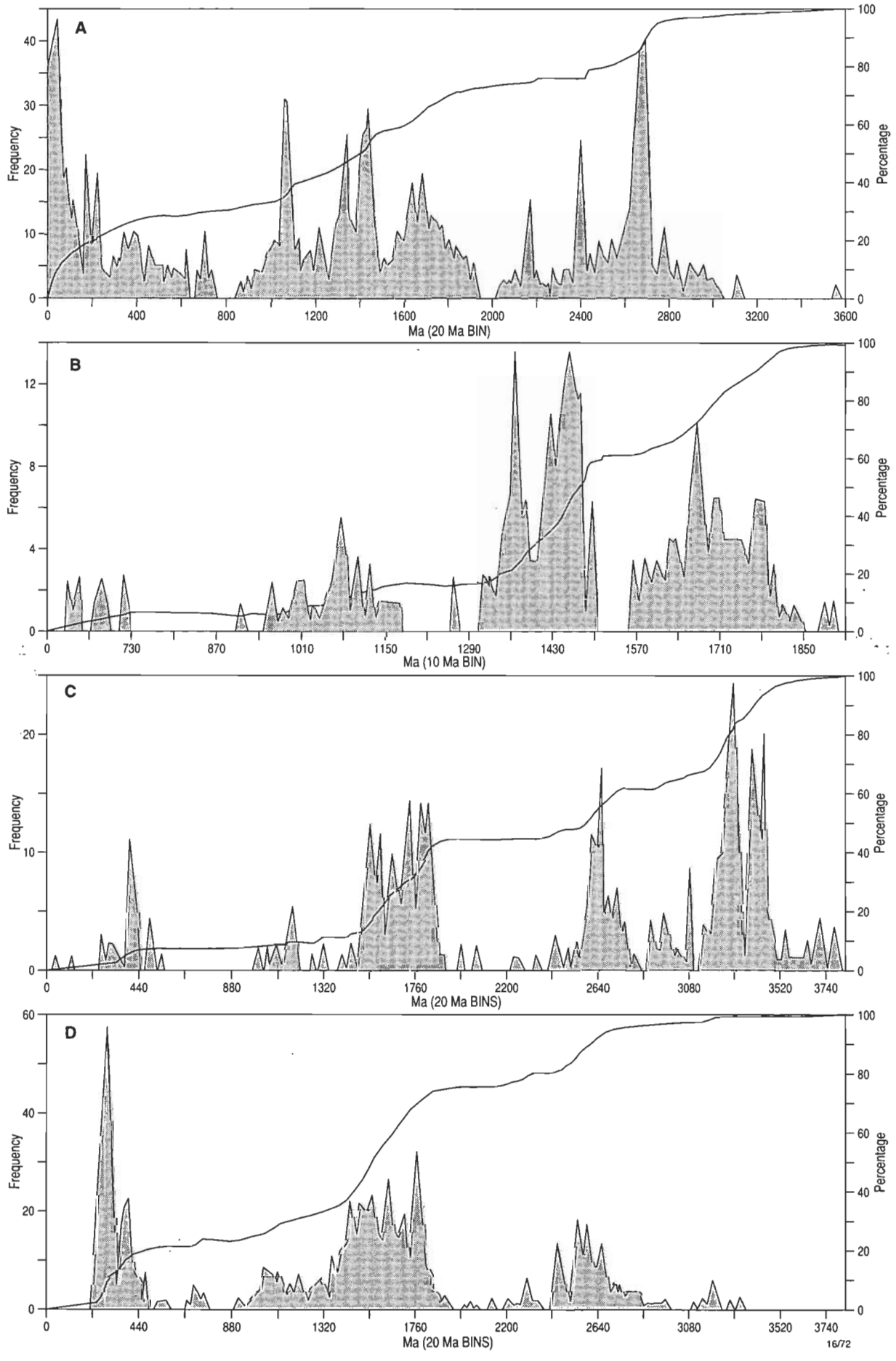
A
Frequency
Percentage
Ma (20 Ma BIN)
B
Frequency
Percentage
Ma (10 Ma BIN)
C
Frequency
Percentage
Ma (20 Ma BINS)
D
Frequency
Percentage
Ma (20 Ma BINS)
16/72

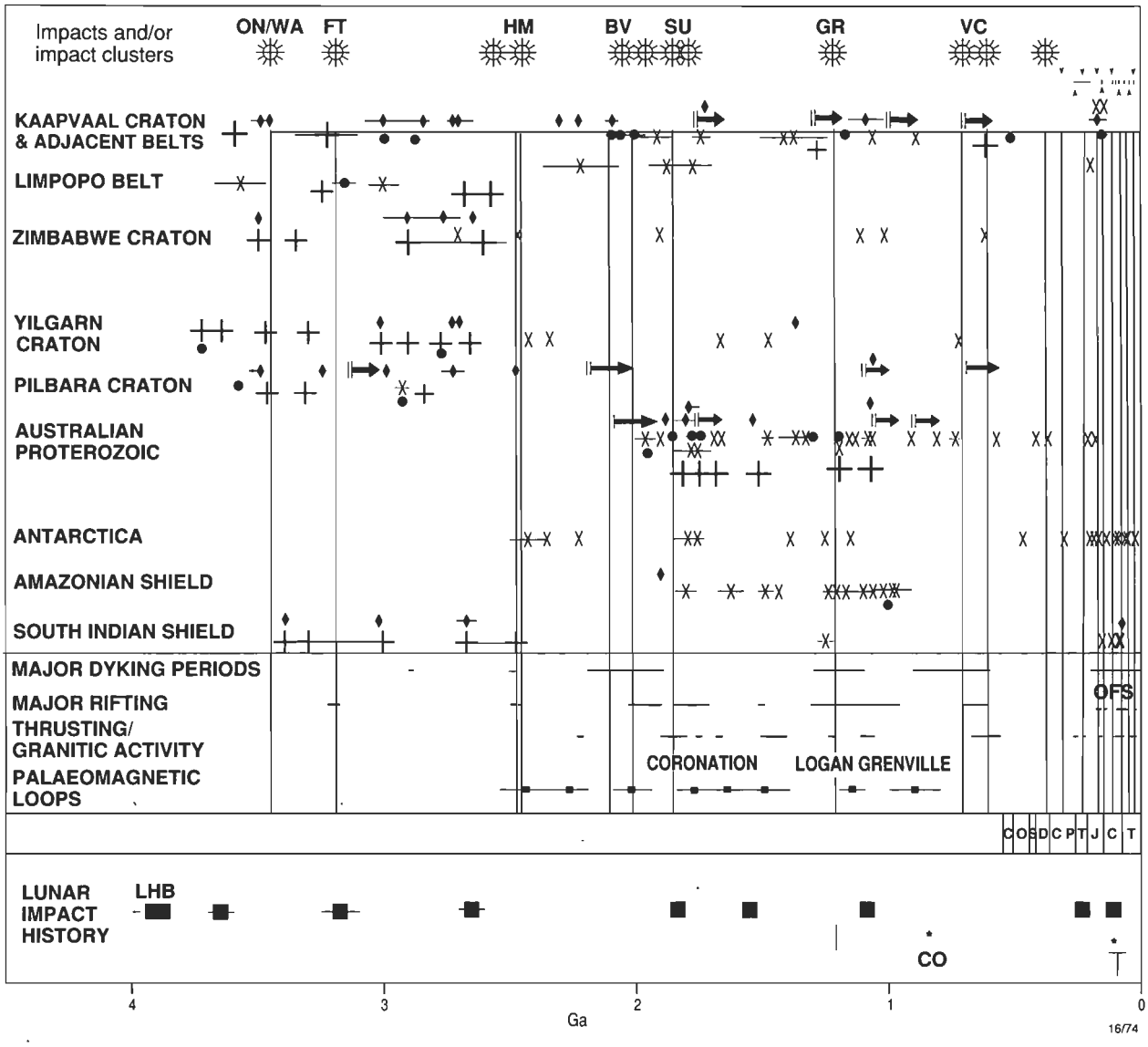

Figure 4. Timescales of mafic and other igneous activity, tectonism, palaeomagnetic anomalies, and impact history of the Moon and the Earth's southern-hemisphere shields. For references and sources of data see Glikson (1993). Stars = impacts; × = mafic dyke swarms; solid diamonds = mafic and ultramafic volcanism; solid circles = mafic plutonism; + = granitoid intrusion; arrows = rifting; horizontal lines represent the durations of events and/or isotopic-age error bars. Abbreviations: ON/WA = Onverwacht Group and Warrawoona Group (mafic–ultramafic volcanic sequences); FT = basal Fig Tree Group possible extraterrestrial impact; HM = Hamersley event (spherules in Wittenoom Formation and Dales Gorge Member); BV = Bushveld event; SU = Sudbury Basin and Uppland impacts; GR = Grenville events (possible impact structures in Sweden); VC = Vendian–early Cambrian (700–540 Ma) impacts (Janisjarvi, Beaverhead, and Acraman). Phanerozoic events are indicated schematically by vertical lines (see Table 2). The lunar impact history is after Baldwin (1985) and Stothers (1992).

Earlier isotopic-age histograms combined with new compilations outline maxima at ca 3.6, 3.45, 3.2, 3.0, 2.75–2.55, 2.45, 2.2, 1.85–1.65, 1.6–1.4, 1.25, 1.2–1.0, and 0.76–0.72 Ga (cf. peaks in Figs. 2a–h and 3a–d, and refer also to Table 1). Whereas some of these peaks are well defined, their interpretation in terms of a primary episodicity of thermal events is *fraught with uncertainties*. Thus, some of the earlier data sets combine ages which were measured by several isotopic systems, and which represent inherited ages, primary igneous ages, reset metamorphic ages, and cooling/uplift ages. Furthermore, the observed age frequency–distribution patterns are influenced by sampling biases which arise from factors such as:

- the overall but non-uniform decrease in the preserved/exposed dimensions of geological terranes with their increase in age;
- the choice of materials of suitable isotopic compositions;
- different degrees of outcrop of contrasted lithologies;
- sampling strategies related to access, and economic and scientific sampling priorities;

Figure 3 (facing page). Frequency–distribution diagrams of isotopic ages from several Precambrian terranes for 20- and 10-Ma age intervals: (a) 1140 isotopic ages from Laurentia (Thurston et al. 1991); (b) 267 U–Pb and Rb–Sr isochron ages from the continental USA (Reed et al. 1993); (c) 548 U–Pb zircon ages from Australian terranes; (d) 976 Rb–Sr isochron ages from Australian terranes.

- a concentration of sampling in technologically developed countries; and
- limits on the mammoth task of assessing the quality and significance of individual age determinations in the database of about 7600 dates used in constructing the histograms (Figs. 2 and 3).

Conceivably the sheer size of the database minimises the sampling biases indicated above; if so, the histograms provide a crude measure of thermal episodicity. However, it is more likely that age correlations based on few accurate isotopic analyses of samples representative of spatially extensive suites are more meaningful in this regard.

For the above reasons, precise isotopic-age determinations in combination with detailed regional geological mapping must be applied to appropriate units to provide both temporal and spatial controls for identifying the episodic distribution of thermal/tectonic events. Significant advances in this regard have been made in Precambrian terranes in North America, Greenland, Fennoscandia, southern Africa, and Australia. Some of these events are compiled in Table 1 and Figures 4 and 5 (principal references: Windley 1993; J.C. Green 1993; Glikson 1993; Von Gruenewaldt & Harmer 1993). The following episodes may be outlined:

- greenstone–granite formation — e.g., 3.45 Ga (Kaapvaal, Zimbabwe, Pilbara), 3.0 Ga (Yilgarn, Superior, Karelian, Ukrainian, Aldan, Sino-Korean), 2.76–2.65 Ga (Slave, Superior, Finland, Zimbabwe, Murchison, central Africa, Brazil, Dharwar, Yilgarn), 2.1–2.07 Ga (Birimian, west Africa; Guiana), and ca 1.8 Ga (circum-Superior Province belts: Flin Flon greenstones, Cape Smith greenstones);
- major dyke swarms — e.g., 3.4 Ga (Ameralik), 3.0–2.9 Ga (west Pilbara), 2.7 Ga (Black Range suite, Pilbara), 2.45 Ga (Matachewan, Zimbabwe Great Dyke, Jimberlana), 2.2, 1.9–1.8, 1.2 Ga (Mackenzie), 0.8, and 0.6 Ga (Gardar);
- major mafic–ultramafic intrusions — e.g., 2.7 Ga (Stillwater Complex), 2.05 Ga (Bushveld Complex), and 1.08 Ga (Giles Complex and near-coeval volcanics);
- plateau flood basalts and rift volcanics — e.g., 3.0 Ga (Pongola) and 2.75–2.65 Ga (Ventersdorp, Fortescue);

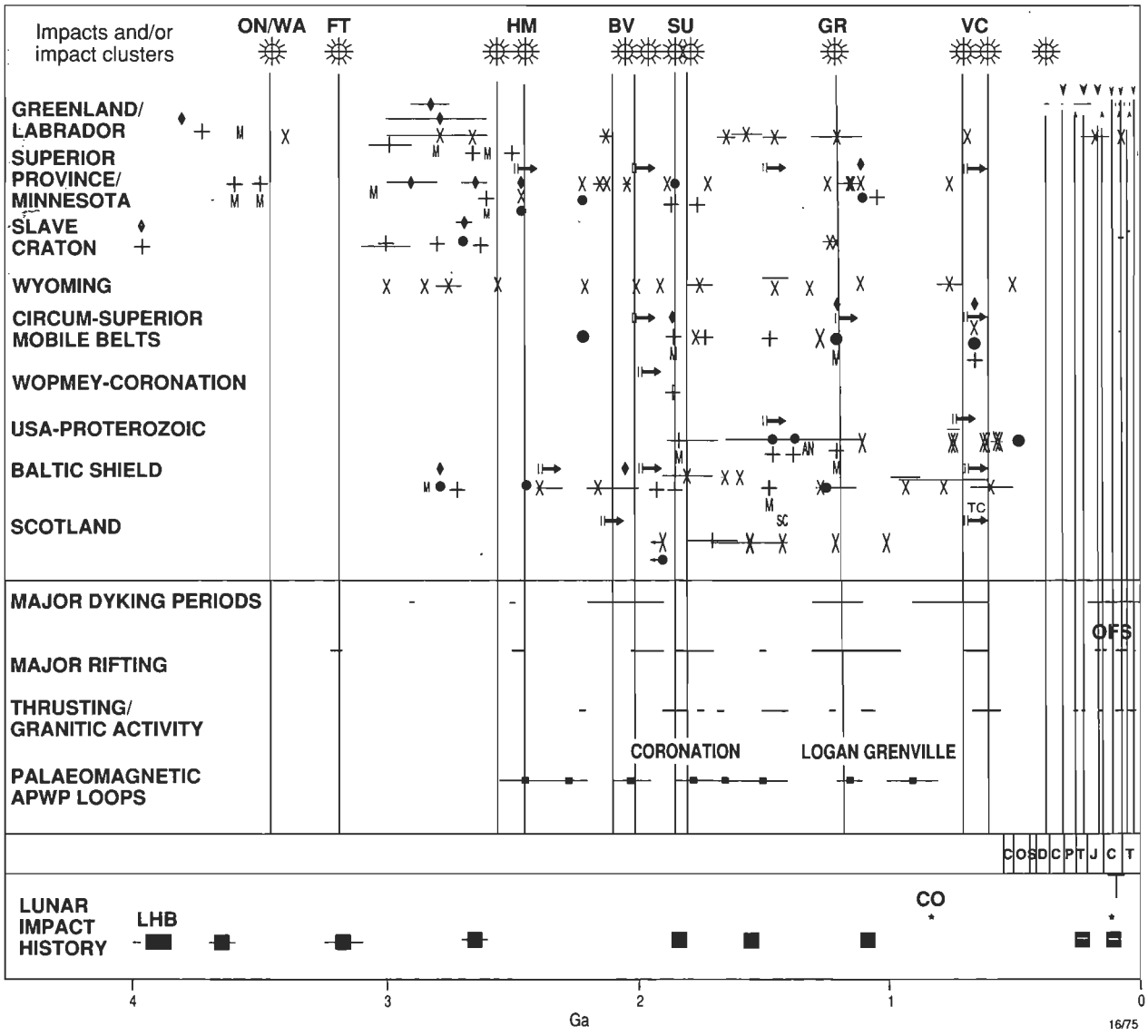

Figure 5. Timescales of basic and other igneous activity, tectonism, and impact history of the Moon and the Earth's northern-hemisphere shields. For references and sources of data see Glikson (1993). For key to symbols and abbreviations, see caption to Figure 4.

- intracratonic and continental-margin rifting — e.g., 3.2 Ga (Fig Tree and Moodies Groups, Kaapvaal; Gorge Creek Group, Pilbara), 2.2–2.0 Ga (Ashburton Trough, Wyloo Group turbidites, Western Australia), 1.5 Ga (Belt rift series), 1.2–1.1 Ga (North American mid-continent rift; Damara), 0.7–0.5 Ga (Appalachian, Caledonides; Table 1); and
- peak granite emplacement, metamorphism, and thrusting in rift-initiated mobile belts — e.g., 2.7 Ga (Limpopo), 1.85–1.7 Ga (Hudsonian/Penokean/Ketilidean/Svecokarelian), 1.3–1.1 Ga (Grenville), 0.6 Ga (Pan-African).

It has been suggested that a selective preservation of particular age domains is an artifact arising from continuous mountain building, erosion, and subduction processes (Gurnis & Davies 1986). However, this is difficult to reconcile with the *repeated superposition of the same mafic igneous/rifting events* in several Precambrian shields (Table 1; Figs. 2–5). Such near-simultaneous events (Table 1) include the following episodes:

- ca 3.5-Ga greenstone–granite formation (Pilbara, Barberton, Zimbabwe, and possibly south India);
- ca 3.2-Ga rifting (Pilbara Block: deposition of Lalla Rookh conglomerates and sandstone in rift zones; Barberton greenstone belt, Transvaal: Moodies conglomerates);
- ca 3.0-Ga greenstone–granite formation (Yilgarn, Zimbabwe, northern Superior, Aldan, southwest Greenland, central Africa);
- ca 2.7-Ga greenstone–granite formation (Yilgarn, Pilbara, Zimbabwe, Superior, Slave, southwest Greenland, Baltic Shield, south India, Brazilian Shield); this is the most extensively preserved Archaean mega-event;
- ca 2.5-Ga global dyke emplacements (Superior, Zimbabwe, Yilgarn, Vestfold Hills complex in Antarctica);
- ca 2.05-Ga greenstone–granite formation (Birimian, west Africa); Bushveld Complex emplacement; initiation of rifts where ca 1.9–1.7-Ga mobile belts developed subsequently;
- ca 1.9–1.8-Ga development of Hudsonian mobile belts (Superior and Slave–Bear provinces in Canada; Greenland; Sweden; Australia; Africa);
- ca 1.5-Ga Belt rift series in western USA; volcanism in South Australia;
- ca 1.3–1.05-Ga Grenville-age mobile belts;
- ca 0.7–0.5-Ga development of Pan-African mobile belts and Caledonian Orogeny; opening of the Iapetus Ocean; alkaline igneous activity (Franklin Province). Further details on some of these events are presented in Glikson (1993) and later in this paper.

These events accord with the concept of an original episodicity for some geological processes during the Archaean — particularly greenstone–granite formation, intracratonic events, and the emplacement of dyke swarms. By contrast, accreted Proterozoic terranes in continental-margin settings may display a more continuous evolution (e.g., central/west USA; Anderson 1983; Condie 1993a, b), although distinct isotopic-age concentrations pertain to some of these events as well (peak events at 1.79–1.67, 1.49–1.43, and 1.39–1.36 Ga; Fig. 2f). However, whereas a general agreement exists among geochronologists regarding the reality of isotopic-age peaks, the root causes of these events remain controversial.

Origin of major crustal mafic igneous events

Explanations of an episodic evolution of the Earth's crust have been advanced in terms of numerous models, including the ones outlined below.

Episodic mantle pulsations

Runcorn (1962) and Dearnley (1966) interpreted isotopic-age irregularities in terms of episodic changes in the mantle-convection-cell pattern. Loper & McCartney (1986) suggested that episodic changes in the magnetic field arise from thermal instabilities at the D" layer. Thermal instabilities result from phase transitions, and provide a mechanism for episodic heat bursts and the resetting of convection patterns (Zhao et al. 1992; Weinstein 1993). Weinstein calculated the thermodynamics of the exothermic olivine-to-spinel and the endothermic spinel-to-perovskite + magnesiowustite transitions at the upper/lower-mantle boundary zone, and inferred that once subducted slabs reach a threshold of thermal buoyancy they will sink into the lower mantle. Consequent phase changes result in catastrophic bursts of whole-mantle convection lasting ca 10 Ma, elevated heat transfer lasting ca 100 Ma, and stabilisation of the geodynamo, which is represented by magnetically quiet superchrons. This mechanism, however, is likely to be confined to linear belts overlying subduction zones overlying descending lithosphere, and is difficult to apply to entire intraplate shield areas as global mantle pulses.

Episodic whole-mantle overturns

In a thought-provoking paper, Davies (1996) tests a kinematic model whose principal elements include:

- endothermic phase transformations at the upper/lower-mantle boundary layer;
- episodic collapse of cool dense upper mantle into hot lower mantle, triggering whole mantle overturn; and
- consequent temporal cyclicity between stable convection-driven plate tectonic regimes and episodes of large-scale mantle upwelling and continental crust formation at intervals of the order of a few 10^8 years; modelled peak activities are apparent at ca 2.7 and 1.9–1.8 Ga.

Assumptions inherent in this model include some weakly constrained factors: efficiency of heat transfer between mantle layers; thermodynamic parameters of mantle phase changes; and the dynamics of subducted plates (Davies 1996). Geological constraints on this model include:

- limits on the distribution of Proterozoic thermal and tectonic activity — for example, the ca 1.9–1.8-Ga signatures are commonly concentrated in mobile-belt networks and along the margins of Archaean cratons, and are dominated by mantle-derived rather than Archaean crust-reworked materials; in contrast, the interiors of Archaean cratons, such as the extensive Yilgarn and Superior cratons, rarely betray thermal/metamorphic imprints of the 1.9–1.8 Ga events. This pattern favours a reticulate, possibly convection-related thermal/tectonic pattern rather than global mantle upwelling; and
- peak activity periods characterised by production of voluminous mafic magmas, and the intervals dominated by plate-tectonic events — this contrasts with the abundance of

island-arc-like volcanic assemblages formed during ca 2.7 and 1.9–1.8 Ga and with the relative scarcity of such assemblages in the intervening period.

Cyclic subcratonic radiogenic heating

Hoffmann (1989) suggested that thermal blanketing of lithosphere by large tracts of radiogenically heated sialic crust culminates in episodic mantle upwelling and consequent rifting. However, the following perceptions are not compatible with this concept:

- Proterozoic mafic igneous/rifting episodes are not confined to the interiors of supercontinents, but occur concomitantly at their accretionary margins. This is demonstrated by the onset of rifting ca 2.1–2.0 Ga and its culmination in major granitic and thrusting activity ca 1.9–1.8 Ga in *both* intrashield-rift settings (Churchill, Cape Smith, Labrador, Wopmay, Mount Isa–Cloncurry) *and* continental-margin settings (Penokean, Ketilidean, Svecokarelian; J.C. Green 1993; Windley 1993; Condie 1993a, b). Likewise, the ca 0.7–0.5-Ga Pan-African events encompass intercratonic mobile belts (Damara, trans-Sahara), intracratonic thrusting (central Australia), ocean-floor spreading (Iapetus Ocean), and rapid terrane accretion (Arabian–Nubian belt; J.C. Green 1993);
- rates of subcrustal lithospheric heating, and therefore thermal blanketing effects, depend on the radiogenic level and geochemical history of the domains in question. Archaean tonalite/trondhjemite/greenstone-dominated sequences, which commonly occupy the central positions of shields, typically have low heat flow due to their low U, Th, and K contents and likely radiogenic-element-depleted coupled lithosphere (Lambert & Heier 1968; Glikson 1983); and
- the consequence of thermal blanketing is questionable, since even small increases in mantle temperature result in sharp reduction in viscosity, convective flow, and thermal homogenisation (Gurnis & Davies 1986).

Hot-spot/mantle-plume models

Models invoking episodic mantle-plume activity (Campbell & Hill 1988) have inherent difficulties regarding their temporal distribution similar to those pertaining to phase-transition-triggered convection. As noted above, the effect of mantle plumes can be expected to be linear rather than global. The question of deep, long-acting mantle hot spots versus migrating faults or structural controls of mantle activity remains the subject of debate (e.g., D.H. Green 1993). On the other hand, structural triggers for large-scale mantle activity may be provided by impacts of large projectiles (D >10 km), which — as indicated by the post-LHB (3.95–3.85 Ga; Wilhelms 1987; Ryder 1990) history of the Moon — inevitably must have affected the Earth.

Possible correlations between mega-impacts and igneous/rifting events

Occurrences of platinum-group-element anomalies and sanidine-quench textures in spherule beds have been interpreted as distal silicate condensates of major impacts (3.48–3.45 Ga, upper Onverwacht Group, Transvaal [Lowe et al. 1989]; 3.47–3.44 Ga, Salgash Subgroup, Pilbara, Western Australia [Lowe & Byerly 1986]; ca 3.2 Ga, basal Fig Tree Group, Transvaal [Lowe et al. 1989]; ca 2.5 Ga, Hamersley Group, Western Australia [Simonson 1992]). Proximal high-velocity-impact effects are preserved as ca 2.0 to post-2.0-Ga structures — including the Vredefort ring (2.016 ± 0.01 Ga; D_c ca 140 km; Dietz 1961b; Colliston & Reimold 1992), Sudbury structure (1.85 Ga; D_c ca 200 km; Dietz 1964; French 1972; Avermann et al. 1992), Uppland structure, central Sweden (ca 1.8 Ga; D_c ca 320 km; Lilljequist & Henkel 1991; Henkel & Lilljequist 1992), and smaller structures (Grieve & Pesonen 1992; Shoemaker & Shoemaker 1990).

Stothers (1992) correlated Baldwin's (1985) post-Imbrium lunar model impact peaks with the orogenic cycles of Fitch et al. (1974), including the intervals 3.8–3.5, 3.15–3.0, 2.85–2.5, 1.95–1.6, 1.2–0.9, and 0.6–0 Ga (Figs. 4 and 5). U–Pb age determinations indicate that these broad intervals consist of numerous distinct igneous and tectonic events (Figs. 4 and 5). Relevant data are tabulated in Table 1, which necessarily presents less than a complete compilation. It is emphasised that, since no distinction is possible between major episodic impact clusters and individual impact related to a continuous 'background' scatter, such correlations are *strictly tentative* at the present state of knowledge. The APWP rates and loops may allow a measure of plate movements and reversals (Irving & Park 1972; Piper 1987). Owing to the redefinition of APWPs by U–Pb baddeleyite analysis of dykes (Krogh et al. 1987), the palaeomagnetic indications are regarded as preliminary.

In the following, potential correlations between Precambrian impact signatures and *certain* rifting and mafic igneous events are considered. However, as the impact record, especially of well-dated mega-impacts, is scant, such comparisons are not regarded as statistically meaningful correlations.

ca 3.2-Ga rifting

The iridium-rich spherule units detected at the base of the ca 3.2-Ga Fig Tree Group (Kaapvaal Craton), interpreted in terms of impact effects by distal asteroids (Lowe et al. 1989; Kyte et al. 1992; Glikson 1993; Koeberl et al. 1993), might coincide with the onset of major felsic volcaniclastic and greywacke sedimentation of the Fig Tree Group, and with ca 3.2-Ga rifting of the Gorge Creek Group (Pilbara Block, Western Australia). Both sequences overlie greenstone–granite terranes with sharp breaks or unconformities. Though no proximal impact effects are apparent in the basement, faults, slumped beds, and the sharp development of turbidity deposits may represent the seismic/tectonic effects of distal impacts.

ca 2.45-Ga dyke emplacements

The Great Dyke suite (Zimbabwe), Matachewan dyke suite (Superior Province), Widgiemooltha dyke suite (Yilgarn), Vestfold Hills complex dykes (Antarctica), and Tornio layered intrusive suite (Finland–Kola) form near-contemporaneous events dated at ca 2.45 Ga. A vestige of contemporaneous impacts, signifying either single or temporally clustered events, is represented by spherule and diamictite units intercalated with the ca 2.45-Ga Wittenoom Formation and Dales Gorge Member (of the Brockman Iron Formation) of the Hamersley Group, Hamersley Basin (WA; Simonson 1992). Very high APWP rates (8–15 cm y^{-1}) are apparent during the ca 2.55–2.35-Ga loop (Piper 1987), signifying rapid crustal movement relative to the dipole.

ca 2.2–2.0-Ga rifting

The 65 000 km^2 Bushveld Complex, Transvaal (2.05 Ga) — consisting of a layered mafic–ultramafic lopolith (Rustenberg suite), coeval granites, and felsites — has been interpreted as the product of a mega-impact (Hamilton 1970; Rhodes 1975), on the basis of:

- a three-lobed structure located north of the possibly contemporaneous 2016 ± 10 Ma Vredefort impact ring;
- megabrecciated central uplifts;
- superheated non-eutectic coeval felsite (Rooiberg felsite) interpreted as instantaneously and non-equilibrated melted sediments (French & Twist 1983); and
- the occurrence of pseudomorphed tridymite (Elston 1992).

Although mesoscale to small-scale mechanical impact signatures have not been detected at the Bushveld Complex (French 1990), they could have been obliterated by thermal recrystallisation (Elston 1992).

Table 1. Approximate peak ages of some tectonic, igneous, and metamorphic episodes suggested in several Precambrian shields and terranes, and tabulated by province and decreasing age

A = amphibolite; B = basic plutonism; C = collision; CH = granulite/charnockite; D = basic dykes; FV = felsic volcanics; G = granite; IV = intermediate volcanics; m = metamorphism; MV = mafic volcanics; N = gneiss; O = anorthosite; R = onset of rift systems; RG = rapakivi granite; T = tonalite–trondhjemite–granodiorite; V = volcanics (undifferentiated); ZX = zircon xenocrysts. For data sources refer to Condie (1993), J.C. Green (1993), Glikson (1993), and Windley (1993).

A. 4.0–2.4 Ga

Superior Province and circum-Superior belts			3.5 N, T, V		3.0–2.8 MV, FV, N		2.7–2.6 MV, IV, FV, G, A	2.5–2.45 MV 2.45 D, B, R
Minnesota River Valley		3.6 T			3.05 MV		2.60 MV, G	
Slave Province	3.96 T, G, A				3.1–2.9 G	2.8 FV	2.72–2.66 MV, IV, FV 2.65–2.6 G	
Labrador	3.9–3.85 ZX 3.8–3.75MV 3.73 T	3.62 m,G	3.4–3.2 D	3.235 G		3.0–2.8 MV 2.76–2.71 m		2.56 G 2.52 G
Greenland	3.82–3.805 MV, FV 3.75-3.7T	3.6–3.55 m	3.4 D		3.07–2.9 T	2.8 m	2.65 G, m, D	2.5 G
Baltic Shield						2.84 m 2.79 MV, B 2.74–2.7 T 2.75–2.73 G, FV		2.44 B 2.4-2.3 D 2.2-2.0 D 2.4-2.0 R, MV
Aldan, Siberia					3.0–2.86 MV, T		2.785 T 2.78–2.75 G, m	
Yilgarn Block								
1. Mt Narryer	<4.27 ZX 3.73 T,B	3.68–3.6G	3.4 G	3.3 G, m			2.78–2.75 G, B	
2. Murchison			3.49–3.44 G		3.0 MV, FV	2.9 G	2.8 MV, FV 2.7 G 2.63 G	
3. Kalgoorlie		3.45–3.0 ZX 2.85–2.75ZX				2.9 FV	2.7–2.69 MV, FV, T, G 2.68–2.61 G	2.42 D 2.37 D
Pilbara		3.72 ZX 3.57 O	3.47–3.45 MV, FV, T 3.49–3.42 G, m	3.3–3.32 T, FV	3.0 FV, MV, m	2.92–2.86 B 2.85–2.83 G	2.77–2.68 MV, FV, D	2.47 IV
North/central Australia								2.4 G
Kaapvaal Craton		3.64–3.55 T	3.5–3.47 MV, FV, T	3.35–3.1 T, G	3.07–2.94 MV, FV, B, G	2.96–2.84 MV; 2.87 B	2.72–2.64 MV	
Limpopo belt				3.29–3.2N	3.1–2.8MV, B 3.06–2.95 D	2.7–2.65 G, m	2.6–2.57 G	2.45 G
Zimbabwe craton	3.8–3.75 ZX		>3.5 MV 3.5 T	3.35 T	2.9 MV, FV 2.93–2.87 T	2.87 m 2.78 m	3.0–2.8 MV 2.76–2.64 MV, FV 2.9–2.6 G	2.51 FV 2.46 D
Dharwar Craton, south India				3.36–3.31 T	3.1–3.0 G, T		2.67 MV, FV 2.6 G 2.57 FV	

B. 2.2-0.6 Ga

Superior Province and circum-Superior belts	2.22 B	2.025–1.92 R, MV	1.89–1.83 MV, IV, FV, N, T, G, m	1.76 FV, G	1.5–1.45 O, RG, CH	1.11–1.086 MV, IV, FV, B	0.74–0.6 R, D, MV, G, m
Minnesota River Valley	2.12 D		1.8 G, D				
Continental USA			1.80–1.68 G, m		1.5–1.43 R, B, G, m 1.4–1.36 G, m	1.2 G, m	0.74–0.6 R, MV, B, G, m
Keewatin, Northwest Territories			1.85–1.76 R, MV				
Wopmay/Coronation Province	2.0–1.9 R	1.97 R	1.88–1.84 G 1.8 C				
Labrador	2.2–2.0 MV, D		1.86 R, MV 1.8 G, m			1.267 D	
Greenland	2.1 D		1.86 R 1.8 G, m	1.64 D 1.56 D	1.45 D	1.3–1.1 D	
Scotland	2.15–1.95 R		1.8–1.6 G, m				0.6 R, G, m
Baltic	2.05 MV 2.0–1.9 R, MV, m	1.95–1.9G 1.9C	1.9–1.8 G	1.7–1.6G		1.2 R 1.1–1.05 G, m	0.6 R, G, m
Aldan, Siberia		1.95–1.9 G, m					
Gascoyne belt, Western Australia	2.1–2.0 R, MV	2.0–1.7 R	1.8–1.6 G				
Northern, northwestern, and central Australia	2.0–1.88 R 2.0–1.9 B		1.87–1.84 G, FV, R 1.81–1.79 MV 1.78 FV 1.8–1.85B 1.80–1.82 G; 1.745 G	1.67G FV 1.69 D	1.56–1.48 G, FV, IV, MV	1.3 B 1.2–1.85 B, G 1.1–1.05 D, MV, FV, G	0.6R
Southern Africa	2.0–1.8 D		1.77–1.75 R, MV 1.75–1.70 R			1.3–1.25 R, G, m 1.0–0.8 R	0.66–0.55 G, m 0.6 R, G, m

The ca 2.2–2.0-Ga onset of a global network of ensialic (subsequently collisional) rift belts (Wopmay–Thelon, Kola–Karelia, north/central Australia) and continental-margin (subsequently accretionary) troughs (Penokean, Svecofennian, Ketilidean, Birimian; Windley 1977; J.C. Green 1993) may be interpreted as major shock-induced rifting and continental splitting triggered by the Bushveld event. The volcanic and plutonic activity that produced the Birimian granite–greenstone terrane of western Africa (Liegeois et al. 1991; Sylvester & Attoh 1992) is dated as ca 2.1–2.07 Ga, within error of the Rb–Sr age of the Bushveld Complex. The APWP migration rates were very high (13 cm y^{-1}) during 2.1–1.95 Ga.

ca 1.9–1.8-Ga Hudsonian mobile belts

The Sudbury impact structure (D_c = 200 km; Dietz 1964) and the possibly near-contemporaneous ca 1.8-Ga Uppland structure, central Sweden (D_c = 320 km; Lilljequist & Henkel 1991; Henkel & Lilljequist 1992) might have been important factors in relation to the peak ca 1.9–1.8-Ga Penokean, Hudsonian, Wopmay, Svecofennian, Ketilidean, north/central Australian, and Birimian plutonic/thrusting episodes. These include extensive mafic magmatism — e.g., the Lamboo Complex, eastern Kimberley province, Western Australia; in the Mount Isa province, northwest Queensland; and in circum-Superior greenstone belts (cf. Flin Flon and northwest Labrador trough). Two suggested Proterozoic impact structures in Finland (Nunjes, D_c = 200 km; Unari, D_c = 250 km; Henkel & Pesonen 1992) might belong to the same cluster. However, APWP migration rates were low (4 cm y^{-1}) during this period.

ca 1.3–1.05-Ga Grenville rifting and mobile belts

Impact structures of ca 1.2 Ga suggested in Sweden on the basis of geophysical evidence and breccia occurrence (S. Bjorkfjarden, Landsortsdjupet; Henkel & Pesonen 1992; Table 2) might offer clues to a bombardment period which triggered rifting and mafic plutonic and dyke emplacements — e.g., Keweenawan mid-continental rifting and mafic igneous activity (1.14 Ga; Krogh et al. 1987); ca 1.2-Ga McKenzie dyke swarm, covering ca 2.7 × 10^6 km^2 in the Slave, Superior, and Churchill provinces (Fahrig 1987); and the ca 1.3–1.05 Ga Grenville system, including the Albany/Fraser–Musgrave mobile belts (e.g., the mafic–ultramafic Giles Complex [Glikson et al. 1995], dated as 1.08 Ga [S.S. Sun, AGSO, personal communication 1995]; Fraser mafic igneous complex, ca 1.3 Ga; and the 1.3–1.1-Ga Sveconorvegian and Namaqualand–Natal-rift mobile belts). The period 1.2–1.1 Ga overlaps an APWP loop with high mean migration rates of 6–7 cm y^{-1} (Table 2).

ca 0.7–0.5-Ga Iapetus Ocean opening and igneous activity

The Vendian–Early Cambrian global rifting, continental splitting, opening of the Iapetus Ocean represented by the Appalachian–Caledonian sutures, and associated mafic and alkaline igneous activity (Franklin igneous province, 675–625 Ma; Doig 1970) could have been genetically linked to clustered impacts represented by:

- the ca 0.7-Ga Janisjarvi structure (D_c = 14 km), Karelia (Grieve & Pesonen 1992);

- the ca 0.59-Ga Acraman structure (D_c = 35 km) and related Bunyeroo ejecta, South Australia (Gostin et al. 1992; Wallace et al. this issue; Williams et al. this issue); and
- the ca 0.6-Ga Beaverhead structure (D_c = 60 km), USA (Grieve & Pesonen 1992).

Several Precambrian impact structures with poor age constraints (e.g., Kelly West, Northern Territory, D_c <20 km; Spider, Western Australia, D_c <13 km; Lawn Hill, Queensland, D_c = 20 km) could belong to the Late Proterozoic–earliest Cambrian bombardment period, as some of them are buried by Cambrian limestones. The period 590–550 Ma is characterised by extremely high APWP migration rates of 20 cm y^{-1}. The major thrusting and formation of thrust-bounded basins in central Australia ca 600 Ma (Petermann Ranges Orogeny) might have been related to north–south compression induced by these plate movements.

Many or all the aforementioned igneous and tectonic phenomena could be of purely endogenic origin. Whether some of them were triggered by mega-impacts, however, remains one of the most challenging questions in Earth science.

Periodicity of Precambrian episodes

Proposed correlations between impacts and mass extinctions (Alvarez et al. 1980; Alvarez 1986; Raup & Sepkosky 1984), continental volcanic events (Rampino & Stothers 1984; Alt et al. 1988; Stothers & Rampino 1990; Stothers 1993a, b), high ocean-ridge-spreading rates, tectonic activity peaks, high eustatic levels, and sedimentary facies (Stothers 1992; Rampino & Caldeira 1993; Rampino 1993) for the Mesozoic–Cainozoic have been interpreted in terms of a periodic cycle in the ranges of 24–35 Ma (Rampino & Stothers 1984) and 26–27 Ma (Rampino & Caldeira 1993). A 33-Ma period accords with the solar system's vertical oscillation across the galactic plane (Bahcall & Bahcall 1985), reflecting periodic gravitational perturbations of the Oort comet cloud as the solar system passes through dense gas clouds of the Galaxy (Rampino & Stothers 1984).

Longer periodicities are suggested by isotopic-age histograms (Gastil 1960; Sutton 1963; Stockwell 1968; Dearnley 1966; Fitch et al. 1974; Moorbath 1977) and by the ages of alkaline igneous events (Rampino & Stothers 1984). Age periodicities on a timescale of 350–500 Ma have been suggested on the basis of broad Rb–Sr, K–Ar, and U–Th–Pb age maxima of early Archaean (3.8–3.5 Ga), middle Archaean (3.2–3.1 Ga), Superior (2.8–2.5 Ga), Churchill (2.0–1.6 Ga), Grenville (1.3–0.9 Ga), and Phanerozoic (0.54–0 Ga) intervals. Although these age ranges are now resolved into a large number of precisely dated events, the possibility of a low-frequency episodicity remains. The 350–500-Ma age periodicities have a similar order of magnitude to the geomagnetic-variation cycle of 250 ± 50 Ma (Negi & Tiwari 1983), which is of a similar order to the galactic rotation period (Stothers 1992). The mean interval between Precambrian impact episodes (both observed and inferred; Table 1; Figs. 4 and 5) at ca 3.47, 3.2, 3.0, 2.7, 2.45, 2.05, 1.8, 1.5, 1.2, and 0.7 Ga is 303 ± 65 Ma. This is of a similar order to the periodicity of Middle to Upper Proterozoic carbonatite intrusions

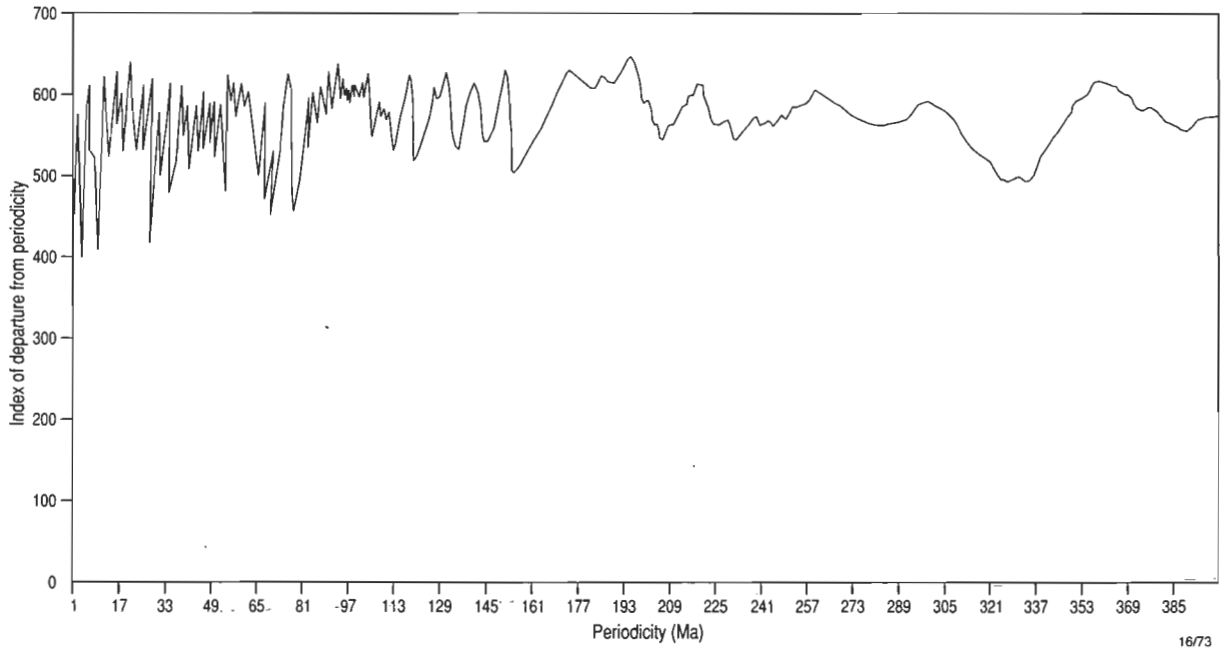

Figure 6. Plots of departures from perfect periodicity (Dmin = 0) values (y-axis) against a range of periodicity values (x-axis) according to a moving-windows/least-departure method (Appendix I) for selected isotopic ages derived from Precambrian ensialic mafic and intermediate igneous activity in Canada, Australia, and South Africa: 3153 ± 47 Ma (Rb–Sr isochron; Messina layered intrusion, Limpopo); 3005 ± 61 Ma (Rb–Sr isochron; Stockford dykes, Limpopo); 2925 ± 16 Ma (U–Pb zircon; Munni Munni layered intrusion, Pilbara); 2860 ± 20 Ma (Pb–Pb isochron; Millindina dykes, Pilbara); 2775 ± 10 Ma (U–Pb zircon; Mount Roe Basalt, Pilbara); 2721 ± 18 Ma (U–Pb zircon; Ventersdorp basalts, Transvaal); 2702 ± 4 Ma (base of Kambalda komatiites, Yilgarn); 2514 ± 16 Ma (Great Dyke, Zimbabwe); 2452 ± 3 Ma (U–Pb baddeleyite; Matachewan dykes, Superior); 2370 ± 30 Ma (Rb–Sr isochron; Widgiemooltha dyke, Yilgarn); 2219 ± 3.6 Ma (U–Pb baddeleyite; Nipissing diabase, Superior); 1884 ± 2 Ma (U-Pb zircon; Cross Lake dyke, Manitoba); 1850 ± 3 Ma (U–Pb zircon; Sudbury granophyre, Superior); 1790 ± 9 Ma (U–Pb zircon; mafic volcanics, Mount Isa–Cloncurry); 1740 ± 24 Ma (U–Pb zircon; gabbro, Mount Isa–Cloncurry); 1530 ± 20 Ma (Gawler volcanics, South Australia); 1267 ± 2 Ma (U–Pb baddeleyite; Mackenzie dykes, Churchill); 1238 ± 4 Ma (U–Pb zircon; Sudbury dykes, Superior) ; 1078 ± 3 Ma (U–Pb zircon; Giles Complex, Musgrave); 1141 ± 2 Ma (U–Pb baddeleyite; Abitibi dykes, Superior); 1109 ± 3 Ma (U–Pb baddeleyite; Logan sill, Superior); 1060 Ma (U–Pb zircon; Tollu volcanics, Musgrave).

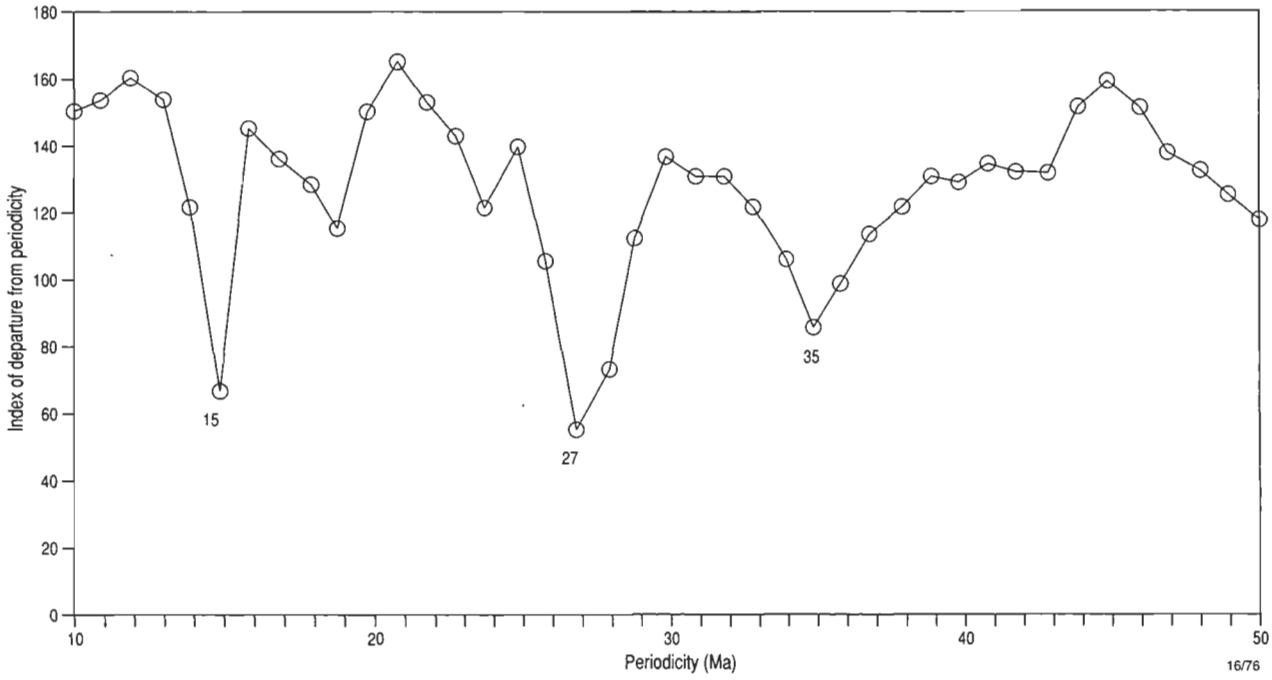

Figure 7. Plots of departures from perfect periodicity (Dmin = 0) values (y-axis) against a range of periodicity values (x-axis) according to a moving-windows/least-departure method (Appendix I) for selected isotopic ages derived from Precambrian least-deformed orthogneisses in southwest Greenland (Nutman et al. 1993): 3870 Ma, 3820–3810 Ma, 3760 Ma, 3730 Ma, 3700 Ma, 3660–3650 Ma, and 3625 Ma (errors mostly <<10 Ma).

(280 Ma; N = 21; Rampino & Stothers 1984), Phanerozoic kimberlite and lamprophyre intrusions (280 Ma; N = 38), carbonatite intrusions (235 Ma; N = 28), geomagnetic reversals (285 Ma; N = 24; Negi & Tiwari 1983), and impact craters (260 Ma; N = 65), which are interpreted in terms of an overall periodicity of 260 ± 25 Ma (Rampino & Stothers 1984).

An attempt to detect potential periodicities must overcome the single greatest difficulty — namely, distinguishing semicontinuous intermittent events from peak-clustered events, which are likely to be in combination. Thus, preserved impacts may include both episodic and non-episodic occurrences that may not be distinguishable. An example is the periodicity of 30 Ma obtained for Phanerozoic impact structures >10 km in diameter; this periodicity is not apparent when craters >5 km in diameter are considered (Grieve et al. 1988). This question can be resolved only by time-series analyses of comprehensive data sets containing precise isotopic-age data.

The detection of hidden or quasiperiodic events in geological data sets needs to take the following criteria into account:

- the incompleteness of isotopic-age data sets owing to limits associated with sampling and dating biases. Ideally, widely distributed formations are preferable to units that may represent purely local events. Major mantle-melting events may have been of shield-wide to global extent. Initially, it is preferable to analyse time series for individual terranes, and this should be followed by studies of units on a continental or global scale;
- the significance of the different isotopic-age methods, and the magnitude of dating errors, which should not exceed the trial period applied to those data. For example, testing of Rb–Sr isochron ages with errors of ± 30 Ma against a trial period of 10 Ma must yield uncertain results, whereas testing U–Pb baddeleyite ages of dykes with errors <5 Ma against such a trial period would be more fruitful; and
- the need to specify the type and extent of geological units analysed. The selection of isotopic-age data sets should take into account factors such as the petrological and geochemical nature of the dated materials (to avoid comparisons between rock units of different origin); the type of event reflected by the isotopic age (whether relict xenocrystal, precursor, magmatic, metamorphic, diagenetic or cooling/uplift); and the locations of sampled units (the rationale for including local, regional, shield-wide, or global data in any single trial data set).

The geological record suggests that, in general, certain units represent continuous or near-continuous to intermittent events, whereas other events are more distinctly episodic. The first type is represented, for example, by ophiolites and by some granite series signifying ongoing accretion–subduction processes. Intermittent events are represented by continental volcanism, related dyke intrusion, and alkaline igneous activity. Attempts at time-series analysis should focus on the intermittent events, although the first type must not be neglected.

Overlapping age determinations of specific events should be resolved either by averaging age groups pertaining to the same event or by choosing the most precise age. For long-acting processes spanning extended intervals, the oldest or initiation age has been selected here.

Several methods can be applied for detecting hidden periodicities in sequential incomplete time series. They include:

- linear and circular digital spectral analysis of serial data (Stothers 1991);
- a moving-windows analysis smoothing data-distribution patterns in terms of varying bin sizes and chosen increments (Rampino & Caldeira 1993);

- Gaussian filtering of high-frequency noise (Rampino & Caldeira 1993); and
- fast Fourier transform (Rampino & Caldeira 1993; Raup & Sepkosky 1984).

The results of a preliminary time-series analysis according to the moving-windows/least-departure time series (Appendix I) are shown in Figures 6 and 7. This method was tested on trial data sets containing one or more introduced periodicities. The results indicate a first approximation of the order of magnitude of the periodicities of the data sets, and agree with those obtained by Stothers's linear spectral analysis method (Stothers 1991) and J. Wood's (CSIRO, personal communication 1995) circular spectral analysis method.

A data set of 22 isotopic ages (whose errors range from ±2 to ±61 and reflect a mean error of 14 Ma) includes mafic intrusions emplaced in continental crust of the Laurentian shield, Pilbara and Yilgarn Cratons (Western Australia), and Kaapvaal Craton (South Africa). The results (Fig. 6) outline periodicities at 30, 10, and 5 Ma, of which the last two probably represent spurious fractional intervals.

Nutman et al. (1993) reported a sequence of episodic granitic events in the Amitsoq Gneiss, southwest Greenland, from which the least deformed tonalitic and granitic gneisses yield precise (error <<10 Ma) U–Pb zircon ion-probe primary igneous ages representing seven distinct magmatic episodes. Time-series analysis of the data yield possible periodicities at 35, 27, and 15 Ma, the middle one being the best defined (Fig. 7).

These results *tentatively* suggest that periodicities in the order of 30 ± 5 Ma may be detectable in the Precambrian record. With colleagues C. Tarlowski and J. Wood, I am currently applying numerous data sets, and several time-series analysis methods suggested by R.B. Stothers, to test these periodicities.

Conclusions

Precambrian models that hinge exclusively on mantle dynamics overlook the predicted effects of extraterrestrial impacts, and have not to date been able to explain the origin of mafic igneous/rifting episodicity. In principle, the deep-crustal and lithospheric faulting triggered by high-velocity impact of large projectiles (Jones 1987), releasing energy in the order of $>>10^9$ Mt (Grieve & Pesonen 1992), is capable of inducing:

- asthenospheric updoming, partial melting, and diapiric activity;
- continental mafic dyke swarms, and plutonic and volcanic activity, including maria-type extrusions (Green 1972, 1981; Glikson 1976, 1993);
- intracontinental rifting and the inception of oceanic spreading;
- accelerated plate movement; and
- consequent compression and thrusting in pre-impact rifts and mobile zones, which in turn can result in orogenic activity.

Although this model remains unproven, it is nevertheless consistent with the bulk of the evidence observed in the Precambrian record, considering that:

- signatures of small to moderate-size impacts are prone to destruction by uplift, erosion, subduction, deformation, and partial melting processes; and
- for large impacts, the thermal and anatectic consequences conceal and overprint mechanical impact signatures by (i) volcanic flooding of impact aureoles, (ii) isostatic subsidence of impacted crust into infracrustal levels, and (iii) the penetrative deformation, recrystallisation, and anatexis of the impacted crust; least-deformed relics may be represented by agmatite structures in Precambrian gneiss complexes.

Owing to the scarce record of Precambrian impacts, the theory outlined in this paper requires testing by means of the following methods:

- a search for further proximal impact clues (breccias, shatter cones, pseudotachylite veins, pseudomorphic vitrification, shock lamellae in quartz and zircon, and high-pressure polymorphs);
- a search for further distal impact clues (microtektite/spherule-condensate units, diamictites, slumping and turbidity current features, and geochemical anomalies including platinum group elements);
- precise isotopic-age determinations of proximal melting effects and of distal microtektite/spherule condensates;
- precise isotopic-age determinations of igneous units and tectonic events potentially correlated with impact events; and
- statistical analysis of the age distribution and possible periodicities of impact events and of igneous, tectonic, sedimentary, and climatic episodes.

The Precambrian impact theory predicts that distal impact-related diamictites, spherule beds, and iridium anomalies will be found in Precambrian stratigraphic records corresponding to identified proximal impact effects. It further predicts that similar evidence will be found in relation to the 3.0–2.9, 2.75–2.65, and 1.5 Ga mafic igneous/rifting events for which no impact connections are known at present. As is the fate of any hypothesis, this model will stand or fall depending on the confirmation of these and other predictions.

Acknowledgments

I am indebted to the late Robert S. Dietz for encouraging me in connection with the concepts presented in this paper. I thank the following people for discussion, correspondence and/or provision of published material: B.M. French, R.A.F. Grieve, C. Koeberl, R. Lilljequist, H.J. Melosh, V.R. Oberbeck, J.D.A. Piper, M.R. Rampino, E.M. Shoemaker, C.S. Shoemaker, B.M. Simonson, and R.B. Stothers. I thank J. Giddings for assistance with the world palaeomagnetic database. I am grateful to R.B. Stothers for kindly providing me with a copy of his spectral time-series program, to C. Tarlowski for writing a Fortran program of a moving-windows periodicity program, and to J. Wood for designing a circular-function time-series program. I thank A.W.R. Bevan, D.M. Hoatson, J.F. Lindsay, J.W. Sheraton, and A.J. Stewart for their comments on this paper.

Table 2. Impact structures (mostly with D_c >10 km) listed in increasing age sequence, and data (*not necessarily genetically related*) from near-contemporaneous basic igneous events, tectonic events, and palaeomagnetic studies

Impact structures for which no age or age limits are known are not included. Principal references: J.C. Green (1993); Grieve (1982); Grieve & Pesonen (1992); Grieve & Pilkington (this issue); Hall & Fahrig (1987); Hall & Hughes (1990); Parker et al. (1990); Piper (1987); Shoemaker & Shoemaker (1988, this issue); Stothers (1993a, b); Von Gruenewaldt & Harmer (1993); Windley (1993).

Impact structure and locality	*Diameter (km)*	*Age of impact signature; stratigraphic boundary*	*Possibly temporally correlated basic igneous activity*	*Broadly near-contemporaneous tectonism and palaeomagnetic signatures*
Bosumtwi, Ghana	10.5	0.3 ± 0.02 Ma; Piacenzian–Calabrian boundary (1.67–1.60 Ma)		
Zamanshin, Russia	13.5	0.9 ± 0.1 Ma		
Elgygytgyn Chukotsk, Russia	19	3.5 ± 0.5 Ma; Zanclean–Piacenzian boundary		
Karla, Russia	10	10 Ma		
Ries, Germany	24	15.1 ± 1 Ma; Langhian–Serravallian boundary	Columbia Plateau Basalts (16 ± 1 Ma)	Red Sea opening — lineament no. 5c: 17 Ma
Haughton, NWT, Canada	24	23.4 ± 1.0 Ma; Chattian–Aquitanian boundary (24–23 Ma)		
Popigai, Siberia	100	35 ± 5 Ma	Ethiopian basalts (36.9 ± 0.9 Ma)	
Chesapeake Bay, USA	85	35.5 ± 0.6 Ma		
Mistastin, Labrador	28	38 ± 4 Ma		40 Ma — rise in Pacific Ocean-floor-spreading (OFS) rate to 5 cm y^{-1}
Montagnais, Canada	45	50.5 ± 0.8 Ma; Ypresian–Lutetian boundary (52–50 Ma)		Kola Peninsula/Scandinavia split of the Arctic ocean — lineament no. 24: 55 Ma
Connolly, Canning Basin, WA, Australia	9	<60 Ma		
Kamensk, Russia	25	65 Ma		
Chicxulub, Yucatan, Mexico	180–220	64.98 ± 0.05 Ma	Deccan basalts and dykes (65.5 ± 2.5 Ma); SW India dykes (61 ± 9 Ma); Greenland (Peary Lake) dykes (~ 65 Ma)	Indian peninsula split — lineament no. 27: 63 Ma
Manson, Iowa	35			
Ust Kara, Russia	>70	73 ± 3 Ma		
Kara, Russia	65	73 ± 3 Ma		Greenland–Labrador split — lineament no. 33: 74 Ma
Lappajarvi, Finland	23	77.3 ± 0.4 Ma		
Boltysh, Ukraine	24	88.3 Ma		
Dellen, Sweden	8	89 ± 2.7 Ma		Australia–Antarctica split — 85 Ma
Yallalie Basin, Western Australia	13	~90 Ma		
Steen Lake, Alberta	25	95 ± 7 Ma	Madagascar basalts (94.5 ± 1.2 Ma)	
Avak, USA	12	>95 Ma		
Sierra Madera, Texas	13	100 Ma		
Logoisk, BSSR, Russia	17	100 ± 20 Ma		
Deep Bay Saskatchewan	12	100 ± 50 Ma		
Boltysh, Ukraine	25	100 ± 5 Ma		

Table 2 *(continued)*

Impact structure and locality	*Diameter (km)*	*Age of impact signature; stratigraphic boundary*	*Possibly temporally correlated basic igneous activity*	*Broadly near-contemporaneous tectonism and palaeomagnetic signatures*
Carswell, Canada	39	115 ± 10 Ma	Rajmahal basalts (117 ± 1 Ma)	110 Ma — sharp jumps in Pacific (to 7 cm y^{-1}) and Atlantic (to 2.5 cm y^{-1}) OFS rates
Oasis, Libya	11.5	<120 Ma		
Mien, Sweden	7	120 Ma		
Tookoonooka, Queensland (buried structure)	55	128 ± 5 Ma		
Talundilli, Queensland (buried structure)	30	128 ± 5Ma		
Gosses Bluff, NT, Australia	24	142.5 ± 0.8M (J/C boundary)	dykes, SW India (144 ± 6 Ma); ?Serra Geral (132 ± 1 Ma).	northwest Africa/North America split (lineament M25 — 157 Ma); southern Africa split (lineament M11 — 133 Ma)
Mjolnir, Norway	40	143 ± 20 Ma		
Rochechouart France	23	160 ± 5 Ma		oldest Pacific Ocean crust (lineament M38 — 169 Ma); high Pacific Ocean spreading rate (4 cm y^{-1}; 165 Ma); oldest Atlantic Ocean crust (157 Ma)
Obolon, Ukraine	15	160 Ma	Antarctic Ferrar basalts (176 ± 1 Ma)	
Redwing Creek, Dakota	9	200 ± 25 Ma		
Wells Creek, Tennessee	14	200 ± 100 Ma		
Puchezh-Katunki, Russia	80	220 ± 10 Ma (Late Triassic)	Karoo volcanics and dykes (190 ± 5 Ma); Antarctic dykes (192 ± 8 Ma); Messina dykes (184 Ma); Greenland TD swarm (225–116 Ma); Newark basalts (201 ± 1 Ma); tholeiitic basalts, west Africa (203.7 ± 1.7 Ma); Wrangellia flood basalt (Ladinian–Carnian boundary; ~230 Ma)	
Manicouagan, Quebec	100	212 ± 2 Ma		
Saint Martin, Manitoba	40	220 ± 32 Ma		
Araguainha Dome, Brazil	40	<250 Ma (P/T boundary)	Siberian traps (248.4 ± 2.4 Ma)	high OFS rates ~200–240 Ma (6 cm y^{-1})
Clearwater twin craters, Quebec	22, 32	290 ± 20 Ma		
Serra da Canghala, Brazil	12	<300 Ma		
Kentland, Indiana	13	300 Ma		
Slate Islands, Ontario	30	<350 Ma		
Charlevoix, Quebec	54	357 ± 15 Ma		
Kaluga, RSFSR, Russia	15	360 ± 10 Ma		
Siljan, Sweden	53	368 ± 1.1 Ma		
Couture, Canada	8	430 ± 25 Ma		
Nicholson Lake, NWT	12.5	<450 Ma		high seafloor-spreading rates during 450–400 Ma (18 cm y^{-1})
Brent, Canada	3	450 ± 3 Ma		
Ames, Oklahoma	16	470 ± 30 Ma		
Lockne, Sweden	7	455 Ma		
Presqu'Ile, Canada	12	<500 Ma		

Table 2 *(continued)*

Impact structure and locality	*Diameter (km)*	*Age of impact signature; stratigraphic boundary*	*Possibly temporally correlated basic igneous activity*	*Broadly near-contemporaneous tectonism and palaeomagnetic signatures*
Gardnos, Norway	5	500 ± 10 Ma		
Saaksjarvi, Finland	6	560 Ma		
Misarai, Lithuania	3	570 ± 50 Ma		
Strangways, NT, Australia	24	<600 Ma		
Beaverhead, USA	60	~600 Ma		
Acraman and contemporaneous ejecta in Bunyeroo Formation, South Australia	35	~590 Ma	Antrim Plateau Basalt; Franklin igneous province (675–625 Ma); south Siberia; Pakistan; Morocco; NW Argentina; British Columbia; late Vendian dolerites along the Scandinavian Caledonides; extensive alkaline magmatism (St Lawrence graben, Labrador, Greenland, Scandinavia, southern rifted margins of Siberia, NE Africa, Iran, Turkey)	Initiation of global rift systems — 625>575 Ma (Yukon, N British Columbia, Alberta, Utah, NW Virginia, SW Virginia, SW Newfoundland, SE Turkey, N. Australia, NW Argentina); extensive rifting; tillites; divergence of APWP indicating continental break-up; high seafloor-spreading rates during 590–550 Ma (20 cm y^{-1})
Lawn Hill, NW Qld	20	600<1670 Ma		
Janisjarvi, Karelia	14	698 ± 22 Ma		
Kelly West, NT, Australia	10–20	Late Proterozoic		
Spider, WA	10–13	>700 Ma		
Strangways, NT, Australia	26–40	~1000 Ma		APWP loop 8 (1.0–0.8Ga)
S. Bjorkfjarden Landsortsdjupet, Sweden	9 30	~1210 Ma ~1200 Ma	1.3–1.1Ga: anorthosites, layered mafic–ultramafic intrusions, rapakivi granites	Grenville (1.3–1.1 Ga), Keweenawan (1.14 Ga); Sveconorvegian (1.09–0.95 Ga); Musgrave–Fraser–Albany (1.3–1.05 Ga); Namaqualand–Natal (1.35–1.0 Ga); 1.1–1.15Ga — high APWP rate (6–7 cm y^{-1}); APWP loop 7 (1.2–1.1 Ga)
Goyder, NT, Australia	7–25	<1400 Ma		
Teague, WA	30	~1600 Ma		APWP loop 6 (1.6–1.4 Ga) APWP loop 5 (1.7–1.6 Ga)
Uppland structure, central Sweden: concentric geological formations, central tonalite, annular breccia troughs, geophysical signature, suspected impact melts	~320	~1800 Ma		continental-margin subduction and ensialic mobile belts: 1.86–1.82 Ga (Penokean); 1.8–1.7 Ga (Hudsonian); 1.72–1.65 Ga (SW USA); 1.8–1.65 Ga (Ketilidian); 1.9–1.6 Ga (Kimberley, Mount Isa–Broken Hill, Arunta, Patterson, Gascoyne). 1.75–1.8 Ga — high APWP rate (12 cm y^{-1}); APWP loop 4 (1.85–1.7 Ga)
Sudbury, Ontario	200	1850 ± 3 Ma		concomitant with the Penokean orogeny (>1.85–1.75 Ga) and parallel events in circum-Superior, Baltic, and Australian shields

Table 2 *(continued)*

Impact structure and locality	*Diameter (km)*	*Age of impact signature; stratigraphic boundary*	*Possibly temporally correlated basic igneous activity*	*Broadly near-contemporaneous tectonism and palaeomagnetic signatures*
Vredefort, Transvaal	140	2016 ± 10 Ma	Kimberley dykes (1.91 ± 0.06 Ga); N Transvaal dykes (~1.9 Ga)	low APWP migration rate (4 cm y^{-1})
Bushveld structure, Transvaal	65 000 km^2	2061 ± 27 Ma	?Palabora intrusive suite (2.06 ± 0.1 Ga); Kapuskasing dyke swarm (2043 ± 14 Ma); Greenland BN and MD dykes (~2.1 Ga, 2.15 Ga; Scotland Loch Maree Group (ca 2.0 Ga); Wyoming dykes	2.1 — high APWP migration rate (13 cm y^{-1}); APWP loop 3 (2.1–1.95Ga)
				APWP loop 2 (2.35–2.20 Ga)
Dales Gorge Member (Brockman Iron Formation) spherule bed, Hamersley Basin, WA		>2470 Ma		
Wittenoom Formation and Carawine Dolomite spherule bed and diamictite (sanidine quench textures), Hamersley Basin, WA		>2470 Ma<2640 Ma	Matachewan dyke swarm (2452 ± 3 Ma); Zimbabwe Great Dyke and satellites (2461 ± 16 Ma); Yilgarn YA and YE dykes and Ravensthorpe dykes (~2.45 Ga); Jimberlana dyke (2.41 Ga); Vestfold Hills dykes (2424 ± 72 Ma); Georgetown Coboid dolerite (<2.49 Ga); Scourie dykes, Scotland (2.42 Ga); Tornio layered intrusion, Finland (2.44 Ga); Wyoming dykes (2.55 Ga)	2.4 Ga — very high APWP migration rate (15 cm y^{-1}); 2.55 Ga — high APWP rate (8 cm y^{-1}). APWP loop 1 (2.55–2.35 Ga)
			~2.7 ± 0.05 Ga major mafic–ultramafic volcanism: Superior Province, Yilgarn, Pilbara (Fortescue Group), Zimbabwe (Bulawayan), Transvaal (Ventersdorp Group)	2.7 Ga — high APWP rates (6 cm y^{-1})
basal Fig Tree Group, Transvaal: 3 spherule units (S1, S2, S3)		~3200 Ma	Messina layered intrusion (3153 ± 47 Ma)	
Warrawoona Group spherule bed, Pilbara Block, WA		~3450 Ma	upper Warrawoona Group basic volcanism (3454 ± 1 Ma)	extensive submarine volcanism
Hooggenoeg Formation spherule bed, Transvaal		~3450 Ma	upper Onverwacht Group basic volcanism (3445 ± 8 Ma)	extensive submarine volcanism

References

Alt, A.D., Sears, J.W. & Hyndman, D.W., 1988. Terrestrial maria: The origins of large basalt plateaus, hotspot tracks and spreading ridges. Journal of Geology, 96, 647–662.

Alvarez, W., 1986. Toward a theory of impact crises. Eos, 67, 649–658,

Alvarez, L.W., Alvarez, W., Asaro, F. & Michel, H.V., 1980. Extraterrestrial cause for the Cretaceous–Tertiary extinction. Science, 208, 1095–1108.

Anderson, J.L., 1983. Proterozoic anorogenic granite plutonism of North America. Geological Society of America, Memoir 161, 133–154.

Anhaeusser, C.R., 1973. The evolution of the early Precambrian crust of southern Africa. Philosophical Transactions of the Royal Society of London, A273, 359–388.

Archibald, N.J. & Bettenay, L.F., 1977. Indirect evidence for a reactivation of a pre–greenstone sialic basement in Western Australia. Earth and Planetary Science Letters, 33, 370–378.

Avermann, M., Bischoff, L., Brockmeyer, P., Buhl, D., Deutsch, A., Dressler, B.O., Lakomy, R., Muller-Mohr, V. & Stoffler, D., 1992. Sudbury project: summary of results — an updated impact model. In: Sudbury, 1992. Lunar and Planetary Institute, Contribution 790, 5

Bahcall, J.N. & Bahcall, S., 1985. The sun's motion perpendicuar to the galactic plane. Nature, 316, 706–708.

Baldwin, R.B., 1985. Relative and absolute ages of individual craters and the rates of infalls on the Moon in the post-Imbrium period. Icarus, 61, 63–91.

Barringer, D.M., 1905. Coon Mountain and its crater. Proceedings of the Academy of Natural Sciences, Philadelphia, 57, 861–886.

Blake, T.S. & Groves, D.I., 1987. Continental rifting and the Archaean–Proterozoic transition. Geology, 15, 229–232.

Campbell, I.H. & Hill, R.I., 1988. A two-stage model for the formation of the granite–greenstone terranes of the Kalgoorlie–Norseman area, Western Australia. Earth and Planetary Science Letters, 90, 11–25.

Card, K.D., 1990. A review of the Superior Province of the Canadian Shield, a product of Archaean accretion. Precambrian Reserch, 48, 99–156.

Colliston, W.P. & Reimold, W.U., 1992. A structural review of the Vredefort dome. In: Sudbury, 1992. Lunar and Planetary Institute, Contribution 790, 16.

Condie, K.C. (editor), 1993a. Proterozoic crustal evolution. Developments in Precambrian Geology, 10, Elsevier, Amsterdam.

Condie, K.C., 1993b. Proterozoic terranes and continental accretion in southwestern North America. In: Condie, K.C. (editor), Proterozoic crustal evolution. Elsevier, Amsterdam, 447–480.

Crook, K.A. & Cook, P.J., 1966. Gosses Bluff — diapir, crypto-volcanic structure or astrobleme? Journal of the Geological Society of Australia, 13, 495–516.

Davies, G.F., 1996. Punctuated tectonic evolution of the Earth. Earth and Planetary Science Letters (in press).

Dearnley, R., 1966. Orogenic fold belts and a hypothesis of Earth evolution. In: Aherns, L., Press, F., Runcorn, S.K & Urey, H.C. (editors), Physics and chemistry of the Earth. Pergamon Press, Oxford, 1–114.

de Wit, M.J. & Hart, R.A., 1993. Earth's earliest continental lithosphere, hydrothermal flux and crustal recycling. Lithos, 30, 309–335.

Dietz, R.S., 1961a. Astroblemes. Scientific American, 295, 51–58.

Dietz, R.S., 1961b. Vredefort ring structure: meterorite impact scar? Journal of Geology, 69, 499–516.

Dietz, R.S., 1964. Sudbury structure as an astrobleme. Journal of Geology, 72, 412–434.

Doig, R., 1970. An alkaline igneous province linking Europe and North America. Canadian Journal of Earth Science, 7, 22–28.

Elston, W.E., 1992. Does the Bushveld–Vredefort system record the largest known terrestrial impact catastrophe? In: Sudbury, 1992. Lunar and Planetary Institution, Contribution 790, 23–24.

Engel, A.E.J., 1966. The Barberton Mountain Land: clues to the differentiation of the Earth. University of Witwatersrand, Johannesburg, Informmation Circular 27.

Fahrig, W.F., 1987. The tectonic setting of continental mafic dyke swarms: failed arm and early passive margin. Geological Association of Canada, Special Paper 34, 331–360.

Fitch, F.J., Forster, S.C. & Miller, J.A., 1974. Geological time scale. Report of Progress in Physics, 37, 1433–1496.

Folinsbee R.E., Baadsgaard, H., Cumming, G.L. & Green, D.C., 1968. A very ancient island arc. In: Knopoff et al. (editors), The crust and upper mantle of the Pacific island arcs. American Geophysical Union, Monograph 12, 441–448.

French, B.M., 1972. Shock metamorphic features of the Sudbury structure, Ontario: a review. In: New developments in Sudbury geology. Geological Association of Canada, Special Paper 10, 19–28.

French, B.M., 1990. Absence of shock metamorphic effects in the Bushveld Complex, South Africa: results of an intensive search. Tectonophysics, 171, 287–301.

French, B.M. & Twist, D., 1983. Status of the Rooiberg felsite in the Bushveld Complex: a review. Report of the Institute of Geological Research, University of Pretoria, 39.

Gastil, G., 1960. Distribution of mineral dates in time and space. American Journal of Science, 258, 1–35.

Glikson, A.Y., 1969. The outer rim of the Gosses Bluff cryptoexplosion structure, N.T. Bureau of Mineral Resources, Australia, Record 1969/42.

Glikson, A.Y., 1972. Early Precambrian evidence of a primiive ocean crust and island nuclei of sodic granite. Geological Society of America, Bulletin 83, 3323–3344.

Glikson, A.Y., 1976. Earliest Precambrian mafic/ultramafic volcanic rocks: ancient oceanic crust or relic terrestrial maria? Geology, 4, 202–205.

Glikson, A.Y., 1983. Geochemical, isotopic and palaeomagnetic tests of early sial–sima patterns: the Precambrian crustal enigma revisited. Geological Society of America, Memoir 161, 95–118.

Glikson, A.Y., 1984. Significance of early Archaean mafic–ultramafic xenolith patterns. In: Kroner, A., Goodwin, A.M. & Hanson, G.N. (editors), Archaean geochemistry. Springer–Verlag, Berlin, 263–280.

Glikson, A.Y., 1993. Asteroids and early Precambrian crustal evolution. Earth Science Reviews, 35, 285–319.

Glikson, A.Y., Ballhaus, C.G., Clarke, J.L., Sheraton, J.W., Stewart, A.J. & Sun, S.S., 1995. Geological framework and crustal evolution of the Giles mafic–ultramafic complex and environs, western Musgrave Block, central Australia. AGSO Journal of Australian Geology & Geophysics, 16, 41–68.

Gostin, V.A., Keays, R.R. & Wallace, M.W., 1992. The Acraman impact and its widespread ejecta, South Australia. In: Sudbury, 1992. Lunar and Planetary Institute, Contribution 790, 30–31.

Green, D.H., 1972. Archaean greenstone belts may include equivalents of terrestrial maria? Earth and Planetary Science Letters, 15, 263–270.

Green, D.H., 1981. Petrogenesis of Archaean ultramafic magmas and implications for Archaean tectonics. In: Kroner, A. (editor), Precambrian plate tectonics. Developments in Precambrian Geology, 4, Elsevier, Amsterdam, 469–489.

Green, D.H., 1993. The mantle solidus for intraplate and passive margin volcanism and implications for mantle dynamics and mantle metasomatism. General Assembly of the International Association of Volcanology and Chemistry of the Earth's Interior, Canberra, Abstracts, 41.

Green, J.C., 1993. Proterzoic rifts. In: Condie, K.C. (editor), Proterozoic crustal evolution. Elsevier, Amsterdam, 97–149.

Grieve, R.A.F., 1980. Impact bombardment and its role in proto-continental growth of the early Earth. Precambrian Research, 10, 217–248.

Grieve, R.A.F, 1992. The record of impact on Earth: implications for a major Cretaceous/Tertiary impact event. Geological Society of America, Special Publication 190, 25–38.

Grieve, R.A.F. & Dence, M.R., 1979. The terrestrial cratering record: II. The crater production rate. Icarus, 38, 230–242.

Grieve, R.A.F. & Pesonen, L.J., 1992. The terrestrial impact cratering record. Tectonophysics, 216, 1–30.

Grieve, R.A.F., Sharpton, V.L., Rupert, J.D. & Goodacre, A.K., 1988. Detecting a periodic signal in the terrestrial cratering record. Proceedings of the Lunar and Planetary Science Conference, Houston, Texas, 18, 375–382.

Gurnis, M. & Davies, G.F., 1986. Apparent episodic crustal growth arising from a smoothly evolving mantle. Geology, 14, 396–399.

Hall, H.C. & Fahrig, W.F. (editors), 1987. Mafic dyke swarms. Geologicao Survey of Canada, Paper 34.

Hall, R.P. & Hughes, D.J. (editors), 1990. Early Precambrian basic magmatism. Blackie, Glasgow.

Hamilton, W., 1970. Bushveld Complex: product of impacts? Geological Society of South Africa, Special Paper 1, 367–374.

Henkel, H. & Lilljequist, R., 1992. Large impacts in the Baltic shield with special attention to the Uppland structure. In: Sudbury, 1992. Lunar and Planetary Institute, Contribution 790, 38–39.

Henkel, H. & Pesonen, L.J., 1992. Impact craters and craterform structures in Fennoscandia. Tectonophysics, 216, 31–40.

Hoffmann, P.F., 1989. Speculations on Laurentia's first gigayear (2.0–1.0 Ga). Geology, 17, 135–138.

Hoffmann, P.F. & Ranalli, G., 1988. Archaean ocean flake tectonics. Geophysical Research Letters, 15, 1077–1080.

Irving, E. & Park, J.K., 1972. Hairpins and superintervals. Canadian Journal of Earth Science, 9, 1318–1324.

Jakes, P.J. & White, A.J.R., 1971. Composition of island arcs and continental growth. Earth and Planetary Science Letters, 12, 224–230.

Jones, A.G., 1987. Are impact-generated lower crustal faults observable? Earth and Planetary Science Letters, 85, 248–252.

Koeberl, C., Reimold, W.U., & Boer, R.H., 1993. Geochemistry and mineralogy of early Archaean spherule beds, Barberton Mountain Land, South Africa: evidence for origin by impact doubtful. Earth and Planetary Science Letters, 119, 441–452.

Krogh, T.E., Corfu, F., Davies, D.W., Dunning, G.R., Heaman, L.M., Kamo, S.L., Machado, N., Greenbough, J.D. & Nakamura, E., 1987. Precise U–Pb isotopic ages of diabase dykes and mafic to ultramafic rocks using trace amounts of baddeleyite and zircon. In: Hall, H.C & Fahrig, W.F. (editors), Mafic dyke swarms. Geological Association of Canada, Special Paper 34, 147–152.

Kyte, F.T., Zhou, L. & Lowe, D.R., 1992. Noble metal abundances in an early Archaean impact deposit. Geochimica et Cosmochimica Acta, 56, 1365–1372.

Lambert, I.B. & Heier, K.S., 1968. Estimates of crustal abundances of thorium, uranium and potassium. Chemical Geology, 3, 235–238.

Liegeois, J.P., Claessens, W., Camara, D. & Klerkx, J., 1991. Short-lived Eburnian orogeny in southern Mali: geology, tectonics, U–Pb and Rb–Sr geochronology. Precambrian Research, 50, 111–136.

Lilljequist, R. & Henkel, H., 1991. Mass redistribution of rocks and elements resulting from a giant impact in central Sweden. 16th General Assembly of the European Geological Societies, Wiesbaden, Germany, Program and Abstracts, C56.

Lock, J. & McElhinny, M.W., 1991. The global palaeomagnetic database. Kluwer Acadmic Publishers, Dordrecht.

Loper, D.E. & McCartney, K., 1986. Mantle plumes and the episodicity of magnetic field reversals. Geophysical Research Letters, 13, 1525–1528.

Lowe, D.R. & Byerly, G.R., 1986. Early Archaean silicate spherule of probable impact origin, South Africa and Western Australia. Geology, 14, 83–86.

Lowe, D.R., Byerly, G.R., Asaro, F. & Kyte, F.J., 1989. Geological and geochemical record of 3400 million year old terrestrial meteorite impacts. Science, 245, 959–962.

Melosh, H.J., 1989. Impact cratering: a geological process. Oxford University Press, New York.

Milton, D.J., Glikson, A.Y. & Brett, P.R., 1996. Gosses Bluff — an end–Jurassic impact structure in central Australia. Part 1: geology. AGSO Journal of Australian Geology & Geophysics (this issue).

Moorbath, S., 1977. Ages, isotopes and evolution of the Precambrian crust. Chemical Geology, 20, 151–187.

Muir, T.L., 1984. The Sudbury structure: considerations and models for an endogenic origin. In: Pye, E.G., Naldrett, A.J. & Giblin, P.E. (editors), The geology and ore deposits of the Sudbury structure. Ontario Geological Survey, Special Publication 1, 449–490.

Negi, J.G. & Tiwari, R.K., 1983. Matching long term periodicities of geomagnetic reversals and galactic motions of the solar system. Geophysical Research Letters, 10, 713–716.

Nicolaysen, L. & Ferguson, J., 1990. Cryptoexplosion structures, shock deformation and siderophile concentrations related to explosive venting of fluids associated with alkaline ultramafic magmas. Tectonophysics, 171, 303–335.

Nutman, A.P., Friend,, C.R.L., Kinny, P.D. & McGregor, V.R., 1993. Anatomy of an Archaean gneiss complex: 3900 to 3600 Ma crustal evolution in southern west Greenland. Geology, 21, 415–418.

Parker, A.J., Rickwood, P.C. & Tucker, D.H. (editors), 1990. Mafic dykes and emplacement mechanisms. A.A. Balkema, Rotterdam.

Peredery, W.V. & Morrison, G.G., 1984. Discussion of the origin of the Sudbury structure. In: Pye, E.G., Naldrett, A.J. & Giblin, P.E. (editors), The geology and ore deposits of the Sudbury structure. Ontario Geological Survey, Special Publication 1, 491–512.

Pidgeon, R.T. & Wilde, S.A., 1990. The distribution of 3.0 Ga and 2.7 Ga volcanic episodes in the Yilgarn Craton of Western Australia. Precambrian Research, 48, 309–325.

Piper, J.D.A., 1987. Palaeomagnetism and the continental crust. Open University Press, Milton Keynes.

Rampino, M.R., 1993. Extraterrestrial forcing of intraplate volcanism? Correlation of flood basalts, large impacts and mass extinctions. General Assembly of the International Association of Volcanology and Chemistry of the Earth's Interior, Canberra, Abstracts; 88.

Rampino, M.R. & Caldeira, K., 1993. Major episodes of geologic change: correlation, time structure and possible causes. Earth and Planetary Science Letters, 114, 215–227.

Rampino, M.R. & Stothers, R.B., 1984. Geological rhythms and cometary impacts. Science, 226, 1427–1431.

Raup, D.M. & Sepkosky, J.J., 1984. Periodicity of extinctions in the geological past. Proceedings of the National Academy of Science, 81, 801–805.

Reed, J.C., Bickford, M.E., Houston, R.S., Link, O.K., Rankin, D.W., Sims, P.K. & Van Schmus, W.R. (editors), 1993. Precambrian: conterminous United States. Geological Society of America, Monograph C-2.

Rhodes, R.C., 1975. New evidence for impact origin of the Bushveld Complex. Geology, 3, 549–554.

Ronca, L.B., 1966. Meteoritic impact and volcanism. Icarus, 5, 515–520.

Runcorn, S.K., 1962. Convection currents in the Earth's mantle. Nature, 195, 1248.

Ryder, G., 1990. Lunar samples, lunar accretion and the early bombardment of the Moon. Eos, 71, 313–322.

Salisbury, J.W. & Ronca, L.B., 1966. The origin of continents. Nature, 210, 669–670.

Shoemaker, E.M. & Shoemaker, C.S., 1990. Proterozoic impact record of Australia. International Workshop on Meteorite Impacts on the Early Earth, Perth. Lunar and Planetary Institute, Contribution 647, 47–48

Shoemaker, E.M. & Wolfe, R.F., 1994. Mass extinctions, crater ages and comet showers. In: Smoluchowski, R., Bahcall, J.N. & Matthews, M.S. (editors), The Galaxy and the Solar System. The University of Arizona Press, 338–386.

Simonson, B.M., 1992. Geological evidence for an early Precambrian microtektite strewn field in the Hamersley Basin of Western Australia. Geological Society of America, Bulletin 104, 829–839.

Stockwell, C.H., 1968. Geochronology of stratified rocks of the Canadian Shield. Canadian Journal of Earth Science, 5, 693–698.

Stothers, R.B., 1991. Linear and circular digital spectral analysis of serial data. Astrophysical Journal 375, 423–426.

Stothers, R.B., 1992. Impacts and tectonism in Earth and Moon history of the past 3800 million years. Earth, Moon and Planets, 58, 145–152.

Stothers, R.B., 1993a. Impact cratering at geologic stage boundaries. Geophysical Research Letters, 20, 887–890.

Stothers, R.B., 1993b. Flood basalts and extinction events. Geophysical Research Letters, 20, 1399–1402.

Stothers, R.B. & Rampino, M.R., 1990. Periodicity in flood basalts, mass extinctions and impacts: a statistical view and a model. Geological Society of America, Special Paper 247, 9–18.

Sutton, J., 1963. Long term cycles in the evolution of continents. Nature, 198, 731–735.

Sylvester, P.J. & Attoh, K., 1992. Lithostratigraphy and composition of 2.1 Ga greenstone belts of the west African craton and their bearing on crustal evolution and the Archaean–Proterozoic boundary. Journal of Geology, 100, 377–393.

Tarney, J., Dalziel, I.W.D. & de Wit, M.J., 1976. Marginal basin 'Rocas Verde' complex from south Chile: a model for Archaean greenstone belt formation. In: Windley, B.F. (editor), Early history of the Earth. Wiley, London, 405–418.

Thurston, P.C., Williams, H.R., Sutcliffe, R.H. & Stott, G.M., 1991. Geology of Ontario. Ontario Geological Survey, Ministry of Northern Development and Mines, Special Volume 4.

Urey, H.C., 1963. Cometary collisions and geological periods. Nature, 242, 32–33.

Von Gruenewaldt, G. & Harmer, R.E., 1993. Tectonic setting of Proterozoic layered intrusions with special reference to the Bushveld Complex. In: Condie, K.C. (editor), Proterozoic crustal evolution. Elsevier, Amsterdam, 181–208.

Wallace, M.W., Gostin, V.A. & Keays, R.R., 1996. Sedimentology of the Neoproterozoic Acraman impact-ejecta horizon, South Australia. AGSO Journal of Australian Geology & Geophysics, this issue.

Weinstein, S.A. 1993. Catastrophic overturn of the Earth's mantle driven by multiple phase changes and internal heat generation. Geophysical Research Letters, 20, 101–104.

Wetherill, G.W. & Shoemaker, E.M., 1982. Collision of astronomically observed bodies with the Earth. Geological Society of America, Special Paper, 190, 1–14.

Wichman, R.W. & Schultz, P.H., 1990a. Implications of early crater-centred volcanism and tectonism at the Sudbury structure, Ontario. Lunar and Planetary Institute, Contribution 746, 56–57.

Wichman, R.W. & Schultz, P.H., 1990b. Implications of impact into viscous mantle rheologies for crater preservation and mantle evolution. Lunar and Planetary Institute, Contribution 746, 58–59.

Wilhelms, D.E., 1987. The geological history of the Moon. United States Geological Survey, Professional Paper 1348.

Williams, G.E., Schmidt, P.W. & Boyd, D.M., 1996. Magnetic signature and morphology of the Acraman impact structure, South Australia. AGSO Journal of Australian Geology & Geophysics (this issue).

Windley, B.F., 1977. The evolving continents. Wiley, London.

Windley, B.F., 1993. Proterozoic collisional and accretionary orogens. In: Condie, K.C. (editor), Proterozoic crustal evolution. Elsevier, Amsterdam, 419–445.

Zhao, W., Yuen, D.A. & Honda, S. 1992. Multiple phase transitions and the style of mantle convection. Physics of the Earth and Planetary Interiors, 72, 185–210.

Appendix I. Moving-windows/least-departure time-series analysis

I devised a time-series method and C. Tarlowski (AGSO) wrote a corresponding Unix program to apply a moving-windows method that would use selected parameters to identify one or more possible periodicities in age-data sets. Chosen parameters include (1) a starting-point age (epoch = To); (2) trial period (Tp = a single bin width); and (3) even-stepped or incremental (I) window-movement rates, expressed as chosen fractions (F) of a single bin width (I = Tp × F). One cycle is defined by a series of incremental shifts of the entire windows overlay over the age-data set for a single bin interval (= trial period) — i.e., To moves to t_min in Tp/F increments (I = Tp × F). A repetition of such cycles for a sequence of trial periods (Tp1, Tp2 ... Tpn) can scan any matches between sequential, complete, or incomplete data sets for chosen sequential ranges and movement increments of trial periods. For an ideal periodic data set, the sum of least departures (min_sum_Tdn) of age values from the period value (defined at the middle of each bin) will be zero, and these values will increase in proportion to increased departures from an ideal periodicity. The normalisation of departures (Td) from mid-bin ([Tn + Tn + 1]/2) positions to the bin width prevents a potential bias arising from the generally increased sum_Td values with increased Tp values in a random data set. The method was tested by several trial data sets containing incomplete time series with one or more introduced periodicities.

The procedure involves the following steps:

1. Data-set age values are defined as t1, t2 ... tn.
2. The range between the youngest age (t1 = t_min) and oldest age (tn = t_max) in a given data set is subjected to an incremental moving-windows overlay.
3. The starting age/epoch (To) of the moving-windows overlay is defined as To = t_min – Tp.
4. The uppermost limit (Tu) of the moving-windows overlay must always comply with: Tu >t_max.
5. The mean (midpoint) of every trial period (Tp) or single bin: Tm
6. In any one cycle, for a chosen Tp (= bin width) value, To on the windows overlay is moved to t_min (= t1) in user-specified increments. The increments are defined in terms of a fraction (F) of the bin width (I = Tp × F), each increment equalling Tp/F. This ensures a proportionality between the size of increments and the size of trial periods (Tp).
7. As the bins overlay moves incrementally over the data set, the departure (Td) of each particular age value (t_x) from the midpoint (Tm = [Tn + Tn + 1]/2) of the bin within which this particular age value happens to fall is measured. Departures (Td) are always given a positive sign, whether t_x >Tm or t_x <Tm), and are normalised to the trial period (Tp): Tdn = 100Td/Tp. Where more than one age value occurs within a single bin, the sum of Tdn values applies to that bin. The normalisation procedure prevents a bias arising from the general increase in Td departure values with increased Tp bin width in random data sets.
8. Commencing with To, for each increment I = Tp/X the sum of normalised departures is calculated for each incremental moving-window position: sum_Tdn = Tdn1 + Tdn2 + Tdnn. (X = the chosen number of increments per bin.)
10. The sum_Tdn departure values for each incremental movement are listed against the corresponding increment number (I1, I2 ... IX).
11. A new trial period (Tp) is chosen and steps 6 to 10 are repeated.
12. An interactive program allows calculation of sum_Tdn values for any chosen range of trial periods (Tp) and chosen number of increments per bin (X).
13. Plots of minimum Tdn values (Y axis) against Tp values allow identification of possible first to nth order periodicities within the data set.

AGSO Journal of Australian Geology & Geophysics, 16 (4), 609–619

Structural interpretations of the Wonga Belt in the Proterozoic Mount Isa Inlier of northwest Queensland—a review

D.H. Blake[1]

Two contrasting interpretations have been put forward recently for the structural evolution of the Wonga Belt, a north–south-trending anticlinal zone of strongly deformed metamorphic rocks, more than 80 km long and up to 5 km wide, in the central part of the Mount Isa Inlier. One interpretation involves major mid-crustal subhorizontal ductile extension with upper plate to the north, and the other involves north–south strike-slip faulting accommodating differential lateral transport of thrust sheets to either side, both the extension and strike-slip faulting taking place before the main folding event. A third interpretation—relatively minor low-angle brittle extensional faulting and subsequent north–south strike-slip faulting predating folding—has been proposed for the southern continuation of the Wonga Belt. Stratigraphic continuity along the Wonga Belt and abrupt changes in stratigraphy across the belt are difficult to reconcile with the south-over-north mid-crustal extension hypothesis, but can be accounted for by the strike-slip faulting component of the other two interpretations. The postulated strike-slip displacement would have exceeded 80 km, and taken place between about 1780 Ma, the maximum age of the youngest metasediments affected, and 1115 Ma, the age of a dolerite dyke that post-dates cross-cutting faults.

Introduction

The Wonga Belt is a north–south-trending anticlinal zone of strongly deformed Proterozoic rocks within the Kalkadoon–Leichhardt Belt, in the central part of the Mount Isa Inlier (Fig. 1). Two contrasting structural interpretations for the main part of the belt have been put forward recently: one by Holcombe and co-workers (Holcombe et al. 1991, 1992, 1993; Oliver et al. 1991; Pearson et al. 1992; and also numerous conference abstracts and unpublished theses not referred to in this review), and the other by Bell, Hammond & Reinhardt (1992), to account for the present disposition of rock units and a doubly plunging lineation and down-dip mineral elongation lineation on the dominant subvertical foliation, which is subparallel to most compositional layering. Holcombe and co-workers consider that, before it was folded into an anticlinorium, the Wonga Belt was part of a subhorizontal extensional shear zone, whereas Bell et al. suggest it was a vertical shear zone. A variation of these interpretations, involving early brittle low-angle extensional faulting and later ductile strike-slip faulting, has been proposed by Passchier (1992) for the southern continuation of the Wonga Belt. The purpose of this paper is to review these structural interpretations and discuss their implications for the regional geology.

The Wonga Belt, which was named by Derrick (1980), extends for more than 80 km north from the Fountain Range Fault (Fig. 1) and is up to 5 km wide. The Fountain Range Fault displaces a southern continuation of the belt about 25 km to the southwest. This continuation is termed the Shinfield Zone in this review, following Passchier (1986a, 1986b, 1992; Passchier & Williams, 1989); it was referred to as the Duchess Belt by Bell et al. (1992) and corresponds to the western part of the Duchess Belt of Blake et al. (1984).

Geological framework

Two major tectonostratigraphic cycles have been identified in the Mount Isa Inlier, as in most other Proterozoic regions in northern Australia (Etheridge et al. 1987). The earlier cycle is represented by basement rocks, which were deformed and metamorphosed before about 1870 Ma, during the Barramundi Orogeny. The later cycle, represented by cover sequences 1–3 (Blake 1987; Blake & Stewart 1992a), was terminated by the Isan Orogeny of Blake et al. (1990). An early phase of this orogeny, D1 of this paper, was dominated by thrusting, according to Bell (1983, 1991). A later phase, D2, at about 1550 Ma, involved open to tight, upright folding about north–south trending axes and regional high-temperature low-pressure metamorphism to upper amphibolite facies. Large granite plutons were emplaced at around 1860 Ma (Kalkadoon Batholith), 1760–1720 Ma (Wonga Batholith), and 1670 Ma (Sybella Batholith), before the Isan Orogeny, and at around 1500 Ma (Williams and Naraku Batholiths). Mafic intrusions of various ages occur throughout the inlier. Several large-scale strike-slip faults trending north–south postdate the D2 folding and metamorphism of the Isan Orogeny. They include the Pilgrim Fault to the east and the Quilalar Fault to the west of the Wonga Belt, which mark the eastern and western boundaries of the Kalkadoon–Leichhardt Belt, separating this tectonic unit from the Western and Eastern Fold Belts of the Mount Isa Inlier (Fig. 1). The Fountain Range Fault separating the Wonga Belt from the Shinfield Zone to the south is one of several major southwest-trending dextral strike-slip faults representing possible splays off the Pilgrim Fault.

The youngest intrusions in the Mount Isa Inlier are dykes of unmetamorphosed dolerite which cut across Isan structures. One of these, the Lakeview Dolerite, has been dated by Page (1983b) at about 1115 Ma (Rb–Sr age). This dyke trends north-northeast across part of the Wonga Belt and, to the south, cuts faults that displace the Shinfield Zone (see Duchess region map of Bultitude et al. 1982, where the dyke is labelled db6), providing a minimum age for the Wonga Belt and Shinfield Zone structures.

The north–south structural grain characteristic of most of the Mount Isa Inlier is an obvious consequence of the D2 Isan folding event and subsequent major strike-slip faulting. However, there is also evidence that the structural grain may have been north–south prior to the Isan Orogeny, as a result of east–west extension. The evidence includes (a) two north–south-trending basins in the west, containing units of cover sequence 2—the Leichhardt River Fault Trough of Glikson et al.(1976) and Derrick (1982), west of the Kalkadoon–Leichhardt Belt, and the Quilalar basin of Jackson et al. (1990), which extended across this belt as far east as the Wonga Belt—and (b) north–south-trending swarms of metamorphosed mafic dykes, especially in the Leichhardt River Fault Trough, and the highly elongate Kalkadoon and Wonga Batholiths, which extend for more than 180 km from south to north, but are less than 20 km across (e.g. Blake 1987).

[1] Australian Geological Survey Organisation, GPO Box 378, Canberra, ACT 2601.

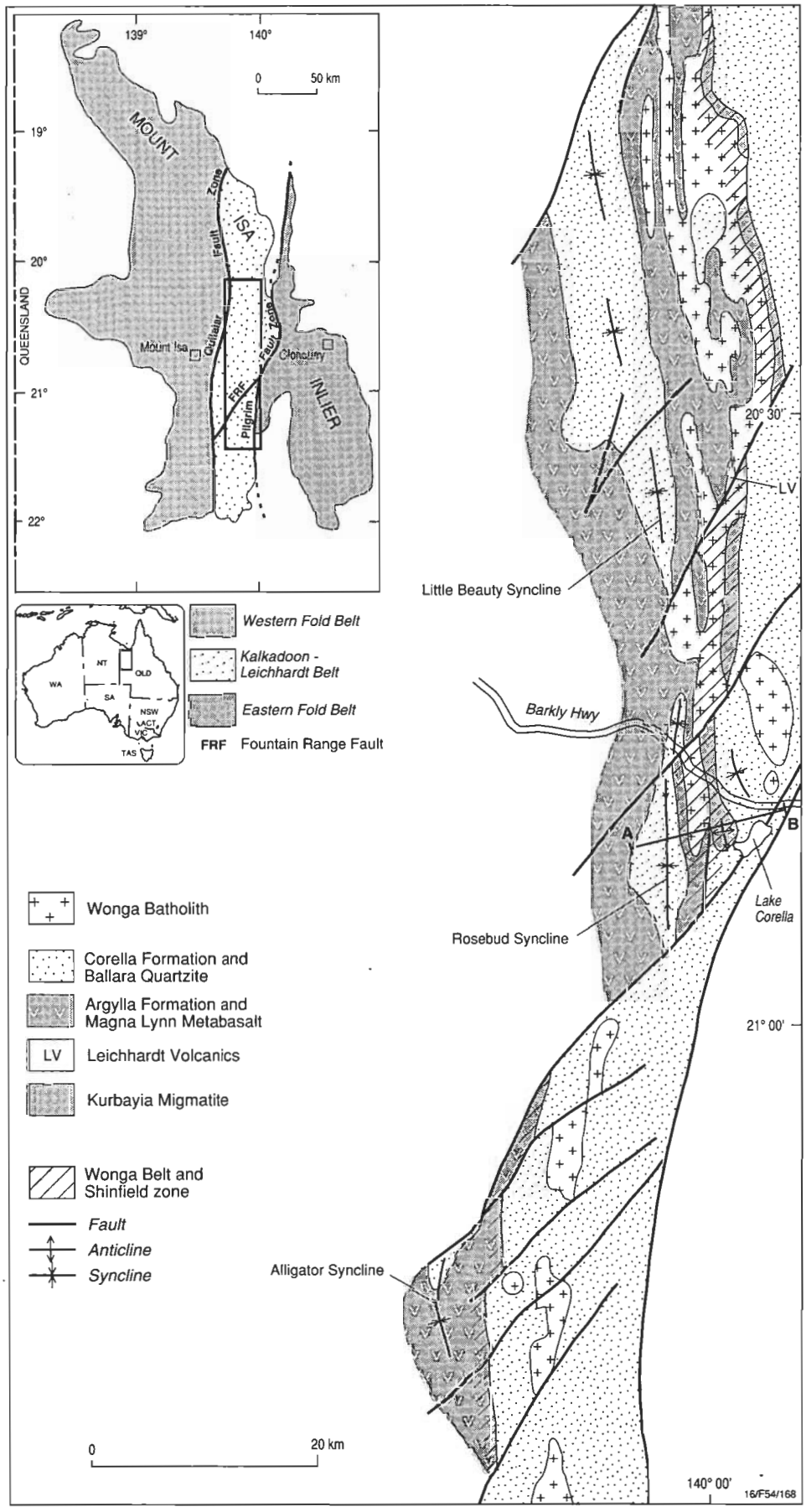

Figure 1. Geological map of the Wonga Belt and its southern continuation, the Shinfield Zone, Mount Isa Inlier. A cross-section from A to B is shown in Fig. 3.

There is also some evidence indicating a north–south structural grain during the earlier Barramundi Orogeny, at least in part of the Kalkadoon–Leichhardt Belt. For example, 20 km east of Mount Isa, near grid reference 630110, Mary Kathleen 1:100 000 sheet (Derrick et al. 1977), three mapped east–west-trending metamorphosed mafic dykes, with a pronounced subvertical north–south-trending foliation attributed to D2 of the Isan Orogeny, cut across subvertical north–south migmatitic banding in basement Kurbayia Migmatite, showing that, here, the Isan D2 foliation and the much earlier Barramundi migmatitic foliation are close to coaxial.

The Wonga Belt contains exposures of basement, cover sequences 1 and 2, granites of the Wonga Batholith, and possibly also granites of the Kalkadoon Batholith (Blake 1992a, 1992b, 1995). Cover sequence 2, younger granite, and possibly also older granite crop out in the Shinfield Zone to the south (Passchier 1992). There is general agreement that the most prominent structural features in this part of the Kalkadoon–Leichhardt Belt—north–south-trending tight upright folds of the Wonga Belt anticlinorium, a subvertical foliation parallel to the axial planes of these folds, and a down-dip mineral elongation lineation on this foliation—and the prevailing amphibolite facies metamorphism were formed during the 1550 Ma D2 phase of the Isan Orogeny (e.g. Oliver et al. 1991; Reinhardt 1992).

Stratigraphy

The stratigraphy of the Wonga Belt is illustrated in Figure 2, and details of the units are summarised in the Appendix. A notable feature is stratigraphic continuity from south to north, along the entire length of the Wonga Belt, but an abrupt change in stratigraphy from west to east, across the belt (see also

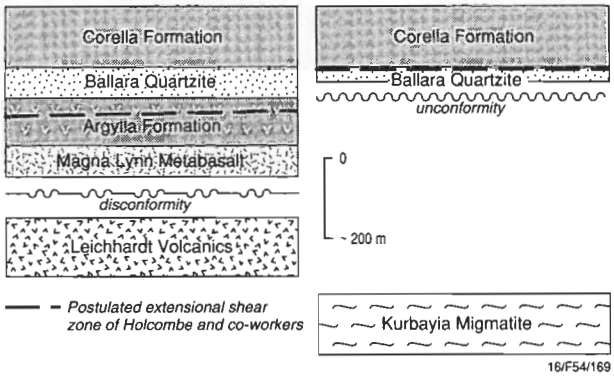

Figure 2. Schematic stratigraphy of the Wonga Belt, showing contrasting successions west and east of the Wonga Belt Fault. Also shown is the position of the postulated extensional shear zone of Holcombe and co-workers (e.g., Holcombe et al. 1993).

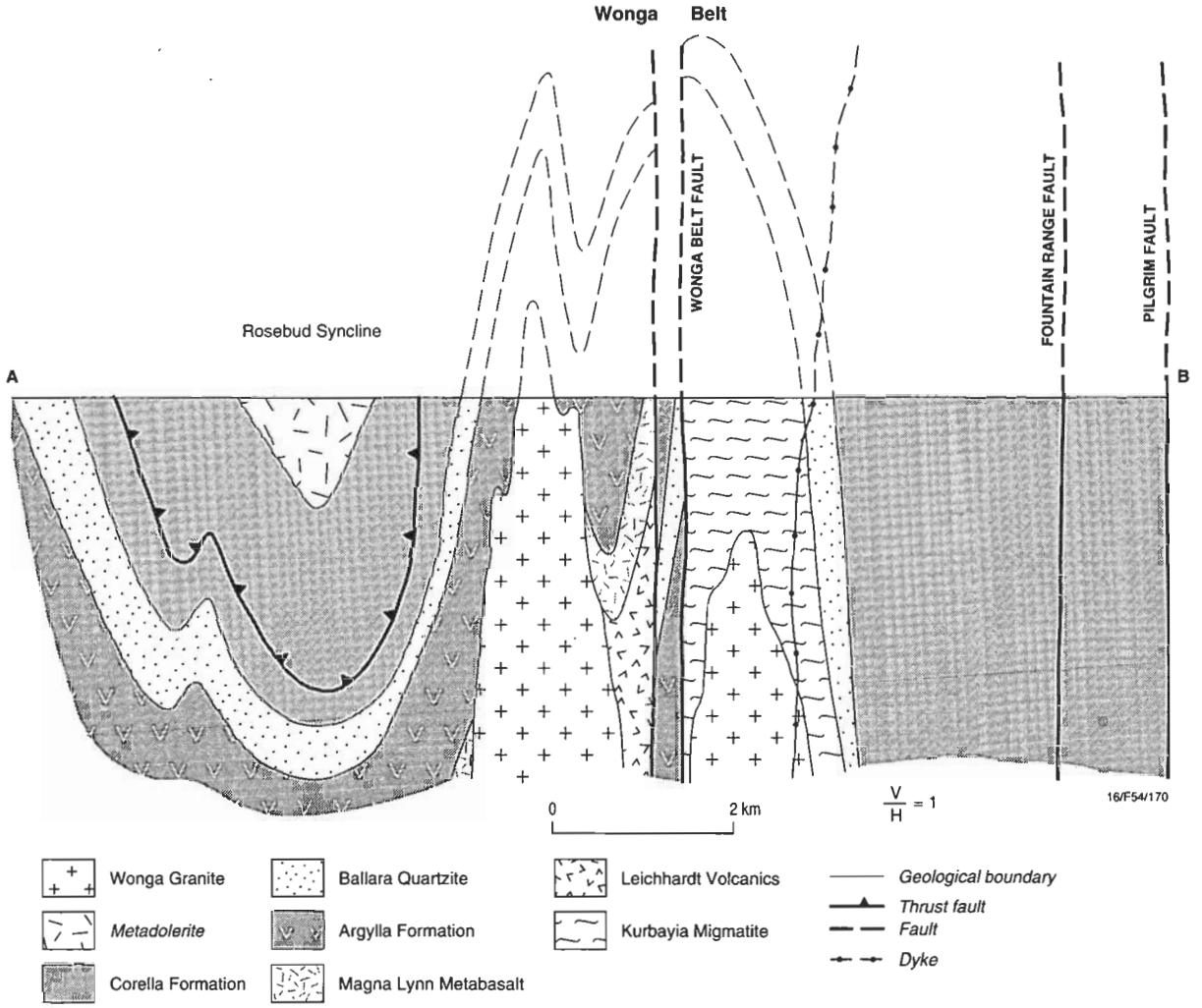

Figure 3. West to east section across the Wonga Belt. Location of section line AB is shown in Fig. 1. The Rosebud Syncline part of the cross-section is based on Reinhardt (1992).

Fig. 3). This change takes place either at a fault (Wonga Belt Fault of Blake & Stewart 1988), as is the case west of Lake Corella (Blake, 1992a), or is masked by metagranite bodies of the Wonga Batholith. Nowhere along the length of the belt can the western sequence be shown to merge into the eastern sequence. Significant differences in stratigraphy between the western and eastern parts of the Wonga Belt are listed below.

- The Argylla Formation and underlying Magna Lynn Metabasalt of cover sequence 2 and the Leichhardt Volcanics of cover sequence 1 crop out in the Wonga Belt only to the west of the Wonga Belt Fault and its inferred continuation to the north. Their combined thickness in this part of the Wonga Belt may be several thousand metres.
- The basement Kurbayia Migmatite (Figs 4–7) in the Wonga Belt crops out only along the eastern side. The rocks of this unit have been regarded by some as belonging to the Argylla Formation (e.g. Derrick 1980; Holcombe et al. 1992; Wilson 1995), but I assign them to the basement because they do not include A-type felsic volcanics of Argylla type (Blake 1995) and show evidence of being folded and metamorphosed to migmatite before they were overlain by Ballara Quartzite (Blake 1992a; but see Holcombe et al. 1993 and Wilson 1995 for alternative explanations of the field evidence) and intruded by granite of the Wonga Batholith (Figs 6 & 7).
- The Ballara Quartzite in the western part is conformable to disconformable on Argylla Formation and includes basal conglomerate in which most of the large clasts are Argylla-type felsic volcanics. In the eastern part, it rests directly on Kurbayia Migmatite, it includes amygdaloidal mafic lava (near Lake Corella), and conglomerate, where present, contains clasts of probable basement rocks, but not Argylla-type volcanics (Fig. 8).

Figure 4. Folded thinly bedded pelitic metasediments of the Kurbayia Migmatite in the Wonga Belt (at GR 972097, Marraba 1:100 000 Sheet). This folding is attributed by the author to the Barramundi Orogeny rather than to the much younger Isan Orogeny.

Figure 5. Vertical foliation planes with doubly plunging intersection lineations in pelitic schist of Kurbayia Migmatite at "Schist Hill" (at GR 982218, Marraba 1:100 000 Sheet): a result of very tight early (Barramundi Orogeny?) folds being overprinted by the axial planar S2 foliation of close-to-coaxial folds during the D2 phase of the Isan Orogeny.

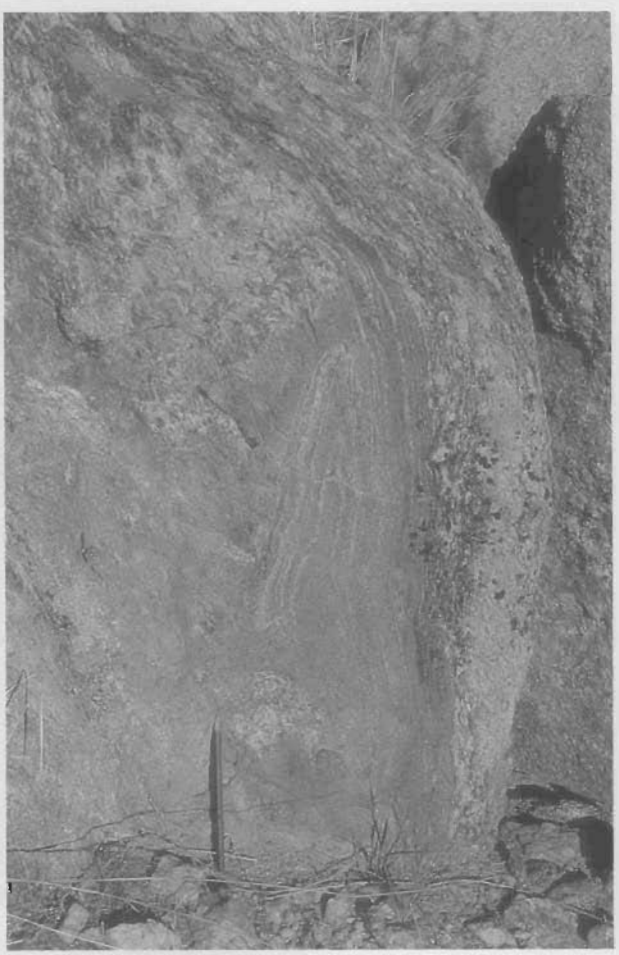

Figure 6. Xenolith in gneissic Wonga Granite of Kurbayia Migmatite showing refolded fold, Wonga Belt (at GR 985229, Marraba 1:100 000 Sheet). The fold is inferred to be a Barramundi structure, much older than the enclosing granite.

Figure 7. Folds in pelitic metasediments, mapped as Kurbayia Migmatite, cut by vein of Wonga Granite (GR 977309, Marraba 1:100 000 Sheet). The folds are probably Barramundi structures, as they predate the granite.

Figure 8. Deformed clasts of probably basement rocks in vertically foliated subvertical conglomerate at the base of the Ballara Quartzite, east side of the Wonga Belt (at GR 978130, Marraba 1:100 000 Sheet). The conglomerate is inferred to be unconformable on Kurbayia Migmatite exposed to the west.

- The Corella Formation to the west can be subdivided into three lithological units (e.g. Derrick et al. 1977), and consists solely of metasediments. The three units cannot be identified with any confidence to the east, where the Corella Formation includes mafic lavas and (east of the Shinfield Zone) felsic metavolcanics as well as metasediments.

Stratigraphic differences are less marked across the anticlinal Shinfield Zone to the south. In this zone (i) no basement or units of cover sequence 1 have been positively identified (although Passchier, 1992, suggests that part of the Bushy Park Gneiss of Bultitude et al. 1982 and Blake 1987 may be basement rather than part of the Wonga Batholith); (ii) Magna Lynn Metabasalt and Argylla Formation have been mapped in both the eastern and western parts of the zone; and (iii) Ballara Quartzite within the zone is confined to thin lenses along the eastern side. However, as pointed out by Passchier (1986, 1992), the Argylla Formation and Ballara Quartzite show a dramatic decrease in thickness across the zone, from at least 1000m to the west, on the western limb of the anticlinal structure, to less than 100m on the eastern limb.

Structural interpretations

According to the interpretation of Holcombe and co-workers (Holcombe et al. 1991, 1992, 1993; Oliver et al. 1991; Pearson et al. 1992), the Wonga Belt represents a mid-crustal (8–10 km depth) subhorizontal extensional shear zone at least 1.5 km thick which was subsequently tightly folded to form the present anticlinorium. In this interpretation, the extension was north–south, with the upper plate moving northwards for many kilometres relative to the lower plate, and involved the development of shear-dominated fabrics and subhorizontal stretching lineations. The extension postdated deposition of the Corella Formation and was broadly synchronous with the emplacement of granites of the Wonga Batholith, taking place between about 1760 and 1730 Ma, more than 100 Ma before the onset of the Isan Orogeny. Later tight folding accompanied regional east–west shortening during the D2 phase of the Isan Orogeny at around 1550 Ma, the time of peak regional metamorphism. The subvertical foliation characteristic of the Wonga Belt is an axial planar D2 structure. The crux of this interpretation is that the original orientation of the extensional shear-dominated fabric was parallel, to within 2°, to subhorizontal stratigraphic layering (Holcombe et al. 1992).

Bell et al. (1992) suggest that the Wonga Belt and its southern continuation, the Shinfield Zone, developed during the D1 phase of the Isan Orogeny as a major vertical ductile strike-slip zone, accommodating differential lateral transport of thrust sheets to either side—north to south thrusting in the west and south to north thrusting in the east. In their interpretation, a subvertical foliation, S1, with a subhorizontal lineation was formed during ductile D1 strike-slip faulting and was subsequently overprinted by the S2 foliation, which was parallel to S1. The D2 phase of the Isan orogeny, at around 1550 Ma, produced the down-dip mineral elongation lineation developed on the main foliation, S2, largely obliterating the D1 foliations and lineations. However, inclusion trails in D2 porphyroblasts in schists of the Corella Formation indicate the presence of three separate, but synchronous, foliations that formed during the D1 thrusting event. From the geometry of the relict foliations and from regional structural considerations, Bell et al. suggest that the Wonga Belt was a zone of strike-slip shearing towards the end of D1, before the D2 folding event. Of the two stretching linea-

tions commonly preserved on the subvertical S2 foliation, the one with variable plunges is considered to be an intersection lineation at some localities and a stretching lineation related to thrusting at others. D1 thrusting, an integral part of the interpretation, has been documented by Reinhardt (1992) on the west side of the Wonga Belt (in the Rosebud Syncline), and is reported on the east side of the belt by Bell et al. (1992).

Passchier (1992) describes the Shinfield Zone as a north–south trending D2 anticlinal zone of highly strained rocks, like the Wonga Belt to the north. He considers the strain evident in the Shinfield Zone to be insufficient to account for the amount of thinning of the Argylla Formation and Ballara Quartzite from west to east across the anticline, and suggests, therefore, that this thinning is mainly due to low-angle brittle faulting of dominantly extensional character predating any ductile deformation. The sense of movement of the extensional faulting was probably hanging wall to the south or southeast (not to the north, as postulated for the Wonga Belt by Holcombe and co-workers). The brittle extension took place after deposition of cover sequence 2 and before the Isan Orogeny, and was probably associated with emplacement of the Wonga Batholith, like extensional structures described from several other localities in the central part of the Mount Isa Inlier (Passchier 1986a, 1986b, 1987, 1991, 1992; Stewart 1987, 1989, 1992; Passchier & Williams 1989; Holcombe et al. 1991, 1992; Pearson et al. 1992). According to Passchier (1992), the brittle extension in the Shinfield Zone predates a north-trending linear shape fabric with variable plunges, which he attributes to ductile north–south strike-slip shearing before D2. The variations in plunge of the lineation are attributed to the overprinting effects of later D2 upright folding and axial planar foliation.

Discussion

In assessing the different structural interpretations, several interrelated problems need to be taken into account. These result from the different experiences, specialities, and abilities of the geologists who have worked in the area, and highlight the need to question so-called 'evidence' and resulting interpretations. Such problems include the following.

- Identifying in the Wonga Belt the protoliths of what are now gneissic rocks. One geologist's metagranite or mylonite may be another geologist's metamorphosed hypabyssal felsic porphyry, or flow-banded rhyolite lava, or ignimbrite flow, or even re-metamorphosed migmatitic basement. My admitted bias for such rocks is commonly towards felsic volcanics; others have a bias towards mylonitised granites.

- Distinguishing different generations of foliations and lineations in complexly deformed terrains. In the Wonga Belt there is a wide variety of rock types with different pre-existing structures and orientations and, consequently, different responses to changing temperature and pressure conditions during deformation. The inhomogeneity is such that distinguishing between the effects of several separate periods of deformation may not always be feasible.

- Correlating rock types and structures from one exposure to the next, let alone across major faults and shear zones, in any area of heterogeneous deformations involving complex folding and faulting. This problem has been highlighted by detailed structural studies in the Mount Novit area south of Mount Isa by Connors et al. (1992).

- Correctly assigning rocks to stratigraphic units: for example, do metasediments on the east side of the Wonga Belt belong to the Argylla Formation (Derrick 1980; Holcombe et al. 1992; Wilson 1995) of cover sequence 2 or to basement Kurbayia Migmatite (Blake 1992a, 1992b, 1995)? (According to Holcombe et al. 1993, this particular question is immaterial for the structural interpretation.)

- Recognising unconformities in highly deformed terrains. For example, an angular unconformity described by Blake (1992a) between basement (Kurbayia Migmatite) and cover sequence 2 (Ballara Quartzite) in the south of the Wonga Belt is dismissed by Holcombe et al. (1993) as an effect of the D2 deformation, with no original angular discordance or different structural histories across the boundary being proved. Another example is a comparable unconformity between basement and cover sequence 2 in the Western Fold Belt about 35 km west of the Wonga Belt (Bultitude et al. 1977; Blake et al. 1984).

- Separating fact (e.g. 'the granite is seen to intrude the sandstone') from interpretation (e.g. 'the granite is inferred to intrude the sandstone')—a perennial problem in geology. An example relevant to the Wonga Belt is the assertion by Holcombe et al. (1993, p. 214) that many granite plutons in the Mount Isa Inlier, including several belonging to the Wonga Batholith, are sill-like bodies of kilometre-scale thickness. This may be a valid interpretation on current evidence, but cannot be proved beyond reasonable doubt.

- Seeing through the overprinting and obscuring effects of the last major deformation and metamorphism to affect the Wonga Belt—the D2 phase of the Isan Orogeny at about 1550 Ma—firstly to identify and secondly to interpret any earlier structures and metamorphisms. Hence, the different views of Holcombe and co-workers, Bell et al., and Passchier on the pre-D2 structural history of the Wonga Belt and Shinfield Zone.

- Distinguishing, in granites of the Wonga Belt, foliations formed during emplacement and crystallisation from foliations formed during post-crystallisation deformation.

- Assessing to what extent small-scale structures mirror the large scale structures. Does the presence of outcrop-scale extensional structures in the Wonga Belt imply the presence of a comparable region-wide structure?

As previously discussed (Blake 1992b), the major north–south extension postulated by Holcombe and co-workers cannot be readily reconciled with a demonstrable stratigraphic continuity of pre-extension rock units from south to north (both above and below the postulated detachment zone) along the entire length of the Wonga Belt, a distance of at least 80 km, and an abrupt change in stratigraphy (according to Blake) from east to west across the belt—over distances ranging from less than 5 metres (across a fault, Fig. 3) to about a kilometre or so where there are separating outcrops of Wonga Granite. In their reply, Holcombe et al. (1993) stressed two features of their model. Firstly, the detachment shear zone separating the upper and lower plates cuts up-section eastwards, coincidently lying entirely within the Argylla Formation on the west side of the Wonga Belt and at the top of the highly attenuated and mylonitic Ballara Quartzite on the east side (Fig. 2). Secondly, the pre-folding discordance between the detachment and stratigraphic boundaries was less than 2°, presumably for the whole length of the Wonga Belt and

for unspecified distances across the belt. They further state that only units above the detachment will preserve any sense of stratigraphic continuity, and that the differences in stratigraphy in the upper plate across the belt are minor and can be accounted for by facies variations. These views conflict with mappable stratigraphic continuity below the Argylla Formation on the west side of the Wonga Belt and below the Corella Formation on the east side, and with my view that the differences in stratigraphy across the belt are much too great and over too short a distance (Fig. 2) to be due simply to facies variations. If the stratigraphic evidence I have put forward (Blake 1992a, 1992b) is confirmed by future work, special pleading is needed for the major detachment zone interpretation of Holcombe and co-workers to remain viable.

To support their extensional model, Holcombe and co-workers cite the structural evidence for relatively minor extension in the central part of the Mount Isa Inlier documented by Passchier (1986a), Passchier & Williams (1989), and Stewart (1989, 1992)—see also Passchier (1986b, 1987, 1991, 1992) and Stewart (1987). The evidence consists mainly of imbricate fault slices of extensional type with cumulative displacements of up to 0.5 km resulting in stratigraphic omissions, listric normal faults, and tourmaline-rich breccias and dolerite intrusions along the faults. This extension took place after deposition of the cover sequence 2 units and before the onset of the Isan Orogeny, so is tentatively correlated with emplacement of the Wonga Batholith. It was essentially brittle in character and appears to be confined to the upper plate of Holcombe et al.'s model. Evidence for movement sense and direction has been largely obscured by overprinting effects of the Isan Orogeny.

Bell et al. (1992) use Rb–Sr isotope data and evidence from inclusion trails in D2 porphyroblasts in schists of the Corella Formation in the Rosebud Syncline, on the west side of the Wonga Belt, to support their view that the earliest foliations and lineations preserved in the cover sequence 2 rocks of the Wonga Belt postdate emplacement of the Wonga Batholith and were formed during the D1 thrusting phase of the Isan Orogeny, not during any earlier extension. This clearly conflicts with the view of Holcombe and co-workers. The suggestion by Bell et al. that the present prevailing subvertical foliation originated as a steep S1 shear zone along which a subhorizontal extensional lineation was formed during strike-slip displacement is in accord with the stratigraphic evidence, in that major north–south strike-slip faulting (but not north–south thrusting) can readily account for the abrupt change in stratigraphy across the Wonga Belt and across the Shinfield Zone.

Some of the doubly plunging intersection lineations on the S2 foliation in the Wonga Belt (e.g., Fig. 5) could be due to overprinting of an early S1 foliation related to thrusting during either later D1 faulting, as suggested by Bell et al., or D2 folding. Other possibilities include S2 overprinting of (i) an earlier ductile extensional foliation, as suggested by Holcombe and co-workers, (ii) coaxial Barramundi folds in basement rocks, as suggested by Blake (1992b; see also Fig. 5), and even, in some cases, (iii) primary flow-banding and igneous foliations in Argylla volcanics and Wonga Granite.

Evidence for thrusting during the Isan Orogeny is widespread in the Mount Isa Inlier, lending support for the thrusting component of the interpretation of Bell et al. (1992). West of the Wonga Belt, inferred directions of thrusting include from north to south for D1 thrusts (e.g. Bell 1983; Loosveld & Schreurs 1987; Blake 1992c; Reinhardt 1992) and east to west for possible D2 thrusts (e.g. Blake 1992d). East of the Wonga Belt, south-over-north thrusting associated with major D1 recumbent folds has been described by Loosveld (e.g. 1992), but only east of the Pilgrim Fault. This fault is a possible terrane boundary and may have a transcurrent displacement of more than 200 km (Blake & Stewart 1988, 1992b), hence the thrusts east of the Pilgrim Fault may not be relevant to the Wonga Belt story.

Major strike-slip faulting along the Wonga Belt and Shinfield Zone before D2 folding, as suggested by Passchier (1992) and Bell et al. (1992), but not minor extension or north–south thrusting alone, can account for the abrupt changes in stratigraphy from west to east and also for some of the structural features. The amount of strike-slip displacement would presumably have to be at least 80 km, as nowhere along the 80 km exposed length of the Wonga Belt can the stratigraphy on the west side be matched in detail with that on the east side. Bell et al. suggest that the strike-slip displacement was sinistral and occurred during the D1 phase of the Isan Orogeny. Blake & Stewart (1988), on the other hand, have suggested that strike-slip faulting along the belt took place before emplacement of Wonga Granite, i.e. between about 1760 and 1750 Ma, as the Wonga Belt Fault appears to predate granite.

There is general agreement that the Wonga Belt and Shinfield Zone anticlinal structure was formed at around 1550 Ma, during the D2 phase of the Isan Orogeny. Some strike-slip movement possibly occurred after the main folding event, as major synclines on the west side of the anticlinorium do not match up closely with major synclines on the east side. However, such faulting may have ceased before the end of the D2 metamorphism, as there is no indication of post-metamorphic north–south faulting along the belt. In any case, all deformation along the belt, including the latest north–south strike-slip faulting, took place before about 1115 Ma, when the Lakeview Dolerite dyke that cuts faults displacing the Shinfield Zone was intruded.

Conclusions

- The structural interpretation of Holcombe and co-workers, that the Wonga Belt represents a major mid-crustal, subhorizontal, extensional shear zone, with the upper plate moving north relative to the lower plate, which was subsequently folded into an anticlinorium, needs to be questioned on several accounts. For example, the interpretation appears to conflict with evidence of stratigraphic continuity along the belt and abrupt changes in stratigraphy across the belt. Also, the postulated extensional shear zone lying at one stratigraphic level on the east side of the belt and at a different stratigraphic level on the west side, for the length of the belt, can be considered an unfortunate coincidence. And, because of differences in style, scale, and movement sense, the proposed major extension in the Wonga Belt cannot be readily linked with the relatively minor extensional structures documented in the Shinfield Zone and elsewhere in the Kalkadoon–Leichhardt Belt.

- The structural interpretation of Bell et al. (1992), that the Wonga Belt and Shinfield Zone represent a vertical shear zone accommodating differential displacement between separate thrust belts to either side, is in accord with the stratigraphic evidence and accounts for at least some of the structural features of the belt.

- The structural interpretation of Passchier (1992), that the deformation prior to D2 (Isan) folding in the Shinfield Zone was partly extensional, but had a significant component of north–south strike-slip movement, is also in accord with the stratigraphic evidence.

- Extensional deformation between 1760 and 1730 Ma, post-dating deposition of cover sequence 2 and predating the Isan Orogeny, may have been an important factor in the development of the Wonga Belt and Shinfield Zone, as it could have led to the apparent concentration of Wonga Granite intrusions in what is now the core of a D2 anticlinorium. However, the amount of displacement caused by extension may have been insignificant compared with that resulting from major strike-slip faulting.

- The main stratigraphic and structural features of the Wonga Belt and Shinfield Zone can be attributed to a combination of north–south strike-slip faulting and D2 Isan folding and metamorphism. If this is correct, the strike-slip faulting probably started after the deposition of the Corella Formation, but possibly before emplacement of the 1760–1720 Ma Wonga Batholith, and may have continued intermittently until after the 1550 Ma D2 folding event. Such faulting had ceased, though, by the time the Lakeview Dolerite was intruded at around 1115 Ma.

Acknowledgements

This paper has benefited from critical reviews by Ken Plumb, Peter Stuart-Smith, and Alastair Stewart of AGSO, Tim Bell (who drew my attention to a major factual error), and Cees Passchier. Comments from other reviewers who strongly criticised the paper have also been taken into account.

References

Bell, T.H., 1983. Thrusting and duplex formation at Mount Isa, Queensland, Australia. Nature, 304, 493–497.

Bell, T.H., 1991. The role of thrusting in the structural development of the Mount Isa Mine and its relevance to exploration in the surrounding region. Economic Geology, 86, 1602–1625.

Bell, T.H., Reinhardt, J. & Hammond, R.L., 1992. Multiple foliation development during thrusting and synchronous formation of vertical shear zones. Journal of Structural Geology, 14, 791–805.

Blake, D.H., 1987. Geology of the Mount Isa Inlier and environs, Queensland and Northern Territory. Bureau of Mineral Resources, Australia, Bulletin, 225.

Blake, D.H., 1992a. Documentation and significance of a major unconformity in the Wonga Belt of the Mt Isa Inlier, northwest Queensland. Australian Journal of Earth Sciences, 39, 671–673.

Blake, D.H., 1992b. Discussion: Tectono-metamorphic evolution of the Mary Kathleen Fold Belt, northwest Queensland: a reflection of mantle plume processes? Australian Journal of Earth Sciences, 39, 675–676.

Blake, D.H., 1992c. Stratigraphy, folding and faulting within the Quilalar Fault System, Mount Isa Inlier. In: Stewart, A.J. & Blake, D.H., (editors), Detailed studies of the Mount Isa Inlier. Bureau of Mineral Resources, Australia, Bulletin 243.

Blake, D.H., 1992d. The compressional Lake Mary Kathleen Fold and Thrust Zone, Mount Isa Inlier. In: Stewart, A.J. & Blake, D.H. (editors), Detailed studies of the Mount Isa Inlier. Bureau of Mineral Resources, Australia, Bulletin 243.

Blake, D.H., 1995. Reply to Discussion, Documentation and significance of a major unconformity in the Wonga Belt of the Mount Isa Inlier, northwest Queensland. Australian Journal of Earth Sciences, 42, 226–227.

Blake, D.H. & Page, R.W., 1988. Early Proterozoic migmatitic basement in the Kalkadoon–Leichhardt Belt of the Mount Isa Inlier, northwest Queensland. BMR Journal of Australian Geology & Geophysics, 10, 323–328.

Blake, D.H. & Stewart, A.J., 1988. Block and possible terrane boundaries in the Mount Isa Inlier. BMR Research Newsletter, 9, 2–3.

Blake, D.H. & Stewart, A.J., 1992a. Stratigraphic and tectonic framework, Mount Isa Inlier. In: Stewart, A.J. & Blake, D.H. (editors), Detailed studies of the Mount Isa Inlier. Bureau of Mineral Resources, Australia, Bulletin 243.

Blake, D.H. & Stewart, A.J., 1992b. The BMR 1983–1990 Mount Isa project: results, some remaining problems, and bibliography. In: Stewart, A.J. & Blake, D.H. (editors), Detailed studies of the Mount Isa Inlier. Bureau of Mineral Resources, Australia, Bulletin 243.

Blake, D.H., Bultitude, R.J., Donchak, P.J.T., Wyborn, L.A.I. & Hone, I.G., 1984. Geology of the Duchess–Urandangi region, Mount Isa Inlier, Queensland. Bureau of Mineral Resources, Australia, Bulletin 219.

Blake, D.H., Etheridge, M.A., Page, R.W., Stewart, A.J., Williams, P.R. & Wyborn, L.A.I., 1990. Mount Isa Inlier—regional geology and mineralisation. Australasian Institute of Mining and Metallurgy, Monograph 14, 1, 915–925.

Bultitude, R.J. & Wyborn, L.A.I., 1982. Distribution and geochemistry of volcanic rocks in the Duchess–Urandangi region. BMR Journal of Australian Geology & Geophysics, 7, 99–112.

Bultitude, R.J., Gardner, C.M. & Noon, T.A., 1977. A recently discovered unconformity near the base of the Proterozoic Cloncurry Complex south of Mount Isa, northwestern Queensland. BMR Journal of Australian Geology & Geophysics, 2, 311–314.

Bultitude, R.J., Blake, D.H. & Donchak, P.J.T., 1982. Duchess region, Queensland. Bureau of Mineral Resources, Australia, 1:100 000 Geological Map Commentary.

Connors, K.A., Proffett, J.M., Lister, G.S., Scott, R.J., Oliver, N.H.S. & Young, D.J., 1992. Geology of the Mount Novit Ranges, southwest of Mount Isa mine. In: Stewart, A.J. & Blake, D.H. (editors), Detailed studies of the Mount Isa Inlier. Bureau of Mineral Resources, Australia, Bulletin 243.

Derrick, G.M., 1980. Marraba, Queensland. Bureau of Mineral Resources, Australia, 1:100 000 Geological Map Commentary.

Derrick, G.M., 1982. A Proterozoic rift zone at Mount Isa, Queensland, and implications for mineralisation. BMR Journal of Australian Geology & Geophysics, 7, 81–92.

Derrick, G.M., Wilson, I.H., Hill, R.M., Glikson, A.Y. & Mitchell, J.E., 1977. Geology of the Mary Kathleen 1:100 000 Sheet area, northwest Queensland. Bureau of Mineral Resources, Australia, Bulletin 193.

Etheridge, M.A., Rutland, R.W.R. & Wyborn, L.A.I., 1987. Orogenesis and tectonic process in the Early to Middle Proterozoic of northern Australia. In: A. Kroner (editor), Proterozoic lithospheric evolution. Geodynamic Series 17, 131–147. American Geophysical Union and Geological Society of America, Washington, D.C.

Glikson, A.Y., Derrick, G.M., Wilson, I.H. & Hill, R.M., 1976. Tectonic evolution and crustal setting of the Middle Proterozoic Leichhardt River Fault Trough, Mount Isa Region, northwestern Queensland. BMR Journal of Australian Geology & Geophysics, 1, 115–129.

Holcombe, R.J., Pearson, P.J. & Oliver, N.H.S., 1991. Geometry of a Middle Proterozoic extensional decollement in northeastern Australia. Tectonophysics, 191, 255–274.

Holcombe, R.J., Pearson, P.J. & Oliver, N.H.S., 1992. Structure of the Mary Kathleen Fold Belt. In: Stewart, A.J. & Blake, D.H. (editors), Detailed studies of the Mount Isa Inlier. Bureau of Mineral Resources, Australia, Bulletin 243.

Holcombe, R.J., Oliver, N.H.S., Hill, E.J. & Pearson, P.J., 1993. Reply to discussion on: Tectono-metamorphic evolution of the Mary Kathleen Fold Belt, northwest Queensland: a reflection of mantle plume processes? Australian Journal of Earth Sciences, 40, 213–215.

Jackson, M.J., Simpson, E.L. & Eriksson, K.A., 1990. Facies and sequence stratigraphic analysis in an intracratonic thermal-relaxation basin: the Early Proterozoic, Lower Quilalar Formation and Ballara Quartzite, Mount Isa Inlier, Australia. Sedimentology, 37, 1053–1078.

Loosveld, R.J.H., 1992. Structural geology of the central Soldiers Cap Belt, Mount Inlier, Australia. In: Stewart, A.J. & Blake, D.H. (editors), Detailed studies of the Mount Isa Inlier. Bureau of Mineral Resources, Australia, Bulletin 243.

Loosveld, R. & Schreurs, G., 1987. Discovery of thrust klippen northwest of Mary Kathleen, Mt Isa inlier, Australia. Australian Journal of Earth Sciences, 34, 387–402.

Oliver, N.H.S., Holcombe, R.J., Hill, E.J. & Pearson, P.J., 1991. Tectono-metamorphic evolution of the Mary Kathleen Fold Belt, northwest Queensland: a reflection of mantle plume processes? Australian Journal of Earth Sciences, 38, 425–455.

Page, R.W., 1983a. Timing of superposed volcanism in the Proterozoic Mount Isa Inlier, Australia. Precambrian Research, 21, 223–245.

Page, R.W., 1983b. Chronology of magmatism, skarn formation and uranium mineralization, Mary Kathleen, Queensland, Australia. Economic Geology, 78, 838–853.

Passchier, C.W., 1986a. Evidence for early extensional tectonics in the Proterozoic Mount Isa inlier, Australia. Geology, 14, 1008–1011.

Passchier, C.W.,1986b. Proterozoic deformation in the Duchess belt, Australia. Geologie en Mijnbouw, 65, 47–56.

Passchier, C.W., 1987. Reply to comment by A.J. Stewart on: Evidence for early extensional tectonics in the Proterozoic Mount Isa inlier, Australia. Geology, 15, 977–979.

Passchier, C.W., 1991. Deformation in the Revenue granite pluton, Mount Isa, Australia. Geologie en Mijnbouw, 70, 275–285.

Passchier, C.W., 1992. Geology of the Myubee area, Mount Isa Inlier, Queensland. In: Stewart, A.J. & Blake, D.H. (editors), Detailed studies of the Mount Isa Inlier. Bureau of Mineral Resources, Australia, Bulletin 243.

Passchier, C.W. & Williams, P.R., 1989. Proterozoic extensional deformation in the Mount Isa inlier, Queensland, Australia. Geological Magazine, 126, 43–53.

Pearson, P.J., Holcombe, R.J. & Page, R.W., 1992. Synkinematic emplacement of the Middle Proterozoic Wonga Batholith into a mid-crustal extensional shear zone, Mount Isa Inlier, Queensland, Australia. In: Stewart, A.J. & Blake, D.H. (editors), Detailed studies of the Mount Isa Inlier. Bureau of Mineral Resources, Australia, Bulletin 243.

Reinhardt, J., 1992. The Corella Formation of the Rosebud Syncline (central Mount Isa Inlier): deposition, deformation, and metamorphism. In: Stewart, A.J. & Blake, D.H. (editors), Detailed studies of the Mount Isa Inlier. Bureau of Mineral Resources, Australia, Bulletin 243.

Stewart, A.J., 1987. Comment on: Evidence for early extensional tectonics in the Proterozoic Mount Isa Inlier, Australia. Geology, 15, 976–977.

Stewart, A.J., 1989. Extensional faulting as the explanation for the Deighton 'Klippe' and other Mount Albert Group outliers, Mount Isa Inlier, northwestern Queensland. Australian Journal of Earth Sciences, 36, 405–421.

Stewart, A.J., 1992. Stratigraphy, extension, and contraction in the Ballara–Mount Frosty area, Mount Isa Inlier, Queensland. In: Stewart, A.J. & Blake, D.H. (editors), Detailed studies of the Mount Isa Inlier. Bureau of Mineral Resources, Australia, Bulletin 243.

Wilson, I.H., 1983. Geochemical discrimination of acid volcanic units in the Mount Isa region, Queensland. BMR Journal of Australian Geology & Geophysics, 8, 109–117.

Wilson, I.H., 1995. Discussion: Documentation and significance of a major unconformity in the Wonga Belt of the Mount Isa Inlier, northwest Queensland. Australian Journal of Earth Sciences, 42, 225–226.

Appendix: Rock units of the Wonga Belt and Shinfield Zone

	Distribution	*Thickness*	*Lithology*	*Relationships*	*Structures*	*Age*
BASEMENT						
Kurbayia Migmatite	Eastern part of Wonga Belt; not present in Shinfield Zone. Extensive exposures west of the Wonga Belt, but none to east.		Partly migmatitic pelitic metasediments (Figs 4–7), subordinate grey felsic metavolcanics, minor foliated grey granodiorite of possibly Kalkadoon type. Leucosomes and layering in metasediments are complexly folded.	Overlain unconformably by Ballara Quartzite according to Blake (1992a); intruded by pink feldspar metaporphyry of Argylla type (forming central parts of two composite dykes with mafic margins), amphibolite dykes, Wonga Granite (Figs 6, 7), and possibly Kalkadoon Granite, all of which postdate migmatisation and associated complex minor folding.	Complex tight to isoclinal minor folds outlined by leucosomes and lithologic layering (interpreted as mainly bedding), mostly about north–south-trending subvertical axial planes; similarly oriented foliation with down-dip mineral elongation lineation generally prominent, and a doubly plunging (folded) intersection lineation (bedding/layering and main foliation) present in places (e.g., Fig. 5).	Migmatisation of Kurbayia Migmatite exposed to west is older than 1860 Ma (Blake & Page 1988).
COVER SEQUENCE 1						
Leichhardt Volcanics	Small outcrop in western part of Wonga Belt, east of the Little Beauty Syncline (Fig. 1). Extensive exposures farther west, but none to east.	>100 m, base not exposed.	Grey foliated fine-grained felsic volcanic rocks with small augen/phenocrysts; I-type chemistry (e.g., Blake et al. 1990).	Overlain disconformably by Magna Lynn Metabasalt; intruded by Wonga Granite.	Subvertical north–south Trending foliation and down-dip mineral elongation lineation.	Leichhardt Volcanics west of Wonga Belt dated at around 1865 Ma (e.g. Page 1983).
COVER SEQUENCE 2						
Magna Lynn Metabasalt	Western part of Wonga Belt and in Shinfield Zone to south. Extensive exposures farther west, but none to east.	> 100 m.	Metabasalt and interlayered mafic and minor felsic metasediments.	Overlain conformably, and in places interfingers with basal part of, Argylla Formation; intruded by Wonga Granite and, in Shinfield Zone, by leucocratic phase of Bushy Park Gneiss (Passchier 1992).	Steep westerly dipping to subvertical bedding and subparallel foliation trending north-south.	Essentially same as overlying Argylla Formation.
Argylla Formation	Western part of Wonga Belt and in Shinfield Zone to south. Extensive exposures farther west and in Eastern Fold Belt to east.	>1000 m	Pinkish purple strongly to weakly foliated felsic metavolcanics, including meta-ignimbrite and flow-banded metarhyolite; typically appreciably magnetic, A-type chemistry (e.g., Blake et al., 1990). Minor bedded arkosic metasediments and quartzite. Felsic volcanics generally readily distinguished from those of Leichhardt Volcanics on field and chemical criteria (Bultitude & Wyborn 1982; Wilson 1983).	Overlain conformably to disconformably by Ballara Quartzite; intruded by amphibolite and Wonga Granite.	Bedding, where evident, moderately to steeply dipping; subvertical strong to weak gneissic foliation generally present, with down-dip mineral elongation lineation.	About 1780 Ma (for example, page 1983)

Ballara Quartzite	Western and eastern parts of Wonga Belt, and eastern side of Shinfield Zone. Extensive exposures to west, but none to east. Outlines major folds (Little Beauty, Rosebud and Alligator Synclines) in west, but mostly confined to narrow lenses (megaboudins) on east side of Wonga Belt and Shinfield Zone.	> 500m (where not structurally disrupted) in west; generally 0–80m in east, but up to 300m in closure of south-plunging anticline near Lake Corella.	In west: metamorphosed cross-bedded quartz sandstone, commonly with conglomerate containing abundant felsic volcanic clasts of Argylla type at or near base. In east: quartzite, generally intensely foliated; conglomerate (no Argylla-type clasts) locally at base (Fig. 8); altered mafic lava in lower part near Lake Corella.	Conformable and disconformable on Argylla Formation in west, unconformable on Kurbayia Migmatite in east (Blake 1992a); overlain conformably by Corella Formation; intruded by granites of Wonga Batholith.	Tight upright major and meso folds in west, doubly plunging, with north–south-trending axial planar cleavage; forms strongly foliated north–south-trending vertical boudin-like bodies in east, except near Lake Corella, where, in closure of southerly plunging anticline, a well developed foliation, subparallel to bedding, dips south and southeast (Fig. 2a in Blake 1992a).	Inferred to be around 1780 Ma, only slightly younger than underlying Argylla Formation.
Corella Formation	Western and eastern parts of Wonga Belt and eastern part of Shinfield Zone. Extensive exposures to east and west.	> 1000m.	Metamorphosed pelitic and calcareous metasediments; includes cordierite–anthophyllite rock, marble, and scapolitic and amphibolitic calc-silicate rocks; mafic volcanics on east side of Wonga Belt and mafic and felsic volcanics on east side of Shinfield Zone.	Conformable on Ballara Quartzite in west and presumably also in east; intruded by large mafic sills in west (in centres of Rosebud and Little Beauty synclines) and by granites of Wonga Batholith (e.g. Burstall Granite) and amphibolite in east.; cut by dyke of Lakeview Dolerite.	Major tight to isoclinal doubly plunging synclines, axial planar foliation, steeply plunging lineations; intrafolial and parasitic folds.	Younger than 1780 Ma (Argylla Formation) and older than 1760 Ma (Wonga Batholith).
GRANITE						
Wonga Batholith (taken to include Wonga Granite and Bushy Park Gneiss)	Wonga Belt and Shinfield Zone and to east.		Gneissic granite and leucogranite, augen gneiss.	Granites of batholith intrude Leichhardt Volcanics, Magna Lynn Metabasalt, Argylla Formation, and Ballara Quartzite in west, and Kurbayia Migmatite (Figs 6, 7), Ballara Quartzite and Corella Formation in east; intruded by metamorphosed mafic dykes and by dyke of unmetamorphosed Lakeview Dolerite.	Generally prominent north–south-trending subvertical foliation and down-dip mineral elongation lineation superimposed on mostly weaker earlier foliation and lineation which could be of either igneous or metamorphic origin.	Dated phases range in age from about 1760 to 1720 (Pearson et al., 1992).

AGSO JOURNAL

OF AUSTRALIAN GEOLOGY & GEOPHYSICS

VOLUME 16
1995

AUSTRALIAN GEOLOGICAL SURVEY ORGANISATION
CANBERRA

REVIEWERS OF MANUSCRIPTS FOR VOLUME 16

The Editorial Board of the AGSO Journal of Australian Geology & Geophysics sincerely thanks the following reviewers for their efforts at maintaining the Journal's standard and in selecting papers for publication.

Bob Abell
Ravi Anand
A.W.R. Bevan
P.N. Bierwirth
Lance Black
R.S Blewett
Simon Bolster
Bob Bourman
D.M. Boyd
Albert Brakel
Charles Butt
Richard Carver
David Champion
Colin Chartres
X.Y. Chen
Lee Chenoweth
Max Churchward
J. Claoué-Long
Geoffrey Clarke
Jon Clarke
Dave Cohen
J. Creasey
John Dohrenwend
M.B. Duggan
Tony Eggleton
Pauline English
Bob Galloway
Andrew Glikson
R.A.F. Grieve
Ken Grimes
Reiner Grun
A.R. Hildebrand
Mark Hinman
Dean Hoatson
Mart Idnurm
R.W. Johnson
Bernie Joyce
J.R. Leven
J.F. Lindsay
Steve Lucas
L.F. Macias
Doug Mackenzie
Ken McQueen
Jon Nott
Cliff Ollier
Brian Oversby
Colin Pain
John Percival
M. Pilkington
Brad Pillans
Ian Robertson
R.D. Shaw
John Sheraton
E.M. Shoemaker
A.J. Stewart
P.G. Stuart-Smith
Shen-su Sun
S.R. Taylor
A.M. Therriault
David Tilley
M.W. Wallace
J. Webb
A.T. Wells
A. Whitaker
Lisa Worrall
G.E.Williams
Bob Young

VOLUME 16, NUMBERS 1 & 2, 1995

Thematic issue: The Giles mafic ultramafic complex and environs, western Musgrave Block, central Australia

Guest associate editor: Andrew Glikson
Preface: The Giles mafic ultramafic complex and environs, western Musgrave Block, central Australia 1

A. Davidson
A review of the Grenville orogen in its North American type area 3

G.L. Clarke, S.-S. Sun & R.W. White
Grenville-age belts and associated older terranes in Australia and Antarctica 25

A.Y. Glikson, C.G. Ballhaus, G.L. Clarke, J.W. Sheraton, A.J. Stewart & S.-S. Sun
Geological framework and crustal evolution of the Giles mafic-ultramafic complex and environs, western Musgrave Block, central Australia 41

Chris Ballhaus & Andrew Y. Glikson
The petrology of layered mafic–ultramafic intrusions of the Giles Complex, western Musgrave Block, Western Australia 69

A.J. Stewart
Resolution of conflicting structures and deformation history of the Mount Aloysius granulite massif, western Musgrave Block, central Australia 91

John W. Sheraton & Shen-Su Sun
Geochemistry and origin of felsic igneous rocks of the western Musgrave Block 107

G.L. Clarke, I.S. Buick, A.Y. Glikson & A.J. Stewart
Structural and pressure-temperature evolution of host rocks of the Giles Complex, western Musgrave Block, central Australia: evidence for multiple high-pressure events 127

A.J.Stewart
Western extension of the Woodroffe Thrust, Musgrave Block, central Australia 147

J.H. Leven & J.F. Lindsay
A geophysical investigation of the southern margin of the Musgrave Block, South Australia 155

L.F. Macias
Remote sensing of mafic–ultramafic rocks: examples from Australian Precambrian terranes 163

A.Y. Glikson & J.W. Creasey
Application of Landsat-5 TM imagery to mapping of the Giles Complex and associated granulites, Tomkinson Ranges, western Musgrave Block, central Australia 173

VOLUME 16, NUMBER 3, 1995

Thematic issue: Australian Regolith Conference `94

Guest associate editors: Colin Pain & Mike Craig

Colin Pain, Mike Craig & Graham Taylor
Australian Regolith Conference `94 195

C.F. Pain & C.D. Ollier
Regolith stratigraphy: principles and problems 197

Clinton J. Rivers, Tony Eggleton & Simon D. Beams
Ferricretes and deep weathering profiles of the Puzzler Walls, Charters Towers, north Queensland 203

Jonathan D.A. Clarke & Lee Chenoweth
Classification, genesis and evolution of ferruginous surface grains 213

Aro V. Arakel
Quaternary vadose calcretes revisited 223

R.P. Bourman
Towards distinguishing transported and *in situ* ferricretes: data from southern Australia 231

David C. Lawie & Paul M. Ashley
Geochemical characterisation of iron-rich regolith materials in the Olary Block of South Australia 243

S. Alipour, A.C. Dunlop & D.R. Cohen
Morphology of lag in the Cobar region, New South Wales....253

D.M. Robertson
Interpretation of fabrics in ferruginous lag....263

S.M. Hill
The differential weathering of granitic rocks in Victoria, Australia....271

R.S.B. Greene & W.D. Nettleton
Soil genesis in a longitudinal dune–swale landscape, New South Wales, Australia....277

Brad Pillans & Robert Bourman
The Brunhes/Matuyama Polarity Transition (0.78 Ma) as a chronostratigraphic marker in Australian regolith studies....289

G.H. McNally & I.R. Wilson
Silcretes of the Mirackina Palaeochannel, Arckaringa, South Australia....295

Jonathan Nott
Long-term landscape evolution on Groote Eylandt, Northern Territory....303

I.C. Roach, K.G. McQueen & Graham Taylor
Discussion: Landscape evolution and tectonics in southeastern Australia (Ollier & Pain 1994)....309

Paul Bishop
Discussion: Landscape evolution and tectonics in southeastern Australia (Ollier & Pain 1994)....315

J.F. Nott
Discussion: Landscape evolution and tectonics in southeastern Australia (Ollier & Pain 1994)....319

Shu Li, J.A. Webb & B.L. Finlayson
Discussion: Landscape evolution and tectonics in southeastern Australia (Ollier & Pain 1994)....323

C.D. Ollier & C.F. Pain
Reply: Landscape evolution and tectonics in southeastern Australia (Ollier & Pain 1994)....325

General Papers

Samir Shafik
Calcareous microplankton biostratigraphy of the Eocene Browns Creek Clay in the Aire District, Otway Basin of southeastern Australia: an update....333

John W. Sheraton, Andrew G. Tindle & Robert J. Tingey
Geochemistry, origin, and tectonic setting of granitic rocks of the Prince Charles Mountains, Antarctica....345

VOLUME 16, NUMBER 4, 1995

Thematic issue: Australian impact structures

Guest associate editor: Andrew Y. Glikson

A.Y. Glikson
Preface....371

A.Y. Glikson (compiler)
A compendium of Australian impact structures, possible impact structures, and ejecta occurrences....373

R.S. Dietz
The significance of extraterrestrial impacts with reference to Australia....377

E.M. Shoemaker & C.S. Shoemaker
The Proterozoic impact record of Australia....379

R.A.F. Grieve & M. Pilkington
The signature of terrestrial impacts....399

A.W.R. Bevan
Australian crater-forming meteorites....421

G.E. Williams, P.A. Schmidt, & D.M. Boyd
Magnetic signature and morphology of the Acraman impact structure, South Australia....431

M.W. Wallace, V. Gostin, & R.R. Keays
Sedimentology of the Neoproterozoic Acraman impact-ejecta horizon, South Australia 443

D.J. Milton, A.Y. Glikson, & R. Brett
Gosses Bluff — a latest Jurassic impact structure, central Australia.
Part 1: geological structure, stratigraphy and origin 453

D.J. Milton, B.C. Barlow, A.R. Brown, F.J. Moss, E.A. Manwaring, E.C.E. Sedmik, G.A. Young, & J. Van Son
Gosses Bluff — a latest Jurassic impact structure, central Australia.
Part 2: seismic, magnetic, and gravity studies 487

P.R. Tingate, J.F. Lindsay, & S.J. Marshallsea
Impact structures as potential petroleum exploration targets: Gosses Bluff, a Late Jurassic example in central Australia 529

J.D. Gorter, R.J. Korsch, & R.S. Nicoll
Thermal history of the Gosses Bluff impact structure, central Australia, from conodont colour-alteration indices: implications for hydrocarbon prospectivity and erosional history 553

P.W. Haines
Goyder impact structure, Arnhem Land, Northern Territory 561

F.L. Sutherland
The Cretaceous/Tertiary-boundary impact and its global effects with reference to Australia 567

A.Y. Glikson
Mega-impacts and mantle-melting episodes: tests of possible correlations 587

General paper

D.H. Blake
Structural interpretation of the Wonga Belt in the Proterozoic Mount Isa Inlier of northwest Queensland — a review 609

Map

D.J. Milton
Geology of the central uplift, Gosses Bluff impact structure, Northern Territory (1:7500 geological map)

GEOLOGY OF THE CENTRAL UPLIFT

GOSSES BLUFF IMPACT STRUCTURE

NORTHERN TERRITORY

1978

Scale 1:7500

100 0 100 200 300 400 500 metres

132° 17′ 132° 18′ 132° 19′

23° 48′ 23° 49′ 23° 50′

Scattered outcrops of Dd not shown

GOSSES BLUFF NORTH

Esso Gosses Bluff No. 1

A A′ B B′

St 38 Flow breccia

St BMR Hermannsburg 32

Sections

Scale $\frac{V}{H} = 1$

Elevation in metres

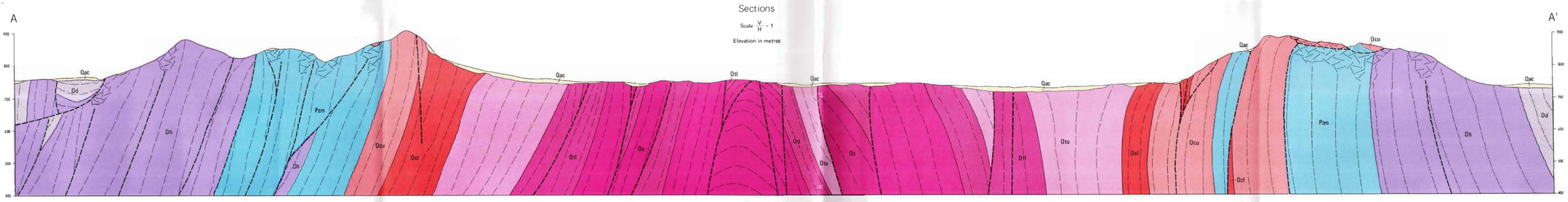

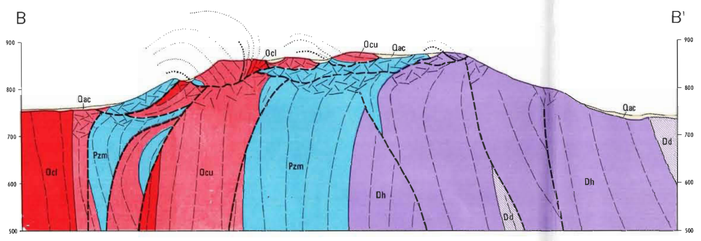

CAINOZOIC	QUATERNARY		Qac — *Alluvium and colluvium*
PALAEOZOIC	DEVONIAN	Pertnjara Group: Parke Siltstone Member, Dare Siltstone Member, Harajica Sandstone Member	Dd — *Siltstone and shale; some fine grained sandstone in upper part* Dh — *Red-brown fine to medium grained sandstone, massive or cross-bedded; red siltstone near base*
	SILURIAN (?) AND DEVONIAN	Mereenie Sandstone	Pzm — *Light-coloured medium and fine grained sandstone, commonly cross-bedded, Scolithus tubes abundant; red coarse-grained sandstone and siltstone near base*
	ORDOVICIAN	Larapinta Group: Carmichael Sandstone, Upper unit	Ocu — *White medium and fine grained sandstone, even-bedded or cross-bedded at low angles*
		Lower unit	Ocl — *Sandstone and siltstone, thickly interbedded, predominantly red*
		Stokes Siltstone, Upper unit	Otu — *Shale and siltstone; some limestone near base*
		Lower unit	Otl — *Bimodal calcareous sandstone, limestone and siltstone*
		Stairway Sandstone	Os — *Fine and very fine grained sandstone*

- *Breccia: clasts showing nearly random attitudes*
- *Flow breccia, clasts highly shocked, many have melted and flowed*
- *Broken rock: clasts roughly retaining local attitudes*
- *Breccia and broken rock (section only)*
- *Geological boundary*
- *Boundary of allochthonous block; teeth are on block*
- *Fault*

Where location of boundaries and faults is approximate, line is broken; where concealed boundaries are dotted, faults are shown by short dashes

- *Strike and dip of strata*
- *Vertical strata*
- *Horizontal strata*
- *Strike and dip of overturned strata*
- *Trend lines*
- WH *Water hole*
- *Petroleum exploration well, abandoned*
- *Contour, in metres*
- St *BMR stratigraphic hole*
- *Vehicle track*

LOCALITY MAP

Mapping 1968-69 by D. J. Milton, USGS
P. R. Brett, USGS
A. Y. Glikson, BMR
Compiled 1974 by D. J. Milton
Drawn by Mercury-Walch, Hobart, Australia
Printed by Mercury-Walch, Hobart, Australia

Reprinted 1996 by Land Information Centre, Bathurst, NSW

Published by the Bureau of Mineral Resources, Geology and Geophysics, Department of National Development. Issued under the authority of the Minister for National Development.
Base map compiled by the US Geological Survey from aerial photography at 1 : 24 000 scale

Copies of this map may be obtained from the Bureau of Mineral Resources, Geology and Geophysics, Canberra, ACT

GOSSES BLUFF IMPACT STRUCTURE

NORTHERN TERRITORY

Burst, J.F., 1965. Subaqueously formed shrinkage cracks in clay. Journal of Sedimentary Petrology, 35, 348–353.

Davies, G.R., 1970. Algal-laminated sediments, Gladstone Embayment, Shark Bay, Western Australia. *In*: Logan, B.W., Davies, G.R., Read, J.F. & Cebulski, D.E. (editors), Carbonate sedimentation and environments, Shark Bay, Western Australia. American Association of Petroleum Geologists, Memoir 13, 169–205.

Friedman, G.M. & Sanders, J.E., 1978. Principles of sedimentology. Wiley, New York.

Wellman, P. & McDougall, I., 1974. Cainozoic igneous activity in eastern Australia. Tectonophysics, 23, 49–65.

Illustrations

Line diagrams or maps should be professionally drafted. (AGSO can provide a full professional drafting service to *Journal* standards at competitive rates. See advertisement below.) Figures should be designed for reproduction at either single column (80mm) or double column (165mm) width. Final versions of line drawings should be supplied as high-contrast photographic prints, but photocopies of draft figures may be submitted initially (see **Submissions** above).

All illustrations, both line drawings and photographs, are referred to as figures.

Figures should be numbered consecutively, in the order in which they are referred to in the text, with parts of an individual figure identified, if necessary, by upper case letter.

Do not draft figure titles on the figure. Captions are typeset and should be listed on a separate sheet.

Photographs should be good quality glossy prints. Scale in photographs should be indicated by either a recognisable object or a plain bar scale whose length is given in the figure caption.

Figures are reproduced in black and white unless special arrangements for use of colour have been made with the editor.

Tables

Tables should be set out on separate sheets. When preparing tables, if possible, please use the Tables function of your word-processor rather than use tabs to align columns.

Providing a disk version

When your manuscript has been accepted, you will be asked to provide a copy on disk.

The disk can be either 3.5 or 5.25 inch MS-DOS or Apple Macintosh format. The Journal is edited using MS Word for Windows version 6, which can convert from most other word-processing programs. Please check with the editor if you have any doubts, or send an ASCII file as backup.

Proofs

Authors will receive one proof of their manuscript, in its final formatted version, but without illustrations, to check before it goes for printing. Authors may be charged for the cost of major changes.

Reprints

The author(s) will receive a total of 50 free reprints of their paper.

Authors may buy extra reprints, which should be ordered when proofs are returned. The cost for 50 additional reprints is $100; special rates apply if more are required.

Please address all correspondence to

The Editor,
AGSO Journal of Australian Geology & Geophysics
Australian Geological Survey Organisation
GPO Box 378
ACT 2601

Tel. (06) 249 9771
Fax (06) 249 9990

AGSO
AUSTRALIAN GEOLOGICAL SURVEY ORGANISATION

AGSO Journal of Australian Geology & Geophysics

Volume 16, Number 4, 1996

Thematic issue: Australian impact structures*

* In honour of Robert S. Dietz (1914-1995) - pioneer of astrobleme research - and of Eugene M. Shoemaker and Carolyn S. Shoemaker for their major contributions to the study of Australian impact structures.

Guest associate editor: Andrew Y. Glikson

A.Y. Glikson
Preface 371
A.Y. Glikson (compiler)
A compendium of Australian impact structures, possible impact structures, and ejecta occurrences 373
R.S. Dietz
The significance of extraterrestrial impacts with reference to Australia 377
E.M. Shoemaker & C.S. Shoemaker
The Proterozoic impact record of Australia 379
R.A.F. Grieve & M. Pilkington
The signature of terrestrial impacts 399
A.W.R. Bevan
Australian crater-forming meteorites 421
G.E. Williams, P.W. Schmidt, & D.M. Boyd
Magnetic signature and morphology of the Acraman impact structure, South Australia 431
M.W. Wallace, V. Gostin, & R.R. Keays
Sedimentology of the Neoproterozoic Acraman impact-ejecta horizon, South Australia 443
D.J. Milton, A.Y. Glikson, & R. Brett
Gosses Bluff - a latest Jurassic impact structure, central Australia. Part 1: geological structure, stratigraphy, and origin 453
D.J. Milton, B.C. Barlow, A.R. Brown, F.J. Moss, E.A. Manwaring, E.C.E. Sedmik, G.A. Young, & J. Van Son
Gosses Bluff - a latest Jurassic impact structure, central Australia. Part 2: seismic, magnetic, and gravity studies 487
P.R. Tingate, J.F. Lindsay, & S.J. Marshallsea
Impact structures as potential petroleum exploration targets: Gosses Bluff, a Late Jurassic example in central Australia 529
J.D. Gorter, R.J. Korsch, & R.S. Nicoll
Thermal history of the Gosses Bluff impact structure, central Australia, from conodont colour-alteration indices: implications for hydrocarbon prospectivity and erosional history 553
P.W. Haines
Goyder impact structure, Arnhem Land, Northern Territory 561
F.L. Sutherland
The Cretaceous/Tertiary-boundary impact and its global effects with reference to Australia 567
A.Y. Glikson
Mega-impacts and mantle-melting episodes: tests of possible correlations 587

General paper

D.H. Blake
Structural interpretations of the Wonga Belt in the Proterozoic Mount Isa Inlier of northwest Queensland - a review 609

Map (in back pocket):

D.J. Milton
Geology of the central uplift, Gosses Bluff impact structure, Northern Territory (1:7500 geological map)